Related titles

Understanding the rheology of concrete
(ISBN 978-0-85709-028-7)

Non-destructive evaluation of reinforced concrete structures
Volume 1: Deterioration processes and standard text methods
(ISBN 978-1-84569-560-6)

Non-destructive evaluation of reinforced concrete structures
Volume 2: Non-destructive testing methods
(ISBN 978-1-84569-950-5)

Toxicity of building materials
(ISBN 978-85709-122-2)

Building materials in civil engineering
(ISBN 978-1-84569-955-0)

Building decorative materials
(ISBN 978-0-85709-257-1)

Woodhead Publishing Series in Civil and Structural Engineering: Number 55

Eco-efficient Masonry Bricks and Blocks

Design, Properties and Durability

Edited by

F. Pacheco-Torgal, P.B. Lourenço, J.A. Labrincha, S. Kumar and P. Chindaprasirt

ELSEVIER

AMSTERDAM • BOSTON • CAMBRIDGE • HEIDELBERG
LONDON • NEW YORK • OXFORD • PARIS • SAN DIEGO
SAN FRANCISCO • SINGAPORE • SYDNEY • TOKYO
Woodhead Publishing is an imprint of Elsevier

Woodhead Publishing is an imprint of Elsevier
80 High Street, Sawston, Cambridge, CB22 3HJ, UK
225 Wyman Street, Waltham, MA 02451, USA
Langford Lane, Kidlington, OX5 1GB, UK

British Library Cataloguing-in-Publication Data
A catalogue record for this book is available from the British Library

Library of Congress Control Number: 2014949117

ISBN 978-1-78242-305-8 (print)
ISBN 978-1-78242-318-8 (online)

Typeset by TNQ Books and Journals
www.tnq.co.in
Printed and bound in the United Kingdom

List of contributors

H. Abanda Oxford Brookes University, Oxford, UK

M.M.A. Abdullah Universiti Malaysia Perlis, Perlis, Malaysia

S. Ahmari Cornerstone Engineering Inc., Louisville, KY, USA

E.M. Alawadhi Kuwait University, Kuwait

R. Alonso-Santurde Universidad de Cantabria, Cantabria, Spain

A. Andrés Universidad de Cantabria, Cantabria, Spain

C.C. António Universidade de Porto, Porto, Portugal

T. Blanco Universidad de Cantabria, Cantabria, Spain

M. Bruggi Politecnico di Milano, Milan, Italy

T. Cao Surface Design Consulting Pty Ltd, Sydney, NSW, Australia

C.F. Castro Universidade de Porto, Porto, Portugal

R. Černý Czech Technical University, Prague, Czech Republic

A. Chaipanich Chiang Mai University, Chiang Mai, Thailand

P. Chindaprasirt Khon Kaen University, Khon Kaen, Thailand

M. Coronado Universidad de Cantabria, Cantabria, Spain

M. D'Orazio Universitá Politecnica delle Marche, Ancona, Italy

H. de Sousa Universidade de Porto, Porto, Portugal

G. Elambo Nkeng Ecole Nationale Supérieure des Travaux Publics, Cameroun, Africa

A.D. González CONICET and Universidad Nacional del Comahue, Bariloche, Argentina

J.N.F. Holanda Northern Fluminense State University, Rio de Janeiro, Brazil

D. Hotza Federal University of Santa Catarina, Florianópolis, Brazil

W.M.W. Ibrahim Universiti Malaysia Perlis, Perlis, Malaysia

M.C. Juárez Universidad de La Rioja, Logroño, Spain

J.M. Kinuthia University of South Wales, Pontypridd, UK

V. Kočí Czech Technical University, Prague, Czech Republic

S. Kumar CSIR-National Metallurgical Laboratory, Jamshedpur, India

S. Lenci Universitá Politecnica delle Marche, Ancona, Italy

P.B. Lourenço University of Minho, Guimaraes, Portugal

B.G.O. Maia Federal University of Santa Catarina, Florianópolis, Brazil

M.P. Morales Universidad Autónoma de Chile, Santiago, Chile

F. Pacheco-Torgal University of Minho, Braga, Portugal

N. Phonphuak Rajabhat Maha Sarakham University, Maha Sarakham, Thailand

E. Quagliarini Universitá Politecnica delle Marche, Ancona, Italy

N. Quijorna Universidad de Cantabria, Cantabria, Spain

Radhakrishna R V College of Engineering, Bangalore, India

I.A. Rahman Universiti Tun Hussein Onn Malaysia, Jalan, Malaysia

F.V. Riza Universiti Tun Hussein Onn Malaysia, Jalan, Malaysia

L. Sousa Universidade de Porto, Porto, Portugal

R. Sousa Universidade de Porto, Porto, Portugal

J.H.M. Tah Oxford Brookes University, Oxford, UK

M.F.M. Tahir Universiti Malaysia Perlis, Perlis, Malaysia

A. Taliercio Politecnico di Milano, Milan, Italy

G. Vasconcelos University of Minho, Guimaraes, Portugal

L. Zhang University of Arizona, Tucson, AZ, USA

Woodhead Publishing Series in Civil and Structural Engineering

1 **Finite element techniques in structural mechanics**
C. T. F. Ross
2 **Finite element programs in structural engineering and continuum mechanics**
C. T. F. Ross
3 **Macro-engineering**
F. P. Davidson, E. G. Frankl and C. L. Meador
4 **Macro-engineering and the earth**
U. W. Kitzinger and E. G. Frankel
5 **Strengthening of reinforced concrete structures**
Edited by L. C. Hollaway and M. Leeming
6 **Analysis of engineering structures**
B. Bedenik and C. B. Besant
7 **Mechanics of solids**
C. T. F. Ross
8 **Plasticity for engineers**
C. R. Calladine
9 **Elastic beams and frames**
J. D. Renton
10 **Introduction to structures**
W. R. Spillers
11 **Applied elasticity**
J. D. Renton
12 **Durability of engineering structures**
J. Bijen
13 **Advanced polymer composites for structural applications in construction**
Edited by L. C. Hollaway
14 **Corrosion in reinforced concrete structures**
Edited by H. Böhni
15 **The deformation and processing of structural materials**
Edited by Z. X. Guo
16 **Inspection and monitoring techniques for bridges and civil structures**
Edited by G. Fu
17 **Advanced civil infrastructure materials**
Edited by H. Wu
18 **Analysis and design of plated structures Volume 1: Stability**
Edited by E. Shanmugam and C. M. Wang

19 **Analysis and design of plated structures Volume 2: Dynamics**
Edited by E. Shanmugam and C. M. Wang
20 **Multiscale materials modeling**
Edited by Z. X. Guo
21 **Durability of concrete and cement composites**
Edited by C. L. Page and M. M. Page
22 **Durability of composites for civil structural applications**
Edited by V. M. Karbhari
23 **Design and optimization of metal structures**
J.Farkas and K. Jarmai
24 **Developments in the formulation and reinforcement of concrete**
Edited by S. Mindess
25 **Strengthening and rehabilitation of civil infrastructures using fiber-reinforced polymer (FRP) composites**
Edited by L. C. Hollaway and J. C. Teng
26 **Condition assessment of aged structures**
Edited by J. K. Paik and R. M. Melchers
27 **Sustainability of construction materials**
J. Khatib
28 **Structural dynamics of earthquake engineering**
S. Rajasekaran
29 **Geopolymers: Structures, processing, properties and industrial applications**
Edited by J. L. Provis and J. S. J. van Deventer
30 **Structural health monitoring of civil infrastructure systems**
Edited by V. M. Karbhari and F. Ansari
31 **Architectural glass to resist seismic and extreme climatic events**
Edited by R. A. Behr
32 **Failure, distress and repair of concrete structures**
Edited by N. Delatte
33 **Blast protection of civil infrastructures and vehicles using composites**
Edited by N. Uddin
34 **Non-destructive evaluation of reinforced concrete structures Volume 1: Deterioration processes**
Edited by C. Maierhofer, H.-W. Reinhardt and G. Dobmann
35 **Non-destructive evaluation of reinforced concrete structures Volume 2: Non-destructive testing methods**
Edited by C. Maierhofer, H.-W. Reinhardt and G. Dobmann
36 **Service life estimation and extension of civil engineering structures**
Edited by V. M. Karbhari and L. S. Lee
37 **Building decorative materials**
Edited by Y. Li and S. Ren
38 **Building materials in civil engineering**
Edited by H. Zhang
39 **Polymer modified bitumen**
Edited by T. McNally
40 **Understanding the rheology of concrete**
Edited by N. Roussel
41 **Toxicity of building materials**
Edited by F. Pacheco-Torgal, S. Jalali and A. Fucic

42 **Eco-efficient concrete**
Edited by F. Pacheco-Torgal, S. Jalali, J. Labrincha and V. M. John
43 **Nanotechnology in eco-efficient construction**
Edited by F. Pacheco-Torgal, M. V. Diamanti, A. Nazari and C. Goran-Granqvist
44 **Handbook of seismic risk analysis and management of civil infrastructure systems**
Edited by F. Tesfamariam and K. Goda
45 **Developments in fiber-reinforced polymer (FRP) composites for civil engineering**
Edited by N. Uddin
46 **Advanced fiber-reinforced polymer (FRP) composites for structural applications**
Edited by J. Bai
47 **Handbook of recycled concrete and demolition waste**
Edited by F. Pacheco-Torgal, V. W. Y. Tam, J. A. Labrincha, Y. Ding and J. de Brito
48 **Understanding the tensile properties of concrete**
Edited by J. Weerheijm
49 **Eco-efficient construction and building materials: Life cycle assessment (LCA), eco-labeling and case studies**
Edited by F. Pacheco-Torgal, L. F. Cabeza, J. Labrincha and A. de Magalhães
50 **Advanced composites in bridge construction and repair**
Edited by Y. J. Kim
51 **Rehabilitation of metallic civil infrastructure using fiber-reinforced polymer (FRP) composites**
Edited by V. Karbhari
52 **Rehabilitation of pipelines using fiber-reinforced polymer (FRP) composites**
Edited by V. Karbhari
53 **Transport properties of concrete: Measurement and applications**
P. A. Claisse
54 **Handbook of alkali-activated cements, mortars and concretes**
Edited by F. Pacheco-Torgal, J. A. Labrincha, C. Leonelli, A. Palomo and P. Chindaprasirt
55 **Eco-efficient masonry bricks and blocks: Design, properties and durability**
Edited by F. Pacheco-Torgal, P. B. Lourenço, J. A. Labrincha, S. Kumar and P. Chindaprasirt
56 **Eco-efficient materials for mitigating building cooling needs: Design, properties and applications**
Edited by F. Pacheco-Torgal, J. A. Labrincha, L. F. Cabeza and C.-G. Granqvist

Foreword

Brickwork and blockwork are very usual construction systems, mainly for houses and apartment buildings. These construction technologies are extensively employed worldwide both in developed and developing countries, sometimes due to strong cultural aspects, long time tradition or even as a symbol of solid construction. Moreover the good performance of masonries is well known by the users, including its strength, thermal and acoustical properties. In developing countries besides the former reasons, brickwork or blockwork are the only suitable methods for self-construction in non-industrialized circumstances.

However the traditional masonry units are usually non-eco-friendly products, mainly because of their high energy consuming components due to their production method (fired-clay bricks) or their compounds (high Portland cement consumption in the concrete or earth-based blocks). That is why for a sustainable construction these traditional and usual building systems are avoided. Nevertheless sustainability is not restricted to environmental aspects, it has to take into account the social requirements and economic feasibility. Therefore the search for eco-efficient masonry units is of utmost importance for the building industry. For this reason this book fulfills an important gap in the building knowledge and provides the designers, architects and engineers with important up-to-date information to re-establish the masonry as a suitable system for eco-efficient buildings.

This publication analyzes the subject in a very comprehensive approach. The traditional masonry units, fired-clay bricks and concrete blocks, are intensively studied in 10 chapters, including the optimized concrete design for the blocks and highly perforated shape for the bricks, paying attention for their thermal performance and pointing out the possibility of using industrial and agricultural wastes as replacement for the raw materials, with emphasis on the fly-ash to the bricks and pozzolana to the blocks. The lightweight concrete blocks have also been considered, mainly those produced with autoclaved aerated concrete. In addition, the millenary adobe blocks are evaluated as suitable products for masonry in the present days, adopting modern techniques for production and of course with much care for their durability. The possibility of the use of PCM (phase change materials) into building envelop has been discussed, mainly for the thermal performance of the masonry.

Geopolymeric blocks, considered a new family of masonry units, have been presented extensively, as they can consume large amount of residues such as fly-ash, mine-tailings, red-mud, blast furnace slag, silica fume and metakaolins.

Theoretical aspects are also presented, primarily regarding the optimization of the topology of the units and their environmental performance, mainly for the energy assessment and carbon dioxide production during the manufacture of the units.

In my opinion, this publication is an important tool for the revival of masonry in several countries where the environmental constraints have restricted their use not in favor of the consumers' wishes. It provides significant collaboration to the society as it gives the professionals of the building industry enough confidence that the use of masonry can be as eco-efficient as other products developed during the last decades that are already available in large scale for the use in buildings and constructions.

Vahan Agopyan
Professor of Building Materials and Components
University of S. Paulo, Escola Politécnica
Vice-President of the University of S. Paulo

Introduction to eco-efficient masonry bricks and blocks

1

F. Pacheco-Torgal
University of Minho, Braga, Portugal

1.1 Brief historical considerations on masonry bricks and blocks: past, present and future

The first masonry units were based on dried mud and were used for the first time around 8000 BC in Mesopotamia, an area bordered by the Tigris and Euphrates rivers stretching from Southeast Turkey, Northern Syria, and Iraq reaching the Persian Gulf (Pacheco-Torgal & Jalali, 2011).

Today, earth masonry units (adobe or compressed earth blocks) still represent a large share of the built environment. Between one-third up to 50 percent of the world's population lives in earth-based dwellings (Guillaud, 2008). The majority of earth construction is located in less developed countries, however, this kind of construction can also be found in Germany, France or even the United Kingdom (Hall, Lindsay, & Krayenhoff, 2012).

As to the fired-clay bricks, their use goes back to around 3000 BC (Lynch, 1994). Even the Roman civilization has left several buildings constructed with fired-clay bricks, for example, the library of Celsus in Ephesus built in 117 AD.

The compressive strength and durability to weathering of fired-clay bricks have made them a widely used construction material for thousands of years. An excellent source on brick history can be found in the book *Brick: A World History* by Campbell and Pryce (2003). It's worth mentioning that this book has an excessive focus on brick masonry's grand architectural features and is less focused on the engineered aspects of brick masonry. Common clay-fired bricks still serve as the base of recent and amazing buildings (Figure 1.1), highlighting the notorious words of the architect Louis Khan on this building material (Scully, 1993).

With the appearance of Portland cement in the twenty-first century, masonry concrete blocks emerged as an alternative to fired-clay bricks, although the latter are still predominant to a large extent. For instance in the United Kingdom, concrete blocks represent only around five percent of the total masonry units production (Bingel & Bown, 2009).

Because of the high kiln-firing temperatures, the fired-clay industry has high energy consumption and is responsible for high greenhouse gas emissions (GHG). Creation of fired-clay bricks has an energy consumption that is almost 300% higher than the energy consumption of concrete blocks (Reddy & Jagadish, 2003). Taking into account the lower embodied energy of concrete blocks, it's expected that in the future this material will gain a higher market share. Still, masonry fired-clay bricks and

Eco-efficient Masonry Bricks and Blocks. http://dx.doi.org/10.1016/B978-1-78242-305-8.00001-2

Figure 1.1 Indian Institute of Management, Ahmedabad (Louis Khan, 1962−1974).

concrete blocks are and will continue to be widely used construction materials around the world, even in highly developed countries. According to a report forecast (Freedonia Group, 2010), US demand for fired-clay brick and concrete block products is projected to increase nearly twelve percent annually from a weak 2009 base to 12.4 billion units in 2014 (66% clay bricks and 37% concrete blocks). This represents just a small proportion of the annual worldwide production. Machine-made brick production, using automated kilns, is approximately 125 billion bricks. China alone is responsible for 100 billion units. Around 91% of the total brick production (1391 billion units) concerns handmade bricks. China and India are the major producers of handmade bricks, respectively, with 700 billion and 144 billion units respectively. The remaining countries are responsible for the production of 422 billion units (Habla, 2014; Sabapathy & Maithel, 2013). This leads to the exploitation of hundreds of millions of tons of nonrenewable resources and, to make things worse, in the next decades the brick (and block) demand will continue to rise just because the building construction industry in less developed countries will also rise steadily (until 2030 urban land cover will increase by 1.2 million km^2 (Seto, Buneralp, & Hutyra, 2012)) to deal with the dramatic increase of urban population (in the next 40 years, urban population will be about 3000 million people (WHO, 2014)).

1.2 Contributions of masonry bricks and blocks for eco-efficient construction

The concept of eco-efficiency was firstly coined in the book *Changing Course* (Schmidheiny, 1992) in the context of the 1992 Earth Summit process. This concept includes "*the development of products and services at competitive prices that meet the needs of humankind with quality of life, while progressively reducing their environmental impact and consumption of raw materials throughout their life cycle, to a level compatible with the capacity of the planet.*"

In the last 10 years, around 1000 papers were published in Scopus journals related to masonry units. The terms "eco-efficiency" or "eco-efficient" were mentioned in only in 0.3% of those papers, meaning that the eco-efficiency concept has not yet successfully entered in the masonry research field. This is especially disturbing in the context of the major environmental threats faced by our planet and the major environmental impacts of the construction industry. Since energy efficiency improvements have the greatest potential of any single strategy to abate global GHG emissions, a major worldwide environmental problem, from the energy sector (IEA, 2012), and since the building sector is a large energy user responsible for about 40% of the European Union's total final energy consumption (Lechtenbohmer and Schuring, 2011), this means that energy efficiency is a priority for eco-efficient construction. The Energy Road Map 2050 (COM (2011), 885/2) confirmed that higher energy efficiency in new and existing buildings is key for the transformation of the EU's energy system. The European Energy Performance of Buildings Directive 2002/91/EC (EPBD) was recast in the form of the 2010/31/EU by the European Parliament on 19 May 2010. One of the new aspects of the EPBD, which reflects an ambitious agenda on the reduction of the energy consumption, is the introduction of the concept of nearly zero-energy building (Pacheco-Torgal, Cabeza, Mistretta, Kaklauskas, & Granqvist, 2013).

Since walls are the major surface areas of the buildings through which considerable amounts of heat are exchanged between the interior and the external environment, the use of masonry units with improved thermal conductivity contributes to the reduction of heat losses in buildings. Therefore, reducing heat energy needs represents an important contribution for eco-efficient construction. A simple way to achieve that concerns the pore forming technique. It takes advantage of the fact that during the firing stage the combustion of organic matter (sawdust, tobacco residues, grass waste, sawdust, cork dust, paper sludge) leads to the formation of micro-pores. This technique allows for the reduction of the density of fired-clay bricks with organic additions resulting in new bricks with an increased thermal resistance. A more efficient technique encompasses the improvement of the design of the cross-section of masonry units in order to reduce their mass and increase the thermal resistance (minimize their thermal transmittance or U-value). Intense research efforts in this field have turned traditional, thick masonry units into highly perforated ones. This subject is important enough to merit the attention of several chapters in this book. State-of-the-art technology on the cross-section design of fired-clay bricks and lightweight concrete blocks allows single-leaf masonry walls with high thermal performance to be built (Figure 1.2).

In some European countries, these masonry units allow for walls without any additional thermal insulation materials like extruded polystyrene, rigid foam of poly-isocyanurate or polyurethane. These insulation materials are associated with negative impacts in terms of toxicity. Polystyrene, for example, contains antioxidant additives and ignition retardants. Additionally, its production involves the generation of benzene and chlorofluorocarbons. On the other hand, polyurethane is obtained from isocyanates, which are widely known for their tragic association with the Bhopal disaster. Besides, it releases toxic fumes when subjected to fire (Pacheco-Torgal, Fucic, & Jalali, 2012). These masonry units are also specially indicated for

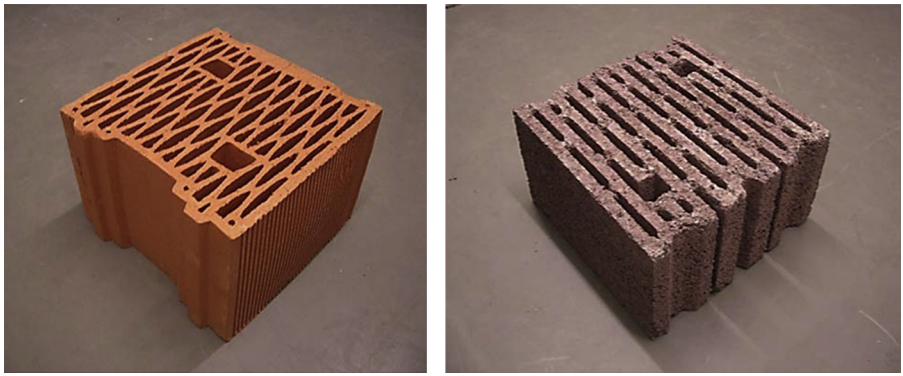

Figure 1.2 Examples of masonry units with enhanced thermal performance. Left: lightweight concrete block; Right: fired-clay brick (Sousa, Castro, Antonio, & Sousa, 2011).

load-bearing structures, even those located in areas prone to seismic risks (Lourenço, Vasconcelos, Medeiros, & Gouveia, 2010).

However, as Sandrolini and Franzoni (2010) recognized, energy savings by means of more efficient thermal insulation is an insufficient approach, further suggesting the inclusion of embodied energy as an important parameter for sustainable construction. A recent review by Cabeza et al. (2013) highlights research efforts to develop building materials with less embodied energy. In a future of a near zero operational energy context, the percentage of the embodied energy in the total energy consumption of the buildings will become increasingly prevalent, and then the use of building materials with lower embodied energy will become a priority area. The energy embodied in construction and building materials (embodied energy) covers the energy consumed during its service life. There are, however, different approaches to this definition, namely: including the energy consumed from the extraction of raw materials to the factory gate (cradle to gate), from extraction to site works (cradle to site) or from extraction to the demolition and disposal (cradle to grave). Berge (2009) considers as embodied energy only the energy needed to bring the material or product to the factory gate (first case), and the transport energy and the energy related to the work execution as being both included in the construction phase of the building. According to this author, the embodied energy represents 85−95% of the material total energy (the remaining 5−15% being related to the construction, maintenance and demolition of the building). As to the third case, the embodied energy includes all energy consumption phases from the production to the cradle. As to the transport energy, it depends on the mode of transport: sea, air, road or rail. Recently Pacheco-Torgal, Faria, and Jalali (2013) studied a 97 apartment-type building (27.647 m^2) located in Portugal, concerning both embodied energy as well as operating energy. The results show that the embodied energy in masonry fire brick units represented 16% of the total energy consumption. If the buildings were in the AA+ energy class, this would mean that the embodied energy in masonry fire brick units could only represent more than 60% of the operating energy for a service life of 50 years. An excellent example of low-embodied-energy masonry units concerns

adobe or compressed earth blocks, which consume as much as 15 times less energy than fired-clay bricks (Zami & Lee, 2010).

The replacement of only 5% of concrete blocks used in the UK masonries by earth masonry would mean a reduction in CO_2 emissions of approximately 100,000 tons (Morton, 2008). Unfortunately, climate change impacts (EEA, 2012) like rivers flooding due to extreme precipitation may pose some limitations to the future use of the earth masonry blocks in the major portion of Europe. Since earth construction is labor intensive, this kind of construction is specially indicated for less developed countries in which the higher housing needs will take place and in which the labor is available for a very low cost (Pacheco-Torgal & Jalali, 2012; Sanya, 2007). That's why earth block masonry constitutes the subject of three chapters of this book.

Last, but not least, another positive way for the brick and block industry to contribute to a more eco-efficient construction encompasses the incorporation of wastes from other industries. This option not only prevents an increase of the area needed for waste disposal, but most important, avoids the exploitation of nonrenewable raw materials used in the production of masonry units, thus reducing its environmental impacts such as deforestation, top-soil loss, air pollution and pollution of water reserves. It is worth remembering that around 1.2 billion people live in areas of physical scarcity, and 500 million people are approaching this situation (Pacheco-Torgal & Labrincha, 2013).

According to the Waste Management Acts 1996 and 2001, wastes can be defined as "any substance or object belonging to a category of waste which the holder discards or intends or is required to discard, and anything which is discarded or otherwise dealt with as if it were waste shall be presumed to be waste until the contrary is proved". In Europe, the milestone related to waste recycling can be found in the Roadmap to a Resource Efficient Europe:

> *By 2020, waste is managed as a resource. Waste generated per capita is in absolute decline. Recycling and reuse of waste are economically attractive options for public and private actors due to widespread separate collection and the development of functional markets for secondary raw materials. More materials, including materials having a significant impact on the environment and critical raw materials, are recycled. Waste legislation is fully implemented. Illegal shipments of waste have been eradicated. Energy recovery is limited to non-recyclable materials, landfilling is virtually eliminated and high quality recycling is ensured.*

So far, a wide variety of waste materials have been studied for fired-clay bricks, including fly ash, mine tailings, slags, construction and demolition waste (CDW), wood sawdust, cotton waste, limestone powder, paper production residue, petroleum effluent treatment plant sludge, kraft pulp production residue, cigarette butts, waste tea, rice husk ash, crumb rubber and cement kiln dust (Zhang, 2013).

Because of its high volume, CDW and mine wastes merit a few additional comments. Eurostat estimates the total for Europe to be 970 million tons/year, representing an average value of almost 2.0 ton/per capita (Sonigo, Hestin, & Mimid, 2010). Currently, the average recycling rate for EU-27 is just 47%. The need to recycle at least

70% of nonhazardous construction and demolition waste by 2020, expressed in COM 571, was set by the Revised Waste Framework Directive 2008/98/EC and does not include naturally occurring material defined in category 170,504 (soil and stones not containing dangerous substances) in the European Waste Catalog. Eurostat estimates the total for Europe to be 970 million tons/year, representing an average value of almost 2.0 ton/per capita. As the current average recycling rate of CDW for EU-27 is only 47%, increasing it to 70% in just a decade seems an ambitious goal, further stressing the need for new and more effective recycling methods (Pacheco-Torgal, Labrincha, Tam, Ding, & de Brito, 2013). Besides, in the next decades, waste recycling will be more and more challenging on the zero-waste scenario (Zaman & Lehmann, 2013).

In other parts of the world (especially in Asia) industrial waste reuse will be even more dramatic just because by 2030, urban land cover will increase by 1.2 million km^2, and that will happen concomitant with an enormous infrastructure boom (Seto et al., 2012).

Mining and quarrying wastes represent a worrying waste responsible for more than 700 million tons/year just in Europe. Mineral waste can be defined as the "residues, tailings or other non-valuable material produced after the extraction and processing of material to form mineral products" (Harrison et al., 2002). Not very long ago, the failure cases of Aznalcollar mine in Spain (1998) which affected 2656 ha of Donana Nature Park with pyrite sludge and Baia Mare mine (2000) in Romania clearly showed that in the short term and environmentally speaking, mine wastes represent a clear and present danger (Pacheco-Torgal & Labrincha, 2013).

Since most mining wastes have toxic substances, research efforts capable of immobilizing these wastes on masonry units would be very important. That is why waste reuse represents an important part of this book, being the subject of five chapters.

Most books already published in masonry have a low-technology approach on this subject, failing to embody any scientific-updated information on masonry units. Those are more suitable for a craftsmanship audience. Others are authored by structural experts and focused on structural details having nothing on masonry units or at maximum a superficial coverage of this issue. The most relevant gap in the literature of masonry units concerns its environmental performance, which is the main reason that led to the making of this book. Assembled by a team of leading international expert contributors, this book constitutes an innovative eco-efficiency approach to masonry units.

1.3 Outline of the book

This book provides an updated state-of-the-art review on the eco-efficiency of masonry units; particular emphasis is placed on the design, properties, performance, durability and environmental performance of these materials.

The first part encompasses an overview on the design, properties and thermal performance of large and highly perforated fired-clay masonry bricks (Chapters 2–4).

Chapter 2 concerns the design and mechanical performance of large and highly perforated fired masonry bricks. The mechanical performance of the units and of the masonry assemblages under distinct loading conditions is discussed. An emphasis is

given to the seismic behavior of hollow, clay brick masonry under combined vertical and lateral in-plane loading, the main seismic performance parameters being discussed.

Chapter 3 addresses the influence of thermal conductivity of clay in the equivalent thermal transmittance of walls built with large and highly perforated fired-clay bricks. The factors that influence heat transfer in single-leaf walls, namely, the geometry of the block (internal voids and vertical joint), the execution of the wall (horizontal joint) and the thermal conductivity of clay are discussed. An equation that enables the calculation of the decrease in the equivalent thermal transmittance of a wall when the thermal conductivity of the clay is decreased is presented.

Chapter 4 covers the influence of several types of clay bricks on the thermal performance of a designed building. These include traditional fired-clay bricks, highly perforated fired-clay bricks without cavity filling and highly perforated fired-clay bricks with expanded polystyrene as cavity filling material. The design, properties and durability of fired-clay masonry bricks containing industrial wastes are the subject of Part Two (Chapters 5–7).

Chapter 5 is concerned with the properties and durability of clay fly ash-based fired masonry bricks. The fly-ash characteristics and its influence on the physical and mechanical properties are analyzed. The durability of the clay-based fired masonry bricks is also covered.

Chapter 6 covers the types of waste, properties and durability of pore-forming waste-based fired-clay masonry bricks. The different types of waste, properties and durability of pore-forming waste-based fired masonry bricks are reviewed.

The different types of waste, properties and durability of toxic waste-based fired masonry bricks are the subject of Chapter 7. It includes a waste classification according to the European Waste List and the distinctive role of wastes in the ceramic process. Its influence on the technical properties of the product as well as on atmospheric emissions are discussed. Its immobilization in the ceramic matrix is also discussed. Considerations on environmental behavior and commercialization are also covered.

Part Three (Chapters 8–11) deals with the design, properties and durability of Portland cement concrete masonry blocks.

Chapter 8 covers the properties and durability of high pozzolanic, industrial by-product content, concrete masonry blocks. The several types of pozzolanic by-products and the fresh and hardened concrete properties, as well as their durability, are reviewed.

Chapter 9 analyses the properties and durability of autoclaved, aerated concrete masonry blocks. It includes an overview on the different types of lightweight concrete, the manufacture and the mechanism of autoclaved, aerated concrete, its physical and mechanical properties, microstructure, thermal conductivity and durability assessed by freeze–thaw resistance.

Chapter 10 covers the design, properties and performance of concrete masonry blocks with phase change material (PCM). Selection criteria, as well as PCM types, are reviewed. The design of PCM-based masonry bricks is discussed. The thermal performance of bricks with PCMs, using either numerical analysis or experimental measurements, is also discussed.

Chapter 11 addresses the design, properties and performance of shape-optimized concrete masonry blocks. It includes a review of innovative masonry blocks developed in recent years, as well as an example of an optimized lightweight concrete masonry unit for single-leaf enclosure walls with no external insulation. Numerical simulations and laboratory tests of two new wall solutions are reported.

Part Four (Chapters 12−15) deals with the design, properties and durability of geopolymeric masonry blocks.

Chapter 12 reviews the properties and durability of fly ash-based geopolymeric masonry blocks, also including a discussion on their production process.

Chapter 13 analyses the properties and durability of mine tailing-based geopolymeric masonry blocks. It includes physical and mechanical properties, durability performance concerning aggressive environments and the effectiveness of immobilization of mine-tailing contaminants.

Chapter 14 looks at the properties and performance of red mud-based geopolymeric masonry blocks. The chemical and mineralogical characteristic of red mud and its suitability for geopolymerization are analyzed. Geopolymerization synergy between red mud and fly ash are studied, as well as properties, durability and leachability of red mud−fly ash.

Chapter 15 is concerned with the design and properties of fly ash, ground granulated blast furnace slag, silica fume and metakaolin geopolymeric-based masonry blocks. A phenomenological model that allows for estimation of the geopolymer blocks compressive strength according to the initial mix design is presented.

The properties and durability of earth-based masonry blocks are the subjects of Part Five (Chapters 16−18).

Chapter 16 concerns the properties and durability of adobe-earth-based masonry blocks. A brief historical digression is presented. Manufacturing details, block dimensions, soil selection and stabilization materials are included. Mechanical and hygro-thermal properties, as well as durability testing procedures of adobe blocks, are discussed. Environmental and economic benefits associated with the use of adobe masonry blocks are also included.

Chapter 17 addresses the properties of compressed earth-based masonry blocks (CEB) including compressed strength, density, water absorption, and moisture buffering capacity, shrinkage and thermal conductivity. The production of CEBs containing agro-waste materials such as rice husk ash (RHA), palm oil fuel ash (POFA) and cassava peels are also reviewed.

Chapter 18 covers the durability of compressed earth-based masonry blocks. A detailed analysis of the factors at play in the determination of durability are presented. Tests and durability indicators are reviewed. The durability of masonry blocks containing industrial, agricultural wastes and by-products is also reviewed.

Finally, Part Six concerns topology optimization and environmental performance (Chapters 19−22).

Chapter 19 is concerned with topology optimization for the development of eco-efficient masonry units. The influence of the design constraints and the geometry of the boundary on the optimal layout of the blocks are numerically investigated.

The decrease in thermal transmittance of the optimized units is compared to that of the commercially available blocks.

Chapter 20 addresses environmental performance and energy assessment of fired-clay brick masonry. The use of alternative fuels is analyzed. Process efficiency and environmental impacts are assessed and compared.

Chapter 21 covers the case of energy and carbon embodied in straw and fired-clay masonry bricks. The manufacturing of wall blocks with straw and clay by small enterprises is introduced. Energy and carbon embodied is assessed. Comparisons with energy and carbon embodied of current fired-clay bricks and concrete blocks are included. Thermal resistance comparisons are also included.

Chapter 22 closes Part Six with a case study concerning the assessment of embodied energy and CO_2 of earth-block and concrete masonry-block houses.

References

Berge, B. (2009). *The ecology of building materials* (2nd ed.). Architectural Press, ISBN 978-1-85617-537-1. Elsevier Science.

Bingel, P., & Bown, A. (2009). Sustainability of masonry in construction. In J. Khatib (Ed.), *Sustainability of construction materials*. Cambridge: Woodhead Publishing Limited.

Cabeza, L. F., Barreneche, C., Miró, L., Morera, J., Bartolí, E., & Fernández, A. (2013). Low carbon and low embodied energy materials in buildings: a review. *Renewable and Sustainable Energy Reviews, 23*, 536−542.

Campbell, J., & Pryce, W. (2003). *Brick: A world history*. Thames & Hudson.

E.E.A. Report 12. (2012). *Climate change, impacts and vulnerability in Europe 2012*. Copenhagen: European Environment Agency.

European Commission. COM 571. (2011). Roadmap to a resource efficient Europe.

Freedonia Group. (2010). *Brick & block to 2014-industry market research, market share, market size, sales, demand forecast, market leaders, company profiles, industry trends*. Cleveland. http://www.freedoniagroup.com/Brick-And-Block.html.

Guillaud, H. (2008). Characterization of earthen materials. In E. Avrami, H. Guillaud, & M. Hardy (Eds.), *Terra literature review—an overview of research in earthen architecture conservation* (pp. 21−31). Los Angeles (United States): The Getty Conservation Institute.

Habla. (2014). *The brick industry*. Zig-Zag Kilns Technology. http://www.hablakilns.com/industry.htm.

Hall, M., Lindsay, R., & Krayenhoff, M. (2012). *Modern earth buildings*. Cambridge: Wood-Head Publishing.

Harrison, D. J., Bloodworth, A. J., Eyre, J. M., Macfarlane, M., Mitchell, C. J., Scott, P. W., et al. (2002). *Utilisation of mineral waste: case studies*. British Geological Survey Commissioned Report CR/02/227 N.

IEA. (2012). *World Energy Outlook 2012*. Paris: OECD/IEA.

Lechtenbohmer, S., & Schuring, A. (2011). The potential for large-scale savings from insulating residential buildings in the EU. *Energy Efficiency, 4*, 257−270.

Lourenço, P., Vasconcelos, G., Medeiros, P., & Gouveia, J. (2010). Vertically perforated clay brick masonry for loadbearing and non loadbearing masonry walls. *Construction and Building Materials, 24*, 2317−2330.

Lynch, G. (1994). *Brickwork: history, technology (in italics) and practice*. London: Donhead.

Morton, T. (2008). *Earth masonry − design and construction guidelines*. HIS BRE Press.
Pacheco-Torgal, F., Cabeza, L., Mistretta, M., Kaklauskas, A., & Granqvist, C. G. (2013). *Nearly zero energy building refurbishment. A multidisciplinary approach*. London, UK: Springer Verlag.
Pacheco-Torgal, F., Faria, J., & Jalali, S. (2013). Embodied energy versus operational energy. Showing the shortcomings of the energy performance building directive (EPBD). *Materials Science Forum, 730−732*, 587−591.
Pacheco-Torgal, F., Fucic, A., & Jalali, S. (2012). *Toxicity of building materials*. Cambridge, UK: Woodhead Publishing Limited, Abington Hall.
Pacheco-Torgal, F., & Jalali, S. (2011). *Eco-efficient construction and building materials*. London: Springer Verlag. p. 247.
Pacheco-Torgal, F., & Jalali, S. (2012). Earth construction: lessons from the past for future eco-efficient construction. *Construction and Building Materials, 29*, 512−519.
Pacheco-Torgal, F., & Labrincha, J. (2013). The future of construction materials research and the seventh UN millennium development goal: a few insights. *Construction and Building Materials, 40*, 729−737.
Pacheco-Torgal, F., Labrincha, J., Tam, V., Ding, Y., & de Brito, J. (2013). *Handbook of recycled concrete and other demolition waste*. Cambridge: Woodhead Publishing Limited.
Reddy, B., & Jagadish, K. (2003). Embodied energy of common and alternative building materials and technologies. *Energy Build, 35*, 129−137.
Sabapathy, A., & Maithel, S. (2013). A multi-criteria decision analysis based assessment of walling materials in India. *Building and Environment, 64*, 107−117.
Sandrolini, F., & Franzoni, E. (2010). Embodied energy of building materials: a new parameter for sustainable architectural design. *International Journal of Heat and Technology, 27*, 163−167.
Sanya, T. (2007). *Living earth. The sustainability of earth architecture in Uganda* (Ph.D. thesis). Norway: The Oslo School of Architecture and Design.
Scully, V. (1993). *Louis I. Khan and the ruins of Rome*. Engineering & Science. pp. 3−13, Winter.
Seto, K. C., Buneralp, B., & Hutyra, L. R. (2012). *Global forecasts of urban expansion to 2030 and impacts on biodiversity and carbon pools*. PNAS. pp. 17−21.
Sonigo, P., Hestin, M., & Mimid, S. (2010). *Management of construction and demolition waste in Europe*. Brussels: Stakeholders Workshop.
Sousa, L. C., Castro, C. F., Antonio, C. C., & Sousa, H. (2011). Topology optimisation of masonry units from the thermal point of view using a genetic algorithm. *Construction and Building Materials, 25*(5), 2254−2262.
Stephan Schmidheiny with BCSD. (1992). *Changing course: A global perspective on development and the environment*. Cambridge, MA: MIT Press.
WHO. (2014). *Urban population growth. Global Health observatory*. http://www.who.int/gho/urban_health/situation_trends/urban_population_growth_text/en/.
Zaman, A. U., & Lehmann, S. (2013). The zero waste index: a performance measurement tool for waste management systems in a 'zero waste city'. *Journal of Cleaner Production, 50*(2013), 123−132.
Zami, M., & Lee, A. (January, 2010). Stabilised or un-stabilised earth construction for contemporary urban housing? In *5th international conference on responsive manufacturing 'green manufacturing'* (pp. 11−13) China: Ningbo Higher Education Park, the University of Nottingham Ningbo.
Zhang, L. (2013). Production of bricks from waste materials − a review. *Construction and Building Materials, 47*, 643−655.

The design and mechanical performance of high-performance perforated fired masonry bricks

2

P.B. Lourenço, G. Vasconcelos
University of Minho, Guimaraes, Portugal

2.1 Introduction

The use of fired clay hollow bricks in the construction of masonry walls, both in load-bearing and non-load-bearing walls is very common in Europe (Mosele et al., 2006). In Portugal and in other south Mediterranean countries, where reinforced concrete technology prevails in the construction of low- to medium-rise buildings, the use of hollow clay masonry walls is mostly used in the construction of non-load-bearing walls (partitions and enclosures). Typical advantages of a hollow clay masonry system as a load-bearing solution are the reduction of execution time, the solution for thermal and acoustic insulation, the significant reduction of thermal bridges, the fire protection, and the reduction of coating thickness. In fact, the energy efficiency of buildings and energy saving are aspects to take into consideration when construction materials are designed both from the economical and environmental point of view. The building stock is responsible for large amount of energy consumption, representing almost one-third of the total amount of energy (Sutcu, Coz Dias, Rabanal, Gencel, & Akkurt, 2014), which is related mainly to cooling and heating of the indoor environment. Because hollow clay bricks are one of the main units used for the enclosure masonry walls, if they are improved by proper processing, they can significantly reduce the thermal conductivity, which results in lower heat losses through the masonry walls. Aiming at improving the thermal behavior of masonry walls, different geometries and geometrical configurations for the hollow clay bricks have been proposed over the last few years (Del Coz Diaz, Neto, Sierra, & Biempica, 2008; Morales, Juárez, López-Ochoa, et al., 2011), together with the use of more efficient raw materials that are able to induce internal porosity, thus reducing the thermal conductivity and transmittance through the walls (Sutcu et al., 2014).

The design of hollow clay brick walls should comply with distinct physical and mechanical requirements. Given that the masonry walls (load-bearing and non-load-bearing) are acted on by in-plane and out-of-plane loadings due to seismic events, it is important that the clay hollow bricks give the masonry walls an adequate mechanical behavior when they are built in seismic-prone regions (Tomaževič, Lutman, & Bosiljkov, 2006). Besides the resistance, it is also important that masonry

Eco-efficient Masonry Bricks and Blocks. http://dx.doi.org/10.1016/B978-1-78242-305-8.00002-4

walls exhibit adequate deformation capacity to accommodate the deformations imposed by the external loading without the development of extensive damage that prevents its repair after earthquakes.

This chapter aims at giving an overview of the fired hollow clay units mostly used in the construction of masonry walls, namely with respect to the geometric, physical, and mechanical requirements. The traditional raw materials and the production technology are reviewed and an overview of the recent trends for the incorporation of waste materials in the composition of the brick is provided. Often, the introduction of waste materials aims not only at improving the environmental sustainability of clay bricks by reducing the quantity of clay but also at improving the thermal capabilities of the brick that results in more cost-effective solutions. The mechanical performance of hollow bricks and its influence on the mechanical behavior of masonry is analyzed. In terms of the mechanical behavior of hollow clay masonry, distinct loading configurations are also highlighted, namely compression and cyclic lateral shear. In addition, the main mechanical parameters describing the seismic performance are also pointed out.

2.2 Conception of fired clay units

Masonry units (concrete blocks, bricks, stone pieces, etc.) are fundamental elements in the definition of geometry and the modularity of dimensions, which should be a multiple of the dimensions of the half unit. The clay and concrete are by far the most common raw materials used in structural masonry units.

In particular, the hollow clay units commonly have a rough, rectangular shape and are characterized geometrically by the global (nominal) dimensions (length $\times$ height $\times$ thickness). The length and height should be selected to allow for modular construction, as they are usually multiples of 200 mm (nominal dimensions), including the 10 mm for the mortar thickness. The modularity is an important characteristic of the masonry units to make the construction technology and geometrical implementation of the structural elements (walls) with openings easier.

2.2.1 Design requirements for fired perforated clay units

The design of clay units should comply with distinct requirements at the level of physical and mechanical properties. Basically, the geometry of the clay brick should be defined based on three main parameters: (1) structural behavior associated to requirements of the constructive system, (2) thermal performance, and (3) ergonomics. Additionally, physical parameters should also be taken into account, particularly to control the conditions of use and durability.

In terms of mechanical properties, the quality of the units is based on the compressive strength in the perpendicular and parallel direction to the bed joints. According to European code requirements, in case clay units are to be used in buildings located in high seismic prone regions, minimal values for the compressive strength in the perpendicular and parallel direction to the bed face of respectively 5.0 N/mm^2 and 2.0 N/mm^2

should be ensured (EC8, 2004). Additionally, an adequate robustness of the units should also be ensured to allow for a suitable behavior of masonry walls submitted to combined vertical and horizontal in-plane loading. This can be achieved by adequate raw material mix and adequate mold design, avoiding straight angles between shells and webs (Tomaževič et al., 2006). In terms of the geometry of clay bricks, the European code (EC6, 2005) provides requirements related to the geometry of the units, namely the percentage of holes (both vertical and horizontal holes), from which it is possible to define a masonry unit group (see Table 2.1). The masonry unit group is also an important characteristic in the point of view of the hollow clay brick masonry design as some fundamental mechanical parameters such as shear, flexural, and compressive strength of clay masonry can be estimated once the group unit is known. Other geometrical features of the hollow clay units are related to the

Table 2.1 Geometry requirements for clay units according to EC6 (2005)

	Group 1	Group 2		Group 3		Group 4	
		Vertical holes				Horizontal holes	
Volume of all holes (% of the gross volume)	≤25	>25; ≤55		≥25; ≤70		>25; ≤70	
Volume of any hole (% of the gross volume)	≤12.5	Each of multiple holes ≤2 grip holes up to a total of 12.5		Each of multiple holes ≤2 grip holes up to a total of 12.5		Each of multiple holes ≤30	
Declared values of thickness of webs and shells (mm)	No requirement	Web ≥5	Shell ≥5	Web ≥3	Shell ≥6	Web ≥5	Shell ≥6
Declared value of combined thickness of webs and shells (% of the overall width)	No requirement	≥16		≥12		≥12	

transversal surface of any hole (both deep and through holes), the thickness of the webs and shells, and the combined thickness of the webs and shells (see Table 2.1). The flatness of the faces of brick masonry units should also be ensured. This property can be determined through European standard EN 772-20 (2000).

The physical requirements needed to be considered in the design of clay masonry units are summarized in Table 2.2. Regarding the density of the clay masonry units,

Table 2.2 Physical requirements for clay units

Requirement	Testing method	Code requirement performance
Aspect (cracks, lumps, flaking, and other defects)	UNI 8942-3 (1986) (retired) clay bricks and blocks. Test methods—exam of the aspect (in Italian)	(EN 771-1, 2005)
Density	EN 772-13 (2002) methods of test for masonry units—determination of net and gross dry density of masonry units (except for natural stone)	LD $\leq$ 1000 kg/m^3 HD $>$ 1000 kg/m^3 (EN 771-1, 2005)
Water vapor permeability	EN 772-15 (2001) methods of test for masonry units—determination of water vapor permeability of autoclaved aerated concrete masonry units	Diffusion coefficient of water vapor $\mu = 5 \div 10$ (EN 1745, 2002)
Efflorescence	ASTM C 67−2005 standard test methods for sampling and testing brick and structural clay tile—efflorescence	(EN 771-1:2005)
Thermal conductivity	–	For normal clay $\lambda \leq 0.55$ W/(m K) For lightened clay $\lambda = 0.20 \div 0.30$ W/(m K) (EN 1745:2002)
Moisture movement	EN 772-19:2000 methods of test for masonry units—determination of moisture expansion of large horizontally perforated clay masonry units	(EN 771-1, 2005)
Freeze-thaw resistance	EN 772-18:2001 methods of test for masonry units—determination of freeze-thaw resistance of calcium silicate masonry units	Only for HD: F0 passive exposure F1 moderate F2 severe (EN 771-1, 2005)

Table 2.2 Continued

Requirement	Testing method	Code requirement performance
Soluble salts content	EN 772-5:2003 methods of test for masonry units—determination of the active soluble salts content of clay masonry units.	For HD units not protected (EN 771-1, 2005)
Reaction to fire	EN 13823:2002 reaction to fire tests for building products—building products excluding floorings exposed to the thermal attack by a single burning item EN ISO 1182:2002 reaction to fire tests for building products—non combustibility test EN 13501-1 fire classification of construction materials and building elements—Part 1—classification using test data from reaction to fire tests.	Euroclass A1 (EN 771-1: 2005)

two classes are identified, namely low gross dry density (LD units with a gross dry density less than or equal to 1000 kg/m^3) and clay units with high gross dry density (HD units with a gross dry density higher than 1000 kg/m^3). Some typical units of each class, defined according to EN 771-1 (2005) are shown in Figures 2.1 and 2.2. The porosity can also be determined when it is intended to know the distribution of pores volume in respect to their diameter. The porosity can influence the freeze-thaw resistance. However, when the intended use of the units assures a complete protection against water penetration, no reference to freeze-thaw is required. On the other hand, when the intended use of the units assures only a partial protection against water penetration and in countries where there is a requirement for freeze and thaw resistance, it shall be evaluated and declared according to the provisions valid for the place where units are applied (see Table 2.2). In the case of HD units, due to its potential use in exterior walls, the freeze-thaw resistance should be declared.

The requirement to declare the active-soluble salts content is intended to ensure that under particular service conditions, the damage to the masonry units does not occur. The soluble salts inducing sulfate attack are sodium, potassium, and magnesium. The damage is dependent on the risk of moisture exposition. Three categories are defined according to the requirement associated to the limitation of the soluble sulfates (EN 771-1, 2005), which are also associated to the risk of exposure to moisture.

Immediately after firing, clay products begin to absorb moisture from the environment. This moisture absorption causes complex chemical reactions within vitrified clay itself, leading to moisture expansion. The moisture expansion is increasing

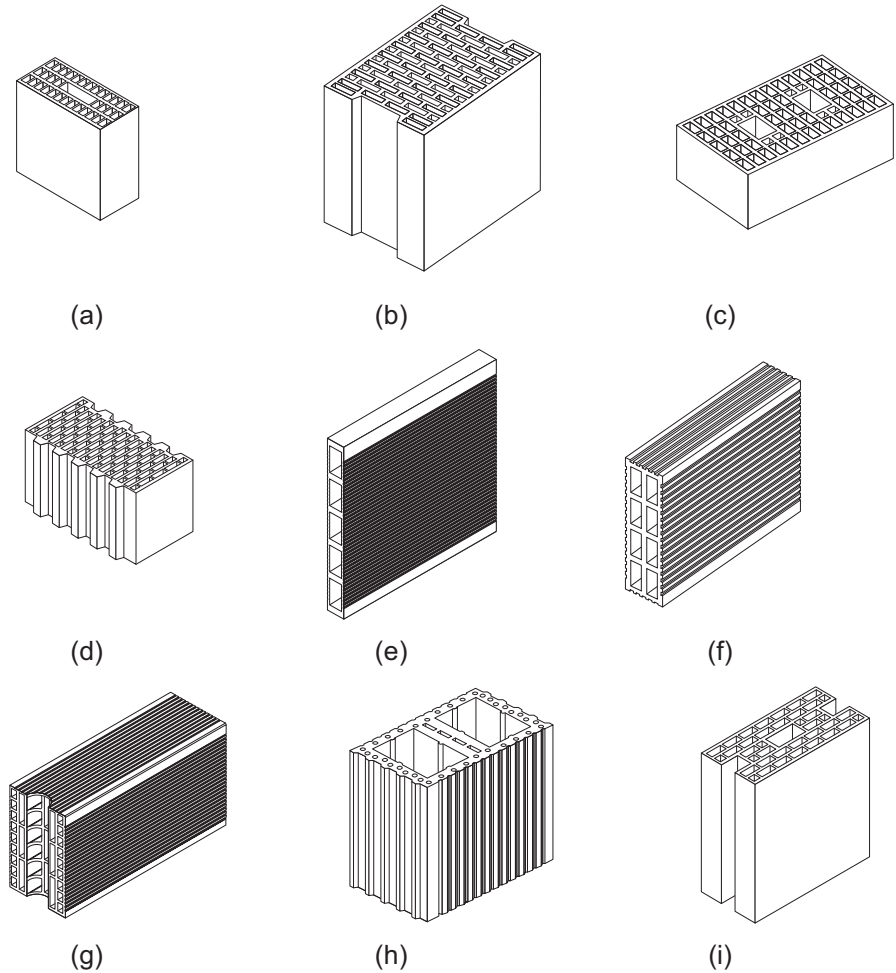

Figure 2.1 LD clay units: (a) vertically perforated unit; (b) vertically perforated unit with mortar pockets; (c) vertically perforated unit with grip holes; (d) vertically perforated unit with tongue and groove; (e) horizontally perforated unit for partition walls; (f) horizontally perforated unit with rendering keyways; (g) horizontally perforated unit with mortar pocket; (h) unit for concrete or mortar infill; (i) unit for masonry panels.

with time, as it is high at early ages and continues to increase very slowly even after many years (Drysdale & Hamid, 2005; Hall & Hoff, 2012). The raw materials, firing temperature, and firing time affect the amount of moisture expansion.

The absorption of moisture by capillary action (initial rate of absorption) in the unit produces a suction effect that draws water from mortar to the unit. Too low or too high values can be detrimental in terms of bond strength at the brick−mortar interfaces, resulting in cracks, delamination, and soluble salts concentration leading to irreversible deterioration processes (Anand, Vasudevan, & Ramamurthy, 2003). High values of the initial absorption of the units results in the formation of a dry, thin layer of mortar

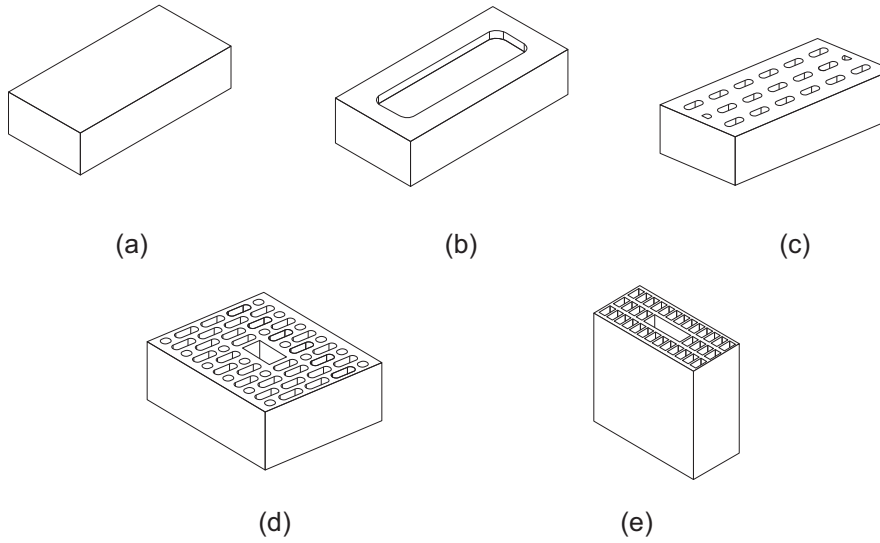

Figure 2.2 HD clay units: (a) solid unit; (b) frogged units; (c) vertically perforated unit; (d) vertically perforated unit; (e) vertically perforated unit.

next to the unit. The mortar can stiffen rapidly avoiding a proper setting of units. Thus, an appropriate value of initial rate of absorption should be ensured.

For units intended to be used in external elements, the water vapor permeability can be important. This is related to water vapor diffusion coefficient (EN 1745, 2002). Knowledge of the thermo-hygrometric performance of building materials is fundamental to avoid the formation of superficial moisture due to environmental and or construction factors (e.g., humidity absorption from air, capillary rise), as well as to assess the extent of condensation phenomena (Dondi, Principi, Raimondo, & Zanariniaba, 2003).

For units to be used in elements subject to fire requirements, the classification of the clay units should be provided. If the percentage of organic compounds is lower than 1% (in volume or weight) the units are classified as Class A1 without the need of testing. The masonry units with organic compounds higher than 1% (in volume or weight) need to be classified according to EN 13501-1 (2002).

Complementary to the mechanical requirements, the thermal efficiency takes a major role on conception of the clay bricks. With the new thermal regulations aiming at achieving more sustainable solutions that result in the saving of energy consumption, additional demand was put in the design of the geometry of the perforated bricks. For example, in Portugal the reference values for the global thermal performance of enclosure walls doubled, with respect to the previous thermal regulation. The environmental sustainability of the hollow clay units is much related to the geometry and internal arrangement of the internal cells aiming at obtaining an adequate thermal conductibility coefficient, which is an important criterion as it influences the heat losses from building enclosure walls. Values of thermal conductibility, λ less than

0.55 W/(m K) can be found for normal clay bricks, but for lightened clay bricks the thermal conductivity can be less than 0.3 W/(m K) (EN1745, 2002).

2.2.2 On the design of the geometry and shape for hollow clay bricks

The geometry and shape of the hollow clay brick units is directly related to the thermal efficiency required for a certain climatic region. According to Li, Wu, He, and Tao (2008), the equivalent thermal conductivity depends on the heat transfer processes, namely by convection within the enclosures, radiation between holes surfaces, and heat conduction through the solid clay. The optimum number of holes and their arrangements depend on the dominated heat transfer process. With the increase in number of holes, generally the natural convection and the surface radiation will be deteriorated in some extent due to the increased thermal radiation shield or space limitation for the developing of natural convection. On the other hand, the increase in holes leads to the increase of heat conduction area in solid skeleton with higher thermal conductivity. The final outcome depends on which factor is prevailing. With respect to the internal configuration of the internal voids (either vertical or horizontal perforations), it is important that thermal bridges are avoided to improve the thermal performance of the brick (Antoniadis, Assael, Tsiglifisi, & Mylona, 2012; Del Coz Diaz et al., 2008; Morales, Juárez, López-Ochoa, et al., 2011). The shape of vertical holes can have distinct configurations, from rectangular voids to triangular or rhomboid voids. Nonrectangular shapes of the voids tend to present greater resistance to the heat transfer and thus to exhibit lower thermal conductivity. Besides, nonrectangular shapes allow for more rows in the same brick leading to lower percentage of voids keeping the same partition thickness and enabling to achieve lower values for the equivalent conductivity coefficient (Lourenço, Vasconcelos, Medeiros, & Gouveia, 2010; Morales, Juárez, Munoz, et al., 2011). In Figure 2.3, an example of clay bricks with different internal voids shape is given to which different thermal conductivity coefficients are associated. An equivalent thermal conductivity, U, of 0.57 W/m^2 K was achieved for rice shape, 0.56 W/m^2 K for lozenges shape, and 0.60 W/m^2 K for the

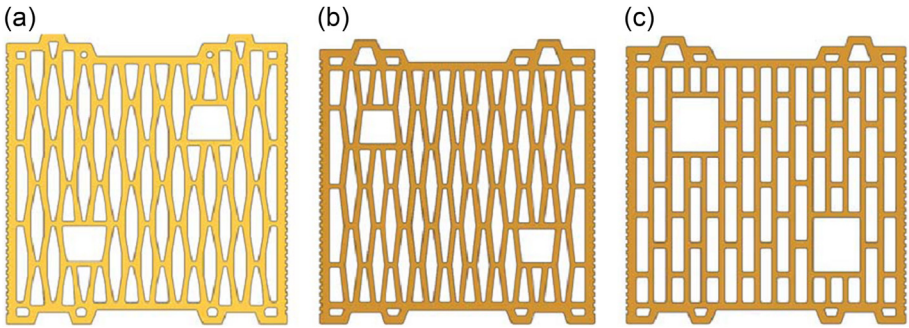

Figure 2.3 Distinct shapes for the internal voids of a brick masonry: (a) rice grain shape; (b) lozenge shape; (c) rectangular shape.

rectangular shape of the internal cells (Lourenço et al., 2010). In relation to horizontal perforation, studies have been also carried out in the analysis of the internal configuration of the voids (Antoniadis et al., 2012; Costa, 2014). In this case variable configurations of rectangular perforations can be found.

Other aspects that can affect the thermal efficiency are the presence of tongue and grooves at the vertical joints and the assembly at the bed joints. The design of dry vertical joints (tongue and groove) is more common, aiming at simplifying the construction technology and avoiding the addition of mortar at the head joints. The tongue and groove head joint tends to decrease the thermal efficiency as it works as a continuous thermal bridge, like the continuous internal ribs (Morales, Juárez, López-Ochoa, & Munoz, 2012). Thus, a way to avoid the thermal bridges is to break it by extending the voids to the tongue and grove area, thus improving the thermal behavior remarkably. The more breaks there are in the heat flux through the tongue and groove system, the better the thermal performance of the brick assemblages.

Usually, ordinary cement mortars (general purpose mortars) used for building walls constitute approximately about 5−7% of the total surface area. As the ordinary cement mortar has high thermal conductivity compared to the masonry bricks, the type of mortar joints and the conductivity of the mortar used for laying the brick units also take an important role in the thermal transmittance of brick walls. The results pointed out by Al-Hadhrami and Ahmad (2009) showed that thermal resistance of the walls prepared with insulating mortar increased by about 23−46% compared to the one obtained in samples prepared with ordinary cement mortar. On the other hand, thin layer joints with bond mortar with low thermal conductivity can reduce the thermal transmittance of a brick wall considerably (Juárez, Morales, Munoz, & Mendívil, 2012; Morales, Juárez, Munoz, Mendívil, & Ruiz, 2014). According to Juárez et al. (2012), the thermal performance of a wall built with a particular type of brick using thin horizontal joints improves by 30−37% in relation to a wall made of the same bricks with standard mortar and full bed joints, depending on their internal geometry. The obtaining of fired clay bricks with perfect laying faces implies a more accurate production technology, which can increase the prices of the units. Besides, the possibility for grinding the bed joint surfaces is related to the clay used in the manufacture of the clay blocks.

2.3 Raw materials used in the production of perforated fired bricks

2.3.1 Conventional raw materials and production technology

The raw materials used in the manufacturing process of fired clay masonry units are a mixture of natural clay, silt, and sand. The clays (recent sedimentary formations) and shales formed from clays under pressure or fire clay, mined at deeper levels, are commonly used in the production of fired hollow clay units. All these clays are equivalent in terms of silica and alumina chemical composition, which are the main chemical compounds of clay, with smaller amounts of iron, calcium, sodium, and other

elements. The surface clays present a great variability and in some cases a mixture of clay of distinct locations can be used to reduce the variability (Drysdale and Hamid, 2005).

The production process of hollow clay bricks encompasses the following steps: (1) Disassembly of clay—after the assessment of the quality of raw material, the clay is laid in layers on stockpile and is kept outside for a certain period of time to ensure consistency. (2) Processing of clay—in this stage, the clay is collected from the stockpile and shoveled into the box feeder, where it is mixed with sand, other additive materials, and water in the mixer to achieve a correct consistency. After this, the clay is fed into the grinder, where it is reduced in size to small granules and after the transport, the mixed clay is dropped into the extruder. (3) Extrusion—the brick mass is pushed through a die and then cut into individual bricks. (4) Drying—after the extrusion, the drying takes up to 36 h for thinner bricks and up to 45 h for thicker bricks. Moisture content of a brick drops from about 20% to 2%. After the process of drying, the bricks are automatically transferred to the kiln by kiln cars. (5) Firing—the dried bricks are then fired for 6−36 h in the kiln, which is usually heated by natural gas or coal at a temperature higher than 900 °C. The firing of the clay bricks intends to improve durability through sintering, which can be seen as the bonding mechanism of clay particles.

2.3.2 Use of by-products and other additives in the production of fired bricks

As the production technology based on the firing process contains high embodied energy, due to the need of reducing the natural source material and aiming at obtaining more efficient solutions in the thermal point of view, several research studies have been studying the possibility of adding distinct by-products as a substitution of part of the raw clay material. In fact, the conventional bricks are produced from clay with high temperature kiln firing, leading to high energy consumption and release of greenhouse gases. The clay bricks have an embodied energy of 2.0 kWh and release an average 0.41 kg of carbon dioxide (CO_2) per brick (Venkatarama Reddy & Jagadish, 2003). On the other hand, the quarrying operations for obtaining clay are energy consuming and generate high levels of wastes. Therefore, the idea is often to obtain modified clay brick blends with waste and by-products and use the traditional technology for the production of hollow bricks. It is also expected that no remarkable differences on the general properties of hollow clay bricks, such as compressive strength and water absorption, are obtained.

With this respect, very different by-products have been used to replace the clay with reasonable results in terms of physical and mechanical properties, mainly as related to compressive strength of the fired material. A general overview of the different residues that have been used in the past can be found in Raut, Ralegaonkar, and Mandavgane (2011) and in Zhang (2013). It should be stressed that fly ash (particularly class F) has been largely used by different authors (Demir, Baspinar, & Orhan, 2005; Gorhan & Simsek, 2013; Sutcu & Akkurt, 2009). All the authors found that the fly ash can replace clay at high volume ratios. In general, the compressive strength of modified clay bricks is higher than in standard clay bricks and the water absorption presents

lower values. Additionally, it was observed that the bond strength and durability (resistance to freeze-thawing cycles) is also better than in standard clay bricks. The use of stone residues such as granite-sawing wastes (Menezes, Ferreira, Neves, Lira, & Ferreira, 2005), granite-basalt fine quarry residues (Sutcu & Akkurt, 2009), and waste-marble powder (Bilgin et al., 2012) revealed also to be adequate for replacing conventional clay raw material. The granite sawing wastes have similar physical and mineralogical characteristics to conventional clay raw materials and demonstrated to lead to final products with characteristics fitting the requirements of Brazilian standardization. In general, the use of these residues revealed to be adequate, taking into consideration the needed physical and mechanical requirements.

The thermal conductivity of a hollow brick is related to the geometry of the hollow cells, and can be optimized according to different geometries of the hollow cells, as discussed in Section 2.2. Additionally, the thermal performance of hollow clay bricks is also dependent on the thermal conductivity of the bulk of the material that constitutes the brick. In this way, the thermal performance of the hollow clay bricks can also be improved by acting on the thermal conductivity of the solid part. The enhancement (reduction) of the thermal conductivity of the material can be obtained by the addition of pore-forming agents to the brick material before firing, like wood sawdust, polymers, leather residues, paper-making sludge, powered limestone, and polystyrene (Zhang, 2013). Lourenço et al. (2010) refers to the use of organic wastes from the wood and paper industry, namely sawdust from wood (SD), cork dust (CD) and paper mill sludge (PM). In this work, distinct percentages of the organic wastes were added to the paste in order to decide for an optimum composition. From Figure 2.4 it is observed that an increase on the percentage of organic waste leads to a reduction of the specific mass and of the thermal conductivity. The introduction of industrial paper residues was also investigated by other authors (Raut et al., 2011; Sutcu et al., 2014). The raw materials blends containing up to 30 wt% of wastes experienced a reduction of the thermal conductivity of approximately 50% without decreasing the compressive strength below the recommended values. Of course, a balance between mechanical performance and thermal insulation of the brick has to be found as, in general, the addition of wastes results in the decrease of the compressive strength. In the work carried out by Demir et al. (2005), it was confirmed that the addition of kraft pulp residues in clay brick production can be effectively used as an organic pore forming in clay body without any detrimental effect on the other brick manufacturing properties. Both density and compressive strength reduce but these are still higher than the ones required by codes. After the work carried out by Gorhan and Simsek (2013), it was observed that the thermal conductivity can also be improved by adding rice husk, which is effective as a pre-forming agent in the clay body, in a proportion between 2.5% and 5% to the clay.

2.4 Mechanical characteristics of perforated fired bricks

The most important mechanical characteristic of masonry units and particularly of hollow clay units is the compressive strength. This property is an indication of the quality of the brick and provides information about the adequacy for the use of hollow clay

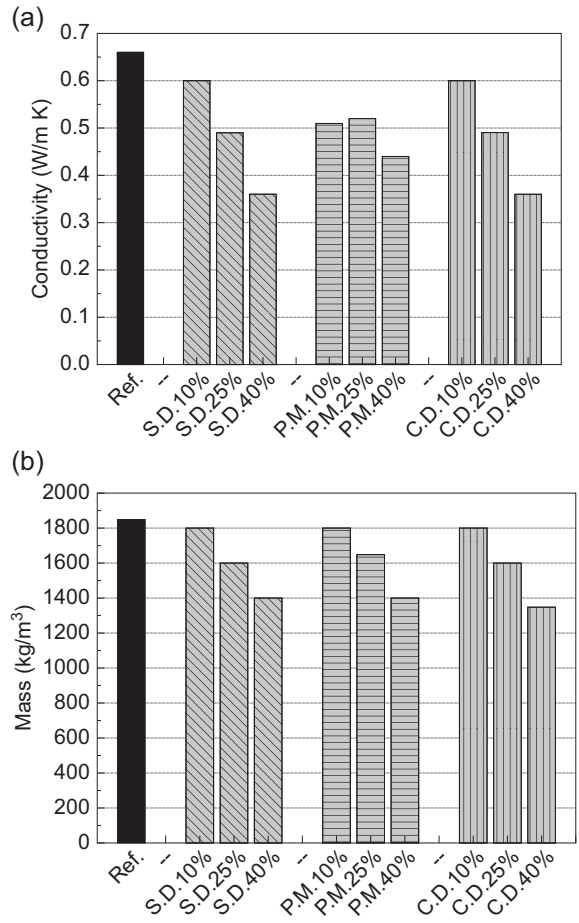

Figure 2.4 Evaluation of different additives on the physical and mechanical behavior of the clay material: (a) conductivity; (b) mass. Here, the reference solution is a clay paste without any additives.

bricks in load-bearing or in non-load-bearing walls. As already discussed, the masonry units should comply with compressive strength requirements when used in seismic prone regions (EC8, 2004).

The compressive strength of masonry units is obtained from uniaxial compression tests based on standardization that defines the loading protocols, equipment, and procedure (EN 772-1, 2000). The uniaxial compression tests can be carried out in force or displacement control, but the latter is preferred if the behavior of the hollow brick after the peak load is required. An example of the typical uniaxial compressive behavior of hollow clay bricks ($300 \times 300 \times 200$ mm), considering two distinct configurations according to the process for the laying of the masonry units on full mortar bed joints (FBM) or as partly ("shell") bedded (SBM), is presented in Figure 2.5 (Lourenço et al., 2010). The shell bedded joints can be preferred to ensure an adequate behavior to water infiltration from rain by avoiding humidity bridges, for example. For partly bedded

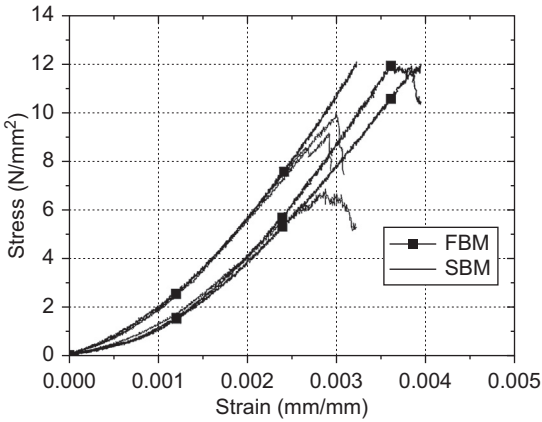

Figure 2.5 Typical stress−strain diagrams under uniaxial compression.

units, two strips of 90 mm of general purpose mortar were considered, with the vertical load applied only in the thickness of the mortar strips through two steel plates with the same thickness. Normalized compressive strengths, f_b, of 13.9 N/mm^2 and 10.5 N/mm^2 were obtained for full bedded units and shell bedded units respectively, meaning that the shell bedded brick presents a reduction of about 25% on the compressive strength. The lower compressive strength of the shell bedded masonry unit is associated to the higher tensile stresses developed in the perpendicular direction to the applied load as is shown in Figure 2.6, where the distribution of the tensile principal stresses obtained from numerical simulation is illustrated (Lourenço et al., 2010). The highest tensile stresses are distributed on the vertical perforations along lines corresponding to the end of the loaded area. These tensile stresses are associated to tensile strains, which leads to the cracking and lateral splitting of the units, according to what was observed from the experimental failure modes.

The analysis of the stress−strain diagrams indicates that the postpeak behavior of the hollow bricks could not be recorded due to its brittle nature under compression. In fact, both types of bedding exhibit brittle behavior accompanied by vertical cracking and splitting of the internal webs, with failure occurring by splitting the external shells of the units. The prepeak regime is also similar, even if the scatter on the compressive strength is higher and the cracking before failure is more extensive for partial bedded clay units.

In spite of the compressive loading parallel to the vertical perforations (perpendicular to bed joints) corresponding to the major loading solicitation, it should be noticed that the compressive strength in the parallel direction to bed joints is important for masonry beams and spandrels, which are considered as structural elements connecting the masonry piers between openings (Haach, Vasconcelos, & Lourenço, 2012). The compressive numerical behavior of clay units with rice grain and rectangular shape of the vertical perforations pointed out in Lourenço et al. (2010) for the three main loading directions (one perpendicular and two parallel to bed joints) is shown in Figure 2.7. It is observed that hollow clay units present a considerable anisotropic

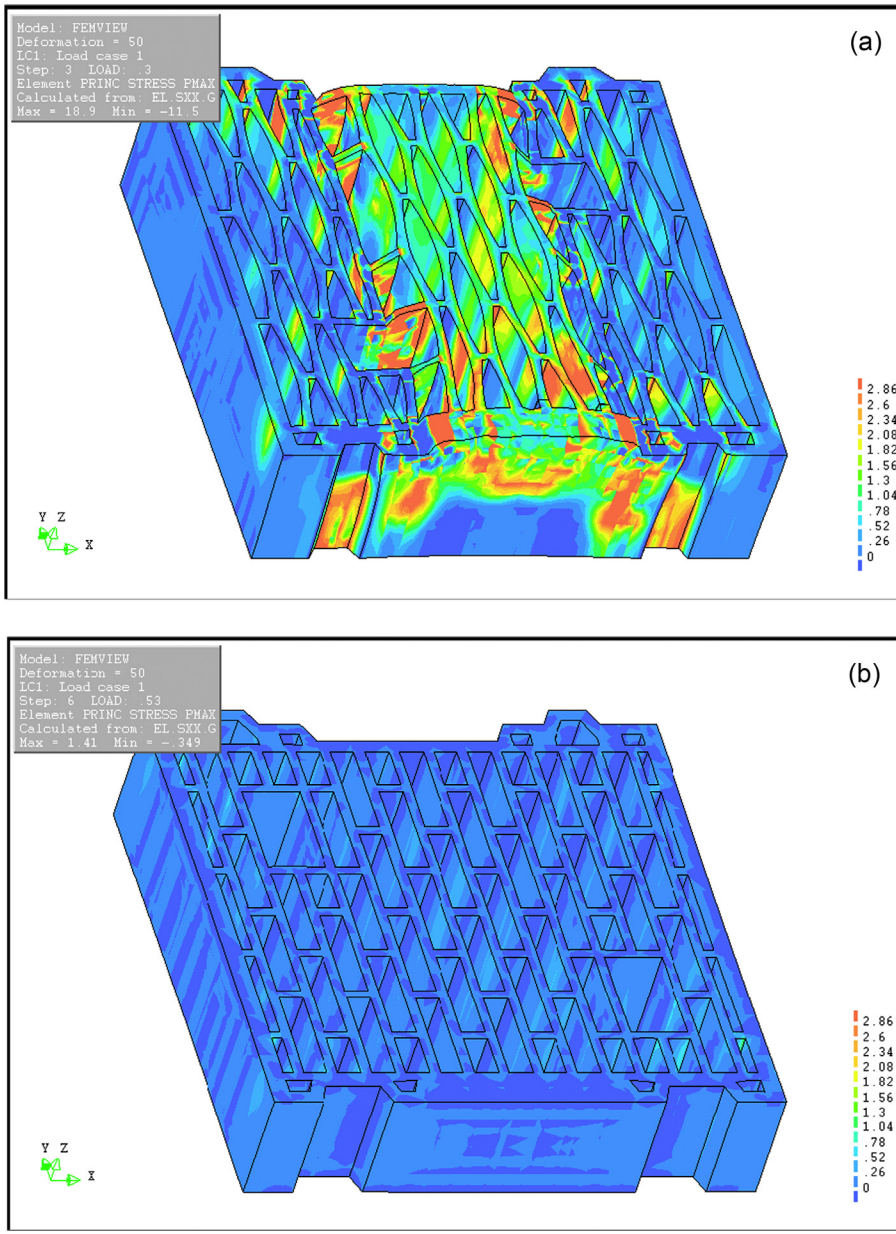

Figure 2.6 Distribution of principal tensile stresses (units in N/mm^2): (a) shell bedded clay unit; (b) full bedded clay unit.

behavior, being the strongest direction parallel to the vertical perforations as expected. The response under uniaxial compressive loading of both clay units is similar in the direction perpendicular to bed joints. However, the hollow clay unit with rectangular perforations presents higher stiffness and compressive strength in both directions

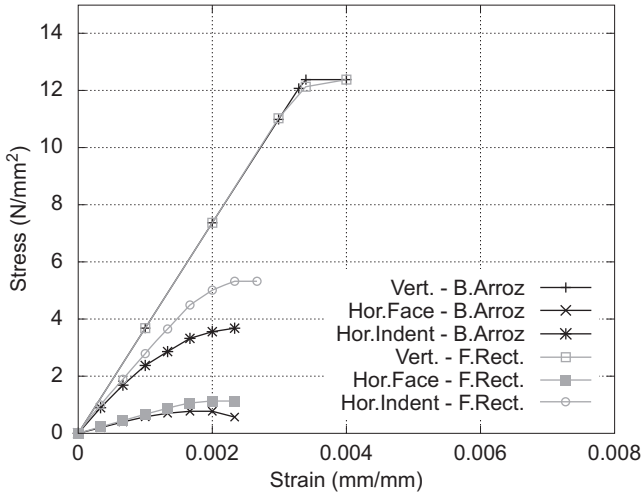

Figure 2.7 Stress−strain diagrams in three main loading directions.

parallel to bed joints. The anisotropic behavior is a result of the geometry of the clay units and is essentially associated to the higher stiffness and higher net area in each distinct direction. The anisotropy degree between the compressive strength normal and parallel to the bed joints is close to the value of 0.3 presented by Tomaževič and Weiss (2012) for the ratio between the compressive strength in the parallel and perpendicular direction to the bed joints.

Although it is not usual to obtain the tensile and shear strength of the masonry units, Tomaževič and Weiss (2012) presented the values of the tensile and shear strength of different hollow clay blocks obtained based on splitting and diagonal compression (tensile strength) and shear tests (shear strength). It was found that the values of the shear strength of hollow clay units are higher than the tensile strength, with the ratio between the normalized shear and compressive strength in range between 0.10 and 0.20. The ratio between the normalized tensile and compressive strength is the range between 0.03 and 0.09. Both shear and tensile strength appears to be related to the combined thickness of the shells and webs, presenting a trend for increasing with higher percentage of the combined thickness and decreasing volume of holes.

It should be stressed that the mechanical characteristics of hollow clay units are particularly important when walls are submitted to combined in-plane vertical and horizontal loading (Tomaževič et al., 2006), as the ductility and energy dissipation of the walls depends on the local behavior of the clay bricks.

2.5 Masonry assemblages with fired perforated brick masonry

The masonry is considered as a composite material composed of units and mortar and unit−mortar interfaces, and its mechanical behavior depends on the mechanical characteristics of the elements and also on its arrangements. The loading configurations to

which masonry is submitted depend on the structural element to which it belongs. In the case of masonry walls, where hollow clay units are almost exclusively used, compressive and in-plane lateral loads are the most important loading configurations when the mechanical behavior of masonry is analyzed.

2.5.1 Mechanical performance of brick masonry under compression

Several experimental, numerical, and simplified analytical studies have been carried out in order to increase the knowledge about the compressive behavior of masonry (Gihad & Lourenco, 2007; Khalaf, Hendry, & Fairbairn, 1994; McNary & Abrams, 1985; Page & Shrive, 1988). As masonry is a composite material made of units and mortar, it has been largely accepted that its failure mechanism and resistance is governed by the interaction between the components. The evaluation of compressive behavior plays a major role in the characterization of masonry as a structural element since compression is a primary loading to which structural walls are subjected. Compressive behavior is also important when masonry is subjected to lateral loading since the in-plane behavior depends on the compressive properties of masonry, especially if flexural resistance mechanisms predominate (Haach, Vasconcelos, & Lourenço, 2011). The finite element numerical analysis of masonry walls based on macromodeling also requires the data regarding the mechanical behavior of masonry under compression and the key mechanical properties, namely the compressive strength, elastic modulus, and fracture energy.

The compressive behavior of masonry is usually determined based on experimental testing, generally according to the standards (EN 1052-1, 1999). An example of the typical compressive behavior of hollow clay masonry is shown in Figure 2.8. The stress–strain diagrams were obtained under displacement control and describe the compressive behavior of full bedded masonry specimens (FBM)

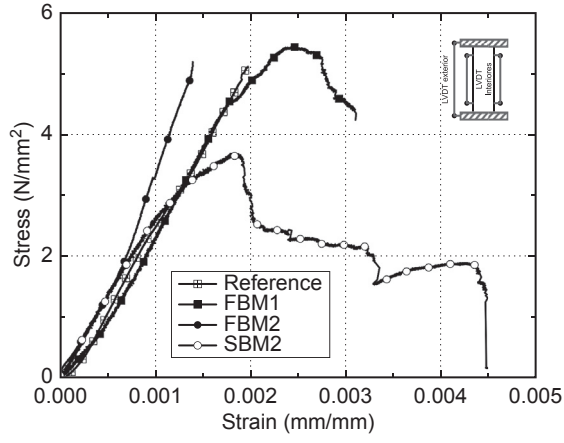

Figure 2.8 Typical stress–strain diagrams of clay brick masonry under compression.

and partial ("shell") bedded masonry (SBM) built with prebatched mortar M10 (group 2 units) and unfilled vertical joints. From the stress−strain diagrams it is possible to determine the compressive strength and modulus of elasticity of masonry. It appears that the behavior of the full bedded masonry is relatively brittle, as no postpeak behavior was found. The response of partly bedded masonry is more ductile in the sense that no abrupt failure occurs, which corresponds to a higher capacity to redistribute compressive stresses within the specimen. A considerable reduction on the compressive strength of the shell bedded masonry was recorded, even if no significant change on the shape of the prepeak behavior (and thus on the initial stiffness) was detected in relation to full bedded masonry. The stress−strain diagrams are very close to the stress−strain diagram obtained by Tomaževič and Weiss (2012) on hollow clay masonry made of different hollow bricks with a distinct arrangement of the internal holes. The prepeak behavior is characterized by some nonlinearity close to the peak resistance and almost no postpeak was recorded. Similar behavior was also pointed out on clay masonry (with clay blocks with rectangular vertical perforations with a percentage of holes of about 46% in group 2) tested by Mojsilovic (2006). In this case, the normalized compressive strength of units is considerably high (between 28.6 and 42.0 MPa), which should result in a brittle failure. It is interesting to notice that the masonry built with clay units belonging to the group 1 (EC6, 2005) present a more ductile behavior under compression, which should be associated to a lower percentage of volume of holes and higher combined thickness of the shells and webs (Tomaževič and Weiss, 2012).

Cracking of the hollow clay masonry is predominantly vertical, developing in the internal webs and shells of the units (Da Porto, Mosele, & Modena, 2011a; Lourenço et al., 2010; Mojsilovic, 2006; Tomaževič et al., 2006), and the failure is characterized by spalling, buckling, and separation of the shells and vertical splitting and crushing of the webs (see Figure 2.9). This behavior can also be attributed to the lateral tensile stresses induced in the units by the distinct deformation characteristics of masonry units and mortar at the bed joints (Khalaf et al., 1994; McNary & Abrams, 1985) and to the buckling of the vertical webs in case of horizontal perforation.

Figure 2.9 Typical failure modes of clay masonry under compression.

2.5.1.1 Prediction of the elastic properties of masonry under compression

The compressive strength of masonry can be estimated through empirical formulas generally based on the results of experimental tests (ACI, 1999; Dymiotis & Gutlederer, 2007; Kaushik, Rai, & Jain, 2007). European masonry code (EN 1996-1-1, 2005) proposes the Eqn (2.1) to estimate the compressive strength of masonry:

$$f_k = k f_b^{0.7} f_m^{0.3} \tag{2.1}$$

where k depends on the type and shape of units and mortar at bed joints, f_b is the normalized compressive strength of the unit, and f_m is the characteristic compressive strength of mortar. For hollow clay units of group 2 and general purpose mortar, the value of k is 0.45. The application of this formula resulted in the overestimation of the compressive strength of group 2 units (Lourenço et al., 2010) and particularly in case of bricks of group one (Tomaževič and Weiss, 2012). However, it was shown that several empirical formulas applied to a great amount of experimental data generally gives compressive strength values of masonry on the safe side (Garzon-Roca, Marco, & Adam, 2013).

The modulus of elasticity of masonry can be determined based on the experimental results, generally by taking the tangent value at one-third of the compressive strength of masonry in the stress−strain diagrams or by considering the secant values in a range between 0.1 and 0.4 of the compressive strength (Da Porto et al., 2011a). It can also be estimated from the compressive strength of masonry. According to EC6 (EN 1996-1-1, 2005), the elastic modulus can be obtained from Eqn (2.2):

$$E = k_E f_k \tag{2.2}$$

where k_E is recommended to be 1000.

The comparison of the values of the elastic modulus estimated based on Eqn (2.2) and the experimental values obtained in full and partial bedded hollow clay brick masonry provided by Lourenço et al. (2010) revealed that the difference is reasonable, at 15% and 3% for full and partly bedded masonry, respectively.

On the other hand, the values of shear modulus, G, used for example in the calculation of the lateral stiffness of masonry walls, can be estimated by multiplying the modulus of elasticity by 0.4 (EN 1996-1-1, 2005). However, according to Tomaževič (2009), the values of the shear modulus of clay brick masonry are considerably lower, and can be fixed in 10% of the modulus of elasticity.

2.5.2 Mechanical performance of brick masonry under shear

In the case of modern masonry, where the connections between walls and between walls and rigid diaphragms are ensured, the global stability of the masonry buildings, when submitted to seismic action, is essentially guaranteed by the resisting mechanism of masonry walls that behaves predominantly in shear. This justifies the relevance that

has been given to the analysis of the behavior of masonry walls under in-plane cyclic loading.

2.5.2.1 Solutions for hollow clay brick masonry walls

Several constructive systems based on hollow clay units for new masonry have been proposed (Mosele et al., 2006). To make the construction technology easier, different types of head and bed joints have been defined. The advances on the production technology of hollow clay units and accurate dimension of the units led to the use of thin layer mortar instead of general purpose mortar (Da Porto, Grendene, & Modena, 2009). Besides, given that structural masonry walls or even enclosure non-load-bearing hollow clay masonry walls are composed of only one leaf, due to the great width of the brick to comply with thermal requirements, it is proposed that the mortar at bed joints is placed by strips to improve the performance of the walls to humidity (face shell masonry) (Lourenço et al., 2010) (see Figure 2.10). On the other hand, there is a trend to use unfilled vertical joints to make the construction faster, and novel shapes for the hollow clay tongue and groove for head joints are adopted (Da Porto et al., 2009; Da Porto, Mosele, & Modena, 2011b; Lourenço et al., 2010

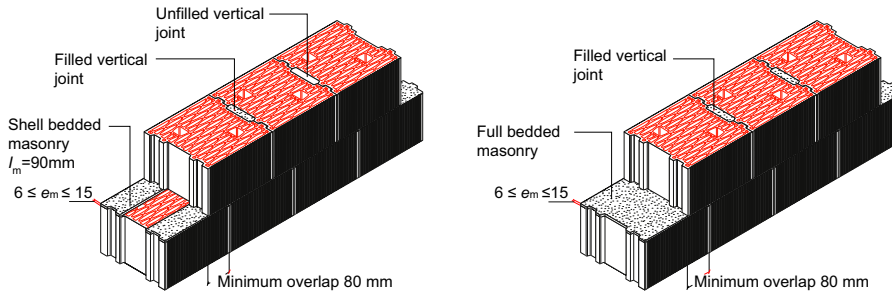

Figure 2.10 Constructive system with hollow clay units fully and partly (shell) bedded with unfilled and filled vertical joints.

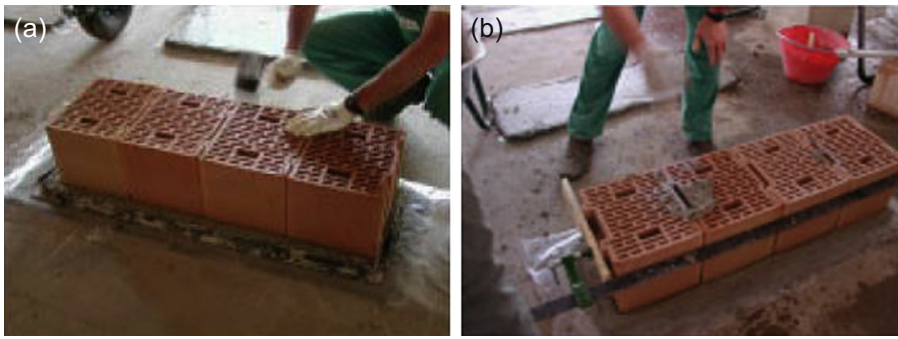

Figure 2.11 Ty Constructive system with hollow clay units; (a) tongue and groove head joints; (b) mortar pockets at head joints.

see Figure 2.11). The hollow clay units with tongue and groove head joints enable the consideration of dry masonry head joints due to the interlocking between units at the head joints to ensure the resistance of the walls for out-of-plane loading. Even if unfilled vertical joints are not recommended in masonry walls built in seismic prone regions (EN 1998-1-1, 2004), there has been an attempt to study the possibility of using unfilled joints, unfilled joints with interlocking, or partially filled head joints with mortar into pockets, as some freedom is given in the national annexes of European countries (Tomaževič et al., 2006).

It is also common to reinforce hollow clay masonry by adding steel reinforcement at bed joints or in the vertical direction located in vertical holes formed by the frogged ends of the masonry units (Da Porto, Guidi, Garbin, & Modena, 2010; Lourenço et al., 2010), where mortar is introduced to ensure appropriate adherence of the reinforcements to the masonry. The addition of reinforcement at the walls intends not only to improve the lateral resistance of the walls, but also the deformation capacity in the nonlinear range and the ability to dissipate energy during cyclic loading. The hollow brick masonry with mortar pockets can be classified as having fully filled head joints as mortar is provided over a minimum of 40% of the unit width. Hollow clay bricks with C shape and H shape have been proposed to make the construction of the reinforced masonry easier (Da Porto et al., 2011a). The horizontal reinforcements can also be placed in recesses made in the brick units (Da Porto et al., 2011b) to improve the in-plane cyclic performance.

2.5.2.2 *Experimental characterization of hollow clay brick masonry walls*

In the scope of seismic experimental research, distinct testing approaches have been used for unreinforced masonry structures, namely quasistatic monotonic or cyclic tests, dynamic shaking table tests, and pseudodynamic tests. According to Calvi, Kingsley, and Magenes (1996), although dynamic tests simulate with more accuracy the seismic action, cyclic quasistatic tests enable more accurate measurements of forces and displacements and the record of damage evolution becomes easier. The quasistatic cyclic tests are typically carried out on walls submitted to a combination of vertical loads, simulating the permanent loads, and monotonic or cyclic horizontal loads simulating the seismic loading in a simple way. Typical fixed-fixed or fixed-free cantilever walls are adopted in the static tests. Although the latter does not represent real boundary conditions, it renders the interpretation of results and testing setup easier. This testing configuration has been adopted in several research programs (Bosiljkov, Page, Bokan-bosiljkov, & Žarnić, 2003; Haach, Vasconcelos, & Lourenço, 2010; Vasconcelos & Lourenço, 2009).

The main resisting mechanisms that are characteristic of the response of the masonry walls submitted to combined in-plane loading are shear and flexure, which result in distinct failure modes (Figure 2.12). The predominance of the shear or flexure is associated to distinct factors, namely the geometry of the walls (height to length ratio), level of precompression loading, boundary conditions, masonry materials, and masonry bonds. In general, in squat walls, the shear resisting mechanism predominates

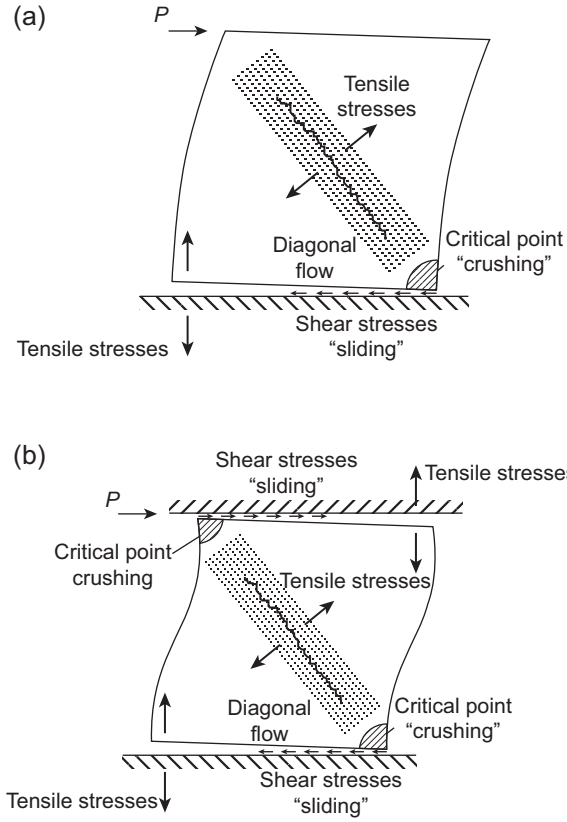

Figure 2.12 Typical failure modes of masonry shear walls: (a) fixed-free boundary conditions; (b) fixed-fixed boundary conditions.

and in slender walls, the flexural resistance mechanism plays the major role. Low precompression load levels are associated to flexural resisting mechanisms and high precompression load levels are in general associated to the development of more important shear resisting mechanisms. In case of cantilever walls, the lateral load applied at the top of the wall leads to the generation of a diagonal flow of compressive stresses from the load application point up to the opposite bottom corner. Diagonal tensile cracks develop often in the alignment of the compressive strut associated to the tensile stresses developed in the perpendicular direction of the strut (Figure 2.12(a)). The progressive concentration of compressive stresses at bottom corners results in most cases in their crushing. Fixed end walls present also the diagonal flow of compressive stresses, but here the stresses concentration can occur at the top and bottom corners of the wall, resulting in the possible crushing. On the other hand, this configuration of stresses results in more common diagonal tensile cracks, meaning that for this boundary condition the shear behavior is more predominant (Haach et al., 2011).

The typical experimental behavior of masonry walls is described based on the force-displacement diagrams relating the force applied at the top of the wall and the displacement at the top of the wall. Figure 2.13 shows the typical force-displacement diagrams obtained in unreinforced hollow clay brick masonry with full and partially bedded masonry and with filled and unfilled vertical joints with an aspect ratio of 0.91 and tested in cantilever boundary configuration under a precompression load of 0.07% and 0.1% of the compressive strength. The full bedded masonry wall with filled vertical joints (FBM-FVJ) presents clearly a predominant flexural (rocking) mechanism associated to the S shape of the force-displacement diagrams. The limitation of the lateral displacement is associated to masonry crushing of the bottom corners. The maximum lateral displacement of shell bedded masonry (SBM-FVJ and SBM-UVJ) is lower than the full bedded masonry in the case of unfilled vertical joints and particularly in the case of filled vertical joints, which exhibits a very brittle behavior. The maximum lateral force is attained for low lateral displacements and failure occurs soon after the maximum load is reached. The in-plane cyclic behavior of full and shell bedded masonry with filled vertical joints is characterized by (1) an opening of the horizontal crack at the bottom bed joint, (2) a rocking mechanism over the lower corners, and (3) the crushing of the bottom corners (see Figure 2.14).

It should be mentioned that in general the in-plane behavior of the unreinforced hollow clay masonry with units belonging to group 2 (EN 1996-1-1, 2005) is described by force-displacement diagrams close to the ones presented in Figure 2.13, with a predominant S shape and somewhat narrow hysteretic loops, at least up to peak lateral resistance (Da Porto et al., 2009; Tomaževič et al., 2006). After the peak load resistance is attained, there is a sudden degradation of the lateral resistance, corresponding to the brittle failure of the masonry walls. This behavior is in part explained by the brittle nature of the hollow blocks. It should be stressed that an important issue related to the in-plane behavior of hollow clay masonry walls is the robustness of the hollow clay bricks as the local failure of the bricks can result in a brittle collapse of the walls and lead to deficient responses in terms of energy dissipation and ductility. The robustness of hollow clay units can be particularly relevant in reinforced masonry, in which the exploitation of the tension capacity of reinforcements is desired. The idea for the need of robustness of the hollow clay bricks was introduced in EC8 (EN 1998-1-1, 2004), when dealing with the seismic behavior of new masonry structures, even if no quantitative criterion is given to evaluate the robustness. However, according to the results of Tomaževič and Weiss (2012), it was concluded that the requirements and recommendations for sufficient robustness of the hollow clay units for the intended use in seismic regions are only partly a function of the unit type as they behave reasonably in the walls submitted from low to moderate levels of precompression load and present a brittle response for high levels of precompression load.

2.5.2.3 *Seismic performance indexes for hollow clay brick masonry*

The evaluation of the seismic performance of unreinforced stone masonry shear walls is carried out in terms of performance indexes, including the ductility and energy

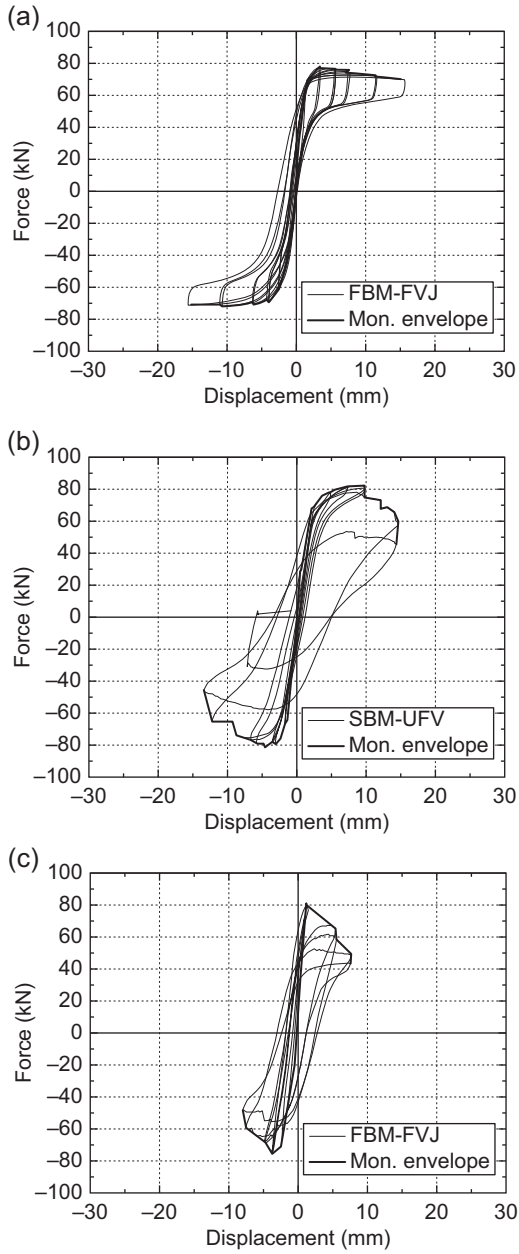

Figure 2.13 Typical force-lateral displacement of masonry walls: (a) full bedded masonry with filled vertical joints; (b) full bedded masonry with unfilled vertical joints; (c) full bedded masonry with filled vertical joints.

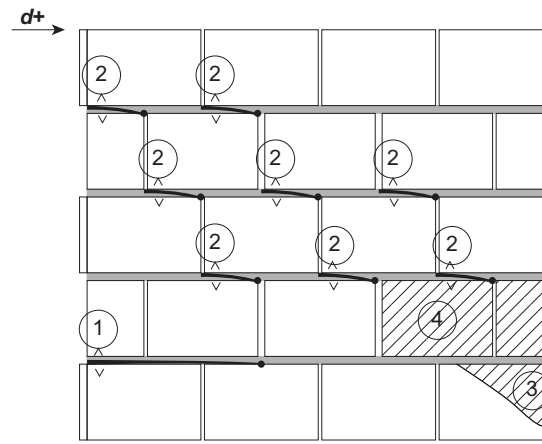

Figure 2.14 Typical crack patterns for hollow clay masonry under in-plane loading.

dissipation capacity. The ductility is a useful measure that makes possible the reduction of elastic seismic design actions by means of a behavior factor, since it gives an indication of the ability of the structure to dissipate energy (Da Porto et al., 2009; Tomaževič, 1999).

The idealized bilinear envelope of the force-lateral displacement diagrams has been widely reported in the literature as a simplified method of evaluating the in-plane seismic performance (stiffness, strength, and ductility) of masonry walls under cyclic loading (Bosiljkov et al., 2003; Magenes & Calvi, 1997; Shing, Noland, Klamerus, & Spaeh, 1989). The experimental envelope is defined by considering the force-displacement points of the hysteresis loops for which the displacement exceeds the previous maximum displacement (Schultz, Hutchinson, & Cheok, 1998). According to Tomaževič (1999), three limit states need to be defined in order to idealize the experimental envelope (see Figure 2.15), which are identified through three characteristic points in the force-displacement diagrams. The crack limit state corresponding to the formation of the first significant cracks is defined with the point (H_{cr}, d_{cr}). The maximum resistance is identified by the couple (H_{max}, d_{Hmax}), and the ultimate state is related to the maximum displacement attained during the cyclic test and is associated to the point (H_{dmax}, d_{max}). The initial secant slope in the elastic plastic diagram, K_e, at the formation of flexural cracks, is calculated as the ratio between the lateral force, H_{cr}, and lateral deformation, d_{cr}. The value of the ultimate resistance of the elastic plastic diagram, H_u, is obtained by ensuring equal energy dissipation of the idealized diagram and the monotonic experimental envelope. The ultimate idealized displacement, d_u, is commonly defined as the displacement measured in the experimental envelope at 80% maximum force degradation (Tomaževič, 1999).

Table 2.3 summarizes the values of indicative points of the nonlinear response of hollow clay masonry walls tested under in-plane cyclic loading by different authors, namely the ratio between H_u and H_{max}, and the rotation angles corresponding to the maximum load, θ_{Hmax}, and to the ultimate load, θ_u, calculated as the ratio between

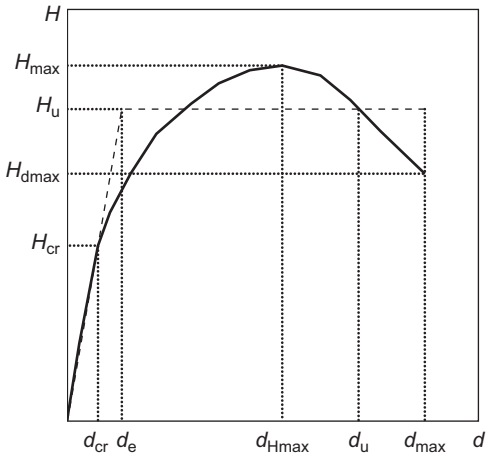

Figure 2.15 Bilinear idealization of the monotonic experimental envelope.

Table 2.3 Characteristics of the bilinear envelope for all specimens

Type of wall	H_u/H_{max}	θ_{Hmax} (%)	θ_u (%)
FBM-FVJ (Lourenço et al., 2010)	0.95	0.54	1.4
SBM-UVJ (Lourenço et al., 2010)	0.89	0.65	1.3
SBM-FVJ (Lourenço et al., 2010)	0.83	0.66	0.7
TM (Da Porto et al., 2009)	0.94	0.82	1.1
TG (Da Porto et al., 2009)	0.87	1.26	1.6
Po (Da Porto et al., 2009)	0.82	1.49	2.2
BM0.3 (Tomaževič and Weiss, 2012)	–	0.28	0.7
BM0.15 (Tomaževič and Weiss, 2012)	–	0.52	1.1

the top displacement measured in the walls and the height of the wall. In terms of ultimate load, H_u, obtained in the idealized bilinear diagram for the hollow clay brick masonry, equivalent to monotonic experimental envelope, it is observed that a value of 0.89 (H_u/H_{max}) was obtained for partly bedded masonry SBM-UVJ (Lourenço et al., 2010), which is close to the value pointed out by Tomaževič (1999) for walls failing in shear. For the specimen FBM-FVJ, a value of 0.95 was observed, which is directly related with the typical flexural envelope. For specimen SBM-FVJ, the value of 0.83 is associated to the very brittle behavior found, which means that a higher reduction of the experimental maximum load should be considered. These values are very close to the ones pointed out by Da Porto et al. (2009) for hollow clay brick masonry walls with tongue and groove head joints and walls with mortar pockets. In relation to

the deformation, it can be observed that apart from the low value of the rotation angle at the maximum resistance (θ_{Hmax}) for the hollow clay brick masonry walls submitted to precompression levels of 30% of the compressive strength (walls BM0.3), in all the other cases the rotation angle at the maximum lateral resistance are in the range of 0.3−0.6 mentioned in Tomaževič and Weiss (2012). It is also observed that the hollow clay brick masonry walls BM0.3 present a rotation angle at the ultimate state, θ_u, of 0.7, which appears not to be acceptable when compared to the range mentioned also by Tomaževič and Weiss (2012) of 1.0−1.2% for the ultimate rotation angle. This value is lower than the one recorded in walls submitted to a compression vertical load of 15% of the compressive strength (BM0.15). It is interesting to notice the remarkable influence of the vertical precompression level on the in-plane behavior of hollow clay brick masonry walls (BM), for which a great difference on the lateral deformation of the walls were found. Higher values of precompression levels are associated to a much brittle behavior of the masonry walls under in-plane lateral loading. According to Da Porto et al. (2009), for nonlinear analysis of shear walls, the Italian code proposes a maximum horizontal displacement of 0.4% of the wall height in walls failing in shear and a maximum horizontal displacement of 0.8% of the wall height in walls failing in flexure.

Another index for the evaluation of the seismic performance of masonry walls under in-plane loading is the dissipation of energy during the hysteretic response of the wall. A dissipative structure can mean the reduction of the seismic response and, consequently, the reduction of the ductility demand (Shing et al., 1989). On the other hand, more dissipative structures have associated higher reduction factors used for the calculation of the reduced elastic seismic forces when using the equivalent elastic static method of analysis for structural analysis. The energy that is dissipated at each loading cycle, E_{diss}, is obtained by integrating numerically the force-displacement hysteresis loop between two consecutive displacement peaks (see Figure 2.16). The input energy is the energy needed to deform the masonry walls from the equilibrium position until a certain level of displacement previously defined. It is calculated as the area under the straight line connecting the origin and the peak force of the hysteresis loop (see Figure 2.14). The values of hysteretic-dissipated energy are low in case of narrow hysteresis loops of the force-displacement diagrams or when the "pinching" effect is visible, which happens when force-displacement diagrams present an S shape. This is the case of the results pointed out by Da Porto et al. (2009) for hollow clay brick masonry walls with different types of bed and head joints and also in case of walls tested by Lourenço et al. (2010). The relation between dissipated and input energy pointed out by Tomaževič et al. (2006) for the hollow clay brick masonry walls with distinct head joints was also low, which could be attributed to the brittle nature of the walls resulting from the local failure of the hollow clay bricks. In fact, the premature collapse of the hollow clay bricks resulted in average values of ratio of the dissipated and input energy of about 0.17 at maximum resistance and of about 0.26 at ultimate state. These values were clearly lower than the values of 0.3 and of 0.4−0.5 at maximum and ultimate states respectively when the walls do not present local brittle failure of the bricks. The study carried out by Tomaževič and Weiss (2012) on the influence of the geometry of the units on the performance of in-plane

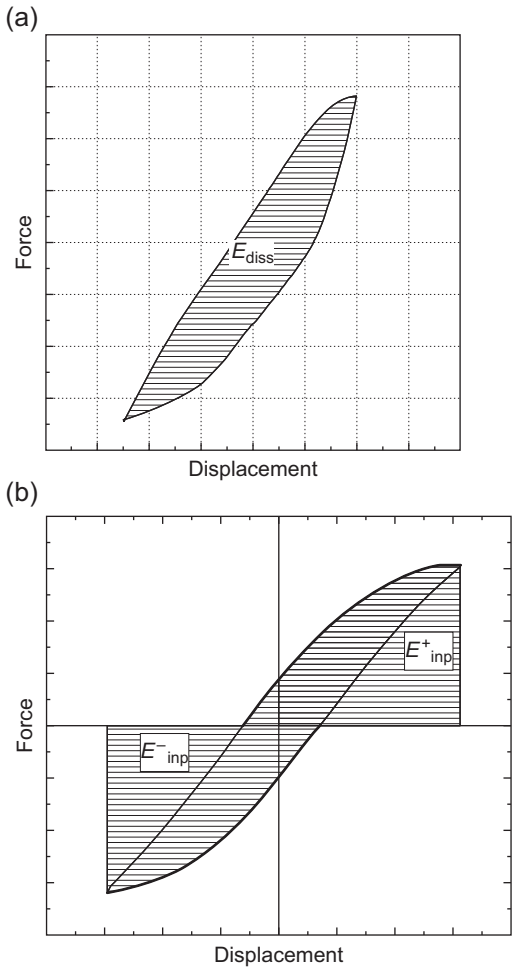

Figure 2.16 (a) Schematic representation of the energy dissipated in a hysteresis loop; (b) schematic representation of the input energy.

behavior of brick masonry walls indicated that the ratio between dissipated and input energy, both at maximum resistance and at ultimate load, does not depend on the geometry of the units, at least if the hollow clay bricks belong to the same group according to EC6 (EN 1996-1-1, 2005). This study concluded also that the dissipated energy is more related to the levels of precompression that determine the failure mode of the masonry walls, and thus the ability of the walls to dissipate energy.

2.6 Conclusions

The hollow brick masonry is a material widely used in the construction of masonry walls of buildings that work as load-bearing and non-load-bearing walls. As enclosure

walls, the hollow brick masonry walls should comply with appropriate physical properties that assure its functional behavior under service loads. This chapter discussed the main physical and mechanical requirements that should be taken into account in the design of hollow brick masonry units so that an appropriate physical and mechanical behavior of masonry is achieved. An overview of the behavior of hollow brick masonry under distinct loading configurations was also provided and the relation with the mechanical performance of the brick was established.

Among the physical properties, the thermal conductivity plays a central role as it is required that the masonry walls present heat losses that result in low energy consumption. The thermal efficiency of the hollow brick can be enhanced at the level of geometry, by designing an appropriate internal arrangement of the perforations and by introducing changes on the compound raw materials. With this respect, organic materials have been considered as pore-forming porosity materials as after the firing process they naturally induce porosity that reduces the thermal conductibility and thus the transmittance of the brick masonry walls.

Another aspect that should be taken into account when designing the hollow brick units consists of the mechanical performance, mainly as related to the compressive strength. The compressive strength of units is mobilized not only under vertical loading but also under lateral in-plane and out-of-plane loading. For in-plane loading, besides the resistance, it is important that walls have adequate deformation capacity in the nonlinear range so that premature damage is developed and brittle response of the brick masonry walls is prevented. This is related to the mechanical properties of brick masonry, which are directly related to the mechanical performance of the hollow brick.

2.7 Future trends

The need for a more sustainable construction has been putting additional demand on the design of more efficient construction materials. In this scope, two main approaches have been followed by researchers, namely (1) achieving more sustainable materials with the incorporation of wastes and by-products (Vasconcelos et al., 2013), by the reduction of natural raw materials, and by reducing the embodied energy; and (2) reducing energy consumption in cooling and heating to create more energy efficient solutions. Both approaches have resulted in several studies on alternative raw materials and on the geometrical configurations (internal holes arrangement) of hollow brick masonry units aiming to optimize the thermal efficiency of the bricks.

It is considered that in the point of view of the physical and mechanical efficiency of hollow bricks, additional work is expected to be carried out in the evaluation of the possibility of using nanotechnology for achieving smart hollow bricks, namely (1) to improve its resistance and deformation ability that ensures more effective responses of masonry walls under earthquake induced loads, (2) to enhance its thermal insulation ability, (3) to control the cracking that develops under service loading conditions, and (4) to give sensing and self-repairing abilities after damage that can be induced by low to medium earthquakes. In the case of hollow blocks used in veneer walls, it should also be possible to combine new geometries with functionalized

surfaces by acting either on the raw materials or on the surface coatings that promote self-cleaning and hydrophilic surfaces aiming at improving thermal performances through the skin of the buildings (Carneiro et al., 2014).

It is also stressed that the development of improved hollow bricks to be used in load-bearing and non-load-bearing walls should be thought of in an integrated context of a development of a constructive system for masonry walls.

References

ACI committee 530. (1999). *Building code requirements for masonry structure*. Farmington Hills, MI: American Concrete Institute.

Al-Hadhrami, L. M., & Ahmad, A. (2009). Assessment of thermal performance of different types of masonry bricks used in Saudi Arabia. *Applied Thermal Engineering, 29*, 1123−1130.

Anand, K. B., Vasudevan, V., & Ramamurthy, K. (2003). Water permeability of alternative masonry systems. *Building and Environment, 38*, 947−957.

Antoniadis, K. D., Assael, M. J., Tsiglifisi, C. A., & Mylona, S. K. (2012). Improving the design of Greek hollow clay bricks. *International Journal of Thermophysics, 33*, 2274−2290.

Bilgin, N., Yeprem, H. A., Arslan, S., Bilgin, A., Günay, E., & Marsoglu, M. (2012). Use of waste marble powder in brick industry. *Construction and Building Materials, 29*, 449−457.

Bosiljkov, V., Page, A., Bokan-Bosiljkov, V., & Žarnić, R. (2003). Performance based studies of in-plane loaded unreinforced masonry walls. *Masonry International, 16*(2), 39−50.

Calvi, G. M., Kingsley, G. R., & Magenes, G. (1996). Testing masonry structures for seismic assessment. *Earthquake Spectra, Journal of Earthquake Engineering Research Institute, 12*(1), 145−162.

Carneiro, J. O., Vasconcelos, G., Azevedo, S., Jesus, C., Palha, C., Gomes, N., et al. (2014). The evaluation of the thermal behaviour of a mortar based brick masonry wall coated with TiO_2 nanoparticles: an experimental assessment towards energy efficient buildings. *Energy and Buildings, 81*, 1−8.

Costa, V. A. F. (2014). Improving the thermal performance of red clay holed bricks. *Energy and Buildings, 70*, 352−364.

Da Porto, F., Grendene, M., & Modena, C. (2009). Estimation of load reduction factors for clay masonry walls. *Earthquake Engineering and Structural Dynamics, 38*, 1155−1174.

Da Porto, F., Guidi, G., Garbin, E., & Modena, C. (2010). In-plane behavior of clay masonry walls: experimental testing and finite-element modeling. *Journal of Structural Engineering, 136*(11), 1379−1392.

Da Porto, F., Mosele, F., & Modena, C. (2011a). Compressive behavior of a new reinforced masonry system. *Materials and Structures, 44*, 565−581.

Da Porto, F., Mosele, F., & Modena, C. (2011b). In-plane cyclic behaviour of a new reinforced masonry system: experimental results. *Engineering Structures, 33*, 2584−2596.

Del Coz Diaz, J. J., Neto, P. J. G., Sierra, J. L. S., & Biempica, C. B. (2008). Nonlinear thermal optimization of external light concrete multi-holed brick walls by finite element method. *International Journal of Heat and Mass Transfer, 51*, 1530−1541.

Demir, I., Baspinar, M. S., & Orhan, M. (2005). Utilization of kraft pulp production residues in clay brick production. *Building and Environment, 40*, 1533−1537.

Dondi, M., Principi, P., Raimondo, M., & Zanariniaba, G. (2003). Water vapour permeability of clay bricks. *Construction and Building Materials, 17*, 253−258.

Drysdale, R., & Hamid, A. A. (2005). *Masonry structures: Behavior and design* (Canadian ed.), ISBN 0-9737209-0-5.

Dymiotis, C., & Gutlederer, B. M. (2007). Allowing for uncertainties in the modeling of masonry compressive strength. *Construction and Building Materials, 16*(7), 1385−1393.

EN 13501-1. (2002). *Classification using test data from reaction to fire tests*.

EN 1996-1-1. (2005). *Eurocode 6: Design of masonry structures − Part1-1: Rules for reinforced and unreinforced masonry*.

EN 1998-1-1. (2004). *Eurocode 8: Design of structures for earthquake resistance − Part 1: General rules, seismic actions and rules for buildings*.

EN 1745. (2002). *Masonry and masonry products. Methods for determining thermal properties*.

EN 1052-1. (1999). *Methods of test for masonry − Part 1: Determination of compressive strength*.

EN 772-1. (2000). *Methods of tests for masonry units − Part 1: Determination of compressive strength*.

EN 772-20. (2000). *Methods of tests for masonry units − Part 20: Determination of flatness of faces of aggregate concrete, manufactured stone and natural stone masonry units*.

EN 771-1. (2005). *Specification for masonry units − Part 1: Clay masonry units*.

Garzon-Roca, J., Marco, C. O., & Adam, J. M. (2013). Compressive strength of masonry made of clay bricks and cement mortar: estimation based on neural networks and fuzzy logic. *Engineering and Structures, 48*, 21−27.

Gihad, M., & Lourenco, P. B. (2007). Mechanics of hollow concrete block masonry prisms under compression: review and prospects. *Cement and Concrete Composites, 29*(3), 181−192.

Gorhan, G., & Simsek, O. (2013). Porous clay bricks manufactured with rice husks. *Construction and Building Materials, 40*, 390−396.

Haach, V. G., Vasconcelos, G., & Lourenço, P. B. (2010). Experimental analysis of reinforced concrete block masonry walls subjected to in-plane cyclic loads. *Journal of Structural Engineering, 136*(4), 452−462.

Haach, V. G., Vasconcelos, G., & Lourenço, P. B. (2011). Parametric study of masonry walls subjected to in-plane loading through numerical modeling. *Engineering Structures, 33*(4), 1377−1389.

Haach, V. G., Vasconcelos, G., & Lourenço, P. B. (2012). Experimental analysis of reinforced concrete block masonry beams using pre-fabricated planar trussed bars. *Construction and Buildings Materials, 26*, 156−166.

Hall, C., & Hoff, W. D. (2012). Moisture expansivity of fired clay ceramics. *Journal of American Ceramic Society, 95*(4), 1204−1207.

Juárez, M. C., Morales, M. P., Munoz, P., & Mendívil, M. A. (2012). Influence of the horizontal joint on the thermal properties of single-leaf walls with lightweight clay blocks. *Energy and Buildings, 49*, 362−366.

Kaushik, H. B., Rai, D. C., & Jain, S. K. (2007). Stress−strain characteristics of clay brick masonry under uniaxial compression. *Journal of Materials in Civil Engineering, 19*(9), 728−739.

Khalaf, F. M., Hendry, A. W., & Fairbairn, D. R. (1994). Study of the compressive strength of block work masonry. *ACI Structural Journal, 91*(4), 367−374.

Li, L. P., Wu, Z. Y., He, Y. L., & Tao, W. Q. (2008). Numerical thermal optimization of the configuration of multi-holed clay bricks used for constructing building walls by the finite volume method. *International Journal of Heat and Mass Transfer, 51*, 3669−3682.

Lourenço, P. B., Vasconcelos, G., Medeiros, P., & Gouveia, J. (2010). Vertically perforated clay brick masonry for loadbearing and non-loadbearing masonry walls. *Construction and Building Materials, 24*(11), 2317−2330.

Magenes, G., & Calvi, G. M. (1997). In-plane seismic response of brick masonry walls. *Earthquake Engineering and Structural Dynamics, 26*, 1091−1112.

McNary, W. S., & Abrams, D. P. (1985). Mechanics of masonry compression. *Journal of Structural Engineering, 111*(4), 857−870.

Menezes, R. R., Ferreira, H. S., Neves, G. A., Lira, H. dL., & Ferreira, H. C. (2005). Use of granite sawing wastes in the production of ceramic brick sand tiles. *Journal of European Ceramic Society, 25*(7), 1149−1158.

Mojsilovic, M. (2006). Masonry elements with chases: behaviour under compression. *Construction and Building Materials, 20*(10), 1028−1039.

Morales, M. P., Juárez, M. C., López-Ochoa, L. M., & Doménech, J. (2011). Study of the geometry of a voided clay brick using rectangular perforations to optimize its thermal properties. *Applied Thermal Engineering, 31*, 2063−2065.

Morales, M. P., Juárez, M. C., López-Ochoa, L. M., & Munoz, P. (2012). Influence of the tongue and groove system on the thermal properties of large-format voided clay bricks for single-leaf walls. *Construction and Building Materials, 30*, 169−173.

Morales, M. P., Juárez, M. C., Munoz, P., & Gómez, J. A. (2011). Study of the geometry of a voided clay brick using non-rectangular perforations to optimize its thermal properties. *Energy and Buildings, 43*, 2494−2498.

Morales, M. P., Juárez, M. C., Munoz, P., Mendívil, M. A., & Ruiz, J. A. (2014). Possibilities for improving the equivalent transmittance of single-leaf walls for buildings. *Energy and Buildings, 69*, 473−480.

Mosele, F., da Porto, F., Modena, C., di Fusco, A., di Cesare, G., Haach, V. G., et al. (2006). Developing innovative systems for reinforced masonry walls. In *Proc. 7th international masonry conference*. London, UK: CD-ROM, 6 pp.

Page, A. W., & Shrive, N. G. (1988). A critical assessment of compression tests for hollow block masonry. *Masonry International, 5*(2), 64−70.

Raut, S. P., Ralegaonkar, R. V., & Mandavgane, S. A. (2011). Development of sustainable construction material using industrial and agricultural solid waste: a review of waste-create bricks. *Construction and Building Materials, 25*, 4037−4042.

Schultz, A. E., Hutchinson, R. S., & Cheok, G. C. (1998). *Seismic performance of masonry walls with bed joint reinforcement, paper T119-4*. Elsevier Science Ltd, ISBN 0-08-042845-2.

Shing, P. B., Noland, J. L., Klamerus, E., & Spaeh, H. (1989). Inelastic behavior of concrete masonry shear walls. *Journal of Structural Engineering, 115*(9), 2204−2225.

Sutcu, M., & Akkurt, S. (2009). The use of recycled paper processing residues in making porous brick with reduced thermal conductivity. *Ceramics International, 35*, 2625−2631.

Sutcu, M., Coz Dias, J. J., Rabanal, F. P. A., Gencel, O., & Akkurt, S. (2014). Thermal performance optimization of hollow clay bricks made up of paper waste. *Energy and Buildings, 75*, 96−108.

Tomaževič, M. (1999). *Earthquake-resistant design of masonry buildings*. London: Imperial College Press, ISBN 1-86094-066-8.

Tomaževič, M. (2009). Shear resistance of masonry walls and Eurocode 6: shear versus tensile strength of masonry. *Materials and Structures, 42*, 889−907.

Tomaževič, M., Lutman, M., & Bosiljkov, V. (2006). Robustness of hollow clay masonry units and seismic behavior of masonry walls. *Construction and Building Materials, 20*(10), 1028−1039.

Tomaževič, M., & Weiss, P. (2012). Robustness as a criterion for use of hollow clay masonry units in seismic zones: an attempt to propose the measure. *Materials and Structures, 45*, 541−559.

Vasconcelos, G., & Lourenço, P. B. (2009). In-plane experimental behaviour of stone masonry walls under cyclic loading. *ASCE, Journal of Structural Engineering, 135*(10), 269−1277.

Vasconcelos, G., Lourenço, P. B., Mendonça, P., Camões, A., Mateus, R., Bragança, L., et al. (2013). Proposal of an innovative solution for partition walls: mechanical, thermal and acoustic validation. *Construction and Building Materials, 48*, 961−979.

Venkatarama Reddy, B. V., & Jagadish, K. S. (2003). Embodied energy of common and alternative building. *Energy and Buildings, 35*, 129−137.

Zhang, L. (2013). Production of bricks from waste materials − a review. *Construction and Building Materials, 47*, 643−655.

3 Influence of large and highly perforated fired-clay bricks in the improvement of the equivalent thermal transmittance of single-leaf masonry walls

M.P. Morales[1], *M.C. Juárez*[2]
[1] Universidad Autónoma de Chile, Santiago, Chile; [2] Universidad de La Rioja, Logroño, Spain

3.1 Introduction

Current buildings are not ecologically sustainable. They are not environmentally friendly and damage the environment due to the high consumption of energy resources, which carries a large amount of harmful emissions (Theodosiou & Papadopoulos, 2007).

Buildings are great consumers of thermal energy. In fact, the residential sector demands about 25% of the total energy consumed in the EU-28, which is equivalent to 275 Mtoe (million tonnes of oil equivalent) (Eurostat, 2013). A large part of this energy is used in the air conditioning of buildings.

Sustainability in global energy generation depends mainly on three lines of action: the use of renewable energy sources (López González, Sala Lizarraga, La Peña Aranguren, & Míguez Tabarés, 2000; López González, Sala Lizarraga, Míguez Tabarés, & López Ochoa, 2007), energy saving and the energy efficiency of machinery and buildings.

Regarding this last line of action, the building sector has had to improve the techniques and properties of the materials used in the construction of enclosure walls so as to minimize energy loss and reduce energy requirements.

Low-density, large and highly perforated materials are now being used. Recent studies have shown the influence that the cladding materials used in building walls have on CO_2 emissions and energy consumption (Raimondo, Dondi, Mazzanti, Stefanizzi, & Bondi, 2005). Seeking to explore further improvements in wall construction materials, other studies have shown how the porous nature of fired-clay bricks can improve thermal performance (Antar, 2010; Morales, Juárez, López-Ochoa, & Doménech, 2010).

Large and highly perforated fired-clay bricks in single-leaf walls (García, 2003) meet these new requirements well. Masonry walls built with such bricks combine good sound insulation, high mechanical strength, exceptional fire resistance and high levels of heat insulation and comfort (thermal inertia).

Eco-efficient Masonry Bricks and Blocks. http://dx.doi.org/10.1016/B978-1-78242-305-8.00003-6

The advantages of these walls, which are usually built with large format pieces, are evident from the point of view of labour requirements and even of costs in building the house. The walls are built with a single layer, eliminating the need for labour and stocks of materials on the site.

The first of these materials for single-layer walls that appear in our market was the Termoarcilla® brick, which, despite its advantages compared to conventional solutions within the framework of current legislation, encountered and continues to encounter great difficulties to find an entry in the market. The Termoarcilla® brick is a voided brick with a great macroscopic porosity (about 50% of voids) with air cells between layers of ceramic material that prevents its convective movements, to which a porosity on a smaller scale is added, formed by air bubbles within the material itself, generated during firing by the volatizing of other materials mixed with the clay for this purpose. Additionally, in the arrangement of these bricks on the site, the vertical joints of mortar are eliminated and the horizontal ones are arranged discontinuously, leaving an air gap between them. Thus low thermal conductivity is achieved using the high thermal resistance of air in any thermal transfer path through the brick.

Of all the different construction solutions for enclosures or envelopes, we focus on the single leaf with no inner cavity, characterized by large-format bricks with appropriate interior and exterior cladding. There are three sections in these single-leaf walls that can affect their thermal performance: the cross-section of the bricks with their air-filled voids (the "clay/air cross-section"), where the geometry of voids and the type of tongue and groove system are influential; the cross-section of the bricks with the voids filled with bonding mortar (the "clay/mortar cross-section"); and the cross-section of the layer of bonding mortar itself (the "bed joint cross-section").

Researchers have recently increased interest in all the components of these sections. The resulting papers have individually characterized the influence of the type of internal void of the large-format brick (Termoarcilla & Tecnalia, 2005; Del Coz Diaz, Neto, Sierra, & Biempica, 2008; Li et al., 2008a,b; Lourenco, Vasconcelos, Medeiros, & Gouveia, 2010; Morales, Juárez, Muñoz, & Gómez, 2011; Sastre, 2008) and the type of tongue and groove arrangement (Ghazi Wakili & Tanner, 2003; Morales, Juárez, López-Ochoa, & Muñoz, 2012) in the clay/air cross-section and clay/mortar cross-section and, finally, the influence of the horizontal joint on the bed joint (Juárez, Morales, Muñoz, & Gómez, 2012).

Other research has sought to reduce the fired-clay thermal conductivity by including additives, and has shown that this decreases thermal conductivity by generating gas micropores in the volume of clay (Alonso-Santurde, Coz, Viguri, & Andrés, 2012; Bilgin et al., 2012; Luciana et al., 2012; Muñoz, Juárez, Morales, & Mendívil, 2013; Raut, Ralegaonkar, & Mandavgane, 2011). These researchers have also studied variations of the mechanical properties (bulk density, water absorption, compressive strength, etc.) versus clay thermal conductivity.

This work seeks to analyse comprehensively the influence of all these factors so that it can be decided which parameter to act on to reduce the equivalent thermal transmittance of the wall.

Finally, an attempt is made to find a relationship between the equivalent thermal transmittance of a wall and the fired-clay thermal conductivity used, since this is a

parameter on which it is possible to act easily by using a dispenser to add suitable quantities of pore-forming additive to the clay during the manufacturing process, prior to the extrusion of the clay.

Single-leaf walls with large and highly perforated fired-clay bricks were chosen for this study.

The numerical calculation method used to obtain the equivalent thermal transmittance U_{eq} (W/m^2-K) of a wall complies with Spanish UNE (Spanish Standard, 2006) and AENOR (Spanish Standard, 2008) standards as well as EN (International Standard, 2007; ISO 8990:1994, 2006; EN 12939:2000, 2000; EN 12664:2001, 2001; European Standard, 2002; European and International Standard, 1996; European and International Standard, 1995) and ISO (European and International Standard, 1995; European and International Standard, 1996; European and International Standard, 2002).

In this work, the mechanical properties of the bricks (bulk density, water absorption, compressive strength, etc.) are not studied, but only the influence of the thermal conductivity of clay in the equivalent thermal transmittance of the wall is studied. Once the improvement in thermal aspects is studied, it should be checked that the bricks and the wall meet all the requirements required by current legislation.

3.2 Materials and methods

Figure 3.1 shows, on a perforated ceramic brick, all elements on which we can act to reduce the equivalent transmittance of an enclosure:

- Internal geometry of voids
- Vertical joint (tongue and groove)

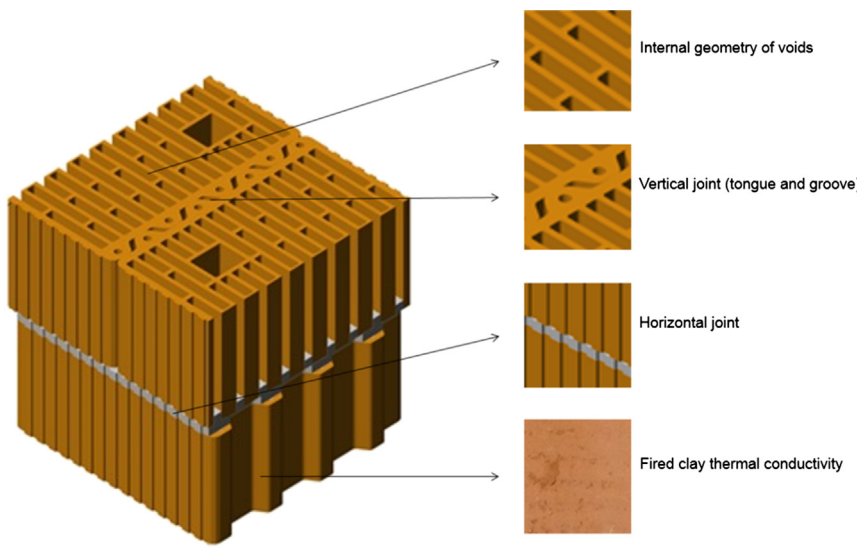

Figure 3.1 Factors influencing the thermal transmittance of a wall.

- Horizontal joint
- Fired-clay thermal conductivity

In the following sections, two types of internal and external geometries of the bricks, as well as three types of horizontal joints, are proposed. For each case, the dependence of the equivalent thermal transmittance of the wall regarding the fired-clay thermal conductivity is studied.

3.2.1 Bricks to study

Figure 3.2 shows the large brick model to be studied, which has the following specifications:

1. Brick dimensions: 300 × 290 × 250 mm.
2. Interior wall thickness: 5 mm.
3. Exterior wall thickness: 8 mm.
4. Length of tongue and groove arrangement: 16 mm, avoiding a vertical joint in the wall.

Two different types of brick are considered:

1. The first (block a) with rectangular internal voids consists of 17 rows perpendicular to the heat flow, in a quincunx, and with a voided tongue and groove arrangement, since this is the layout most widely used commercially and it has been studied previously (Antar, 2010; Termoarcilla & Tecnalia, 2005; García, 2003; Sastre, 2008; Li et al., 2008a; Morales et al., 2010, 2011). The cross-section of this brick is shown in Figure 3.3(a).
2. The second (block b) with rhomboidal internal voids, consists of 25 rows perpendicular to the heat flow and a simple tongue and groove arrangement. This brick has recently begun to appear on the market after several studies (Del Coz et al., 2008; Juárez et al., 2012; Li et al., 2008b; Lourenco et al., 2010; Morales et al., 2012). The cross-section of this brick is shown in Figure 3.3(b).

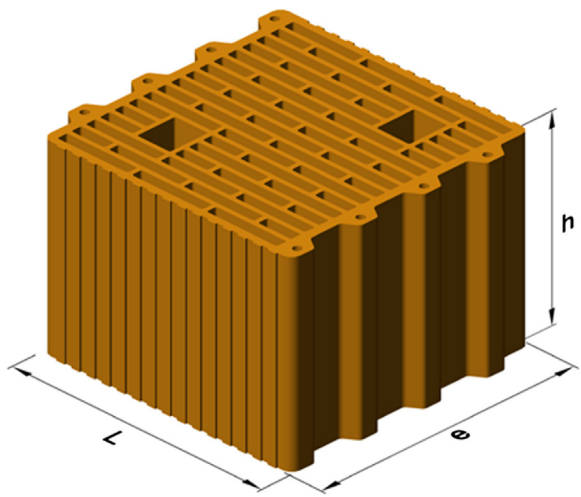

Figure 3.2 Large and highly perforated fired-clay brick.

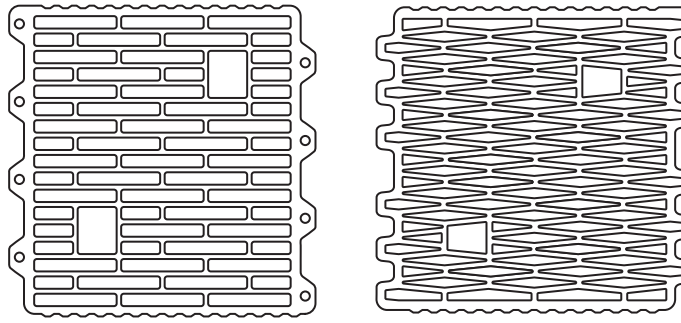

Figure 3.3 (a,b) Cross-sections of the bricks studied.

3.2.2 Horizontal joint in brickwork wall

The bricks described are examined with three different types of horizontal joint:

1. A horizontal joint made with standard mortar (Spanish Standard, 2008) and penetration, called a *full-bed joint.*
2. A discontinuous joint with an air chamber (this type of arrangement is the one most widely used in building), called a *furrowed-bed joint.*
3. A thin horizontal joint that uses a type of mortar grip that does not penetrate the junction bricks of consecutive rows, called a *thin joint.*

In this last arrangement, the clays used in the brick should allow easy grinding, as the bonding mortar is applied in very thin layers of 3 mm, according to the standard (Spanish Standard, 2013). This arrangement requires proper alignment of the bricks, suitable flatness between them and precision workmanship.

Each wall was built as follows:

1. Normal arrangement using standard mortar ($\lambda_m = 1.3$ W/m-K), with 10-mm bed joint thickness and 10 mm of penetration in each brick. Two different horizontal joints were assessed:
   a. Full-bed joint
   b. Furrowed-bed with a 30-mm gap
2. Assembly with a thin horizontal joint made of bonding mortar ($\lambda_m = 0.83$ W/m-K), with 3-mm bed joint thickness and no penetration.

3.2.3 Fired-clay thermal conductivity

As mentioned above, clays today are lightened with various materials in order to reduce their thermal conductivity. Several studies have been conducted on this matter (Demir, 2006; Sutcu & Akkurt, 2010), but they are all based on a clay with a specific composition and a given thermal conductivity.

A recent study (Muñoz et al., 2013) has shown that adding up to 15% additive to a clay with no additive and $\lambda = 0.745$ W/m-K can reduce its thermal conductivity to $\lambda = 0.445$ W/m-K, i.e. by 40%.

Considering this background of studies, we set out to check for a relationship between the thermal conductivity of fired-clay bricks (regardless of how they were made) and the equivalent thermal transmittance of a wall, built using the bricks and arrangement proposed above.

The starting point for the study was a clay with a thermal conductivity of $\lambda = 0.600$ W/m-K, decreasing in steps of 0.05 W/m-K to thermal conductivity values of 50%, that is, to a figure of $\lambda = 0.300$ W/m-K.

3.2.4 Boundary conditions for solving by finite element method

The model analysed by numerical methods is the part of the wall represented by the assembly of two bricks, as is shown in Figure 3.4.

In this figure can be observed the three characteristic sections of the assembly and the heights of each one of them: the cross-section of the bricks with their air-filled voids (the "clay/air cross-section"), height h_1; the cross-section of the bricks with the voids filled with bonding mortar (the "clay/mortar cross-section"), height h_2; and the cross-section of the layer of bonding mortar itself (the "bed joint cross-section"), height h_3. These indicated heights relate to a standard type of assembly with gripping mortar and penetration into the bricks.

3.2.5 Thermal calculations

The finite elements method (COMSOL 4.2a; ANSYS 14.0) was used to obtain the heat fluxes for the boundary conditions as per the standards, thus enabling the equivalent thermal transmittance of the envelope wall to be calculated.

The finite elements method was used to solve each of the first two characteristic sections of the wall (the "clay/air cross-section" and the "clay/mortar cross-section")

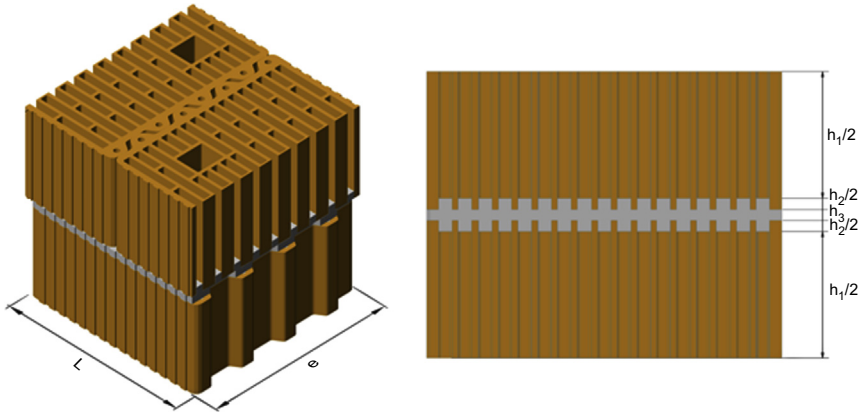

Figure 3.4 Part of the wall representing the assembly of two bricks and the three heights of characteristic sections.

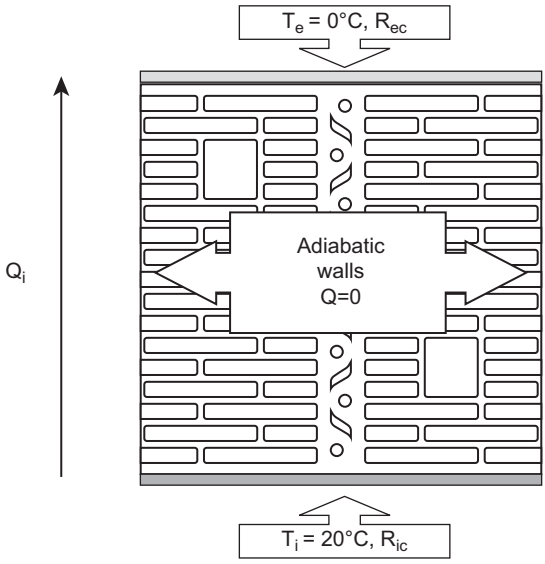

Figure 3.5 Boundary conditions for obtaining the heat flow, Q_i.

with the boundary conditions specified by the aforementioned standards, as shown in Figure 3.5. The heat flow through each characteristic section, Q_i, was obtained.

Once the heat flow, Q_i, was calculated, the thermal resistance, R_i, was obtained via the following expression:

$$R_i = \frac{L \cdot \Delta T}{Q_i} - R_{ic} - R_{ec}$$

Where R_{ic} and R_{ec} are the resistances of the interior and exterior cladding, respectively.

This gave the thermal resistances for the clay/air cross-section (R_1) and for the clay/mortar cross-section (R_2).

The thermal resistance of the horizontal joint (the "bed joint cross-section") can be calculated straightforwardly, since the conductivity of the bonding mortar and the size of the air gap are known:

1. For a horizontal joint with standard mortar furrowed with a 30-mm air gap

$$R_3 = \frac{e - 0,03}{\lambda_m} + \frac{0,03}{\lambda_{air}}$$

2. For a thin horizontal joint

$$R_3 = \frac{e}{\lambda_m}$$

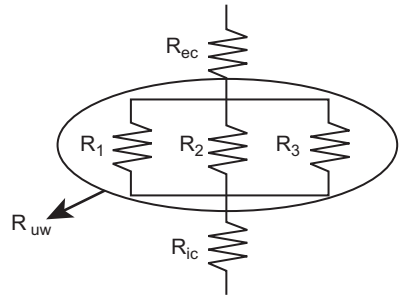

Figure 3.6 Thermal network.

Once the resistance of each characteristic section has been found, the total resistance of the unclad wall can be determined as follows:

$$R_{\text{uw}} = \frac{h_1 + h_2 + h_3}{\frac{h_1}{R_1} + \frac{h_2}{R_2} + \frac{h_3}{R_3}}$$

where h_1, h_2 and h_3 are the heights of the aforementioned sections.

Finally, the equivalent thermal transmittance of the entire wall was calculated:

$$U_{\text{i}} = \frac{1}{R_{\text{T i}}} = \frac{1}{R_{\text{ic}} + R_{\text{ec}} + R_{\text{uw}}}$$

For the sake of clarity, a schematic layout of the thermal network is shown in Figure 3.6.

3.3 Results

3.3.1 *Equivalent transmittance of the wall made of bricks with rectangular voids (block a) and the three types of horizontal joint*

Table 3.1 shows the equivalent thermal transmittance of the wall made using "block a" for different fired-clay conductivities and for the three types of assembly.

As expected, the better the assembly system, the lower the thermal transmittance: in other words, the lower the thermal conductivity of the mortar used, the lower the height of the joint.

Data from Table 3.1 enable builders to choose the most appropriate method of assembly according to the remaining parameters.

For example, a "good" large and highly perforated fired clay with low thermal conductivity (0.300 W/m-K) with a "bad" assembly system (continuous-type assembly using mortar with high thermal conductivity) would yield a thermal transmittance of

Table 3.1 Table comparing equivalent thermal transmittance levels using bricks with rectangular voids depending on the type of horizontal joint

Block a	U_{eq} (W/m^2-K)		
Fired clay	Joint with standard mortar $\lambda_m = 1.3$ (W/m-K)		Joint of bonding mortar $\lambda_m = 0.83$ (W/m-K)
λ (W/m-K)	Full-bed joint	30-mm furrowed-bed joint	Thin joint
0.600	0.7783	0.6654	0.5425
0.550	0.7558	0.6454	0.5245
0.500	0.7322	0.6246	0.5059
0.450	0.7072	0.6027	0.4867
0.400	0.6806	0.5797	0.4666
0.350	0.6521	0.5551	0.4456
0.300	0.6211	0.5286	0.4232

the wall of 0.6211 W/m^2-K. However, a "good" assembly system (thin bonding mortar joint) with a "bad" fired clay with high thermal conductivity (0.600 W/m-K) would give a thermal transmittance of 0.5425 W/m^2-K.

A plot of the values of Table 3.1 (Figure 3.7) shows a decreasing linear trend in thermal transmittance in all cases. This clearly shows the importance of the type of assembly, an aspect that has been studied in earlier papers (Juárez et al., 2012).

Both the table and the graph give an idea of the range of thermal transmittance values depending on the fired-clay thermal conductivity and the type of assembly. We believe that this may prove to be a useful tool for the prior design of walls.

3.3.2 *Equivalent transmittance of the wall made of bricks with rhomboidal voids (block b) and the three types of horizontal joint*

Table 3.2 shows the equivalent thermal transmittance of the wall made using "block b" for different fired-clay conductivities and for the three types of assembly.

It is worth noting that the thermal transmittance values for brick b were found to be very low at 0.3546 W/m^2-K in the best case, i.e. the fired clay with the lowest thermal conductivity and a horizontal bonding mortar joint (a thin layer of mortar with low thermal conductivity).

It is also noteworthy that relatively low thermal transmittance levels are recorded for the wall in this case (0.5478 W/m^2-K) with a continuous joint made of standard

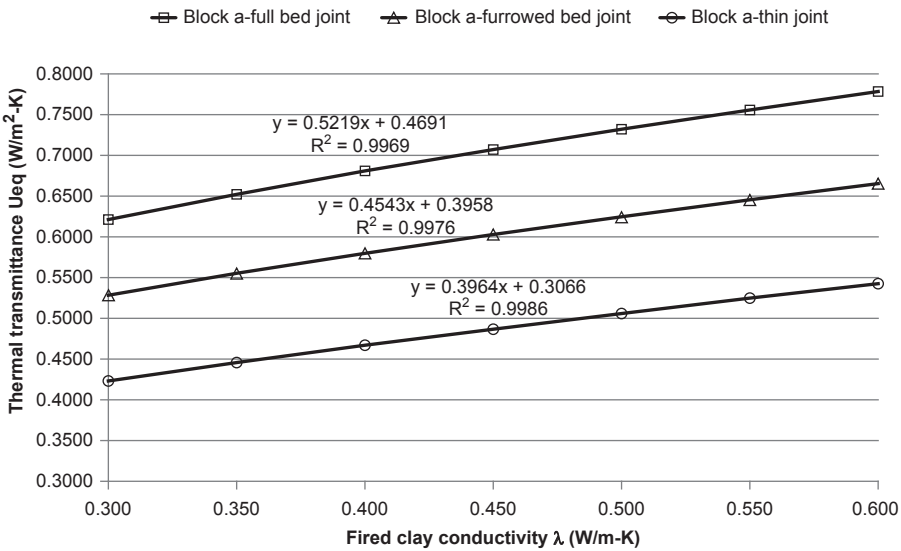

Figure 3.7 Fired-clay thermal conductivity vs. wall thermal transmittance for a brick with rectangular voids.

Table 3.2 Table comparing equivalent thermal transmittance levels using bricks with rhomboidal voids, depending on the type of horizontal joint

Block b	**U_{eq} (W/m^2-K)**		
Fired clay	**Joint with standard mortar λ_m = 1.3 (W/m-K)**		**Joint of bonding mortar λ_m = 0.83 (W/m-K)**
λ (W/m-K)	**Full-bed joint**	**30-mm furrowed-bed joint**	**Thin joint**
0.600	0.6782	0.5594	0.4344
0.550	0.6595	0.5446	0.4226
0.500	0.6399	0.5291	0.4103
0.450	0.6192	0.5127	0.3976
0.400	0.5972	0.4954	0.3843
0.350	0.5735	0.4767	0.3700
0.300	0.5478	0.4564	0.3546

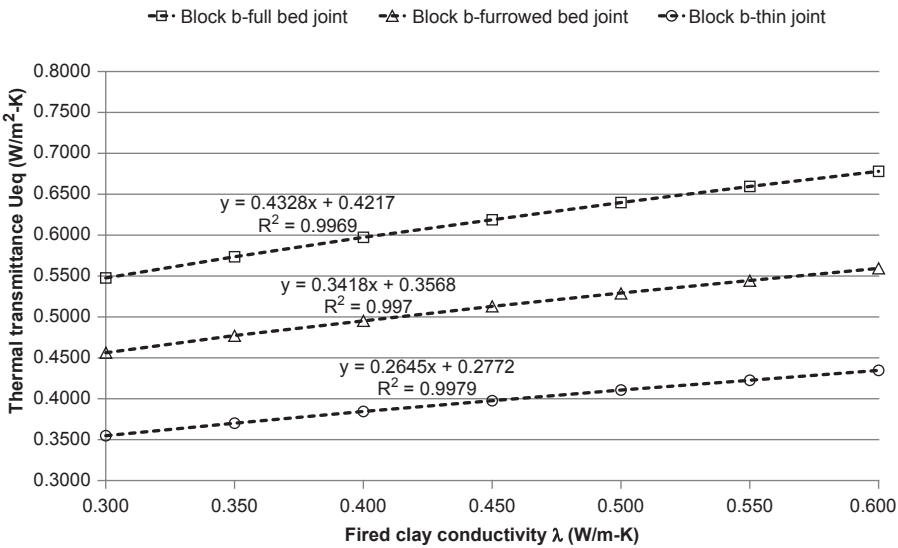

Figure 3.8 Fired-clay thermal conductivity vs. wall thermal transmittance for a brick with rhomboidal voids.

mortar and lightened low fired-clay thermal conductivity due to the good geometrical configuration of the brick.

As in the previous case, the table enables the parameters that are to be adjusted to be chosen with a view to obtaining a specific wall thermal transmittance.

The values plotted in Table 3.2 (Figure 3.8) once again record a linear trend for each type of assembly.

Like the previous brick, this gives the range of wall thermal transmittance values depending on the fired-clay thermal conductivity and the type of assembly.

3.4 Comparative analysis

Combining Tables 3.1 and 3.2 for the different bricks and plotting them together (Figure 3.9) reveals a pronounced linear trend regardless of the type of brick or assembly.

The aforementioned graph reveals that the equivalent thermal transmittance of the wall depends largely on the type of brick and the type of assembly, as shown previously (Juárez et al., 2012; Morales et al., 2011, 2012).

As expected, the lowest equivalent thermal transmittance levels for the wall are obtained using the best brick with the best assembly, and the highest with the worst brick and the worst assembly. However, in the intermediate zones, any of the parameters could be changed when a particular thermal transmittance is required. It should be noted there are other parameters that influence the design of a wall, e.g. mechanical strength limits and the density of the bricks (which prevent the conductance of the fired

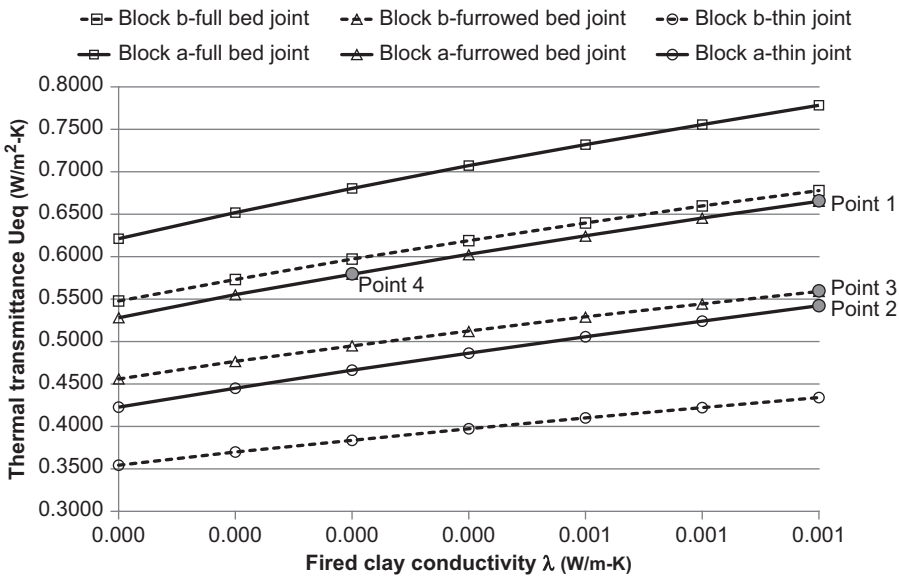

Figure 3.9 Wall thermal transmittance vs. fired-clay thermal conductivity.

clay from being reduced), manufacturing processes that require using a particular brick type, difficulties in ensuring thin joint assembly and financial considerations.

Here is an example. A manufacturer has a clay with a thermal conductivity of 0.600 W/m-K and produces a rectangular brick, without grinding (i.e. the brick is not suitable for assembly with a thin horizontal joint). The best equivalent thermal transmittance that can be obtained for the wall under these conditions is 0.6654 W/m^2-K (point 1 in Figure 3.9). There are three options for improving the equivalent thermal transmittance of the wall:

1. Grinding the brick surface to enable wall assembly with a thin horizontal joint. This gives an equivalent thermal transmittance of 0.5425 W/m^2-K (point 2 in Figure 3.9). The grinding of the bricks may require considerable investment in machinery and a significant modification of the manufacturing process.
2. Changing the geometry of the brick from a rectangular to a rhomboid shape. This would give an equivalent thermal transmittance of the wall of 0.5594 W/m^2-K (point 3 in Figure 3.9) with a horizontal furrowed joint with a 30-mm air gap, i.e. with no grinding required. This modification would involve changing the extrusion mold on the machinery and the production of a different brick, which would also require major investment.
3. Increasing the proportion of the pore-forming additive, reducing the thermal conductivity of the clay to 0.400 W/m-K. This would lead to an equivalent thermal transmittance of the wall of 0.5797 W/m^2-K (Point 4 in Figure 3.9) with a horizontal furrowed joint with a 30-mm air gap. In this case, the manufacturer would only have to check whether the brick complies with the mechanical requirements, and no major investment would be necessary.

In view of the similarity of the slopes, we considered studying the quantities expressed as percentages in order to compare the percentage decrease in the fired-clay thermal

conductivity with the percentage decrease in the thermal transmittance of the wall depending on the type of brick and joint executed. The resulting values are shown in Tables 3.3 and 3.4.

From these values it can be deduced that the improvement in the equivalent thermal transmittance resulting from the decrease in fired-clay thermal conductivity ranges between 2.9% and 22% for bricks with rectangular voids, regardless of the type of assembly. For bricks with rhomboidal voids, the decreases are very similar, ranging between 2.6% and 19.2%, also regardless of the type of assembly.

The plot of the results from Tables 3.3 and 3.4 (Figure 3.10) shows that the trend line is reliably close to the results of the thermal calculations, with an error of ±3%. The trend line corresponds to the equation:

$$\Delta U_{eq} = 0.4040 \cdot \Delta\lambda_{clay} - 0.008$$

This equation, with a Pearson's correlation coefficient of 0.98 (Lehmann & Romero, 2008), enables a rapid estimate to be made of the thermal transmittance of a wall once the variation in the fired-clay thermal conductivity is known and the brick and assembly types have been selected. In other words, if the thermal transmittance value of a wall for a given brick is known and the specifications of the clay and the specific assembly type are factored in, the variation in thermal transmittance based on the variation in fired-clay thermal conductivity can be estimated, maintaining the same brick and type of assembly, and builders can proceed accordingly by lightening the clay as much as possible.

Table 3.3 Percentage improvement in the equivalent thermal transmittance of the wall according to the decrease in fired-clay thermal conductivity for bricks with rectangular voids

	% Improvement in U_{eq} for "block a"		
	Joint with standard mortar $\lambda_m = 1.3$ (W/m-K)		Joint of bonding mortar $\lambda_m = 0.83$ (W/m-K)
Decrease λ_{clay} (%)	Full-bed joint	30-mm furrowed-bed joint	Thin joint
8.33%	2.89%	3.01%	3.32%
16.67%	5.92%	6.14%	6.75%
25.00%	9.13%	9.42%	10.29%
33.33%	12.55%	12.88%	13.98%
41.67%	16.22%	16.58%	17.86%
50.00%	20.20%	20.56%	21.99%

Table 3.4 Percentage improvement in the equivalent thermal transmittance of the wall according to the decrease in fired-clay thermal conductivity for bricks with rhomboidal voids

	% Improvement in U_{eq} for "block b"		
	Joint with standard mortar $\lambda_m = 1.3$ (W/m-K)		Joint of bonding mortar $\lambda_m = 0.83$ (W/m-K)
Decreased λ_{clay} (%)	Full-bed joint	30-mm furrowed-bed joint	Thin joint
8.33%	2.75%	2.65%	2.72%
16.67%	5.64%	5.43%	5.53%
25.00%	8.69%	8.35%	8.46%
33.33%	11.94%	11.45%	11.54%
41.67%	15.43%	14.78%	14.81%
50.00%	19.22%	18.42%	18.36%

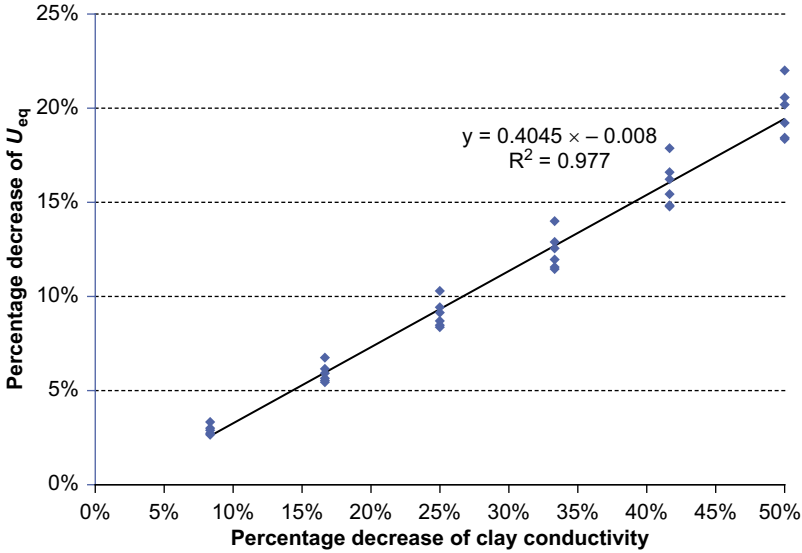

Figure 3.10 Percentage decrease of U_{eq} versus percentage decrease in fired-clay thermal conductivity.

3.5 Conclusions and future trends

The equivalent thermal transmittance of a wall depends on several parameters: the type of brick used (including the specific type of internal void and the type of tongue and groove arrangement), the type of assembly (horizontal joint type and thermal conductivity of its materials), and the type of clay used to make the brick.

Obviously, the lower the thermal conductivity of the materials the lower the equivalent thermal transmittance of the whole wall will be. However, for a given type of brick and assembly, the thermal transmittance of the wall depends linearly on fired-clay thermal conductivity.

The best thermal performance is obtained in walls that use a geometrically optimized brick and are assembled with bonding mortar and a thin joint. Nevertheless, using either of these solutions (or indeed both of them together) entails significant investment in the brick manufacturing process and the wall building process.

The equivalent thermal transmittance of a wall can be decreased by up to 20% by reducing the conductivity of the clay by up to 50% without changing the type of brick or the type of wall assembly. All that is required is to ensure that the mechanical parameters (density and compressive strength) are fulfilled.

This study has found that the percentage improvement in the thermal transmittance of walls depends linearly on the percentage improvement in the fired-clay thermal conductivity, regardless of the type of brick and assembly.

An equation is obtained for estimating the percentage improvement in the thermal transmittance of a wall in terms of the percentage improvement in the thermal conductivity of the clay with an error of less than 3% in all cases − a figure that can be considered negligible in the range of values in which the trade usually works.

As previously mentioned, the mechanical parameters (bulk density, water absorption, compressive strength, etc.) have not been considered in this study. It would be desirable to relate the thermal conductivity of the clay with the mechanical parameters, which are those that limit the reduction in thermal conductivity, making it impossible to improve on the equivalent thermal transmittance. This study is not elementary since it depends on the type of clay used and the pore-forming additives employed.

Moreover, the use of additives in the clays increases water absorption and the block requires the use of external cladding.

Other lines of work may include repeating this study in other types of wall assemblies, as multilayer walls, ventilated facades, etc.

References

Alonso-Santurde, R., Coz, A., Viguri, J. R., & Andrés, A. (2012). Recycling of foundry by-products in the ceramic industry: Green and core sand in clay bricks. *Construction and Building Materials, 27*, 97−106. http://dx.doi.org/10.1016/j.conbuildmat.2011.08.022.

ANSYS 14.0. (April 2014). *Multiphysics modeling and engineering simulation software*. http://www.ansys.com.

Antar, M. A. (2010). Thermal radiation role in conjugate heat transfer across a multiple-cavity building block. *Energy, 35*(8), 3508−3516. http://dx.doi.org/10.1016/j.energy.2010.04.055.

Bilgin, N., Yeprem, H. A., Arslan, S., Bilgin, A., Günay, E., & Marsoglu, M. (2012). Use of waste marble powder in brick industry. *Construction and Building Materials, 29*, 449−457. http://dx.doi.org/10.1016/j.conbuildmat.2011.10.011.

COMSOL 4.2a. (2005). *Multiphysics modeling and engineering simulation software*. [CD ROM] COMSOL AB. http://www.comsol.com (April 2014).

Termoarcilla, C., & Tecnalia, L. (2005). *Investigación de las condiciones del Bloque Termoarcilla para el cumplimiento de las exigencias del nuevo CTE. Propiedades térmicas*. www.termoarcilla.com.

Del Coz Diaz, J. J., Neto, P. J. G., Sierra, J. L. S., & Biempica, C. B. (2008). Nonlinear thermal optimization of external light concrete multi-holed brick walls by finite element method. *International Journal of Heat and Mass Transfer, 51*, 1530−1541. doi: 10.1016.ijheatmasstransfer.2007.07.029.

Demir, I. (2006). An investigation on the production of construction brick with processed waste tea. *Building and Environment, 41*, 1274−1278. http://dx.doi.org/10.1016/j.buildenv.2005.05.004.

EN 12939:2000. (2000). *Thermal performance of building materials and products − Determination of thermal resistance by means of guarded hot plate and heat flow meter methods − Thick products of high and medium thermal resistance*. European Committee for Standardization.

EN 12664:2001. (2001). *Thermal performance of building materials and products − Determination of thermal resistance by means of guarded hot plate and heat flow meter methods − Dry and moist products of medium and low thermal resistance*. European Committee for Standardization.

European and International Standard. (1996). *Building components and building elements. Thermal resistance and thermal transmittance. Calculation method*. EN ISO 6946.

European and International Standard. (1995). *Thermal bridges in building construction. Heat flows and surface temperatures. Part 1: General calculation methods*. EN ISO 10 211-1.

European and International Standard. (2002). *Thermal bridges in building construction. Heat flows and surface temperatures. Part 2: Thermal linear bridges*. EN ISO 10 211-2.

European Standard. (2002). *Masonry and masonry products. Methods for determining design thermal values*. EN 1745.

Eurostat. (2013). *Energy, transport and environment indicators*, ISBN 978-92-79-33105-3. http://dx.doi.org/10.2785/4663. ISSN:1725-4566.

García, X. (2003). *Idoneidad de los cerramientos monocapa para viviendas Bioclimáticas en emplazamientos de elevada severidad climática*. Universidad Pontificia Comillas de Madrid. Instituto de Investigación Tecnológica. http://www.iit.upco.es.

Ghazi Wakili, K., & Tanner, Ch (2003). U-value of a dried wall made of perforated porous clay bricks: hot box measurement versus numerical analysis. *Energy and Buildings, 35*(7), 675−680. doi:10.16.S0378-7788(02)00209-8.

International Standard. (2007). *Building materials and products-hygrothermal properties-tabulated design values and procedures for determining declared and design thermal values*. ISO 10456 http://www.iso.org/iso/catalogue_detail.htm?csnumber=40966 (April 2014).

ISO 8990:1994. (2006). *Thermal insulation − Determination of steady-state thermal transmission properties − Calibrated and guarded hot box*. International Standard Organization, 50748.

Juárez, M. C., Morales, M. P., Muñoz, P., & Gómez, J. A. (2012). Influence of horizontal joint on the thermal properties of single-leaf walls with lightweight clay blocks. *Energy and Buildings, 49*, 362−366. http://dx.doi.org/10.1016/j.enbuild.2012.02.033.

Lehmann, E. L., & Romero, J. P. (2008). *Testing statistical hypotheses* (3rd ed.). New York: Springer, ISBN 0-387-98864-5.

Li, L. P., Wu, Z. G., He, Y. L., Lauriat, G., & Tao, W. Q. (2008a). Optimization of the configuration of 290 × 140 × 90 hollow clay bricks with 3-D numerical simulation by finite volume method. *Energy and Buildings, 40*(10), 1790−1798. http://dx.doi.org/10.1016/j.enbuild.2008.03.010.

Li, L. P., Wu, Z. G., He, Y. L., Lauriat, G., & Tao, W. Q. (2008b). Numerical thermal optimization of the configuration of multi-holed clay bricks used for constructing building walls by the finite volume method. *International Journal of Heat and Mass Transfer, 51*, 3669−3682. doi:10.1016.ijheatmasstransfer.2007.06.008.

López González, L. M., Sala Lizarraga, J. M., La Peña Aranguren, V. de, & Míguez Tabarés, J. L. (2000). Proposal for the use of renewable energy in the La Rioja autonomous community (LRAC) (Spain). *Renewable Energy, 20*(3), 289−304. http://dx.doi.org/10.1016/S0960-1481(99)00111-1.

López González, L. M., Sala Lizarraga, J. M., Míguez Tabarés, J. L., & López Ochoa, L. M. (2007). Contribution of renewable energy sources to electricity production in the La Rioja Autonomous Community, Spain. A review. *Renewable and Sustainable Energy Reviews, 11*(6), 1244−1259. http://dx.doi.org/10.1016/j.rser.2005.09.002.

Lourenco, P. B., Vasconcelos, G., Medeiros, P., & Gouveia, J. (2010). Vertically perforated clay brick masonry for loadbearing and non-loadbearing masonry walls. *Construction and Building Materials, 24*, 2317−2330. doi:10.1016.j.conbuildmat.2010.04.010.

Herek, L. C. S., Hori, C. E., Reis, M. H. M., Mora, N. D., Granhem Tavares, C. R., & Bergamasco, R. (2012). Characterization of ceramic bricks incorporated with textile laundry sludge. *Ceramics International, 38*(2), 951−959. http://dx.doi.org/10.1016/j.ceramint.2011.08.015.

Morales, M. P., Juárez, M. C., López-Ochoa, L. M., & Doménech, J. (2010). Study of the geometry of a voided clay brick using rectangular perforations to optimize its thermal properties. *Applied Thermal Engineering, 31*(11−12), 2063−2065. http://dx.doi.org/10.1016/j.applthermaleng.2011.02.033.

Morales, M. P., Juárez, M. C., Muñoz, P., & Gómez, J. A. (2011). Study of the geometry of a voided clay brick using non-rectangular perforations to optimise its thermal properties. *Energy and Building, 43*(9), 2494−2498. http://dx.doi.org/10.1016/j.enbuild.2011.06.006.

Morales, M. P., Juárez, M. C., López-Ochoa, L. M., & Muñoz, P. (2012). Influence of tongue and groove system on the thermal properties of large-format voided clay bricks for single-leaf walls. *Construction and Building Materials, 30*, 169−173. http://dx.doi.org/10.1016/j.conbuildmat.2011.12.006.

Muñoz, P., Juárez, M. C., Morales, M. P., & Mendívil, M. A. (January 3, 2013). Improving the thermal transmittance of single-brick wall built of clay bricks lightened with paper pulp. *Energy & Buildings, 59*, 171−180. http://dx.doi.org/10.1016/j.enbuild.2012.12.022. Available on line:.

Raimondo, M., Dondi, M., Mazzanti, F., Stefanizzi, P., & Bondi, P. (2005). Equilibrium moisture content of clay bricks: the influence of the porous structure. *Building and Environment, 42*(2), 926−932. http://dx.doi.org/10.1016/j.buildenv.2005.10.017.

Raut, S. P., Ralegaonkar, R. V., & Mandavgane, S. A. (2011). Development of sustainable construction material using industrial and agricultural solid waste: a review of waste-create bricks. *Construction and Building Materials, 25*, 4037−4042. http://dx.doi.org/10.1016/j.conbuildmat.2011.04.038.

Sastre, V., &, Con arquitectura. (2008). *Bloques cerámicos de alto aislamiento térmico, Termoarcilla ECO*. http://www.conarquitectura.com/articulos/24-10-2012-12-50-07-26.pdf (April 2014).

Spanish Standard. (2006). *Código Técnico de la Edificación. Documento Básico. Ahorro de Energía*. *Cte-db-he*. http://www.codigotecnico.org (April 2014).

Spanish Standard. (2009). *Reglamento particular de la marca AENOR para piezas de arcilla cocida para fábricas a revestir*. AENOR RP 34−14.

Spanish Standard. (2009). *Reglamento particular de la marca AENOR para piezas de arcilla cocida para fábricas a revestir*. AENOR RP 34-14. http://www.aenor.es/documentos/certificacion/reglamentos/w_RP_34-14_2009-06-01.pdf (April 2014).

Sutcu, M., & Akkurt, S. (2010). Utilization of recycled paper processing residues and clay of different sources for the production of porous anorthite ceramics. *Journal of the European Ceramic Society, 30*, 1785−1793. http://dx.doi.org/10.1016/j.jeurceramsoc.2010.01.038.

Theodosiou, T. G., & Papadopoulos, A. M. (2007). The impact of thermal bridges on the energy demand of buildings with double brick wall constructions. *Energy and Buildings, 40*(11), 2083−2089. http://dx.doi.org/10.1016/j.enbuild.2008.06.006.

Traditional fired-clay bricks versus large and highly perforated fired-clay bricks masonry: influence on buildings thermal performance

4

R. Černý, V. Kočí
Czech Technical University, Prague, Czech Republic

4.1 Introduction

According to several objective indicators, energy-saving efforts became apparent in the past several decades (Gökce & Gökce, 2013; Mata, Kalagasidis, & Johnsson, 2013; Ralegaonkar & Gupta, 2010; Uygunoglu & Kecebas, 2011). The average share of buildings' energy consumption reaches almost 40% (Chwieduk, 2003; EuroACE, 2004) and its rise is expected in the future. Additionally, 69% of the energy used in buildings is consumed in heating in the European Union (EEA, 2012); thus, a significant reduction in energy demands can be achieved by promoting buildings with better thermal insulating capabilities of their envelopes. This process has already been started because new thermal standards prescribe more and more stringent requirements aiming at improvement of the thermal insulating skills of external walls. For example, in United Kingdom, the requested U-value for external walls was reduced from 1.70 W/(m^2K) in 1965 (Jäger, 1984) to the current 0.30 W/(m^2K) (L1A, 2010). For better imagination, this means that although in the not very distant past brick masonry with a thickness of 0.45 m was considered sufficient from a thermal point of view, according to the current thermal standards this wall should be over 2 m thick. The increase of wall thickness can present a solution to a certain extent, but in modern building practice it is surely unthinkable. There are several definite ways how the increasing demands of thermal standards can be met: by involving thermal insulations into the composition of building envelopes, finding better constructional solutions, or by developing building materials with improved thermal insulating properties. This also concerns the bricks.

Since its establishment, brick production went through a large development, reflecting current trends in the technical, economical, or scientific field. After industrial production was started, the increase of the quality and quantity of brick products was perceptible. Energy-savings effort, as another tendency common for the whole building industry (Al-Sanea, Zedan, & Al-Hussain, 2012; Ascione, Bianco, DeMasi, & Vanoli, 2013; Boyano, Hernandez, & Wolf, 2013; Suarez, Prieto, & Fernández, 2013), was also reflected in the brick industry. Therefore, traditional bricks were gradually replaced by brick blocks with cavities filled with air during the last few decades

Eco-efficient Masonry Bricks and Blocks. http://dx.doi.org/10.1016/B978-1-78242-305-8.00004-8

(Alhazmy, 2010; Arendt, Kraczek, & Florczuk, 2011; da Silva Almeida et al., 2013) because there is clear evidence of good thermal insulating skills of air-contained materials (Jerman & Černý, 2012; Kim, Leon, & Lee, 2010). Depending on the specific ratio of the air/brick body and the parameters of the brick body, perforating solid bricks led to a decrease in the values of thermal conductivity up to ~0.20−0.12 W/(mK) (Pavlík, Jerman, Trník, Kočí, & Černý, 2014) from the original ~0.90−0.50 W/(mK) (Pavlík, Fiala, Pavlíková, Pernicová, & Černý, 2010; Principi & Fioretti, 2012; Sala et al., 2008).

Although dry, nonflowing air has the best thermal insulating property from all traditional insulating materials (Jelle, 2011), a new type of highly perforated bricks filled with other insulating materials appeared in the last few years (Bouchair, 2008; Zukowski & Haese, 2010). It might seem ineffective, but filled cavities reduce radiative heat transport, which is, together with convection and conduction, one of the heat transport modes (Ait-taleb, Abdelbaki, & Zrikem, 2008; Badruddin, Zainal, Narayana, & Seetharamu, 2007). The highest efficiency of insulating skills of air is achieved when it covers a large number of small pores, which is not the case for highly perforated bricks. According to Pavlík et al. (2014), application of insulating materials as cavity filling can lead to an improvement in thermal properties up to 29.6%, and effective thermal conductivity of highly perforated clay bricks filled with expanded polystyrene can be reduced to 0.088 W/(mK). In comparison with traditional fired clay bricks, for which body thermal conductivity lies usually between ~0.5 and 0.9 W/(mK) (Pavlík et al., 2010; Principi & Fioretti, 2012; Sala et al., 2008), it presents a substantial improvement leading to significant savings of heating energy.

In addition to the improvement of material properties, the constructional solution of buildings went through large enhancements. It resulted in the introduction of so-called "passive houses," which can be currently assumed as the top of building design. The houses built-in passive standards are characterized by very low-energy consumption while standard construction materials and technologies are used. According to Feist (2007) and generally accepted criteria, the space heating demand of passive houses has to be lower than 15 kWh/(m^2a) and specific primary energy demand for heating, cooling, hot water, auxiliary electricity, and domestic and common area electricity have to be lower than 120 kWh/(m^2a). To achieve this standard, in addition to excellent thermal insulating building materials, it is necessary to use windows with very low heat losses and very high solar gains, a ventilation system with highly efficient heat recovery, etc.

Since 1992, when the first passive house was built (Passivhaus Institute, 1997), most passive houses were built only on a timber basis (Audenaert, DeCleyn, & Vankerckhove, 2008; Dodoo & Gustavsson, 2013; Feist, 2001; Fux, Ashouri, Benz, & Guzzella, 2014; Janson, 2010; Mlakar & Štrancar, 2013). The main reason why it was so is the stud system of timber structures with boarding allowing the thermal insulation to be implemented into the wooden frame between the studs. This fact reduces the thickness of the building envelope, which would be unfeasible with other building materials. However, after more than 20 years since the first passive house was built, the share of brick-based passive houses was increased to 15%, according to Kuzman, Grošelj, Ayrilmis, and Zbašnik-Senegačnik (2013). This fact only proves the progress

of brick development. Probably the best way to demonstrate the progress in the brick industry aimed at the improvement of thermal insulating properties is to perform a case study comparing the influence of traditional fired clay bricks and highly perforated clay bricks with and without cavity filling on thermal performance of reference building. Therefore, this comparison is the main objective of this chapter.

4.2 Simulation tools for the assessment of energy performance of buildings

There are several simulation tools suitable for the assessment of buildings' energy demands or their thermal performance. As examples, the dynamic simulation software used by Thiers and Peuportier (2008), the computer-aided design tool for passive solar systems applied by Yakubu (1996), the simulation software for zero energy building design used by Wang, Gwilliam, and Jones (2009), or the optimization tools Building Energy Optimization (Christiansen, Horowitz, Anderson, & Barker, 2005) and EGUSA (Fairey et al., 2002) can be quoted.

There are also several nondynamic software tools for the calculation of building energy performance mostly related to passive or low-energy houses. One of the most advanced and detailed models with an accuracy of ± 0.5 kWh is PHPP (Passive House Planning Package, 2007), which was created by W. Feist at Passivhaus Institut in Germany. It is based on European standards related to the thermal protection of buildings, passive house design, or energy performance calculations, converting them to a more convenient and user-friendly form. Therefore, it is one of the most frequently used design tools, not only for passive houses. For example, for scientific purposes it was used by Ridley et al. (2013) or Stephan, Crawford, and de Myttenaere (2013).

In the case study performed within the frame of this chapter, Design Builder software was used. It allows building modeling together with dynamic energy simulations. It was developed for the creating or assessing of building designs at any stage of the design process. Some typical uses are evaluating a range of facade options for the effect on overheating, energy use, and visual appearance; checking for optimal use of natural light; modeling lighting control systems; calculating savings in electric lighting; calculating temperature, velocity, and pressure distribution in and around buildings using computational fluid dynamics (CFD) visualizing site layouts and solar shading; thermal simulation of naturally ventilated buildings; and heating, ventilation, and air conditioning design, including heating and cooling equipment sizing.

4.3 Reference building

The reference building presented in this study follows the principles of passive house design. Regarding the commitment to implement the European directive 2010/31/EC (2010), more likely known as EPBD II, into national thermal standards, it is apparent that the passive standard will become quite common in the near future. Therefore, our

design is directed in this way, although reaching the passive standard is not the main design objective in this case.

4.3.1 Architectural solution and technical equipment

The designed family house is self-standing and has two stories without a basement. The bottom story is partially embedded in a hillside, and there is a garage connected to the upper floor. The disposition of the family house is designed as 7 + 1. The main entrance is situated on the second floor. Behind the main door, there is a small vestibule that can also be connected with the garage. Next to the vestibule, there is a hall with the stairs connecting both stories of the house. The hall is connected with particular rooms on this floor, which are intended for active living. Between the hall and main living room, there is a glass wall with a sliding door. Also between the main living room and workroom or kitchen, there are glass sliding doors that can optically enlarge the internal space. The plan view of the second floor is depicted in the upper part of Figure 4.1, and a list of rooms with their area is summarized in Table 4.1.

Rooms on the first floor are intended mostly for resting. There is a parents' bedroom with its own bathroom and dressing room and two children's bedrooms separated by a playroom that can be later changed into a dressing room. The children also have their own bathroom. The plan view of the first floor is shown in the bottom part of Figure 4.1. The list of rooms with their area is summarized in Table 4.2. Three-dimensional visualizations of the southeast, northeast, and southwest views of the designed family house are shown in Figure 4.2.

It is supposed that the house will be used by a family of five members. It will be occupied permanently except on workdays, when it will be empty from 8:00 until 18:00. This occupancy schedule will be used for the calculation of internal heat gains, which are important for the estimation of energy performance.

As in case of other passive houses, a standard heating system is not installed in this house. Space heating is ensured by a ground source heat pump (GSHP), which uses earth as the heat source. Similar to a refrigerator or air conditioner, these systems use a heat pump to force the transfer of heat from the ground. Heat pumps can transfer heat from a cool space to a warm space, against the natural direction of flow, or they can enhance the natural flow of heat from a warm area to a cool one. The core of the heat pump is a loop of refrigerant pumped through a vapor-compression refrigeration cycle that moves heat. Unlike air source heat pumps, GSHP exchanges heat with the ground. This is much more energy-efficient because underground temperatures are more stable than air temperatures through the year. According to Self, Reddy, and Rosen (2013), the coefficient of performance (COP) of GSHPs usually lies between 3 and 5; therefore, a COP equal to 3.5 was chosen in this case study. The COP expresses the efficiency of the GSHP and is calculated as heat output from the condenser divided by power supplied to the compressor. According to the ČSN EN 73 0540-2 (2011), the highest allowed cooling set point is 27 °C, and this value was used also in this case. The domestic hot water system provides the household with hot water at 55 °C. The exchange of fresh air is ensured by mechanical ventilation with a heat recovery system with an efficiency of 80%, which is in compliance with Roulet, Heidt,

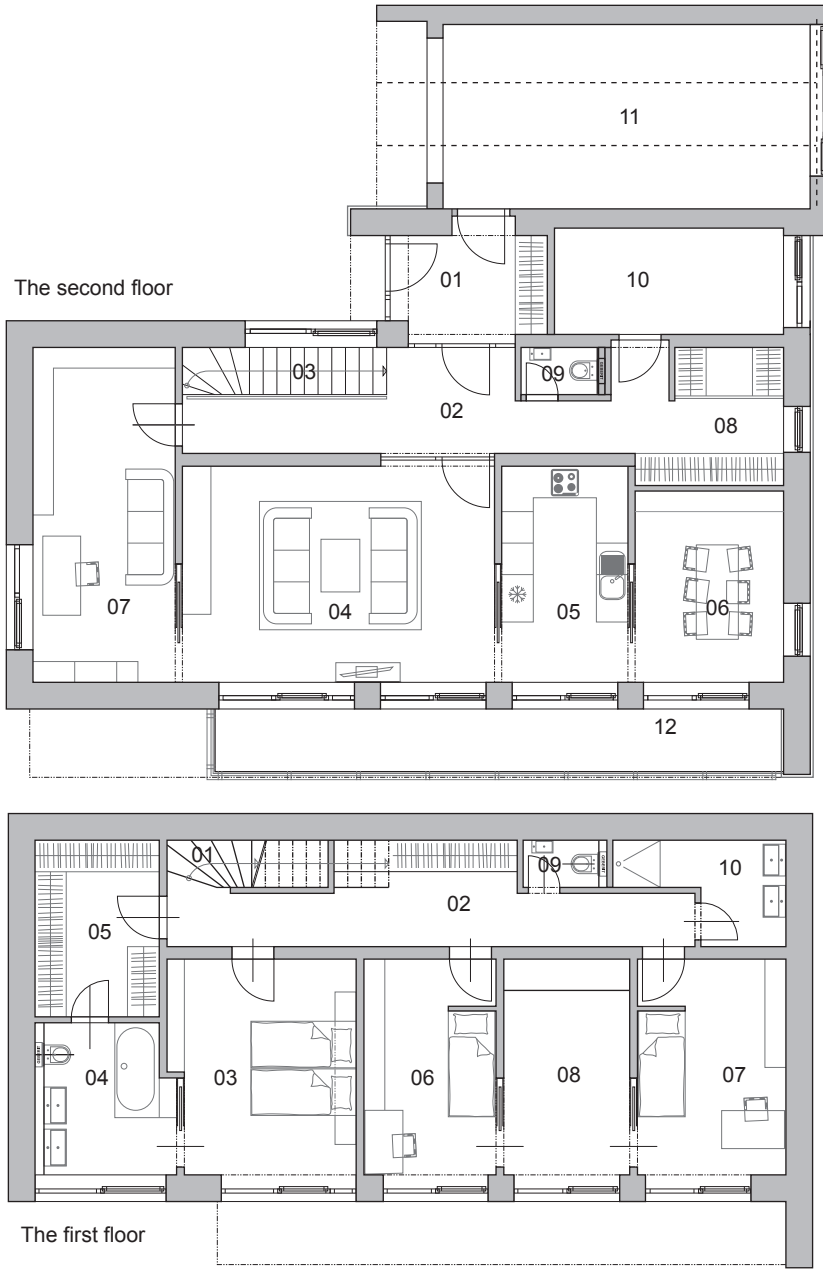

Figure 4.1 Plan view of the first and second floor of the designed family house.

Table 4.1 List of rooms on the second floor

No.	Room	Area (m^2)
01	Vestibule	6.34
02	Hall	11.28
03	Stairway	3.48
04	Living room	25.70
05	Kitchen	10.51
06	Dining room	10.94
07	Workroom, library	17.26
08	Dressing room	8.38
09	Toilet	1.30
10	Technical room	8.81
11	Garage	24.50
12	Balcony	14.74

Table 4.2 List of rooms on the first floor

No.	Room	Area (m^2)
01	Stairway	2.61
02	Hall with dressing room	13.95
03	Parents' bedroom	14.89
04	Bathroom	7.00
05	Dressing room	7.97
06	Bedroom 1	10.78
07	Bedroom 2	12.00
08	Playroom/dressing room	10.37
09	Toilet	1.30
10	Bathroom	4.78

Foradini, and Pibiri (2001) describing heat recovery efficiency mostly between 30% and 90%. The ventilation system is operated continuously at a ventilation rate of 0.30/h. This provides the required amount of fresh air necessary for a five-member family according to ČSN EN 13829 (2001).

Figure 4.2 Southeast, northeast, and southwest views of the designed family house.

4.3.2 Constructional solution

To investigate the influence of traditional and highly perforated clay bricks on the thermal performance of the designed building, the external walls are built of three different materials. In the first case, the traditional solid clay bricks present the construction material. The second variation of the family house assumes highly perforated clay bricks with cavities filled with air. In the last variation, the external walls are made of highly perforated clay bricks with cavities filled with expanded polystyrene. The last brick represents the most advanced brick currently available in the building market. Both perforated clay bricks with dimensions 500 × 250 × 247 mm are depicted in Figure 4.3.

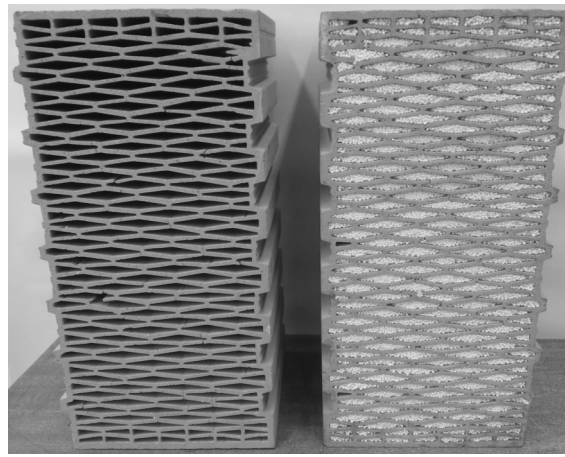

Figure 4.3 Highly perforated clay bricks with and without cavity filling.

In this case, the cavities cover approximately 56% of the cross-section area. The external walls are provided from both sides with thermal insulating plaster 25 mm thick. The thermal conductivity of solid clay brick was taken from Sutcu, del Coz-Díaz, Rabanal, Gencel, and Akkurt (2014), and the effective thermal conductivity of highly perforated clay bricks was taken from Pavlík et al. (2014). The composition of external walls, including the thickness of the particular layers and their thermal conductivity, is summarized in Table 4.3.

The remaining constructional parts (i.e., ground floor, roof, windows, and doors) are identical for all of the investigated variations, which means that only the influence of material of external walls is taken into account. The composition of the ground floor and roof, including thickness and thermal conductivity of the particular layers, is summarized in Tables 4.4 and 4.5. The design values of the thermal conductivity of particular materials were taken from ČSN EN 73 0540-3 (2005). Because the roof is designed as two-layered with a ventilated air gap, only the bottom part of the roof (between the interior and the air gap) is included into the U-value calculations.

The U-value of the particular parts of the building envelope can be calculated according to the equation

$$U = \frac{1}{R_{\mathrm{si}} + \frac{d_j}{\lambda_j} + R_{\mathrm{se}}}, \tag{4.1}$$

where R_{si} and R_{se} ($\mathrm{m^2K/W}$) are the thermal resistances of internal and external surface prescribed in ČSN EN 73 0540-2 (2011), d_j (m) is the thickness of a particular layer, and λ_j (W/(mK)) is its thermal conductivity. Under real conditions, the calculated U-values will be probably higher because of the presence of thermal bridges, the elimination of which is a very difficult task. Elimination would be possible if the insulation layer was completely homogeneous without distance anchors or any

Table 4.3 Composition of external walls

Material	Thickness (m)	Thermal conductivity (W/(mK))
Thermal insulating plaster	0.025	0.097
Traditional clay brick	0.500	0.830
Highly perforated clay brick	0.500	0.124
Highly perforated clay brick with cavities filled with expanded polystyrene	0.500	0.088

Table 4.4 Composition of the ground floor

Material	Thickness (m)	Thermal conductivity (W/(mK))
Foam glass gravel	0.250	0.050
Concrete	0.080	1.230
Polyethylene waterproofing	0.002	0.330
Concrete	0.250	1.230
Expanded polystyrene	0.050	0.035
Concrete	0.050	1.230

Table 4.5 Composition of the bottom part of the roof

Material	Thickness (m)	Thermal conductivity (W/(mK))
Ceramic joists with brick inserts and concrete topping	0.230	1.100
Hydrophobic mineral wool	0.480	0.039
Oriental strand board	0.015	0.130

pervading elements. However, it is difficult to achieve in practice; therefore, the calculated U-values of the particular parts of the building envelope, summarized in Table 4.6, were in the calculations increased by 0.02 W/(m^2K), as recommended in ČSN EN ISO 6946 (2008).

According to Grynning, Gustavsen, Time, and Jelle (2013), windows can be responsible for as much as 45% of overall heat losses, which means their selection

Table 4.6 Parameters of the particular components of the analyzed building envelope

	Area (m^2)	U-value (W/m^2K)		
		Var. A	Var. B	Var. C
External walls	267.49	0.776	0.212	0.157
Ground floor	129.17		0.146	
Roof	126.66		0.080	
Windows	54.76		0.700 (frame 1.100)	
Doors	2.86		0.900	

can significantly affect the thermal performance of a building. This is the reason why in the presented case study windows with triple glazing were assumed.

4.3.3 Model of the building for computer simulations

The model of the building for energy calculations, created using Design Builder software, is shown in Figure 4.4. In several countries, such as Ireland or Great Britain, Design Builder was approved as an official tool for the building's energy analysis. After the building model was created, dynamic simulation of energy performance was carried out using the EnergyPlus (2011) built-in module with input parameters taken from European standards (ČSN EN 15217, 2008; ČSN EN 15603, 2009; ČSN EN ISO 13829, 2001; ČSN EN ISO 6946, 2008; ČSN EN ISO 13370, 2009; ČSN EN ISO 13789, 2009; ČSN EN ISO 13790, 2009), which are also contained in the PHPP model. EnergyPlus is a complex simulation tool allowing heating, cooling, lighting, ventilation, or water use to be modeled. As boundary conditions, it contains climatic data for more than 2100 locations, which are appropriate for energy simulations (Crawley, 1998). In this simulation, climatic data for Prague, Czech Republic were chosen. Because EnergyPlus is a stand-alone simulation program without a user-friendly graphical interface, its implementation into the Design Builder environment allows for performing simulations easily without any fuss, defining building model and input parameters, which were precalculated in accordance with a PHPP model. The flowchart of the simulation process, including the necessary input parameters, is shown in Figure 4.5.

To calculate heating energy, in addition to the thermal properties of the building envelope, it is also necessary to include internal heat gains into calculations because they can significantly reduce the required amount of energy for heating. Internal heat gains are generated by the activity of occupants as metabolic heat, by utilization of electrical devices, or by thermal emission of artificial lighting. Their amount mainly depends on the number of occupants and the time they spend in the building. In this case study, we assumed their presence for 70% of the year. According to ČSN EN

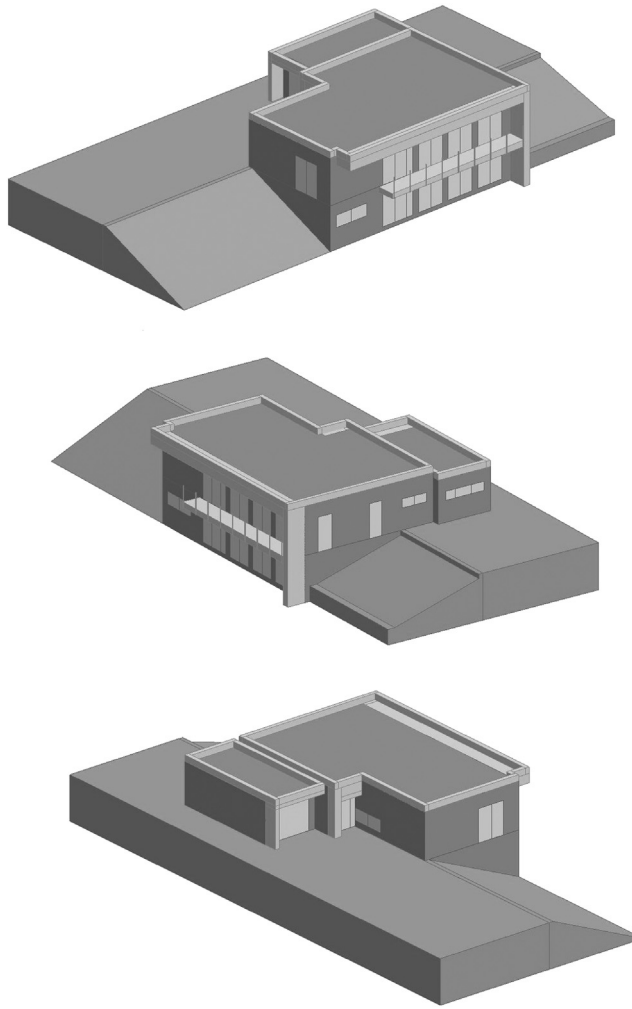

Figure 4.4 Southeast, northeast, and southwest views of the building model of the designed family house.

ISO 13790 (2009), specific internal heat gains comprising metabolic heat, heat produced by electrical devices, and artificial lighting can be calculated in a simplified estimate as 100 W per person plus 100 W per building unit, regardless of the presence of occupants. In this case study, specific internal heat gains can be set to 2.98 W/m^2. Moreover, heat gains can also be achieved because of solar insolation through windows. Therefore, the biggest glass area is oriented to the south whereas opaque parts of buildings are mostly oriented to the north. Anyway, the amount of solar gains depends on the properties of windows. In addition to the U-values of frame and glass, which are particularly responsible for heat losses, the solar factor of windows is very important from the point of view of solar gains. According to Jelle (2013), the

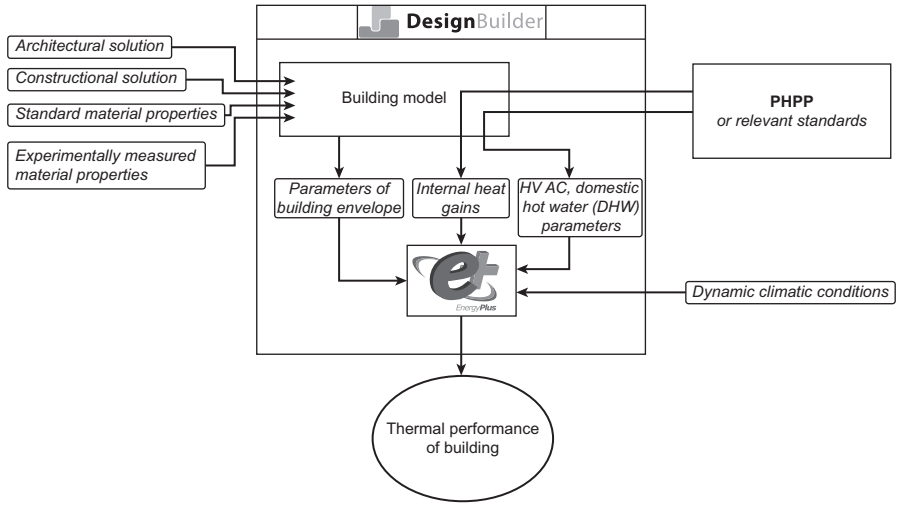

Figure 4.5 Flowchart of the simulation process. HVAC, heating, ventilation, and air conditioning.

solar factor lies between 0.11 and 0.85. In this case study, we used the solar factor of windows equal to 0.61.

In this case study, the dynamic simulation of energy performance of the designed building provides the results of required heating energy per year, among others. This value subsequently serves as an effective indicator showing the influence of traditional and highly perforated clay bricks on the thermal performance of the designed building.

4.4 Computational results and discussion

From the point of view of thermal performance and according to the expectations, the designed family house made of traditional clay bricks shows the worst results. The annual heating energy demand at given input parameters is equal to 20,279 MJ, which corresponds approximately to 27.98 kWh/m^2. When highly perforated brick with air-filled cavities is used, the annual heating energy demand is reduced to 9958 MJ, which is approximately 13.74 kWh/m^2. The best results are obtained when highly perforated brick with cavities filled with expanded polystyrene is used. The annual heating energy demand is only 8922 MJ, which represents approximately 12.31 kWh/m^2. The results are summarized in Figure 4.6.

The differences between the heating energy demands follow, in a certain way, the differences between the thermal conductivities of the particular bricks, but they are limited by the constructional solution and materials of the other parts of the building envelope. Because brick-based external walls of the designed family house represent only 46% of its building envelope, the improvement of energy savings cannot be as

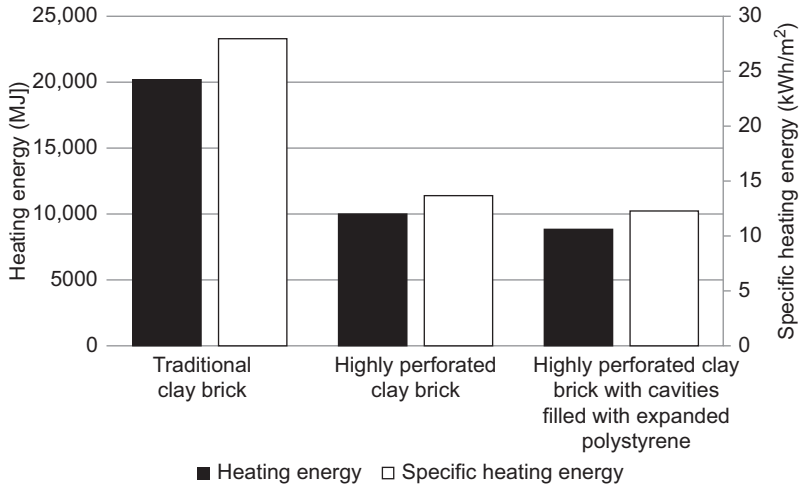

Figure 4.6 Comparison of heating energy demands.

high as the improvement of the thermal insulating properties of highly perforated bricks because of the heat losses through windows, doors, roof, or ground floor, which remain unchanged in all of the investigated variations.

Comparing the values of thermal conductivity presented in Table 4.3, one can notice that the development of traditional brick into a new type of highly perforated brick went along with a substantial reduction of its thermal conductivity, reaching up to 89.4%. The improvement of the thermal insulating properties of new bricks, on the one hand, consisted in an enhancement of the thermal insulating properties of the brick body by addition of combustible admixtures before firing, such as sawdust, paper residues, or other combustible wastes (Eliche-Quesada, Corpas-Iglesias, Pérez-Villarejo, & Iglesias-Godino, 2012; Sutcu & Akkurt, 2009; Sutcu et al., 2014). On the other hand, the system of internal cavities effectively reduces the conductive heat transfer. Moreover, subsequent application of cavity filling can also reduce the radiative heat transfer. As it was mentioned before, there are generally three modes of heat transfer: conduction, convection, and radiation. Although the conduction and convection heat transfers are taken into account very frequently, radiative heat transfer remains often underestimated in building physics. Radiative heat transfer in hollow clay brick cavities was studied by Kočí et al. (2012). They referred to Modest (1993) and expressed it as

$$\lambda_{\text{rad}} = \varepsilon\sigma_{\text{SB}} \cdot \frac{\left(T_1^4 - T_2^4\right)}{T_1 - T_2} \cdot \Delta x, \tag{4.2}$$

where λ_{rad} is the radiative thermal conductivity (W/(mK)), ε is the emissivity of the material (dimensionless), σ_{SB} is the Stefan−Boltzmann constant (W/(m^{2}K^4)), T_1 and T_2 are the temperatures of the opposite surfaces in the cavity (K), and Δx is distance

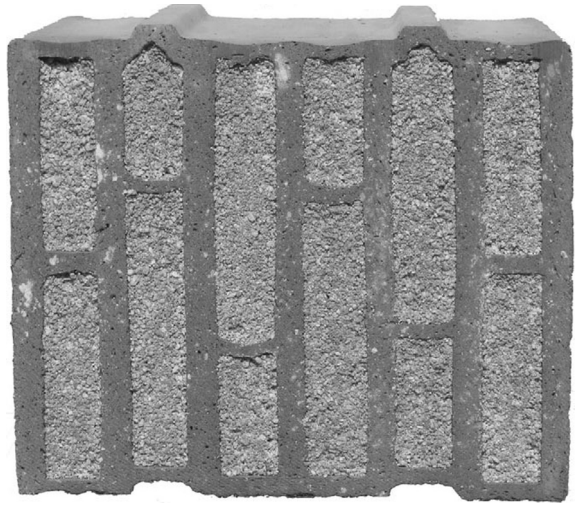

Figure 4.7 Hollow brick filled with perlite insulation tested by Zukowski and Haese (2010). *Source*: Reprinted from Zukowski and Haese (2010), Copyright (2010), with permission from Elsevier.

between the opposite pore/cavity walls (m). In common building materials, such as concrete, wood, mineral wool, polystyrene etc., radiative heat transfer does not play a significant role because, regarding the pore size distribution, the temperature difference between the opposite pore walls is very small. However, when highly perforated bricks with their large cavities are exposed to the weather conditions, the temperature gradient in these cavities can be very high, especially when the brick is insolated from one side. Thus, the radiation heat transfer is perceptible. Summarizing all of these facts together, the best improvement of the thermal insulating skills of highly perforated clay bricks can be achieved only when materials with low thermal conductivity and low median pore size will be applied as cavity filling.

Pavlík et al. (2014) reported that after the application of expanded polystyrene as cavity filling, the effective thermal conductivity reduction reached 29% in comparison with air-filled cavities. Similar results demonstrating the progress that has been done in the field of the brick industry during the last few decades were also presented by other investigators. Using perlite as cavity filling (Figure 4.7), Zukowski and Haese (2010) reduced the thermal conductivity of highly perforated brick from 0.41 to 0.09 W/(mK). Al-Hadhrami and Ahmad (2009) investigated several types masonry bricks used in Saudi Arabia (Figure 4.8), and they showed that the application of mineral wool as cavity filling of hollow brick reduced the thermal conductivity by 24.5%.

According to the results presented in this case study, the utilization of highly perforated bricks with or without cavity filling instead of traditional clay bricks can lead to substantial energy savings. In the case of a designed family house made of highly perforated bricks with cavity filling, it led to the reduction of heating energy of 56.0%; in the case of highly perforated clay brick without cavity filling, it was

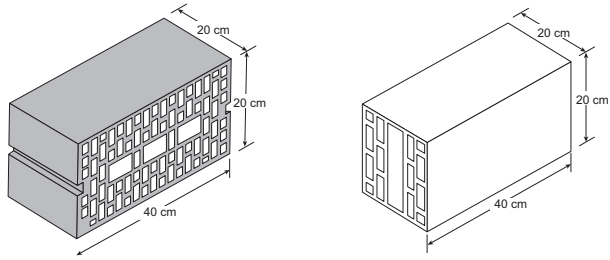

Type 1: normal hollow red clay brick, ordinary concrete mortar
Type 2: type 1 with body added polystyrene insulation
Type 3: type 1 with body added perlite insulation
Type 4: type 1 with center holes filled w/polystyrene insulation
Type 5: normal hollow clay brick, insulating mortar
Type 6: type 5 with center hole filled w/perlite + cement mix
Type 7: type 5 with center hole filled w/mineral wool insulation
Type 8: type 5 with center hole filled w/perlite + cement mix, ordinary concrete mortar
Type 9: type 5 with center hole filled w/mineral wool, ordinary concrete mortar

Figure 4.8 Hollow clay brick types tested by Al-Hadhrami and Ahmad (2009).
Source: Reprinted from Al-Hadhrami and Ahmad (2009), Copyright (2009), with permission from Elsevier.

50.9%. The reduction of heating energy was significant to such an extent that even conditions of passive standard were met because the annual heating energy was lower than 15 kWh/m^2.

4.5 Future trends

The influence of traditional fired clay bricks versus highly perforated clay bricks on the thermal performance of common buildings was found very significant. Highly perforated clay bricks either with or without cavity filling represent the most advanced bricks that are currently available on the building market. Unlike traditional clay bricks, the thermal properties of highly perforated bricks are substantially improved. Therefore, their positive influence on building thermal performance is apparent.

According to the results of the assessment of the thermal performance of a reference family house in this chapter, the utilization of highly perforated bricks can lead to a reduction in annual heating energy up to 56.0% in a comparison with traditional bricks. This represents an appreciable number taking into account the rising prices of energy. It also illustrates well the wide development and progress made in the field of the brick industry during the last few decades, which involved the material of the brick body as well as the geometry of the cavities and their filling.

The improved thermal insulation function of highly perforated clay bricks is the first important factor revealing their potential for the application in low-energy houses. The second one may be the tradition in certain geographical areas of Europe. For instance, in the Central European countries, ceramic brick was a building material most frequently used for many centuries.

Another argument for using the advanced types of brick as construction materials in low-energy buildings as a replacement for most commonly used timber can be found if a building-physics point of view is adopted (Kočí, Bažantová, & Černý, 2014). The brick-based structures of any type have fewer problems with moisture condensation

because most bricks are characterized by fast water vapor transport. The relatively low value of the water vapor diffusion resistance factor of bricks in a comparison with wood allows faster transport of water vapor through a construction. This is very important because it leads to prevention of water vapor accumulation and its subsequent possible condensation. The problems of water vapor condensation during the winter period are well known in general and, of course, water vapor condensation can also occur in this case, but the high vapor permeability of bricks helps to increase the evaporation so that the overall condensation/evaporation balance is better than in the case of less permeable materials.

The bricks also have a good thermal accumulation function that cannot be achieved for timber-based buildings. In addition, contrary to the timber structures, which may face problems with a poor fire resistance or the possibility of biological degradation, the brick-based houses, by their nature, are well-resistant to high temperatures. They are also rarely affected by microorganism attacks.

As it follows from the arguments given above, the advanced highly perforated bricks can be considered very promising construction materials in the nearest future, when the passive standard is supposed to become quite common.

Acknowledgments

This research has been supported by the Czech Science Foundation under project No P105/12/G059.

References

Ait-taleb, T., Abdelbaki, A., & Zrikem, Z. (2008). Numerical simulation of coupled heat transfers by conduction, natural convection and radiation in hollow structures heated from below or above. *International Journal of Thermal Sciences, 47*, 378−387.

Al-Hadhrami, L. M., & Ahmad, A. (2009). Assessment of thermal performance of different types of masonry bricks used in Saudi Arabia. *Applied Thermal Engineering, 29*, 1123−1130.

Al-Sanea, S. A., Zedan, M. F., & Al-Hussain, S. N. (2012). Effect of thermal mass on performance of insulated building walls and the concept of energy savings potential. *Applied Energy, 89*, 430−442.

Alhazmy, M. M. (2010). Numerical investigation on using inclined partitions to reduce natural convection inside the cavities of hollow bricks. *International Journal of Thermal Sciences, 49*, 2201−2210.

Approved Document L1A. *Conservation of fuel and power in new dwellings* (2010). London: RIBA Enterprises.

Arendt, K., Kraczek, M., & Florczuk, J. (2011). Numerical analysis by FEM and analytical study of the dynamic thermal behavior of hollow bricks with different cavity concentration. *International Journal of Thermal Sciences, 50*, 1543−1553.

Ascione, F., Bianco, N., De Masi, R. F., & Vanoli, G. P. (2013). Rehabilitation of the building envelope of hospitals: achievable energy savings and microclimatic control on varying the HVAC systems in Mediterranean climates. *Energy and Buildings, 60*, 125−138.

Audenaert, A., De Cleyn, S. H., & Vankerckhove, B. (2008). Economic analysis of passive houses and low-energy houses compared with standard houses. *Energy Policy, 36*, 47−55.

Badruddin, I. A., Zainal, Z. A., Narayana, P. A. A., & Seetharamu, K. N. (2007). Numerical analysis of convection conduction and radiation using a non-equilibrium model in square porous cavity. *International Journal of Thermal Science, 46*, 20−29.

Bouchair, A. (2008). Steady state theoretical model of fired clay hollow bricks for enhanced external wall thermal insulation. *Building and Environment, 43*, 1603−1618.

Boyano, A., Hernandez, P., & Wolf, O. (2013). Energy demands and potential savings in European office buildings: case studies based on EnergyPlus simulations. *Energy and Buildings, 65*, 19−28.

Christiansen, C., Horowitz, S., Anderson, R., & Barker, S. (2005). BEopt: software for identifying optimal building designs on the path to zero net energy, NREL CP-0550−3733. In *Proceedings of the ISES solar world energy congress, Orlando, FL.*

Chwieduk, D. (2003). Towards sustainable-energy buildings. *Applied Energy, 76*, 211−217.

Crawley, D. B. (1998). Which weather data should you use for energy simulations of commercial buildings. *ASHRAE Transactions, 104*, 498−515.

ČSN EN 15217. (2008). *Energy performance of buildings − methods for expressing energy performance and for energy certification of buildings*. Prague: Czech Office for Standards, Metrology and Testing.

ČSN EN 15603. (2009). *Energy performance of buildings − overall energy use and definition of energy ratings*. Prague: Czech Office for Standards, Metrology and Testing.

ČSN EN 73 0540-2. (2011). *Thermal protection of buildings − part 2: Requirements*. Prague: Czech Office for Standards, Metrology and Testing.

ČSN EN 73 0540-3. (2005). *Thermal protection of buildings − part 3: Design value quantities*. Prague: Czech Office for Standards, Metrology and Testing.

ČSN EN ISO 13370. (2009). *Thermal performance of buildings − heat transfer via ground − calculation methods*. Prague: Czech Office for Standards, Metrology and Testing.

ČSN EN ISO 13789. (2009). *Thermal performance of buildings − transmission and ventilation heat transfer coefficients − calculation method*. Prague: Czech Office for Standards, Metrology and Testing.

ČSN EN ISO 13790. (2009). *Energy performance of buildings − calculation of energy use for space heating and cooling*. Prague: Czech Office for Standards, Metrology and Testing.

ČSN EN ISO 13829. (2001). *Thermal performance of building − Determination of air permeability of buildings − fan pressurization method*. Prague: Czech Office for Standards, Metrology and Testing.

ČSN EN ISO 6946. (2008). *Building components and building elements − thermal resistance and thermal transmittance − calculation method*. Prague: Czech Office for Standards, Metrology and Testing.

Dodoo, A., & Gustavsson, L. (2013). Life cycle primary energy use and carbon footprint of wood-frame conventional and passive houses with biomass-based energy supply. *Applied Energy, 112*, 834−842.

Eliche-Quesada, D., Corpas-Iglesias, F. A., Pérez-Villarejo, L., & Iglesias-Godino, F. J. (2012). Recycling of sawdust, spent earth from oil filtration, compost and marble residues for brick manufacturing. *Construction and Building Materials, 34*, 275−284.

EnergyPlus. (2011). *EnergyPlus homepage*. http://apps1.eere.energy.gov/buildings/energyplus/ Accessed 21.04.14.

EU Directive 2010/31/EC of the European Parliament and of the Council of 19 May 2010 on the energy performance of buildings. *Official Journal of the European Communities*, (June 2010), 13−35.

EuroACE. (2004). *Towards Energy efficient buildings in Europe*. final report June (ec.europa.eu).

European Environment Agency. (2012). *Energy efficiency and energy consumption in the household sector (ENER 022) − Assessment published April 2012*. www.eea.europa.cz.

Fairey, P., Vieira, R., Parker, D., Hanson, B., Broman, P., Grant, J., et al. (2002). EnergyGauge USA: a residential energy simulation design tool, Florida solar energy center. In *Presented at the 12th Symposium on improving building systems in hot and humid climates, Houston, TX*.

Feist, W. (2001). Das passivhaus 2001: Fakten, Entwicklung, Tendenzen. In *Passivhaustagung 2001 Proceedings, Böblingen* (pp. 3−11) (in German).

Feist, W. (2007). Passive houses in practice. In *The building physics calendar* (pp. 675−741). Berlin: Ernst & Sohn.

Fux, S. F., Ashouri, A., Benz, M. J., & Guzzella, L. (2014). EKF based self-adaptive thermal model for passive house, Energy and Buildings, 68 (Part C), 811−817.

Gökce, H. U., & Gökce, G. U. (2013). Holistic system architecture for energy efficient building operation. *Sustainable Cities and Society, 6*, 77−84.

Grynning, S., Gustavsen, A., Time, B., & Jelle, B. P. (2013). Windows in the buildings of tomorrow: energy losers or energy gainers? *Energy and Buildings, 61*, 185−192.

Jäger, F. (1984). *Solar energy applications in houses: Performance and economics in Europe* (1st ed.). New York: Published for the Commission of the European Communities by Pergamon Press.

Janson, U. (2010). *Passive houses in Sweden − from design to evaluation of four demonstration projects*. Lund, Sweden: Lund University.

Jelle, B. P. (2011). Traditional, state-of-the-art and future thermal building insulation materials and solutions − properties, requirements and possibilities. *Energy and Buildings, 43*, 2549−2563.

Jelle, B. P. (2013). Solar radiation glazing factors for window panes, glass structures and electrochromic windows in buildings − measurement and calculation. *Solar Energy and Materials & Solar Cells, 116*, 291−323.

Jerman, M., & Černý, R. (2012). Effect of moisture content on heat and moisture transport and storage properties of thermal insulation materials. *Energy and Buildings, 53*, 39−46.

Kim, H. K., Leon, J. H., & Lee, H. K. (2010). Workability, and mechanical, acoustic and thermal properties of lightweight aggregate concrete with a high volume of entrained air. *Construction and Building Materials, 29*, 193−200.

Kočí, J., Maděra, J., Pavlík, Z., Fiala, L., Vejmelková, E., & Černý, R. (2012). Determination of effective thermal conductivity of hollow bricks using a computational approach and its verification in a semi-scale experiment. In *Proceedings of the 5th international building physics conference* (pp. 143−147). Kyoto: Kyoto University.

Kočí, V., Bažantová, Z., & Černý, R. (2014). Computational analysis of thermal performance of a passive family house built of hollow clay bricks. *Energy and Buildings, 76*, 211−218.

Kuzman, M. K., Grošelj, P., Ayrilmis, N., & Zbašnik-Senegačnik, M. (2013). Comparison of passive house construction types using analytic hierarchic process. *Energy and Buildings, 64*, 258−263.

Mata, E., Kalagasidis, A. S., & Johnsson, F. (2013). A modeling strategy for energy, carbon, and cost assessments of building stocks. *Energy and Buildings, 56*, 100−108.

Mlakar, J., & Štrancar, J. (2013). Temperature and humidity profiles in passive-house building blocks. *Building and Environment, 60*, 185−193.

Modest, M. F. (1993). *Radiative heat transfer*. New York, USA: McGraw-Hill.

Passivhaus Institute. (1997). Nutzerverhalten. In *Protokollband Nr. 9 des Arbeitskreis kostengünstige Passivhäuser, Darmstadt*.

Pavlík, Z., Fiala, L., Pavlíková, M., Pernicová, R., & Černý, R. (2010). Hygric and thermal properties of historical masonry. In *Structural faults and repair 2010 [CD-ROM]*. Edinburgh: Engineering Technics Press Edinburgh.

Pavlík, Z., Jerman, M., Trník, A., Kočí, V., & Černý, R. (2014). Effective thermal conductivity of hollow bricks with cavities filled by air and expanded polystyrene. *Journal of Building Physics, 37*(4), 436−448.

Passive House Planning Package PHPP. (2007). *Requirements for quality approved passive houses*. Germany: Passivhaus Institut Darmstadt.

Principi, P., & Fioretti, R. (2012). Thermal analysis of the application of PCM and low emissivity coating in hollow bricks. *Energy and Buildings, 51*, 131−142.

Ralegaonkar, R. V., & Gupta, R. (2010). Review of intelligent building construction: a passive solar architecture approach. *Renewable and Sustainable Energy Reviews, 14*, 2238−2242.

Ridley, I., Clarke, A., Bere, J., Altamirano, H., Lewis, S., Durdev, M., et al. (2013). The monitored performance of the first new London dwelling certified to the Passive House standard. *Energy and Buildings, 63*, 67−78.

Roulet, C. A., Heidt, F. D., Foradini, F., & Pibiri, M. C. (2001). Real heat recovery with air handling units. *Energy and Buildings, 33*, 495−502.

Sala, J. M., Urresti, A., Martín, K., Flores, I., & Apaolaza, A. (2008). Static and dynamic thermal characterisation of a hollow brick wall: tests and numerical analysis. *Energy and Buildings, 40*, 1513−1520.

Self, S. J., Reddy, B. V., & Rosen, M. A. (2013). Geothermal heat pump systems: status review and comparison with other heating options. *Applied Energy, 101*, 341−348.

da Silva Almeida, G., da Silva, J. B., de Silva, C. J., Swarnakar, R., de Arújo Neves, G., & de Lima, A. G. B. (2013). Heat and mass transport in an industrial tunnel dryer: modeling and simulation applied to hollow bricks. *Applied Thermal Engineering, 55*, 78−86.

Stephan, A., Crawford, R. H., & de Myttenaere, K. (2013). A comprehensive assessment of the life cycle energy demand of passive houses. *Applied Energy, 112*, 23−34.

Suarez, I., Prieto, M. M., & Fernández, F. J. (2013). Analysis of potential energy, economic and environmental savings in residential buildings: solar collectors combined with microturbines. *Applied Energy, 104*, 128−136.

Sutcu, M., & Akkurt, S. (2009). The use of recycled paper processing residues in making porous brick with reduced thermal conductivity. *Ceramics International, 35*, 2625−2631.

Sutcu, M., del Coz-Díaz, J. J., Rabanal, F. P. A., Gencel, O., & Akkurt, S. (2014). Thermal performance optimization of hollow clay bricks made up of paper waste. *Energy and Buildings, 75*, 96−108.

Thiers, S., & Peuportier, B. (2008). Thermal and environmental assessment of a passive building equipped with an earth-to-air heat exchanger in France. *Solar Energy, 82*(9), 820−831.

Uygunoglu, T., & Kecebas, A. (2011). LCC analysis for energy-saving in residential buildings with different types of construction masonry blocks. *Energy and Buildings, 43*, 2077−2085.

Wang, L., Gwilliam, J., & Jones, P. (2009). Case study of zero energy house design in UK. *Energy and Buildings, 41*, 1215−1222.

Yakubu, G. S. (1996). The reality of living in passive solar homes: a user-experience study. *Renewable Energy, 8*, 177−181.

Zukowski, M., & Haese, G. (2010). Experimental and numerical investigation of a hollow brick filled with perlite insulation. *Energy and Buildings, 42*, 1402−1408.

The properties and durability of clay fly ash-based fired masonry bricks

5

J.N.F. Holanda
Northern Fluminense State University, Rio de Janeiro, Brazil

5.1 Introduction

The thermal power stations worldwide produce huge amounts of solid waste material in the form of a fine powder, namely fly ash (Joshi & Lothia, 1997). It is noteworthy that there are other types of fly ashes originated from processes such as agricultural biomass and incineration (Barbieri, Andreola, Lancellotti, & Taurino, 2013; Cheng, Tu, Ko, & Ueng, 2011; Faria, Gurgel, & Holanda, 2012; Quaranta et al., 2011; Thy, Jenkins, Grundvig, Shiraki, & Lesher, 2006). In this chapter, however, emphasis is given mainly to the coal combustion fly ashes produced in the thermal power stations.

Fly ash is a coal combustion by-product with large chemical, mineralogical, and physical variability, depending on the coal origin and kind, and also on the combustion process. According to the ASTM C618-92a standard (ASTM, 2005) two classes of coal fly ash are defined based on the chemical composition: (1) F Class: the fly ashes of this group usually present $SiO_2 + Al_2O_3 + Fe_2O_3 > 70\%$, $SO_3 < 5\%$, moisture content $<3\%$, and loss on ignition $<6\%$; and (2) C Class: bothfly ashes of this group usually present $SiO_2 + Al_2O_3 + Fe_2O_3 < 70\%$. In addition, the fly ashes contain toxic trace elements and are considered to be highly polluting (Ahmaruzzaman, 2010). For this reason, the thermal power stations that use coal as a combustible are usually confronted worldwide with the environmental pollution problems. A significant amount of the coal combustion fly ashes produced worldwide have been primarily disposed of in landfills and ash lagoons (Alam & Akhtar, 2011; Sarkar, Singh, & Das, 2007), causing significant environmental impacts. In addition, such methods are very expensive. Significant impacts of improper disposal of fly ashes include land, water, and air pollution. This means that the use of safe methods for fly ash recycling that are consistent with current needs is of high economical, environmental, and social interest.

In recent years, the fired clay masonry bricks have become a highly promising technological approach for the reuse of solid wastes (Dondi, Guarini, Raimondo, & Venturi, 2002a; Faria et al., 2012; Kadir & Sarani, 2012; Quaranta et al., 2011). The waste reuse is possible if it is compatible from the technical, environmental, and economical viewpoints. Some reasons in favor of reuse of solid wastes as alternative raw materials to produce fired clay masonry bricks are: (1) availability of the clay

Eco-efficient Masonry Bricks and Blocks. http://dx.doi.org/10.1016/B978-1-78242-305-8.00005-X

brick industry that utilizes large volumes of natural raw materials; (2) less use of virgin raw materials; (3) the use of low-cost raw material; (4) use of common clays with large chemical and mineralogical variability; (5) the ceramic processing is not greatly modified; (6) inertization of toxic substances in the fired clayey matrix; and (7) destroying any pathogens during the firing step at high temperature.

The fired clay masonry bricks are considered one of the oldest building materials, whose use began about 5000 BC (Kadir & Sarani, 2012). Since that time, the fired clay masonry bricks are being widely used for building due to the following factors (Christine, 2004; Lynch, 1994): (1) good physical and mechanical properties; (2) durability; (3) beauty; (4) little maintenance; and (5) low cost. The industrial processing of fired clay masonry bricks consists of three main steps: (1) preparation of the clayey body; (2) conformation; and (3) thermal treatment. The clay bricks are produced in a wide firing temperature range (~600−1100 °C), using a slow-firing cycle. The raw materials for clay bricks are mainly common clays or shales with varied colors after firing, and they also have large compositional variation. For this reason, the clay body formulations can tolerate the incorporation of different solid wastes in significant amounts.

A considerable effort is being made worldwide on the reuse of coal combustion fly ashes as a source of alternative raw materials to produce new materials such as cement, concrete, zeolites, glass-ceramics, adsorbents for cleaning of flue gas, lightweight aggregate, road subbase, and clay bricks (Ahmaruzzaman, 2010; Alam and Akhtar, 2011; Moreno et al., 2005). However, in spite of the increasing interest in using fly ash as a ceramic raw material to produce fired clay masonry bricks, more research is still needed.

This chapter is to give an overview of the current literature on the reuse of fly ash from thermal power stations to produce fired clay masonry bricks. Special emphasis is given to the fly ash characteristics and its effect on the technical properties and durability of the fired clay masonry bricks.

5.2 Fly ash characterization

The reuse of fly ash into a clay brick body requires its prior characterization (John & Zordan, 2001). In particular, the characterization of the fly ash helps to define the composition of the clayey formulation, and also helps to preview the effects of its addition during the ceramic processing and final properties. The following characteristics of the fly ash should be evaluated: chemical composition, mineral phases, physical characteristics, thermal behavior, and environmental analysis.

5.2.1 Chemical and mineralogical compositions

Table 5.1 gives the chemical composition of the fly ashes produced in several countries. As can be observed, the fly ashes present complex chemical composition. The very different chemical composition they present is related to various factors such as coal composition, pulverization degree, design of the furnace, combustion process

Table 5.1 Chemical compositions of several fly ashes

Oxides	Fly ashes (wt%)					
	European fly ash	Indian fly ash	American fly ash	Brazilian fly ash	Chinese fly ash	Malaysia fly ash
SiO_2	28.50–59.60	45.00–65.25	35.00–52.00	58.80–71.00	56.58	56.58
Al_2O_3	17.60–35.60	14.00–31.10	15.00–32.00	19.00–26.30	27.83	27.83
Fe_2O_3	2.60–16.00	3.00–15.00	8.00–25.00	2.34–8.00	4.05	4.00
CaO	0.50–27.30	0.10–6.50	0.70–8.00	0.20–3.78	4.31	4.30
MgO	0.60–3.80	0.20–3.90	0.30–1.50	0.20–180	1.49	1.40
Na_2O	0.10–1.80	–	–	0.10–0.70	–	–
K_2O	0.40–4.50	–	–	0.40–1.76	–	–
P_2O_5	0.10–1.70	–	–	0.04–0.06	–	–
TiO_2	0.50–2.60	–	–	1.18–1.21	–	–
MnO	0.02–0.10	–	–	0.02–0.04	–	–
SO_3	0.10–8.60	0.40–1.80	0.10–2.80	0.10–0.70	–	–
LOI	1.10–8.10	1.00–11.30	1.30–13.00	0.20–2.71	2.82	2.53

Sources: Silva et al., 1999; Lingling et al., 2005; Moreno et al., 2005; Sabedot et al., 2011; Shakir et al., 2013.

conditions, and nature of ash collection (Reddy, Abhishek, & Babu, 2012; Sukala, Singh, Solanki, Sutariya, & Thakur, 2012). The fly ashes are essentially composed of silica (SiO_2), alumina (Al_2O_3), and iron oxide (Fe_2O_3) with lesser amounts of Ca, Mg, Na, K, P, Ti, and Mn oxides. This makes the fly ashes potentially valuable sources of oxides for the manufacture of fired clay masonry bricks. In fact, the common clays and shales used in the production of fired clay bricks also are rich in SiO_2, Al_2O_3, and Fe_2O_3 (Gomes, 1988).

The fly ashes present very complex mineralogical composition with both amorphous and crystalline phases (Moreno et al., 2005; Queralt, Querol, Soler, & Plans, 1997; Reddy et al., 2012; Silva, Calarge, Chies, Mallmann, & Zwonok, 1999). The fly ashes are, from a mineralogical viewpoint, compounds of (1) a main amorphous phase (48−90% depending on the type of fly ash) in the form of alumino-silicate glass, and (2) mineral phases such as quartz (SiO_2), cristobalite (SiO_2), mullite ($Al_6Si_2O_{13}$), hematite (Fe_2O_3), magnetite (Fe_3O_4), anhydrite ($CaSO_4$), ettringite ($3CaOAl_2O_33CaSO_432H_2O$), feldspars ($(Ca,Na)(Al,Si)_4O_8$), calcite ($CaCO_3$), and calcium oxide (CaO). In addition, the fly ashes also contain unburned carbon (coal).

5.2.2 Physical characterization

The fly ash is a fine powdery waste material with color varying from gray to black, depending on the amount of unburned carbon. The fly ash particles exhibit distinct morphologies of various sizes (Chusid, Miler, & Rapoport, 2009; Reddy et al., 2012) such as spherical (cenosphere or plerosphere) and irregular, with a predominance of spherical particle morphology. The specific gravity of fly ash usually ranges from 2.1 to 3.0 (Ahmaruzzaman, 2010), depending on the iron oxide content (hematite and magnetite). The specific surface area of fly ash usually ranges from 0.17 to 12.40 m^2/g (Cultrone & Sebastián, 2009; Dondi et al., 2002a; Moreno et al., 2005; Silva et al., 1999), which is within the specific surface area range of the kaolinitic clays (Gomes, 1988). The real density of fly ash may vary from 1.3 to 2.7 g/cm^3 (Cultrone & Sebastián, 2009; Moreno et al., 2005; Silva et al., 1999), depending on the mineral phase composition. The fly ashes exhibit a wide range of particle size distribution (0.10−250 μm) (Cultrone & Sebastián, 2009; Moreno et al., 2005; Queralt et al., 1997; Silva et al., 1999). This particle size range is compatible with the size range of common clays used to produce fired clay masonry bricks. In terms of soil mechanics, the fly ash can be classified as a nonplastic material (Silva et al., 1999). Thus, when added to a clay or shale, it influences the plastic behavior, conformation, and drying of the clayey body. This means that a clay or shale of high plasticity should be selected for use in the clay/fly ash mixes.

5.2.3 Thermal behavior

The thermal behavior of the coal combustion fly ashes strongly reflects their chemical and mineralogical compositions. In addition, the thermal behavior of fly ashes exhibits

complex exothermic and endothermic events at different temperature ranges, which can influence the sintering behavior of a clay−fly ash mix. The main thermal event observed in the DTA curve of Brazilian fly ash was an exothermic peak at 530 °C associated with the presence of carbonaceous material (Silva et al., 1999). Orimulsion fly ashes (Dondi et al., 2002a) show complex thermal behavior, whose main exothermic and endothermic reactions are: (1) high weight loss at 1000 °C (41.8% ash B-Apulia; 39.6% ash F-Sardinia); (2) wide exothermic trend of the DTA curve up to about 500 °C; and (3) an endothermic event between 500 and 1000 °C. The DTA curve of coal gasification fly ash (Aineto, Acosta, & Iglesias, 2006) shows two exothermic peaks at 450 and 700 °C due to oxidation processes.

5.2.4 Environmental characterization

It is well known that the fly ashes contain heavy metals. However, their classification as a hazardous material is controversial. Some European fly ashes showed high levels of leachable trace elements (As, B, Ba, Cr, and Sr) according to the DIN-38414 standard (Moreno et al., 2005). Leaching tests in municipal solid waste incineration (MSWI) fly ash showed that the leaching concentrations of As, Hg, Pb, Zn, and Cd exceeded the Chinese standard limits (Haiying, Youcai, & Jingyu, 2011). Hence, this type of fly ash presents a high potential for environmental pollution. It was found that Brazilian fly ashes presented leaching concentrations of As, Pb, and total Cr above Brazilian leaching limits (Sabedot et al., 2011). This means that the fly ash sample can be classified as a hazardous material according to the NBR 10004 standard. On the other hand, the vast majority of the American fly ashes present low concentrations of heavy metals (Chusid et al., 2009), being considered nonhazardous materials.

5.3 Fly ash-based fired clay masonry brick processing

The processing flow diagram in Figure 5.1 summarizes the main steps used to produce fired clay masonry bricks incorporated with different fly ashes. As can be observed, all research works have been conducted to follow the conceptual flowchart for the industrial production of fired clay masonry bricks (Gomes, 1988; Santos, 1989): common clays, preparation of the clayey body, shaping, drying, and firing. However, the researchers have used different fly ashes and common clays and also adopted different processing conditions to produce fired clay masonry bricks.

The common clays and fly ashes used to produce fired clay masonry bricks present a very broad range of chemical, mineralogical, and physical characteristics. The coal combustion fly ashes are chemically very similar to the natural common clays. Thus, a good chemical compatibility between fly ash and common clay should be expected.

Table 5.2 gives the different processing conditions used to produce fired clay masonry bricks containing fly ash. The clay bodies could tolerate the incorporation of a variety of coal combustion fly ashes in the form of fine powder.

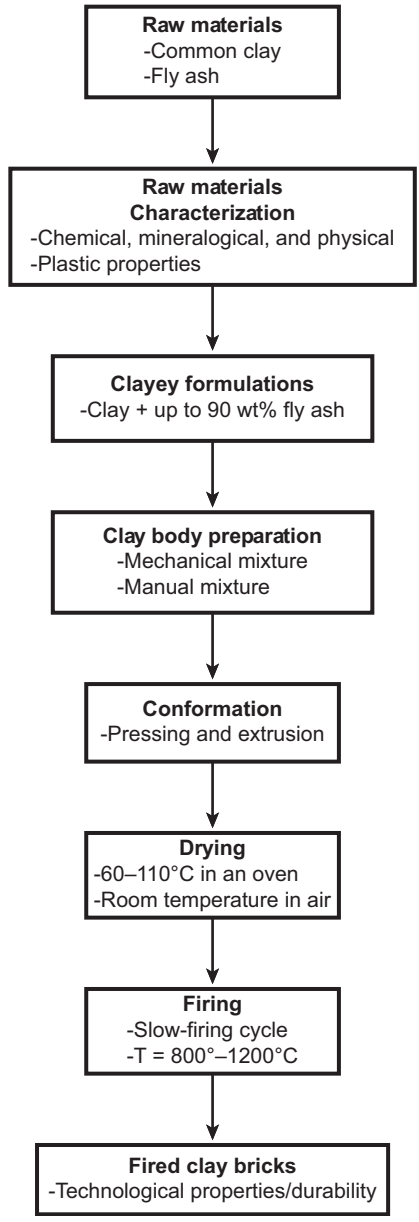

Figure 5.1 Methodology used for manufacturing fly ash-based fired clay masonry bricks.

The common clay was replaced by up to 90 wt% of fly ash. It can be seen that different mixing methods (mechanical and manual), different shaping methods (pressing and extrusion), different drying methods, and different firing process (different heating/coaling rates and firing temperatures) have been used.

Table 5.2 Processing conditions used in the production of fly ash-based fired clay masonry bricks

Fly ash	Fly ash amount (wt%)	Mixing method	Forming method	Drying	Firing
Teruel fly ash	40	Mechanical/ 5 wt% Water	Pressing/100 MPa	Not defined	Fired between 900−1200 °C for 3 h
Orimulsion fly ash	Up to 6	Manual	Extrusion	Dried at room temperature for 48 h, and then dried at 100 °C for 24 h in an oven	Fired in an electrical kiln at 900 °C
Nanjing fly ash	Up to 80[a]	Not defined	Not defined	Dried at room temperature for 48 h, and then at 60 °C for 4 h and 100 °C for 6 h	Fired in an electrical kiln between 1000 and 1100 °C for 8 h
IGCC fly ash	20	Not defined/5 wt% Water	Pressing/20 MPa	Dried at 110 °C	Fired at 900 °C for 5 h
ESP fly ash	Up to 90	Mechanical/7 wt% Water	Pressing/40 MPa	Dried at room temperature for 24 h, and then dried at 110 °C for 24 h in an oven	Fired in an electrical kiln at 1000 °C for 2 h
High-sulfate-containing fly ash	85−90	Mechanical	Pressing/10 MPa	Dried at room temperature for 72 h, and then dried at 110 °C in an oven	Fired in an electrical kiln between 800−1000 °C

[a]Vol %.
Sources: Aineto et al., 2006; Baspinar et al., 2010; Dondi et al., 2002b; Lingling et al., 2005; Queralt et al., 1997; Sarkar et al., 2007.

5.4 Effects of fly ash on the technological properties

The quality of the fly ash-based clay masonry bricks after firing has been evaluated in terms of the main technological properties (linear shrinkage, water absorption, apparent density, apparent porosity, and mechanical strength). Table 5.3 summarizes the technological properties of fly ash-based clay masonry bricks incorporated with different coal combustion fly ashes.

Queralt et al. (1997) reported on the firing behavior of fly ash and plastic clay (60 wt%)−fly ash (40 wt%) mixture between 900 and 1200 °C. Substantial changes to the mineralogical evolution of fly ash with increasing firing temperature (Figure 5.2) were found. The main changes suffered by the fly ash during the firing process at high temperature were: (1) decreasing the amount of the glassy phase (alumino-silicate glass); (2) increasing the amount of mullite; (3) the iron-based minerals are converted to hematite; and (4) the development of feldspar minerals and cristobalite. By increasing the firing temperature, important changes to the physical properties (linear shrinkage, water absorption, and apparent density) of plastic clay (60 wt%)−fly ash (40 wt%) mixture were observed. The linear shrinkage and the apparent density increase, while the water absorption (open porosity) decreases, mainly above 1000 °C. In addition, all these changes were favored by the mineralogical evolution of the fly ash on firing. The ceramic pieces with plastic clay (60 wt%)−fly ash (40 wt%) could be used in the production of ceramic building materials, including fired clay masonry bricks. It was also found the fired clay pieces change color from pale brown to dark brown.

Dondi, Guarini, Raimondo, and Venturi (2002b) investigated the use of up to 6 wt% of two Orimulsion fly ashes (ash B−Apalua and ash F−Sardinia) in the manufacture of fired clay masonry bricks. The use of Orimulsion fly ashes has caused several changes to the technical properties of both unfired and fired clay bricks. The preparation of a homogeneous clay−Orimulsion fly ash mixture is very difficult due to the fly ash being highly hygroscopic. Orimulsion fly ashes have caused detrimental effects on the plasticity, drying rate, and drying sensibility of the plastic clay−fly ash mixtures. Increasing the amount of fly ash tends to change the firing color, resulting in a more yellow color of clay masonry bricks. The technological properties (linear shrinkage, water absorption, bulk density, total porosity, and flexural strength) of clay masonry bricks fired at 900 °C depend to a large extent on the added Orimulsion fly ash amount. It was found that the Orimulsion fly ash could be used in fired clay masonry bricks, in the range of 1 to 2 wt%, as a partial replacement for common clay.

Lingling, Wei, Tao, and Nanru (2005) reported on the influence of fly ash with a high replacing ratio (up to 80% vol) of clay on the physical properties of fired clay masonry bricks. The plasticity index of clay−fly ash mixtures was found to be strongly decreased by the fly ash addition. This substantial decrease in plasticity is in line with the nonplastic nature of the fly ash. When the proportion of fly ash in clayey formulation is 80% by volume, the plasticity index reaches 3.8%. The improvement of the plasticity characteristics of clay−fly ash mixtures with a high volume ratio of fly ash can be done with the use of additives. The results showed that significant changes

Table 5.3 Physical and mechanical properties of fly ash-based fired clay masonry bricks

Fly ash	LS (%)	AD (g/cm^3)	AP (%)	WA (%)	CS (MPa)
Teruel fly ash	2.00–3.00	2.00–2.40	–	0.50–9.25	–
Orimulsion fly ash (B)	0.10–1.30	1.79–1.81	26.00–34.00	14.50–19.00	19.00–25.00[a]
Orimulsion fly ash (F)	0.00–2.10	1.91–2.04	26.00–30.50	12.50–16.00	11.00–14.00[a]
Nanjing fly ash	–	1.35–2.20	1.34–42.12	0.61–31.26	14.70–98.50
IGCC fly ash	Negligible	–	–	10.38–14.13	0.71–2.20
ESP fly ash	–	1.426–1.430	35.6–36.2	24.4–25.2	18.6–19.1
High-sulfate-containing fly ash	–	1.02–1.27	32.31–48.90	25.46–48.00	1.90–8.65
Jalna fly ash	–	–	–	3.74–14.23	2.18–953
Indian fly ash	–	1.20–1.85	–	10.00–21.00	6.50–30.00

LS–linear shrinkage; AD–apparent density; AP–apparent porosity; WA–water absorption; CS–compressive strength.
[a]Flexural strength.
Sources: Queralt et al., 1997; Dondi et al., 2002b; Lingling et al., 2005; Aineto et al., 2006; Sarkar et al., 2007; Baspinar et al., 2010; Bansode, 2012.

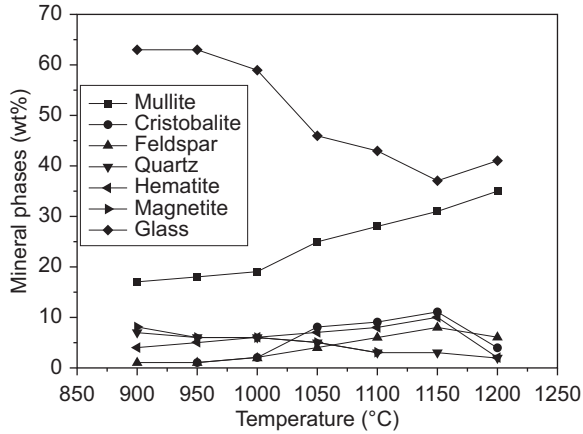

Figure 5.2 Mineralogical evolution (wt%) of fly ash on firing.
Adapted from Queralt et al. (1997).

to the physical and mechanical properties (Figures 5.3–5.5) of clay–fly ash fired masonry bricks with a high volume ratio of fly ash occurred. It was observed that the water absorption increases (Figure 5.3), apparent density decreases (Figure 5.4), and compressive strength (Figure 5.5) decreases with increasing the ratio of fly ash in fired clay bricks. Despite this, the clay–fly ash fired masonry bricks with a high ratio of fly ash met the requirements in the Chinese standard specifications.

Aineto et al. (2006) reported on the use of coal gasification fly ash in the production of fired clay-based ceramics. The results showed that the addition of coal gasification fly ash has caused only a slight reduction of the plasticity of the clay–fly ash mixes.

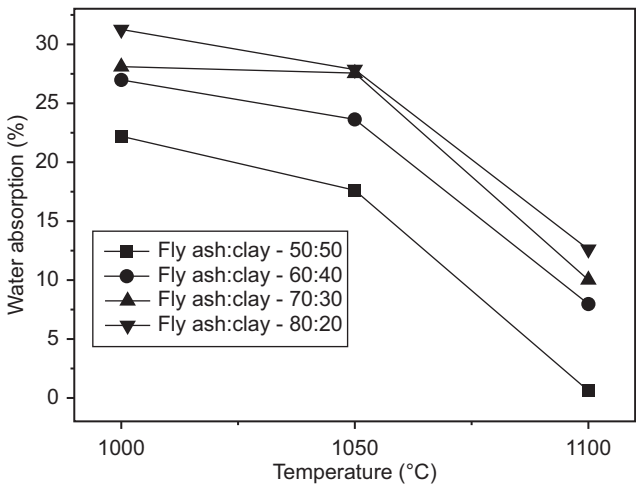

Figure 5.3 Water absorption of clay–fly ash fired masonry bricks with a high volume ratio of fly ash.
Adapted from Lingling et al. (2005).

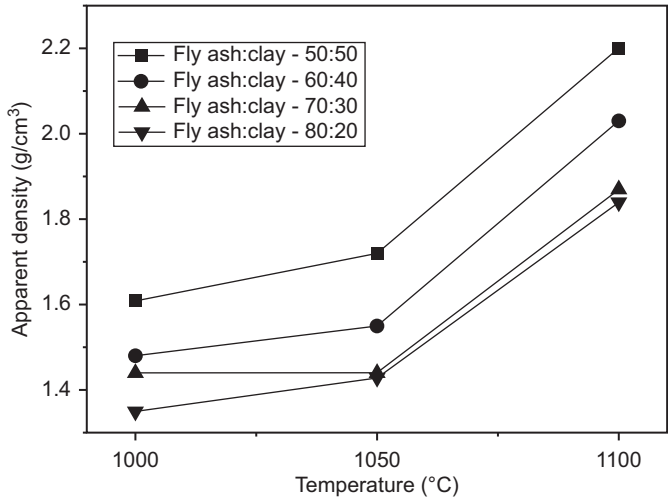

Figure 5.4 Apparent density of clay–fly ash fired masonry bricks with a high volume ratio of fly ash. Adapted from Lingling et al. (2005).

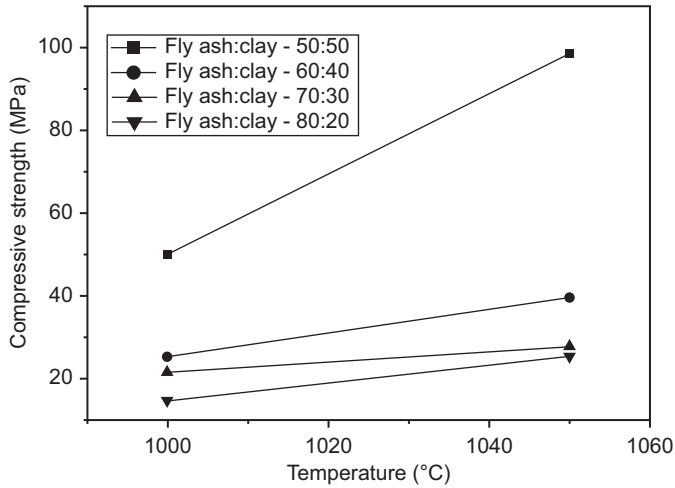

Figure 5.5 Compressive strength of clay–fly ash fired masonry bricks with a high volume ratio of fly ash.
Adapted from Lingling et al. (2005).

It was found that the coal gasification fly ash (added up to 20 wt%) acts as an active additive that improves the densification behavior and technical properties of the clay masonry bricks fired at 900 °C. This behavior can be explained by the chemical and mineralogical compositions that tend to favor the formation of a liquid phase at lower firing temperatures than the fly ash-free clay bodies. The results also showed that the

introduction of coal gasification fly ash had a beneficial effect on the technical properties (lower absorption, lower saturation coefficient, and higher mechanical strength) of the fired bricks. In addition, the coal gasification fly ash containing clay masonry bricks showed only a slightly darker reddish coloration, as well as no efflorescence observed.

Sarkar et al. (2007) investigated the effect of the electro-static precipitator (ESP) fly ash addition on the technological properties of clay masonry bricks fired at 1000 °C. Addition of EPS fly ash to common clay was found to reduce the apparent density and increase the water absorption. During the firing process, the EPS fly ash remains inert and negatively influences the densification behavior of the EPS fly ash containing fired clay masonry bricks. Despite this, up to 80 wt.% of EPS fly ash could be incorporated to clay to produce fired clay masonry bricks with good technical properties (apparent density = 1.426−1.430 g/cm^3, water absorption = 24.4−25.2%, apparent porosity = 35.6−36.2%, and mechanical strength = 18.6−19.1 MPa).

Baspinar, Kahraman, Gorhan, and Demir (2010) reported on the use of high-sulfate-containing fly ash with boric acid (H_3BO_3) addition in the production of fired clay bricks. The test pieces were fired between 800 and 1000 °C, which is the industrial clay brick firing temperature range. Increasing the firing temperature improved the technological properties (water absorption, apparent density, apparent porosity, and compressive strength) of the fired high-sulfate-containing fly ash−clay bricks. In addition, an increase in the firing temperature also contributed to improving the sintering behavior of the fly ash particles. The experimental results indicated that it was possible to produce fired bricks with good technological properties (Figures 5.6 and 5.7) from high-sulfate-containing fly ash by adding clay and boric acid simultaneously. The

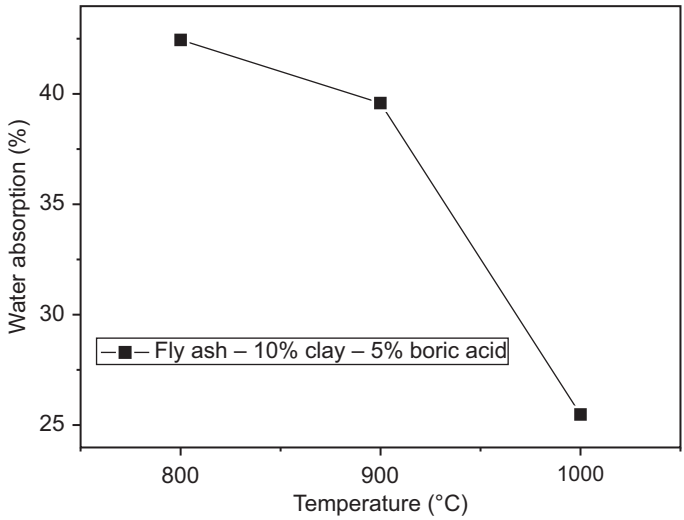

Figure 5.6 Water absorption of high-sulfate-containing fly ash−10% clay−5% boric acid fired bricks.
Adapted from Baspinar et al. (2010).

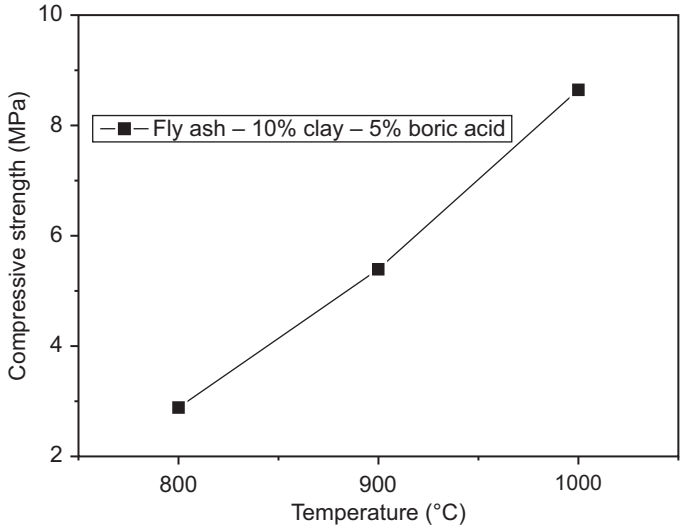

Figure 5.7 Compressive strength of high-sulfate-containing fly ash−10% clay−5% boric acid fired bricks.
Adapted from Baspinar et al. (2010).

better clayey formulation was that composed of high-sulfate-containing fly ash with the addition of 10% clay and 5% boric acid. Such behavior was mainly due to the increase of alkali and earth alkali oxides present in the fly ash and clay with B_2O_5, which tends to accelerate the vitrification process. This formulation also had a denser well-sintered microstructure.

Haiying et al. (2011) investigated the use of MSWI fly ash as an alternative raw material to produce fired ceramic bricks. The leaching characteristics of the fired bricks also were determined. The fly ash is rich in SiO_2, Al_2O_3, and CaO, as well as having a low plasticity index (3.7%). The orthogonal test and performance analysis indicated that the optimal clayey formulation (named R20) was fly ash: 20%, red ceramic clay: 60%, feldspar: 10%, and gang sand: 10%. The results showed that the technological properties (shrinkage, water absorption, and compressive strength) of the R20 formulation are strongly influenced by the firing temperature. It was found that the firing shrinkage decreased with increase of firing temperature (900−1050 °C). The compressive strength of the ceramic bricks tends to increase with the increase of firing temperature. However, the water absorption presented different behaviors, depending on the firing temperature. Between 900 and 1000 °C, the water absorption decreased, and then rose with an increase of firing temperature from 1000 to 1050 °C. This behavior was well correlated with the appearance quality. The results also showed that the sintered microstructure was strengthened with the increase of firing temperature. The open porosity was strongly reduced. In terms of mineralogical evolution during the firing process the following trends were found: (1) the amount of crystalline phases of the sintered ceramic matrix first increased and then decreased; and (2) the glassy phase amount presented a reverse trend. The following crystalline phases

were found: quartz, cordierite, enstatite, mullite, and andradite. Leaching results of heavy metals (As, Cd, Cr, Cu, Ni, Pb, Hg, and Zn) from sintered ceramic matrix were reduced considerably in comparison with those from unfired ceramic matrix.

Bansode (2012) investigated the influence of fly ash and steel slag on the technological property behavior of solid bricks. The fly ash sample used met specification ASTM C618 for Class C fly ash. The results showed that the addition of fly ash and steel slag have strongly influenced the technological properties of clay bricks, particularly for water absorption (3.74−14.23%) and compressive strength (2.18−9.53 MPa). However, the use of a high amount of fly ash in the clayey formulations is very problematic due to the less adhesive effect of clay. Despite this, a clayey formulation containing 40% fly ash with 60% clay could be a good formulation to produce clay−fly ash masonry bricks.

Resourceefficientbricks (2013) has reported on the processing and technological properties of clay−fly ash masonry bricks fired at 1000 °C. Indian fly ashes and alluvial, black, and red soils in different proportions were used. It was found that the fly ash reduces the plasticity of the clay−fly ash mixes, as well as reducing the drying time and shrinkage cracks. The technological properties (water absorption, bulk density, and compressive strength) of the fired bricks are strongly influenced depending on the fly ash amount and soil type used. In this report, the following advantages of clay−fly ash fired masonry bricks were found: (1) bricks conforming to IS:3102 can be produced; (2) fuel saving in the range of 15−35% (coal composition) or coal savings up to 3−7 tons per lakh bricks; (3) drying losses are checked in the case of plastic black and red soils. Excessive linear drying shrinkage is reduced; (4) brick strength in the case of black and red soil is increased by almost one and a half times (30−50%); (5) waste material is used 30−40 tons per lakh in the case of alluvial soils and 100−125 tons per lakh bricks in the case of red and black soils; and (6) clay savings in brick manufacture is 10−40 wt%.

As described previously, different results have been obtained. However, a direct comparison between the several results is very complex and difficult. This is related primarily to three main factors: (1) the use of various types of fly ashes in different proportions; (2) the use of different common clays; and (3) the use of different processing conditions. Despite this, some observations are given below:

- In general, the introduction of fly ash into a clay body has a positive effect on the ceramic processing and technological properties. The clay−fly ash masonry bricks present good dimensional stability (low firing shrinkage), lower open porosity (lower water absorption), and higher mechanical strength (higher compressive strength).
- The amount of fly ash that could be added to a clay depends on two factors: common clay nature and fly ash chemical, mineralogical, and physical characteristics.
- The common clays and fly ashes present large chemical and mineralogical variability from one source to another. This means that no general rule can be applied for their use in fired clay masonry bricks.
- The fly ash in fine powder form (<250 μm) tends to favor good mixture and packaging of the clay−fly ash mixes in the forming step.
- The fly ash is a nonplastic material rich in glass, quartz, and mullite particles. Thus, the fly ash could be used to improve the plasticity characteristics (plastic extrusion) of common clays used in most of the clay masonry brick factories.

- The firing temperature of fly ash-containing fired clay masonry bricks is usually higher than that of fly ash-free fired clay bricks. This indicates that the addition of fly ash into fired clay masonry bricks could be problematic in many countries because it tends to increase the manufacturing cost.
- The firing color is an important criterion used to qualify fired clay masonry bricks. The fly ash addition tends to cause a gradual shift from light to dark or vice versa on the firing color. The greater the amount of fly ash added, the greater the shift in color.

5.5 Durability

Durability is one of the major requirements to be considered in the use of building materials. The durability of fired clay masonry bricks is strongly dependent on the common clays and processing conditions (Koroth, Fazio, & Feldman, 1998). In particular, this property is considered to be closely related to the densification degree (lower water absorption and higher density) of the clay bricks. The main factors that influence the durability of fired clay masonry bricks are: (1) cycles of heat and cold; (2) cycles of wetting and drying; and (3) soluble salt crystallization.

Despite its practical importance, the durability of clay−fly ash fired masonry bricks has been little investigated. However, Cultrone and Sebastián (2009) have shown that the incorporation of fly ash into clay tends to improve the durability of fired clay masonry bricks. This behavior is due to a reduction of the volume of the smallest pores in the sintered microstructure of clay bricks. In particular, the smallest pores are primarily responsible for most damage caused to the fired clay bricks due to soluble salt crystallization.

5.6 Future trends

In this chapter, it has been shown that coal combustion fly ash can be a good alternative raw material as a partial replacement of common clay in the manufacture of fired clay masonry bricks. However, more research should be conducted in this area in order to clarify several aspects of the incorporation of fly ash into the clay body, such as:

1. A key issue in the manufacture of clay−fly ash based fired masonry bricks is the clayey body formulation. In general, an empirical approach has been used. Thus, the use of experimental design to optimize the clayey formulation must be studied.
2. The phase composition and sintered microstructure of the fired masonry bricks can change substantially with the incorporation of the fly ash. Thus, more research must be done in order to understand the complex interactions between clay and fly ash during firing.
3. The coal combustion fly ashes have toxic components, such as heavy metals, which are hazardous to the environment and health. Thus, the environmental assessment (leaching and solubilization tests) of the fired bricks and gaseous emissions during the thermal treatment step (drying and firing) must be studied.
4. It has been observed that there is a lack of studies about the evaluation of the life cycle of the fly ash-based fired clay masonry bricks.

Acknowledgments

This work has been supported by CNPq and FAPERJ.

References

Ahmaruzzaman, M. (2010). A review on the utilization of fly ash. *Progress in Energy and Combustion Science, 36*, 327−363. http://dx.doi.org/10.1016/j.pecs.2009.11.003.

Aineto, M., Acosta, A., & Iglesias, I. (2006). The role of a coal gasification fly ash as clay additive in building ceramic. *Journal of the European Ceramic Society, 26*, 3783−3787. http://dx.doi.org/10.1016/j.jeurceramsoc.2006.01.011.

Alam, J., & Akhtar, M. N. (2011). Fly ash utilization in different sector in Indian scenario. *International Journal of Emerging Trends in Engineering and Development, 1*, 1−7.

ASTM C618. (2005). *Standard specification for coal fly ash and raw or calcined natural pozzolan for use in concrete*. American Society for Testing Materials.

Bansode, S. S. (2012). Comparative analysis between properties of steel slag, fly ash and clay bricks. *GeoCongress*, 3816−3825.

Barbieri, L., Andreola, F., Lancellotti, I., & Taurino, R. (2013). Management of agricultural biomass wastes: preliminary study on characterization and valorisation in clay matrix bricks. *Waste Management, 33*, 2307−2315. http://dx.doi.org/10.1016/j.wasman.2013.03.014.

Baspinar, M. S., Kahraman, E., Gorhan, G., & Demir, I. (2010). Production of fired construction brick from high sulfate-containing fly ash with boric acid addition. *Waste Management & Research, 28*, 4−10. http://dx.doi.org/10.1177/0734242X08096529.

Cheng, T. W., Tu, C. C., Ko, M. S., & Ueng, T. H. (2011). Production of glass-ceramic from incinerator ash using lab-scale and pilot-scale thermal plasma systems. *Ceramics International, 37*, 2437−2444. http://dx.doi.org/10.1016/j.ceramint.2011.05.088.

Christine, B. (2004). *Masonry design and detailing: For architects and contractors*. New York: McGraw Hill.

Chusid, M., Miler, S. H., & Rapoport, J. (2009). The building brick of sustainability. *The Construction Specifier*, 30−41.

Cultrone, G., & Sebastián, D. (2009). Fly ash addition in clayey materials to improve the quality of solid bricks. *Construction and Building Materials, 23*, 1178−1184. http://dx.doi.org/10.1016/j.conbuildmat.2008.07.001.

Dondi, M., Guarini, G., Raimondo, M., & Venturi, I. (2002a). Orimulsion fly ash in clay bricks − part 1: composition and thermal behavior of ash. *Journal of the European Ceramic Society, 22*, 1729−1735.

Dondi, M., Guarini, G., Raimondo, M., & Venturi, I. (2002b). Orimulsion fly ash in clay bricks − part 2: technological behavior of clay/ash mixtures. *Journal of the European Ceramic Society, 22*, 1737−1747.

Faria, K. C., Gurgel, R. F., & Holanda, J. N. F. (2012). Recycling of sugarcane bagasse ash waste in the production of clay bricks. *Journal of Environmental Management, 101*, 101−107. http://dx.doi.org/10.1016/j.jenvman.2012.01.032.

Gomes, C. F. (1988). *Argilas − O que são e para que servem*. Fundação Calosute Gulbenkian.

Haiying, Z., Youcai, Z., & Jingyu, Q. (2011). Utilization of municipal solid waste incineration (MSWI) fly ash in ceramic brick: product characterization and environmental. *Waste Management, 31*, 331−341.

John, V. M., & Zordan, S. E. (2001). Research & development methodology for recycling residues as building materials − a proposal. *Waste Management, 21*, 213−219.

Joshi, R. C., & Lothia, R. P. (1997). Fly ash in concrete: production, properties and uses. In *Advances in concrete technology* (Vol. 2). Gordon and Breach Science Publishers.

Kadir, A. A., & Sarani, N. A. (2012). An overview of wastes recycling in fired clay bricks. *International Journal of Integrated Engineering, 4*, 53−69.

Koroth, S. R., Fazio, P., & Feldman, D. (1998). Comparative study of durability indices for clay bricks. *Journal of Architectural Engineering, 4*, 26−33.

Lingling, X., Wei, G., Tao, W., & Nanru, Y. (2005). Study on fired bricks with replacing clay by fly ash in high volume ratio. *Construction and Building Materials, 19*, 243−247. http://dx.doi.org/10.1016/j.conbuildmat.2004.05.017.

Lynch, G. C. J. (1994). Bricks: properties and classifications. *Structural Survey, 13*, 15−20.

Moreno, N., Querol, X., Andrés, J. M., Saatanton, K., Towler, M., Nugteren, H., et al. (2005). Physico-chemical characteristics of European pulverizad coal combustión fly ashes. *Fuel, 84*, 1351−1363.

Quaranta, N., Unsen, M., López, H., Giansiracusa, C., Roether, J. A., & Boccaccini, A. R. (2011). Ash from sunflower husk as raw material for ceramic products. *Ceramics International, 37*, 377−385. http://dx.doi.org/10.1016/j.ceramint.2010.09.015.

Queralt, I., Querol, X., Soler, A. L., & Plans, F. (1997). Use of coal fly ash for ceramics: a case study for a large Spanish power station. *Fuel, 76*, 787−791.

Reddy, K. S., Abhishek, C. H., & Babu, M. H. (2012). *Role of fly-ash bricks in construction*. India: Bachelor of Technology in Civil Engineering.

Resourceeffcientbricks. (2013), Use of fly ash for brick making (clay-fly ash bricks). http://resouceefficientbricks.org/resource.php. Accessed 10.10.13.

Sabedot, S., Sundstron, M. G., Böet, S. C., Sampaio, C. H., Dias, R. G. O., & Ramos, C. G. (2011). Caracterização e aproveitamento de cinzas da combustão de carvão mineral geradas em usinas termelétricas. In *Anais do III Congresso Brasileiro de Carvão Mineral (VB06)* (pp. 1−15) (Brazil).

Santos, P. S. (1989). *Ciência e tecnologia das argilas* (Vol. 2). Edgard Blücher Ltda.

Sarkar, R., Singh, N., & Das, S. K. (2007). Effect of addition of pond ash and fly ash on properties of ash-clay burnt bricks. *Waste Management & Research, 25*, 566−571.

Shakir, A. A., Naganathan, S., & Mustapha, K. N. (2013). Properties of bricks made using fly ash, quarry dust and billet scale. *Construction and Building Materials, 41*, 131−138. http://dx.doi.org/10.1016/j.conbuildmat.2012.11.077.

Silva, N. I. W., Calarge, L. M., Chies, F., Mallmann, J. E., & Zwonok, O. (1999). Caracterização de cinzas volantes para aproveitamento cerâmico. *Cerâmica, 45*, 1−8. http://dx.doi.org/10.1590/S0366-69131999000600004.

Sukala, R., Singh, D., Solanki, P., Sutariya, J., & Thakur, K. (2012). *Fly ash bricks*. Ahmedabad: Shantilal Shah Engineering College, Gujarat Technological University.

Thy, P., Jenkins, B. M., Grundvig, S., Shiraki, R., & Lesher, C. E. (2006). High temperature elemental losses and mineralogical changes in common biomass ashes. *Fuel, 85*, 783−795.

Types of waste, properties, and durability of pore-forming waste-based fired masonry bricks

6

N. Phonphuak[1], *P. Chindaprasirt*[2]
[1]Rajabhat Maha Sarakham University, Maha Sarakham, Thailand; [2]Khon Kaen University, Khon Kaen, Thailand

6.1 Introduction

One of the oldest construction materials is brick, and it continues to be one of the most popular building materials because it is durable, easy to handle, aesthetic in look, and inexpensive. Clay bricks are used for exterior and interior walls, partitions, piers, footings, and other load-bearing structures (Duggal, 2008). The history of masonry construction can be considered as the beginning of the history of civil engineering. Naturally available stone was the oldest building masonry material known to humans. Some of the most significant building structures in terms of architectural look in the world, such as the Great Wall of China, Colosseum in Rome, pyramids in Egypt, and the Taj Mahal in India, were built with brick. The masonry structure not only provides strong structure that can stand the wear and tear of nature, such as wind, flood, earthquake, and fire, but also looks elegant and impressive. To improve the quality of the brick, several techniques were employed over the years. Initially, natural heat was utilized in the making of sun-baked brick. The addition of chopped straw and grass to the clay mixture was employed to reduce the distortion and cracking of bricks. The next big step in enhancing the brick properties occurred around 4000 BC (The Mason Contractors Association of America, 2012). The firing of brick was used to improve the strength and durability of brick.

As urbanization expands, the demand for bricks increases (Karaman, Gunal, & Ersahin, 2006). Good-quality brick is now a basic commodity for modern housing and other structures. Bricks are now developed to become homogeneous and strong. This is achieved with the ceramic bonding from the fusion phase of silica and alumina clay constituents (Adeola, 1977). Compressive strength and water absorption are two major physical properties of bricks that are potential predictors of their ability to sustain weathering. The main factors involved in manufacturing bricks are the type of raw material used and the firing temperatures, both of which affect the final product (Cultrone, Sebastián, & De La Torre, 2005). In order to obtain bricks with appropriate physical and mechanical properties, additives are frequently used in brick production. The selection of additives depends on the characteristics required. Lightweight bricks with high compressive strength and low water absorption are desirable. One way to increase such capacity of bricks is to create porosity in the clay body

Eco-efficient Masonry Bricks and Blocks. http://dx.doi.org/10.1016/B978-1-78242-305-8.00006-1

through the addition of pore former materials, which are either organic or inorganic pore generators.

Organic pore formers are generally cheaper than inorganic ones and also have the advantage of ensuring a heat contribution to the firing (Demir, 2008). Thus, their use is more fuel efficient and environmentally friendlier than firing pure clay bricks or bricks with inorganic pore formers. However, inorganic pore formers are also used, as their contribution to environmental problems is minimal. Their uses may adversely affect the plasticity of clay and increase the amount of water required to produce a mixture with acceptable plasticity (Demir, 2008; Dondi, Marsigli, & Fabbri, 1997; Schmidt-Reinholz, 1990).

The pore formers used in clay brick manufacturing can be classified into two groups: organic and inorganic pore generators (Karaman, Gunal, & Ersahin, 2008). This chapter reviews various waste materials in different compositions as additional raw materials at different dosage levels for the making of fired masonry bricks. The advantages and disadvantages of the incorporation of different waste materials to the brick manufacturing process are discussed.

6.2 Industrial waste pore former and the properties of bricks

6.2.1 Sludge

There are a variety of sludges from different sources, such as sludges from sewage treatment plants, paper industry, tannery industry, and arsenic-iron industry (Kadir & Mohajerani., 2011). The strategy on sludge management is important to the success of achieving long-term sustainability and the strategy should be based on the actual needs of the community (Campbell, 2000). The main chemical components of sludge are silica (SiO_2), alumina (Al_2O_3), calcium oxide (CaO), and iron oxide (Fe_2O_3). The typical XRD pattern spectrum of sludge is shown in Figure 6.1. The compositions include some quartz, calcite, mica, and dolomite.

The use of sludge as an additive to construction and building materials such as building bricks, lightweight artificial aggregates, and cement-like materials is a win−win strategy because it converts the waste into useful materials and helps reduce the waste disposal problem (Weng, Lin, & Chiang, 2003). The benefits of using sludge as an additive in the fired clay matrix for making brick and tile have been studied by several authors (Jordán, Almendro-Candel, Romero, & Rincón, 2005; Merino, Arévalo, & Romero, 2007; Monteiro, Alexandre, Margem, Sánchez, & Vieria, 2008; Montero, Jordan, Hernandez-Crespo, & Sanfeliu, 2009). These authors agreed that the incorporation of sludge adversely affects the mechanical strength of brick, and thus the right amount of sludge needs to be used in order to meet the relevant standards applied to specific construction materials (Eliche-Quesada et al., 2011). Liew et al. (2004) studied the incorporation of sewage sludge as pore former into clay brick. The physical and mechanical properties of bricks containing 10−40 wt% of dried sludge generally complied with the technical Malaysian Standard MS 7.6:1972 for

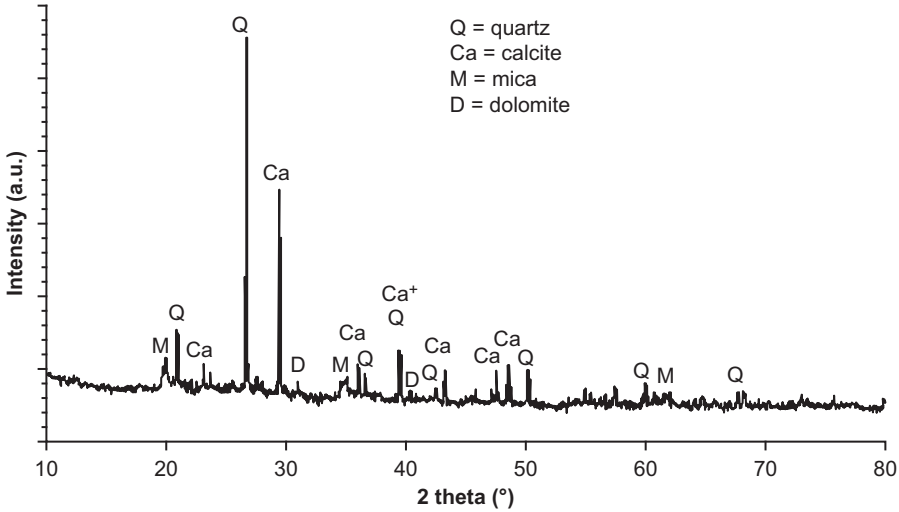

Figure 6.1 XRD pattern of sludge ash.
Source: García et al. (2012).

general wall construction. As shown in Table 6.1, the high amount of 10−40% sludge in clay brick adversely affected the drying shrinkage, but the firing shrinkage was decreased. The water absorption increased to 37% compared to 23.6% of the control brick and the compressive strength decreased to 2 MPa compared to 15.8 MPa of the control brick. The decrease in compressive strength and increase in water absorption with increasing sludge content are due to the increase in pores, gradual pore coarsening, and formation of crack. Thus, bricks with high sludge content have poor surface finishing and may not be suitable for use as facing brick. The incorporation of 10% sludge seems to produce bricks with low shrinkage and water absorption with relatively high compressive strength of 8.9 MPa.

Table 6.1 Effects of sewage sludge addition on the properties of clay bricks

Sludge additions (%)	Drying shrinkage (%)	Firing shrinkage (%)	Water absorption (%)	Compressive strength (N/mm^{-2})
0	0.075	2.55	23.6	15.8
10	0.058	2.07	26.7	8.9
20	0.081	2.08	29.0	5.4
30	0.092	1.34	33.1	3.1
40	0.102	1.10	37.0	2.0

Source: Liew et al. (2004).

Basegio, Berutti, Bernades, & Bergmann (2002) investigated the utilization of tannery sludge as a raw material for clay products. The results showed that the compressive strength of brick increased with increasing firing temperature but decreased with increasing amount of sludge. The maximum compressive strength of brick with 0−10% sludge addition was 25 MPa at firing temperature of 1180 °C. The same authors suggested that the incorporation of 10% tannery sludge was an appropriate amount to be used, considering the environmental aspects and the minimum requirement for the building industry. Monteiro et al. (2008) used 0, 3, 5, and 10 wt% of sludge from water treatment plants for making red ceramic with firing temperatures of 700, 900, and 1000 °C. The results indicated that the incorporation of up to 10% sludge into clay slightly increases the water absorption and reduces the mechanical strength of the fired ceramic. This is caused by the change in porosity with the high weight loss during the firing stage. The incorporation of sludge into the clay body should be done with care and a small percentage should be used in order not to interrupt the ceramic processing. Rouf & Hossain (2003) used iron and arsenic sludge at dosage levels of 5%, 15%, 25%, and 50% in clay bricks with firing temperatures of 950, 1000, and 1050 °C. The results indicated that 15% by mass is the optimum amount of sludge with firing temperature of 1000 °C. However, the strength of brick can be improved to a value comparable to that of normal clay brick with a slightly higher firing temperature of 1050 °C. Hassan, Fukushi, Turikuzzaman, & Moniruzzaman (2014) studied the use of 3%, 6%, 9%, and 12% arsenic−iron sludge in brick making. Bricks were determined on the basis of laboratory tests (ASTM C67). The durability of clay bricks is largely dependent upon their water absorption. The water absorptions of control clay bricks were between 10.0% and 11.2% and increased to 15.2−19.6% for the prepared clay bricks with sludge ranges of 3−6%. The compressive strength of 3%, 6%, 9%, and 12% sludge bricks were 14.1, 15.1, 9.4, and 7.1 MPa, respectively. The 6% sludge brick met the AASHTO standard's strength requirement of 14.7 MPa for a first-class brick. Moreover, the water absorption capacity of the prepared bricks increased with the gradual increase in sludge content. The optimum amount of clay sludge of 6% by weight is therefore recommended. García, Quesada, Villarejo, Iglesias-Godino, & Corpas-Iglesias (2012) studied the effect of sludge from Jaen (south Spain) on the properties and microstructure of fired clay brick manufacturing. Sludge content in the clay mixture varied from 1% to 15% of dry weight and the bricks were fired at 950 °C. Water absorption was determined in accordance with the standard UNE 67-027. Compressive strength was measured for fired samples in accordance with the standard UNE 67-026. The incorporation of 1−15 wt% sludge resulted in an increase in water absorption from 22.7% to 27.9%. They observed that there was a limit in the incorporation of sludge due to an increase in water absorption and a decrease in mechanical strength as a result of the increase in porosity caused by the decrease in bulk density (Figure 6.2). Results indicated that incorporating up to 5 wt% sludge is beneficial for clay bricks.

Weng et al. (2003) studied the utilization of sludge collected from an industrial wastewater treatment plant. The results indicated that the amount of sludge and firing temperature are the two key factors determining the quality of brick, as shown in Figure 6.3. With firing temperature of 1000 °C, first-class brick is obtained with the

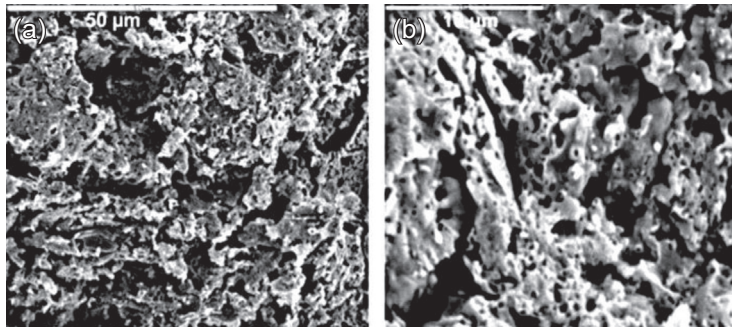

Figure 6.2 Scanning electron microscope micrographs of (a) clay and (b) clay containing 5 wt% sludge.
Source: García et al. (2012).

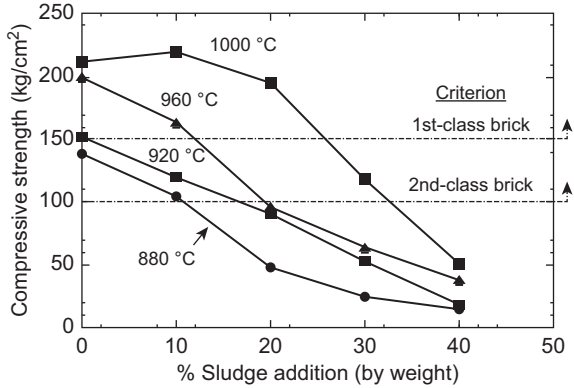

Figure 6.3 The compressive strength of bricks containing sludge collected from an industrial wastewater treatment plant.
Source: Weng et al. (2003).

use of up to 25% sludge and second-class brick is obtained with up to 33% sludge. For a firing temperature of 960 °C, first-class brick is obtained with the use of up to 12% sludge and second-class brick is obtained with up to 20% sludge. It was suggested that the waste offered economic benefits while maintaining the properties of the manufacturing clay brick (Zani, Tenaglia, & Panigada, 1990).

6.2.2 Textile sludge

The textile industry generally uses several chemicals and dyes at high concentration to obtain the required characteristics, such as softness, brightness, and color in clothes or textiles. The textile industry thus generates a large amount of wastewater. This wastewater is reported to contain a substantial amount of sand and grit, lint-free and emulsified oil grease, heavy metals, and volatile organic compounds (Barredo-Damas et al., 2010). Solid waste from textile production has the potential for use as an additive

in building material (Pappu, Saxena, & Asolekar, 2007; Senthilkumar, Sivakumar, & Akilamudhan, 2008). Balasubramanian, Sabumon, Lazar, & Ilangovan (2006) reported the use of textile effluent treatment plant sludge as a pore former in fired clay brick. The incorporation of 10% textile sludge results in bricks with compressive strength higher than the minimum requirement of 3.5 MPa for compressive strength of load-bearing bricks, as per IS: 1077−1979. The increase in the amount of sludge to 20% and 30% results in bricks with lower compressive strengths than that prescribed in IS: 1077−1979. The bricks with 10% textile sludge, however, do not meet the strength requirements for "Grade NW" bricks as specified in the ASTM standard (C62−80). It should be noted here that the minimum compressive strength requirement for commercial bricks as specified in the ASTM standard is almost three times that of the Indian standard (BIS, 1979).

Baskar, Meera Sheriffa Begum, & Sundaram (2006) studied the production of fired clay bricks with 0−30% of sludge from textile water treatment plants. The fired clay bricks were tested to evaluate their shrinkage, weight loss, and compressive strength. The results indicated that the increase in amount of waste results in a loss in compressive strength. The maximum amount of sludge that can be added is in the range of 6−9% to produce brick with acceptable compressive strength between 3.5 and 4.2 MPa satisfying the Bureau of Indian Standards.

Jahagirdar, Shrihari, & Manu (2013) also studied the use of textile sludge in making burnt clay bricks and reported a slightly higher amount of sludge addition of 15% to produce brick with compressive strength greater than 3.5 MPa (tested in accordance with IS 3495 (Part-I)-1992). Durability of the bricks can be judged by water absorption test (IS 3495 (Part-II)-1992). The density, compressive strength, and ringing sound of

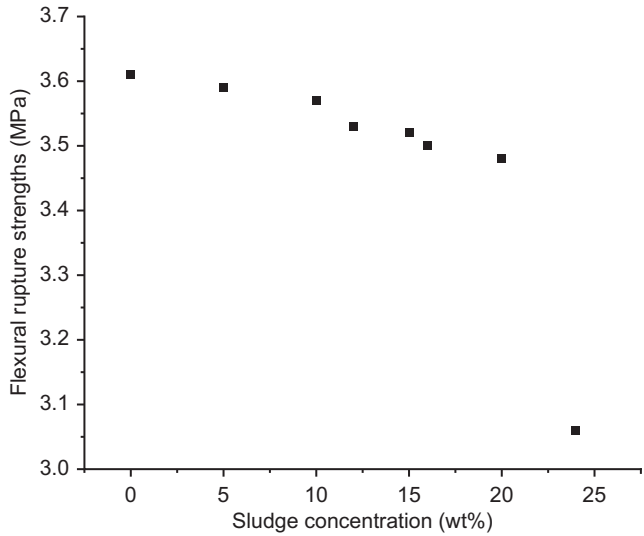

Figure 6.4 Average values of flexural strengths of ceramic bricks with sludge.
Source: Herek et al. (2012).

bricks reduce, whereas water absorption and efflorescence increase, as the sludge content in brick increases. High firing temperature and firing period (i.e., 800 °C and 24 h) give good results in terms of compressive strength.

Herek et al. (2012) used textile laundry wastewater sludge to produce bricks and reported that sludge can be incorporated up to 20% (by mass) in producing bricks with suitable mechanical properties. The incorporation of more than 20% sludge results in significant reduction in the flexural rupture strength of brick, as shown in Figure 6.4. The incorporation of sludge decreased the flexural strength of brick, but it is still higher than the 1.5 MPa limit specified by the Brazilian standard. An applied leaching test and a solubilization test were also performed on the produced bricks and indicated that they are sufficiently safe and inert. The scanning electron microscope images of the ceramic bricks with and without sludge incorporation are shown in Figure 6.5. The sample with sludge shows increases in pore sizes that are in line with the results of the water absorption test.

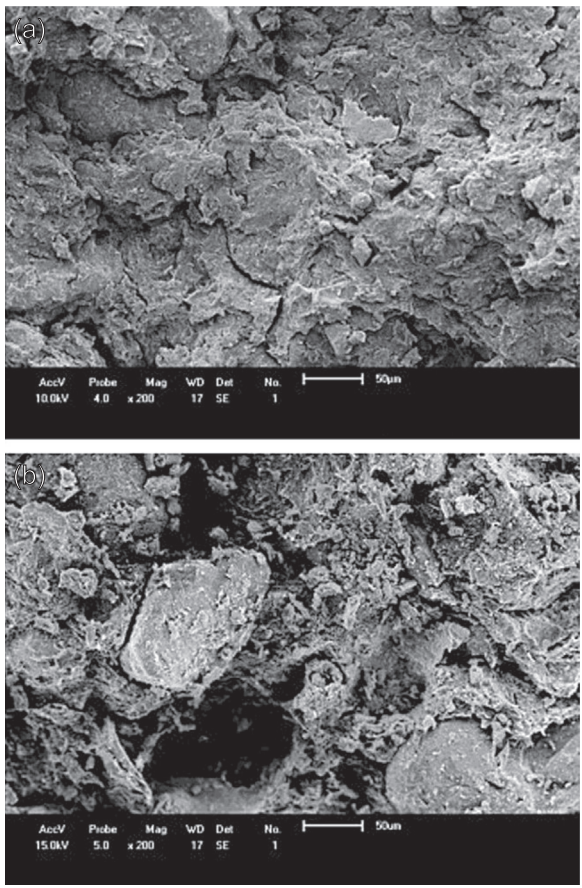

Figure 6.5 Scanning electron photomicrographs of ceramic bricks (a) without sludge and (b) with sludge.
Source: Herek et al. (2012).

6.2.3 Waste from marble industry

The marble industry generates a large quantity of residue during the process of cutting and polishing the material, in the form of dust and white mud. This waste is a concern to the general public, as it can leak into public waterways and is posing a serious environmental threat to the public. Attempts are being made to utilize marble wastes in different applications, such as a source material for calcium silicates (Felipe-Sese, Eliche-Quesada, & Corpas-Iglesias, 2011), as material in road construction, as aggregates in concrete and asphalt, and as an additive in cement or other building materials (Montero et al., 2009; Saboya, Xavier, & Alexandre, 2007). The main chemical composition of waste from marble industry is calcium oxide (55%). The waste also contains smaller amounts of impurities such as magnesium, ferrous, silicon, and aluminum oxides (Eliche-Quesada, Corpas-Iglesias, Pérez-Villarejo, & Lglesias-Godino, 2012). The XRD pattern (Figure 6.6) of marble residue showed magnesium calcite ($Mg_{0.03}Ca_{0.97}$) (CO_3) as the major crystalline phase, and the presence of dolomite ($CaCO_3 \cdot MgCO_3$) and traces of quartz.

The incorporation of waste from marble industry in the matrix of fired clay brick has been studied by several authors and proved to be very efficient for improving the brick's mechanical properties (Balint & Mattyasovszky-Zsolnay, 1982; Bozadgiev, 1996; Freire & Mota, 1997; Saboya et al., 2007; Vincenzini & Fiori, 1976). Saboya et al. (2007) showed that the incorporation of 15−20% marble waste is appropriate for the manufacturing of ceramic brick. As water absorption is one of the most critical properties for ceramic brick, the incorporation of 20% or higher content of marble waste produced bricks with higher water absorption than that allowed for construction purposes. The marble residue is also used in conjunction with recycled sawdust, spent earth from oil filtration, and compost for brick manufacturing (Eliche-Quesada et al., 2012). The optimum sintering temperature was shown to be 1050 °C. At a low firing temperature of 950 °C, the bricks contained a large amount of open pores and this adversely affected the compressive strength of the bricks. Based on the results obtained, the same authors suggested the optimum proportion of 5 wt% sawdust, 10 wt% compost, and 15 wt% spent earth from oil filtration and 70% marble waste.

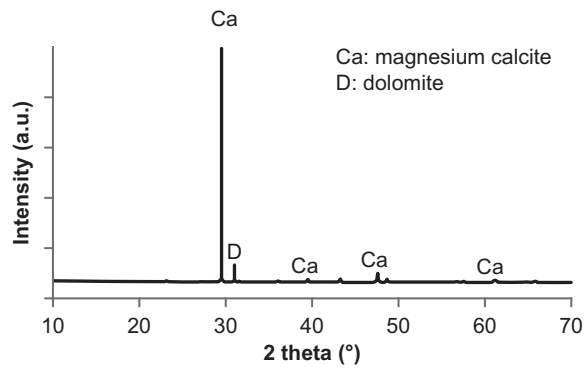

Figure 6.6 The XRD pattern of marble.
Source: Quesada et al. (2012).

6.2.4 Waste from paper industry

Paper industry produces a significant amount of different wastes. The pulp residue contains high cellulose fiber (Demir, Baspınar, & Orhan, 2005) and the other contains high calcium oxide (Sutcu & Akkurt, 2009) and both can be used in fired clay brick production. The crystalline and phase analyses of paper processing residues are shown in Figure 6.7. The by-products and residue pulp from paper industry are managed using several approaches, including land filling, incineration, use in cement plants and brickworks, agricultural use and compost, anaerobic treatment, and recycling (Huet, 1982; Shao, Qui, & Shah, 2001; Seminar, 1994).

Demir et al. (2005) showed that kraft pulp fiber residue could be used as pore former in fired brick. The thickness of the cellulose fiber is around 5−20 μm with a small amount of inorganic content deposited at its surfaces. The main chemical components are 52% SiO_2, 21% A_2O_3, 9% Fe_2O_3, and 9% loss on ignition (LOI). Up to 5% pulp residue could be effectively used as pore former in producing clay brick at a firing temperature of 900 °C. The increase in the dosage beyond this level was not effective in decreasing the bulk density of the clay body. The compressive strength of the samples decreased with the increase in amount of residue added. It has also been shown that the residues can be easily utilized as pore-forming additives into bricks bodies to facilitate production of vertically perforated insulation bricks.

Muñoz, Juárez, Morales, & Mendívil (2013) studied the use of paper pulp as a lightening additive and its influence on the thermal and mechanical properties of fired clay brick. The results indicated that the use of paper pulp increases the porosity of bricks and has a more significant impact in terms of reducing compressive strength than on the thermal conductivity. The incorporation of 15% paper pulp has improved the thermal conductivity at 10 °C by 39.7% compared to a conductivity value of clay brick without additive of 0.45 W/m K. The thermal conductivity behavior is not linear and decreases appreciably only with addition of more than 5% paper pulp.

Porous and lightweight anorthite ceramics from the mixtures of fired clay and paper waste with sawdust addition were also studied and successfully produced

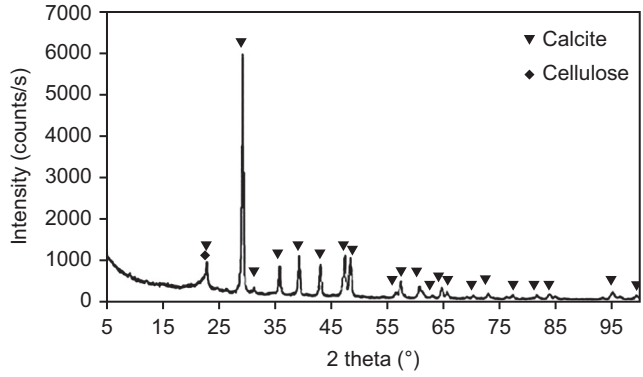

Figure 6.7 X-ray diffraction pattern of paper processing residues.
Source: Sutcu & Akkurt (2009).

(Sutcu & Akkurt, 2010). Recycled paper processing residues (PPR) and clay of different sources for production of porous anorthite ceramics were fired at 1100−1300 °C and PPR contents of 20−50 wt%. Results from this study demonstrated that clay mixture with 30−40 wt% of PPR fired at 1200−1400 °C contained anorthite as a major phase and some minor secondary phases such as mullite or gehlenite phase in the mixtures. The compressive strength of the samples ranged from 8 to 43 MPa. It was claimed that upon completion of this study, porous thermally insulating anorthite ceramics were successfully produced (Sutcu, Akkurt, Bayramb, & Uluca, 2012). An anorthite refractory insulating brick was produced from clay, recycled paper waste, and sawdust with firing temperature of 1200 °C. Pores in the brick were created from the burning of cellulose fiber and the decomposition of calcium carbonate. Depending on the porosity of bricks, the bulk densities ranged from 1.12 to 0.64 g/cm^3, and the thermal conductivities varied from 0.25 to 0.13 W/m K. The same authors also indicated that the strengths were sufficiently high for use as an insulating fired brick. In conclusion, paper residues can potentially be used in the production of lighter and economical new brick material and in this way it can be utilized in an environmentally safe way (Demir et al., 2005; Raut, Sedmake, Dhunde, Ralegaonkar, & Mandavgane, 2012).

The other waste from paper industry contains high amounts of CaO and can also be used in making fired clay porous brick with reduced thermal conductivity (Sutcu & Akkurt, 2009). Inorganic content of this residue is largely calcite. The ingredients were powdered, mixed, and hydraulic pressed under a pressure of 10 MPa, and then fired at 1100 °C. The results indicated the normal trend that the increase in the residue addition resulted in the increase in porosity content and the decrease in the compressive strength of samples, but compressive strength was still higher than the strength values required by standard. It has also been shown that the thermal conductivity values of the produced porous brick (<0.4 W/m K) showed more than 50% reduction compared to local brick of the same composition (0.8 W/m K). Preliminary trials were successfully conducted on industrial-scale-product bricks with this high CaO waste from paper industry.

6.3 Agricultural waste pore formers and properties of bricks

6.3.1 Rice husk

Rice husk is an organic waste and is produced in large quantities. It is a major by-product of the rice milling and agro-based biomass industry. Rice husk is a cellulose-based fiber and contains approximately 20% silica in amorphous form (Hu et al., 2008; Mansaray & Ghaly, 1998; Nair, Fraaij, Klaassen, & Kentgens, 2008; Ndazi, Karlsson, Tesha, & Nyahumwa, 2007). In addition, it consists of 60−65% volatile matter, 10−15% fixed carbon, and 17−23% ash (Hu et al., 2008; Kwong, Christopher, Chao, Wang, & Cheung, 2007; Mansaray & Ghaly, 1998). It contains approximately 40% cellulose, 30% lignin group, and 20% silica

(Chindaprasirt, Kanchanda, Sathonsaowaphak & Cao, 2007). Rice husk can absorb water ranging from 5% to 16% of unit weights, and the unit weight of rice husk is 83−125 kg/m^3 (Mansaray & Ghaly, 1998). The ash of rice husk contains approximately 90% silica, which is a highly porous structure and is lightweight, with high specific surface area. Rice hulk ash has been applied as an additive in many materials and applications, such as refractory brick, manufacturing of insulation, and materials for flame retardants (Boateng & Skeete, 1990; Chaudhary & Jollands, 2004; Choi, Mori, & Ohama, 2006; Rice Husk Ash Website, 2008). This is due to its highly porous structure and its good insulating property. The properties of rice husk ash silica vary according to the firing temperature and time. The rice husk addition increased the porosity of sintered samples (see Figure 6.8) (Chiang, Chou, Hua, Chien, & Cheeseman, 2009). Furthermore, the increase in the sintering temperatures increased the compressive strength of the fired brick.

Figure 6.9 shows that the total porosity of fired clay brick increased with the increasing dosage of rice husk and decreased with the increasing sintering temperature. With 1100 °C sintering temperature, the total porosity of brick increased from 5% to 38% with a corresponding increase in rice husk from 0% to 20%. As sintering progresses, pores become rounded and smaller than those obtained with no rice

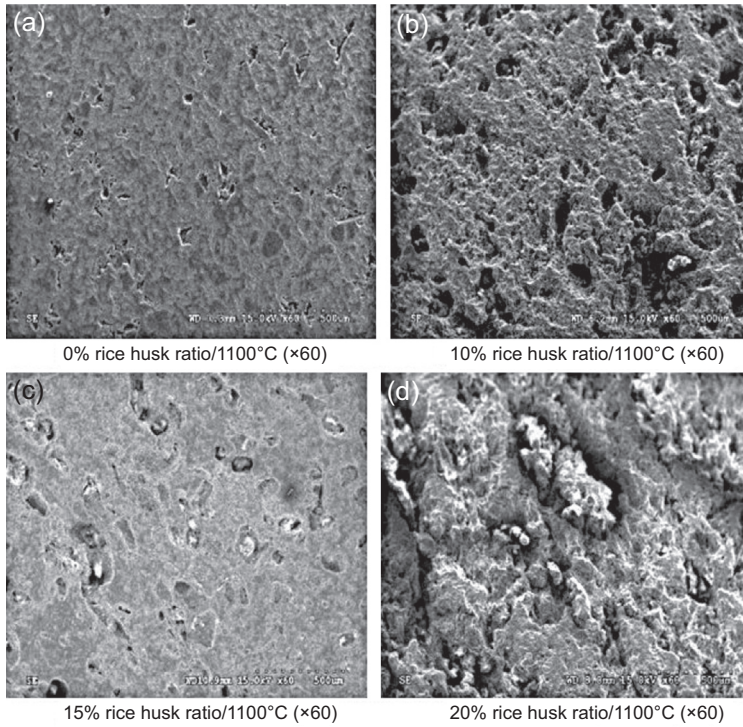

Figure 6.8 Scanning electron micrograph images of fired clay brick with rice husk sintered at 1100 °C: (a) 0%, (b) 10%, (c) 15%, (d) 20%.
Source: Chiang et al. (2009).

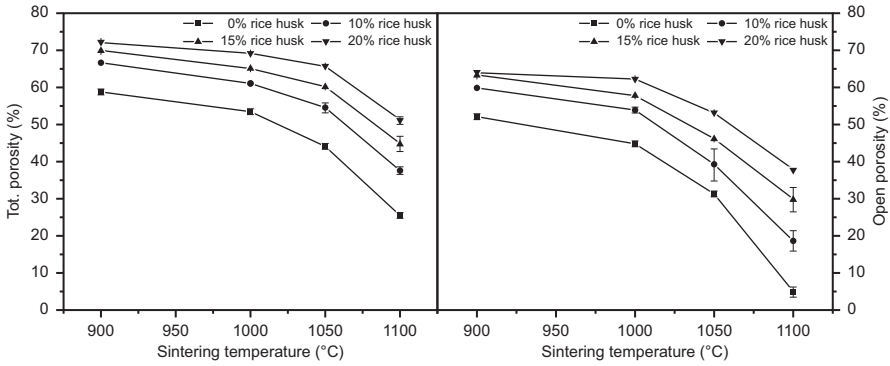

Figure 6.9 Sintering temperature effect on the total porosity and open porosity of specimens. *Source*: Chiang et al. (2009).

husk addition. The pores are completely isolated from the surface at the end of sintering, and then closed. Sintering is accelerated at firing temperatures over 950 °C because of the vitreous phase formations. This phase penetrates into pores and closes them, and then separates them from neighboring pores (Milheiro, Ferire, Silva, & Holanda, 2005). The mechanism can explain the reduction in water absorption with increasing sintering temperature.

Görhan & Şimşek (2013) investigated the effects of rice husk addition on the porosity and thermal conductivity properties of fired clay bricks. The dosages of 0−15% rice husk and firing temperature 700−1000 °C were employed. Figure 6.10 shows the variation of water absorption rate for the firing temperatures of 700, 800, 900, and 1000 °C. The effect of rice husk content on water absorption is more significant than the effect of firing temperature. For the BG series, the incorporation of 0%, 5%, 10%, and 15% rice husk resulted in samples with water absorption rates in the

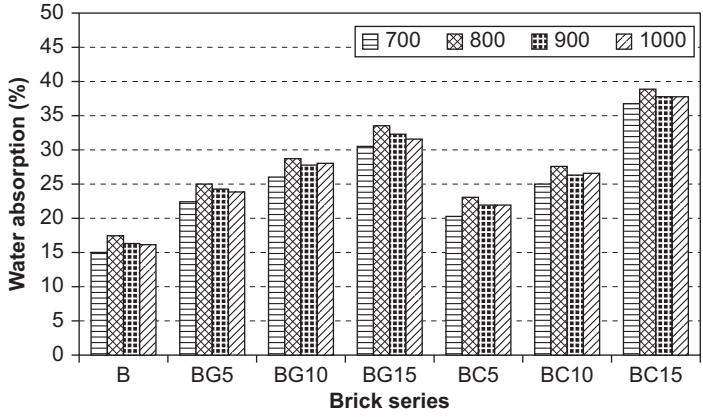

Figure 6.10 Water absorption of the specimens.
Source: Görhan & Şimşek (2013).

order of 15%, 24%, 27%, and 32%. The rate of water absorption for the BC series also increased in a similar fashion with the increase in rice husk content. The water absorption for bricks with 10% rice husk is slightly higher than 25%, the boundary value for water absorption. The incorporation of 5% and 10% of rice husk resulted in clay bricks with slightly lower compressive strengths of 7−10 MPa, which are lower than the reference clay bricks but nevertheless satisfy the requirements of TS EN 772-1 for disaster regulation for a building material to be used in indoor structural applications. The use of 10% of rice husk is the optimum composition for production of clay bricks. Rice husk could thus be used as a good pore former additive in clay body.

6.3.2 Sugarcane bagasse

In the process of making sugar, sugarcane is crushed to extract the juice. The fibrous residue is called bagasse and is used as a fuel source for feeding a boiler. Sugarcane bagasse ash (SCBA) is thus a residue obtained from the burning of bagasse in the sugar industry. In general, the ash with high silica content contains a high portion of quartz (Faria, Gurgel, & Holanda, 2010). It is characterized as a solid waste and is usually disposed of as landfill. The SCBA contains a large amount of silica (62%) and some Al_2O_3, CaO, Fe_2O_3, and potassium oxide (K_2O). LOI of about 10% implies the high content of unburnt organic matter. The major crystalline phases found in sugarcane bagasse ash are quartz (SiO_2) and cristobalite (SiO_2), as shown in Figure 6.11 (Ganesan, Rajagopal, & Thangavel, 2007).

Souza, Teixeira, Santos, Costa, & Longo (2011) indicate that the SCBA is rich in crystalline silica and thus is possible for use as ceramic raw material. Also, with a sufficient amount of amorphous silica and with proper grinding, it has been used as

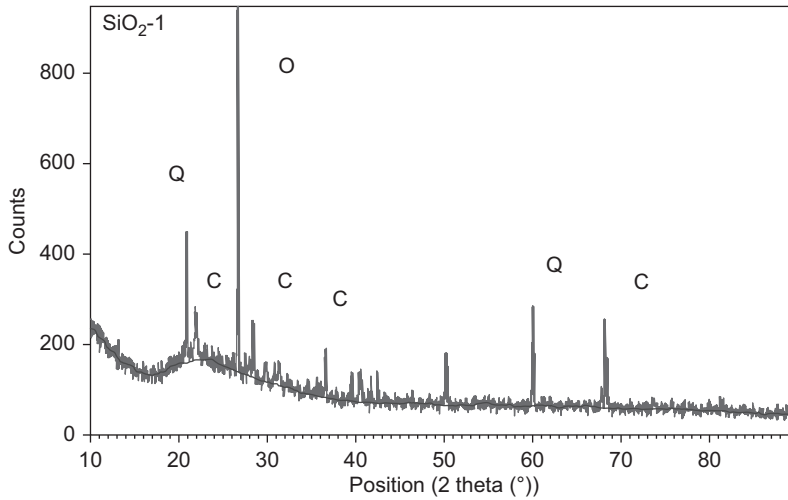

Figure 6.11 X-ray diffraction pattern of bagasse ash.
Source: Ganesan et al. (2007).

a pozzolan in cement, mortar, and concrete mixtures (Frías & Villar-Cocina, 2007; Ganesan et al., 2007; Payá, Monzó, Borrachero, Diaz-Pinzón, & Ordónez, 2002). The use of SCBA waste in clay ceramics has also been recently suggested (Borlini et al., 2006; Teixeira, Souza, Santos, & Peña, 2008; Vieira, Soares, Sánchez, & Monteiro, 2004). Faria, Gurgel, & Holanda (2012) reported that the incorporation of SCBA into clay bricks resulted in an increase in water absorption and a decrease in strength of the fired clay brick. However, with a sufficiently high firing temperature of 1000 °C, the water absorption for clay bricks still conforms to the specifications. The same authors recommended the use of SCBA up to 10 wt% into clay brick body to limit the adverse effect on the strength of fired bricks, thus ensuring the safe and sustainable use of SCBA in the brick industry.

Souza et al. (2011) use SCBA as an additive in ceramic materials. The raw material used in roof tile production was mixed with 0%, 20%, 40%, and 60% ash by weight. The samples were fired at 800, 900, 1000, 1100, and 1200 °C. The incorporation of 0−60% SCBA in the samples decreased the water absorption. Water absorption did not change much at the firing temperatures below 1000 °C, but was pronounced at 1100 °C and 1200 °C. The formation of the liquid phase resulted in a decrease in the open pores at the high firing temperatures. The addition of SCBA also decreased the flexural strength; however, the flexural strength of samples increased with increasing firing temperature due to a decrease in porosity and an increase in bulk density with an increasing temperature. The result showed that the 20−60% weight of SCBA can be incorporated in clay bricks and roof tiles at firing temperatures up to 1000 °C. Conclusively, the results revealed that in terms of environmental protection, waste management practices, and saving of raw materials, SCBA can be regarded as a potential raw material as a pore former in the manufacturing of clay bricks with improved thermal conductivity.

Kadir & Maasom (2013) studied the use of sugarcane bagasse (SB) in fired clay bricks. Fired clay bricks were tested for thermal conductivity and compressive strength. The densities of 1%, 2%, and 3% of SB bricks decreased compared to control brick to 1790, 1640, and 1520 kg/m^3 with corresponding decrease in the thermal conductivities to 0.0117, 0.0111, and 0.0107 W/m K and compressive strengths to 22.8, 14.2, and 5.8 MPa. The strength significantly reduces with the increase in the content of the bagasse ash, but with the 3% addition the strength is still sufficient.

6.3.3 Sawdust

Sawdust is a waste from the wood and timber industry. As it possesses a firing capacity, it is normally used as a fuel source in thermal processes (biomass). It is also used as insulating material. Little work has been attempted, however, regarding use of these wastes in the production of building materials (Demir, 2008; Duchan & Kopar, 2001; Low, Fazio, & Guite, 1984). The main chemical components of sawdust are carbon (60.8%), hydrogen (5.2%), oxygen (33.8%), and nitrogen (0.9%). Dry wood is primarily composed of cellulose, lignin, hemicelluloses, and minor amounts (5−10%) of extraneous materials (Horisawa et al., 1999). The sawdust residue can be incorporated in clay as a pore-forming agent in ceramics technology. Furthermore,

such combined products give the fired clay a more porous microstructure. This results in the decrease in clay density and improves the clay thermal insulating capacity. The optimum sintering temperature has been shown to be around 1050 °C. At sintering temperature of 950 °C, open porosity increased, which resulted in the decrease in the compressive strength of the bricks (Eliche-Quesada et al., 2012).

Okunade (2008) used wood ash in conjunction with sawdust as admixtures in laterite clay bricks. Sawdust (for burning out) and wood ash admixtures at a ratio of 70:30 by weight was incorporated into laterite clay. The testing was done in accordance with ASTM C67. The admixtures were added in various combinations of proportions by volume (from 0% to 10%). The results indicated that the dry and wet compressive strength of bricks made from the control mix were 18.40 and 15.20 MPa, respectively. The average water absorption of bricks made from the control mix was 13.0−15.0%. Conclusively, the results revealed that wood ash on its own would also result in production of lightweight and more porous products.

6.3.4 Charcoal

Charcoal is normally obtained from the burning of wood, peat, bones, cellulose, or other carbonaceous substances with little or insufficient air. It is an amorphous carbon in the form of highly porous microcrystalline graphite. When charcoal is used as an additive to clay, it can help save energy in brick production. The major crystalline phases found in charcoal are quartz and cristobalite, as shown in Figure 6.12.

Phonphuak & Thiansem (2011) tested the physical and mechanical properties of fired clay briquettes containing 0%, 2.5%, 5%, 7.5%, and 10% of charcoal by weight. Charcoal particles of 2−3 mm (size 1), 1−2 mm (size 2), and less than 0.5 mm (size 3) and a firing temperature of 950 °C were used. The charcoal additives in the specimens

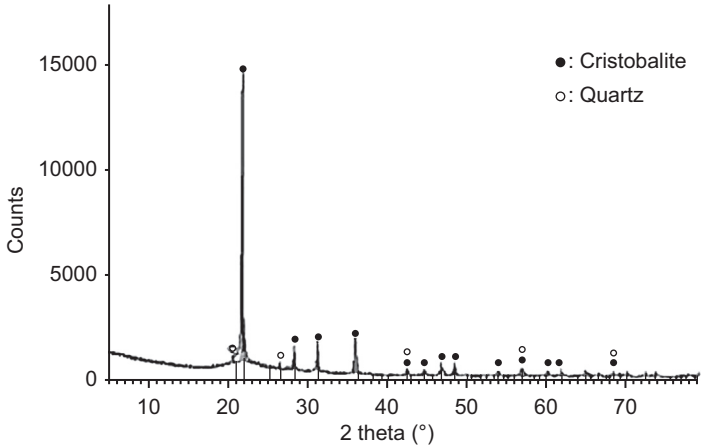

Figure 6.12 X-ray diffraction patterns of charcoal.
Source: Phonphuak & Thiansem (2012).

were burnt out through the process of firing, leaving abundant pores in the clay bricks. The water absorption of the briquette specimens was in the range of 18−40% and was directly proportional to apparent porosity (Table 6.2). The highest apparent porosity was 53% (10% of charcoal size 1) and the lowest was 31% (2.5% of charcoal size 3), suggesting that the high percentage of charcoal in the specimens caused an increase in porosity. In addition, compressive strength of clay briquette specimens decreased with an increase in the amount of charcoal (Table 6.2).

Figure 6.13(a)−(d) shows the surface texture of fired clay specimens with charcoal. The fired briquette specimens with the addition of fine charcoal exhibited the fine pore structure and those with coarser-size charcoal exhibited coarser pores; the brick with fine pores also showed a low water absorption capacity. Charcoal is thus regarded as an appropriate additive to raw materials used in producing lightweight fired clay bricks.

The effect of firing temperature of fired clay brick with addition of charcoal was also studied by Phonphuak & Thiansem (2012). In order to determine the extent of the pore-forming effects of charcoal, additive was added into raw brick clay and divided into five different batches of specimens mixed with five different percentages of charcoal additives: 0%, 2.5%, 5.0%, 7.5%, and 10% by weight. Specimens were fired at four different temperatures: 900, 950, 1000, and 1100 °C. The water absorption was found to increase with the increase in the amount of charcoal, as shown in Table 6.3. The highest porosity was 48.0% with 10% charcoal addition, and the lowest was 20.3% with 2.5% charcoal addition. The strengths of the fired briquettes were reduced with the increase in the charcoal content due to the increased porosity.

Table 6.2 Effect of charcoal size and proportion on the physical and mechanical properties of fired briquette specimens (fired at 950 °C)

Properties	Size	Charcoal proportion (% by weight)				
		0%	2.5%	5.0%	7.5%	10%
Water absorption (%)	1[a]	17.2	21.8	27.8	34.8	40.7
	2[b]	17.2	19.2	22.6	29.9	35.7
	3[c]	17.2	18.3	20.0	24.3	33.2
Apparent porosity (%)	1	29.0	35.35	38.3	47.2	53.9
	2	29.0	33.8	35.5	46.0	48.8
	3	29.0	31.5	35.1	38.9	46.6
Compressive strength (kg/cm^2)	1	152.7	77.8	77.4	47.7	29.0
	2	152.7	107.0	64.7	41.9	73.8
	3	152.7	143.5	90.6	85.7	78.6

[a]Charcoal size 1 (2−3 mm).
[b]Charcoal size 2 (1−2 mm).
[c]Charcoal size 3 (less than 0.5 mm).
Source: Phonphuak & Thiansem (2011).

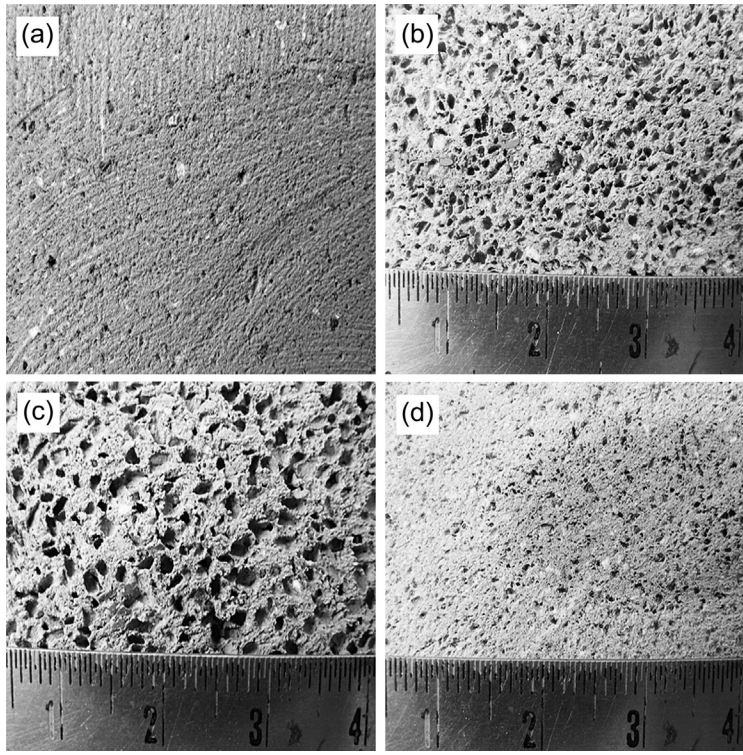

Figure 6.13 Surface texture of briquette specimens fired at 950 °C. (a) Original clay, (b) mixed with charcoal size 1 (2−3 mm), (c) mixed with charcoal size 2 (1−2 mm), and (d) mixed with charcoal size 3 (less than 0.5 mm).
Source: Phonphuak & Thiansem (2011).

However, the strength was also found to increase with firing temperature. The increase in firing temperature from 900 to 950 °C substantially increases the strength of briquettes.

The authors suggested that the briquettes consisting of 2.5% charcoal with sizes less than 0.5 mm fired at 950 °C are desirable in terms of mechanical and physical properties. The briquettes were more porous and stronger compared to the commercial bricks.

6.4 Other waste pore formers

Other agricultural wastes such as sawdust, tobacco residues, grass (Demir, 2008), processed waste tea (Demir, 2006), sunflower seed shell (Bánhidi & Gömze, 2008), and spent grains from brewing industry (Russ, Mörtel, & Meyer-Pittroff, 2005) can also be used as pore former additives in the production of fired clay bricks. Demir (2008) investigated the use of sawdust, tobacco residues, and grass (0%, 2.5%, 5%, and 10% weight) in making fired clays at firing temperature of 900 °C.

Table 6.3 Mechanical properties of fired test briquettes produced under different firing temperatures and varying charcoal concentrations

Properties	Temperature (°C)	Percent charcoal additions by weight 0%	2.5%	5.0%	7.5%	10.0%
Water absorption (%)	900	17.38	18.90	20.60	25.16	35.98
	950	17.18	18.27	19.98	24.34	33.21
	1000	16.96	16.89	19.36	23.49	30.56
	1100	12.89	13.54	18.67	22.32	28.67
Apparent porosity (%)	900	31.16	31.56	35.68	41.09	47.96
	950	28.96	31.45	35.14	38.93	46.85
	1000	22.56	23.96	32.45	37.76	42.29
	1100	20.38	20.27	29.73	32.51	36.34
Compressive strength (kg/cm^2)	900	97.63	66.96	35.58	32.27	31.77
	950	152.66	143.45	90.57	85.70	78.59
	1000	173.09	147.31	123.25	119.78	105.59
	1100	265.87	152.42	128.96	120.62	110.52

Source: Phonphuak & Thiansem (2012).

The incorporation of all three wastes increases the apparent porosity and water absorption of the fired bricks and the strengths are reduced as expected. The incorporation of 5% waste additives resulted in apparent porosity of around 36−37% and water absorptions of around 25−26% compared with 30% and 17%, respectively, for the control bricks. The compressive strengths were reduced to around 10−11 MPa compared to 15.5 of the control brick. The results thus indicated that the three organic residues could be effectively used as pore formers with dosage of up to 5% addition by weight. The waste residues increased the open porosity and decreased the bulk density.

Processed waste tea (PWT) is a by-product from green tea processing. It is used to produce mushroom, as fertilizer, and for making particleboard. Demir (2006) studied the incorporation of PWT of up to 5% by weight to the fired clay brick. No cracking and bloating were observed on the fired clay brick samples. For the PWT of 0%, 2.5%, and 5.0%, high porosities of 30%, 35%, and 41.45% were obtained with the corresponding water absorption of 18.0%, 22.5%, and 27.3% and compressive strengths of 15.5, 19.5 and 22.7 MPa. The high porosity is due to the pore-forming ability of the PWT. The increase in strength with the increase in the amount of PWT is due to the increased burning caused by burning of the PWT in the clay body, which generated extra heating. The increase in strength with the increase in the amount of the PWT additive is quite attractive for producing high-strength fired clay bricks.

Sunflower seed shell has also been shown to be a good pore former additive. Bánhidi & Gömze (2008) show that the sunflower seed shell can be used as additive in the manufacturing of clay brick and the thermal conductivity of brick is significantly decreased, from 0.27 to 0.17 W/m K, when 7% weight of sunflower seed shell was used. Under the same conditions, the incorporation of sunflower seed shell gave much better performance than the incorporation of sawdust, with the corresponding reduction in thermal conductivity of brick to 0.23 W/m K.

Spent grain from brewing industry is also a possible pore former additive. Russ et al. (2005) investigated the using of spent grains and showed that the use of both dry and moist spent grains as additives (3.5% by mass) to clay body increases the porosity of brick. The dry spent grain resulted in higher-porosity brick compared with the use of moist spent grain. Both dry and moist spent grain increased the porosity of the brick more than the use of sawdust with the same 3.5% by weight addition. The water absorption of bricks is directly proportional to the porosity. However, the strength of bricks with both dry and moist spent grains of 9.25 and 8.78 MPa were slightly lower than the value of 9.51 MPa of the brick with sawdust. The incorporation of spent grain produced only a slightly lower-strength brick with high porosity and low density compared to the use of sawdust as additive.

Other industrial wastes such as coal wastes (Jung, Yoo, Lee, & Kim, 2005), urban sewage sludge, bagasse, sludge from the brewing industry, olive mill wastewater, and coffee grounds (Eliche-Quesada et al., 2011) have also been studied, with promising results. Jung et al. (2005) studied the addition of 10−50% coal wastes to clay bricks calcined at 900−1400 °C. The water absorption of the brick specimens increased with the amount of additive and decreased with increasing calcination temperature. Increased coal waste content generally increased the water absorption and decreased the compressive strength. When up to 30% of coal waste is mixed into clay at 1300 °C, the water absorption and compressive strength satisfy the requirements of first-class brick under Korea standard.

Eliche-Quesada et al. (2011) investigated the use of urban sewage sludge, bagasse, sludge from the brewing industry, olive mill wastewater, and coffee ground wastes in the manufacture of ceramic. The samples with 15% sludge, 2.5% bagasse, 5% sludge from the brewing industry, 6.5% olive mill wastewater, and 3% coffee grounds were mixed to produce bricks with firing temperature of 950 °C. It was reported that the water absorption increased to over 35% and the thermal insulation increased by more than 8% when urban sewage sludge, brewing industry sludge, and bagasse were incorporated into the clay body with the corresponding reduction in compressive strength by a maximum of 19%. The incorporation of coffee grounds and of olive wastewater was even more beneficial, showing compressive strengths comparable to bricks without waste and a 19% improvement in thermal conductivity.

Cigarette butts (CB) have also been shown to be suitable for use as pore former in making lightweight fired bricks (Aeslina, Abbas, Felicity, & John, 2009; Aeslina & Abbas, 2008). The brick samples were prepared with the incorporation of 0%, 2.5%, 5.0%, and 10.0% (by weight) CB (corresponding to about 0%, 10%, 20%, and 30% by volume) with firing temperature of 1050 °C. The water absorptions and initial rate of absorptions increased and the densities and strengths decreased with

the increasing CB content. The density values of fired bricks were reduced by 8−30%. The compressive strengths of bricks were 12.6, 5.2, and 3.0 MPa for bricks with 2.5%, 5.0%, and 10% CB, respectively. Thermal conductivity performance of bricks was also improved by 51−58%.

The above-mentioned literature confirmed that the agricultural and some industrial wastes could be advantageously used in the improvement of the thermal insulation properties and low dead load in buildings. Good-quality bricks are obtained with the added benefit of waste utilization.

6.5 Future trends

The use of clay brick in the construction of housing and other structures has been with us for a very long time and continues to grow as the need for good building structures for dwelling and working places expands. The importance of manufacturing of good-quality brick and brick structures in a sustainable way is, therefore, a key issue. The manufacturing of fired clay brick has raised some concerns in terms of energy consumption and emission of greenhouse gas. The utilization of waste-based pore formers is very attractive in terms of the waste utilization and its associated benefits. Good-quality brick with lighter weight could be manufactured with fuel efficiency. The reduction in wastage in the fired brick production, the improved energy efficiency in the firing, and the improved strength and durability will enhance the sustainability of the brick. The correct use of waste-based pore formers in terms of types and dosages and the required properties will improve the attractiveness of fired brick utilization.

6.6 Sources of further information and advice

The basic process of making of fired clay brick is quite simple, and this knowledge is shared by various craftsmen throughout the world. However, the brick production process can be quite diverse, ranging from modern mechanized and automated processes in developed countries to a relatively simple process with no major changes in brick-making technology in developing countries. The knowledge of fired clay brick can, therefore, be obtained through both classical and modern books on the subject, such as those by Bucci and Mollo (2010), p. 533, NPCS Board of Consultants & Engineers (2007), Duggal (2008), Bonapace & Sestini (2007), and Ward-Harvey (2008). The references given in this chapter are also very useful and can provide detailed knowledge on the subject.

References

Adeola, J. O. (1977). *A Review of masonry block/brick types used for building in Nigeria* (M. Eng. Thesis). University of Benin.

Aeslina, A. K., & Abbas, M. (2008). Possible utilization of cigarette butts in light-weight fired clay bricks. *World Academy of Science, Engineering and Technology, 45*, 153−157.

Aeslina, A. K., Abbas, M., Felicity, R., & John, B. (2009). Density, strength, thermal conductivity and leachate characteristics of light-weight fired clay bricks incorporating cigarette butts. *World Academy of Science, Engineering and Technology, 53*, 1035−1040.

Balasubramanian, J., Sabumon, P., Lazar, J., & Ilangovan, R. (2006). Reuse of textile effluent treatment plant sludge in building materials. *Waste Management, 26*, 22−28.

Balint, P., & Mattyasovszky-Zsolnay, T. (1982). Indicators of raw material properties and technological parameters and the density of brick. *Epitoanyag, 34*, 23−27.

Bánhidi, V., & Gömze, L. A. (2008). Improvement of insulation properties of conventional brick products. *Materials Science Forum, 589*, 1−6.

Barredo-Damas, S., Alcaina-Miranda, M. I., Bes-Pia, A., Iborra-Clar, M. I., Iborr-Clar, A., & Mendoza-Roca, J. A. (2010). Ceramic membrane behavior in textile wastewater ultrafiltration. *Desalination, 250*, 623−628.

Basegio, T., Berutti, F., Bernades, A., & Bergmann, C. P. (2002). Environmental and technical aspects of the utilization of tannery sludge as a raw material for clay products. *European Ceramic Society, 22*, 2251−2259.

Baskar, R., Meera Sheriffa Begum, K. M., & Sundaram, S. (2006). Characterization and reuse of textile effluent treatment plant waste sludge in clay bricks. *University of Chemical Technology and Metallurgy, 41*, 473−478.

Boateng, A. A., & Skeete, D. A. (1990). Incineration of rice hull for use as a cementitious material: the Guyana experience. *Cement and Concrete Research, 20*, 795−802.

Bonapace, C., & Sestini, V. (2007). *Traditional materials and construction technologies used in the Kathmandu Valley*. United Nations Educational, Scientific and Cultural Organization.

Borlini, M. C., Mendonca, J. L. C. C., Conte, R. A., Pinatti, D. G., Vieira, C. M. F., & Monteiro, S. N. (2006). Effect of particle size of an ash from sugarcane bagasse in the properties of red ceramic. *Materials Science Forum, 530−531*, 538−543.

Bozadgiev, L. (1996). Single-fired tile bodies containing carbonate waste. *Tile and Brick International, 12*, 116−117.

Bucci, A., & Mollo, L. (2010). *Regional architecture in the Mediterranean area*. Alinea Editrice, ISBN 9788860552938.

Campbell, H. W. (2000). Sludge management-future issues and trends. *Water Science and Technology, 41*, 1−8.

Chaudhary, D. S., & Jollands, M. C. (2004). Characterization of rice hull ash. *Applied Polymer Science, 93*, 1−8.

Chiang, K. Y., Chou, P. H., Hua, C. R., Chien, K. L., & Cheeseman, C. (2009). Lightweight bricks manufactured from water treatment sludge and rice husks. *Journal of Hazardous Materials, 171*, 76−82.

Chindaprasirt, P., Kanchanda, P., Sathonsaowaphak, A., & Cao, H. T. (2007). Sulfate resistance of blended cements containing fly ash and rice husk ash. *Construction and Building Materials, 21*, 1356−1361.

Choi, N. W., Mori, I., & Ohama, Y. (2006). Development of rice husks-plastics composites for building materials. *Waste Management, 26*, 189−194.

Cultrone, G., Sebastián, E., & De La Torre, M. J. (2005). Mineralogical and physical behavior of solid bricks with additives. *Construction and Building Materials, 19*, 39−48.

Demir, I. (2006). An investigation on the production of construction brick with processed waste tea. *Building and Environment, 41*, 1274−1278.

Demir, I. (2008). Effect of organic residues addition on the technological properties of clay bricks. *Waste Management, 28*, 622−627.

Demir, I., Baspınar, M. S., & Orhan, M. (2005). Utilization of kraft pulp production residues in clay brick production. *Building and Environment, 40*(11), 1533−1537.

Dondi, M., Marsigli, M., & Fabbri, B. (1997). Recycling of industrial and urban wastes in brick production: a review. *Tile and Brick International, 13*, 218−225.

Duchan, V., & Kopar, T. (2001). Sawdust and paper-making sludge as pore forming agents for lightweight clay bricks source. *Industrial Ceramics, 21*, 81−86.

Duggal, S. K. (2008). *Building materials* (3rd revised ed.). New Age International (P) Ltd., Publishers.

Eliche-Quesada, D., Corpas-Iglesias, F. A., Pérez-Villarejo, L., & Iglesias-Godino, F. J. (2012). Recycling of sawdust, spent earth from oil filtration, compost and marble residues for brick manufacturing. *Construction and Building Materials, 34*, 275−284.

Eliche-Quesada, D., Martínez-García, C., Martínez-Cartas, M. L., Cotes-Palomino, M. T., Pérez-Villarejo, L., Cruz-Pérez, N., et al. (2011). The use of different forms of waste in the manufacture of ceramic bricks. *Applied Clay Science, 52*, 270−276.

Faria, K. C. P., Gurgel, R. F., & Holanda, J. N. F. (2010). Characterization of sugarcane bagasse ash for use in ceramic bodies. *Materials Science Forum, 660-661*, 1049−1052.

Faria, K. C. P., Gurgel, R. F., & Holanda, J. N. F. (2012). Recycling of sugarcane bagasse ash waste in the production of clay bricks. *Environmental Management, 101*, 7−12.

Felipe-Sese, M., Eliche-Quesada, D., & Corpas-Iglesias, F. A. (2011). The use of solid residues derived from different industrial activities to obtain calcium silicates for use as insulating construction materials. *Ceramics International, 37*, 3019−3028.

Freire, A. S., & Mota, J. F. (1997). *Potentiality of utilization of marble and granite waste*. Brazil: Quality Rocks Magazine [in Portuguese].

Frías, M., & Villar-Cocina, E. (2007). Influence of calcining temperature on the activation of sugar-cane bagasse: kinetic parameters. *Advances in Cement Research, 19*(3), 109−115.

Ganesan, K., Rajagopal, K., & Thangavel, K. (2007). Evaluation of bagasse ash as supplementary cementitious material. *Cement and Concrete Composites, 29*(6), 515−524.

García, C. M., Quesada, D. E., Villarejo, L. P., Iglesias-Godino, F. J., & Corpas-Iglesias, F. A. (2012). Sludge valorization from wastewater treatment plant to its application on the ceramic industry. *Environmental Management, 95*, 343−348.

Görhan, G., & Şimşek, O. (2013). Porous clay bricks manufactured with rice husks. *Construction and Building Materials, 40*, 390−396.

Hassan, K. M., Fukushi, K., Turikuzzaman, K., & Moniruzzaman, S. M. (2014). Effects of using arsenic-iron sludge wastes in brick making. *Waste Management, 34*, 1072−1078.

Herek, L. C. S., Hori, C. E., Reis, M. H. M., Mora, N. D., Tavares, C. R. G., & Bergamasco, R. (2012). Characterization of ceramic bricks incorporated with textile laundry sludge. *Ceramics International, 38*, 951−959.

Horisawa, S., Sunagawa, M., Tamai, Y., Matsuoka, Y., Tohru Miura, T., & Terazawa, M. (1999). Biodegradation of nonlignocellulosic substances II: physical and chemical properties of sawdust before and after use as artificial soil. *Journal of Wood Science, 45*, 492−497.

Huet R. J. (1982). *Disposal of primary paper mill sludge on sandy cropland soil* (Ph.D. thesis). University of Wisconsin-Madison.

Hu, S., Xiang, J., Sun, L., Xu, M., Qiu, J., & Fu, P. (2008). Characterization of char from rapid pyrolysis of rice husk. *Fuel Processing Technology, 89*, 1096−1105.

Jahagirdar, S. S., Shrihari, S., & Manu, B. (2013). Utilization of textile mill sludge in burnt clay bricks. *Environmental Protection, 3*, 6−13.

Jordán, M. M., Almendro-Candel, M. B., Romero, M., & Rincón, J. M. (2005). Application of sewage sludge in the manufacturing of ceramic tile bodies. *Applied Clay Science, 30*, 219−224.

Jung, J. H., Yoo, J. W., Lee, J. U., & Kim, H. T. (2005). Application of coal wastes to clay bricks and investigation of their physical properties. *Industrial and Engineering Chemistry, 11*, 175−179.

Kadir, A. A., & Maasom, N. (2013). Recycling sugarcane bagasse waste into fired clay brick. *Zero Waste General, 1*, 21−26.

Kadir, A. A., & Mohajerani, A. (2011). Bricks: an excellent building material for recycling wastes−a review. In *Proceeding of the IASTED International conference environmental management and engineering (EME 2011) July 4−6, 2011 Calgary, AB, Canada* (pp. 108−115).

Karaman, S., Gunal, H., & Ersahin, S. (2006). Assessment of clay brick compressive strength using quantitative values of colour components. *Construction and Building Materials, 20*, 348−354.

Karaman, S., Gunal, H., & Ersahin, S. (2008). Quantitative analysis of pumice effect on some physical and mechanical properties of clay bricks. *Applied Science, 8*, 1340−1345.

Kwong, P. C. W., Christopher, Y. H., Chao, J. H., Wang, C. W., & Cheung, G. K. (2007). Co-combustion performance of coal with rice husks and bamboo. *Atmospheric Environment, 41*, 7462−7472.

Liew, A. G., Idris, A., Samad, A., Calvin, A., Wong, H. K., Jaafar, M. S., et al. (2004). Incorporation of sewage sludge in clay brick and its characterization. *Waste Management and Research, 22*, 226−233.

Low, N. M. P., Fazio, P., & Guite, P. (1984). Development of light-weight insulation clay products from the clay-sawdust-glass system. *Ceramics International, 10*, 59−65.

Mansaray, K. G., & Ghaly, A. E. (1998). Physical and thermochemical properties of rice husk. *Energy Sources Part A: Recovery Utilization and Environmental Effects, 19*, 989−1004.

Merino, I., Arévalo, L. F., & Romero, F. (2007). Preparation and characterization of ceramic products by thermal treatment of sewage sludge ashes mixed with different additives. *Waste Management, 27*, 1827−1844.

Milheiro, F. A. C., Ferire, M. N., Silva, A. G. P., & Holanda, J. N. F. (2005). Densification behavior of a red firing Brazilian kaolinitic clay. *Ceramics International, 31*, 757−763.

Monteiro, S. N., Alexandre, J., Margem, J. I., Sánchez, R., & Vieria, C. M. F. (2008). Incorporation of sludge waste from water treatment plant into red ceramic. *Construction and Building Materials, 22*, 1281−1287.

Montero, M. A., Jordan, M. M., Hernandez-Crespo, M. S., & Sanfeliu, T. (2009). The use of sewage sludge and marble residues in the manufacture of ceramic tile bodies. *Applied Clay Science*, 404−408.

Muñoz, P., Juárez, M. C., Morales, M. P., & Mendívil, M. A. (2013). Improving the thermal transmittance of single-brick walls built of clay bricks lightened with paper pulp. *Energy and Building, 59*, 171−180.

Nair, D. G., Fraaij, A., Klaassen, A. A. K., & Kentgens, A. P. M. (2008). A structural investigation relating to the pozzolanic activity of rice husk ashes. *Cement and Concrete Research, 38*(6), 861−869.

Ndazi, B. S., Karlsson, S., Tesha, J. V., & Nyahumwa, C. W. (2007). Chemical and physical modifications of rice husks for use as composite panels. *Composites Part A, 38*, 925−935.

NPCS Board of Consultants & Engineers. (2007). *The complete technology book on bricks, cement and asbestos*. Dehli, India: Niir Project Consultancy Services.

Okunade, E. A. (2008). The effect of wood ash and sawdust admixtures on the engineering properties of a burnt laterite-clay brick. *Journal of Engineering and Applied Science, 8*, 1042−1048.

Pappu, A., Saxena, S., & Asolekar, S. R. (2007). Solid waste generation in India and their recycling potential in building material. *Building and Environment, 42*, 2311−2320.

Payá, J., Monzó, J., Borrachero, M. V., Diaz-Pinzón, L., & Ordónez, L. M. (2002). Sugarcane bagasse ash (SCBA): studies on its properties for reusing in concrete production. *Journal of Chemical Technology and Biotechnology, 77*, 321−325.

Phonphuak, N., & Thiansem, S. (2011). Effects of charcoal on physical and mechanical properties of fired test briqettes. *SciAsia, 37*, 120−124.

Phonphuak, N., & Thiansem, S. (2012). Using charcoal to increase properties and durability of fired test briqettes. *Construction and Building Materials, 29*, 612−618.

Raut, S. P., Sedmake, R., Dhunde, S., Ralegaonkar, R. V., & Mandavgane, S. A. (2012). Reuse of recycle paper mill waste in energy absorbing light weight bricks. *Construction and Building Materials, 27*, 247−251.

Rice Husk Ash Website. (2008). http://www.ricehuskash.com/ Accessed 20.12.13.

Rouf, M. A., & Hossain, M. D. (2003). Effects of using arsenic-iron sludge in brick making. In *Fate of arsenic in the environment, proceedings of the BUET-UNU international symposium, February 5−6, Dhaka, Bangladesh* (pp. 193−208).

Russ, W., Mörtel, H., & Meyer-Pittroff, R. (2005). Application of spent grains to increase porosity in bricks. *Construction and Building Materials, 19*, 117−126.

Saboya, F., Xavier, G. C., & Alexandre, J. (2007). The use of the powder marble by-product to enhance the properties of brick ceramic. *Construction and Building Materials, 21*, 1950−1960.

Schmidt-Reinholz, C. H. (1990). Suggestions for the reduction of bulk density through additives. *Tile and Brick International, 6*, 23−27.

Seminar, I. Z. F. (1994). Brick making raw materials properties, treatment, product quality. Part 1 *Ziegelindustrie International, 2*(11), 779−790.

Senthilkumar, K., Sivakumar, V., & Akilamudhan, P. (2008). Experimental studies on disposal of various industrial solid wastes. *Modern Applied Science, 2*, 128−132.

Shao, Y., Qui, J., & Shah, S. S. (2001). Microstructure of extruded cement bonded fiber board. *Cement and Concrete Research, 31*, 1153−1161.

Saboya, F., Jr, Xavier, G. C., & Alexandre, J. (2007). The use of the powder marble by-product to enhance the properties of brick ceramic. *Construction and Building Materials, 21*, 1950−1960.

Souza, A. E., Teixeira, S. R., Santos, G. T. A., Costa, F. B., & Longo, E. (2011). Reuse of sugarcane bagasse ash (SCBA) to produce ceramic materials. *Environmental Management, 92*, 2774−2780.

Sutcu, M., & Akkurt, S. (2009). The use of recycled paper processing residues in making porous brick with reduced thermal conductivity. *Ceramics International, 35*(7), 2625−2631.

Sutcu, M., & Akkurt, S. (2010). Utilization of recycled paper processing residues and clay of different sources for the production of porous anorthite ceramics. *European Ceramic Society, 30*, 1785−1793.

Sutcu, M., Akkurt, S., Bayramb, A., & Uluca, U. (2012). Production of anorthite refractory insulating firebrick from mixtures of clay and recycled paper waste with sawdust addition. *Ceramics International, 38*, 1033−1041.

Teixeira, S. R., Souza, A. E., Santos, G. T. A., & Peńa, A. F. V. (2008). Sugarcane bagasse ash as a potential quartz replacement in red ceramic. *American Ceramic Society, 91*, 1883−1887.

The Mason Contractors Association of America. (2012). *History of masonry*. http://www.masoncontractors.org/aboutmasonry/historyofmasonry Accessed on 20/12/2013.

Vieira, C. M. F., Soares, T. M., Sánchez, R., & Monteiro, S. N. (2004). Incorporation of granite waste in red ceramics. *Materials Science Engineering, 373*, 115−121.

Vincenzini, P., & Fiori, C. (1976). Expansion characteristics of some Italian brick clays by moisture re-hydration. *La Ceramic (Florence), 19*, 19−27.

Ward-Harvey. (2008). *Fundamental building materials* (4th ed.). WHO Presentation Services NSW.

Weng, C. H., Lin, D. F., & Chiang, P. C. (2003). Utilization of sludge as brick materials. *Advances in Environmental Research, 7*, 679−685.

Zani, A., Tenaglia, A., & Panigada, A. (1990). Reuse of paper making sludge in brick production. *Ziegelindustries International, 12*, 682−690.

Types of waste, properties and durability of toxic waste-based fired masonry bricks

7

M. Coronado, T. Blanco, N. Quijorna, R. Alonso-Santurde, A. Andrés
Universidad de Cantabria, Cantabria, Spain

7.1 Introduction

Masonry product construction industry traditionally has used natural raw materials such as clay and sand from mineral extraction to manufacture construction products. However, natural resources are consumed more rapidly than the natural system can replace them, causing their scarcity and worries about the security of raw materials supply. On the other hand, the environmental impacts associated with the extraction and processing of raw materials is creating an ecological global unbalance that requires action to be taken.

Resources efficiency is essential for sustainable growth. One of the flagship initiatives under the Europe 2020 strategy is "Exploiting synergies and addressing trade-offs" (EU, 2011). In this way, increasing recycling rate will reduce the pressure on demand for primary resources, energy consumption and greenhouse emissions as well as avoiding the wastage of valuable materials. The manufacture of waste-based fired masonry bricks is a practical example of industrial symbiosis (Quijorna and Andrés, 2013).

In order to achieve a more sustainable waste and resources management, new philosophies and practices have been implemented. Eco-innovation aims to reduce the use of natural resources and the release of harmful substances across the whole life cycle. This helps to enable an evolution through a combination of technological and non-technological changes that can yield substantial environmental improvements. The methods for introducing technological changes such as cleaner production, pollutant control and eco-efficiency are focused on products and processes modification or redesign. Non-technological changes are based on life cycle analysis, closed loop cycles and industrial ecology, which imply modification or redesign of organizations and institutions (Eco-innovation Observatory, 2010). In this way industrial ecology conceptualizes industry as a man-made ecosystem that operates in a similar way to natural ecosystems, where the waste or by-product of one process is used as an input into another process. Industrial ecology interacts with natural ecosystems and attempts to move from linear to cyclical or closed loop systems.

There are a wide variety of solid wastes susceptible to becoming new resources in the manufacturing of construction products. Ceramic processes designed to obtain useful products for different applications such as bricks, tiles or roofing tiles are

Eco-efficient Masonry Bricks and Blocks. http://dx.doi.org/10.1016/B978-1-78242-305-8.00007-3

considered as good potential receptors for the recycling of waste. This chapter presents an updated review of the available literature on the incorporation of different solid wastes as secondary resources in the ceramic industry since the year 2000. The wastes have been classified according to their specific nature and origin (European Waste Catalogue) as well as the different roles that the alternative raw materials can play in the ceramic process.

Due to the industrial origin of the waste, its incorporation into ceramic processes should be assessed from an integral point of view, the emissions during firing, the technological and environmental properties, as well as the durability of these new materials. Moreover, this takes into account that the Construction Products Regulation (CPR), Life Cycle Assessment (LCA) and the Environmental Product Declaration (EPD) are the basic requirements on sustainability that define relevant and specific information about the product and the environmental associated impacts throughout its entire life cycle.

7.2 Industrial waste classification used in fired masonry bricks

The basis for this overview was a classification of the wastes used in the ceramic industry according to two criteria: (1) the European Waste Catalogue (EWC) that categorizses them, taking into account what they are and how they were produced (EWC, 2002) and (2) their behavior or role in the ceramic process, as well as the main effects caused to the ceramic product.

7.2.1 According to the European Waste Catalogue

The EWC (2002) is a hierarchical list of 20 codes of waste descriptions established by Commission Decision 2000/532/EC which classifies and categorizes waste materials (Table 7.1). Figure 7.1 shows the classification of the studied wastes into these 20 different codes. The studies analyzed in this review usually mix clay with one or more wastes from different EWC codes to obtain ceramic products. However, the incorporation of some wastes corresponding to EWC codes of wastes 08, 09, 12, 14 and 15 into ceramic products is not usually studied. Ceramic products containing wastes that belong to different wastes have been classified according to the EWC code of the waste introduced in higher proportion or to the waste that affects most properties of the product.

Fifty percent of the studied papers introduce residues classified under the EWC codes 01, 10 and 19. Wastes classified in the EWC code 01 are wastes resulting from exploration, mining, quarrying and physical and chemical treatment of minerals. The main source processes generating this type of waste are physical and chemical processing of ornamental rocks, mining and quarrying works and alumina production. Wastes belonging to the EWC code 10 are wastes from thermal processes: power stations and other combustion plants (except those classified as EWC 19), iron and steel

Table 7.1 European waste catalogue and hazardous waste list

Chapters of the list			
01	Wastes resulting from exploration, mining, quarrying, physical and chemical treatment of minerals.	11	Wastes from chemical surface treatment and coating of metals and other materials; non-ferrous hydrometallurgy.
02	Wastes from agriculture, horticulture, aquaculture, forestry, hunting and fishing, food preparation and processing.	12	Wastes from shaping and physical and mechanical surface treatment of metals and plastics.
03	Wastes from wood processing and the production of panels and furniture, pulp, paper and cardboard.	13	Oil wastes and wastes of liquid fuels (except edible oils, 05 and 12).
04	Wastes from the leather, fur and textile industries.	14	Waste organic solvents, refrigerants and propellants (except 07 and 08).
05	Wastes from petroleum refining, natural gas purification and pyrolytic treatment of coal.	15	Waste packaging; absorbents, wiping cloths, filter materials and protective clothing not otherwise specified.
06	Wastes from inorganic chemical processes.	16	Wastes not otherwise specified in the list.
07	Wastes from organic chemical processes.	17	Construction and demolition wastes (including excavated soil from contaminated sites).
08	Wastes from the manufacture, formulation, supply and use (MFSU) of coatings (paints, varnishes and vitreous enamels), sealants and printing inks.	18	Wastes from human or animal health care and/or related research (except kitchen and restaurant wastes not arising from immediate health care).

Continued

Table 7.1 Continued

Chapters of the list			
09	Wastes from the photographic industry.	19	Wastes from waste management facilities, off-site waste water treatment plants and the preparation of water intended for human consumption and water for industrial use.
10	Wastes from thermal processes.	20	Municipal wastes (household waste and similar commercial, industrial and institutional wastes) including separately collected fractions.

Source: EWC, 2002.

industry and aluminum, lead and zinc thermal metallurgy. In this category are included, among others, coal or biomass fly ash, metallic sludge and slag and foundry sand. Wastes classified in the EWC code 19 are wastes from waste management facilities, off-site wastewater treatment plants and the preparation of water intended for human consumption and water for industrial use such as sewage sludge or incinerated sewage sludge ash. In addition, a high percentage of the wastes introduced into ceramics comes from agriculture (EWC 02) and from construction and demolition waste including excavated soil from polluted sites such as waste bricks or river and marine sediments (EWC 17).

7.2.2 Roles in the ceramic matrix

Another more general classification based not only on the specific nature and origin of the waste but also on the different roles that the alternative raw materials can play in the brick-making process is proposed (Petavratzi & Barton, 2007).

Figure 7.2 shows seven different categories of roles (A = fluxing agents, B = fillers, C = clay substitutes, D = body fuels, E = pore formers, F = property affecting wastes) that the waste could play in the ceramic matrix during the firing process. A single alternative material may have different roles in the firing step. For instance, fly ash with high content of carbonaceous matter and alkaline compounds may act as both body fuel and fluxing agent, forming liquid phases at relative low temperatures, contributing to the sintering consolidation. On the other hand, fly ash with low carbon content and negligible content of alkaline compounds may act as clay

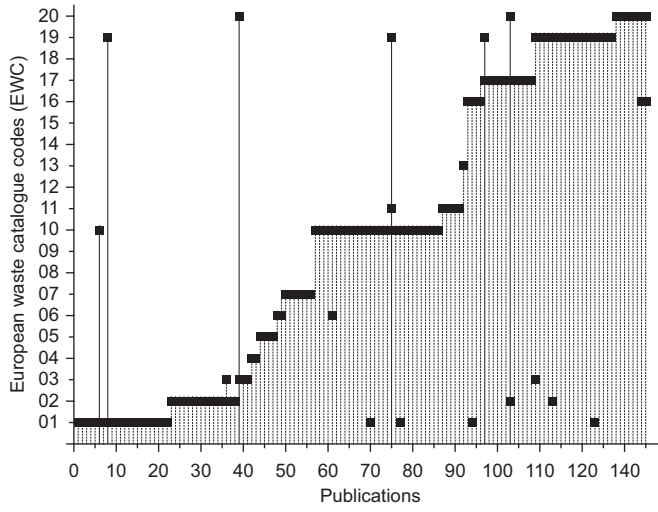

1 (Acchar et al., 2006)
2 (Campos et al., 2007)
3 (Das et al., 2000)
4 (Dhanapandian and Shanthi, 2009)
5 (Ducman et al., 2005)
6 (El-Mahllawy, 2008)
7 (He et al., 2012a)
8 (Junkes et al., 2011)
9 (Lemeshev et al., 2004)
10 (Menezes et al., 2002)
11 (Menezes et al., 2005)
12 (Menezes et al., 2008)
13 (Menezes et al., 2009)
14 (Monteiro et al., 2004)
15 (Moreira et al., 2008)
16 (Ozkan et al., 2010)
17 (Ramadan et al., 2001)
18 (Saboya et al., 2007)
19 (Segadaes et al., 2005)
20 (Sviderskii et al., 2007)
21 (Torres et al., 2007)
22 (Vieira, 2007)
23 (Acchar et al., 2013)
24 (Aripin et al., 2011)
25 (Barbieri et al., 2013)
26 (Chan, 2011)
27 (De la casa et al, 2009)
28 (Demir, 2006)
29 (Demir, 2008)
30 (Demir et al., 2005)
31 (Eliche quesada et al., 2011)
32 (Ibanga and Ahmed, 2007)
33 (La rubia, 2010)
34 (Martínez et al., 2012)
35 (Mekki et al., 2008)
36 (Mothé and Ambrósio, 2007)
37 (Teixeira et al., 2008)
38 (Valenciene, 2011)
39 (Maschio et al., 2009)
40 (Shukla et al., 2010)
41 (Suctu and Akkurt, 2009)
42 (Basegio et al., 2002)
43 (Herek et al., 2012)
44 (Acchar et al., 2009)
45 (Monteiro et al., 2006)
46 (Pinheiro and Holanda, 2009)
47 (Souza et al., 2003)
48 (Baspinar et al., 2010a)
49 (Dondi et al., 2010)
50 (Abali et al., 2007)
51 (Christogerou et al., 2009)
52 (Kavas, 2006)
53 (Kurama et al., 2006)
54 (Kurama et al., 2007)
55 (Uslu and Arol, 2004)
56 (Vichaphud et al., 2012)
57 (Acosta et al., 2002)
58 (Alonso-Santurde et al., 2010)
59 (Alonso-Santurde et al., 2011)
60 (Bantsis et al., 2011)
61 (Baspinar et al., 2010b)
62 (Cultrone and Sebastián, 2009)
63 (Dondi et al, 2002a)
64 (Dondi et al, 2002b)
65 (Faria et al., 2006)
66 (Faria et al, 2011)
67 (Fernández-Pereira et al., 2011)
68 (Furlani et al., 2010)
69 (García-Ubaque et al., 2007)
70 (Karamanova et al., 2011)
71 (Koukouzas et al, 2011)
72 (Kute and Deodhar, 2002)
73 (Lingling et al., 2005)
74 (Little et al., 2008)
75 (Martelon et al., 2000)
76 (Monteiro et al., 2008b)
77 (Olgun et al., 2005)
78 (Oliveira et al., 2004)
79 (Ozdemir and Yilmaz, 2007)
80 (Pérez-Villarejo et al., 2010)
81 (Quaranta et al., 2010)
82 (Quijorna et al., 2011)
83 (Quijorna et al., 2012)
84 (Rego, 2009)
85 (Shih et al., 2004)
86 (Zimmer and Bergmann, 2007)
87 (Corpas iglesias et al., 2011)
88 (Couto et al., 2001)
89 (Dominguez et al., 2011)
90 (Sikalidis and Zaspalis, 2007)
91 (Singh et al., 2007)
92 (Eliche Quesada et al., 2012)
93 (Adie and Osibanjo, 2013)
94 (Adylov et al., 2010)
95 (Dondi et al., 2009)
96 (Zhu et al., 2014)
97 (Baruzo et al., 2006)
98 (Blanco et al., 2005)
99 (Demir and Orham, 2003)
100 (Hammer and Karius, 2002)
101 (Karius and Hammer, 2001)
102 (Lafhaf et al., 2008)
103 (Malaskiene et al., 2011)
104 (Romero et al., 2008)
105 (Romero et al., 2009)
106 (Samara et al., 2008)
107 (Vieira et al., 2004)
108 (Vieira and Monteiro, 2007)
109 (Anderson et al., 2002)
110 (Arsenovic et al., 2012)
111 (Cusido et al., 2003)
112 (Cusido and Soriano, 2011)
113 (Devant et al., 2011)
114 (Haiying et al., 2011)
115 (Jordan et al., 2005)
116 (Kizinievic et al., 2013)
117 (Lin and Weng, 2001)
118 (Lin et al., 2006)
119 (Martínez-García et al., 2012)
120 (Merino et al., 2007)
121 (Monteiro et al., 2008b)
122 (Montero et al., 2009)
123 (Shin and Kim, 2009)
124 (Souza et al., 2008)
125 (Szoke and Muntean, 2009)
126 (Teixeira et al., 2011)
127 (Weng et al., 2003)
128 (Aeslina and Mohajerani, 2012)
129 (Chidiac and Federico, 2007)
130 (Kadir and Mohajerani, 2012)
131 (Kadir and Mohajerani, 2011)
132 (Loryuenyong et al., 2009)
133 (Sarani and Kadir, 2013)
134 (Vu et al., 2001a)
135 (Vu et al., 2001b)

Figure 7.1 Industrial wastes used in the manufacture of fired masonry bricks, classified according to the European Waste Catalogue and hazardous waste list (EWC) (EWC, 2002).

substitute or as a filler when these ashes are predominantly composed of quartz (Vieira & Monteiro, 2009).

The role A of **fluxing agents** is composed of materials with a relatively high amount of alkaline oxides, mainly K_2O and Na_2O, which in reaction with silica and alumina promote liquid phase formation at relatively low firing temperatures and, thus, contribute to the sintering consolidation and densification of the ceramic structure. Among the wastes included in this category are glassy wastes, boron-containing

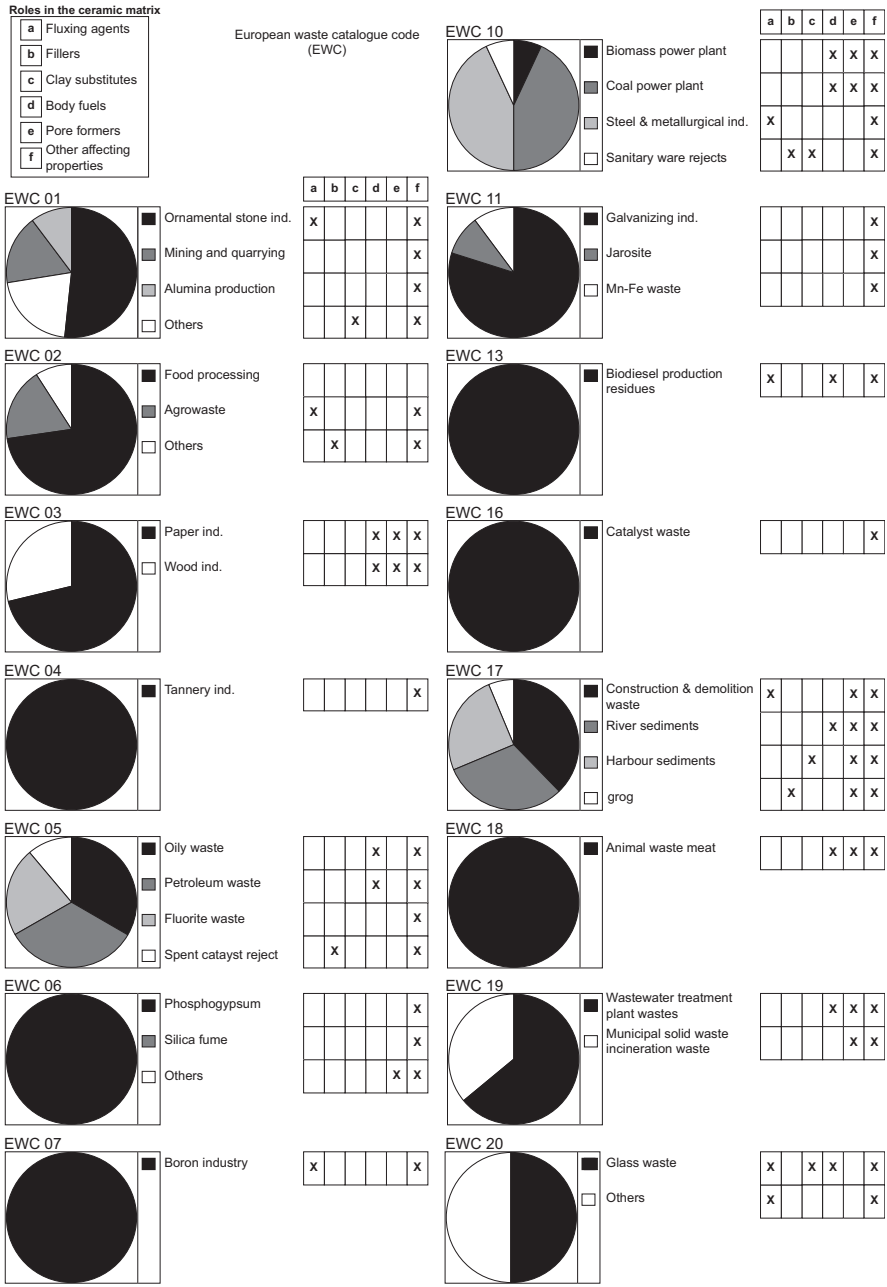

Figure 7.2 Industrial wastes classification according to the role played in the ceramic matrix.

residues, Waelz slag, steel slag, bone ash, ash from the gasification of coal and sludge from the ornamental stone industry. For instance, granite is considered a flux material due to its large amount of alkaline oxides. These oxides derive from feldspars and micaceous minerals that are common constituents of granite rock.

The role B of **fillers** includes wastes which can partially substitute the effect caused by the sand in the vitrification process; this means the dissolution of the inorganic waste material in the glassy phase that occurs during the sintering of clay or the reaction with clay minerals to form new mineral phases in the fired clay structure. Among the wastes possibly found in this category are sewage sludge, ash generated in the incineration of sewage sludge, steel dust, steel refining sludge, foundry sand and spent catalyst rejects.

The role C of **clay substitutes** is made up of waste with a certain amount of clay minerals that confer the plastic behavior to the ceramic matrix. Among the wastes included in this category are municipal solid waste incineration slag, grog or chamotte, water treatment residues and fly ash from the paper industry. The role D of **body fuel** agents contains wastes including combustible carbon-containing matter, which has a relative heating power, and is therefore desirable for saving energy. Among the wastes included in this category are oily residues, blast furnace sludge which still has a significant amount of coke, sludge from the paper industry, ash with high carbon content, sewage sludge and sawdust.

The role E of **pore formers** includes wastes that usually possess a high content of organic matter that burn out to form pores. It is important to observe that the inclusion of alternative materials in the ceramic process normally changes the properties of the fired product with substances that modify the ceramic behaviour and cannot be included in the previous role categories. Therefore, an additional role **F** of **property affecting** wastes has been included that contains all the summarized wastes.

The most common roles played by wastes in the ceramic matrix are role E of pore formers, role A of fluxing agents and role D of body fuels. Porosity is a desirable property to obtain acoustic and thermal isolating products, while fluxing agents and body fuels promote energy savings by reducing considerably the firing temperature of the bricks. This leads not only to a much lower heat requirement as compared to the traditional process but also to higher economic profits.

7.3 Comparison between clay minerals and the alternative raw materials

The great majority of natural raw materials for the ceramic industry mainly contain clay minerals, quartz, feldspar, carbonates and iron. This composition is responsible for the distinctive roles that materials play during ceramic processing, as previously described in Section 7.2.2, and it is also responsible for the final properties of the ceramic products. In addition, ceramic materials also contain minor amounts of components such as iron oxides that, given the long firing cycles used, might act also as fluxing agents during the firing process affecting the ceramic process (Segadães, 2006).

Taking into account the major components (expressed as oxides) and their roles during firing, the ceramic industry uses ternary phase diagrams to interpret the firing behavior and property development of the products. The joint fluxing oxides (K_2O, Na_2O, CaO, MgO and Fe_2O_3) are used as "equivalent CaO" content in the $SiO_2-Al_2O_3-CaO$ phase diagram. These ternary diagrams are equilateral triangles that represent the chemical composition of ceramics. In these diagrams, the composition axes run from each vertex (pure component/s, weight fraction = 1) to the opposite side (mixtures without the component from the opposite vertex, weight fraction = 0). Phase diagrams are extremely useful to obtain information of ceramic processes. For a given temperature and composition, it is possible to determine the phases that are present, the compositions of the phases and the relative fractions of these phases, which are responsible for the ultimate properties of the ceramic products (Segadães, 2006). It is assumed that waste materials that might be easily used as alternative ceramic raw materials might be those whose compositions are not so far apart from the natural conventional raw materials composition (Elías, 2009).

In order to assess the potential incorporation of different types of waste into ceramic products and their compatibility with the clays, the composition of the waste from the codes most frequently used in ceramics, EWC 01, 10 and 19, have been located in the ceramic ternary phase diagram according to their relevant components: SiO_2 as inert, Al_2O_3 as plastic and K_2O, Na_2O, CaO, MgO and Fe_2O_3 as "equivalent CaO" fluxing components. Figure 7.3 shows six triangular diagrams. In the three diagrams on the left side is illustrated the compositions of wastes from mining exploration (EWC 01) (Figure 7.3(a)), thermal processes (EWC 10) (Figure 7.3(b)) and waste management facilities (EWC 19) (Figure 7.3(c)), while the three diagrams on the right side show the mixtures of clay and these wastes used in the studied publications.

Wastes from **mining exploration activities (EWC 01)** (Figure 7.3(a); left side) show a similar chemical composition as the natural clays used in the ceramic industry. They contain major components expressed as oxides, silica (SiO_2), alumina (Al_2O_3) and lime CaO, as in the great majority of ceramic products. This is the reason why the composition of these wastes lies in or close to the restricted area of compositions of the clays used in the manufacturing of ceramic products. Wastes located in this area are considered compatible alternative ceramic materials that can successfully be upgraded in high amounts in ceramic formulations playing a similar role to the clays during the ceramic processing. As expected, mixes containing these compatible wastes and natural clay are also located in the restricted area (Figure 7.3(a); right side).

Chemical composition of **waste from thermal treatments (EWC 10)** (Figure 7.3(b); left side) **and from waste management facilities (EWC 19)** (Figure 7.3(c); left side) depends on the kind of thermal industries involved, biomass and carbon power plants or metal industries, and the source of the waste that has been managed in the waste management facility, respectively. Due to the different origins compared to the clays, their composition might be different from the composition of the traditional clays. This is especially true in the case of metallurgical slag and foundry sand belonging both to EWC code 10 and in the case of sludge from industrial wastewater facilities (EWC 19). For instance, metallurgical wastes and foundry sand are located far from the restricted area established for the clays. Due to the high fluxing

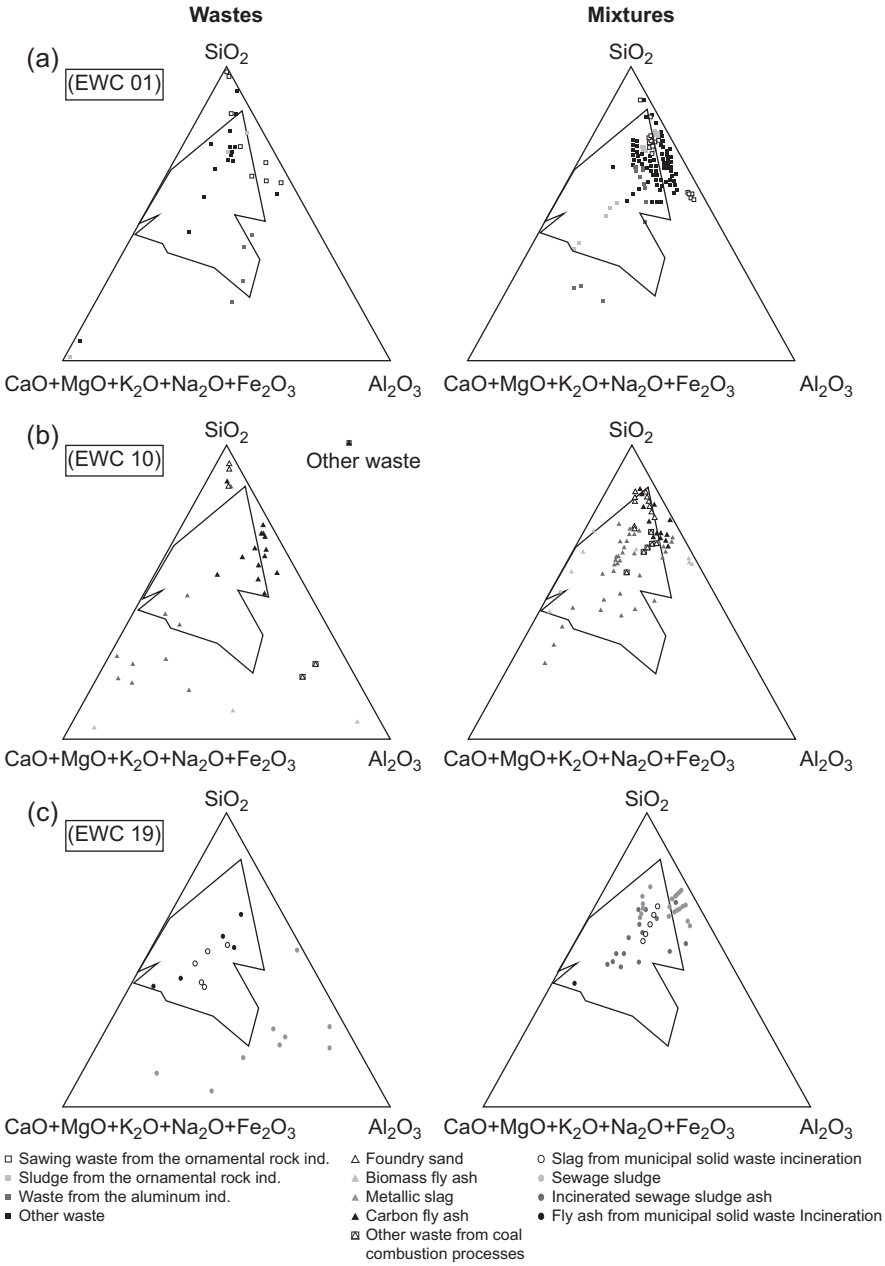

Figure 7.3 Location of the wastes and waste-based mixtures from EWC: (a) 01, (b) 10 and (c) 19, in the ternary phase diagram according to the relevant components SiO_2-Al_2O_3-(K_2O, Na_2O, CaO, MgO and Fe_2O_3) in ceramics.

oxide contents in metallurgical wastes, the compositions are located close to the SiO_2-CaO side of the triangle and to the fluxing vertex. In the same way, the high silica content of the foundry sand, higher than 70% in most of the cases, almost places this waste in the silica vertex.

Despite the differences in the chemical composition of some waste from thermal processes and waste management facilities and the clays, the composition of mixtures containing these wastes fall within or close to the restricted area for the natural clays. This means that these wastes can be used as alternative materials in ceramic processes up to certain proportions in the mixtures. In this case, the relative amount of waste in the mixture plays an important role that might affect the final properties due to the compositional differences between the clays and these wastes.

7.4 Firing conditions used in the manufacture of waste-based fired bricks

The firing process is the key step in the manufacturing of ceramic products because it controls their properties. The materials experience irreversible structural changes reaching the proper ceramic structure that is responsible for the final properties of the product. Depending on the initial materials and the desired product, the firing conditions, firing temperature, firing rate and soaking time in the kiln are different. The temperature at which the liquid phase is created varies according to the composition and mineralogy of the clay. The Reference Document on Best Available Techniques in the ceramic manufacturing industry (EU, 2007) establishes that vitrification usually starts at about 900 °C and is completed at about 1050 °C. However, fluxing agents such as iron oxides, lime and alkalis lead to lower initial melting temperatures, promoting the amount of liquid phase formed at any given temperature contributing to a lower consumption of energy. This is particularly true when the clays are calcareous in nature.

Tables 7.2–7.4 show the firing conditions used in the studied works incorporating waste from the EWC codes 01, 10 and 19. Most of these works have studied the behavior of mixtures containing different amounts of clay and waste using constant heating rates in electric laboratory kilns up to temperatures between 800 and 1200 °C. In some of these publications, the authors select the amount of waste to be introduced in the process and study the effect of the firing conditions on the properties of the products. Some works assess the effect of the amount of waste added at a fixed temperature, while others vary not only the temperature and/or the firing conditions but also the proportion of waste in the mixtures. There are works that simulate the industrial firing cycle on a laboratory scale, while others are carried out on a pilot or even at an industrial scale.

7.4.1 Gaseous emissions during the firing process

The firing process inevitably leads to the release of gaseous compounds, mainly derived from the raw materials due to the decomposition of minerals present in these

Table 7.2 Firing conditions used during firing products containing wastes from exploration, mining, quarrying, physical and chemical treatment of minerals (EWC 01)

Source	Waste	% Waste	Furnace	Firing temperature	Firing rate	Soak time	Reference
Ornamental stone industry	Granite waste	≤30%	Laboratory kiln	920 °C	1 °C/h	n/a	Ducman, Kopar, and Sanchez (2005)
		20–60%	Laboratory kiln	800–1200 °C	9 °C/min	2 h	Menezes, Ferreira, Neves, and Ferreira (2002)
			Pilot kiln	1150–1200 °C		30 min	
		20–60%	Laboratory and industrial kiln	1150–1200 °C	9 °C/min	30 min	Menezes, Ferreira, Neves, Lira, and Ferreira (2005)
		≤40%	Laboratory kiln	850–1100 °C	4 °C/min	3 h	Monteiro, Peçanha, and Vieira (2004)
		≤40%	Hoffman ind. Kiln	970 °C	n/a	6 h	Vieira and Monteiro (2004)
	1. Granite waste **2.** Kaolin waste	**1.** ≤ 50% **2.** ≤ 50%	Laboratory kiln	1000–1150 °C	36–39 °C/min	5 min	Campos et al. (2007)
		1. ≤100% **2.** ≤100%	Laboratory kiln	1000–1150 °C	36 °C/min	5 min	Menezes et al. (2008)
		1. 25–35% **2.** 10–38%	Laboratory kiln	1000–1150 °C 1180–1240 °C	36 °C/min 38 °C/min	5 min	Menezes et al. (2009)
	1. Kaolin waste	**1.** 50% **2.** 10–40%	Laboratory kiln	1100–1175 °C	5 °C/min	4 h	El-Mahllawy (2008)

Continued

Table 7.2 Continued

Source	Waste	% Waste	Furnace	Firing temperature	Firing rate	Soak time	Reference
	2. Granite waste **3.** Blast furnace slag (EWC 10)	**3.** 10–40%					
	Granite and marble rejects	30%	Laboratory kiln	950–1100 °C	5 °C/min	2 h	Acchar, Vieira, and Hotza (2006)
		≤50%	Laboratory kiln	500–900 °C	10 °C/min	2 h	Dhanapandian and Shanthi (2009)
		≤30%	Laboratory kiln	1100–1150 °C	8 °C/min	2 h	Segadaes et al. (2005)
	1. Granite sludge **2.** Quartzite sludge	**1.** 35–70% **2.** 35–70%	Laboratory kiln	1100–1200 °C	n/a	1 h	Torres et al. (2007)
	Marble waste	≤20%	Laboratory kiln	750–950 °C	5 °C/min	n/a	Saboya, Xavier, and Alexandre (2007)
		15–35%	Laboratory kiln	975–1050 °C	n/a	n/a	Montero, Jordán, Hernández-Crespo, and Sanfeliu (2009)
	Powder rock	≤20%	Laboratory kiln	850–1150 °C	n/a	2 h	Moreira, Manhães, and Holanda (2008)

Quarrying and mining	Coal-mining waste	20–50%	Laboratory kiln	950 °C	n/a	2 h	Lemeshev, Gubin, Savelev, Tumanov, and Lemeshev (2004)
	Clay waste	5–20%	Laboratory kiln	1140–1200 °C	n/a	n/a	Özkan, Çolak, and Oyman (2010)
	Iron ore tailing waste	30–50%	Laboratory kiln	1060–1200 °C	10 °C/min	n/a	Das, Kumar, and Ramachandrarao (2000)
	Residual clay	40–80%	Laboratory kiln	950 °C	n/a	4 h	Ramadan, Saleh, Taha, and Moharam (2001)
	1. Mineral wastes **2.** Sewage sludge (EWC 19)	**1.** 5–65% **2.** 10–65%	Laboratory kiln	1100–1150 °C	5 °C/min	40 min	Junkes, Carvalho, Segadães, and Hotza (2011)
Aluminum industry	Red mud	10–80%	High temperature box resistance furnace	1000–1100 °C	2.5 °C/min	2 h	He et al. (2012)
	1. Red mud **2.** Mining waste	**1.** 38–75% **2.** 15–38%	n/a	1150–1200 °C	n/a	n/a	Sviderskii, Strashnenko, and Chernyak (2007)

Table 7.3 Firing conditions used during firing products containing wastes from thermal processes: power stations and other combustion plants, iron and steel industry and aluminum, lead and zinc thermal metallurgy (EWC 10)

Source	Waste	% Waste	Furnace	Firing temperature	Firing rate	Soak time	Reference
Biomass thermal power plant	Fly ash	≤50%	Laboratory kiln	950 °C	10 °C/min	n/a	Pérez-Villarejo et al. (2012)
	Gasification ashes	15−20%	Pilot-scale kiln (electric)	1000−1075 °C	1−3 °C/min 3−4 °C/min	4 h	Fernández-Pereira et al. (2011)
Coal power plant	Fly ash	85−90%	Laboratory kiln	800−1000 °C	3 °C/min	1 h	Baspinar, Kahraman, et al. (2010)
		≤15%	Laboratory kiln	800−1000 °C	n/a	n/a	Cultrone and Sebastián (2009)
		1.5−6%	Laboratory kiln	750−890 °C	n/a	3−5 h	Dondi et al. (2002a) Dondi et al. (2002b)
		≤20%	Pilot-scale kiln	1050 °C	4.5 °C/min	15 min	Koukouzas et al. (2011)
		≤60%	Laboratory kiln	850−1000 °C	n/a	n/a	Kute and Deodhar (2002)
		≤80%	Laboratory kiln	1000 °C	0.8−1.6 °C/h	8 h	Lingling, Wei, Tao, and Nanru (2005)

		10–50%	Laboratory kiln	850–1150 °C	5 °C/min	2 h	Monteiro, Lima, et al. (2008)
		25–40%	Industrial kiln	950–1050 °C	n/a	n/a	Rego, 2009
		20–80%	Laboratory kiln	1125–1200 °C	150 °C/h	6 min	Zimmer and Bergmann (2007)
	1. Fly ash **2.** Tincal ore waste	**1.** ≤10% **2.** ≤10%	Refractory roller furnace	1020 °C	n/a	34 min	Olgun, Erdogan, Ayhan, and Zeybek (2005)
	1. Fly ash **2.** Metal finishing waste (EWC 11)	**1.** ≥90% **2.** ≤10%	Laboratory kiln	1000–1250 °C	20 °C/min	1 h	Little, Adell, Boccaccini, and Cheeseman (2008)
Metallurgical and steel industry	Foundry sand	Green or core sand ≤50%	Industrial kiln	1020–1030 °C	1.4 °C/min	3.5 h	Alonso-Santurde, Coz, Quijorna, Viguri, and Andrés (2010)
		≤50%	Laboratory kiln	800–900 °C	1.6 °C/min	4 h	Alonso-Santurde et al. (2011)
			Industrial kiln	850 °C	n/a	n/a	
		10–50%	Laboratory kiln	n/a	n/a	n/a	Quaranta, Lalla, Caligaris, Boccaccini, and Vieira (2010)

Continued

Table 7.3 Continued

Source	Waste	% Waste	Furnace	Firing temperature	Firing rate	Soak time	Reference
	Waste olivine powders (foundry industry)	20–100%	Laboratory kiln	1100–1350 °C	10 °C/min	1 h	Furlani, Aneggi, and Maschio (2013)
	Blast furnace slag	30–70%	Laboratory kiln	1200–1220 °C	10 °C/min	30 min	Karamanova, Avdeev, and Karamanov (2011)
		≤100%	Laboratory kiln	1150–1200 °C	n/a	1 h	Ozdemir and Yilmaz (2007)
	Steel slag	≤20%	Box kiln	800–1000 °C	n/a	4 h	Bantsis, Sikalidis, Betsiou, Yioultsis, and Bourliva (2011)
		5–10%	Laboratory kiln	1100 °C	2–4 °C	n/a	Faria et al. (2012)
		5–30%	Laboratory kiln	800–1100 °C	2–3 °C/min	6 h	Shih, Wu, and Chiang (2004)
		20–30%	Industrial kiln	850–930 °C	Ind. Process	3.5 h	Quijorna, Miguel, and Andrés (2011)
		20–40%	Industrial kiln	850 °C	0.85 °C/min	n/a	Quijorna, Coz, and Andrés (2012)
	Siderurgical waste	≤3%	Industrial kiln	950 °C	0.85 °C/min	n/a	Oliveira and Holanda (2004)

Ceramic manufacturing	**1.** Sanitary ware sludge **2.** Anodizing sludge (EWC 11) **3.** Glass waste (EWC 19)	**1.** 50% **2.** 25% **3.** 25%	Laboratory kiln	1100−1300 °C	5 °C/min	5 h	Martelon, Jarrige, Ribeiro, Ferreira, and Labrincha (2000)
	1. Sanitary ware waste **2.** Steel slag	**1.** 30% **2.** 5−20%	Laboratory kiln	1100 °C	2−4 °C/min	n/a	Faria (2011)

materials, but fuels, if used, also contribute to gaseous pollutants. The chemical and mineralogical composition, as well as the specific firing conditions, firing temperature, time and rate, during the ceramic process play important roles in the emission of atmospheric pollutants. In general, increasing the temperature promotes an increase in the release of contaminants to the atmosphere, while faster firing cycles generally result in reduced emissions.

The Integrated Pollution Prevention and Control Directive (IPPC) (IPPC, 2007) and the reference document on best available techniques in the ceramic manufacturing industry (EU, 2007) establish the pollutants to be assessed in ceramic processes: fluorine, chlorine, sulfur and nitrogen oxides, carbon monoxide and dioxide, volatile organic compounds (VOC), metals and particulate matter. In addition, the document on best available techniques in the ceramic manufacturing industry also determines the range of temperature over which emissions of pollutants are released during firing (Figure 7.4).

The temperature at which these emissions occur depends on the mineral phases containing the pollutant and other phases that contain compounds that may affect emissions. Fluorine emissions generally depend primarily on the firing temperature and, to a lesser extent, on its content in the raw material, which at the same time is a function of mineralogy (González, Galán, & Miras, 2006). In the ceramic industry, the emissions of fluorine are observed at two main intervals of temperature, the first one at about 600 °C due to the clay mineral de-hydroxylation and the second one at higher temperatures (>900 °C) from the decomposition of fluorite (CaF_2) formed by the chemical reaction of the fluorine released during the clay mineral de-hydroxylation with the CaO liberated from the decomposition of carbonates (Eqns (7.1) and (7.2)).

$$CaCO_3 \rightarrow CaO + CO_2 \tag{7.1}$$

$$CaO + 2HF \rightarrow CaF_2 + H_2O \tag{7.2}$$

Sulfur emissions are conditioned by the mineralogy and the possible reactions that take place during firing that form stable compounds, avoiding the emissions up to certain temperatures. When mixtures contain high amounts of calcite and sulfur, anhydrite and/or efflorescence in the fired product can be formed during firing, and there will be no emissions, at least none of those that depend on the raw materials. The emission of sulfur is derived from the decomposition of pyrite and organic matter at low temperatures (~400−550 °C) and gypsum and anhydrite at higher temperature (~1200 °C). Anhydrite ($CaSO_4$) is formed, as shown in Eqn (7.3), under oxidizing conditions by reaction of CaO evolved from the dissociation of $CaCO_3$ (Eqn (7.1)) and the SO_2 produced from the decomposition of sulfur containing compounds.

$$SO_2 + {}^1\!/_2\, O_2 + CaO \rightarrow CaSO_4 \tag{7.3}$$

The emission of chlorine at low temperature is caused by the decomposition of micas, halite and organic matter, while at temperatures above 850 °C, the

Table 7.4 Firing conditions used during firing masonry bricks containing wastes from waste management facilities, off-site waste water treatment plants and the preparation of water intended for human consumption and water for industrial use (EWC 19)

Source	Waste	% Waste	Furnace	Firing temperature	Firing rate	Soak time	Reference
Wastewater treatment plant	Sewage sludge	≤15%	Propane kiln	1000 °C	2.6 °C/h	3 h	Cusidó, Cremades, and González (2003)
		15%	Propane lab. kiln	1050 °C	Standard heating cycle	1 h	Cusidó and Soriano (2011)
		≤24%	Propane kiln	980 °C	2.6 °C/min	3 h	Devant, Cusidó, and Soriano (2011)
		≤10%	Laboratory kiln	Standards cycle for porous materials			Jordán, Almendro-Candel, Romero and Rincón (2005)
		5–40%	Laboratory kiln	1000–1050 °C	n/a	4 h	Kizinievic, Žurauskiene, Kizinievic, and Žurauskas (2013)
		1–15%	Laboratory kiln	950 °C	10 °C/min	n/a	Martínez-García, Eliche-Quesada, Pérez-Villarejo, Iglesias-Godino, and Corpas-Iglesias (2012)

Continued

Table 7.4 Continued

Source	Waste	% Waste	Furnace	Firing temperature	Firing rate	Soak time	Reference
		≤10%	Laboratory kiln	700−1100°C	3°C/min	1 h	Monteiro, Alexandre, et al. (2008)
		≤100%	Special tubular oven for gas detection	150−1100 °C	2−4 °C/min	20 min	Souza, Toledo, Holanda, Vargas, and Faria (2008)
		≤10%	Laboratory kiln	900−1000 °C	n/a	2 h	Szoke and Muntean (2009)
		≤30%	Laboratory kiln	850−1200 °C	n/a	n/a	Teixeira et al. (2011)
		≤40%	Combustion chamber	880−1000 °C	n/a	6 h	Weng, Lin, and Chiang (2003)
Municipal solid waste incineration plant	Municipal sewage sludge ash	15−30%	n/a	950 °C	n/a	n/a	Haiying, Youcai, and Jingyu (2011)
		≤50%	Laboratory kiln	950−1050 °C	n/a	n/a	Lin and Weng (2001)
		13−100%	Laboratory kiln	900−1200 °C	2 °C/min	1 h	Merino, Arévalo, and Romero (2007)

	1. Sewage sludge ash **2.** Sewage sludge **3.** Carpet yarn (EWC 04)	**1.** 5−10% **2.** 4−6% **3.** ≤5%	Industrial kiln	980 °C, 72 h	n/a	n/a	Anderson, Elliott, and Hickson (2002)
	Municipal solid waste incinerator fly ash slag	≤40%	Laboratory kiln	800−1000 °C	10 °C/min	6 h	Lin (2006)
		≤50%	Laboratory kiln	800−1050 °C	n/a	2 h	Shin and Kim (2009)
	Fly ash	≤40%	Laboratory kiln	1100 °C	n/a	n/a	Garcia-Ubaque, Giraldo, and Moreno-Piraján (2013)

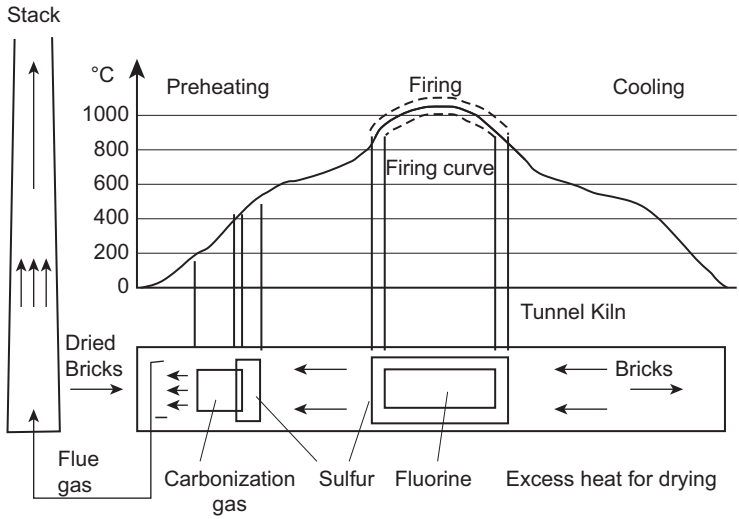

Figure 7.4 Temperature ranges for the release of pollutants during the firing of bricks (BREF, 2007).

decomposition of chlorine-containing mineral salts is responsible for the second emission of chlorine. Due to the high temperatures used in ceramic processes (normally above 850 °C), all the chlorine is emitted, and thus, emission mainly depends on the initial content in the raw material.

The emissions of CO_2 from the clays are observed in two main temperature ranges. The first emission peak occurs at temperatures between 350 and 500 °C, due to the combustion of the organic matter. The second emission peak at temperatures above 800 °C is attributed to the decomposition of carbonates. Due to the high temperatures used in ceramic processes, the all-carbon content in the materials is emitted, and thus, emission mainly depends on the initial content in the raw material.

Most of the publications are focussed on the assessment of the technical and environmental performance of the new ceramic products. It is important to stress that less than 10% of the total number of reviewed publications have studied the emissions during the firing process. Table 7.5 shows the emissions during the firing of alternative ceramic containing waste from the EWC codes 01, 10 and 19 and summarizes the information about the method of assessment, the studied pollutants and the regulatory emission threshold limits used to evaluate the potential environmental impact during firing waste-based products. Some of these works have been carried out on an industrial or semi-industrial scale, but most of them have been simulated at laboratory scale. The most studied compounds are fluorine (HF), chlorine (HCl), sulfur (SO_2) and carbon (CO_2) dioxides.

The emissions from the firing process can be assessed by different techniques, as shown in Table 7.5. The main methods are analyzing off-gases, using evolved gas analysis (EGA) and using a mass balance approach. Analysis of the off-gas emissions of HF, HCl, SO_2 and CO_2, is frequently used at industrial scale. Evolved gas analysis

Table 7.5 Gaseous emissions during firing waste-based fired masonry bricks (methods and the regulatory emission threshold limits)

EWC	Source	Waste	Method	Studied compounds	Regulations threshold limits	Reference
	Coal power plant	Fly ash	Mass balance: chemical analysis before/after firing by ICP/OES/MS ISE (Electron selective)	SO_X and V	n/a	Dondi et al. (2002b)
10	Metallurgical and steel industry	Foundry sand and Waelz slag	Mass balance: chemical analysis before/after firing by ICP/OES/MS ISE (Electron selective)	CO_2, NO_X, SO_2, HF, HCl	n/a	Quijorna et al. (2012)
		Steel slag (Waelz slag)	Mass balance: chemical analysis before/after firing by ICP/OES/MS ISE (Electron selective)	CO_2, NO_X, SO_2, HF, HCl	n/a	Quijorna et al. (2011)
		Siderurgical solid waste	Thermal analysis and mass spectrometer (DTG-MS)	CO_2, H_2O	n/a	Oliveira and Holanda (2004)
			Gas capturing by simulating a stack sampling	SO_2, CO, NO_2, HCl, PM_{10}	Argentinian emissions regulations	Quaranta et al. (2010a)

Continued

Table 7.5 Continued

EWC	Source	Waste	Method	Studied compounds	Regulations threshold limits	Reference
19	Wastewater treatment plant	Sewage sludge	Gas sampling and analysis (US EP, 1994)	VOCs, SO_2, CO, NO_X, HCl, HF and metals	Royal Decree 833/1975 and Decree 323/1994 Generalitat de Catalunya (DOGC, 1994)	Cusido et al. (2003)
			European Space Agency: ESA PSS-01-729 - ESA PSS-01-702	WLM, VCM CO, TOC	European Space Agency	Cusidó and Soriano (2011)
			European Space Agency: ESA PSS-01-729 - ESA PSS-01-702	CO, TOC, VCM, TLM	European Space Agency	Devant et al. (2011)
			Infrared gas analyzer system URAS 14	CO, CO_2, CH_4	n/a	Souza et al. (2008)
	Municipal solid waste incineration plant	Sewage sludge ash	Ion selective electrode, optical emission spectrometry, NLP standards, non-dispersive infrared analyzer, hydrocarbon analyzer	HF, SO_2, HCl, NO_X, VOC, PM_{10} and metals	Environmental Protection Act EPA 1190	Anderson et al. (2002)

involves the combination of different thermal techniques which usually are: thermogravimetry (TGA), quadrupole mass spectrometer (QMS) and Fourier transform infrared spectrometer (FTIR). On the other hand, the mass balance approach can be used to estimate the emission values (Ψ), taking into account the concentration of the element in the materials before and after the firing process, using the following equation:

$$\Psi_i = 10,000 * \frac{M_{wi}}{A_{mj}} * \left[\frac{100}{100 - \text{LOI}} * C_{\text{o}}^{j} - C_{\text{f}}^{j}\right] \tag{7.4}$$

where i = polluting compounds; j = constituting elements of the polluting compounds; Ψ_i = emission (in mg of compound i per kg of ceramic produced); LOI = loss on ignition (%); M_{wi} = molecular weight of the polluting compounds; A_{mj} = atomic mass of the element; C_{o}^{j} = concentration of element (j) in the raw material, and C_{f}^{j} = concentration of element (j) in fired product.

7.5 Characteristics of waste-based fired bricks

The evaluation of the applicability of waste in the ceramic sector is assessed by the study of the technical suitability, durability and the environmental compliance of the ceramic waste-based products.

7.5.1 Technological properties of the waste-based fired products

From a technological perspective, the possibility of reusing or recycling a given waste depends on the desired quality of the final products into which it is introduced. The ceramic process involves physical and chemical changes that affect the properties of ceramic products. Due to the different characteristics of some waste materials compared to the traditional ceramic raw materials the technical suitability of the incorporation of waste in ceramic products needs to be assessed by measuring different technological properties. In addition to the technological properties, the phase composition analysis and/or the surface morphology structures are analyzed in the studied works using X-ray diffraction (XRD) and scanning electron microscopy (SEM) techniques.

The most common properties measured by the authors are water absorption (WA), linear firing shrinkage (LFS), rupture flexural strength or module of rupture (σ_{f}), compressive strength (σ_{c}), weight loss during firing (WL), density (ρ), and porosity (P). The standards methods used to measure these properties vary as a function of the country and its quality standard regulations. Most of the works studied have used Standards from Europe (CEN standards or National Standards), America (ASTM or National Standards) and Asia (National Standards).

Water Absorption (WA) is the ability of porous materials to retain a certain amount of liquid (water) in their air spaces, which is a key property when it comes

to the resistance of the product in the environment. The determination of the water absorption is usually done by the immersion of the fired specimens into water at atmospheric pressure and room temperature until saturation. The samples are weighted every 24 h until the mass difference is less than 0.1%, which means that the specimen is completely saturated. Water absorption is measured as a percentage of the saturated mass of the specimen using the following equation:

$$\mathrm{WA}\ (\%) \ = \ 100 * \frac{M_\mathrm{f} - M_\mathrm{o}}{M_\mathrm{f}} \tag{7.5}$$

where: WA (%) = water absorption; M_o = initial dry weight; and M_f = final weight after absorption.

Flexural strength or module of rupture (σ_f) is an important test to assess the mechanical quality of the material. Normally, this test is conducted using a three-point loading method. Before the test, the length of the specimen is measured, then the specimen is located in the centre-point loading. The load speed is fixed, and the test is performed by applying an initial load that is increased continuously until no greater load can be sustained. The maximum load applied to the specimen is recorded, and the average values of flexural strength are calculated by the equation:

$$\sigma_\mathrm{f} \ = \frac{3F_\mathrm{m}l}{2bh^2} \tag{7.6}$$

where: σ_f: flexural strength, N/mm^2; F_m: breaking load, N; b: sample width; h: sample thickness, mm; width, mm; l: distance between supports, mm; d: mean value of distance between the centre of load rollers and support rollers, mm.

Compressive strength (σ_c) is the bulk unit charge against the breakage under axial compressive strength, and it is one of the most important properties. Normally, this test is conducted using a progressively increasing normal strength with the load applied centered on the upper surface of the sample until breakage. Before the test, the area of both bearing surfaces is measured and the average taken. The compressive strength is calculated by dividing the maximum load by the average surface of both bearing surfaces using the equation:

$$\sigma_\mathrm{c} \ = \frac{G}{A} \tag{7.7}$$

where: σ_c: compressive strength, N/mm^2; G: breaking load, N; and A: average surface of both bearing surfaces, mm^2.

Weight loss during firing (WL) is associated with clay minerals, hydroxides, organic matter and volatile components, and it is an important parameter in ceramic processing with implications for the development of porosity and affecting all the technological properties, as well as the release of contaminants to the atmosphere.

The weight loss is obtained by measuring the weight of the samples before and after firing as a percentage of the weight of the specimen using the following equation:

$$\mathrm{WL}\ (\%) = 100 * \frac{P_o - P_f}{P_o} \tag{7.8}$$

where: WL (%) = weight loss; P_o: initial weight; and P_f: final weight after firing. Positive values are observed for weight loss and negative ones for weight gain.

Linear firing shrinkage (LFS) is the change in length measurements of the specimens upon firing, and it is a very important test in ceramic industries because it is related to the formation of the glassy phase and the degree of densification during sintering. The linear firing shrinkage is obtained by measuring the length of the samples before and after firing as a percentage of the length of the specimen using the following equation:

$$\mathrm{LFS}\ (\%) = 100 * \frac{L_o - L_f}{L_o} \tag{7.9}$$

where: LFS (%) = linear shrinkage; L_o: initial length of the ceramic body; and L_f: final length of the ceramic body.

Positive values are observed for linear contraction and negative ones if expansive processes take place.

The bulk density is calculated as the ratio of dry mass of the specimens to its volume using the following equation:

$$\rho = \frac{\text{dry mass}}{\text{volume}} \tag{7.10}$$

where: ρ = density; dry mass (g) and volume of the specimen (cm^3).

Porosity is the amount of voids in a material proportional to its volume. Open pores to the exterior allow the water flow through them while closed pores are those not connected to the exterior and thus water cannot flow through them. Open porosity is closely related to the quality of the ceramic product decreasing its strength as well as altering the thermal and acoustic properties. Different techniques are used to measure the open porosity such as Archimedes method, Mercury Intrusion Porosimetry and BET methods.

Tables 7.6–7.8 summarize the technological properties that have been assessed in the specimens obtained using waste from the EWC codes 01, 10 and 19. In order to assure the reproducibility of the results, the tests are usually performed in different replicates (from three up to 10, depending on the property).

The key factors affecting the properties of ceramic products are the roles played by the raw materials (see Figure 7.2) and the temperature during the firing process. Wastes containing high contents of alkaline oxides that mainly act as **fluxing agents**, such as boron-rich waste, facilitate the densification process, increasing the structural

Table 7.6 Technological properties measured in fired masonry bricks containing wastes from exploration, mining, quarrying, physical and chemical treatment of minerals (EWC 01)

Source	Waste	% Waste	Mechanical properties	Reference
Ornamental stone industry	Granite waste	≤30%	Porosity	Ducman et al. (2005)
		20−60%	Water absorption, modulus of rupture	Menezes et al. (2002)
		20−60%	Water absorption, modulus of rupture, compressive strength	Menezes et al. (2005)
		≤40%	Water absorption, bulk density, linear shrinkage, mechanical strength, weight loss	Monteiro et al. (2004)
		≤40%	Water absorption, flexural rupture strength, linear shrinkage, bulk density	Vieira and Monteiro (2004)
	1. Granite waste **2.** Kaolin waste	**1.** ≤50% **2.** ≤50%	Water absorption and flexural strength	Campos et al. (2007)
		1. ≤100% **2.** ≤100%	Linear shrinkage, modulus of rupture, water absorption	Menezes et al. (2008)
		1. 25−35% **2.** 10−38%	Water absorption, porosity, density and flexural strength	Menezes et al. (2009)
	1. Kaolin Waste **2.** Granite waste **3.** Blast furnace slag (EWC 10)	**1.** 50% **2.** 10−40% **3.** 10−40%	Water absorption, weight loss, compressive strength	El-Mahllawy (2008)
	Granite and marble rejects	30%	Density, volume changes, weight loss, water absorption, compressive strength	Acchar et al. (2006)

		≤50%	Water absorption, porosity, density, compressive and flexural strength	Dhanapandian and Shanthi (2009)
		≤30%	Water absorption, density, flexural strength, shrinkage	Segadaes et al. (2005)
	1. Granite sludge **2.** Quartzite sludge	**1.** 35−70% **2.** 35−70%	Water absorption, flexural strength, density	Torres et al. (2007)
	Marble waste	≤20%	Water absorption, porosity, linear shrinkage, apparent specific gravity, flexural strength	Saboya et al. (2007)
		15−35%	Water absorption, flexural strength, linear contraction	Montero et al. (2009)
	Powder rock	≤20%	Linear shrinkage, water absorption, density, flexural strength	Moreira et al. (2008)
Quarrying and mining	Coal-mining waste	20−50%	Shrinkage, water absorption, density, porosity, compressive strength	Lemeshev et al. (2004)
	Clay waste	5−20%	Water absorption, bending strength, shrinkage	Ozkan et al. (2010)
	Iron ore tailing waste	30−50%	Water absorption, bulk density, flexural strength, shrinkage	Das et al. (2000)
	Residual clay	40−80%	Compressive strength, water absorption	Ramadan et al. (2001)
	1. Mineral wastes **2.** Sewage sludge (EWC 19)	**1.** 5−65% **2.** 10−65%	Flexural strength, water absorption, firing shrinkage	Junkes et al. (2011)
Aluminum industry	Red mud	10−80%	Bulk density, weight loss, shrinkage, water absorption, compressive strength	He et al. (2012)
	1. Red mud **2.** Mining waste	**1.** 38−75% **2.** 15−38%	Water absorption, flexural strength density, porosity, fraction of closed pores	Sviderskii et al. (2007)

Table 7.7 Technological properties measured in fired masonry bricks containing wastes from thermal processes: power stations and other combustion plants, iron and steel industry and aluminum, lead and zinc thermal metallurgy (EWC 10)

Source	Waste	% Waste	Technological properties	Reference
Biomass thermal power plant	Fly ash	≤50%	Water absorption, compressive strength, density, firing shrinkage, weight loss	Pérez-Villarejo et al. (2012)
	Gasification ashes	15–20%	Weight loss, linear shrinkage, flexural strength, density, water absorption	Fernández-Pereira et al. (2011)
Coal power plant	Fly ash	85–90%	Porosity, bulk density, water absorption, weight loss and flexural strength	Baspinar, Kahraman, et al. (2010)
		≤15%	Pore size distribution and volume, compressive strength	Cultrone and Sebastián (2009)
		1.5–6%	Water absorption, porosity, density, flexural strength, SEM, XRD	Dondi et al. (2002a)
		≤20%	Water absorption, flexural strength	Koukouzas et al. (2011)
		≤60%	Compressive strength, water absorption	Kute and Deodhar (2002)
		≤80%	Porosity, water absorption, density, compressive strength	Lingling et al. (2005)
		10–50%	Bulk density, porosity, water absorption, flexural strength, shrinkage	Monteiro, Lima, et al. (2008)
		25–40%	Weight loss, water absorption, porosity, flexural strength, shrinkage	Rego (2009)
		20–80%	Linear shrinkage, water absorption, loss of ignition, flexural strength, porosity	Zimmer and Bergmann (2007)

	1. Fly ash **2.** Tincal ore waste	**1.** ≤10% **2.** ≤10%	Shrinkage, water absorption, weight loss, flexural strength	Olgun et al. (2005)
	1. Fly ash **2.** Metal finishing waste (EWC 11)	**1.** ≥90% **2.** ≤10%	Density, water absorption, shrinkage	Little et al. (2008)
Metallurgical and steel industry	Foundry sand	≤50%	Compressive strength, shrinkage, bulk density, open porosity, water absorption, density, efflorescence	Alonso-Santurde et al. (2011)
		≤50%	Weight loss, porosity, volume changes, compressive and flexural strength	Quaranta et al. (2010a)
	Waste olivine powders (foundry industry)	20−100%	Water absorption, firing shrinkage, XRD	Furlani et al. (2013)
	Blast furnace slag	30−70%	Density, water absorption, porosity, flexural strength, Vickers hardness, linear shrinkage	Karamanova (2011)
		≤100%	Linear shrinkage, density, porosity and water absorption	Ozdemir and Yilmaz (2007)
	Steel slag	≤20%	Water absorption, shrinkage, compressive and flexural strength	Bantsis et al. (2011)
		5−10%	Density, porosity flexural strength	Faria et al. (2011)
		5−30%	Shrinkage, weight loss, water absorption, compressive strength	Shih et al. (2004)

Continued

Table 7.7 Continued

Source	Waste	% Waste	Technological properties	Reference
		20–30%	Porosity, bulk density, water absorption, flexural strength	Quijorna et al. (2011)
		20–40%	Water absorption, density, porosity, flexural strength	Quijorna et al. (2012)
Ceramic manufacturing	**1.** Sanitary ware sludge **2.** Anodizing sludge (EWC 11) **3.** Glass waste (EWC 19)	**1.** 50% **2.** 25% **3.** 25%	Water absorption, shrinkage, flexural strength	Martelon et al. (2000)
	1. Sanitary ware waste **2.** Steel slag	**1.** 30% **2.** 5–20%	Density, porosity, shrinkage, flexural strength	Faria et al. (2006)

Table 7.8 Technological properties measured in waste-based fired masonry bricks containing wastes from waste management facilities, off-site waste water treatment plants and the preparation of water intended for human consumption and water for industrial use (EWC 19)

Source	Waste	% Waste	Technological properties	Reference
Wastewater treatment plant	Sewage sludge	15%	Water absorption, density, thermal conductivity, mechanical resistance	Cusidó and Soriano (2011)
		≤24%	Thermal conductivity, porosity, mechanical resistance	Devant et al. (2011)
		≤10%	Water absorption, shrinkage and flexural strength	Jordán et al. (2005)
		5–40%	Water absorption, shrinkage, porosity, density and flexural strength thermal properties (conductivity)	Kizinievic et al. (2013)
		1–15%	Weight loss, bulk density, water absorption, compressive strength, shrinkage	Martínez-García et al. (2012)
		≤10%	Water absorption, density, flexural strength, shrinkage	Monteiro, Alexandre, et al. (2008)
		≤10%	Linear shrinkage, density, water absorption, compressive strength	Szoke and Muntean (2009)
		≤30%	Water absorption, porosity, linear firing shrinkage, flexural strength	Teixeira et al. (2011)
		≤40%	Firing shrinkage, weight loss, density, water absorption, compressive strength, specific surface area	Weng et al. (2003)

Continued

Table 7.8 Continued

Source	Waste	% Waste	Technological properties	Reference
Municipal solid waste incinerator plant	Sewage sludge ash	15−30%	Compressive strength, water absorption, shrinkage	Haiying et al. (2011)
		≤50%	Water absorption, shrinkage, loss on ignition, bulk density, compressive strength	Lin and Weng (2001)
		13−100%	Water absorption, compressive strength, density, loss of mass	Merino et al. (2007)
	1. Sewage sludge ash **2.** Sewage sludge **3.** Carpet yarn (EWC 04)	**1.** 5−10% **2.** 4−6% **3.** ≤5%	Density, water absorption, compressive strength, effloresce, frost resistance	Anderson et al. (2002)
	Municipal solid waste incinerator fly ash slag	≤40%	Water absorption, shrinkage, density, compressive strength	Lin (2006)
		≤50%	Shrinkage, water absorption, bulk density, compressive strength	Shin and Kim (2009)
	Fly ash	≤40%	Water absorption, compressive strength, efflorescence	García-Ubaque et al. (2013)

compactness of the ceramic. In general, products with high densification also show high linear firing shrinkage and mechanical resistance but low weight loss, porosity and water absorption. Contrary to this, products containing other fluxing oxides such as reduced iron oxides (wustite and magnetite) present linear firing expansion. The expansion may be attributed to the transformation of the crystalline phase iron oxide (FeO) into magnetite (Fe_3O_4) during the sintering process due to the larger unit cell size of its crystalline structure (Quijorna, de Pedro, Romero, Andrés, 2014).

Wastes that mainly act as **fillers** used for sand replacement in the ceramic manufacturing process such as foundry sand, industrial incinerated sewage sludge or dredged harbor sediments show high values of water absorption. Wastes which contain high contents of organic matter and carbon such as bottom ash or sewage sludge mainly act as **pore forming agents and/or fuels**, increasing the porosity, water absorption and weight loss but decreasing the linear firing shrinkage and flexural strength.

Besides the role played by the waste material, the temperature also has a significant effect on the final properties. Higher temperatures increase the liquid phase formation, which enhances the densification process, increases the linear firing shrinkage and mechanical resistance and decreases the weight loss, porosity and water absorption.

7.5.1.1 Analysis and modeling of properties of the waste-based fired products

Reusing waste in the ceramic sector generally entails as optimization process the development of waste-based ceramic formulations using a case-by-case study instead of a global assessment that allows a generalization of the results. Usually the traditional approach includes the selection of several trials with different proportion of waste in the mixtures, the assessment of the results, and the adjustment of the proportions of waste in the mixtures to obtain the desired properties. However, to achieve conclusions about the dependence of the output variables of the products (basic characteristics, technical and environmental) on the input variables (raw materials and process) demands a rigorous design of experiments taking into account a wide variety of raw materials, firing cycles and final products. Recently, various studies have demonstrated the viability of using the mixture design of experiments (M-DoE) methodology in ceramic products to predict the final properties of the products (Correia, Hotza, & Segadães, 2008) or to maximize (Campos et al., 2007) or optimize (Correia, Hotza, & Segadães, 2004, 2005; Menezes et al., 2008) the waste content in ceramic mixtures to obtain products with particular desired properties.

The purpose of the design of experiments is to obtain appropriate models to correlate the response variables with the input variables. In the particular case of mixture design of experiments (M-DoE), the input variables are the proportions of the components of the mixture, which must sum to unity. In the development and manufacturing of waste-based ceramic products, the properties of the final products are mainly determined by the combination of the raw materials and the process conditions. The basic assumption of this technique is that, when the

process conditions are kept constant, the properties of the products (response variables) are simply determined by the proportion of the components in the mixture.

The usual ceramic materials can be divided into three different types of components, with different roles during ceramic processing: plastic (clays), fluxing (feldspar) and filler (quartz) as explained before in Section 7.2. This explains the frequent use of the epithet "triaxial" to describe industrial ceramic products and suggests graphical representations based on triangles, usually equilateral. In such diagrams, as in the case of the phase diagrams explained before (Section 7.3.), composition axes run from each vertex (pure component, weight fraction = 1) to the opposite side (mixtures without the component from the opposite vertex, weight fraction = 0). Thus, raw materials, natural or otherwise, with similar nature, which have similar roles and are capable of replacing each other, should be represented in the same vertex of such triangles (Correia, Dienstmann, Folgueras, & Segadães, 2009; Menezes et al., 2007, 2008, 2009). This also suggests the use of a ternary simplex-lattice design of experiments using a minimum number of mixtures strategically located and widely distributed on the equivalent simplex triangle. The most used design to select mixtures is a modified {3,2} centroid simplex-lattice design augmented with interior points where a total of 10 composition points are chosen within the triangle.

Regression equations that best fit the experimental data are iteratively calculated until statistically relevant models (significance level $p < 0.05$, confidence limit 95%) are reached using the analysis of variance (ANOVA). These mathematical equations describe the various technological properties (dependent variables or responses) as functions of the raw materials content in the initial mixture. By comparing the values and signs of the equation coefficients, it is possible to establish potential synergic or/and antagonist effects between the materials. The validity of each model is checked against the properties of a new mixture, and the error percentage is determined as the difference between the experimental and predicted values. The graphic representations of the fitted equations are response surface plots on the mixture composition triangle.

The use of this methodology in the manufacturing of ceramic products allows one to obtain a quick prediction of the effects of possible changes in the raw materials or their proportions in the mixture. This methodology has been widely applied in several scientific and technical areas. Its specific application to the case of ceramic products using alternative materials represents progress in the current knowledge in this research area.

7.5.2 Durability of the waste-based fired products

Durability is defined as the ability of a material to remain serviceable in the surrounding environment during the useful life without damage or unexpected maintenance. Durability depends on the environmental conditions, climate and season, and other factors such as the technical performance of the product. Properties such as porosity, water absorption as well as the microstructure and the mineral phases developed during the firing process affect the resistance and durability of the product. The firing conditions are an essential determinant of brick durability that affect the vitrification

degree (amount of glass formed). Products fired at higher temperature are generally more vitreous and have lower porosity and water absorption capacity but higher degree of durability.

The main deterioration mechanisms that cause damages in the masonry fired bricks are (1) wetting–drying and (2) freezing–thawing mechanisms that can cause stress and deterioration, (3) salts attack that causes efflorescence and/or cracking of the material, (4) acid or basic attack, (5) the action of fire and, (6) the action of wind that causes abrasion.

- **Wetting–drying mechanism:** The permeability to water of most masonry products causes its penetration in the brick structure. The penetration can occur in three ways: directly through rainfall, indirectly when water moves upward by capillary action from foundation, or laterally from retained material (Abu Bakar, Wan Ibrahim, & Megat Johari, 2009), and it may cause problems in the thermal and acoustic properties as well as the durability of the bricks.
- **Freezing–thawing mechanism:** Moisture in the product under temperature changes (seasons and climates) can cause expansion and contraction that produce thermal shock causing thermal stresses that may produce some spalling in the brick. Frost damage arises from the stresses created within bricks by the freezing of water within the pores which leads to cracking of the brick. Resistance to frost damage is a major criterion of durability.
- **Salts attack:** The presence of soluble salts including sulfates, chlorides and/or carbonate compounds of sodium, potassium, magnesium and calcium is one of the main causes of the loss of durability. These salts may be originated from the composition of the raw materials, but they may also have an external origin due to the water in contact with the brick during its life use.

Water in contact with the available salts in the product for sufficient time causes efflorescence on the external walls and/or microstructural damage and deterioration in the ceramic bricks. Efflorescence is caused by the transport of the soluble salts among the material, while the damage can be due to the crystallization of the salts in the pores of the material. The ability to absorb water depends on the number and the size of the open pores and how accessible they are to the water at the surface.

- **Acid or basic attack:** The reactivity of the brick with the chemicals in the environment can deteriorate the bricks. Ceramic bricks are generally very resistant to chemical attack by alkalis and acids and are attacked only under extreme conditions.
- **Fire resistance:** It is defined as the ability of a material to resist the action of high temperature under fire conditions without any appreciable deformation or substantial loss of strength. In general, fire resistance of bricks is generally good because it is itself a fired material. In severe fires, temperatures may approach the vitrification range of brick, causing slight fusion of exposed faces. Neither of these effects seriously diminishes fire resistance. This property is especially important in the case of refractory materials which may resist prolonged high temperatures.
- **Abrasion:** The abrasion process is caused by the wind or water carrying dust particles that can deteriorate the bricks. It strongly depends on the surrounding environment to which the brick is exposed and the surface hardness of the material.

Table 7.9 summarizes the durability properties that have been assessed in the fired bricks obtained using waste from the EWC codes 01, 10 and 19. In bricks containing

Table 7.9 Leaching behavior of waste-based fired masonry bricks

EWC	Waste	% Waste	Durability	Method	Reference
01	**1.** Kaolin waste **2.** Granite waste **3.** Blast furnace slag (EWC 10)	**1.** 50% **2.** 10–40% **3.** 10–40%	Acid resistance	Weight loss due to acid attack	El-Mahllawy (2008)
	Iron ore tailing waste	30–50%	(a) Acid and alkali resistance, (b) Thermal shock	(a) European Standards method, (b) Thermal expansion coefficient	Das et al. (2000)
	1. Red mud **2.** Mining waste	**1.** 38–75% **2.** 15–38)%	Acid and alkali resistance	Acid and alkali resistance indexes	Sviderskii et al. (2007)
	Slate waste (slag and mud)	100%	(a) Permeability, (b) Abrasion	(a) European standards method, (b) Pin-on-disc test	Campos et al. (2004)
10	Biomass fly ash	≤50%	Water suction	UNE 67-031	Pérez-Villarejo et al. (2012)
	Coal fly ash	≤15%	(a) Salt crystallization in the pores, (b) Hydric properties	(a) UNI EN 12370, (b) Hydric tests	Cultrone and Sebastián (2009)
		1.5–6%	(a) Soluble salts (Na, K, Ca, Mg, Ni, SO_4^{2}, CrO_4^{3-}, $vO4^{3-}$, (b) Efflorescence	(a) UNE-EN-772-5, (b) UNI 8942-3	Dondi et al. (2002b)
		≤80%	(a) Frost and melting resistance, (b) Cracking due to lime attack	GB/T2542 (Chinese standards)	Lingling et al. (2005)

		25−40%	Permeability	IS 654-1972 (Indian Standards)	Rego (2009)
	Foundry sand	≤50%	(a) Soluble salts, (b) Efflorescence (Na, K, Ca, Mg, V)	(a) UNE-EN-772-5, 2001; (b) ASTM C67, 1994	Alonso-Santurde et al. (2010)
		≤50%	(a) Soluble salts (Na, K, Cl^-, F^-, SO_4^2, (b) Efflorescence, (c) Frost resistance	(a) UNE-EN-772-5, 2001; (b) ASTM C67, 1994; (c) Maage's durability factor	Alonso-Santurde et al. (2011)
	Blast furnace slag	≤100%	(a) Frost resistance, (b) Efflorescence	TS EN 159 (Turkish Standards)	Ozdemir and Yilmaz (2007)
	Waelz slag	20−30%	Soluble salts	UNE-EN-772-5	Quijorna et al. (2011)
	Waelz slag and foundry sand	20−40%	Soluble salts	UNE-EN-772-5	Quijorna et al. (2012)
19	Sewage sludge	5−40%	Water suction	EN 771-1, 11	Kizinievic et al. (2013)
		1−15%	(a) Frost resistance, (b) Water suction	(a) (UNE 67-028), (b) UNE 67-031	Martínez-García et al. (2012)
	1. Sewage sludge ash **2.** Sewage sludge **3.** Carpet yarn	**1.** 5−10% **2.** 4−6% **3.** ≤ 5%	(a) Frost resistance, (b) Efflorescence	n/a	Anderson et al. (2002)
	Fly ash from municipal solid waste incinerator plant	≤40%	Efflorescence	ASTM C67, 1994	García-Ubaque et al. (2013)

waste from EWC 01, the most commonly studied durability property is the acid and basic resistance using different methods: (1) calculating the weight loss due to acid attack, (2) the acid and alkali resistance indexes or (3) using European standard methods. The most common parameters measured to assess the durability of the waste-based products containing waste from the EWC 10 and 19 are frost resistance, presence of soluble salt, efflorescence phenomenon and water penetration measured using standard tests.

7.5.3 Environmental behavior

The environmental behavior of a construction product is assessed by the study of the properties that influence its environmental sustainability, such as leaching behavior. As there is no harmonization in the tests and components to be studied to determine the environmental performance of the waste-based ceramic products so far, the leaching tests selected in each case are different. Table 7.10 summarizes the different leaching tests of alternative ceramic products containing waste from the EWC codes 01, 10 and 19, as well as the analyzed substances and the regulatory threshold limits taken into account to evaluate the environmental impact of the new products during the useful life and at the end of their life when they can be considered either construction and demolition waste (C&DW) or secondary raw material.

Different leaching procedures have been applied in the studied publications (Figure 7.5). During the useful life of the new ceramic product, the diffusion leaching test (NEN 7345) is commonly used, and the results are compared with the threshold limits established in the Building Material Decree. This test is based on the mass transfer and provides kinetic information on the release of constituents of a monolithic sample before reaching steady-state conditions. At the end of its useful life, whether deposited in landfills or as a secondary raw material, compliance leaching tests are used to assess the environmental impacts of the alternative product from a granular sample. The most used tests are the Toxicity Characteristic Leaching Procedure (TCLP), and the equilibrium batch leaching tests UNE-EN 12457. Results from these tests are compared, respectively, to the threshold limits established by the Environmental Protection Agency (EPA) and those summarized in the 2003/33/EC Council Decision, wherein the criteria for acceptance of waste at landfill are established. Other authors assess the leaching behavior using National standards such as National Brazilian Regulations (NBR) or Chinese National Standard (GB). The influence of pH on leaching is also studied using the acid and base neutralization capacity test (EN 14997).

At present in the European Union, the Construction Products Directive (CPD) of 1989 (OJEU, 1989) that aimed to break down technical barriers to trade in construction products within the European Economic Area was replaced in 2011 by the 305/2011/EC Construction Products Regulation (CPR) (OJEU, 2011). The CPR establishes that the construction works must be designed and built in such way that they will not be a threat to the hygiene health and *environment, throughout their life cycle (both use and demolition)*. The mechanism for implementation adopted by CPR was to set very high level requirements for works known as the Essential Requirements. The European

Table 7.10 Summary of the patents developed for waste-based fired masonry bricks

EWC	Source	Waste	Leaching test	Studied elements	Regulations threshold limits	Reference
10	Biomass	Gasification fly ash	Dutch Diffusion Test (NEN 7345) European Standard UNE-EN 12457	As, Ba, Cd, Co, Cr, Cu, Hg, Mo, Ni, Pb, Sb, Se, Sn, V, Zn	Building Materials Decree European Landfill Directive (2003/33/CE)	Fernández-Pereira et al. (2011)
	Coal power plant	Fly ash	D.M 512/19998 (Italian law)	Mg, SO_4^{2-}, V, Ni	n/a	Dondi et al. (2002b)
			European Standard leaching test (UNE-EN 12457 2 2002)	As, Ba, Cd, Cr, Cu, Mo, Ni, Pb, Zn	European Landfill Directive (2003/33/CE)	Little et al. (2008)
	Metallurgical and steel industry	Foundry sand	Dutch diffusion test (NEN 7345) European Standard UNE-EN 12457	Pb, As, Cr, Cl^-, F^-, SO_4^{2-}	Building Materials Decree European Landfill Directive (2003/33/CE)	Alonso-Santurde et al. (2010)
			Dutch diffusion test (NEN 7345) European Standard (UNE-EN 12457)	As, Ba, Cd, Cr, Cu, Mo, Ni, Pb, Zn, F^-, Cl^-, SO_4^{2-}, Sb, Se	Building Materials Decree European Landfill Directive (2003/33/CE)	Alonso-Santurde et al. (2011)
		Waelz slag	Dutch Diffusion Test (NEN 7345)	Cr, Zn, Cd, Ni, Ba, Mo, Cu, Pb, As	Building Materials Decree	Quijorna et al. (2011)

Continued

Table 7.10 Continued

EWC	Source	Waste	Leaching test	Studied elements	Regulations threshold limits	Reference
			European Standard (UNE-EN 12457)		European Landfill Directive (2003/33/CE)	
		Foundry sand and Waelz slag	Dutch Diffusion Test (NEN 7345)	As, Ba, Cd, Cr, Cu, Ni, Mo, Pb, Zn, Cl^-, F^-, SO_4^{2-}	Building Materials Decree	Quijorna et al. (2012)
			European Standard UNE-EN 12457	As, Ba, Cr, Mo, Cl^-, F^-, SO_4^{2-}	European Landfill Directive (2003/33/CE)	
		Steel slag	pH-static test (EN 1497)	Si, Mn, Al, Zn, Mg, Ca, Cr, B, Ba, Na, K, Sr, Ti, V, Fe, Ni, P, Zr	n/a	Furlani et al. (2010)
			European Standard leaching test (EN 12457 2 2002)	As, Pb, Mn, Cu, Cd, Ni, Cr, Fe, Zn	USEPA limits	Bantsis et al. (2011)
		Siderurgical solid waste	Associação Brasileira de Normas Técnicas (NBR 10005-6. 1987)	Cr, Cd, Zn, Cu, Fe, Pb, Hg	NBR 10004, 1987	Oliveira and Holanda (2004)

19	Wastewater treatment plant	Sewage sludge	Dutch Diffusion Test (NEN 7345)	As, Ba, Cd, Co, Cr, Cu, Mo, Ni, Pb, Sb. Se, Sn, V, Zn, Br^-, F^-, SO_4^{2-}	Building Materials Decree	Cusidó and Soriano (2011)
			EPA Standard (TCLP)	Cr, Ni, Cu, Zn, As, Se, Ag, Cd, Pb	USEPA limits	Martínez-García et al. (2012)
				As, Cd, Cr (VI), Cr (tot.), Cu, Hg, Pb, Zn		Weng et al. (2003)
	Municipal solid incineration plant	Sewage sludge ash	EPA Standard (TCLP)	As, Ba, Cd, Cr, Cu, Hg, Mg, Ni, Pb, Ag, Se	USEPA limits	García-Ubaque et al. (2013)
			China Standard leaching test (GB5085.3−2007)	As, Cd, Cr, Cu, Hg, Ni, Pb, Zn	China Standard GB5085.3−2007 limit	Haiying et al. (2011)
		Fly ash	EPA Standard (TCLP)	Cu, Zn, Pb, Cr	USEPA limits	Singh, Chaturvedi, Morchhale, and Yegneswaran (2007)

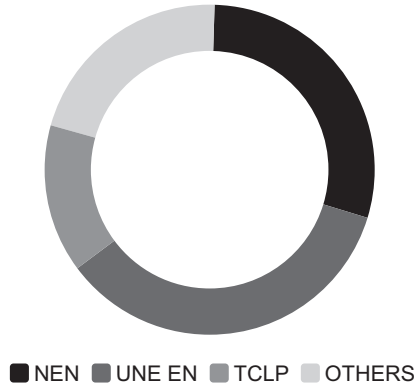

Figure 7.5 Leaching tests used to assess the environmental impact of waste-based fired masonry bricks.

Committee for Standardisation (CEN) was responsible for developing a standard for every construction product (through product technical committees) to support the Essential Requirements. These requirements shall be incorporated into Harmonised European Standards as technical specifications that shall be met by the products for specific use. Technical specifications under the Essential Requirement 3 (ER 3) "Health, safety and environment" that include dangerous substances release require equal consideration such as stability and reaction to fire, but in practice, they are not incorporated and defined yet.

Due to the wide variety of substances that are used in construction products, the European Commission thought about a step-by-step approach to implement the ER 3. At the moment, the work group CEN/TC 351/WG 1 "Horizontal test methods for leaching to soil, ground and surface water" is responsible for the definition of the methods of leaching of construction products. The application of the leaching tests is linked to the scenarios of intended use. The release of dangerous substances, expressed in mg/m^2 or kg per time unit and service life, should be assessed according to the CEN/TC 351 standards: TS-2 dynamic surface leaching test (DSLT) to determine the surface-dependent release of substances from monolithic or plate-like or sheet-like building products and TS-3 up-flow percolation test for determination of the release of substances from granular building products (CEN, 2010b). These documents are under approval and the conditions of the proposed leaching test are currently under discussion and validation.

A list of regulated dangerous substances possibly associated with building products under the Construction Products Regulation (CPR) has been established at a European level (EC, 2011). This list indicates which substances and parameters the evaluation should focus on. No aggregation is foreseen. For each pollutant, limit values are or can be defined at national level (at present only a few member states have quantitative requirements on this issue, e.g. the Dutch "Soil Quality Decree" (VROM, 2007) and the German "Principles for assessing the effects of building products on soil and groundwater" (DIBt, 2009)).

7.6 Current framework

Current trends in policies and marketing strategies for new products aim to provide environmental information about the product. This environmental information allows one to assess the sustainability of the new products before they are available on the market. Life cycle assessment (LCA) and the environmental product declaration are useful tools used to assess and show the environmental information, respectively.

7.6.1 Environmental product declaration: LCA

Construction Products Regulation (CPR) provides a "common technical language", offering uniform assessment methods of the performance of construction products. These methods have been compiled in harmonized European standards (hEN) and European Assessment Documents (EAD). The harmonized European standards on construction products, together with the relevant horizontal standards on assessment methods, for (1) resistance to fire, reaction to fire, external fire performance, noise absorption; (2) construction products in contact with drinking water; and (3) release of dangerous substances into indoor air, soil and (ground) water create a common European technical language to be used by all actors in the construction sector to express requirements (regulatory authorities in member states), to declare the product performance (manufacturers) and to verify compliance with such requirements (design engineers, contractors) (EC, 2013).

The manufacturer shall draw up a Declaration of Performance when a product covered by a harmonized European standard (hEN) or a European Technical Assessment (ETA) is placed on the market. The Declaration of Performance (DoP) is the key concept in the Construction Products Regulation (CPR). It serves to deliver the information about the essential characteristics of the product that a manufacturer wants to make available on the market (EU, 2013). In order to ensure that the declaration of performance (DoP) for specific products is accurate and reliable, a system of Assessment and Verification of Constancy of Performance (AVCP) for each family of construction product is applied (CPA et al., 2012).

One of the new key issues of the CPR is the requirement on sustainability, especially the sustainable use of natural resources, which are the basic requirements for construction works 7 (BRCW 7) and the reduction of life-cycle impacts of greenhouse gases (BRCW 3). Both requirements define relevant product-specific information involving the life cycle approach. Therefore, it is necessary to use the European standards, under development by CEN technical committee (CEN/TC 350), to regulate in these areas of sustainability.

On the other hand, the CPR introduces the life cycle perspective when assessing the performance of a construction product because construction products can have an environmental impact from the extraction of raw materials through processing and manufacture, maintenance, use of the product or at the end of its life. Life cycle assessment, or LCA, is a methodology that measures the environmental impact of a construction product, component or building. The particular type of LCA known as an environmental product declaration (EPD) has been developed to provide

environmental information from LCA studies in a common format, based on common rules, known as product category rules (PCR). PCR have been developed in different European countries. To be comparable, the EPD must have the same PCR to ensure that scope, methodology, data quality and indicators are all the same. All construction EPD Programs should comply with the International Standards for Life Cycle Assessment and the overarching standard for Environmental Product Declaration (CPA et al., 2012). The core PCR EN 15,804 describes the rules regarding how to develop an EPD for construction products in a common way.

7.6.2 Patents and commercial initiatives

During recent years, various patents (Table 7.11) and commercial initiatives for ceramic products containing waste have been developed. In general, these patents jointly introduce wastes from different sources (EWC codes) due to the different roles that they play during the ceramic process that contribute to enhance the final properties of the products. Eighty percent of the patents have been developed in China, while the other 20 percent belong to other countries such as Taiwan, Korea, Japan and Rumania.

Table 7.11 Patents for ceramic products containing waste

Patent no	Title (country)	Inventor (year)	Source material
CN103044009	Archaized bricks produced by using polished brick factory waste materials and preparation method thereof (China)	Jianshun (2013)	Polished brick waste, clay, water
CN102557712	Method for manufacturing water permeable brick by using sugar filter mud (China)	Gao et al. (2012)	Sugar filter mud, power plant fly ash, clay, waste ceramic
CN102515691	Light environment-friendly brick prepared from waste brick powder, and preparation method for light environment-friendly brick (China)	Wen, Liao, Zhao, and Wen (2012)	Polishing brick waste mud, waste brick powder, aluminum ore, mug bean mud and clay
CN102432267	Brick making method capable of saving land resources (China)	Wang, Chen, Wang, and Wang (2012)	Silt, coal slag, fly ash, coal gangue, industrial waste slag and clay

Table 7.11 Continued

Patent no	Title (country)	Inventor (year)	Source material
CN101603346	Sludge brick and preparing method thereof (China)	Lin (2009)	Sludge brick, fly ash, clay and industrial solid waste
CN101525241	Method for preparing water permeable brick with vitrified tile waste and product obtained (China)	Liu and Gu (2009)	Vitrified tile waste, clay, feldspar, water glass
CN101514110	Red mud and fly ash fireproof insulation brick (China)	Ruan (2009)	Red mud, fly ash, lightweight aggregate, clay, water
CN101386528	Method for producing ceramic tile by metallurgical steel slag (China)	Tang and Lu (2009)	Metallurgical steel slag, clay, quartz
CN101284723	Process for preparing low porosity clay brick from waste sagger (China)	Wang and Huang (2008)	Waste sagger, clay water, alumina fine powder, flint fine powder
CN101279839	Solid wall insulating brick made by calcining fly ash coal gangue (China)	Xu (2008)	Fly ash, coal slack bentonite (clay), perlite
CN101255050	Method for sintering bricks by high-doping aluminum hydroxide industrial sludge clay (China)	Yuan (2008)	Industrial sludge and clay
TW397718	The sintered body of continuous through holes using industrial waste and unused resources as major raw materials (Taiwan)	Jiun-Rung and Takahiro (2000)	Glass residue, shale, stones, glass dregs, fly ash, clay
RU2007111319	Ceramic brick and auger extruder carrier used for its manufacturing (Rumania)	Andrej (2007)	Silica sedimentary rock, clay

Continued

Table 7.11 Continued

Patent no	Title (country)	Inventor (year)	Source material
RU2308439	Raw material mix for manufacture of ash-ceramic tiles and brick (Rumania)	Vladimirovich, Georgievich, Karpovna, Nikolaevic, and Aleksandrovich (2007)	Ash-ceramic, clay
RU2243183	Ceramic mass (Rumania)	Svatovskaja, Maslennikova, Zueva, and Abu-Khasan (2007)	Oil-contaminated granite, clay
KR100678365	Porous and lightweight clay bricks sintered at low temperature by using solid wastes and manufacture method thereof (Korea)	Won (2004)	Fly and paper ash, clay
KR100536880	Low-temperature sintered ceramic clay brick or floor clay brick using solid wastes and production method thereof (Korea)	Won (2004)	Fly and paper ash, clay, terra alba
KR20030039390	Construction materials, tripods for breakwater and cubstones using bio-balls made of waste limestone and sludge, and manufacture thereof (Korea)	Moon (2003)	Waste limestone, zeolite, clay, feldspar
KR20010014496	Preparation method of bricks using marine clay (Korea)	Suk (2001)	Excavation waste soil (marine clay)
JP2004243714	Manufacturing method of board such as laminated tile, brick, tile and board such as laminated tile, brick, tile (Japan)	Junnosuke (2004)	Clay, fly ash, grog, tile waste

Currently, there are some commercial initiatives that aim to develop ceramic products containing waste as secondary resources. Among them, the *Green Leaf Bricks* from recycled materials such as sewage wastes, recycled iron oxides, recycled glass, mineral tailings (Green Leaf Bricks, 2014), and other virgin ceramic scrap or '*EcoBrick*' that contains sewage sludge, mainly (Life Project, 2008). A life cycle analysis and the performances have been published in their environmental product declarations. Other certificates that can be applied for these products are the SMaRT© Sustainable Product Standard and the Leadership in Energy & Environmental Design (LEEDs credits).

On the other hand, it is remarkable to review the use of alternative, recycled and secondary sources (MARSS) 2005−2010 in the brick manufacturing sector performed by the company CERAM and requested by the Brick Manufacturing Association (BDA) (Smith, 2010).

7.7 Conclusions and future trends

Industrial symbiosis is a key aspect of sustainable development aiming at increasing the resources efficiency by considering waste streams as new valuable resources in other processes. This chapter presents an updated literature review on the potential use of waste materials as new resources in the fired masonry bricks: benefits, barriers, current and future trends.

The ceramic industry is a good receptor for different waste streams due to the similar composition between mixtures containing waste materials and the natural clays which allow one to obtain ceramic products fulfilling the technical requirements. This is attributed to the key roles that these materials play during the ceramic process: clay substitutes, fillers, body fuels, pore formers, fluxing agents and colorants. A wide variety of waste materials have been assessed for the production of ceramic products. Most of the research has been conducted using residues resulting from exploration, mining, quarrying, physical and chemical treatment of minerals (EWC 01), from thermal processes, iron and steel industry and aluminium, lead and zinc thermal metallurgy (EWC 10) and from waste management facilities (EWC 19).

The technical properties and the durability of products containing these waste materials have been evaluated in the publications studied in this review. The most common measured technological properties are water absorption, porosity, flexural strength, compressive strength, density, weight loss and linear firing shrinkage during firing. Regarding durability, frost resistance, soluble salts and efflorescence are usually assessed. Alternative products containing waste materials are also subjected to different regulations on construction products that establish the technical requirements that a product must fulfil depending on its use. It has been found that, in general, the introduction of certain amounts of waste in the initial mixture does not degrade these properties, meeting the performance requirements or even improving some of them. Mixture design of experiments (M-DoE) can be used to model, predict and optimize the technical properties with a minimum number of experiments.

Beside the technical quality, the increasingly restrictive environmental regulations are forcing the ceramics industry to closely examine their environmental impact. However, less attention has been paid to assess the leaching behavior of the products and the gaseous emissions during the firing process.

In order to assess the market potential of construction products and their effective commercialization, life cycle assessment (LCA) is being used as a tool for determining the environmental aspects and potential impacts associated with a product and consider the entire life cycle: extraction, manufacturing, transportation, use and end-of-life phases. The environmental product declaration (EPD) is a document required by the different regulations on construction products to show the results of the LCA. At the moment, few patents for alternative products containing mixed wastes have been developed, and some commercial products are currently on the market.

The requirements on sustainability established by the Construction Products Regulation make it necessary to provide relevant technical and environmental information about products for market applications. The European Commission is working to solve this situation and new European Standards are currently under approval to assess the impact of the products. In the foreseeable future, the new products containing wastes will probably be regulated by the same criteria used for traditional construction products, and an integrated study will be required to ensure the technical and environmental performance of these products before their introduction into the market.

Acknowledgments

The authors gratefully acknowledge financial support for this research under the framework of the Spanish Education and Science Ministry, Project CTM 2009-11303. M. Coronado was funded by the Spanish Ministry of Education and Science on an F.P.I. fellowship.

References

Abali, Y., Yurdusev, M. A., Zeybek, M. S., & Kumanlioglu, A. A. (2007). Using phosphogypsume and boron concentrator wastes in light brick production. *Construction and Building Materials, 21*(1), 52−56.

Abu Bakar, B. H., Wan Ibrahim, M. H., & Megat Johari, M. A. (2009). A review: durability of fired clay brick masonry wall due to salt attack. *International Journal of Integrated Engineering (Issue on Civil and Environmental Engineering), 1*(2), 52−56.

Acchar, W., Dultra, E. J. V., & Segadães, A. M. (2013). Untreated coffee husk ashes used as flux in ceramic tiles. *Applied Clay Science, 75−76*, 141−147.

Acchar, W., Rulff, B. M., & Segadães, A. M. (2009). Effect of the incorporation of a spent catalyst reject from the petroleum industry in clay products. *Applied Clay Science, 42*(3−4), 657−660.

Acchar, W., Vieira, F. A., & Hotza, D. (2006). Effect of marble and granite sludge in clay materials. *Materials Science and Engineering, 419*(1−2), 306−309.

Acosta, A., Iglesias, I., Aineto, M., Romero, M., & Rincón, J. M. (2002). Utilisation of IGCC slag and clay steriles in soft mud bricks (by pressing) for use in building bricks manufacturing. *Waste Management, 22*(8), 887−891.

Adie, G. U., & Osibanjo, O. (2013). Reusability of slag from automobile battery manufacturing in fired clay building bricks: a waste-to-wealth initiative. *Journal of Solid Waste Technology and Management, 39*(1), 35−42.

Adylov, G. T., Menosmanova, G. S., Riskiev, T. T., Rumi, M. K., & Faiziev, S. A. (2010). Prospects for expanding the raw materials resources for ceramic production. *Glass and Ceramics (English translation of Steklo i Keramika), 67*(1−2), 63−65.

Aeslina, A. K., & Mohajerani, A. (2012). Leachability of heavy metals from fired clay bricks incorporated with cigarette butts. *Symposium on Business, Engineering and Industrial Applications*, 872−877.

Alonso-Santurde, R., Andrés, A., Viguri, J. R., Raimondo, M., Guarini, G., Zanelli, C., et al. (2011). Technological behaviour and recycling potential of spent foundry sands in clay bricks. *Journal of Environmental Management, 92*(3), 994−1002.

Alonso-Santurde, R., Coz, A., Quijorna, N., Viguri, J. R., & Andrés, A. (2010). Valorization of Foundry Sand in Clay Bricks at industrial scale. *Journal of Industrial Ecology, 14*(2), 217−230.

Anderson, M., Elliott, M., & Hickson, C. (2002). Factory-scale proving trials using combined mixtures of three by-product wastes (including incinerated sewage sludge ash) in clay building bricks. *Journal of Chemical Technology and Biotechnology, 77*(3), 345−351.

Aripin, H., Lestari, L., Agusu, L., Sudiana, I. N., Jumsiah, N., Rahmatia, I., Sunendar, B., Nurdiwijayanto, L., Mitsudo, S., & Sabchevski, S. (2011). Preparation of porous ceramic with controllable additive and firing temperature. *Advanced Materials Research, 277*, 151−158.

Arsenovic, M., Radojevic, Z., & Stankovic, S. (2012). Removal of toxic metals from industrial sludge by fixing in brick structure. *Construction and Building Materials, 37*, 7−14.

Bantsis, G., Sikalidis, C., Betsiou, M., Yioultsis, T., & Bourliva, A. (2011). Ceramic building materials for electromagnetic interference shielding using metallurgical slags. *Advances in Applied Ceramics, 110*(4), 233−237.

Barbieri, L., Andreola, F., Lancellotti, I., & Taurino, R. (2013). Management of agricultural biomass wastes: preliminary study on characterization and valorisation in clay matrix bricks. *Waste Management, 33*(11), 2307−2315.

Baruzzo, D., Minichelli, D., Bruckner, S., Fedrizzi, L., Bachiorrini, A., & Maschio, S. (2006). Possible production of ceramic tiles from marine dredging spoils alone and mixed with other waste materials. *Journal of Hazardous Materials, 134*(1−3), 202−210.

Basegio, T., Berutti, F., Bernardes, A., & Bergmann, C. P. (2002). Environmental and technical aspects of the utilisation of tannery sludge as a raw material for clay products. *Journal of the European Ceramic Society, 22*(13), 2251−2259.

Baspinar, M. S., Demir, I., & Orhan, M. (2010). Utilization potential of silica fume in fired clay bricks. *Waste Management and Research, 28*(2), 149−157.

Baspinar, M. S., Kahraman, E., Gökhan, G., & Demir, I. (2010). Production of fired construction brick from high sulfate-containing fly ash with boric acid addition. *Waste Management and Research, 28*(1), 4−10.

Blanco, I., Rodas, M., Sánchez, C. J., Dondi, M., & Alonso-Azcárate, J. (2005). Technological characterization and ceramic application of gravel pit by-products from

middle-course Jarama river deposits (central Spain). *Applied Clay Science, 28*(1−4), 283−295.

BREF. (2007). *European Commission. Reference document on best available techniques in the ceramic manufacturing industry*. Information on http://eippcb.jcr.es.

Campos, L. F. A., Menezes, R. R., Lisboa, D., Santana, L. N. L., Neves, G. A., & Ferreira, H. C. (2007). Experimental design to maximize the waste content in ceramic bricks and tiles. *Cerâmica, 53*, 373−380.

Campos, M., Velasco, F., Martínez, M. A., & Torralba, J. M. (2004). Recovered slate waste as raw material for manufacturing sintered structural tiles. *Journal of European Ceramic Society, 24*(5), 811−819.

Chan, C. (2011). Effect of natural fibres inclusion in clay bricks: physico-mechanical properties. *World Academy of Science, Engineering and Technology, 73*, 51−57.

Chidiac, S. E., & Federico, L. M. (2007). Effects of waste glass additions on the properties and durability of fired clay brick. *Canadian Journal of Civil Engineering, 34*(11), 1458−1466.

Christogerou, A., Kavas, T., Pontikes, Y., Koyas, S., Tabak, Y., & Angelopoulos, G. N. (2009). Use of boron wastes in the production of heavy clay ceramics. *Ceramics International, 35*(1), 447−452.

Construction Products Association (CPA), the British Board of Agreement (BBA), British Standards Institution (BSI), FBE Management Limited in consultation with the Trading Standards Institute (TSI). (2012). *Guidance on products regulations (2012)*. Information on http://www.constructionproducts.org.uk.

Construction Products Regulation (CPR). Methods of the performance of construction products, 305/2011/EC.

Corpas-Iglesias, F. A., Pérez-Villarejo, L., Benítez Guerrero, M., Artiaga Díaz, R., & Pascual Cosp, J. (2011). Use of mud from metallic surface treatment industries as additive to ceramic matrices. *Boletín de la Sociedad Española de Cerámica y Vidrio, 50*(3), 117−124.

Correia, S. L., Hotza, D., & Segadães, A. M. (2004). Simultaneous optimization of linear firing shrinkage and water absorption of triaxial ceramic bodies using experiments design. *Ceramic International, 30*(6), 917−922.

Correia, S. L., Hotza, D., & Segadães, A. M. (2005). Optimizing mechanical strength and bulk density of dry ceramic bodies through mixture design. *Boletin de la Sociedad Espanola de Cerámica y Vidrio, 44*(1), 53−58.

Correia, S. L., Dienstmann, G., Folgueras, M. V., & Segadães, A. M. (2009). Effect of quartz sand replacement by agate rejects in triaxial porcelain. *Journal of Hazardous Materials, 163*(1), 315−322.

Correia, S. L., Hotza, D., & Segadães, A. M. (2008). Predicting porosity content in triaxial porcelain bodies as a function of raw materials contents. *Journal of Materials Science, 43*(2), 696−701.

Couto, D. M. S., Silva, R. F., Castro, F., & Labrincha, J. A. (2001). Attempts of incorporation of metal plating sludges in ceramic products. *Industrial Ceramics, 21*(3), 163−168.

Cultrone, G., & Sebastián, E. (2009). Fly ash addition in clayey materials to improve the quality of solid bricks. *Construction and Building Materials, 23*(2), 1178−1184.

Cusidó, J. A., Cremades, L. V., & González, M. (2003). Gaseous emissions from ceramics manufactured with urban sewage sludge during firing processes. *Waste Management, 23*(3), 273−280.

Cusidó, J. A., & Soriano, C. (2011). Valorization of pellets from municipal WWTP sludge in lightweight clay ceramics. *Waste Management, 31*(6), 1372−1380.

Demir, I. (2006). An investigation on the production of construction brick with processed waste tea. *Building and Environment, 41*(9), 1274−1278.

Demir, I. (2008). Effect of organic residues addition on the technological properties of clay bricks. *Waste Management, 28*(3), 622−627.

Demir, I., Baspinar, M. S., & Orhan, M. (2005). Utilization of kraft pulp production residues in clay brick production. *Building and Environment, 40*(11), 1533−1537.

Demir, I., & Orhan, M. (2003). Reuse of waste bricks in the production line. *Building and Environment, 38*(12), 1451−1455.

Deutches Institut fur Bautechnik (DIBt). (2009). *Principles for assessing the effects of building products on soil and groundwater*.

Devant, M., Cusidó, J. A., & Soriano, C. (2011). Custom formulation of red ceramics with clay, sewage sludge and forest waste. *Applied Clay Science, 53*(4), 669−675.

Dhanapandian, S., & Shanthi, M. (2009). Utilization of marble and granite wastes in brick products. *Journal of Industrial Pollution Control, 25*(2), 155−160.

Dondi, M., Ercolani, G., Guarini, G., Raimondo, M., & Ruffini, A. (2002a). Orimulsion fly ash in clay bricks−part 2: prospects and limitations. *Waste Management and the Environment*, 547−556.

Dondi, M., Ercolani, G., Guarini, G., Raimondo, M., & Ruffini, A. (2002b). Orimulsion fly ash in clay bricks−part 3: chemical stability of ash-bearing products. *Waste Management and the Environment*, 547−556.

Dondi, M., Guarini, G., Raimondo, M., & Zanelli, C. (2009). Recycling PC and TV waste glass in clay bricks and roof tiles. *Waste Management, 29*(6), 1945−1951.

Dondi, M., Guarini, G., Raimondo, M., Zanelli, C., Fabbriche, D. D., & Agostini, A. (2010). Recycling the insoluble residue from titania slag dissolution (tionite) in clay bricks. *Ceramics International, 36*(8), 2461−2467.

Ducman, V., Kopar, T., & Sanchez, E. (2005). Possible use of the rejects from the polishing of granite in the production of bricks. *Applied Clay Science, 36*(1), 1−6.

Das, S. K., Kumar, S., & Ramachandrarao, P. (2000). Exploitation of iron ore tailing for the development of ceramic tiles. *Waste Management, 20*(8), 725−729.

De La Casa, J. A., Lorite, M., Jiménez, J., & Castro, E. (2009). Valorisation of wastewater from two-phase olive oil extraction in fired clay brick production. *Journal of Hazardous Materials, 169*(1−3), 271−278.

Eco-Innovation Observatory. (2010). *The eco-innovation challenge*. Annual report 2010. Information on http://www.eco-innovation.eu.

Elías, X. (2009). Reciclaje de residuos industriales, Residuos sólidos urbanos y fangos de depuradora. *Ed. Díaz de Santos*, Spain, p. 1295.

Eliche-Quesada, D., Martínez-García, C., Martínez-Cartas, M. L., Cotes-Palomino, M. T., Pérez-Villarejo, L., Cruz-Pérez, N., & Corpas-Iglesias, F. A. (2011). The use of different forms of waste in the manufacture of ceramic bricks. *Applied Clay Science, 52*(3), 270−276.

Eliche-Quesada, D., Martínez-Martínez, S., Pérez-Villarejo, L., Iglesias-Godino, F. J., Martínez-García, C., & Corpas-Iglesias, F. A. (2012). Valorization of biodiesel production residues in making porous clay brick. *Fuel Processing Technology, 103*, 166−173.

El-Mahllawy, M. S. (2008). Characteristics of acid resisting bricks made from quarry residues and waste steel slag. *Construction and Building Materials, 22*(8), 1887−1896.

EU. (2011a). European Comminication from the Commision to the European Parliament, the Council, the European Economic and Social Committee, the Committee of the Regions. A resource-efficient Europe-Flagship initiative under the Europe 2020 strategy. *COM, 2011*, 21. Brussels, 26.1.2011a.

European Commission. (2013). *Harmonised European standards. Declaration of performance (DoP) and CE marking*. Information on http://ec.europa.eu/enterprise/sectors/construction/declaration-of-performance/european-standards/index_en.htm.

EWC. (2002). *The European waste catalogue*. Environmental protection agency. Information on http://www.epa.ie.

Faria, R. T., Jr., Souza, V. P., Cosin, S., Toledo, R., & Vargas, H. (2011). Characterization of clay ceramics based on the recycling of industrial residues − on the use of photothermal techniques to determine ceramic thermal properties and gas emissions during the clay firing process. In C. Sikalidis (Ed.), *Advances in ceramics − Characterization, raw Materials, processing, properties, degradation and healing*. ISBN:978-953-307-504-4.

Faria, R. T., Jr., Souza, V. P., Cosin, S., Toledo, R., & Vargas, H. (2012). Gas emission and structural changes in the firing of red clay ceramics with addition of sanitary ware mass wastes. *Advances in Ceramics, 11*, 225−228.

Fernández-Pereira, C., De La Casa, J. A., Gómez-Barea, A., Arroyo, F., Leiva, C., & Luna, Y. (2011). Application of biomass gasification fly ash for brick manufacturing. *Fuel, 90*(1), 220−232.

Furlani, E., Tonello, G., & Maschio, S. (2010). Recycling of steel slag and glass cullet from energy saving lamps by fast firing production of ceramics. *Waste Management, 30*(8-9), 1714−1719.

Furlani, E., Tonello, G., Aneggi, E., & Maschio, S. (2013). Possible use of waste olivine powders from a foundry process into the ceramic industry: sintering behaviour of olivine, kaolin and their blends. *Ceramics International, 39*(2), 1257−1263.

Gao. (2012). *Method for manufacturing water permeable brick by using sugar filter mud*. CN patent application 102557712.

Garcia-Ubaque, C. A., Giraldo, L., & Moreno-Piraján, J. C. (2013). Quality study of ceramic bricks manufacture with clay and ashes from the incineration of municipal solid wastes. *Afinidad, 70*(561), 57−63.

González, I., Galán, E., & Miras, A. (2006). Fluorine, chlorine and sulphur emissions from the Andalusian ceramic industry (Spain)−proposal for their reduction and estimation of threshold emission values. *Applied Clay Science, 32*, 153−171.

Green Leaf Bricks. (2014). Information on http://www.greenleafbrick.com/.

Haiying, Z., Youcai, Z., & Jingyu, Q. (2011). Utilization of municipal solid waste incineration (MSWI) fly ash in ceramic brick: product characterization and environmental toxicity. *Waste Management, 31*(2), 331−341.

Hamer, K., & Karius, V. (2002). Brick production with dredged harbour sediments. An industrial-scale experiment. *Waste Management, 22*, 521−530.

He, H., Yue, Q., Qi, Y., Gao, B., Zhao, Y., Yu, H., et al. (2012). The effect of incorporation of red mud on the properties of clay ceramic bodies. *Applied Clay Science, 70*, 67−73.

Herek, L. C. S., Hori, C. E., Reis, M. H. M., Mora, N. D., Tavares, C. R. G., & Bergamasco, R. (2012). Characterization of ceramic bricks incorporated with textile laundry sludge. *Ceramics International, 38*(2), 951−959.

Ibanga, E. J., & Ahmed, A. D. (2007). Influence of particle size and firing temperature on burnt properties of rice/clay mix. *The Pacific Journal of Science and Technology, 8*(2), 267−271.

IPPC. (2007). *Reference document on best available techniques in the ceramic manufacturing industry*.

IPPC. (2008). *Directive 2008/1/EC of the European Parliament and of the Council of 15 January 2008 concerning integrated pollution prevention and control*.

Jianshun, L. (April 17, 2013). *Archaized bricks produced by using polished brick factory waste materials and preparation method thereof*. CN patent application 20121576952 A.

Jiun-Rung, C., Takahiro, N., & Hocheng Corp. (July 11, 2000). *The sintered body of continuous through holes using industrial waste and unused resources as major raw materials*. TW patent application 397718 B.

Jordán, M. M., Almendro-Candel, M. B., Romero, M., & Rincón, J. M. (2005). Application of sewage sludge in the manufacturing of ceramic tile bodies. *Applied Clay Science, 30*(3−4), 219−224.

Junkes, J. A., Carvalho, M. A., Segadães, A. M., & Hotza, D. (2011). Ceramic tile formulations from industrial waste. *InterCeram: International Ceramic Review, 60*(1), 36−41.

Junnosuke, K., & Junnosuke Yasuhiro. (September 02, 2004). *Manufacturing method of board such as laminated tile, brick, tile and board such as laminated tile, brick, tile*. JP patent applicant 2004243714 A.

Kadir, A. A., & Mohajerani, A. (2010). Possible utilization of cigarette butts in lightweight fired clay bricks. *Proceeding of World Academy of Science, Engineering and Technology, 35*. pp. 153−155.

Kadir, A. A., & Mohajerani, A. (2011). Recycling cigarette butts in lightweight fired clay bricks. *Proceedings of Institution of Civil Engineers: Construction Materials, 164*(5), 219−229.

Karamanova, E., Avdeev, G., & Karamanov, A. (2011). Ceramics from blast furnace slag, kaolin and quartz. *Journal of the European Ceramic Society, 31*(6), 989−998.

Karius, V., & Hamer, K. (2001). pH and grain-size variation in leaching tests with bricks made of harbour sediments compared to commercial bricks. *Science of the Total Environment, 278*(1−3), 73−85.

Kavas, T. (2006). Use of boron waste as a fluxing agent in production of red mud brick. *Building and Environment, 41*(12), 1779−1783.

Kizinievic, O., Žurauskiene, R., Kizinievic, V., & Žurauskas, R. (2013). Utilisation of sludge waste from water treatment for ceramic products. *Construction and Building Materials, 41*, 464−473.

Koukouzas, N., Ketikidis, C., Itskos, G., Spiliotis, X., Karayannis, V., & Papapolymerou, G. (2011). Synthesis of CFB-coal fly ash clay bricks and their characterisation. *Waste and Biomass Valorization, 2*(1), 87−94.

Kurama, S., Kara, A., & Kurama, H. (2006). The effect of boron waste in phase and micro-structural development of a terracotta body during firing. *Journal of the European Ceramic Society, 26*(4−5), 755−760.

Kurama, S., Kara, A., & Kurama, H. (2007). Investigation of borax waste behaviour in tile production. *Journal of the European Ceramic Society, 27*(2−3), 1715−1720.

Kute, S., & Deodhar, S. V. (2002). Effect of fly ash and temperature on properties of burnt clay bricks. *Journal of the Institution of Engineers (India): Civil Engineering Division, 84*(2), 82−85.

Lafhaj, Z., Samara, M., Agostini, F., Boucard, L., Skoczylas, F., & Depelsenaire, G. (2008). Polluted river sediments from the North region of France: treatment with Novosol® process and valorization in clay bricks. *Construction and Building Materials, 22*(5), 755−762.

La Rubia, M. D., Rodríguez, A. Y., Eliche-Quesada, D., & Corpas-Iglesias, F. A. (2010). Efecto de la incorporación de alpeorujo en la fabricación de ladrillos de arcilla. *Revista de la Sociedad Española de Mineralogía, 13*, 135−136.

Lemeshev, V. G., Gubin, I. K., Savelev, Y. A., Tumanov, D. V., & Lemeshev, D. O. (2004). Utilization of coal-mining waste in the production of building ceramic materials. *Glass and Ceramics (English translation of Steklo i Keramika), 61*(9−10), 308−311.

Life Project. (2008). *EcoBrick − Manufacturing sand-limestone. Bricks, recycling energy and organics from sewage sludge (2008)*. LIFE08 ENV/D/000029. Information on http://ec.europa.eu/environment/life/project/Projects/index.cfm?fuseaction=search.dspPage&n_proj_id=3447.

Lin, C., & Huizhou O Meet Environmental. (December 16, 2009). *Sludge brick and preparing method thereof*. CN patent application 101603346 A.

Lin, D., & Weng, C. (2001). Use of sewage sludge ash as brick material. *Journal of Environmental Engineering, 127*(10), 922−927.

Lin, K. L. (2006). Feasibility study of using brick made from municipal solid waste incinerator fly ash slag. *Journal of Hazardous Materials, 137*(3), 1810−1816.

Lingling, X., Wei, G., Tao, W., & Nanru, Y. (2005). Study on fired bricks with replacing clay by fly ash in high volume ratio. *Construction and Building Materials, 19*(3), 243−247.

Little, M. R., Adell, V., Boccaccini, A. R., & Cheeseman, C. R. (2008). Production of novel ceramic materials from coal fly ash and metal finishing wastes. *Resources, Conservation and Recycling, 52*(11), 1329−1335.

Liu, Y., Gu, X., & Jingdezhen Ceramic Inst. (September 09, 2009). *Method for preparing water permeable brick with vitrified tile waste and product obtained*. CN patent applicant 101525241 A.

Loryuenyong, V., Panyachai, T., Kaewsimork, K., & Siritai, C. (2009). Effects of recycled glass substitution on the physical and mechanical properties of clay bricks. *Waste Management, 29*(10), 2717−2721.

Malaiskiene, J., Maciulaitis, R., & Kicaite, A. (2011). Dependence of ceramics physical − mechanical properties on chemical and mineralogical composition. *Construction and Building Materials, 25*(8), 3168−3174.

Martelon, E., Jarrige, J., Ribeiro, M. J., Ferreira, J. M., & Labrincha, J. A. (2000). New clay-based ceramic formulations containing different solid wastes. *Industrial Ceramics, 20*(2), 75−76.

Martínez, M. L., Eliche, D., Cruz, N., & Corpas, F. A. (2012). Utilization of bagasse from the beer industry in clay brick production for building. *Materiales de Construcción, 62*(306), 199−212.

Martínez-García, C., Eliche-Quesada, D., Pérez-Villarejo, L., Iglesias-Godino, F. J., & Corpas-Iglesias, F. A. (2012). Sludge valorization from wastewater treatment plant to its application on the ceramic industry. *Journal of Environmental Management, 95*, S343−S348.

Maschio, S., Furlani, E., Tonello, G., Faraone, N., Aneggi, E., Minichelli, D., Fedrizzi, L., Bachiorrini, A., & Bruckner, S. (2009). Fast firing of tiles containing paper mill sludge, glass cullet and clay. *Waste Management, 29*(11), 2880−2885.

Mekki, H., Anderson, M., Benzina, M., & Ammar, E. (2008). Valorization of olive mill wastewater by its incorporation in building bricks. *Journal of Hazardous Materials, 158*(2−3), 308−315.

Menezes, R. R., De Almeida, R. R., Santana, L. N. L., Neves, G. A., Lira, H. L., & Ferreira, H. C. (2007). Analysis of the use of kaolin processing waste and granite sawing waste together for the production of ceramic bricks and roof tiles. *Cerâmica, 53*(326), 192−195.

Menezes, R., Farias, F., Oliveira, M. F., Santana, L. N. L., Neves, G. A., Lira, H. L., & Ferreira, H. C. (2009). Kaolin processing waste applied in the manufacturing of ceramic tiles and mullite bodies. *Waste Management and Research, 27*(1), 78−86.

Menezes, R. R., Ferreira, H. S., Neves, H. C., & Ferreira, H. C. (2002). Uso de rejeitos de granitos como matérias-primas cerámicas. *Cerâmica, 48*(306), 92−101.

Menezes, R. R., Ferreira, H. S., Neves, G. A., Lira, H. D. L., & Ferreira, H. C. (2005). Use of granite sawing wastes in the production of ceramic bricks and tiles. *Journal of the European Ceramic Society, 25*(7), 1149−1158.

Menezes, R. R., Neto, H. G. M., Santana, L. N. L., Lira, H. L., Ferreira, H. S., & Neves, G. A. (2008). Optimization of wastes content in ceramic tiles using statistical design of mixture experiments. *Journal of the European Ceramic Society, 28*(16), 3027−3039.

Merino, I., Arévalo, L. F., & Romero, F. (2007). Preparation and characterization of ceramic products by thermal treatment of sewage sludge ashes mixed with different additives. *Waste Management, 27*(12), 1829−1844.

Methods of test of burnt clay building bricks. (1992). IS, 3495.

Monteiro, R. C. C., Lima, M. M. R. A., & Alves, S. (2008). Mechanical characteristics of clay structural ceramics containing coal fly ash. *International Journal of Mechanics and Materials in Design, 4*(2), 213−220.

Monteiro, S. N., Alexandre, J., Margem, J. I., Sánchez, R., & Vieira, C. M. F. (2008). Incorporation of sludge waste from water treatment plant into red ceramic. *Construction and Building Materials, 22*(6), 1281−1287.

Monteiro, S. N., Peçanha, L. A., & Vieira, C. M. F. (2004). Reformulation of roofing tiles body with addition of granite waste from sawing operations. *Journal of the European Ceramic Society, 24*(8), 2349−2356.

Monteiro, S. N., Silva, F. A. N., & Vieira, C. M. F. (2006). Microstructural evaluation of a clay ceramic incorporated with petroleum waste. *Applied Clay Science, 33*(3−4), 171−180.

Montero, M. A., Jordán, M. M., Hernández-Crespo, M. S., & Sanfeliu, T. (2009). The use of sewage sludge and marble residues in the manufacture of ceramic tile bodies. *Applied Clay Science, 46*(4), 404−408.

Moon, L. S. (May 22, 2003). *Construction materials, tripods for breakwater and cubstones using bio-balls made of waste limestone and sludge, and manufacture thereof*. KR patent application 20030039390 A.

Moreira, J. M. S., Manhães, J. P. V. T., & Holanda, J. N. F. (2008). Processing of red ceramic using ornamental rock powder waste. *Journal of Materials Processing Technology, 196*(1−3), 88−93.

Mothé, C. G., & Ambrósio, M. C. R. (2007). Processes occurring during the sintering of porous ceramic materials by TG/DSC. *Journal of Thermal Analysis and Calorimetry, 87*(3), 819−822.

OJEU. (February 11, 1989). Official Journal of the European Communities (1989) Council Directive 89/106/EEC of 21 December 1989 on the approximation of laws, regulations and administrative provisions of the Member States relating to construction products. *Official Journal of the European Communities*. L40.

OJEU. (April 4, 2011). Official Journal of the European Unions (2011) Regulation (EU) No 305/2011 of the European Parliament and of the Council of 9 March 2011 laying down harmonized conditions for the marketing of construction products and repealing Council Directive 89/106/EEC. *Official Journal of the European Union*. L 8875−43.

Olgun, A., Erdogan, Y., Ayhan, Y., & Zeybek, B. (2005). Development of ceramic tiles from coal fly ash and tincal ore waste. *Ceramics International, 31*(1), 153−158.

Oliveira, G. E., & Holanda, J. N. F. (2004). Análise do impacto ambiental causado pela utiliçao de residuo sólido do sector siderúrgico em cerámica vermelha. *Cerâmica, 50*, 185−189.

Ozdemir, I., & Yilmaz, S. (2007). Processing of unglazed ceramic tiles from blast furnace slag. *Journal of Materials Processing Technology, 183*(1), 13−17.

Özkan, I., Çolak, M., & Oyman, R. E. (2010). Characterization of waste clay from the Sardes (Salihli) placer gold mine and its utilization in floor-tile manufacture. *Applied Clay Science, 49*(4), 420−425.

Pérez-Villarejo, L., Eliche-Quesada, D., Iglesias- Godino, F. J., Martínez-García, C., & Corpas-Iglesias, F. A. (2012). Recycling of ash from biomass incinerator in clay matrix to produce ceramic bricks. *Journal of Environmental Management, 95*, S349−S354.

Petavratzi, E., & Barton. (2007). *Characterization of mineral wastes, resources and processing technologies*. Heavy ceramic (brick). School of Civil Engineering. University of Leeds.

Pinheiro, B. C. A., & Holanda, J. N. F. (2009). Processing of red ceramics incorporated with encapsulated petroleum waste. *Journal of Materials Processing Technology, 209*(15−16), 5606−5610.

Quaranta, N. E., Lalla, N. S., Caligaris, M. G., Boccaccini, A. R., & Vieira, C. M. (2010). Ceramic tiles adding waste foundry sand to different clays. *WIT Transactions on Ecology and the Environment, 140*, 99−108.

Quijorna, N., & Andrés, A. (2013). *Incorporación de escoria Waelz al sector cerámico al sector cerámico: ejemplo de ecología industrial* (Ph.D. thesis). Departamento de Ingeniería Química y Química Inorgánica. Universidad de Cantabria.

Quijorna, N., Coz, A., & Andrés, A. (2012). Recycling of Waelz slag and waste foundry sand in red clay bricks. *Resources, Conservation and Recycling, 65*, 1−10.

Quijorna, N., de Pedro, M., Romero, M., & Andrés, A. (2014). Characterisation of the sintering behaviour of Waelz slag from electric arc furnace (EAF) dust recycling for use in the clay ceramics industry. *Journal of Environmental Management, 65*, 1−10.

Quijorna, N., Miguel, G. S., & Andrés, A. (2011). Incorporation of Waelz slag into commercial ceramic bricks: a practical example of industrial ecology. *Industrial and Engineering Chemistry Research, 50*(9), 5806−5814.

Ramadan, A. M., Saleh, A. M., Taha, T. A., & Moharam, M. R. (2001). An attempt to improve mechanical properties of brick produced from El-Maghara coal washing plant waste. *Physicochemical Problems of Mineral Processing, 35*, 153−160.

Rego, S. (2009). Utilisation of industrial waste flyash as an adulterant to clay for the manufacture of mangalore roofing tiles. *Journal of Solid Waste Technology and Management, 35*(3), 169−180.

Romero, M., Andrés, A., Alonso, R., Viguri, J., & Rincón, J. M. (2008). Sintering behaviour of ceramic bodies from contaminated marine sediments. *Ceramics International, 34*(8), 1917−1924.

Romero, M., Andrés, A., Alonso, R., Viguri, J., & Rincón, J. M. (2009). Phase evolution and microstructural characterization of sintered ceramic bodies from contaminated marine sediments. *Journal of the European Ceramic Society, 29*(1), 15−22.

Ruan, K. (August 26, 2009). *Red mud and fly ash fireproof insulation brick*. CN patent application 101514110 A.

Saboya, F., Jr., Xavier, G. C., & Alexandre, J. (2007). The use of the powder marble by-product to enhance the properties of brick ceramic. *Construction and Building Materials, 21*(10), 1950−1960.

Samara, M., Lafhaj, Z., & Chapiseau, C. (2009). Valorization of stabilized river sediments in fired clay bricks: factory scale experiment. *Journal of Hazardous Materials, 163*(2−3), 701−710.

Sarani, A. A., & Kadir, A. A. (2013). Thermal conductivity of fired clay bricks incorporated with cigarette butts. *Advanced Materials Research, 690−693*, 919−924.

Segadães, A. M., Carvalho, M. A., & Acchar, W. (2005). Using marble and granite rejects to enhance the processing of clay products. *Applied Clay Science, 30*(1), 42−52.

Segadães, A. M. (2006). Use of phase diagrams to guide ceramic production from wastes. *Advanced Applied Ceramic, 105*(1), 46−54.

Shih, P., Wu, Z., & Chiang, H. (2004). Characteristics of bricks made from waste steel slag. *Waste Management, 24*(10), 1043−1047.

Shin, D., & Kim, K. (2009). Preparation of fired bricks as construction materials by replacing clay with municipal incinerator residue slag. *Journal of Ceramic Processing Research, 10*(6), 739−743.

Shukla, S. K., Kumar, V., Mudgal, M., Morchhale, R. K., & Bansal, M. C. (2010). Utilization of concentrate of membrane filtration of bleach plant effluent in brick production. *Journal of Hazardous Materials, 184*(1−3), 585−590.

Sikalidis, C., & Zaspalis, V. (2007). Utilization of Mn-Fe solid wastes from electrolytic MnO_2 production in the manufacture of ceramic building products. *Construction and Building Materials, 21*(5), 1061−1068.

Singh, I. B., Chaturvedi, K., Morchhale, R. K., & Yegneswaran, A. H. (2007). Thermal treatment of toxic metals of industrial hazardous wastes with fly ash and clay. *Journal of Hazardous Materials, 141*(1), 215−222.

Smith, A., & Materials from Alternative, Recycled and Secondary Sources (MARSS). (2005−2010). *A review of the use of non-primary clay raw materials in the UK brick manufacturing sector*.

Souza, G. P., Santos, R. S., & Holanda, J. N. F. (2003). Recycling of a petroleum waste in ceramic bodies. *Materials Science Forum, 416*, 743−747.

Souza, V. P., Toledo, R., Holanda, J. N. F., Vargas, H., & Faria, R. T., Jr. (2008). Pollutant gas analysis evolved during firing of red ceramic incorporated with water treatment plant sludge. *Ceramica, 54*(331), 351−355.

Suk, L. J. (February 26, 2001). *Preparation method of bricks using marine clay*. KR patent application 20010014496 A.

Sutcu, M., & Akkurt, S. (2009). The use of recycled paper processing residues in making porous brick with reduced thermal conductivity. *Ceramics International, 35*(7), 2625−2631.

Svatovskaja, L. B., Maslennikova, L. L., Zueva, N. A., & Abu-Khasan, M. (October 20, 2007). *Ceramic mass*. RU patent application 2308439 C1.

Sviderskii, V. A., Strashnenko, S. V., & Chernyak, L. P. (2007). Ceramics from mining by-products and alumina production wastes. *Glass and Ceramic, 64*(2), 51−54.

Szoke, A., & Muntean, M. (2009). Sludge recycling in ceramic matrix. *Environmental Engineering and Management Journal, 8*(4), 907−909.

Tang, Q., Lu, B., & Foshan Oceano Ceramics Co Ltd. (April 18, 2009). *Method for producing ceramic tile by metallurgical steel slag*. CN patent application 101386528 A.

Teixeira, S. R., De Souza, A. E., De Almeida Santos, G. T., Peña, A. F. V., & Miguel, A. G. (2008). Sugarcane bagasse ash as a potential quartz replacement in red ceramic. *Journal of the American Ceramic Society, 91*(6), 1883−1887.

Teixeira, S. R., Santos, G. T. A., Souza, A. E., Alessio, P., Souza, S. A., & Souza, N. R. (2011). The effect of incorporation of a Brazilian water treatment plant sludge on the properties of ceramic materials. *Applied Clay Science, 53*(4), 561−565.

Torres, P., Manjate, R. S., Quaresma, S., Fernandes, H. R., & Ferreira, J. M. F. (2007). Development of ceramic floor tile compositions based on quartzite and granite sludges. *Journal of the European Ceramic Society, 27*(16), 4649−4655.

Uslu, T., & Arol, A. I. (2004). Use of boron waste as an additive in red bricks. *Waste Management, 24*(2), 217−220.

Valanciene, V. (2011). Utilization of meat and bone meal bottom ash in ceramics. *Medziagotyra, 17*(1), 86−92.

Vichaphund, S., Intiya, W., Kongkaew, A., Loykulnant, S., & Thavorniti, P. (2012). Utilization of sludge waste from natural rubber manufacturing process as a raw material for clay-ceramic production. *Environmental Technology (United Kingdom), 33*(22), 2507−2510.

Vieira, C. M. F., De Souza, E. T. A., & Monteiro, S. N. (2004). Influence of grog addition on a clay body used in red ceramic products. *Industrial Ceramics, 24*(2), 85−89.

Vieira, C. M. F., & Monteiro, S. N. (2004). Characterization of granite waste for incorporation in red ceramic. *Materials Science Forum, 498*, 728−733.

Vieira, C. M. F., & Monteiro, S. N. (2007). Effect of grog addition on the properties and microstructure of a red ceramic body for brick production. *Construction and Building Materials, 21*(8), 1754−1759.

Vladimirovich, E. G., Georgievich, V. G., Karpovna, S. N., Nikolaevic, K. A., & Aleksandrovich, B. P. (October 20, 2007). *Raw material mix for manufacture of ash-ceramic tiles and brick*. RU patent application 2308439 C1.

Vieira, C. M. F., & Monteiro, S. N. (2009). Incorporation of solid wastes in red ceramics−an updated review. *Revista Materia, 14*(3), 881−905.

VROM − Ministry of Spatial Planning Housing and the Environment. Agency, regulator or other governmental or inter-governmental body, Netherlands 2007.

Vu, D., Wang, K., & Bac, B. H. (2011a). Humidity control porous ceramics prepared from waste and porous materials. *Materials Letters, 65*(6), 940−943.

Vu, D., Wang, K., Nam, B. X., Bac, B. H., & Chu, T. (2011b). Preparation of humidity-controlling porous ceramics from volcanic ash and waste glass. *Ceramics International, 37*(7), 2845−2853.

Wen, J., Liao, Y., Zhao, Y., Wen, Z., & Sichuan Baita Xinlianxing Ceramic Group Co Ltd. (June 27, 2012). *Light environment-friendly brick prepared from waste brick powder, and preparation method for light environment-friendly brick*. CN patent aplication 102515691 A.

Wang, Y., Chen, K., Wang, F., & Wang, Z. (May 02, 2012). *Brick making method capable of saving land resources*. CN patent application 102432267 A.

Wang, Z., Huang, Y., & Xinmi Wanli Industry Dev Co Ltd. (October 15, 2008). *Process for preparing low porosity clay brick from waste sagger*. CN patent application 101284723 A.

Weng, C., Lin, D., & Chiang, P. (2003). Utilization of sludge as brick materials. *Advances in Environmental Research, 7*(3), 679−685.

Won, L. E., & Woosung Ceramics Ind Co. Ltd. (December 02, 2004). *Porous and lightweight clay bricks sintered at low temperature by using solid wastes and manufacture method thereof*. KR patent application 20040099677 A.

Yuan, M. (September 03, 2008). *Method for sintering bricks by high-doping aluminium hydroxide industrial sludge clay*. CN patent applicant 101255050 A.

Xu. (2008). *Solid wall insulating brick made by calcining fly ash coal gangue*. CN patent application CN 101279839 A.

Zhu, P., Cao, Z. B., Wang, L. Y., YE, Y. L., Qian, G. R., Cao, T. H., et al. (2013). Recycling of calcium fluoride sludge as ceramic material using low temperature sintering technology. *Journal of Material Cycles and Waste Management, 16*(1), 156−161.

Zimmer, A., & Bergmann, C. P. (2007). Fly ash of mineral coal as ceramic tiles raw material. *Waste Management, 27*(1), 59−68.

The properties and durability of high-pozzolanic industrial by-products content concrete masonry blocks

8

P. Chindaprasirt[1], *T. Cao*[2]
[1] Khon Kaen University, Khon Kaen, Thailand; [2] Surface Design Consulting Pty Ltd, Sydney, NSW, Australia

8.1 Introduction

Masonry units covered by most standards include those made from normal and lightweight concretes, calcium silicate, natural stone, and fired clay. Concrete masonry units are commonly rectangular prisms and specialized shapes manufactured from pressed, cast, or extruded aggregate concrete. They can be manufactured for virtually any architectural or structural function. Specifications for concrete masonry units are provided in several standards, including BS EN 771-3 (2011), AS/NZS 4455.1 (2008), ASTM C55 (2011), ASTM C90 (2013), ASTM C129 (2011), ASTM C744 (2011), and ASTM C1634 (2011).

In recent years, most concrete masonry units are manufactured by automatic machinery of advanced design and capable of very high output. The concrete mix, consisting of cement and pozzolan, water, additives, coloring agents, and fine and coarse aggregates, is commonly mixed in an automated mixer prior to being transported to the block-making machine. Concrete mixes used in the manufacture of concrete masonry units are dry cohesive concrete mixes, which are needed to provide sufficient "green strength" after compaction in the mold for handling without damage or distortion. The required property in the fresh state is thus the ability of concrete to be cast into a mold or to be formed into a required block size. In a hardened state, strength and durability are important properties. The workability and castability of fresh masonry concrete can be controlled using a parameter such as water requirement. The compactability/castability is gauged by the ease of forming the blocks, with the additional requirement that the blocks retain their required shapes.

After mixing, a period of workable mix is required for the molding of blocks; thus, setting time is an important parameter, especially in the tropics, where high temperature accelerates the setting of concrete. It is therefore important to obtain sufficient workability and compactability, while the mix should be as lean as possible, with sufficient properties in the hardened state (Dowson, 1990). Curing of concrete masonry units is usually achieved by a "curing in the yard" process or by low-pressure steam curing methods, which normally yield better control of mechanical properties and appearance.

Eco-efficient Masonry Bricks and Blocks. http://dx.doi.org/10.1016/B978-1-78242-305-8.00008-5

Portland cement is commonly used as binding material for making masonry concrete. Several classes of cement can be used for masonry concrete. ASTM C 91 (2012) classifies masonry cement according to strength. The required 7-day compressive strength for types N, S, and M are 3.4, 9.0, and 12.4 MPa, respectively, and 6.2, 14.5, and 20 MPa, respectively, for the required 28-day compressive strengths. However, Portland cement production contributes substantially to the emission of greenhouse gas. To reduce the use of Portland cement, the use of a high content of pozzolanic industrial by-products is an attractive choice. The use of pozzolan to replace part of the Portland cement not only reduces the amount of Portland cement and its effect on the global greenhouse gas problem but also increases the durability of products through pore refinement and the reduction of calcium hydroxide in the system (Chindaprasirt, Jaturapitakkul, & Sinsiri, 2005; Kroehong, Sinsiri, Jaturapitakkul, & Chindaprasirt, 2011; Malhotra, 2002). Also, the strength requirement of masonry concrete is not the prime concern, as it is often used for low-strength and non-load-bearing applications. This allows the use of many types of pozzolans: the ones with huge economic and environmental benefit are the industrial by-product pozzolans, due to the large volume obtained annually and their availability.

The topics of mix ingredients and composition, fresh concrete properties, and hardened properties of masonry concrete are the subjects of this chapter, together with the properties of cement and concrete with addition of industrial by-product pozzolans and the properties of masonry blocks.

8.2 Mix composition and fresh and hardened properties of masonry concrete

The mix composition of masonry concrete differs significantly from conventional concrete, as the basic required properties are different. One of the important requirements of masonry concrete mix in the fresh state is the block-forming capability. Zero-slump concrete (sometime called no-slump concrete) is used in the mass production/automated production of concrete products, including masonry blocks. This type of concrete is characterized by its low water content and stiff consistency, which corresponds to a slump of 6 mm or less (ACI 116R-90, 2000; Grant, 1952; Kosmatka, Kerkhoff, Panarese, MacLeod, & McGrath, 2002). Unlike the behavior of normal concrete, zero-slump concrete permits the stripping/demolding of fresh concrete after filling and compacting and its transportation to a location with defined curing conditions. This characteristic is referred to as concrete green strength, which facilitates short processing time and efficient use of molds and block-forming machines.

Workability of no-slump concrete cannot be evaluated with commonly used test methods for normal concrete mixes. Traditionally, the workability of no-slump concrete is judged by its compactability using a method that simulates the actual placement conditions. Some of the tests (Bartos, Sonebi, & Tamimi, 2002; Koehler & Fowler, 2003) that have been used to evaluate the workability of no-slump/low-slump concretes are the standard Proctor test (ASTM D698, 2012) or the modified Proctor test (ASTM D1557, 2012), the Kango Hammer test based on BS 1924 (1975) and BS

1377 (1975), and the Intensive Compaction (IC) test (NT Build 427, 1994). The IC test is known to be fast and sensitive to small changes in mixture proportions (Kappi & Nordenswan, 2007). It is also known to simulate accurately the conditions for roller-compacted concrete. Since this test does not incorporate intense vibration, it may not reflect the conditions commonly used in the placement of concrete masonry units.

Some guidance for mixture proportioning for concrete masonry units manufactured on conventional vibrating block machines are given in ACI 211.3R (2002). The mix design for concrete block work is based on the fineness modulus (FM) method, which consists of six steps (Jablonski, 1996): determining the FM of each aggregate; proportioning aggregates for proper FM; determining aggregate batch proportions; determining the moisture content in aggregate; determining cement content; and determining water content.

There are no specific restrictions on the types of cement or the types and contents of supplementary cementitious materials used in the concrete masonry mix. With normal aggregate complying with ASTM C33 (2013), ACI 211.3R-02 (2002) indicates that the normal range of cement content is about 10% by mass of aggregate for load-bearing masonry units. In higher-strength masonry units, the cement content may exceed 20% by mass of aggregate. Lightweight aggregate can also be used in masonry concrete and must comply with ASTM C331/331M-10 (2010). The mix design method given in ACI 211.3R-02 (2002) is a trial-and-error means of establishing the initial test batch. The water content of the batch is manually adjusted until the mixture "balls" in the hand without exhibiting signs of free moisture. The mix is then put through the machine to verify characteristics such as surface finish/texture, compressive strength, absorption, and green strength.

It has been found that compaction behavior and green strength of zero-slump concrete are largely affected by the granulometric properties and the shape of the fine aggregates (Husken & Brouwers, 2012). Angular fine particles show beneficial effect on the green strength but result in a lower packing condition. Spherical particles, however, increase the packing condition but reduce the green strength as the internal friction and particle interlocking are reduced. Higher packing condition normally results in higher strength and better durability (lower porosity).

The strength requirements for concrete masonry units vary between standards. In ASTM, concrete masonry units are required to have an average compressive strength (minimum net area) of 13.1 MPa (ASTM C90-13, 2013) for load-bearing and 4.14 MPa (ASTM C129-11, 2011) for non-load-bearing units. Typical properties of concrete masonry units of contemporary production can be found in the published article (De Vekey, 2001). Strength and water absorption are often used to determine the class of masonry concrete and its usage (ASTM C 55-11, 2011). Grade N, with minimum average strength of 24.1 MPa, is for high strength, and resistance to severe frost and moisture penetration. Grade S is for general use, with minimum average strength of 17.3 MPa and where moderate strength and resistance to frost action and moisture penetration are required. Concrete masonry units for structural use are also classified by weight; light weight is for block lighter than 1680 kg/m^3, medium weight is 1680−2000 kg/m^3, and normal weight is 2000 kg/m^3 or more.

In regard to durability, the potential problems are deterioration caused by:

- Frost action/freeze−thaw attack;
- Sulfate attack;
- Salt attack (crypto-efflorescence);
- Acid attack; and
- Use of unstable materials as aggregates.

Freeze−thaw attack is one of the main concerns in cold climates, whereas absorption- and expansion-type deteriorations are important in hot and humid climates. General guidance for the selection of concrete masonry units for durability can be found in standards such as BS 5628-3 (2005) and AS 3700 (2011).

8.3 High-pozzolanic industrial by-product content concrete masonry blocks

Many types of industrial by-products are now used as pozzolans to replace part of Portland cement. They can be broadly classified into three types, as follows:

1. Slag,
2. Coal ash, and
3. Agricultural waste or by-product ash.

The most commonly used slag is ground granulated blast furnace slag (GGBFS) for reasons of availability. For coal ash, fly ash (FA) obtained from pulverized coal combustion (PCC) is the most common—again, for reasons of availability. Other types of coal ash, e.g. bottom ash and FAs obtained from other combustion techniques, are also available. For agricultural waste or by-product ashes, rice husk ash (RHA) is the most common one and is used quite extensively for making masonry concrete block (Ettu, Nwachukwu, Arimanwa, Anyanwu, & Okpara, 2013; Oyekan & Kamiyo, 2008; Oyetola & Abdullahi, 2006). The other ashes, such as rice husk bark ash, palm oil fuel ash (POFA), bagasse ash, and cement kiln dust, also possess pozzolanic properties and thus can be used for making masonry concrete block as well. Figure 8.1 shows the morphology of some of the industrial by-product pozzolans. FA is spherical in shape and this helps with the workability of the mix. The other ground pozzolans range from mostly angular in shape to highly irregular, while some have porous surfaces, especially those due to the original cellular structure of the agricultural product.

The use of a high content of industrial by-product pozzolan in masonry cement and concrete masonry block is important. The increase in the usage of this by-product pozzolan offers an eco-friendly alternative by allowing a reduction in the use of Portland cement.

8.3.1 Ground granulated blast furnace slag concrete block

Granulated blast furnace slag is the glassy material formed by water quenching of molten slag discharged from the blast furnaces in the iron-making industry. The water

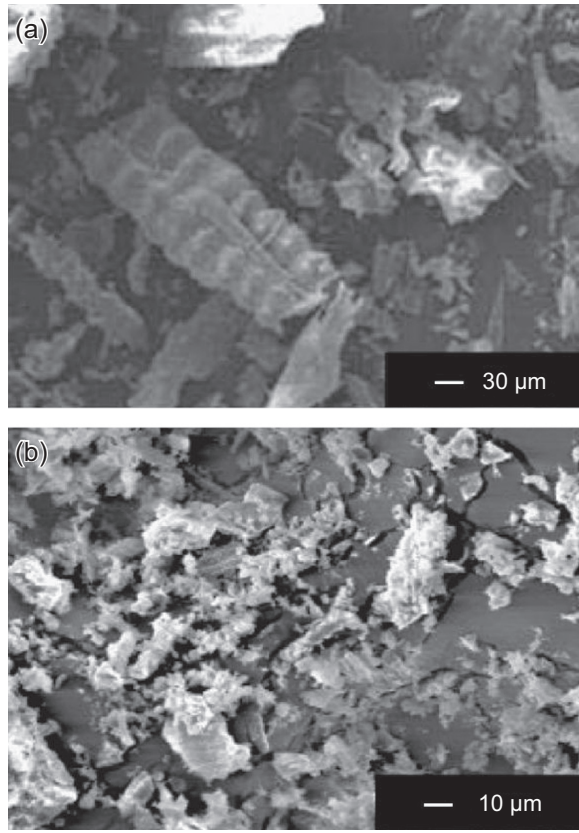

Figure 8.1 Morphology of (a) rice husk ash; (b) ground rice husk ash; (c) palm oil fuel ash; (d) ground palm oil fuel ash; (e) fly ash; (f) fine fly ash (Chindaprasirt, Rukzon, & Sirivivatnanon, 2008); (g) bottom ash (Sathonsaowaphak, Chindaprasirt, & Pimraksa, 2009); (h) ground bottom ash; (i) bagasse ash (Chusilp, Jaturapitakkul, & Kiattikomol, 2009a); (j) ground bagasse ash; (k) ground granulated blast furnace slag (Karim, Zain, Jamil, & Lai, 2013); and (l) cement kiln dust (Peethamparan, Olek, & Diamond, 2009).

quenching process is termed granulation and its product, granulated blast furnace slag, is sand-like in appearance. The granulated slag is then dried and ground in a ball mill or similar equipment to fineness similar to normal Portland cement or greater (approximately 400−650 m^2/kg) before being used as supplementary cementitious material.

Standards that cover GGBFS for use as supplementary cementitious material in cement and concrete include ASTM C989/C989M-12a (2012), BS EN 15167 (2006), GB/T 18046 (2008), and AS 3582.2 (2001). Slag-blended cements are covered in standards such as BS EN 197-1 (2011), BS 146 (2002), and JIS R 5211 (2009). The typical ranges of chemical composition of blast furnace slags in the US and Canada are 32−43% SiO_2, 7−16% Al_2O_3, 32−45% CaO, and 5−15% MgO (ACI 233R-03, 2003).

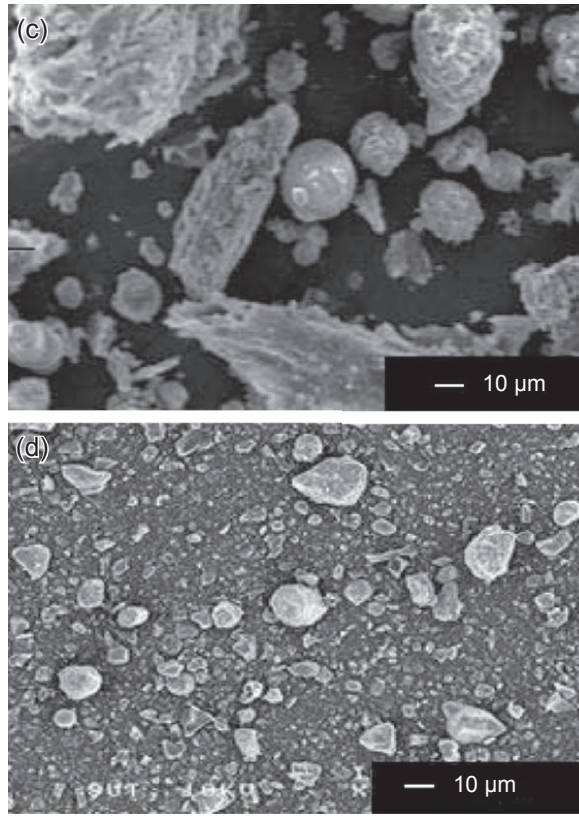

Figure 8.1 Continued.

When the molten slag, on leaving the furnace, is not water quenched, it is directed into ground bays to be air cooled. This material is commonly called blast furnace rock slag, and it is a crystalline rock-like material that has little cementitious value and is essentially inert in concrete. Rock slag is suitable for use as aggregate in concrete, as per ASTM C33 (2013). Crushed air-cooled slag has been used as an aggregate in the manufacture of commercial concrete masonry blocks for many years. The residual strength of the concretes and mortars after exposure to high temperature is higher for products containing air-cooled slag and other slag-based aggregates in comparison to natural sand or aggregates (Cree, Green, & Noumowé, 2013; Shoaiba, Ahmedb, & Balaha, 2001).

The advantages of the use of properly ground blast furnace slag to partially replace Portland cement can be realized for both fresh and hardened concretes. In the fresh state, the workability of fresh concrete is enhanced and the setting time is increased with reduced bleeding. In the hardened state, the concrete durability is improved with increased resistance to sulfate attack and resistance to alkali−silica reactions (ACI 233R-03, 2003). However, some drawbacks such as low early strength development do exist for concrete containing GGBFS as partial replacement of Portland cement. O'Rourke, McNally, and Richardson (2009) suggested the use of a small

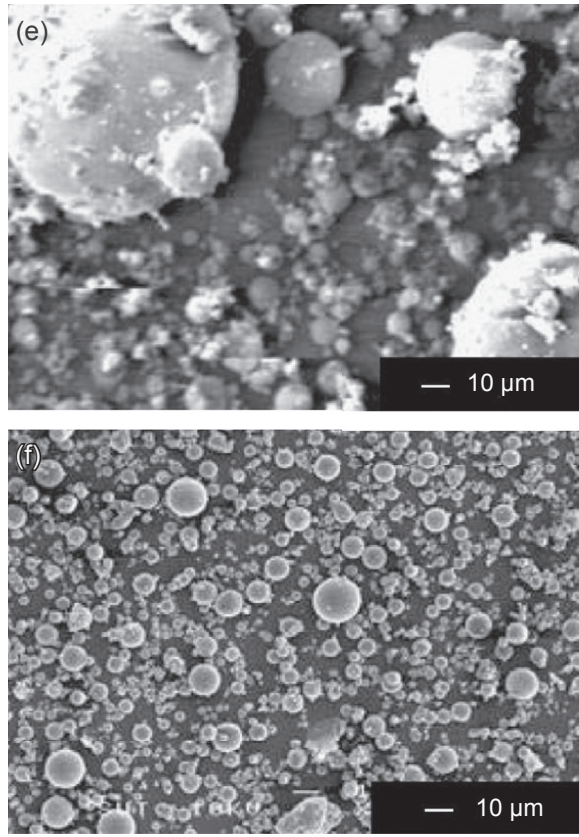

Figure 8.1 Continued.

quantity of gypsum and anhydrite to improve the early strength development of GGBFS—Portland cement binders with only a small effect on the later-age strength development of the mixtures. The mix of GGBFS and Portland cement with 0.5% gypsum and 2.5% anhydrite produced good early strength and high 28-compressive strength, as shown in Figure 8.2. The same author suggested that the formulation could be used to produce painting-quality masonry blocks with good early strength at low binder content.

Slag is often used in combination with other pozzolan in blending with Portland cement for making masonry cement. Fonseca (2012) managed to make good masonry cement with only 20% ordinary Portland cement and the rest consisting of 25% FA and 55% slag. The same author showed that the 28-day compressive strength obtained complied with the requirement for class S masonry mortar as per ASTM C91/C91-M-12 (2012).

In the manufacturing of precast concrete and blocks, the use of slag-blended cement, particularly type IS (65% Portland, 35% slag) as per ASTM C595/C595M-13 (2013), is reported to result in better quality, particularly in regard to reduction in cracking

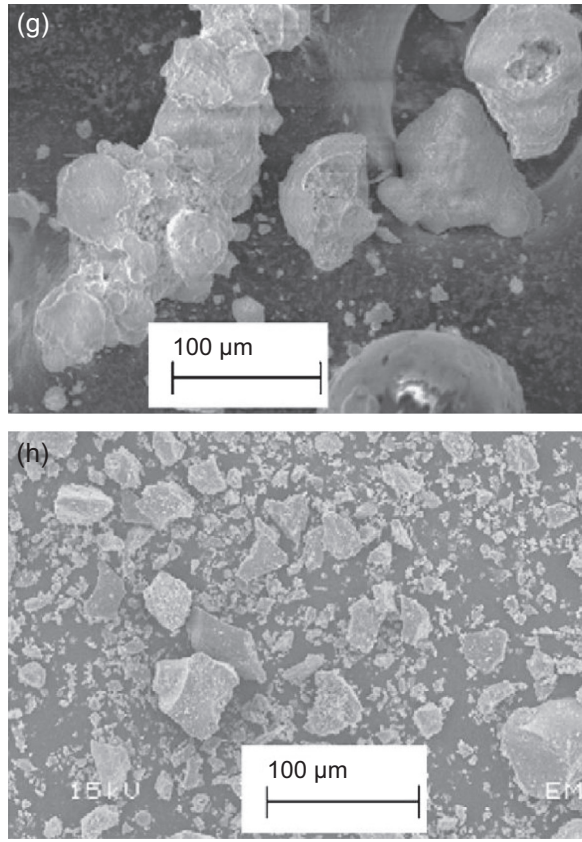

Figure 8.1 Continued.

during block processing (Slagcement.org, 2013). Other benefits that slag-blended cement can impart on concrete blockwork include (Slag Cement Association, 2003):

- An architecturally appealing lighter color;
- A finer, tighter surface texture;
- Reduced efflorescence;
- Decreased permeability; and
- Increased compressive strengths.

The "optimal" replacement percentage of slag in the manufacturing of concrete blocks depends on the block making process and the curing condition, as well as cost/benefit considerations. Currently, the common slag replacement percentage in commercial production is in the range of 20−50% of the cementitious materials.

8.3.2 Fly ash, bottom ash, and other coal ash masonry blocks

FA and bottom ash are by-products obtained from the burning of coal at a temperature of around 1200−1300 °C in PCC units in electricity power plants. During combustion,

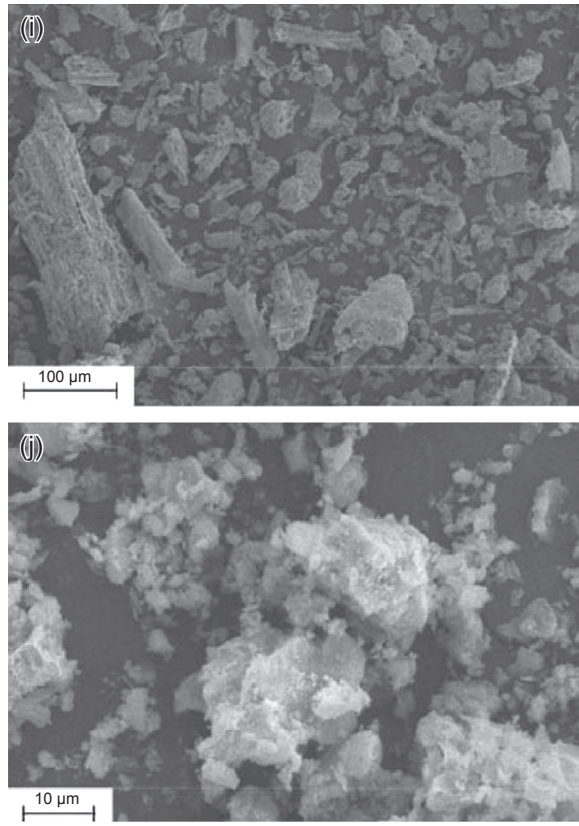

Figure 8.1 Continued.

mineral impurities such as clay, feldspar, quartz, and shale fuse and escape with the exhaust gases. As the fused material flies upwards, it solidifies into mostly fine spherical particles called "fly ash." This is then collected by electrostatic precipitators or bag filters. FA accounts for approximately 85% of the total coal ash. The other 15%, bottom ash, is collected at the bottom of the furnace. Bottom ash consists of agglomerated ash particles that are too heavy to escape with the exhaust gases.

ASTM C618 (2012) categorizes FAs as Class F and Class C. Class F FAs are generally low on CaO and are normally produced from burning anthracite or bituminous coals. Class C FA contains high CaO and is generally produced from burning lignite or sub-bituminous coal. Class C FA has pozzolanic properties and varying degrees of self-hardening/cementitious properties. FA for use in concrete is also covered in standards such as JIS R 5213 (2009) and BS EN 450 (Part 1:2012; Part 2:2005).

FA can be successfully used to blend with mixed cement (comprising approximately 80% OPC and 20% limestone blend) for making masonry cement (Chindaprasirt, Buapa, & Cao, 2005). The cement with 20% FA showed 28-day compressive strength of 18.0 MPa, which satisfied the strength requirement of 14.5 MPa for Type S masonry

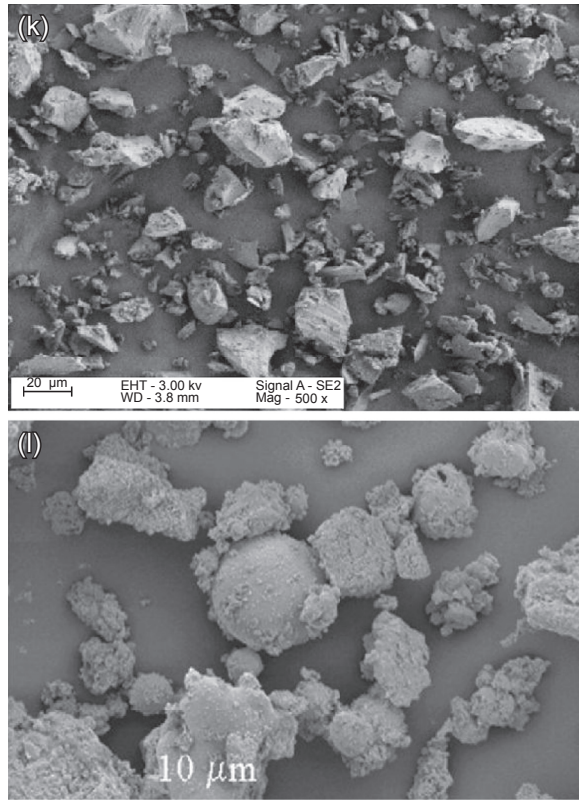

Figure 8.1 Continued.

cement as per ASTM C 91/C91M-12 (2012), and that with 40% FA showed 28-day compressive strength of 14.0 MPa. An increase in setting times with incorporation of FA was also observed; this is quite beneficial, especially in hot tropical climates. FA with very high calcium content possesses self-hardening/cementitious properties and thus can be used as a binder to produce masonry block. Turgut (2010) used high-calcium FA with 32% CaO mixed with limestone powder waste to produce a masonry block without the use of Portland cement using 5% water content and a compression pressure of 20 MPa. The mixture with FA content of 30% by volume showed relatively high 28-day compressive strength of 15.5 MPa (as shown in Figure 8.3) and acceptable water absorption.

FA can also be used as pozzolan in making lightweight masonry concretes. The 15% and 30% high-calcium FA replacement (using cementing efficiency factor of 0.5) showed increased strength and reduced shrinkage for foam lightweight masonry concrete, as shown in Figure 8.4 (Chindaprasirt & Rattanasak, 2011). FA helps disperse both cement and foam bubble and thus enhances the uniformity of mixtures. For lightweight masonry blocks using 0−4 mm volcanic slag aggregate and 20% FA replacement with binder volume content of 10%, the produced lightweight concrete

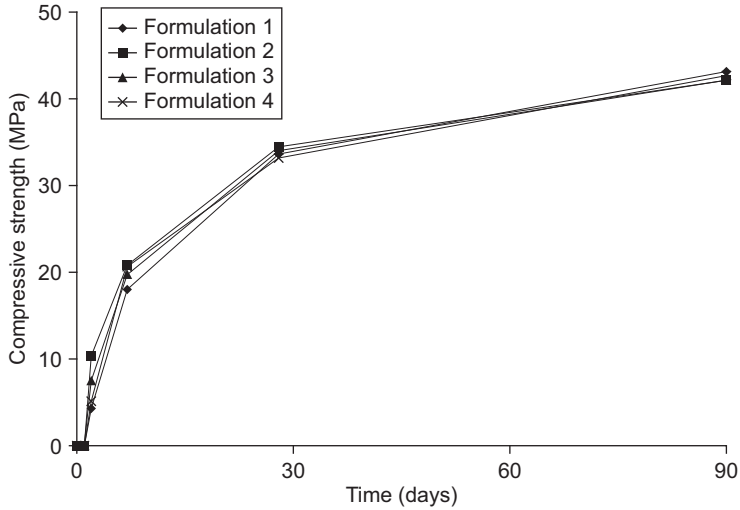

Figure 8.2 Compressive strengths of GGBFS base binders with gypsum (O'Rourke et al., 2009). Formulation 1: Portland cement 30.0%, gypsum 0.0%, lime 0%, GGBFS 70.0%, anhydrite II 0.0%; Formulation 2: Portland cement 29.0%, gypsum 0.5%, lime 0%, GGBFS 68.0%, anhydrite II 2.5%; Formulation 3: Portland cement 28.5%, gypsum 0.6%, lime 0%, GGBFS 67.5%, anhydrite II 3.4%; Formulation 4: Portland cement 27.0%, gypsum 0.6%, lime 3%, GGBFS 66.0%, anhydrite II 3.4%.

gives satisfactory strength and density, as shown in Figure 8.5 (Demirdag, Ugur, & Sarac, 2008). The strength should not be less than 2.8 MPa, as specified in BS 6073-1 (1981). For higher FA replacement, higher binder content is required to offset the reduced cement content of the mixture.

Other FAs can also be used to make masonry concrete blocks. However, the quality of these FAs is not as good as those obtained from the PCC process. These other FAs include those from circulating fluidized bed combustion with a burning temperature around 900−1000 °C and from normal fluidized bed combustion with a burning temperature of 800−900 °C (Homwuttiwong, Jaturapitakkul, & Chindaprasirt, 2012). Kungskulniti, Thaisuchart, Kongmuang, Phornpimolthape, & Charoenca (2011) studied the use of low-quality FA in producing hollow concrete masonry blocks. This FA had low SiO_2, Al_2O_3, and Fe_2O_3 content of 43.5% and a particle size range of 20−70 μm with large particle surface of highly porous texture. The blocks were made from Portland cement, FA, and fine limestone aggregate. The concrete blocks with 70% FA exhibited satisfactory water absorption characteristics and 7-day compressive strength of 4.5 MPa with no problem of leaching of toxic element.

Bottom ash contains similar chemical constituents as FA, but the particle size is larger and contains a large amount of irregular particles with pores and rough surfaces. Ground to fine particles, it can be used as a good pozzolan (Cheriafa, Rochaa, & Pérab, 1999; Jaturapitakkul & Cheerarot, 2003). Since it requires intense grinding to produce reasonable pozzolanic properties, at present bottom ash use is limited to aggregate or

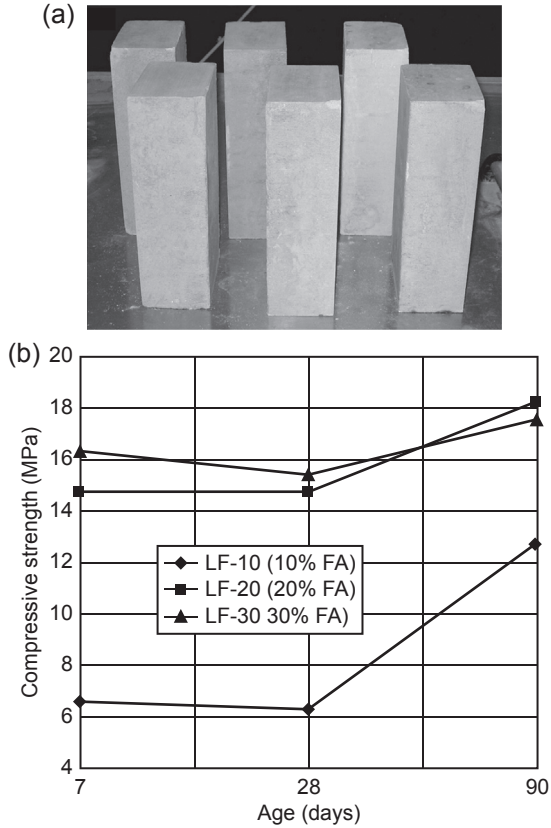

Figure 8.3 Appearance and compressive strength of masonry block from high-calcium fly ash (FA) and limestone powder waste (Turgut, 2010). (a) Appearance of masonry block. (b) Compressive strength development and fly ash content.

sand replacement, especially in masonry concrete (Ozkan Yuksel & Muratoglu, 2007). Ramadoss & Sundararajan (2013) indicated that lignite-based bottom ash can partially replace 20% of fine aggregate in masonry mortar with no adverse effect on strength but with improved sorptivity and coefficient of absorption due to the filler effect. A number of masonry block producers thus use coal combustion by-products in two ways: FA as a partial replacement for cement, and bottom ash as a partial replacement for aggregate (Center for Applied Energy Research, 2013).

8.3.3 Rice husk ash masonry blocks

Rice husk is composed of approximately 40% cellulose, 30% lignin, and 20% silica; when it is burnt, the combustible portion is eliminated. The resulting ash, therefore, contains a substantial amount of silica in the order of 90% (Chindaprasirt, Kanchanda, Sathonsaowaphak, & Cao, 2007; Metha, 1979;

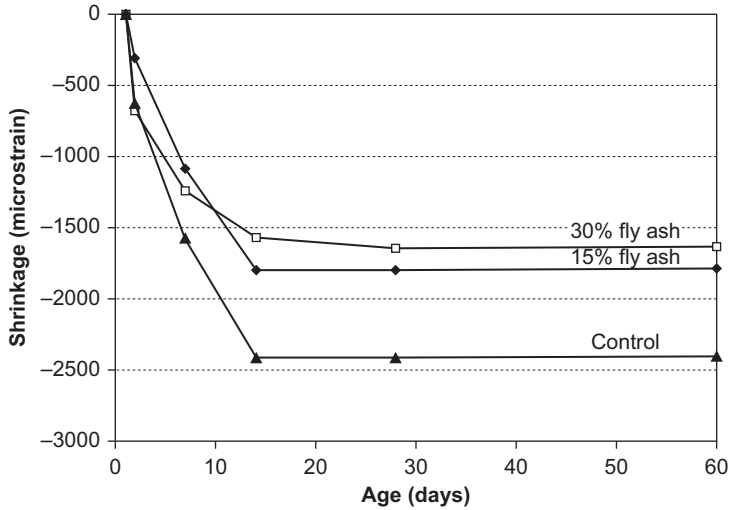

Figure 8.4 Drying shrinkage of lightweight concrete block (density 1600 kg/m^3) (Chindaprasirt & Rattanasak, 2011).

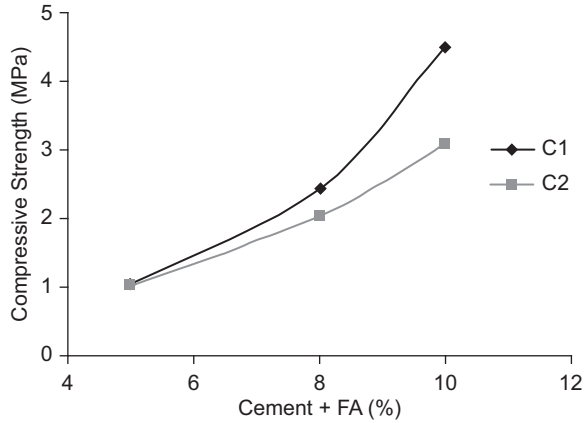

Figure 8.5 Compressive strength of lightweight masonry block with 0−4 mm volcanic slag aggregate and cement with 20% fly ash replacement (Demirdag et al., 2008). C1 = Portland cement; C2 = Portland cement with 20% fly ash replacement.

Stroeven, Bui, & Sabuni, 1999). There are two forms of silica: amorphous and crystalline; the composition is dictated by the temperature and duration of burning. RHA with a high amount of amorphous silica is reactive and is suitable for use as a pozzolan to partially replace cement. The reactive RHA is usually obtained by burning at a temperature lower than 650−700 °C (Chindaprasirt, Kanchanda, Sathonsaowaphak, & Cao, 2007; Della, Kuhn, & Hotza, 2002). At a higher burning temperature, the RHA contains some crystalline silica, but still can be used as good

pozzolan provided that it is properly ground (Ismail & Waliuddin, 1996; Rukzon, Chindaprasirt, & Mahachai, 2009). Rice husk is used extensively as a bio-fuel source for small power generating plants. In the modern plants, *fluidized bed combustors and fluidized bed gasifiers are used for efficient heat recovery*. The burning temperatures vary mostly between 600 and 900 °C (Natarajan, Nordina, & Rao, 1998) with the average temperature of 740 °C. For the fluidized bed, the ash produced is small in particles usually less than 0.375 mm as combustion is accompanied by a simultaneous attrition of ash (Bhattachary, Shah, & Alikhani, 1984; Natarajan et al., 1998).

As shown in Figure 8.1, the morphology of RHA is highly porous texture resulting from the cell structure of the husk. The reactivity of RHA is increased with grinding to a required fineness (Rukzon et al., 2009). The incorporation of RHA requires additional water to maintain the workability of the mix (Chindaprasirt, Kanchanda, et al., 2007; Kene, Domke, Deshmukh, & Deotale, 2011), and this could offset the strength gain due to the higher water-to-cement ratio. The setting of RHA concrete is prolonged with the increase in RHA content. The addition of a proper amount of 20−30% RHA by weight of binder was found to increase the strength and durability of concrete. The incorporation of RHA refines the pore of paste and reduces the $Ca(OH)_2$ content. RHA concrete is therefore more durable than normal concrete, with increased resistance to sulfate, acid, and chloride attack (Chindaprasirt, Kanchanda, et al., 2007; Chindaprasirt & Rukzon, 2008; Coutinho, 2002; Ganesan, Rajagopal, & Thangavel, 2008; Zhang & Mohan, 1996). Figure 8.6 shows the expansion of mortar bars containing RHA and FA immersed in 5% sulfate solution tested in accordance with ASTM C1012/C1012M − 13 (2013) and Chindaprasirt, Kanchanda, et al. (2007). The resistance to sulfate attack of mortars containing RHA and FA are much better than that of normal Portland cement mortar. The mortar containing 40% RHA shows the best result.

RHA is also used in combination with other pozzolans. Most common is the combination of RHA and FA (Chindaprasirt & Rukzon, 2008; Isaia, Gastaldini, & Moraes, 2003; Kene et al., 2011). FA, having spherical particles with smooth surfaces, helps increase the workability of the mix with the ball bearing effect, whereas RHA particles are quite cellular and thus increases the water requirement. FA thus helps the workability of the RHA concrete (Chindaprasirt & Rukzon, 2008; Kene et al., 2011). When RHA is used in combination with FA, concrete with a relatively high strength of 45.0 MPa can be obtained with the mixture of FA to RHA of 2:1 and 30% replacement of Portland cement compared with 40.0 MPa of the control concrete (Kene et al., 2011). This improvement in strength and durability of mixes containing both RHA and FA is due to the synergic effect of the two pozzolans (Chindaprasirt & Rukzon, 2008; Isaia et al., 2003).

As RHA is abundant and available worldwide, it is commonly used as pozzolan in making concrete blocks (Ettu, Nwachukwu et al., 2013; Nasly & Yassin, 2009; Oyetola & Abdullahi, 2006). The effectiveness of RHA depends on its reactivity. High reactivity is associated with proper burning and grinding. When used in masonry concrete, the RHA cement blend with excellent strength and durability characteristics would enhance the properties of the masonry concrete blocks. In many instances, the proper grinding of RHA is not an option in order to reduce the cost and thus lower the

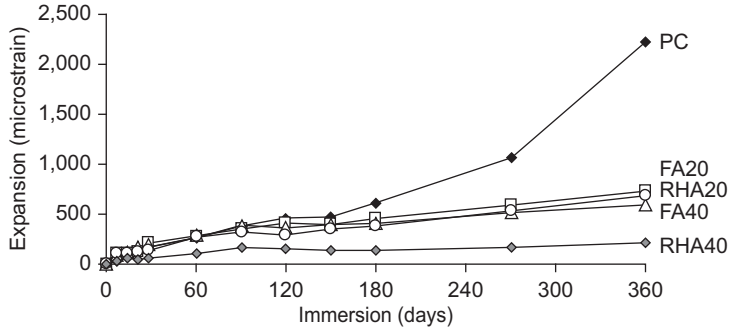

Figure 8.6 Expansion of mortar bars containing RHA and fly ash immersed in 5% sodium sulfate solution (Chindaprasirt, Kanchanda, et al., 2007). PC = Portland cement mortar, FA20 = 20% fly ash mortar, FA40 = 40% fly ash mortar, RHA20 = 20% rice husk ash mortar, RHA40 = 40% rice husk ash mortar.

strength of concretes. Masonry RHA cement concrete blocks were developed and used successfully for load-bearing masonry walls (Nasly & Yassin, 2009). The mix with cement-to-RHA ratio of 1:4 by volume, cement/sand + gravel ratio of 1:8 gave compressive strength of 4.0 MPa. The authors suggested proper compaction, such as a vibrating feeder to vibrate the mold, to obtain high-strength blocks. RHA (passed No. 325 sieve) was also used to replace Portland cement at 50% level to make interlocking blocks with the ratio of cement to sand to lateritic soil of 1:3.5:3.5. The 28-day strength of the block of 6.6 MPa and the water absorption of 10−12% were satisfactory (Greepala & Parichartpreecha, 2011).

Even with low quality such as with a high loss of ignition (LOI), RHA can still be used successfully in making masonry concrete block, but at a low percentage replacement. The RHA with high LOI indicates the incomplete burning with still-high volatile matter, including carbon, and its use will result in a lower cementitious quantity and quality. Oyetola & Abdullahi (2006) used RHA with LOI of 17.8% to make 150 × 450 mm hollow sandcrete blocks. The mix with 20% RHA partially replaced cement using a binder-to-sand ratio of 1:8 produced blocks with a satisfactory compressive strength of 3.65 MPa. The same authors also observed that incorporation of RHA with high LOI also increases the water requirement and the setting time of the mixture. In normal circumstances the LOI should be less than 10%, as specified in ASTM C618-12 (2012). Published results (Cook & Suwanvitaya, 1981; Suriyakumaran & Ismail, 1979) indicate that the use of RHA with carbon content of 10% has no adverse effect on strength. Chik, Bakar, Johari, & Jaya (2011) also found that the use of 20% RHA to replace cement can produce masonry concrete blocks with little effect on strength and water absorption.

8.3.4 Other industrial by-product pozzolans

When burnt, most agricultural by-product ashes contain a high proportion of silica, which is the main ingredient of pozzolan, and after proper grinding they can be

used as good pozzolans. Bagasse ash is obtained from the use of bagasse as a fuel source in sugar mills and, similar to other agricultural waste ash, it can be used as pozzolan (De Paula, Tinoco, Rodrigues, & Saraz, 2010; Ganesan, Rajagopal, & Thangavel, 2007; Rukzon & Chindaprasirt, 2012). The incorporation of bagasse ash results in an increase in resistance to chloride penetration with little or no adverse effect on the strength development of concrete (Amin, 2011; Rukzon & Chindaprasirt, 2012). Bagasse ash is also used in conjunction with other pozzolans in making masonry blocks. Kulkarni, Raje, & Rajgor (2013) used up to 50% bagasse ash mixed with FA as blended pozzolan for use with lime and quarry dust to produce satisfactory masonry blocks with compressive strength of 4.0−7.5 MPa. An added benefit is the reduction in the weight of the blocks with increased addition of bagasse ash. Bagasse ash (passed No. 200 sieve) is also used to replace Portland cement at 40% level to make interlocking blocks with the ratio of cement to sand to lateritic soil of 1:3.5:3.5. The 28-day strength of the block is over 7.0 MPa and the water absorption is satisfactory at 10−12% (Nokkaew, Khobklang, & Greepala, 2008). The incorporation of a proper amount of bagasse ash also improves the resistance to sulfates of mortar (Chusilp, Jaturapitakkul, & Kiattikomol, 2009b). The ability to resist sulfate attack reduces when the level of replacement is too large and the quality of the bagasse ash is low, as indicated by the high LOI, as shown in Figure 8.7.

POFA is obtained from the burning of palm oil fibers, shells, and empty fruit bunches in power plants (Sata, Tangpagasit, Jaturapitakkul, & Chindaprasirt, 2012). With proper grinding, the ground POFA can be used as a pozzolan (Tay, 1990) to partially replace Portland cement up to 40%, with only a small reduction in strength but with improvement in the chloride penetration resistance of mortar (Chindaprasirt et al., 2008) and water permeability of concrete (Chindaprasirt, Homwuttiwong, & Jaturapitakkul, 2007). POFA is even used as a supplementary cementitious material for producing high-strength concrete (Tangchirapat, Jaturapitakkul, & Chindaprasirt, 2009). Up to 50% POFA can be used to replace cement for making masonry concrete blocks with adequate strength and satisfactory water absorption (Kaosol, Tongsuwan, & Kaewsatain, 2010). POFA is used successfully in making aerated masonry concrete block. The mix with 30% POFA partially replaced cement gives masonry blocks with satisfactory compressive strength of 4.0 MPa (Hussin & Abdullah, 2009).

Apart from using rice husk alone as a fuel source in small power plants, rice husk and eucalyptus bark are used in some power plants. The resulting rice husk−bark ash is also rich in silica and thus can be used as good pozzolan (Chindaprasirt, Homwuttiwong, et al., 2007; Tangchirapat, Buranasing, Jaturapitakkul, & Chindaprasirt, 2008). Several other agricultural by-product ashes can also be used. Palm bunch ash (PBA) and saw dust ash (SDA) have been used to replace mixed cement for making masonry mortar blocks (Anang, Tulashie, & Boadu, 2011). After a 14-day curing period, mortar from cement replaced with PBA and SDA at dosages up to 40% gave compressive strengths that complied with the standard compressive strength for class A block of 4.0 MPa. Corn cob ash (CCA) has also been used as pozzolan in making masonry blocks. CCA burnt at 650 °C and passed 600 μm sieve is used to replace part of cement in making sandcrete blocks with a cement-to-sand ratio of 1:6. The resulting sandcrete blocks with 25% CCA exhibit satisfactory

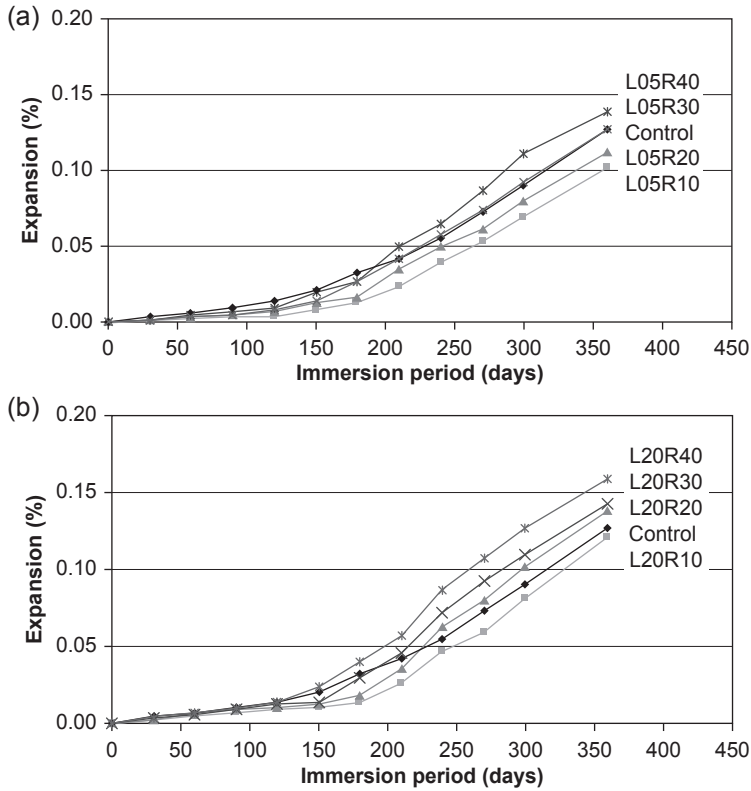

Figure 8.7 Expansion of mortar bars containing bagasse ash immersed in 5% magnesium solution (Chusilp et al., 2009b). (a) Portland cement replaced with 5% LOI bagasse ash. (b) Portland cement replaced with 20% LOI bagasse ash. Control = 100% Portland cement, L05 = bagasse ash with 5% LOI, R10 = 10% replacement with bagasse ash.

strengths of 3.8−4.9 MPa (Ettu, Anya, Arimanwa, Anyaogu, & Nwachukwu, 2013; Ettu, Nwachukwu, et al., 2013).

8.4 Future trends

The increasing use of industrial by-product pozzolans and other alternative pozzolans will be the future trend of using cementing materials, especially in masonry concrete, where strength is not the prime concern. For example, cement kiln dust exists in sizable quantity and can also be exploited for making masonry blocks. It is a highly alkaline solid waste in the form of dust trapped from cement kiln exhaust gas. The cement kiln dust, if not returned to the cement production process, is usually disposed of at landfill sites. A number of patents have been granted for the use of this cement kiln dust in making masonry concrete (Wills, 1983) and for use in combination with FA or with

FA plus GGBFS (Barbour, 2003). Other by-product pozzolanic materials will be used more extensively in the future. For example, calcium carbine residue is used in conjunction with bagasse ash (Rattanashotinunt, Thairit, Tangchirapat, & Jaturapitakkul, 2013) to form a new cementitious material. The trend is for more and more of the alternative pozzolans to be studied for use as eco-cementing materials, especially in the masonry block industry.

8.5 Sources of further information and advice

State-of-the-art of masonry block making is quite diverse, ranging from the old masonry concretes with hand tamping to modern machine molding blocks, and from a standard application such as non-load-bearing and load-bearing blocks to nonstandard architectural applications. In regard to the knowledge of industrial by-product pozzolan masonry blocks, it is therefore advisable to go through the books and articles on alternative cementitious materials and on masonry concrete, such as those by Siddique (2008), Siddique & Khan (2011), Malhotra & Mehta (1996), Cox, Nugteren, & Janssen-Jurkovičová (2008), Kicklighter (2010), ACI 530/530.1-13 (2013), and Trimble & Brisch (2008). The references given in this chapter are quite comprehensive and thus can be used to provide basic knowledge on the subject.

References

ACI 116R-90. (2000). *Cement and concrete terminology*. ACI Committee 116. USA: American Concrete Institute.

ACI 211.3R-02. (2002). *Guide for selecting proportions for no-slump concrete*. ACI Committee 211. USA: American Concrete Institute.

ACI 233R-03. (2003). *Slag cement in concrete and mortar*. ACI Committee 233. USA: American Concrete Institute.

ACI 530/530.1-13. *Building code requirements and specification for masonry structures and companion commentaries*. USA: Joint ACI/ASCE/TMS.

Amin, N. (2011). Use of bagasse ash in concrete and its impact on the strength and chloride resistivity. *Journal of Materials in Civil Engineering, 23*(5), 717−720.

Anang, M. A., Tulashie, S. K., & Boadu, K. O. (2011). Effect of additives on the mechanical properties of some cement products. *Pelagia Research Library, Der Chemica Sinica, 2*(6), 294−303.

AS 3582.2-2001. (2001). *Supplementary cementitious materials for use with Portland and blended cement. Part 2. Slag − ground granulated iron blast furnace*. Standards Australia.

AS 3700-2011. (2011). *Masonry structures*. Standards Australia.

AS/NZS 4455.1:2008. (2008). *Masonry units, pavers, flags and segmental retaining wall units. Part 1: Masonry units*. Standards Australia.

ASTM C33/C33M-13. (2013). Standard specification for concrete aggregate. In *Book of standards* (Vol. 04.02). USA: American Society for Testing and Materials.

ASTM C55-11. (2011). Standard specification for concrete building brick. In *Book of standards* (Vol. 04.05). USA: American Society for Testing and Materials.

ASTM C90-13. (2013). Standard specification for load bearing concrete masonry units. In *Book of standards* (Vol. 04.05). USA: American Society for Testing and Materials.

ASTM C91/C91M-12. (2012). Standard specification for masonry cement. In *Book of standards* (Vol. 04.01). USA: American Society for Testing and Materials.

ASTM C129-11. (2011). Standard specification for non-load-bearing concrete masonry units. In *Book of standards* (Vol. 04.05). USA: American Society for Testing and Materials.

ASTM C331/331M-10. (2010). Standard specification for lightweight aggregates for concrete masonry units. In *Book of standards* (Vol. 04.02). USA: American Society for Testing and Materials.

ASTM C595/C595M-13. (2013). Standard specification for blended hydraulic cements. In *Book of standards* (Vol. 04.01). USA: American Society for Testing and Materials.

ASTM C618-12. (2012). Standard specification for coal fly ash and raw or calcined natural pozzolan for use in concrete. In *Book of standards* (Vol. 04.02). USA: American Society for Testing and Materials.

ASTM C744-11. (2011). Standard specification for prefaced concrete and calcium silicate masonry units. In *Book of standards* (Vol. 04.05). USA: American Society for Testing and Materials.

ASTM C989/C989M-12a. (2012). Standard specification for slag cement for use in concrete and mortars. In *Book of standards* (Vol. 04.02). USA: American Society for Testing and Materials.

ASTM C1012/C1012M − 13. (2013). Standard test method for length change of hydraulic-cement mortars exposed to a sulfate solution. In *Book of standards* (Vol. 04.01). USA.

ASTM C1634-11. (2011). Standard specification for concrete facing brick. In *Book of standards* (Vol. 04.05). USA: American Society for Testing and Materials.

ASTM D689-12. (2012). *Standard test methods for laboratory compaction characteristics of soils using standard effort (600 kN-m/m^3)*. USA: American Society for Testing and Materials. Book of Standards (Withdrawn 2009).

ASTM D1557-12. (2012). Standard test methods for laboratory compaction characteristics of soil using modified effort (2700 kN-m/m^3). In *Book of standards* (Vol. 04.08). USA: American Society for Testing and Materials.

Barbour, R. L. (2003). *Settable composition containing cement kiln dust*, US patent No. 6645290 B1.

Bartos, P. J. M., Sonebi, M., & Tamimi, A. K. (2002). Workability and rheology of fresh concrete; compendium of tests. In P. J. M. Bartos, M. Sonebi, & A. K. Tamimi (Eds.), *Report of RILEM TC 145-WSM*.

Bhattachary, S. C., Shah, N., & Alikhani, Z. (1984). Some aspects of fluidized bed combustion of paddy husk. *Applied Energy, 16*(4), 307−316.

BS 146:2002. (2002). *Specification for blast furnace cements with strength properties outside the scope of BS EN 197-1*. British Standards.

BS 1377:1975. (1975). *Methods of test for soils for civil engineering purposes*. British Standards.

BS 1924:1975. (1975). *Methods of test for stabilized soils*. British Standards.

BS 5628-3:2005. (2005). *Code of practice for the use of masonry − part 3: Materials and components, design and workmanship*. British standards.

BS 6073-1:1981. (1981). *Precast concrete masonry units, specification for precast concrete masonry units*. British Standards.

BS EN 197-1:2011. (2011). *Cement, part 1: Composition, specifications and conformity criteria for common cements*. British Standards.

BS EN 450 (Part 1:2012; Part 2:2005). *Fly ash for concrete*. British Standards.

BS EN 771-3:2011. (2011). *Specification for masonry units. Part 3: Aggregate concrete masonry units, British Standard*. British Standards.

BS EN 15167 (Part 1 and Part 2):2006. (2006). *Ground granulated blast furnace slag for use in concrete mortar and grout*. British Standards.

Center for Applied Energy Research. (2013). *Coal combustion by-products (CCBs): How to evaluating fly ash and bottom ash for concrete block*. University of Kentucky and Center for Applied Energy Research. Available from http://www.caer.uky.edu/kyasheducation/testing-block.shtml Accessed on 01.11.13.

Cheriafa, M., Rochaa, J. C., & Pérab, J. (1999). Pozzolanic properties of pulverized coal combustion bottom ash. *Cement and Concrete Research, 29*(9), 1387−1391.

Chik, F. A. W., Bakar, B. H. A., Johari, M. A. M., & Jaya, R. P. (2011). Properties of concrete block containing rice husk ash subjected to GIRHA. *International Journal of Research and Reviews in Applied Sciences, 8*(1), 57−64.

Chindaprasirt, P., Buapa, N., & Cao, H. T. (2005). Mixed cement containing fly ash for masonry and plastering work. *Construction and Building Materials, 19*, 612−618.

Chindaprasirt, P., Jaturapitakkul, C., & Sinsiri, T. (2005). Effect of fly ash fineness on compressive strength and pore size of blended cement paste. *Cement and Concrete Composites, 27*, 425−428.

Chindaprasirt, P., Homwuttiwong, S., & Jaturapitakkul, C. (2007). Strength and water permeability of concrete containing palm oil fuel ash and rice husk-bark ash. *Construction and Building Materials, 21*, 1492−1499.

Chindaprasirt, P., Kanchanda, P., Sathonsaowaphak, A., & Cao, H. T. (2007). Sulfate resistance of blended cements containing fly ash and rice husk ash. *Construction and Building Materials, 21*, 1356−1361.

Chindaprasirt, P., & Rattanasak, U. (2011). Shrinkage behavior of structural foam lightweight concrete containing glycol compounds and fly ash. *Materials and Design, 32*(2), 723−727.

Chindaprasirt, P., & Rukzon, S. (2008). Strength, porosity and corrosion resistance of ternary blend portland cement, rice husk ash and fly ash mortar. *Construction and Building Materials, 22*(8), 1601−1606.

Chindaprasirt, P., Rukzon, S., & Sirivivatnanon, V. (2008). Resistance to chloride penetration of blended Portland cement mortar containing palm oil fuel ash, rice husk ash and fly ash. *Construction and Building Materials, 22*(5), 932−938.

Chusilp, N., Jaturapitakkul, C., & Kiattikomol, K. (2009a). Utilization of bagasse ash as a pozzolanic material in concrete. *Construction and Building Materials, 23*, 3352−3358.

Chusilp, N., Jaturapitakkul, C., & Kiattikomol, K. (2009b). Effects of LOI of ground bagasse ash on the compressive strength and sulfate resistance of mortars. *Construction and Building Materials, 23*, 3523−3531.

Cook, D. J., & Suwanvitaya, P. (1981). Rice husk ash based cements − a state of the art review. In *Proc. ESCAP/RCTT: Workshop on rice husk ash cement, New Delhi, India*.

Coutinho, J. S. (2002). The combined benefits of CPF and RHA in improving the durability of concrete structures. *Cement and Concrete Composites, 25*(1), 51−59.

Cox, M., Nugteren, H., & Janssen-Jurkovičová, M. (2008). *Combustion residues: Current, novel and renewable applications*. In M. Cox, H. Nugteren, & M. Janssen-Jurkovičová (Eds.). John Wiley & Sons.

Cree, D., Green, M., & Noumowé, A. (2013). Residual strength of concrete containing recycled materials after exposure to fire: a review. *Construction and Building Materials, 45*, 208−223.

De Paula, M. O., Tinoco, I. D. F. F., Rodrigues, C. D. S., & Saraz, J. A. O. (2010). Sugarcane bagasse ash as a partial Portland cement replacement material. *Dyna, 163*, 47−54.

De Vekey, R. C. (2001). Bricks, blocks and masonry made from aggregate concrete: performance requirements. In *BRE Digest 460 Part 1, BRE, Garston, Watford WD25 9XX*. UK.

Della, V. P., Kuhn, L., & Hotza, D. (2002). Rice husk ash as an alternative source for active silica production. *Journal of Materials Letters, 57*, 818−821.

Demirdag, S., Ugur, I., & Sarac, S. (2008). The effects of cement/fly ash ratios on the volcanic slag aggregate lightweight concrete masonry units. *Construction and Building Materials, 22*, 1730−1735.

Dowson, A. (1990). Mix design for concrete block paving. In *Proceedings of the 1st international conference on concrete block paving* (pp. 121−127). UK: S. Marshall & Son Ltd.

Ettu, L. O., Anya, U. C., Arimanwa, J. I., Anyaogu, L., & Nwachukwu, K. C. (2013). Strength of binary blended cement composites containing corn cob ash. *International Journal of Engineering Research and Development, 6*(10), 77−82.

Ettu, L. O., Nwachukwu, K. C., Arimanwa, J. I., Anyanwu, T. U., & Okpara, S. O. (2013). Strength of blended cement sandcrete and soilcrete blocks containing Afikpo rice husk ash and corn cob ash. *International Journal of Modern Engineering and Research, 3*(3), 1366−1371.

Fonseca, F. S. (May 10−12, 2012). *High volume fly ash masonry grout*. Struct Magazine.

Ganesan, K., Rajagopal, K., & Thangavel, K. (2007). Evaluation of bagasse ash as supplementary cementitious material. *Cement and Concrete Composites, 29*, 515−524.

Ganesan, K., Rajagopal, K., & Thangavel, K. (2008). Rice husk ash blended cement: assessment of optimal level of replacement for strength and permeability properties of concrete. *Construction and Building Materials, 22*(8), 1675−1683.

GB/T 18046-2008. (2008). *Ground granulated blast furnace slag used in cement and concrete*. Chinese National Standards.

Grant, W. (1952). *Manufacture of concrete masonry units*. Chicago, IL, USA: Concrete Publishing Corp.

Greepala, V., & Parichartpreecha, R. (2011). Effects of using fly ash, rice husk ash, and bagasse ash as replacement materials on the compressive strength and water absorption of lateritic soil-cement interlocking blocks. In *The 9th Australasian masonry conference Queenstown, New Zealand*.

Homwuttiwong, S., Jaturapitakkul, C., & Chindaprasirt, P. (2012). Strength and water permeability of concrete containing various types of fly ash and filler material. *International Journal of Materials Research, 103*(8), 1058−1064.

Husken, G., & Brouwers, H. (2012). On the early behaviour of zero-slump concrete. *Cement and Concrete Research, 42*, 501−510.

Hussin, M. W., & Abdullah, K. (2009). Properties of palm oil fuel ash cement based aerated concrete panel subjected to different curing regimes. *Malaysian Journal of Civil Engineering, 21*(1), 17−31.

Isaia, G. C., Gastaldini, A. L. G., & Moraes, R. (2003). Physical and pozzolanic action of mineral additions on the mechanical strength of high-performance concrete. *Cement and Concrete Composites, 25*, 69−76.

Ismail, M. S., & Waliuddin, A. M. (1996). Effect of rice husk ash on high strength concrete. *Construction and Building Materials, 10*, 521−526.

Jablonski, N. (1996). *Mix designs for concrete block − proportioning using the fineness modulus method*. The Aberdeen Group.

Jaturapitakkul, C., & Cheerarot, R. (2003). Development of bottom ash as pozzolanic material. *Journal of Materials in Civil Engineering, 15*(1), 48−53.

JIS R 5211:2009. (2009). *Portland blast furnace slag cement*. Japanese Industrial Standards.

JIS R 5213-2009. (2009). *Portland fly ash cement*. Japanese Industrial Standards.

Kappi, A., & Nordenswan, E. (2007). Workability of no-slump concrete. *Concrete International*, 37−41.

Karim, M. R., Zain, M. F. M., Jamil, M., & Lai, F. C. (2013). Fabrication of a non-cement binder using slag, palm oil fuel ash and rice husk ash with sodium hydroxide. *Construction and Building Materials, 49*, 894−902.

Kaosol, T., Tongsuwan, W., & Kaewsatain, S. (2010). Recycling of oil palm ash as partial replacement of cement in concrete block production. In *The 8th Asian-Pacific regional conference on practical environmental technologies (APRC2010)* (pp. 24−27). Ubon-ratchathani, Thailand: Ubon Ratchathani University.

Kene, S. D., Domke, P. V., Deshmukh, S. D., & Deotale, R. S. (2011). Assessment of concrete strength using fly ash and rice husk ash. *International Journal of Engineering Research and Applications, 1*(3), 524−534.

Kicklighter, C. E. (2010). *Modern masonry − Brick, block and stone* (7th ed.). Goodheart-Wilcox.

Koehler, E., & Fowler, D. (2003). Summary of concrete workability test methods. In *Report ICAR 105−1, International Centre for Aggregate Research*. USA: University of Texas at Austin.

Kosmatka, S. H., Kerkhoff, B., Panarese, W. C., MacLeod, N. F., & McGrath, R. J. (2002). *Design and control of concrete mixtures* (7th Canadian ed.). Ottawa, Canada: Cement Association of Canada.

Kroehong, W., Sinsiri, T., Jaturapitakkul, C., & Chindaprasirt, P. (2011). Effect of palm oil fuel ash fineness on the microstructure of blended cement paste. *Construction and Building Materials, 25*(11), 4095−4104.

Kulkarni, A., Raje, S., & Rajgor, M. (2013). Bagasse ash as an effective replacement in fly ash bricks. *Intenational Journal of Engineering Trends and Technology, 4*(10), 4484−4489.

Kungskulniti, N., Thaisuchart, N., Kongmuang, U., Phornpimolthape, C., & Charoenca, N. (2011). Application of bituminous fly ash for partial replacement of cement in producing hollow concrete blocks. *Asia Journal of Public Health, 2*(3), 15−21.

Malhotra, V. M. (2002). Introduction: sustainable development and concrete technology. *ACI Concrete International, 24*(7), 22.

Malhotra, V. M., & Mehta, P. K. (1996). *Pozzolanic and cementitious materials*. Gordon and Breach.

Metha, P. K. (1979). The chemistry and technology of cement made from rice husk ash. In *Proc. UNIDO/ESCAP/RCTT: Workshop on rice husk ash cement, Peshawar, Pakistan* (pp. 113−122). Bangalore, India: Regional Center for Technology Transfer.

Nasly, M. A., & Yassin, A. A. M. (2009). *Sustainable housing using an innovative interlocking block building system*. Meniti Pembangunan Lestari dalam Kejuruteraan Awam, Pusat Pengajian Kejuruteraan Awam, Universiti Sains Malaysia. pp. 130−138.

Natarajan, E., Nordina, A., & Rao, A. N. (1998). Overview of combustion and gasification of rice husk in fluidized bed reactors. *Biomass Bioenergy, 14*(5−6), 533−546.

Nokkaew, K., Khobklang, P., & Greepala, V. (2008). Effect of bagasse ash on water absorption and compressive strength of lateritic soil interlocking block. In *Proc. excellence in concrete construction through innovation*. United Kingdom: Kingston University.

NT Build 427. (1994). *Concrete, Fresh: Compactability with IC-tester (intensive compaction tester)*. Nordtest.

O'Rourke, B., McNally, C., & Richardson, M. G. (2009). The development of calcium sulfate-ggbs-Portland cement binders. *Construction and Building Materials, 23*, 340−346.

Oyekan, G. L., & Kamiyo, O. M. (2008). Effect of Nigerian rice husk ash on some engineering properties of sandcrete blocks and concrete. *Research Journal of Applied Science, 3*(5), 345−351.

Oyetola, E. B., & Abdullahi, M. (2006). The use of rice husk ash in low-cost sandcrete block production. *Leonardo Electronic Journal of Practices and Technology, 8*, 58−70.

Ozkan, O., Yuksel, I., & Muratoglu, O. (2007). Strength properties of concrete incorporating coal bottom ash and granulated blast furnace slag. *Journal of Waste Management, 27*, 161−167.

Peethamparan, S., Olek, J., & Diamond, S. (2009). Mechanism of stabilization of Na-montmorillonite clay with cement kiln dust. *Cement and Concrete Research, 39*, 580−589.

Ramadoss, P., & Sundararajan, T. (2013). Utilization of lignite-based bottom ash as partial replacement of fine aggregate in masonry mortar. *Arabian Journal for Science and Engineering, 39*, 737−745. http://dx.doi.org/10.1007/s13369-013-0703-1.

Rattanashotinunt, C., Thairit, P., Tangchirapat, W., & Jaturapitakkul, C. (2013). Use of calcium carbide residue and bagasse ash mixtures as a new cementitious material in concrete. *Materials and Design, 46*, 106−111.

Rukzon, S., & Chindaprasirt, P. (2012). Utilization of bagasse ash in high-strength concrete. *Materials and Design, 34*, 45−50.

Rukzon, S., Chindaprasirt, P., & Mahachai, R. (2009). Effect of grinding on chemical and physical properties of rice husk ash. *Intenational Journal of Minerals Metallurgy and Materials, 16*(2), 242−247.

Sata, V., Tangpagasit, J., Jaturapitakkul, C., & Chindaprasirt, P. (2012). Effect of W/B ratios on pozzolanic reaction of biomass ashes in Portland cement matrix. *Cement and Concrete Composites, 34*, 94−100.

Sathonsaowaphak, A., Chindaprasirt, P., & Pimraksa, K. (2009). Workability and strength of lignite bottom ash geopolymer mortar. *Journal of Hazardous Materials, 168*, 44−50.

Shoaiba, M. M., Ahmedb, S. A., & Balaha, M. M. (2001). Effect of fire and cooling mode on the properties of slag mortars. *Cement and Concrete Research, 31*(11), 1533−1538.

Siddique, R. (2008). *Waste materials and by-products in concrete*. Berlin Heidelberg: Springer-Verlag.

Siddique, R., & Khan, M. I. (2011). *Supplementary cementing material*. Heidelberg: Springer.

Slag Cement Association. (2003). *Producing concrete block with slag cement, slag cement in concrete, 18*. Slag Cement Association.

Slagcement.org. (2013). *For precast and block, slag makes sense*. Available from http://www.slagcement.org/News/Story_PrecastAndBlock.html Accessed on 21.10.13.

Stroeven, P., Bui, D. D., & Sabuni, E. (1999). Ash of vegetable waste used for economics production of low to high strength hydraulic binders. *Fuel, 78*, 153−159.

Suriyakumaran, R., & Ismail, M. G. M. U. (1979). Rice hull ash cement. In *Proceedings of a joint workshop on production of cement-like materials from agro-wastes, Peshawar, Pakistan, UNIDO, UNESCAP, RCTT*. Pakistan Council of Scientific and Industrial Research Technology.

Tangchirapat, W., Buranasing, R., Jaturapitakkul, C., & Chindaprasirt, P. (2008). Influence of rice husk-bark ash on mechanical properties of concrete containing high amount of recycled aggregates. *Construction and Building Materials, 22*(8), 1812−1819.

Tangchirapat, W., Jaturapitakkul, C., & Chindaprasirt, P. (2009). Use of palm oil fuel ash as a supplementary cementitious material for producing high-strength concrete. *Construction and Building Materials, 23*, 2641−2646.

Tay, J. (1990). Ash from oil-palm waste as a concrete material. *Journal of Materials in Civil Engineering, 2*(2), 94−105.

Trimble, B. E., & Brisch, J. H. (2008). In B. E. Trimble, & J. H. Brisch (Eds.), *Masonry*. USA: STP 1496, ASTM.

Turgut, P. (2010). Masonry composite material made of limestone powder and fly ash. *Powder Technology, 204*(1), 42−47.

Wills, M. H., Jr. (1983). *Concrete masonry units incorporating cement kiln dust*, US Patent No. 4407677 A.

Zhang, M. H., & Mohan, M. V. (1996). High-performance concrete incorporating rice husk ash as a supplementary cementing material. *ACI Materials Journal, 93*(6), 629−636.

The properties and durability of autoclaved aerated concrete masonry blocks

9

A. Chaipanich[1], *P. Chindaprasirt*[2]
[1]Chiang Mai University, Chiang Mai, Thailand; [2]Khon Kaen University, Khon Kaen, Thailand

9.1 Introduction

This chapter describes the different properties and the durability of autoclaved aerated concrete (AAC) masonry blocks and contains the following sections: the types of lightweight concrete, history, utilization, manufacturing, mechanism of AAC, physical properties, mechanical properties, microstructure, characterizations, thermal conductivity and durability of AAC. The types of lightweight concrete section describes different types of lightweight concrete and the different production process used in making lightweight concrete such as aerated concrete and foam concrete, paying particular attention to AAC. The utilization of AAC as masonry blocks is also mentioned. The mechanism involved in the production of AAC in relation to the pore-forming method used and the hydration of AAC is described in the mechanism section. The physical properties section describes the bulk density of AAC and the relation to the air voids. The mechanical properties section describes the compressive strength and flexural strength of the AAC, the relationships with the physical properties and the hydration products. The microstructure section describes the pore size formed and the morphology of the AAC microstructure characterized through the use of scanning electron microscopy (SEM) while the other characterization section involved the use of X-ray diffraction and thermogravimetric analysis techniques. Thermal conductivity is also discussed in the chapter. The durability section of the chapter describes the freeze-thaw resistance of the AAC.

9.2 Types of lightweight concrete

Lightweight concrete can be classed according to its unit weight or density, which normally ranges from 320 to 1920 kg/m^3, according to the ACI Committee 213 Guide for Structural Lightweight Aggregate Concrete (ACI 213, 2001). There are three different lightweight concrete type divisions in terms of strength range, which are low-density concretes (0.7−2.0 MPa), moderate-strength concretes (7−14 MPa) and structural concretes (17−63 MPa). The density of these concretes is in the range of 300−800 kg/m^3, 800−1350 kg/m^3 and 1350−≈1920 kg/m^3 respectively. The use of lightweight concrete has been used since the early 1900s in the United States,

Eco-efficient Masonry Bricks and Blocks. http://dx.doi.org/10.1016/B978-1-78242-305-8.00009-7

and lightweight concrete has been used in multistory buildings, long span bridges, offshore platforms and large structures (Mindess, Young, & Darwin, 2003). A number of advantages in using low-density lightweight concrete in construction are due to its low density, low thermal conductivity, low shrinkage and high heat resistance, in addition to reduction in dead load, lower haulage cost and faster building rate (Wongkeo, Thongsanitgarn, Pimraksa, & Chaipanich, 2012).

A number of ways can be used to produce lightweight concrete mainly using lightweight aggregate or lightweight matrix. The lightweight aggregate that can be used varies from natural pumice aggregate to man-made sintered aggregate such as sintered fly ash (Mindess et al., 2003). The discussion on lightweight aggregate is out of the scope of this chapter and will not be discussed in further detail. The focus will be maintained on the lightweight cement matrix filled with air, which sometimes is referred to as aerated concrete or foam concrete. The classification of different aerated concrete or foam concrete that can be produced were simplified by Just & Middendorf (2009) to be either AAC or air cured foam concrete. Therefore, generally there are two types of aerated concrete: foam concrete and AAC. The foaming agents that can be used are various kinds of detergents, resin soap, glue resins or proteins such as keratin (Narayanan & Ramamurthy, 2000a). The foam can be added by means of mechanical or physical methods as reported by Just & Middendorf (2009). The foams generated mechanically use the method of beating a foaming agent together while the physical method is referred to the addition of the already foamed solution directly in the mixing process. The latter method has been found to produce more regular and stable pores than the former, which generates irregular pores (Just & Middendorf, 2009). This foam concrete is normally air cured. AAC is a class of lightweight concrete that is made by first creating gas bubbles in the fresh concrete and then cured in high-pressure steam curing known as autoclaved. The autoclaved aerated method is generally used in the production of AAC masonry blocks. This is because the aerated concrete, sometimes known as cellular concrete, produced from this method has a uniformly generated cellular structure of air voids in the range of 0.1−1 mm forming in the cement paste or mortars (Mindess et al., 2003).

9.3 Autoclaved aerated concrete (AAC) history and utilization as masonry blocks

The first commercial production of AAC was in 1923 in Sweden. Since then, it has now been used in more than 40 countries in Europe, America, Australia, the Middle East and the Far East. The modern uses of AAC in the United States began in 1990 for residential and commercial buildings (Masonry magazine, 2008; Kočí, Maděra, & Černý, 2012; Radhi, 2011). AAC masonry blocks can be made as precast building blocks and are used in residential construction, hospitals, office buildings and university accommodations (Hess, Kincl, Amasay, & Wolfe, 2010.). AAC masonry blocks have many advantages in comparison to conventional concrete: lighter weight (typically weigh one-sixth to one-third of conventional concrete), lower building costs and provides thermal and acoustic insulation (Hendry, 2001; Hess et al., 2010; Klingner, 2008). The thermal insulation

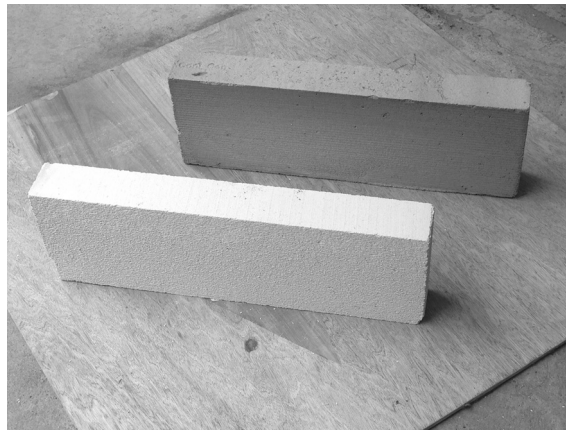

Figure 9.1 Examples of a standard AAC block.

property of AAC would make buildings more energy efficient as it has been reported in a case study in the United Arab Emirates where the use of AAC was found to reduce energy consumption in the residential sector by about 7% (Radhi, 2011). Due to the high porous structure with 60–70% air, AAC has the ability to dampen the mechanical vibration energy giving its excellent sound insulation, therefore the use of AAC would be very suitable for places like schools, hotels and apartments (Technology Brief, 2010). The design and specifications of AAC masonry blocks is covered by the Masonry Standards Joint Committee code and by ASTM C1386. The standard size of an AAC masonry block is larger compared to the concrete masonry unit (CMU) block; the length of an AAC masonry block is 610 mm compared to the 410 mm length of a CMU block (Hess et al., 2010). Although it is larger in size, it is lighter, so the large size of an AAC block is comparable to a medium-sized CMU block in terms of weight (Hess et al., 2010). A standard block is 50–375 mm thick, 200 mm in height and 610 mm in length (Klingner, 2008). A standard AAC block is shown in Figure 9.1. Overall, due to these desired properties of AAC, especially its lightweight, thermal and acoustic properties, AAC masonry block is an ideal construction material for walls in many residential and office buildings.

9.4 Manufacturing and mechanism of autoclaved aerated concrete

AAC is generally made from quartz-rich sand, lime, cement and aluminum powder (Kurama, Topcu, & Karakurt, 2009). Gypsum and fly ash can also be used in the production of AAC (Klingner, 2008). Aluminum powder is used as an air-entraining (aerating) or pore-forming agent and is the most common agent used (Narayanan & Ramamurthy, 2000a). It is based on the reaction of aluminum with the soluble alkalis in the cement to form the small bubbles of hydrogen as in Eqn (8.1) (Mindess et al., 2003). This causes the material to rise in the mold and after curing

for 45 min, the products are cut into the required unit size by wires (Technology Brief, 2010).

$$Al + 2OH^- + 2H_2O \rightarrow Al(OH)_4^- + H_2 \tag{8.1}$$

Calcium aluminate hydrate (C_3AH_6) can also be formed with hydrogen gas through the reaction of the aluminum powder with calcium hydroxide, as can be seen in Eqn (8.2) (Kurama et al., 2009). Thereafter, the aerated concrete is then autoclaved for 8−12 h (Technology Brief, 2010).

$$2Al(S) + 3Ca(OH)_2(S) + 6H_2O \rightarrow 3CaO.Al_2O_3.6H_2O + H_2(g) \tag{8.2}$$

Autoclaved high-pressure steam curing is used to improve compressive strength of aerated concrete. The AAC products are ready for use within 24 h (the strength is generally equivalent to 28 days under ambient curing). The structure of C-S-H phases was found to change under high temperature and pressure when subjected to autoclaved curing. In Portland cement, the α-dicalcium silicate hydrate (α-C_2SH) is formed instead of an amorphous calcium silicate hydrate (C-S-H), which resulted in a reduction in strength (Mindess et al., 2003). However, in the presence of silica, α-C_2SH is converted to tobermorite ($C_5S_6H_5$) on continued heating (Mindess et al., 2003; Yazici, 2007). Additional silica may be available through the use of pozzolanic material as supplementary cementitious material. The tobermorite phase has a larger volume of structure than the α-C_2SH phase, which causes a decrease in the porosity and consequently an increase in the compressive strength. The formation of tobermorite at high temperature curing would depend on the CaO/SiO_2 ratio as well as the temperature as reported by Meller, Kyritsis, & Hall (2009) and Taylor (1997). The typical condition previously used for AAC are in the range of 8−16 h duration and at the pressure in the range of 4−16 MPa (Narayanan & Ramamurthy, 2000a; RILEM, 1993).

$$\underset{\text{Portland cement}}{(C_3S + C_2S)} \xrightarrow{H_2O} \text{C-S-H} + CH + \underset{\text{Silica}}{S} \tag{8.3}$$

$$CH + S \xrightarrow{H_2O} \text{C-S-H} + \rightarrow \underset{\text{Tobermorite}}{C_5S_6H_5} \tag{8.4}$$

9.5 Physical properties of autoclaved aerated concrete

The bulk density of bottom ash (BA) cement AAC specimens has been reported by Wongkeo et al. (2012) by comparing the addition of aluminum powder. The bulk density of autoclaved lightweight concrete without BA replacement decreased up to 23.47% when aluminum (Al) was added. Al addition was therefore found to have a significant effect on the bulk density of autoclaved concrete. Moreover, the bulk density of bottom ash AAC compared to Portland cement AAC increased from 2% to 7% when

BA was used to replace Portland cement at 10% and 30% respectively. The increase in the bulk density of bottom ash AAC was due to the formation of the tobermorite phase when BA is used.

The volume of permeable voids results of all ternary Portland cement-bottom ash-silica fume AAC has been reported by Wongkeo & Chaipanich (2010). It was found that the volume of permeable voids of all bottom ash (BA) AAC specimens decreased with increased BA content and silica fume (SF) addition due to the reduction of hydrogen gas. The unit weight of BA AAC increased with increased BA content. When SF was added at 2.5% and 5%, the unit weight of BA AAC with SF increased. Therefore, the volume of permeable voids is shown to directly affect the unit weight of all bottom ash AAC.

9.6 Mechanical properties of autoclaved aerated concrete

9.6.1 Compressive strength

It is known that the compressive strength is influenced by a number of factors such as extrinsic and intrinsic factors. The extrinsic factors are the testing and curing conditions while the intrinsic factors involve the mixture, such as the water content, cement and aggregate type used, and their content, as well as the aerated agents used. Porosity as a result is created by these factors involved and directly influenced the compressive strength outcome. Consequently, the product density is found to be directly related to the compressive strength. A reduction in the density by the formation of large micropores is reported to cause a significant drop in the compressive strength (CEB, 1977). The compressive strength is reported to be in the range of 3.9−8.5 MPa when the AAC density is 700 kg/m^3 but reduced to 1.3−2.8 MPa when the density is 400 kg/m^3 (CEB, 1977; Narayanan & Ramamurthy, 2000a).

Compressive strength of AAC concrete reported by Huang, Ni, Cui, Wang, & Zhu (2012) is 4.0 MPa with a density of 610 kg/m^3. While Serhat Baspinar, Demir, Kahraman, & Gorhan (2014) reported compressive strength of AAC in the range of 1.91−5.10 MPa when the density range was 590−780 kg/m^3, Albayrak et al. (2007) found the AAC compressive strength in the range of 1.1−5.0 MPa and the density range of 270−500 kg/m^3, showing an increase in the strength with density. Although the autoclave conditions used were different for each method used, in general the compressive strength can be seen to reduce with a decrease in the AAC density and there appears to be a direct relationship between the compressive strength of AAC with its density. Table 9.1 summarizes the compressive strength results and autoclaved conditions from previous published works.

The autoclaving method significantly influences the compressive strength where at higher temperature and pressure a stable form of tobermorite is achieved (Narayanan & Ramamurthy, 2000a).

The types of cement used will result in different compressive strength (Mindess et al., 2003). Normal Portland cement type I would result in a weaker calcium silicate

Table 9.1 Review of compressive strength results

Authors	Compressive strength (MPa)	Density (kg/m^3)	Condition method			
			Binder	Temperature (°C)	Pressure (MPa)	Time (h)
Mostafa (2005)	1.1−3.0 1.8−3.7 1.9−3.6 2.0−3.6	NA NA NA NA	C, L, AS	183	1	2 6 12 24
Albayrak et al. (2007)	1.25−3.25	270−533	Ze	200	1.5	12
Huang et al. (2012)	4.0	610.2	C, SCT, BFS, G	NA	1.35	8
Keriene et al. (2013)	2.24	451	C, L	176	0.8	20
Serhat Baspinar et al. (2014)	1.9−3.7	590−650	C, L, FA	NA	0.4	8
	3.9−5.1	740−780	C, L, FA, SF	NA	0.8	8

C−cement, L−lime, AS−air-cooled slag, Ze−zeolite, SCT−skarn-type copper tailing, BFS−blast furnace slag, G−gypsum, FA−fly ash, SF−silica fume, NA−not available.

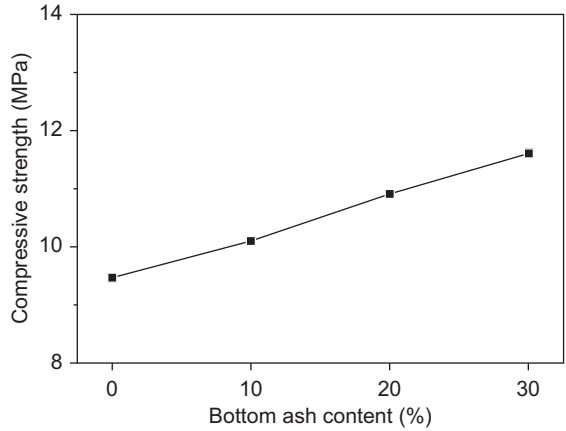

Figure 9.2 Compressive strength of bottom ash autoclaved aerated concrete. Adapted from Wongkeo et al. (2012).

hydrate (α-C_2SH), which resulted in a reduction in strength. But when additional silica is present, α-C_2SH is converted to tobermorite ($C_5S_6H_5$), which increases the compressive strength of AAC (Taylor, 1997; Yazici, 2007). Therefore, the chemical compositions of the amorphous binder used have a significant effect on the compressive strength of AAC.

The compressive strength of bottom ash AAC with BA at up to 30% was found to increase with increasing BA content (Wongkeo et al., 2012), as shown in Figure 9.2. The increased compressive strength is the result of the tobermorite phase being formed under autoclave conditions where tobermorite was formed at a high temperature (above 100 °C) with CaO/SiO_2 in the range between 0.8−1.0 (Meller et al., 2009; Taylor, 1997). The additional silica content was obtained from BA leading to the alteration of CaO/SiO_2 ratio, thus achieving the suitable CaO/SiO_2 ratio for tobermorite formation. The tobermorite phase has a larger volume of structure than α-C_2SH phase, which causes a decrease in porosity and increase in compressive strength when compared to the control Portland cement AAC (Richardson, 2008; Yazici, 2007).

AAC with the use of ternary cement comprising of Portland cement, bottom ash and silica fume has been investigated for compressive strength. It was found that the compressive strength of all bottom ash AAC increased with increased BA and SF content (Wongkeo & Chaipanich, 2010).

Generally the unit weight can be seen to have a direct relationship with that of compressive strength. When SF is added there is a greater pozzolanic reaction which resulted in an increase in the density of bottom ash AAC. Consequently, the early compressive strength of bottom ash AAC with SF was significantly improved. Moreover, when Wongkeo & Chaipanich (2010) compared the compressive strength results of air cured and autoclaved samples, the compressive strength of bottom ash AAC with SF addition and cured in autoclave was found to have higher strength than the corresponding 7 and 14 days air cured bottom ash concrete. The benefit is contributed to the better pozzolanic reaction when autoclaved, which resulted in

the tobermorite phases being formed. The 28 day air cured compressive strength was found to be similar to bottom ash AAC being autoclaved for six hours. It was concluded that one of the major factors affecting strength development is the air voids in the concrete.

In general, compressive strength of AAC at 24 h in general can achieve equal strength of normal cured concrete after 28 days (Mindess et al., 2003). Compressive strength of AAC after 8 and 12 h autoclaved reported by Narayanan & Ramamurthy (2000b) were found to be higher than the corresponding concrete mixes when compared to those of moist cured conditions at 28, 90 and 150 days.

9.6.2 Flexural strength

It is reported that the flexural strength of AAC concrete is in the range of 0.15−0.35 (Valore, 1954). However, it would seem that the ratio would vary depending on the materials and conditions of tests. For example, Wongkeo et al. (2012) reported the flexural strength to be in the range of 2.7−3.2 MPa, and the ratio of flexural strength to compressive strength is between 0.24 and 0.27 depending on the mix (whether it is of Portland cement only or if a pozzolan such as bottom ash is used as supplementary cementitious material).

9.7 Microstructure of autoclaved aerated concrete

The microstructure of AAC consists of macropores and micropores and is influenced by the method of pore formation (Narayanan & Ramamurthy, 2000a). The pore sizes, those are initially formed from the reaction of aluminum with the cement alkalis, are somewhat larger in size typically in the range of 0.1−1.0 mm (Ioannou, Hamilton, & Hall, 2008; Mindess et al., 2003). The pore sizes created by the chemically reacted agent such as aluminum or the foaming methods are therefore large enough to be visible and easily seen. The formation of macropores is reported to be formed from the aeration process while the micropores appear in the wall of the macropores (Alexanderson, 1979). Petrov & Schlegel (1994) summarized the macropore and micropore size as being greater than 60 μm for the former and 50 nm or less for the latter (Alexanderson, 1979). Macropore sizes of 50−500 μm (0.05−0.5 mm) formed during aeration have also been reported (Alexanderson, 1979).

The microstructure of AAC characterized by the SEM were found to show AAC to consist of these two different types of pores. The large pores as observed and reported by several published works are typically round in shape and can therefore be in the range of 0.05−1.0 mm in size (Alexanderson, 1979; Ionnou et al., 2008; Mindess et al., 2003; Narayanan & Ramamurthy, 2000a). The micropores that form between the walls can be seen in between the hydration products. SEM micrographs also show the shape of such hydration products that are formed after being autoclaved. The more common tobermorite platelets are generally found when there is enough silica in the mix. The microstructure of AAC will also depend on the hydration products formed, which consequently depend largely on the cement types and methods used.

The CaO/SiO_2 ratio of 0.83 is the optimum to give 1.1 nm tobermorite (Meller et al., 2009; Richardson, 2008). Portland cement with BA and SF in Bottom ash AAC was found to result in an increase of reactive SiO_2 content in the system and favors tobermorite formation (Wongkeo & Chaipanich, 2010). The tobermorite structure being formed would give a denser microstructure to the overall matrix than the poorly crystalline fibrous like C-S-H that would otherwise form in normal Portland cement AAC.

9.8 Characterizations of autoclaved aerated concrete

9.8.1 X-ray diffraction

The main reaction product of AAC has been detected and confirmed by means of an X-ray diffraction (XRD) technique to be the tobermorite group (Matsui et al., 2011; Narayanan & Ramamurthy, 2000b; Wongkeo et al., 2012). The formation of tobermorite would depend on the cement compositions with a suitable amount of silica and the autoclaving condition such as temperature, as reported by Taylor (1997) and Meller et al. (2009).

XRD traces of bottom ash and Portland cement AAC were reported by Wongkeo et al. (2012). Comparison between XRD traces of the bottom ash cement AAC and Portland cement AAC can therefore be observed showing the different phases presented in each concrete. XRD traces of Portland cement and bottom ash cement AAC showed some minor peaks of C_3S and C_2S, which are dehydrated calcium silicate phases from Portland cement. Moreover, tobermorite ($xCaOSiO_2.zH_2O$) can only be seen detected in bottom ash AAC but was not found in Portland cement where $Ca(OH)_2$ and α-C_2SH ($Ca_2SiO_4.3H_2O$) phases were found instead. In addition, the intensity of $Ca(OH)_2$ peaks was found to decrease with increased BA content. This is due to the pozzolanic reaction and the dilution effect.

Other hydrated phases such as ettringite, hydrogarnet and C_2SH have also been reported in addition to the CSH, $Ca(OH)_2$ and tobermorite found in cement-sand and cement-fly ash AAC (Narayanan & Ramamurthy, 2000b). Kus and Carlsson (2003) carried out XRD analysis on naturally weathered and artificially weathered AAC and detected phases as the main peaks in the binder (when considering only the binder part) are calcite, anhydrite and tobermorite. The calcite peak is noticed to be increased over time. This is caused by carbonation where $Ca(OH)_2$ is converted to calcium carbonate. Although tobermorite and calcite are generally found in the CaO and SiO_2 system, when there is the presence of Al and SO_3, other minor phases can also be found such as monosulfate and kaotite (Matsui et al., 2011).

9.8.2 Thermal gravimetric analysis

Thermal gravimetric analysis (TGA) results of bottom ash cement AAC are plotted as derivative thermogravimatric (DTG) curves in order to identify the detected phases by Wongkeo et al. (2012). The detected phases are calcium silicate hydrate (C-S-H) at

≈71−86 °C, calcium hydroxide ($Ca(OH)_2$) at ≈446−476 °C and calcium carbonate ($CaCO_3$) at ≈697−708 °C. The intensity of C-S-H curves was found to increase with increased BA content. This is due to the increase in the presence of the tobermorite phase formed with increasing BA content, which corresponds to the increased compressive strength of the samples. Moreover, $Ca(OH)_2$ can be seen to reduce with increasing BA content due to the pozzolanic reaction that was used in the reaction to form tobermorite and also due to the dilution effect, where the use of supplementary cementitious materials such as bottom ash was used to replace part of Portland cement.

TGA results of ternary cement AAC concrete of Portland cement-bottom ash-silica fume was reported by Wongkeo & Chaipanich (2010). Results were plotted as derivative showing DTG curves of ternary cement AAC concrete compared with 28 days air cured samples. In ternary cement AAC, the DTG curves showed detection of C-S-H (tobermorite phase), $Ca(OH)_2$ and $CaCO_3$ phases. The weight loss of the tobermorite phase was attributed to the dehydration of the loosely bound molecular interlayer water (Alarcon-Ruiz, Platret, Massieu, & Ehrlacher, 2005). It is believed that ettringite and C_2ASH_8 were not formed in the AAC concrete due to the substitution of Al for Si in the tetrahedral site of tobermorite (Wongkeo & Chaipanich, 2010). This was reported to have a significant effect in the chemical behavior of cement paste, including the cation and anion exchange behavior, solubility and reactions that would result in the delay of ettringite formation (Shaw, Henderson, & Komanschek, 2000). Furthermore, the formation of C-A-S-H (hydrogarnet) groups would not occur at a temperature below 200 °C but tobermorite would form instead where the tobermorite crystallization would be accelerated and the stability of tobermorite increases when alumina is available (Meller et al., 2009; Mostafa, 2005). The tobermorite phase of autoclaved bottom ash increased with increasing BA content up to 20%. The $Ca(OH)_2$ phase was found to reduce with increasing BA content due to the increase in the pozzolanic reaction of BA and SF and the dilution effect.

9.9 Thermal conductivity of bottom ash cement autoclaved aerated concrete

The thermal conductivity of AAC concrete has a direct relationship with its physical properties. The thermal conductivity of bottom ash cement AAC was reported to increase slightly with bottom ash used as supplementary cementitious material in concrete (Figure 9.3), because the BA content increased the overall unit weight or bulk density of the concrete (Wongkeo & Chaipanich, 2010; Wongkeo et al., 2012). Pore structure of the lightweight aggregates, density of concrete and the cement matrix has an effect on the thermal conductivity of concrete (Corinaldesi et al., 2011; Topcu & Uygunoglu, 2007). Thus, the thermal conductivity of BLWC tended to increase due to the decrease in the volume of permeable voids with increasing BA content (Wongkeo & Chaipanich, 2010). Albayrak et al. (2007) reported that the compressive strength and the thermal conductivity of AAC concrete are reduced with the decrease

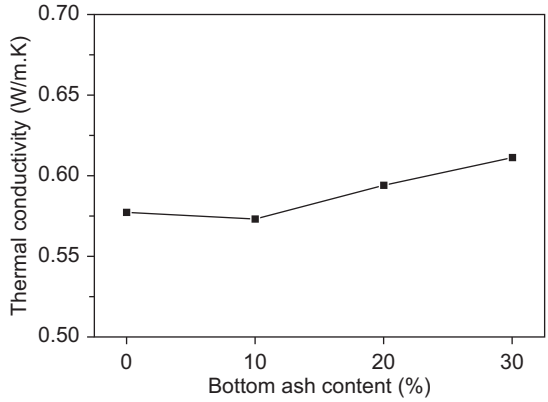

Figure 9.3 Thermal conductivity of bottom ash autoclaved aerated concrete.
Adapted from Wongkeo et al. (2012).

in bulk density. Albayrak et al. (2007) found the thermal conductivity of AAC in the range of 1.1−5.0 MPa and the density range of 270−500 kg/m^3, showing an increase in the strength with density. Several other researchers (Blanco, Garcia, Mateos, & Ayala, 2000; Demirboga, 2003, 2007; Demirboga & Gul, 2003) also reported that the decrease in thermal conductivity is related to the reduction in the concrete density. Jerman, Keppert, Vyborny, & Cerny (2013) showed that the thermal conductivity depends on the density of AAC as well as the moisture content (Figure 9.4), where the increase in moisture content and density leads to an increase in the thermal conductivity. The thermal conductivity is therefore known to increase with the increase in the density of both normal and AAC concrete. The thermal conductivity of AAC can be as low as 0.08 W/m K at 25°C. However, the compressive strength as a consequence is

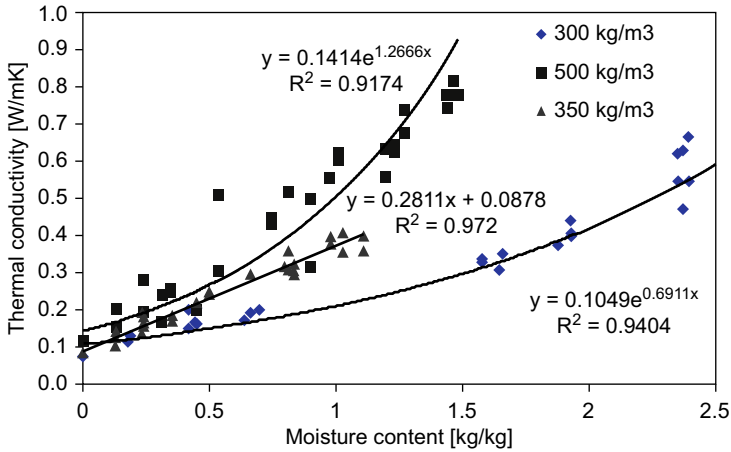

Figure 9.4 Thermal conductivity of autoclaved aerated concrete as a function of moisture content.
Jerman et al. (2013) printed with permission from Elsevier.

very low (2.05 MPa) (Jerman et al., 2013). When AAC with bottom ash is used as supplementary cementitious material, the thermal conductivity is in the range of 0.58−0.61 W/m K (Wongkeo et al., 2012). On the other hand, when bottom ash is used as aggregate, the thermal conductivity of the AAC concrete is reported to be in between 0.220−0.361 W/m K and was found to reduce with increasing BA content used as sand replacement (Kurama et al., 2009).

The thermal conductivity of all bottom ash AAC concrete with SF was found to be higher than that of a Portland cement control concrete and increased with increasing SF (Wongkeo & Chaipanich, 2010). This is due to the decreasing of the volume of permeable voids and density of microstructure in the cement paste matrix. Small changes in the thermal conductivity of ternary Portland cement-bottom ash-silica fume AAC were reported to be similar within the range of 0.61−0.65 W/m K. Therefore, it is observed that there is a direct relationship between the thermal conductivity and the bulk density of AAC concrete.

9.10 Durability of autoclaved aerated concrete

Since the AAC has voids, which are large due to the formation of the initial reaction for aeration, it is expected to be frost resistant (Mindess et al., 2003). However, the degree of saturation is important for freeze-thaw reactions (Roulet, 1983), as aerated concrete is susceptible to liquid and gas penetration due to its high porosity that may cause damage to the concrete (Narayanan & Ramamurthy, 2000a; RILEM, 1993). The maximum degree of saturation is reported to be in the range of 20−40%. With a higher degree of saturation, the concrete would be become brittle and crack completely (Roulet, 1983).

Jerman et al. (2013) reported the freeze-thaw resistance of AAC using the scaling method where the samples were to undergo 25 and 50 cycles of 8 h freezing at −15 °C and thawing of 8 h at 20 °C. They tested samples at different conditions taking into account the nature of different environments such as dry, 10% moisture and complete saturation. The dry and 10% moisture conditions were tested since it would better fit the realistic environment of building use in comparison to the completely saturated condition. The mass loss and compressive strength loss of samples tested at these conditions are plotted as shown in Figures 9.5 and 9.6. Interestingly, the dry samples show no sign of mass loss or compressive strength loss after 25 cycles. Higher percentages of mass loss were found in the samples with 10% moisture and in capillary water-saturated samples.

On the other hand, results of the dry samples after 50 cycles showed some mass loss (0.36−0.50%) and minor loss in compressive strength (max. at 0.10%). In the samples with 10% moisture content, the mass loss is in the range of 1.3−1.5%, while the loss in compressive strength is higher in P1.8-300 sample (16.3%) but seemed to be acceptable at 6−8% for P2-350 and P4-500 samples. For capillary saturated samples, the loss of compressive strength and mass loss are much more severe after 50 freeze/thaw cycles, especially in P1.8-300 and P2-350 samples where the compressive strength loss is 46.0% and 45.7% respectively. These samples, however, have very low compressive strength initially of 2.05 and 2.24 MPa (Jerman et al., 2013). The

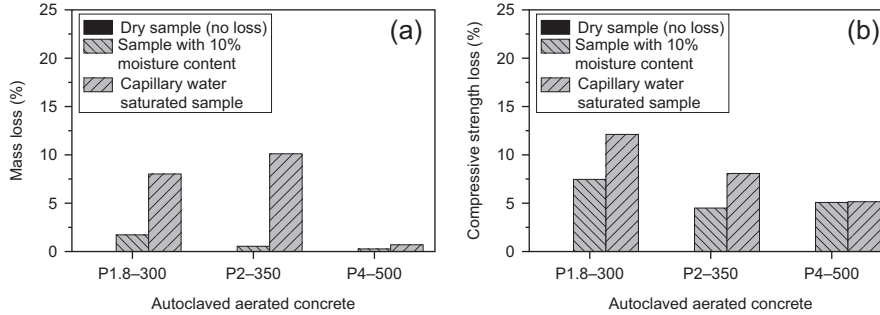

Figure 9.5 (a) Mass loss and (b) compressive strength loss of ACC at 25 cycles. Adapted from Jerman et al. (2013).

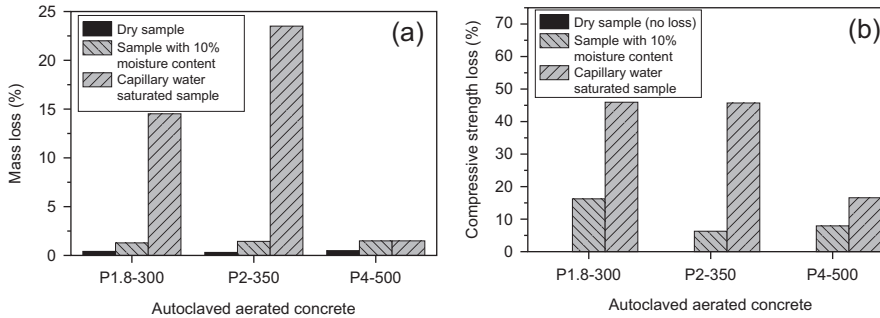

Figure 9.6 (a) Mass loss and (b) compressive strength loss of ACC at 50 cycles. Adapted from Jerman et al. (2013).

P4-500 has compressive strength of 4.0, which suffers lower mass loss of 1.5% and lower compressive strength loss of 16.6%. In both sets of tests at 25 and 50 cycles, the results show that the degree of water saturation has a significant effect on the freeze-thaw resistance of AAC concrete.

It was concluded that in dry and 10% samples, the freeze-thaw is tolerable in the compressive strength range of 1.8−4.0 MPa (Jerman et al., 2013). This appears to agree with the work by Tikalsky, Pospisil, & MacDonald (2004) in achieving good freeze-thaw resistance providing the moisture content is less than 16% AAC concrete with bulk density in the range of 500−600 kg/m^3 and the compressive strength of 1−2 MPa.

Therefore, when considering the freeze-thaw resistance of the AAC concrete, the deciding factors that would significantly affect the AAC performance are the presence of air voids, the degree of saturation and compressive strength.

9.11 Conclusions and future trends

While the focus of this chapter is generally on the properties and durability of AAC, which is a review of past and recent research works on the subject, the future trends

involving AAC would largely depend on the application of the AAC and the specification required by the construction industry, as well as those set by the standards. Research will be heavily focused on new science and technology leading to innovative AAC products, taking into account the specification requirement, application, economical and environmental aspects. As such, new technology and new materials should be used in producing AAC. For example, a different and more suitable source of silica could be used, and if it is environmentally friendly and is also economical, the better. That is probably the reason why the research on pozzolanic materials have been so successful and have attracted many interests. New cost-effective production should be looked at also, not least the new materials such as nano-size or new waste and by-products that can benefit the mechanical and durability properties of AAC.

9.12 Sources of further information and advice

Narayanan & Ramamurthy (2000a) have reviewed the works on AAC, which described a number of properties of AAC. Wongkeo and Chaipanich (2010) and Wongkeo et al. (2012) reported the works on the use of pozzolans as binary and ternary blended cements and the results on the mechanical properties of AAC. Concrete by Mindess et al. (2003) is also a useful book to read to give an overall idea of lightweight concrete in general and the classifications of lightweight concrete. Published works by Meller et al. (2009), Taylor (1997) and Richardson (2008) are other useful reading sources on the hydration of calcium silicate and the hydration products at different temperatures and pressure.

References

ACI Committer 213. (2001). *Guide for structural lightweight aggregate concrete*. Farmington Hills: American Concrete Institute.

Alarcon-Ruiz, L., Platret, G., Massieu, E., & Ehrlacher, A. (2005). The use of thermal analysis in assessing the effect of temperature on a cement paste. *Cement and Concrete Research, 35*, 609−613.

Albayrak, M., Yorukoglu, A., Karahan, S., Atlihan, S., Aruntas, H. Y., & Girgin, I. (2007). Influence of zeolite additive on properties of autoclaved aerated concrete. *Building and Environment, 42*, 3161−3165.

Alexanderson, J. (1979). Relations between structure and mechanical properties of autoclaved aerated concrete. *Cement and Concrete Research, 9*, 507−514.

Baspinar, S. M., Demir, I., Kahraman, E., & Gorhan, G. (2014). Utilization potential of fly ash together with silica fume in autoclaved aerated concrete production. *KSCE Journal of Civil Engineering, 18*, 47−52.

Blanco, F., Garcia, P., Mateos, P., & Ayala, J. (2000). Characteristic and properties of lightweight concrete manufactured with cenospheres. *Cement and Concrete Research, 30*, 1715−1722.

CEB. (1977). *Autoclaved aerated concrete*. Manual of design and technology. The Construction Press.

Corinaldesi, V., Mazzoli, A., & Moriconi, G. (2011). Mechanical behaviour and thermal conductivity of mortars containing waste rubber particles. *Materials and Design, 32*, 1646−1650.

Demirboga, R., & Gul, R. (2003). The effects of expanded perlite aggregate, silica fume, fly ash on the thermal conductivity of lightweight concrete. *Cement and Concrete Research, 33*, 723−727.

Demirboga, R. (2003). Influence of mineral admixtures on thermal conductivity and compressive strength of mortar. *Energy and Buildings, 35*, 189−192.

Demirboga, R. (2007). Thermal conductivity and compressive strength of concrete incorporation with mineral admixtures. *Building and Environment, 42*, 2467−2471.

Hendry, A. W. (2001). Masonry walls: materials and construction. *Construction and Building Materials, 15*, 323−330.

Hess, J. A., Kincl, L., Amasay, T., & Wolfe, P. (2010). Ergonomic evaluation of masons laying concrete masonry units and autoclaved aerated concrete. *Applied Ergonomics, 41*, 477−483.

Huang, X., Ni, W., Cui, W., Wang, Z., & Zhu, L. (2012). Preparation of autoclaved aerated concrete using copper tailings and blast furnace slag. *Construction and Building Materials, 27*, 1−5.

Ioannou, I., Hamilton, A., & Hall, C. (2008). Capillary absorption of water and n-decane by autoclaved aerated concrete. *Cement and Concrete Research, 38*, 766−771.

Jerman, M., Keppert, M., Vyborny, J., & Cerny, R. (2013). Hygric, thermal and durability properties of autoclaved aerated concrete. *Construction and Building Materials, 41*, 352−359.

Just, A., & Middendorf, B. (2009). Microstructure of high-strength foam concrete. *Materials Characterization, 60*, 741−748.

Keriene, J., Kligys, M., Laukaitis, A., Yakovlev, G., Špokauskas, A., & Aleknevicius, M. (2013). The influence of multi-walled carbon nanotubes additive on properties of non-autoclaved and autoclaved aerated concretes. *Construction and Building Materials, 49*, 527−535.

Klingner, R. E. (2008). *Using autoclaved aerated concrete correctly*. MASONRY Magazine: the Voice of the Masonry Industry. http://www.masonrymagazine.com/6-08/autoclaved.html.

Kočí, V., Maděra, J., & Černý, R. (2012). Exterior thermal insulation systems for AAC building envelopes: computational analysis aimed at increasing service life. *Energy and Buildings, 47*, 84−90.

Kurama, H., Topcu, I. B., & Karakurt, C. (2009). Properties of the autoclaved aerated concrete produced from coal bottom ash. *Journal of Materials Processing Technology, 209*, 767−773.

Kus, H., & Carlsson, T. (2003). Microstructural investigations of naturally and artificially weathered autoclaved aerated concrete. *Cement and Concrete Research, 33*, 1423−1432.

Matsui, K., Kikuma, J., Tsunashima, M., Ishikawa, T., Matsuno, S., Ogawa, A., et al. (2011). In situ time-resolved X-ray diffraction of tobermorite formation in autoclaved aerated concrete: influence of silica source reactivity and Al addition. *Cement and Concrete Research, 41*, 510−519.

Meller, N., Kyritsis, K., & Hall, C. (2009). The mineralogy of the $CaO-Al_2O_3-SiO_2-H_2O$ (CASH) hydroceramic system from 200 to 350°C. *Cement and Concrete Research, 39*, 45−53.

Mindess, S., Young, J. F., & Darwin, D. (2003). *Concrete*. USA: Pearson Education.

Mostafa, N. Y. (2005). Influence of air-cooled slag on physicochemical properties of autoclaved aerated concrete. *Cement and Concrete Research, 35*, 1349−1357.

Narayanan, N., & Ramamurthy, K. (2000a). Structure and properties of aerated concrete: a review. *Cement and Concrete Composites, 22*, 321−329.

Narayanan, N., & Ramamurthy, K. (2000b). Microstructural investigations on aerated concrete. *Cement and Concrete Research, 30*, 457−464.

Petrov, I., & Schlegel, E. (1994). Application of automatic image analysis for the investigation of autoclaved aerated concrete structure. *Cement and Concrete Research, 24*, 830−840.

Radhi, H. (2011). Viability of autoclaved aerated concrete walls for the residential sector in the United Arab Emirates. *Energy and Buildings, 43*, 2086−2092.

Richardson, I. G. (2008). The calcium silicate hydrates. *Cement and Concrete Research, 38*, 137−158.

RILEM recommended practice. (1993). *Autoclaved aerated concrete-properties, testing and design*. E&FN SPON.

Roulet, C. A. (1983). Expansion of aerated concrete due to frost—determination of critical saturation. In F. H. Wittmann (Ed.), *Proceedings autoclaved aerated concrete, moisture and properties* (pp. 157−169). Amsterdam: Elsevier.

Shaw, S., Henderson, C. M. B., & Komanschek, B. U. (2000). Dehydration/recrystallization mechanisms, energetics, and kinetics of hydrated calcium silicate minerals: an in situ TGA/DSC and synchrotron radiation SAXS/WAXS study. *Chemical Geology, 167*, 141−159.

Taylor, H. F. W. (1997). *Cement chemistry*. NY: Taylor and Thomas Telford Services Ltd.

Technology Brief. (2010). *Autoclaved aerated concrete masonry units*. Resource Information from The International Masonry Institute. Available from: http://www.imiweb.org/design_tools/tech_briefs/01.02%20AAC%20MASONRY%20UNITS.pdf Accessed 04.02.14.

Tikalsky, P. J., Pospisil, J., & MacDonald, W. (2004). A method for assessment of the freeze-thaw resistance of performed foam cellular concrete. *Cement and Concrete Research, 34*, 889−893.

Topcu, I. B., & Uygunoglu, T. (2007). Properties of autoclaved lightweight aggregate concrete. *Building and Environment, 42*, 4108−4116.

Valore, R. C. (1954). Cellular concretes−physical properties. *Journal of American Concrete Institute, 25*, 817−836.

Wongkeo, W., & Chaipanich, A. (2010). Compressive strength, microstructure and thermal analysis of autoclaved and air cured structural lightweight concrete made with coal bottom ash and silica fume. *Materials Science and Engineering A, 527*, 3676−3684.

Wongkeo, W., Thongsanitgarn, P., Pimraksa, K., & Chaipanich, A. (2012). Compressive strength, flexural strength and thermal conductivity of autoclaved concrete block made using bottom ash as cement replacement materials. *Materials and Designing, 35*, 434−439.

Yazici, H. (2007). The effect of curing conditions on compressive strength of ultra high strength concrete with high volume mineral admixtures. *Buildings and Environment, 42*, 2083−2089.

The design, properties, and performance of concrete masonry blocks with phase change materials

10

E.M. Alawadhi
Kuwait University, Kuwait

10.1 Introduction

Thermal insulation materials are chosen to reduce heat flow across a medium, and they can be made of a single or multiple materials. Thermal insulation materials save the U.S. industry more than $60 billion/year in energy costs (Cengel, 1998, pp. 158−159). Therefore, the significance of the insulation materials motivates energy engineers to enhance the thermal characteristics of the thermal insulation materials toward higher thermal resistance. Fibrous, cellular, and granular substances are commonly used insulation materials in buildings. The selection of thermal insulation material is based on its thermal conductivity, thermal mass, temperature of indoor and outdoor spaces, durability, cost, and other factors. The thermo-physical properties of the materials used in the building envelope strongly affect the heating or cooling energy consumptions. The thermal conductivity affects the heat flow at a steady-state condition. For a transient condition, the specific heat also affects the heat flow by absorbing and storing the heat in the form of sensible heat. The solar intensity and outdoor air temperature vary with time; hence, the thermal conductivity and the specific heat of the materials used in building envelopes affect the heat flow. The preferred thermal insulations are materials with high thermal capacity and low thermal conductivity. A comprehensive review of thermal insulation material design economics was accomplished by Turner & Malley, and Torgal, Mistretta, Kaklauskas, Granqvist, & Cabeza (2013) explained in their book how to tackle the challenges of building refurbishment toward nearly zero energy.

Incorporation of phase change material (PCM) into the building envelope has been investigated as a cost-effective technique for reducing the cooling loads. PCMs are organic or inorganic substances with low melting temperature and high latent heat of fusion, such as paraffin and salt. The PCMs are classified as a capacitive type of insulation materials because they slow down the heat flow by absorbing the heat. During high outdoor temperature times, the PCM melts and stores part of the heat as it transfers from outdoors to indoors, and at low outdoor temperature times, the PCM solidifies and releases the stored heat. During the melting process, the specific heat of the PCM increases to more than 100 times, which enables it to absorb

Eco-efficient Masonry Bricks and Blocks. http://dx.doi.org/10.1016/B978-1-78242-305-8.00010-3

a large amount of energy in a relatively small quantity of PCM. Using PCM in building material was suggested by Barkmann & Wessling (1975). Morikama, Suzuki, Okagawa, and Kanki (1985) introduced the concept of the encapsulation of PCM in an unsaturated polyester matrix for building material. A recent review of the PCM for building envelopes can be found in references (Osterman, Tyagi, Butala, Rahim, & Stritih, 2012; Pomianowski, Heiselberg, & Zhang, 2013; Soares, Costa, Gaspar, & Santos, 2013; Waqas & Din, 2013). Depending on the envelope's component, research for PCM can be classified into three groups: bricks, roofs, and windows. For bricks, Alawadhi (2008) presented a thermal analysis of bricks with cylindrical hollows filled with PCM, and the results indicate that the heat gain can be reduced by 17.55% for certain design and weather conditions. Zhang, Chen, Wu, & Shi (2011) reported the thermal characteristics of brick with PCM under real fluctuating outdoor temperature. The thermal response represented by the inside wall surface temperature of brick wall filled with PCM is evaluated and compared with that of solid brick wall. Chwieduk (2013) published a paper about the possibility of substituting the thick and heavy thermal mass external bricks used in high-latitude countries by thin and light thermal mass bricks. The effect of orientation, position of the PCM layer, phase change temperature, and weather conditions was studied by Izquierdo-Barrientos et al. (2012), and they found that the PCM helps to reduce the maximum and amplitude of the instantaneous heat flux.

For roofs, Alawadhi & Alqallaf (2011) investigated a concrete roof with vertical cone frustum holes filled with PCM. The objective of the PCM roof is to reduce the heat flow from the outdoor to indoor space by increasing the thermal mass of the roof. The shape for the PCM containers maintains the physical strength of the roof, can be replaced easily if needed, and allows the PCM to expand during the melting process in the upward direction. The heat flux at the indoor surface of the roof can be reduced by 39%, as reported. Numerical analysis of heat transfer across the roof structure with PCM is by Ravikumar & Sirinivasan (2011), and approximately 56% reduction in heat gain into the room is obtained with a PCM roof structure when compared with a conventional roof. On the other hand, the concept of double layers of PCM in a building roof was proposed by Pasupathy & Velraj (2008) for a year-round thermal management. The double layer of PCM in the roof is recommended to reduce the heat flow through the roof.

Research for PCM in windows was also accomplished as a technique for reducing the heat gain through windows. Windows account for a large percentage of heat gain during the daytime, and energy penetrates the windows through solar radiation and convection. Therefore, reducing heat gain through windows is the key factor for saving energy in buildings, and to reduce the heat gain, external shutters are installed to eliminate the effect of the solar radiation. A window shutter filled with PCM was proposed and analyzed by Alawadhi (2012), and a parametric study is conducted to assess the effect of different design parameters, such as PCM type and quantity in the shutter. It was reported that the melting temperature of PCM should be close to the maximum outdoor temperature during the daytime, and the quantity of PCM should be sufficient to absorb large quantities of heat gain. Goia et al. (2012) described the thermo-physical behavior of PCM glazing system configurations. PCM-filled

glass windows for reducing the solar radiation entering the indoor space through the windows was also investigated (Ismail, Salinas, & Henriquez, 2008), and the effectiveness of the system is compared with windows filled with reflective gases.

10.2 Phase change material (PCM) candidates for buildings

The selection of the PCM for a building envelope is mainly based on its melting temperature. To have an effective PCM, the melting temperature of the PCM should be within outdoor minima and maxima temperatures to allow the PCM to melt and solidify. Having low cost and being nontoxic, nonflammable, and chemically stable are preferred characteristics of PCMs. PCMs are classified as organic or inorganic substances with a high latent heat of fusion and a relatively low melting temperature (e.g., paraffin, and salt). There are hundreds of potential PCM candidates that are reviewed and listed with their properties in the literature (Cabezaa et al., 2011). However, few PCMs have actually been tested and used for buildings. Several PCM candidates are substantially reduced to only a few because many PCMs have a high latent heat of fusion and a convenient melting temperature, but they are hazardous or highly corrosive. The organic or inorganic PCMs are known to melt with a high heat of fusion in a wide range of melting temperatures. However, the PCM melting temperature and latent heat of fusion are not the only criteria to select the PCM. The PCM must exhibit certain desirable thermodynamic and chemical properties. In addition, economic considerations of the cost and availability in large scales must also be considered.

10.2.1 PCM selection criteria

The PCM selection criteria for building envelopes are listed below. Many researchers highlighted the desirable and undesirable features of the PCM, such as Kenisarin & Mahkamov (2007). The most important properties for selecting the PCM for buildings are PCM melting temperature and latent heat of fusion. To be a successful PCM in a building envelope, the following thermodynamic, chemical, and economic criteria should be considered:

1. Thermodynamic criteria
   - **a.** The thermo-physical properties should be available and accurate.
   - **b.** The PCM melting temperature should be close to outdoor temperature.
   - **c.** The latent heat of fusion and specific heat must be high.
   - **d.** A high thermal conductivity to prevent potential PCM overheating and fast thermal response.
   - **e.** The PCM solid and liquid phase properties are preferred to be close to each other. Large variations in densities between the solid and liquid could cause segregation, resulting in changes in the chemical composition of the material.
   - **f.** The volumetric thermal expansion of PCM during melting should be low.
2. Chemical criteria
   - **a.** Chemically stable, so that the PCM can be in service for a long time.
   - **b.** No chemical decomposition.

   c. Noncorrosive.
   d. The PCM must be nonpoisonous to ensure the safety of the residents.
   e. Nonflammable.
   f. Insulator to electricity to avoid a short circuit if leakage occurs.
3. Economic criteria
   a. Commercially available in large quantities in the market.
   b. PCM pureness should be high to guarantee high performance of the PCM.
   c. Inexpensive, so that the price is comparable to traditional insulation materials.

Unfortunately, a single PCM that possesses all of the above criteria is not available, and there is simply no perfect PCM. However, some of the undesirable PCM characteristics can be corrected. For example, high conductive metals can be incorporated into the PCM to increase its low thermal conductivity if fast thermal response is required. The negative effect of high thermal expansion of the PCM can be corrected by leaving a measured air pocket in the housing to allow the PCM to expand.

10.2.2 PCM types

PCMs are grouped into the families of organic and inorganic. Subfamilies of the organic materials include paraffin and nonparaffin. Salt hydrates may be regarded as alloys of inorganic PCM. Abhat (1983) classified the PCM used for thermal energy systems, and a detailed classification was suggested by Mehling and Cabeza (1997).

1. Paraffin organics
   Paraffin organics are an oil product, and they are a family of saturated hydrocarbons with similar properties. They are characterized by C_nH_{2n+2}, and all series below $n = 5$ are gases at 25 °C. Those between $n = 5$ and $n = 15$ are liquid, and the rest are waxy solids. The thermal conductivity of paraffin is very low and it is comparable to the best insulators. In addition, paraffin is serviced as a PCM for building envelopes because it possesses most of the PCM selection criteria for buildings. Paraffin organics are inexpensive, have high sensible and latent heat storage capacities, and are available in a wide range of melting temperatures, which facilitates the design and optimization of PCM for buildings. However, paraffin should not be exposed to high temperature because it is flammable. The general characteristics of the paraffin are as follows:
   a. High latent heat of fusion, around 240,000 J/kg
   b. Wide range of melting point selection, from −6 to 66 °C
   c. Flammable
   d. Nontoxic
   e. Noncorrosive
   f. Chemically stable
   g. High volumetric thermal expansion
   h. High density, around 750 kg/m^3
   i. Low thermal conductivity, around 0.3 W/m-K
   j. High wetting ability
   k. Low vapor pressure in the melt
   Table 10.1 provides a list of paraffin organics previously used in building components (Hale, Hoover, & O'Neill, 1971; Izquierdo-Barrientos, Belmonte, Rodríguez-Sánchez, Molina, & Almendros-Ibáñez, 2012; Koschenz & Lehmann, 2004). A comprehensive list and other PCMs can be found in Cabeza et al. (2011) and Osterman et al. (2012).

Table 10.1 Previously examined paraffin organics and their properties

Paraffin organics	Formula	Melting point (°C)	Latent heat (kJ/kg)	Density (kg/m^3)	Conductivity (W/m-K)
n-Tetradecane	$C_{14}H_{30}$	5.5	228.0	771	0.15
n-Hexadecane	$C_{16}H_{34}$	16.7	237.0	774	0.25
n-Octadence	$C_{18}H_{38}$	28.0	244.0	774	0.35
Eicosane	$C_{20}H_{42}$	36.8	241.0	778	0.27

2. Nonparaffin organics
   Nonparaffin organic components are characterized by $CH_3(CH_2)_{2n}COOH$, their latent heat of fusions are comparable to that of organic paraffin, and their densities are larger than paraffin organics. However, they are rarely used in building envelopes because of their many unacceptable characteristics. Their cost is twice greater than that of paraffins. In addition, almost all nonparaffin organic materials are flammable and should not be exposed to high temperature media, flame, or storage oxidizer agents. Also, exposure to high heat can cause decomposition and caution is needed in handling nonparaffin organic materials of any type. Another disadvantage of the nonparaffin organics is their thermal conductivity, which is 5−10 times higher than paraffin; therefore, they are considered good thermal conductors.
3. Salt hydrates
   Several paraffin and nonparaffin organics have a melting point within the desired range, but they are flammable and a special housing design is required, adding an additional manufacturing cost. Salts hydrates are successful substitutes for organic PCM, and they were previously used as a PCM for bricks (Principi & Fioretti, 2012). They are nonflammable, have a high heat of fusion, and have a wide range of melting temperature from 18.5 to 116.0 °C. However, the major disadvantage of the salt hydrates as PCM is that they are highly corrosive. Another disadvantage is the significant difference between liquid and solid densities. Therefore, the PCM housing structure must be perfectly designed to overcome the thermal expansion of the salt. Table 10.2 shows the salt hydrates that were previously used as PCMs for building (Waqas & Din, 2013). The general characteristics of salt hydrates are as follows:
   a. High heat of fusion
   b. Relatively low thermal conductivity
   c. Highly corrosive
   d. Relatively more expensive than paraffin and nonparaffin PCMs

10.3 Masonry brick designs for PCM

One of the early designs of masonry bricks with PCM was proposed by Lai & Chiang (2006) and followed by Alawadhi (2008). Basically, the design was bricks containing hollow cylinders filled with PCM. Figure 10.1 shows the geometry configuration of a brick containing three hollow cylinders filled with PCM, and the thermal analysis of

Table 10.2 Previously used salt hydrates and their properties

Material	Melting point (°C)	Heat of fusion (kJ/kg)	Density (kg/m^3)	Specific heat (kJ/kg)	Conductivity (W/m-K)
$CaCl_2$ $6H_2O$	29.7	171	1333	1.45	0.23
Na_2SO_4 $10H_2O$	32.4	254	1485	1.93	0.544
$Zn(NO_3)_2$ $6H_2O$	36.4	147	2065	1.8	0.31

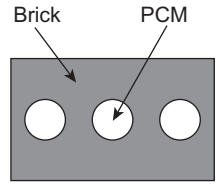

Figure 10.1 Brick containing three hollow cylinders filled with phase change material (PCM).

the design was accomplished using experimental (Lai & Chiang, 2006) and theoretical methods (Mandelbrot, 1983).

For the Lai & Chiang (2006) design, the size of the brick is 172 × 70 × 305 mm, and the brick has three cylindrical holes with a diameter of 45 mm. An acrylic tube, $k = 0.19$ W/m-K, with diameter slightly less than 45 mm, was completely filled with *n*-octadecane, an organic paraffin. The ends of the acrylic tubes were completely sealed by silicone, and they were repeatedly tested at high and low temperatures to ensure there were no leaks. They evaluated the thermal performance of the bricks with PCM by comparing the temperature variations of the top surface, the center of the holes, and the bottom surface with a brick without PCM or just a hollow cylinder. They indicated that when the temperature of the PCM tube exceeded the PCM melting temperature, a liquid zone at the upper region was observed, and the zone grew under the influence of the natural convection flow of liquid PCM. In addition, the experimental results indicated that the temperature at the top surface of the brick with PCM was lower than brick without PCM during the daytime. On the other hand, the brick with PCM became a heat source, resulting in a higher temperature at the top surface at nighttime. In general, the brick with PCM design was capable of reducing the maximum bottom surface temperature by 4.9 °C when the maximum outdoor temperature was 35.5 °C.

A brick with dimensions of 0.25 × 0.15 × 0.15 m with cylindrical holes was evaluated numerically by Alawadhi (2012). The diameter of the holes is 0.03 m, and the effect of the number of PCM cylinders in the brick was investigated. The number of cylinders reflects the PCM quantity in the brick. A brick with one, two, and three

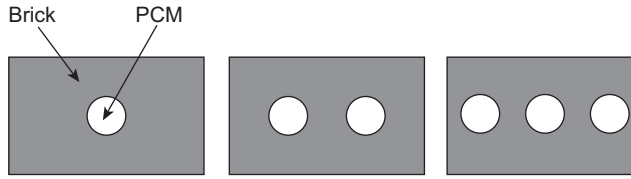

Figure 10.2 A brick with one, two, and three phase change material (PCM) cylinders.

PCM cylinders as well as a brick without PCM were considered as case studies, as shown in Figure 10.2. A brick with a minimum quantity of the PCM is desirable to maintain the physical strength of the brick and to reduce the production cost.

In these designs, the PCM cylinders are located at the middle of the brick. The outdoor surface of the wall is subjected to a time-dependent solar radiation and forced convection boundary conditions, whereas the indoor surface is subjected to a time-independent free convection boundary condition. Three types of organic paraffin were selected for the numerical study, and they are *n*-octadecane, *n*-eicosane, and P116. P116 has a melting temperature of 47°C. These PCMs were selected because their melting temperatures are within the temperature variations of the outdoor space. Real weather data for the month of June for the state of Kuwait were used for the outer boundary condition. The weather data are for the month of June when the temperature and solar radiation are the highest. The thermal performance of the brick with PCM is compared with brick without PCM, and heat flux at the indoor surface of the brick is calculated. The results indicated that the P116 and *n*-octadence are ineffective in reducing the heat flux at the indoor space. The *n*-octadence was in the liquid phase all of the time because of its low melting temperature whereas *n*-eicosane was in the solid phase all of the time because of its high melting temperature. With P117, the rate of change of the heat flux is dramatically decreased during the daytime compared with the brick without PCM, with a maximum heat flux reduction of 24.2%. A brick with one, two and three cylinders, with P116 PCM, was evaluated. For a brick with a one-cylinder design, the maximum heat flux reduced at the indoor space was 11.5%; this value was 17.9% with two cylinders and 24.2% with three cylinders.

Castell, Martorell, Medrano, Perez, & Cabrza (2010) added microencapsulated PCM in conventional and alveolar bricks that were typically used in Mediterranean regions. The experimental wall consisted of convectional bricks with a dimension of $0.29 \times 0.14 \times 0.75$ m, and there were three rows of hollow cylinders each containing seven holes, as shown in Figure 10.3. A panel containing PCM is attached at the outdoor surface of the brick, followed by a spray foam polyurethane, $k = 0.028$ W/m-K and $\rho = 35$ kg/m^3. The PCM is paraffin with a melting temperature of 28°C. Wall temperatures were obtained, as well as heat flux entering the wall, and the results were compared to wall without PCM. The report results indicated that the brick with PCM can smooth out the daily temperature fluctuations. In addition, the energy consumption of the brick with PCM can be reduced by 15% compared with bricks without PCM. The Sierpinski carpet (Mandelbrot, 1983) is used to characterize the geometric structure of a brick filled with PCM. Figure 10.4 shows the schematic of the Sierpinski

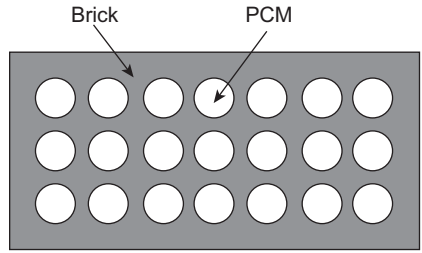

Figure 10.3 Brick with three rows of hollow cylinders each containing seven holes.

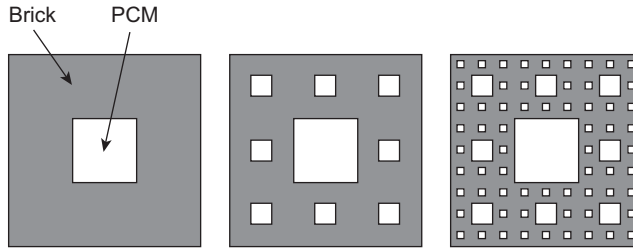

Figure 10.4 A schematic of the Sierpinski carpet.

carpet. The Sierpinski carpet is commonly used to characterize porous objects, and because a brick with hollows is physically considered a porous object, the Sierpinski carpet can be applied to study brick with PCM. The filling amount of PCM in the brick is represented by the porosity of the Sierpinski carpet.

In addition, the effects of the PCM amount and spatial distribution of the PCM on the thermal characteristics of the brick wall can be easily determined by comparing it with that of the brick without PCM. The Sierpinski carpet is a typical self-similar porous fractal object. A square is the general algorithm, and the carpet is constructed by dividing the square into nine congruent smaller squares and removing the central one then repeating the same procedure recursively to the remains. The fractal dimension of the carpet is $D = \ln(8)/\ln(3)$. For the *i*th recirculation, the porosity (ε_i), and pore scale (L_i) of the Sierpinski carpet can be calculated as, respectively,

$$\varepsilon_i = 1 - \left(\frac{3^2 - 1}{3^2}\right)^i$$

$$L_i = \frac{L_o}{3^i}$$

Zhang et al. (2011) present the effect of PCM amount in the brick with a Sierpinski carpet design on the indoor surface temperature. They indicated that with increasing the amount of the PCM, the temperature fluctuation amplitudes indoors was effectively reduced, and the temperature hysteresis was correspondingly enhanced. A simpler design was proposed and analyzed by Silva, Vicente, Soares, & Ferreira (2012).

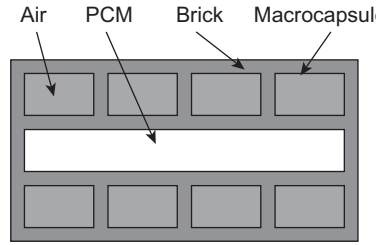

Figure 10.5 Steel macrocapsules were filled with phase change material (PCM) and inserted into the middle brick voids.

In their design, steel macrocapsules were filled with PCM and inserted into the middle brick voids, as shown in Figure 10.5. The bricks are made of clay with dimensions of 30 × 20 × 15 cm, and the steel macrocapsules have dimensions of 30 × 17 × 2.8 cm and 0.75-mm thickness. In this research, organic paraffin was chosen, designated as RT18 with a melting temperature of 18°C.

The experimental results indicated that the brick PCM design contributed to the reduction in the indoor space temperature fluctuations from 10 to 5°C. In addition, the time delay was about 3 h for brick with PCM on the charging mode whereas it was only 1 h for brick without PCM. A flexible plastic container was used, proposed by Principi & Fioretti (2012), to house the PCM in the brick. Then, the container was placed in the cavity and filled with PCM. Finally, the container was sealed to avoid the leakage of liquid PCM. The holes in the brick chosen for the design have a thickness of 0.027 m, as shown in Figure 10.6. The PCM was inserted in only one row in the brick, and the selected row is the closest to the external side of the brick. This position was chosen to effectively store energy coming from outdoors and to allow the release of most of the stored thermal energy toward the outdoor space.

The PCM used in this experimental study was Glauber salt (Na_2SO_4-$10H_2O$), which has a melting temperature of 32.5°C. The design brick with PCM led to not only a delay of about 6 h in the heat flux peak but also a reduction of the heat flux by 25%. A brick of size 30 × 20 × 15 cm with 12 square cavities of 4 × 3.667 cm filled with PCM was designed by Hichem, Noureddine, Nadia, & Djamila (2013), and they optimized the

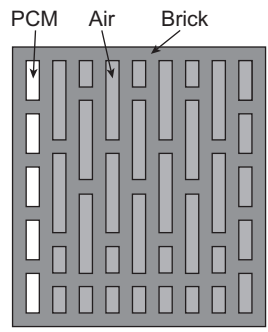

Figure 10.6 Brick with phase change material (PCM) inserted in only one row in the brick.

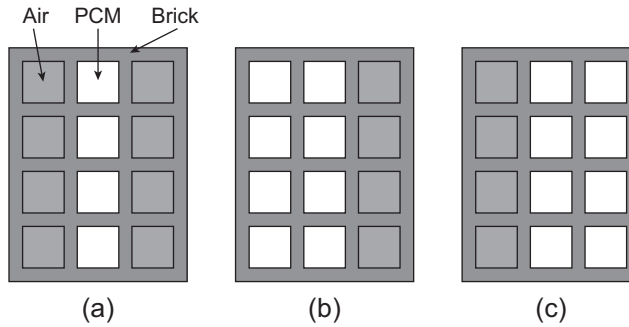

Figure 10.7 Bricks with different positions and quantities of phase change material (PCM): (a) middle; (b) middle and near outer surface; (c) middle and near inner surface.

type of the PCM, the location of the PCM, and the amount of the PCM in the brick. There are three possible positions of PCM in brick: (a) in the middle, (b) in the middle and near the outer surface, and (c) in the middle and near the inner surface. Figure 10.7 shows bricks with different positions and quantities of PCM.

The reduction of total heat flux for 1 day was 82.1% for the (a) PCM position, 90.02% for (b) PCM position, and 69.93% for the (c) PCM position. Hence, if the double quantities of PCM are employed, the (a) PCM position, the efficiency of brick was only enhanced by 7.92%.

10.4 Analysis methods

The thermal performance of bricks with PCM can be evaluated by comparing the heat flux and surface temperature at the indoor surface with a brick without PCM. The heat flux and surface temperature can be determined for a brick with PCM by either numerically solving the heat conduction equation along with the boundary conditions or directly using experimental measurements. The numerical method is commonly employed to perform optimization or paramedic studies to assess the effect of different design parameters, such as the PCM quantity, type, and location in the brick. The design parameters are optimized by minimizing heat flux or surface temperature at the indoor surface. The experimental method is typically employed to validate the numerical method and to ensure that the governing equations and applied boundary conditions are accurate enough for practical implementation.

10.4.1 Numerical method

All structure components in a building, including masonry bricks, are three-dimensional space. However, an approximation can be made to reasonably reduce the size of the computation domain from three- to two- or even one-dimensional space. Computation domain reduction should be considered in numerical simulations to reduce the model size, computational time, and required data storage capacity. If the geometry and thermal boundary condition of the bricks can be completely described

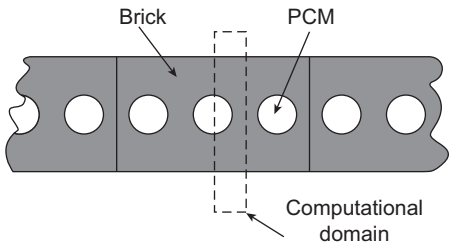

Figure 10.8 Bricks with repetitive symmetry and the computational domain.

in one- or two-dimensional space, then the space can be reduced. When the geometry and boundaries of the model are repeated in a particular direction, then the model has a repetitive symmetry. For example, the simulation of a long wall made of masonry bricks with three holes can be easily modeled using the repetitive symmetry, as shown in Figure 10.8. This wall is relatively long, and if the indoor and outdoor thermal boundary conditions are not varied along the wall direction, then the thermal characteristics do not vary significantly along the wall. Therefore, the line of symmetries should have a zero heat flux. Note that the repetitive symmetry is valid anywhere in the object except at the end of the wall. Additionally, the height of the wall is large compared to its thickness; therefore, the height effect has a negligible effect on the heat transfer. Hence, only a quarter of the masonry brick is considered. Figure 10.8 shows the computational domain.

The thermo-physical properties of the bricks are temperature independent, but it is dependent for the PCM to account for latent heat effect. For simplicity, the thermal expansion of PCM is not considered, and the effect of the natural convection flow of the liquid PCM is neglected in the computations. A significant variation between the solid and liquid densities induces the natural convection flow in the liquid portion of the PCM. The natural convection flow reduces the thermal resistance in the bricks, and hence increases the heat transfer. However, the natural convection effect is significant only if the temperature difference between the boundaries is high (Alawadhi, 2012). The two-dimensional heat conduction equations for the brick and the PCM are expressed in the following mathematical form:

$$\text{Brick}: \quad (\rho C_p)_b \frac{\partial T_{bn}}{\partial t} = k_b \left(\frac{\partial^2 T_b}{\partial x^2} + \frac{\partial^2 T_b}{\partial y^2} \right)$$

$$\text{PCM}: \quad (\rho C_p)_{PCM} \frac{\partial T_{PCM}}{\partial t} = k_{PCM} \left(\frac{\partial^2 T_{PCM}}{\partial x^2} + \frac{\partial^2 T_{PCM}}{\partial y^2} \right)$$

where (ρC_p) is specific heat per unit volume, and (k) is the thermal conductivity. The subscript (b) and (PCM) refer to the property of the brick and PCM, respectively. For modeling the phase change process, there are two main methods: moving mesh and fixed mesh methods. The mesh of the moving mesh method is continuously changing to track the solid/liquid interface. This method is seldom used in modeling phase

change because it will highly complicate the computations. The fixed mesh method is commonly used for modeling phase change. In this method, the geometry of the grid is independent of time, and the latent heat effect of the PCM is simulated by making the specific heat function of the temperature. The definition of the specific heat is as follows:

$$\left(\rho C_{\mathrm{p}}\right)_{\mathrm{PCM}} = \begin{cases} \left(\rho C_{\mathrm{p}}\right)_{\mathrm{PCM}} & \mathrm{T} < \mathrm{T}_m \\ \left(\rho C_{\mathrm{p}}\right)_{\mathrm{PCM}} + \rho_{\mathrm{PCM}}\left(\dfrac{\lambda}{\Delta \mathrm{T}}\right) & \mathrm{T}_m \le \mathrm{T} \le \mathrm{T}_m + \Delta \mathrm{T} \\ \left(\rho C_{\mathrm{p}}\right)_{\mathrm{PCM}} & \mathrm{T} > \mathrm{T}_m + \Delta \mathrm{T} \end{cases}$$

λ is the latent heat of fusion, T_m is the melting temperature of PCM, and $\Delta \mathrm{T}$ is the phase change transition temperature. $\Delta \mathrm{T} = 1\ ^{\circ}\mathrm{C}$ is extensively used in numerical simulations for the PCM and is recommended by many researchers (Alawadhi, 2004). If there are significant variations of the PCM properties between the solid and liquid, then the average should be used. The outdoor surface of the wall is subjected to a time-dependent solar radiation heat flux, Q_{s}, and air convective boundary conditions, with temperature and heat transfer coefficients of T_{o} and h_{o}, respectively. At the indoor surface of the wall, a free convective boundary condition is applied with temperature and heat transfer coefficients of T_{i} and h_{i}, respectively. The heat flux at the outdoor wall surface is expressed as

$$Q_{\mathrm{os}} = h_{\mathrm{o}}(T_{\mathrm{o}} - T_{\mathrm{os}}) + (1 - \rho)Q_s$$

where T_{os} is the outdoor surface temperature and ρ is the solar reflectivity. The heat flux at the indoor surface can be obtained from

$$Q_{\mathrm{is}} = h_{\mathrm{i}}(T_{\mathrm{i}} - T_{\mathrm{is}})$$

where T_{is} is the indoor surface temperature. The average heat flux at the indoor roof surface is calculated to evaluate the performance of the PCM, and it can be expressed as

$$\overline{Q_{\mathrm{is}}} = \int_A h_{\mathrm{i}}(T_{\mathrm{i}} - T_{\mathrm{is}})\mathrm{dAy}$$

The total heat flux can be integrated to obtain the total average heat flux over a specific period:

$$\left(\overline{Q_{\mathrm{is}}}\right)_{\mathrm{ave}} = \frac{1}{\mathrm{t}} \int_{\mathrm{t_o}}^{\mathrm{t}+\mathrm{t_o}} \overline{Q_{\mathrm{is}}}\ \mathrm{dt}$$

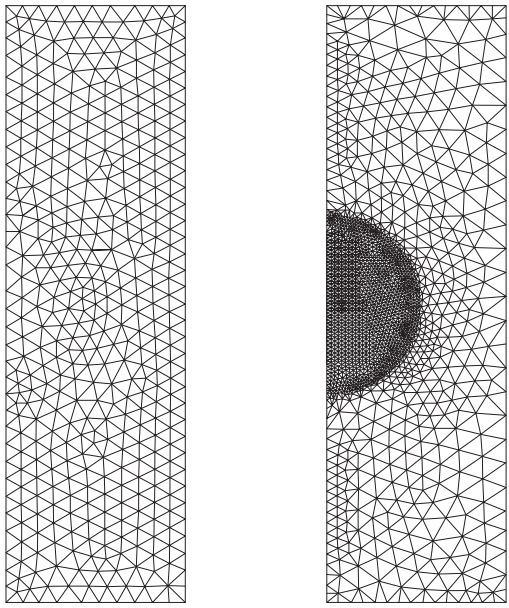

Figure 10.9 The masonry brick discretized with (a) course and (b) fine meshes.

The finite element method is extensively used for thermal analysis of brick with PCM. The computational domain should be first divided into elements, and this process is called "discretization." The element distribution in the computational domain is called the "mesh," and the elements are connected to each other at points called "nodes." The masonry brick with three holes, as shown in Figure 10.9a, is discretized with 1263 elements. The result of the finite element method can be additionally enhanced by increasing the number of elements in the model. On the other hand, increasing the number of elements leads to a proportional increase in the computational time and storage memory. High temperature gradients are expected in the PCM region whereas they are low in the brick region. Therefore, elements must be concentrated at the PCM region to correctly simulate the latent heat effect. In Figure 10.9b, the PCM region has more elements than the first mesh, and the number of elements is increased to 3561. After the computational domain is discretized, the element equations for the thermal analysis must be established.

The element equations are assembled to obtain the global equation for the mesh, which describe the thermal behavior as whole. The first law of thermodynamics states that thermal energy is conserved:

$$\rho C\left(\frac{\partial T}{\partial t}\right) + \{L\}^T\{Q\} = 0$$

where {L} is the vector operator and {Q} is the heat flux vector. Fourier's law is used to relate the heat flux vector to thermal gradients:

$$\{Q\} = -[K]\{L\}\{T\}$$

where [K] is thermal conductivity matrix and {T} is the temperature vector. Therefore, the element equation can be expressed as

$$\rho C\left(\frac{\partial T}{\partial t}\right) - \{L\}^T[K]\{L\}\{T\} = 0$$

The preconditional generalized minimum residual (PGMR) solver is the most effective solver for solving the temperature field. The PGMR method is an iterative method for the numerical solution of a system of nonsymmetric linear equations. At each time step, the temperature result is checked for convergence, and the following condition is used to declare the convergence at each time step:

$$\frac{\left|T_{ij}^{m+1} - T_{ij}^{m}\right|}{T_{ij}^{m}} \leq 10^{-6}$$

The convergence condition represents the sum of the temperature difference calculated from the current (m + 1)th iteration and the previous (m)th iteration and normalized by the sum of the current iteration. This ratio should be small enough for the convergence condition. For more information regarding the numerical method for PCM, Alawadhi (2010) illustrates in his book a melting process of PCM inside of a circular enclosure. The PCM is *n*-eicosane and paraffin wax, and details about theory, modeling, meshing, and analyses are explained.

10.4.2 Experimental method

The experimental technique is extensively utilized for studying the thermal performance of masonry bricks because the experimental results are reliable and reflect real, practical situations. To conduct an experiment, a section of brick with a PCM wall with a dimension of at least 1.0 m^2 should be constructed and ready for experiments. The wall is installed at one of the vertical walls of a testing room whereas other walls are made of brick without PCM. The roof and floor are perfectly insulated. Figure 10.10 shows a typical testing room for evaluating the brick with PCM. The testing room can be freely rotated to study the effect of the facing direction on the thermal performance of the brick with the PCM wall, and direct north, south, east, and west directions are typically considered. To ensure that the testing room will not be shaded, it should be placed in an open field, and the indoor temperature is controlled by a thermostat and air-conditioning unit (Castell et al., 2010). On the other hand, the entire testing can be conducted indoors. In this method, the indoors is heated to simulate the outdoor space whereas the surrounding simulates the

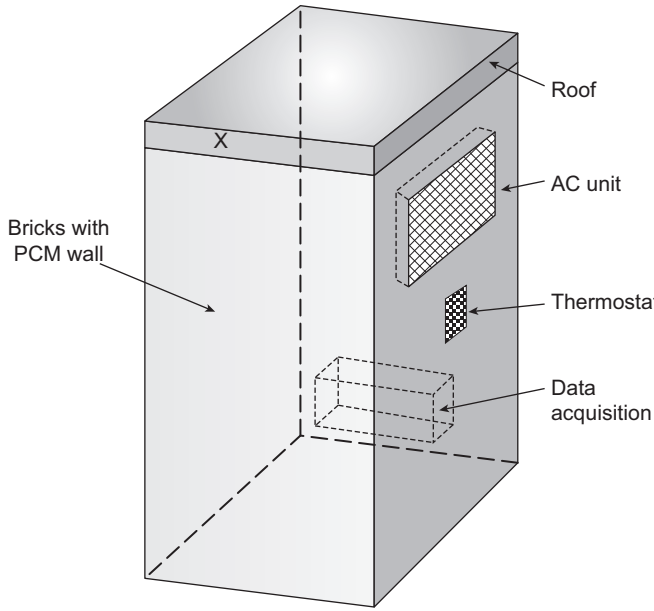

Figure 10.10 A typical testing room for evaluating the brick with the phase change material (PCM).

low-temperature indoor space (Mandelbrot, 1983). Powerful bulbs must be installed in the testing room to simulate solar radiation. In both methods, the experiment should be continuously running for at least 3 days to ensure that a thermal periodic condition is established in the entire testing room. K-type thermocouples are attached to the indoor and outdoor surfaces of the walls as well as inside of the PCM to monitor the melting process of the PCM in the bricks. Heat flux sensors are attached to the indoor and outdoor surfaces to measure the heat flux from the outdoor to indoor spaces and to estimate the heat transfer coefficients. Data acquisition is used to record the temperature and heat flux readings every fixed interval.

The heat flux variations with time at the indoor surface of the testing room are obtained for all walls, and the performance of the brick with the PCM wall is compared to a wall that does not contain PCM. The heat fluxes for all walls are integrated for a specific period, or 1 day, to obtain the net heat gain. If the wall made of brick with PCM is capable of considerably reducing the heat gain, the objective of reducing the heat gain using brick with PCM is achieved. To determine the equivalent specific heat with the temperature of PCM-concrete brick, Cheng, Pomianowski, Wang, Heiselberg, & Zhang (2013) propose a technique in which complex experimental installations are not required. The required needed data are only the top heat flux and the temperature distributions in different layers. The dynamic change of specific heat can be presented by using the proposed method. The environmental impact of construction systems on alveolar bricks and PCMs can be evaluated using life cycle assessment as presented by Castell et al. (2013).

10.4.3 Future trends

Practically, a single PCM type is used with bricks. Future trends involve the bricks filled with PCMs with different melting temperatures (Yang, Zhang, & Xu, 2014). The bricks with different PCMs work more effectively as a thermal barrier at a wide range of outdoor ambient temperatures. Solid packages of PCM in bricks will be replaced by spheres of encapsulated paraffin (Arkar & Medved, 2007). The spheres of encapsulated paraffin have a larger surface area that provides bricks with better thermal response with the outdoor ambient air temperature (Cabeza et al., 2007). The microencapsulated housing design enables PCM to freeze and melt in day and night cycles, in which night cooling is important to achieve this full cycle every day.

References

Abhat, A. (1983). Low temperature latent heat thermal energy storage: heat storage materials. *Solar Energy, 30*, 313−332.

Alawadhi, E. (2004). Phase change with free convection in a circular enclosure: numerical simulations. *Computers and Fluids, 33*, 1335−1348.

Alawadhi, E. (2008). Thermal analysis of a building brick containing phase change material. *Energy Buildings, 40*, 351−357.

Alawadhi, E. (2010). *Finite elements simulations using ANSYS*. Taylor and Frances.

Alawadhi, E. (2012). Using phase change materials in window shutter to reduce the solar heat gain. *Energy and Building, 47*, 421−429.

Alawadhi, E., & Alqallaf, H. (2011). Thermal analysis of a building's roof with cone frustum holes containing PCM. *Energy Conversion and Management, 52*, 2958−2964.

Arkar, C., & Medved, S. (2007). Free cooling of a building using PCM heat storage integrated into the ventilation system. *Solar Energy, 81*, 1078−1087.

Barkmann, H. G., & Wessling, F. C. (1975). Use of building structure components for thermal storage. In *Processing of the workshop on solar energy storage subsystems for heating and cooling of building*. Virginia, USA: Charlottesville.

Cabeza, L., Castellon, C., Nogues, M., Medrano, M., Leppers, R., & Zubillaga, O. (2007). Use of microencapsulated PCM in concrete walls for energy savings. *Energy Buildings, 39*, 113−119.

Cabeza, L. F., Castell, A., Barreneche, C., De Gracia, A., & Fernández, A. I. (2011). Materials used as PCM in thermal energy storage in buildings: A review. *Renewable and Sustainable Energy Reviews, 15*(3), 1675−1695.

Castell, A., Martorell, I., Medrano, M., Perez, G., & Cabrza, L. (2010). Experimental study of using PCM in brick constructive solution for passive cooling. *Energy Buildings, 42*, 534−540.

Castell, A., Menoufi, K., de Gracia, A., Rincon, L., Boer, D., & Cabeza, L. F. (2013). Life cycle assessment of alveolar brick construction system incorporating phase change materials (PCMs). *Applied Energy, 101*, 600−608.

Cengel, Y. (1998). *Heat Transfer, "a practical approach,"* New York: Mc-Graw Hill Book.

Cheng, R., Pomianowski, M., Wang, X., Heiselberg, P., & Zhang, Y. (2013). A new method to determine thermophysical properties of PCM-concrete brick. *Applied Energy, 112*, 988−998.

Chwieduk, D. (2013). Dynamics of external wall structures with a PCM (phase change materials) in high latitude countries. *Energy, 59*, 301−313.

Goia, F., Perino, M., & Hasse, M. (2012). A numerical model to evaluate the thermal behavior of PCM glazing system configurations. *Energy Buildings, 54*, 141−153.

Hale, D., Hoover, M., & O'Neill, M. (1971). *Phase change materials handbook*. USA: Space Sciences Laboratory, George Marshall Space Flight Center.

Hichem, N., Noureddine, S., Nadia, S., & Djamila, D. (2013). Experimental and numerical study of a usual brick filled with PCM to improve the thermal inertia of buildings. *Energy Procedia, 36*, 766−775.

Ismail, K., Salinas, C., & Henriquez, J. (2008). Comparison between PCM filled glass windows and absorbing gas filled windows. *Energy Buildings, 40*, 710−719.

Izquierdo-Barrientos, M., Belmonte, J., Rodríguez-Sánchez, D., Molina, A., & Almendros-Ibáñez, J. (2012). A numerical study of external building walls containing phase change materials (PCM). *Applied Thermal Engineering, 47*, 73−85.

Kenisarin, M., & Mahkamov, K. (2007). Solar energy storage using phase change materials. *Renewable and Sustainable Energy Reviews, 11*, 1913−1965.

Koschenz, M., & Lehmann, B. (2004). Development of a thermally activated ceiling panel with PCM for application in lightweight and retrofitted building. *Energy Buildings, 36*, 567−578.

Lai, C., & Chiang, C. (2006). How phase change materials affect thermal performance: hollow bricks. *Building Research and Information, 34*, 118−130.

Mandelbrot, B. (1983). *The fractal geometry of nature*. New York: Freeman.

Mehling, H., & Cabeza, L. F. (1997). *Heat and cold storage with PCM. Springer*.

Mehling, H., & Cabeza, L. F. (2007). Phase change materials and their basic properties. In H. O. Paksoy (Ed.), *Thermal energy storage for sustainable energy consumption: Fundamentals, case studies and design* (pp. 257−278). Kluwer Academic Publishers Group.

Morikama, Y., Suzuki, H., Okagawa, F., & Kanki, K. (1985). A development of building element using PCM. In *Proceedings of the international symposium on thermal application of solar energy* (Kanagawa, Japan).

Osterman, E., Tyagi, V. V., Butala, V., Rahim, N. A., & Stritih, U. (2012). Review of PCM based cooling technologies for buildings. *Energy and Buildings, 49*, 37−49.

Pasupathy, R., & Velraj. (2008). Effect of double layer phase change material in building roof for year round thermal management. *Energy Buildings, 40*, 193−203.

Pomianowski, M., Heiselberg, P., & Zhang, Y. (2013). Review of thermal energy storage technologies based on PCM application in buildings. *Energy and Buildings, 67*, 56−69.

Principi, P., & Fioretti, R. (2012). Thermal analysis of the application of PCM and low emissivity coating in hollow bricks. *Energy and Buildings, 51*, 131−142.

Ravikumar, M., & Sirinivasan, P. S. S. (2011). Year round performance of PCM filled RCC roof for thermal management. *European Journal Scientific Research, 3*, 424−433.

Silva, T., Vicente, R., Soares, N., & Ferreira, V. (2012). Experimental testing and numerical modelling of masonry wall solution with PCM incorporation: a passive construction solution. *Energy Buildings, 49*, 235−245.

Soares, N., Costa, J. J., Gaspar, A. R., & Santos, P. (2013). Review of passive PCM latent heat thermal energy storage systems towards buildings' energy efficiency. *Energy and Buildings, 59*, 82−103.

Torgal, P. F., Mistretta, M., Kaklauskas, A., Granqvist, C., & Cabeza, L. F. (2013). *Nearly zero energy building refurbishment*. Springer.

Turner, W. C., & Malley, J. F. *Handbook of Thermal Insulation Design Economics for Pipes and Equipment*. New York: McGraw-Hill. pp. 15−30.

Waqas, A., & Din, Z. (2013). Phase change material (PCM) storage for free cooling of buildings—a review. *Renewable and Sustainable Energy Reviews, 18*, 607−625.

Yang, L., Zhang, X., & Xu, G. (2014). Thermal performance of a solar storage packed bed using spherical capsules filled with PCM having different melting points. *Energy Buildings, 68*, 639−646.

Zhang, C., Chen, Y., Wu, L., & Shi, M. (2011). Thermal response of brick wall filled with phase change materials (PCM) under fluctuating outdoor temperatures. *Energy and Buildings, 43*, 3514−3520.

The design, properties and performance of shape optimized masonry blocks

11

L. Sousa, C.F. Castro, C.C. António, H. de Sousa, R. Sousa
Universidade de Porto, Porto, Portugal

11.1 Introduction

Recent European Directives concerning building energy efficiency are imposing the development or improvement of building envelope systems, since the growing importance of well-being, in conjunction with architectural trends, specifically the widespread increase of the glazed area in buildings, has led to an increase in unacceptable energy consumption levels.

These envelope systems are one of the features that needs improvements, because, despite their economic and functional importance, they present a high tendency to develop noticeable defects (e.g. cracking, water infiltrations). On the other hand, the thermal comfort and energy saving are pressuring the construction industry to comply the technical requirements and to increase performance of their products with acceptable costs, thus presenting a challenge to the development of façade systems.

Traditionally, the opaque part of the façades of buildings was generally made of masonry, usually designated by enclosure walls. The thermal efficiency induced important changes for these types of enclosure walls, in particular in south European countries where traditionally the mild winter climate justifies the use of walls with moderate thermal performance.

Now it makes sense to ask if whether or not the masonry will continue to have such a relevant importance in the construction of buildings, since given the technological evolution and development of new materials, masonry could lose importance to other solutions that have better cost/behavior effectiveness.

In order for masonry to continue to have a distinguishing presence in buildings, it would need to evolve, thus ensuring more functions and always at a competitive cost.

One of the ways by which the masonry can answer to these new challenges is by using thick single leaf walls with distributed insulation, by using thermal shaped optimized units made from lightweight materials with good thermal insulation and sufficient mechanical resistance, usually lightweight clay or concrete.

The primary intention of these wall solutions is to achieve, simultaneously, thermal insulation levels without the use of specific thermal insulation materials, adequate mechanical resistance and economic competitiveness.

These purposes must be obtained not only from the unit cost, but also by productivity gains associated with unit laying, since the dimensional increase of the units

Eco-efficient Masonry Bricks and Blocks. http://dx.doi.org/10.1016/B978-1-78242-305-8.00011-5

highlights one of the main problems of construction using masonry, which is the arduous nature of the workmanship in its laying. Also, this type of task is repetitive and physically exhausting, exposing workers to the risk of serious injury, with severe consequences in terms of productivity.

In order to answer adequately to current needs, it will be necessary to

- Develop solutions which are better adapted to environmental issues and to the needs of workmanship, being easier to handle and with less waste.
- Increase industrialization by concentrating multiple roles in a single element, generalizing the concept of the system with a greater emphasis on prefabrication.
- Design construction projects more oriented towards execution difficulties, and more concerned with site conditions.

These overall objectives require a complex optimization process, integrating various aspects, from numerical simulations and laboratory trials to experimental factory productions.

11.2 Searching for the optimal masonry block

Masonry enclosure walls are elements that are most exposed to environmental conditions (rain, temperature, wind loading, seismic vibrations) and to actions related to the use of the occupants. In order to accomplish these functions, masonry walls must be a multifunctional system able to answer to several demands, such as thermal and acoustic comfort, watertightness, fire resistance, safety in use, stability to loading effects, amongst others.

Most of these functions are performed by masonry walls, or can be partially or exclusively performed by other systems applied to the masonry, such as rendering systems to improve watertightness or thermal insulation. The use of these rendering systems with masonry supports increases the construction complexity and the difficulty of the characterization of the behavior of walls. Research and innovation are strongly needed to assess the vulnerability of existing constructions, to define economical rational design rules, to allow for build, novel shapes and novel applications of masonry and to contribute to masonry innovation.

11.2.1 Modern masonry solutions

A building's enclosure constructed in masonry is a very common solution worldwide and single leaf or cavity walls are both frequent. However, modern masonry walls are usually single leaf, made from large units and finishes with a specific behavior in order to significantly improve some specific aspects, for example thermal insulation or/and watertightness (Figures 11.1 and 11.2).

In Europe, clay units (vertically or horizontally perforated) are commonly used, but other units, like those made from concrete, have also large utilization (Figure 11.3).

Modern masonry systems are made from a set of pieces, i.e. units with different topologies and dimensions, which allow various applications and details to be carried

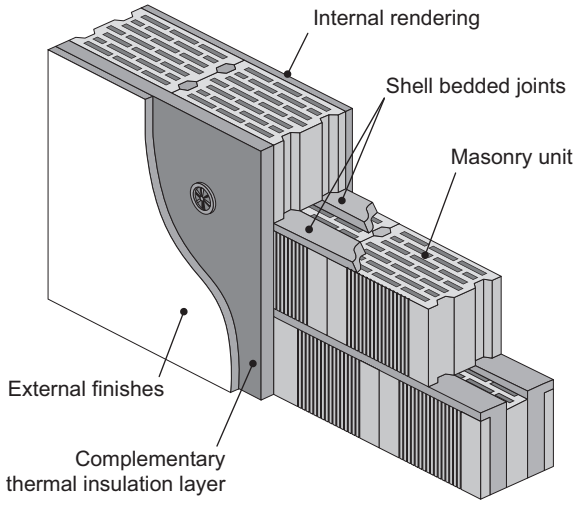

Figure 11.1 Detailed example of a modern masonry solution for enclosure walls.

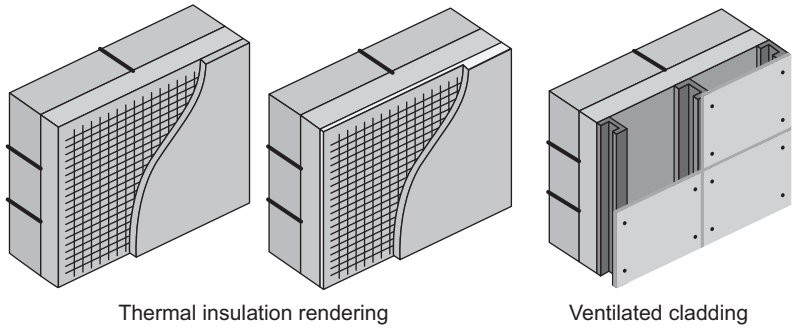

Figure 11.2 General examples of finishes applied to masonry wall.

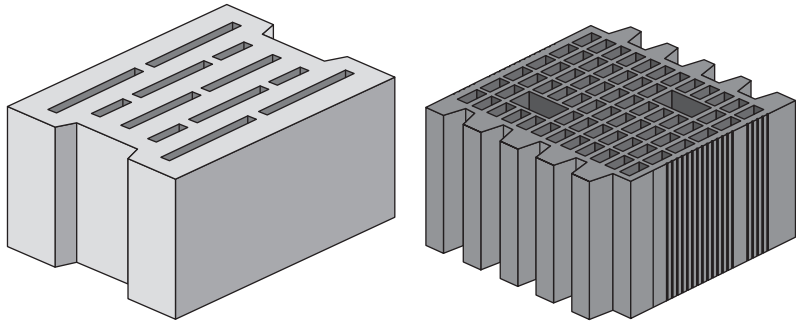

Figure 11.3 Examples of base units made of concrete and clay (vertically perforated).

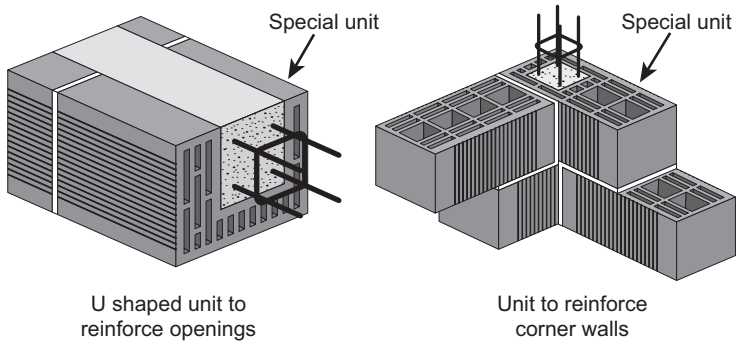

Figure 11.4 Special units to solve particular situations of masonry construction.

out, thus making the wall as a constructive system for which, in addition to the standard base units, special units are also developed to solve particular situations, such as connections between walls, integrations of windows or reinforcements (Figure 11.4), amongst others.

The units are usually laid in general purpose mortar joints, which can have an improved thermal behavior, but can also be laid in thin layer mortars for both better mechanical and thermal performance.

Also ancillary components (e.g. bed joint reinforcement, wall ties) can be used to improve the behavior of masonry in some situations, such as the connection between walls and other structural elements (Figure 11.5), but in general the use of these elements is not very common in some European countries.

11.2.2 External wall requirements

Construction works, including components and materials, must accomplish the basic requirements established in the European Directives (European Parliament, 2011):

1. Mechanical resistance and stability
2. Safety in case of fire
3. Hygiene, health and the environment
4. Safety and accessibility in use
5. Protection against noise
6. Energy economy and heat retention
7. Sustainable use of natural resources

The accomplishment of these requirements is made through the comparison between reference/minimum characteristics and the confirmed performance of the building components. The reference/minimum characteristics are referred in national regulations and design codes, and the performance of the building components are usually determined from laboratory tests or from established practises of design and construction.

When masonry walls are used in façades of buildings, i.e. used as enclosure masonry walls, they must also help to accomplish the basic requirements, including

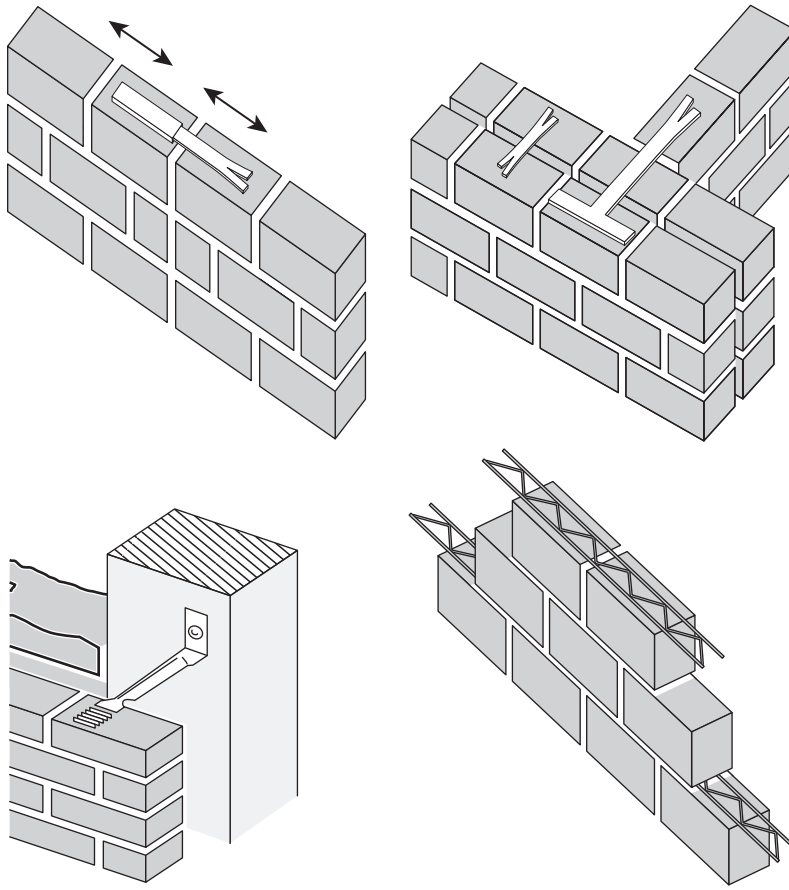

Figure 11.5 Examples of ancillary materials for masonry walls.

the units and the mortar joints. These constituent materials are important since they play an important role in the behaviour of the masonry, since they can influence a diversity of behaviours of the wall, such as thermal, acoustical, watertightness and mechanical performance. Therefore, the basic requirements for enclosure walls used in the building façades are important to be analysed.

11.2.2.1 Mechanical resistance and stability

Structural masonry used for enclosure walls should be checked to avoid collapse under loading of the whole or part of the wall, to avoid major deformations or damage to other elements or installed equipment. Design codes for masonry, such as EC6-Eurocode 6 (CEN, 2005) or EC8-Eurocode 8 (CEN, 2004), can be used.

It is important to underline that although this checking is not required for nonstructural enclosure walls, it is important to ensure the stability and mechanical resistance of these walls for wind loading according to EC6 (CEN, 2005), and also to other possible

actions induced by their support that can originate cracking (e.g. deformation, thermal actions). Also, a seismic verification of nonstructural walls is referred in EC8 (CEN, 2004), including applied coatings and connections to support the walls.

For the constituent materials, EC6 (CEN, 2005) and EC8 (CEN, 2004), together with a vast set of recent European standards, point to requirements for these materials as well as for structural masonry, many of them also applicable to infill/nonstructural masonry. The main objective of these requirements is to ensure a better mechanical behavior of masonry walls. It concerns geometrical characteristics (e.g. volume of holes, thickness of webs and shells for the units), mechanical characteristics (e.g. minimum compressive strengths of units and joints), and also aspects related to masonry detailing practices (e.g. interlocking of units), use of perpend joints, thickness limits for joints, use of shell bedded laying and use of bed joint reinforcement, amongst others.

11.2.2.2 Safety in case of fire

Masonry walls provide good fire resistance performance for the usual thicknesses (30−35 cm). Moreover, the constituent materials have a good reaction to fire (noncombustible materials, usually low in organic aggregates − class A1).

The determination of the class of fire resistance (REI and EI) can be performed through laboratory tests or estimated from tables of EC6 (CEN, 2005) through the thickness and composition of the wall. The determination of the classes of reaction to fire when necessary (different from class A1), is only measurable through testing.

11.2.2.3 Hygiene, health and the environment

To ensure watertightness of rain and lack of condensation on walls improves the health of the internal building environment and durability of the wall and applied materials.

Watertightness normally is achieved by using higher wall thicknesses and an adequate treatment of joints, or through the masonry wall and rendering systems with low permeability, or just by waterproofing membranes/coatings without a specific contribution from the masonry wall. In general, the watertightness can only be evaluated by testing (e.g. ASTM, 2011). However, there are some design/construction practices established in technical documents for assessing the watertightness of some masonry wall solutions (e.g. CSTB, 2008).

On the other hand, ensuring proper heat transfer coefficients, U value and appropriate thermal bridge technical solutions can greatly reduce the risk of condensation on the walls.

Finally, the most common constituent materials for masonry systems do not constitute danger to the users nor to the environment since there is an absence of noxious materials.

11.2.2.4 Safety in use

The walls must be able to guarantee an adequate impact resistance and the suspension of eccentric moderate loading (200−400 kg). In general, masonry is a heavy and rigid

solution, and usually is connected to the building structure. These characteristics usually are enough to ensure all requirements.

On the other hand, the facings of the walls, including applied finishes and installations, must be executed in a way that does not cause injury (contact and safety use).

11.2.2.5 Protection against noise

Since usually masonry is a heavy solution, this aspect is beneficial to airborne sound insulation, easily satisfying the most demanding requirements of sound insulation for exterior walls referred in national regulations. However, these acoustic requirements are more demanding for interior walls (e.g. separation between dwellings). This aspect often requires the use of thicker walls or even double walls with integration of specific acoustic insulation.

11.2.2.6 Energy economy and heat retention

The thermal performance and mitigation of the thermal bridges are one of the most crucial aspects of the façade walls. Thermal comfort requirements demand that the exterior walls contribute towards ensuring comfortable thermal conditions on the inside. To this effect most regulations establish maximum permissible values for the overall heat transfer, U value. These values have become increasingly stricter to ensure higher levels of thermal insulation. An improved performance can be achieved using masonry solutions made with units thermally optimized that can be complemented with specific thermal insulation.

It is important to notice that thermal insulation of building façades depends not only on the masonry (opaque part), but also on other building elements such as glazed elements.

11.2.2.7 Sustainable use of natural resources

The use of masonry systems that integrates pieces/units to solve singular situations (e.g. openings, integrations of reinforced elements, connections between walls) can reduce the amount of construction waste. Moreover, a large part of the waste from the demolition of masonry can be recycled for other uses in the construction industry, since most of the raw materials used are natural.

On the other hand, the use of natural raw materials (e.g. clays, sand, cork, wood powder and rice husk) avoids the use of synthetic materials that are harmful to the environment.

11.3 Enhanced performance of masonry blocks using optimization techniques

The development of new masonry units, possessing properties which match or exceed current existing products, is conventionally performed within a laboratory. The presence of air cells in concrete units and mortar joints affecting the thermal conductivity

of a wall was evaluated by Abdou and Murali (1994). Pierzchlewicz (1996) presented a pioneering research work in which 13 kinds of hollow blocks with different hole geometry (aligned and staggered) were developed, and their thermal and strength properties were analyzed. Bastos, Sousa, & Melo (2005) correlated the mix design with different properties of lightweight concrete masonry blocks, including compressive strength and thermal conductivity through tests on three walls. Later Al-Jabri, Hago, Al-Nuaimi, & Al-Saidy (2005) carried out an experimental investigation on the thermal insulation properties of lightweight concrete hollow blocks.

The time-consuming and laborious process often demands for thousands of samples to be produced and tested. Several authors have addressed the problem of utilizing numerical techniques to enhance the efficiency of the experiment-based development of a new product. The development of mathematical models plays an important role in the simulation and optimization of complex systems leading to efficient and economical designs. With the aim of providing improved layouts for a wide class of structural elements, the information generated by finite element analyses was employed to select the best design among a number of alternative constructive possibilities.

Extensive numerical investigations were carried out by del Coz Díaz et al., in particular, heat-insulating lightweight concrete hollow brick walls (del Coz Díaz, García Nieto, Betegón Biempica, & Prendes Gero, 2007) and slabs floors (del Coz Díaz, García Nieto, Domínguez Hernández, & Suárez Sánchez, 2009), taking into account the nonlinearity deriving from radiation effects (del Coz Díaz, García Nieto, Suárez Sierra, & Betegón Biempica, 2008; del Coz Díaz, García Nieto, Suárez Sierra, & Peñuelas Sánchez, 2008). Furthermore, focusing on new numerical methodologies del Coz Díaz and coworkers have been constantly innovating to access the effects of thermal properties of different constituent materials and the dimensions of recesses on the overall thermal performances of several structural components – floors made up of clay, concrete and lightweight concrete hollow blocks (del Coz Díaz et al., 2010, 2014) and multi-holed lightweight concrete blocks (del Coz Díaz, García Nieto, Álvarez Rabanal, & Domínguez Hernández, 2012; del Coz Díaz, García Nieto, Díaz Pérez, & Riesgo Fernández, 2011). The same authors also carried out experiments focusing on the hygrothermal properties of different mixes of lightweight concrete that are commonly employed in the fabrication of blocks making up the building envelope and provided best fitting numerical studies (del Coz Díaz et al., 2013). Interesting applications of innovative hollow concrete masonry blocks in which new layouts are characterized by reduced weight, adequate strength, and enhanced handling possibility have been presented. Javidan, Safarnejad and Shahbeyk (2013) have numerically observed that inserting a horizontal diaphragm in the middle or the bottom of a block can increase its ultimate effective strength (load resistance/weight).

The possibility of utilizing powerful optimization techniques to reduce the amount of experimental data required to develop a new product has been coupled to empirical modeling focusing on challenges to the masonry industry. Sousa, Sousa, et al. (2011) and Sousa, Castro, et al. (2011) have used a genetic algorithm for the definition of the geometry of lightweight concrete blocks that minimizes their transmittance, by determining the optimum values of a finite number of parameters that define the position, the size and the spacing of the holes within the block. The holes are assumed to be of

rectangular shape and arranged in a regular mesh, either aligned or staggered. A more general approach has been presented by Bruggi and co-workers (Bruggi & Cinquini, 2011; Bruggi, Cinquini, & Taliercio, 2013; Bruggi & Taliercio, 2013a, 2013b) with no a priori assumption made about the geometry of the holes in the block, so as to fully exploit the potentials of topology optimization; nevertheless, the presented two-dimensional problem of topology optimization should be studied as 3D. The search for new environment-friendly masonry products urges for mixes composed entirely of recycled and waste aggregates. Recently, Vu, Forth, Dao, & Toropov (2013) showed that the use of optimization techniques has a potential to provide economies during future scaling-up and manufacturing processes as compared to experimental optimization alone (Forth, Dao, Toropov, & Vu, 2010).

11.3.1 Optimization methodology using a genetic algorithm

Advantageous computational methods of design optimization do not guarantee to arrive at the true optimum, but offer an efficient method that has a high probability of finding the optimum or of getting close to it. There should be no requirement for any of the functions or constraints to be continuous or for differentials to exist allowing continuous and discrete design variables to coexist concerning geometry, materials and systems of construction. Evolutionary algorithms are optimization procedures that apply the Darwinian principle of survival of the fittest by maintaining a population of solutions of which the poorest are eliminated. Each solution is ranked according to a fitness value closely related to the objective function.

Implemented genetic algorithms supported by elitist strategies are based on operators such as selection, crossover, elimination/substitution and mutation, preserving a core of best individuals to be transferred into the next generation. A suitable and efficient elitist genetic algorithm (GA) has been described in the literature (António, 2002; António, Castro, & Sousa, 2005; Sousa, Castro, et al., 2011). Given a population, its individuals are ranked according to their fitness, and the elite group is defined as the best-fit individuals. Selection is performed by randomly choosing pairs of progenitors with one individual from the best-fit group (elite) and another from the least-fit group. The offspring genetic material is obtained using a modification of the parameterized uniform crossover technique. Solutions with similar genetic properties are eliminated and then substituted with new randomly-generated individuals. Implicit mutation is considered by randomly selecting individuals and then, depending on a given probability, one binary digit will mutate. After mutation, the original size population is recovered, the new population is found and the evolutionary process continues. The stopping criterion used is based on the mean fitness value of the best individuals within the population. If the mean fitness value of the elite group does not vary for a defined number of generations, it is assumed that the iterative process has converged; that is to say, the optimal solution was found.

Computational optimization is employed to define the topology of a masonry block that minimizes its thermal transmittance, with the aim of maximizing the thermal insulation of masonry buildings. Block manufacturing is a business that is strongly dependent on demand where standardized sizes are important with block dimensions being

specified by the manufacturer. The specific weight of masonry raw material obviously depends on its components. For lightweight concrete with expanded clay aggregates, the lowest specific weight corresponds to the lowest thermal conductivity and the highest thermal insulation performance. On the other hand, the lowest specific weight corresponds to the worst structural behaviour. A compromise between thermal and structural behaviour should be settled with the manufacturer.

Considering a vector of design parameters, $\mathbf{b} = \{b_1,\ldots,b_D\}$, and a function that measures the masonry wall transmittance, $\Pi(\mathbf{b})$, a single-objective optimization problem can be defined as

$$\text{minimize } \Pi(\mathbf{b}) \tag{11.1}$$

subject to state equations of the thermal problem and to additional side constraints related to weight and topology block $b_{d^-} \leq b_d \leq b_{d^+},\ d = 1,\ldots,D$.

In GA implementation, data codification is very important for further manipulation. Each possible solution is associated with an individual that is to say with a chromosome or string of digits. A mixed code format is adopted for the genotype of each chromosome of the individual or solution. A binary code format using a genotype with five digits will be considered for each design variable taking continuous values on intervals, such as vertical or horizontal shell's and web's thicknesses. An integer coding is considered for each discrete variable assigning a position on its domain. Clearly the dimension of the space design, even for a comparatively small chromosome structure, can be very large. An initial population is obtained by randomly generating different individuals within the solution space. Every individual is evaluated according to its fitness value, which is related to the objective function and defined as

$$F(\mathbf{b}) = \overline{F} - \Pi(\mathbf{b}) \tag{11.2}$$

where $\overline{F}$ is a predefined constant chosen to ensure a positive fitness value. The GA will seek to increase fitness as it operates. The schematic representation of the optimization algorithm is given in Figure 11.6.

11.3.2 Optimal thermal insulation of masonry walls using topology optimization

Using computer-aided simulations, it is possible to compare different building designs and to predict temperature fluctuations with a high degree of accuracy. Search for a new lightweight masonry block that will perform according to today's normative requests and exhibits optimal thermal insulation behavior is an ongoing process (Sousa, Castro, et al., 2011; Sousa et al., 2013; Svoboda & Kubr, 2010). Attention has been focused on the optimal design of masonry blocks in order to minimize their thermal transmittance (i.e. to maximize their thermal resistance).

A general mathematical description of an optimization problem includes objectives and constraints. Single objective formulations are straight-forward and allow detailed exploration. For insulation optimization, the objective function measures the masonry

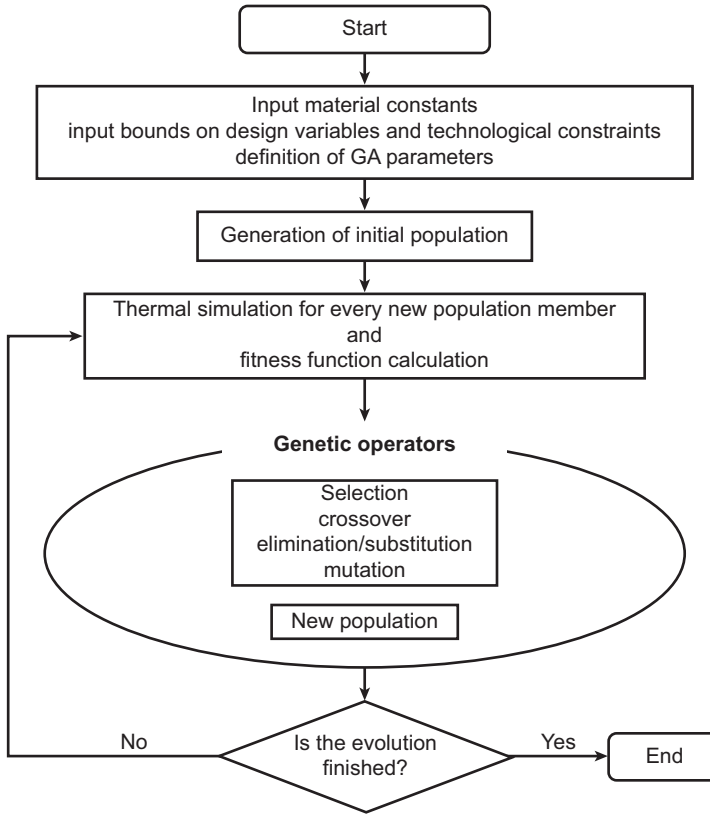

Figure 11.6 Flow diagram for the optimization algorithm.

wall transmittance and then normative requests and technological constraints have to be embodied in the optimization procedure (Evins, 2013; Gosselin, Tye-Gingras, & Mathieu-Potvin, 2009). In this section, an example of thermal optimization of a light-weight concrete masonry block, according to thermal normative requests, is presented.

The thermal behaviour of a wall can be characterized by the thermal transmittance of masonry units according to normative requests (CEN, 1993; CEN, 2002; CEN, 2005). This coefficient can be correctly calculated by three-dimensional finite element simulation considering the heat transfer simulation. Pure conduction is found in the concrete, and heat transfer by conduction, radiation and convection must be in the holes of the units. A detailed description of the thermal behavior of the voids is described in a previous work (Sousa, Castro, et al., 2011; Sousa et al., 2013).

The heat transfer due to the existence of air voids and the temperature gradient between the interior and the exterior surfaces of masonry walls is calculated using the first law of thermodynamics and the isotropic Fourier law for heat flux (Kreith & Bohn, 2001). The analysis of radiation exchange among the surfaces of an enclosure is complicated by the fact that when the surfaces are not black, radiation leaving a surface may be reflected back and forth several times among the surfaces with partial

absorption occurring at each reflection. A proper analysis of the problem, including the effects of these multiple reflections, is presented in a previous work (Sousa, Castro, et al., 2011). The study of the natural or free convection is made considering empirical correlations between the Nusselt (Nu) number, the Prandtl (Pr) and Rayleigh (Ra) numbers in enclosed spaces to determine free convection heat transfer coefficient in the voids (Kreith & Bohn, 2000).

The accuracy of the nonlinear method to predict clear wall thermal conductivity was validated using normative results for masonry units, EN 1745, where maximal discrepancy between referenced and simulated thermal resistance values was below 1% (Sousa, Castro, et al., 2011; Sousa et al., 2013).

In order to get a thermal optimization of vertically perforated lightweight concrete masonry units, the optimization algorithm described in the previous section has been used. The numerical evolutionary algorithm described iterates over the finite element thermal analysis supported by ABAQUS software.

The goal of the study is to find dimensions and distribution of voids that will minimize the thermal transmittance of masonry blocks with the following dimensions: 350 mm length including 5 mm vertical mortar joints on each side, 200 mm height including 10 mm horizontal mortar joint on the top and on the bottom and 350 mm thickness plus 20 mm mortar at internal and external render finish surfaces; total wall thickness becomes 390 mm. These values were provided by the manufacturer according to standard building procedures.

The 3D steady state heat transfer analysis has been performed considering linear solid elements of eight nodes. The internal and external surface temperatures are considered constant and equal to 293 and 273 K respectively. The heat transfer by convection and radiation is considered on the internal and external faces with associated thermal resistances $R_{si} = 0.13$ m^2 K/W and $R_{se} = 0.04$ m^2 K/W. The concrete presents a specific weight equal to 1100 kg/m^3 corresponding to a thermal conductivity, (concrete = 0.38 W/m K), according to Portuguese standard NP EN 1745. The experimental values for mortar thermal conductivity are given:

- Mortar thermal conductivity of interior mortar is equal to $\lambda = 0.80$ W/(m K).
- Mortar thermal conductivity of exterior mortar is equal to $\lambda = 1.00$ W/(m K).
- Mortar thermal conductivity of joint mortar is equal to $\lambda = 0.54$ W/(m K).

The thermal transmittance of the blocks is calculated by the following equation:

$$U = \frac{\mathrm{Fl}}{\Delta T \cdot L \cdot H} \tag{11.3}$$

where Fl is the summation of the node thermal flux at the internal surface as given by ABAQUS, ΔT is the temperature difference between internal and external block surfaces, L measures the block length and H the block height.

Searching an improvement of the thermal resistance of masonry units, the optimization algorithm will iterate as the topology of the unit evolves to an optimum. The project considers a design vector **b** with eight process parameters describing the

Table 11.1 Design side constraints and optimal design vector

Parameters, b_k	b_k^-	b_k^+	Optimal value
b_1	0	8	2
b_2	0	10	10
b_3, b_4, b_5, b_6	18.0	18.0	18.0
b_7	0	1	1
b_8	0	2	2

topology as follows: b_1 − number of vertical webs; b_2 − number of horizontal webs; b_3, b_4 − vertical shell's and web's thicknesses, respectively; b_5, b_6 − horizontal shell's and web's thicknesses; b_7 − voids staggered ($b_7 = 0$) or "in line" ($b_7 = 1$); b_8 − consideration of strip bed joints − no strip bed joints ($b_8 = 0$), strip bed joint on the central row ($b_8 = 1$) or strip bed joints on alternate rows ($b_8 = 2$). The optimization algorithm has been implemented allowing the parameters to vary according to the side constraints given in Table 11.1.

The optimal topology of the block corresponds to 16.5 kg in weight and a thermal transmittance of the masonry wall $U = 0.48$ W/(m^2 K), which is lower than Portuguese standards requests for the more severe climatic zone. This optimal solution exhibits staggered voids and strip bed joints on alternate rows. With this geometry, elongation of the heat flow path through the wall was attained.

This study was completed with some topology changes in order to get an improvement in construction technology and structural behavior. The topology update was made by

- Introducing two large voids in order to improve handling and laying.
- Introducing tongue and groove vertical joints to speed up the construction improving the alignment.
- Filling vertical strip joints with mortar in order to get a better behavior under horizontal loads.

The optimal topology obtained for a lightweight concrete masonry unit is presented in Figure 11.7.

This unit corresponds to a thermal transmittance of the masonry wall $U = 0.50$ W/(m^2 K), which is a good thermal insulation for a single leaf wall made with lightweight concrete blocks. The open surfaces resulting from strip bed joints need proper technology, already available and used in the building industry, in order to avoid mortar filling the air spaces and consequent performance deterioration.

This type of wall can be an interesting alternative to cavity walls, which are expensive components as a single leaf wall with good thermal insulation properties was obtained, with economic and technical advantages due to quicker and easier construction and less dependence on workmanship quality. The area of total holes as a

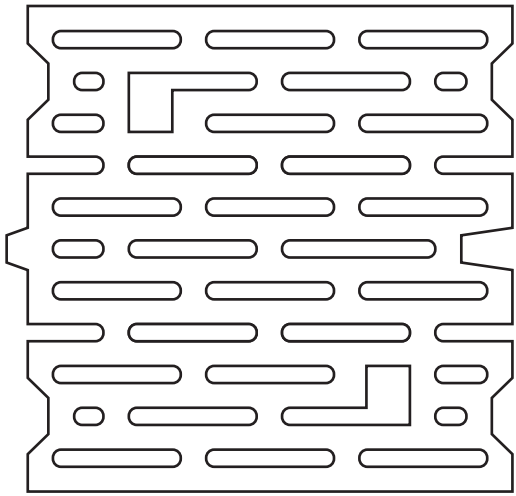

Figure 11.7 Optimized geometry of the block.

percentage of the gross area is equal to approximately 30%, which is acceptable for good structural behavior.

11.3.3 Industrial developments

At the moment, these concerns are important and two different industrial projects, both with the same aim, have been concluded with the participation of Oporto University, Portugal. The main objective of these projects was to develop wall solutions that answer adequately to the actual requirements, both with regard to thermal standards, as well as to mechanical behavior, watertightness and acoustic comfort, and aiming to rely on solutions based on a single leaf wall, reinforced, confined or only simple infill. The use of structural masonry is limited to small buildings.

Through these projects two masonry systems were developed: concrete masonry system made from lightweight concrete units and mortar (expanded clay aggregates), which fulfils the value of $U \leq 0.5$ W/(m^2 C), enough for all Portuguese climate zones, and a ceramic masonry, made from a block whose raw material is a porous ceramic paste, which fulfils the value of $U \leq 0.6$ W/(m^2 C), corresponding to the two climate zones where most construction work takes place.

The units were developed according to numerical processes referred to in 11.3 and 11.4, i.e. a study of the thermal behavior of both masonry systems was made through FEM, and an optimization of the thermal transmittance of masonry was made through modifications on the geometry of the units (considering different shapes for the holes, number of holes and rows and unit width) and the density of the materials intended to be used on those units.

In this optimization process, the requirements to be applied to masonry walls, units and mortar according to Portuguese regulations, European Standards and other references were considered.

Some of the most important requirements considered in the development of both masonry systems were:

- Portuguese reference values for thermal transmittance of walls, U value (Portugal – Leis, Decretos, 2006).
- Density of the unit materials to control thermal conductivity, which was estimated through EN1745 (CEN, 2002).
- Minimum compressive strength of the units defined in the Portuguese NDP – National Determined Parameters of EC8 (CEN, 2004).
- Geometrical requirements for group two units defined in EC6 (CEN, 2005) and in the Portuguese NDP of EC8 (CEN, 2004).
- Maximum weight of the unit to ensure minimum safety and health in manual handling work referred in Portuguese regulations (Portugal – Leis, Decretos, 2006).
- Maximum slenderness of the wall referred in the Portuguese NDP of EC8 (CEN, 2004).
- Minimum thickness of the wall to ensure watertightness defined according to French standard (CSTB, 2008).

Considering these aspects, the result was the development of two masonry systems made from large units with lightweight materials, such as clay and lightweight concrete (clay density lower than 1850 kg/m^2, mixed with polystyrene aggregates and concrete density lower than 1200 kg/m^2, mixed with lightweight expanded clay aggregates).

The main characteristics of clay and lightweight concrete masonry are:

- The width clay and lightweight concrete units is 300 and 350 mm, respectively.
- Both units have vertical holes and are classified as group two units according to EC6 geometrical requirements (CEN, 2005).
- Both units have two grip holes to help handling the units during construction works.
- The concrete unit has a blind face (5 mm thick) for laying the mortar joints.
- The units are bedded on mortar strips joints with an overlap of half of the length of the unit.
- The thickness of the horizontal joints is 10 mm.
- The vertical joints represent 40% of the width of the unit and are filled with mortar to the full height of the joints.
- The vertical and horizontal joints in the clay masonry are made from general purpose mortar, and in the lightweight concrete masonry, the joints are made from lightweight mortar (factory made mortar).

Considering these characteristics, final numerical simulations of the thermal behavior were made for both masonry systems (Figure 11.8), and no significant changes in the U value were recorded, thus maintaining the main objective for thermal transmittance of the wall ($U \leq 0.5$ W/(m^2 C) for the concrete masonry and $U \leq 0.6$ W/(m^2 C) for the clay masonry). Moreover, mechanical simulations were made to estimate the compressive behaviour of masonry through an FEM nonlinear model (Figure 11.8), and details about the numerical model can be found in available literature (Sousa & Sousa, 2012; Sousa et al., 2013).

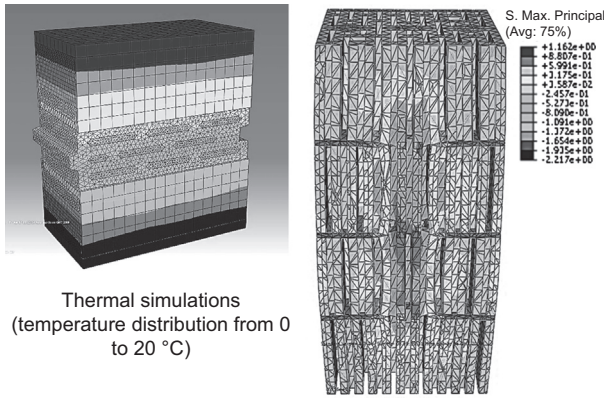

Figure 11.8 Examples of FEM simulations made for the concrete masonry.

After these simulations, several experimental productions of these units were made in factory by the manufacturers until the desired values for compressive strength and density of the units were achieved. Examples of clay and lightweight concrete units are presented in Figure 11.9, and examples of masonry details are presented in Figure 11.10 and in Figure 11.11 for both masonry systems.

Laboratory tests were made, according to European and American standards, to determine the main mechanical characteristics of the masonry systems (Figure 11.12), and the results obtained were within the expected values for shell bedded masonry. Details on laboratory set-ups for compressive, shear and diagonal tension tests and results for lightweight concrete and clay masonry are available in Sousa & Sousa (2010, 2011).

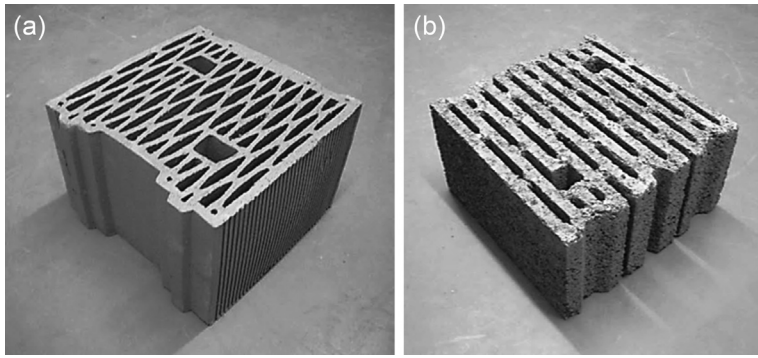

Figure 11.9 Masonry units developed: (a) clay unit and (b) lightweight concrete unit.

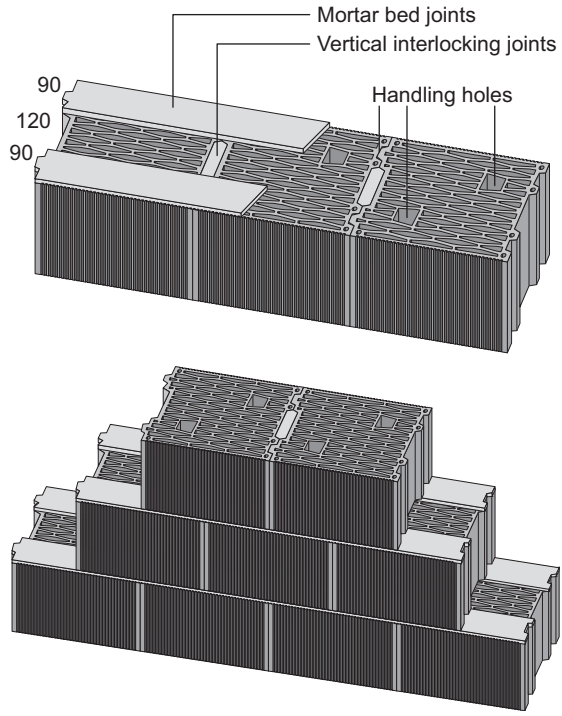

Figure 11.10 Masonry details schematics for clay masonry (dimensions in mm).

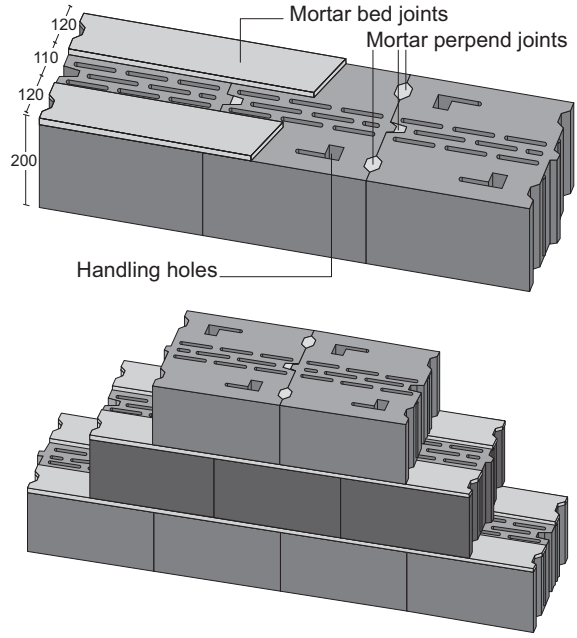

Figure 11.11 Masonry details schematics for lightweight concrete masonry (dimensions in mm).

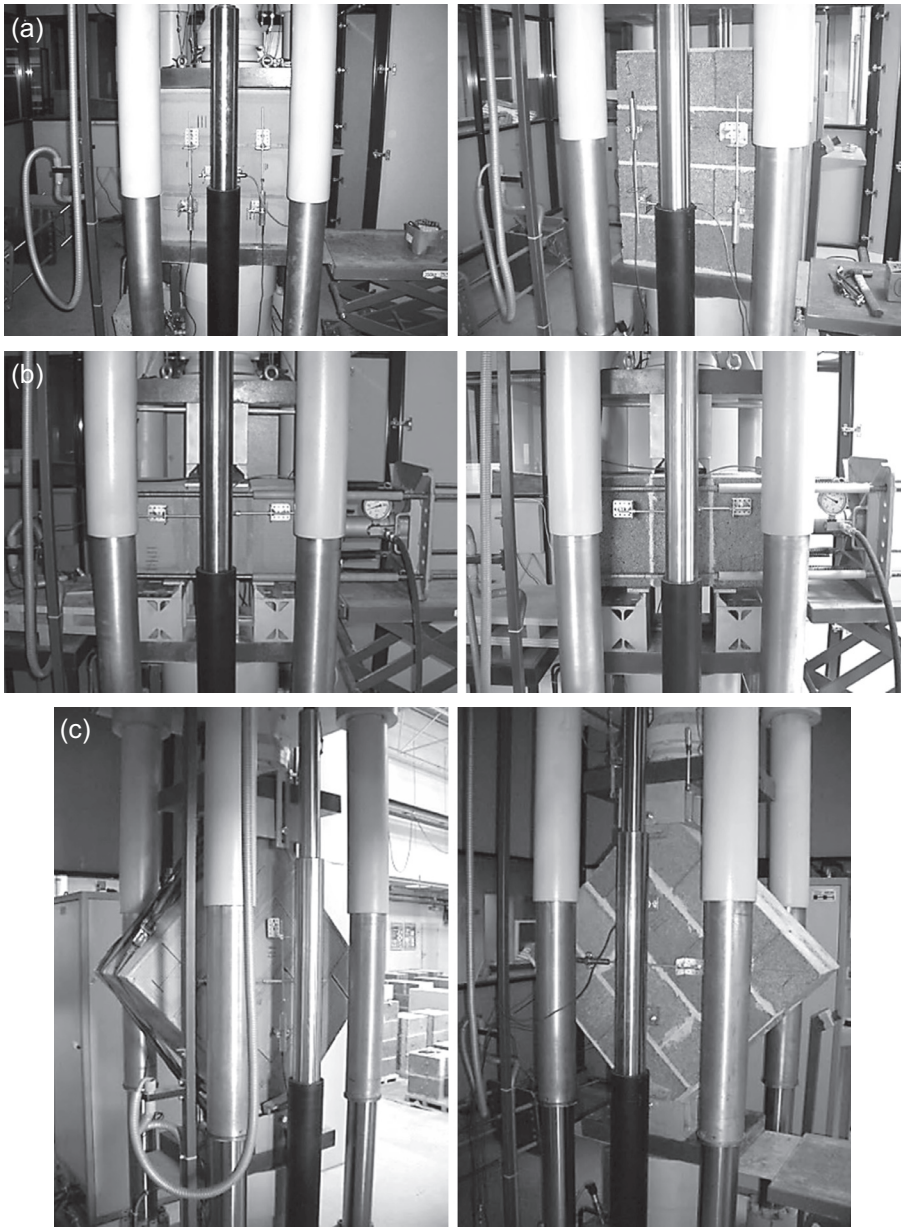

Figure 11.12 Example of laboratory tests set-ups for lightweight concrete and clay masonry: (a) compressive test, (b) shear tests and (c) diagonal tension test.

11.4 Conclusions and future trends

Sustainability and energy saving are the request of today. The hollow block with advantages of high strength, lightness and high performance should be used.

Economy and productivity improvements suggest the usage of building systems that reduce cost, due to the reduction of labour and to increasing geometric accuracy, such as the use of rectified units and special purpose mortars. Masonry unit mortar systems and mechanical aids have been developed, which ensure a fast, simple and qualitatively better construction of the walls. The new generation of masonry systems should be developed by taking modular coordination into account in order to ensure that the constituent materials can adapt better to the length and height of panels and to the layout of spans, finishes or other building materials; new techniques for reinforced masonry seem to be of relevance.

There is a growing emphasis in terms of quality of interior spaces, which leads to higher demands in the building enclosures, in particular in relation to thermal and acoustic comfort requirements without minimizing the requirements related to security, stability and durability of the buildings.

As masonry blocks can be used without rendering, aesthetics innovation calls for increased cooperation between material scientists, architects and civil engineers, combining efficiency and quality-enhanced constructions technologies.

References

Abdou, O. A., & Murali, K. S. (1994). The effect of air cells and mortar joints on the thermal resistance of concrete masonry walls. *Energy and Buildings, 21*(2), 111−118.

Al-Jabri, K. S., Hago, A. W., Al-Nuaimi, A. S., & Al-Saidy, A. H. (2005). Concrete blocks for thermal insulation in hot climate. *Cement and Concrete Research, 35*(8), 1472−1480.

António, C. C. (2002). A multilevel genetic algorithm for optimization of geometrically non-linear stiffened composite structures. *Structural and Multidisciplinary Optimization Research Journal, 124*(5), 372−386.

António, C. C., Castro, C. F., & Sousa, L. C. (2005). Eliminating forging defects using genetic algorithms. *Materials and Manufacturing Processes, 20*, 509−522.

ASTM. (2011). *ASTM 514E/514M − Standard test method for water penetration and leakage through masonry*. West Conshohocken, USA.

Bastos, A. M., Sousa, H., & Melo, A. F. (2005). Methodology for the design of lightweight concrete with expanded clay aggregates. *Masonry Society Journal, 23*(1), 73−84.

Bruggi, M., & Cinquini, C. (2011). Topology optimization for thermal insulation: an application to building engineering. *Engineering Optimization, 43*(11), 1223−1242.

Bruggi, M., Cinquini, C., & Taliercio, A. (2013). Topology optimization of masonry blocks with enhanced thermomechanical performances. In *Proceedings of the 10th world congress on structural and multidisciplinary optimization, Orlando, Florida, USA*.

Bruggi, M., & Taliercio, A. (2013a). Design of masonry blocks with enhanced thermo-mechanical performances by topology optimization. *Construction and Building Materials, 48*, 424−433.

Bruggi, M., & Taliercio, A. (2013b). Minimization of the thermal transmittance of masonry blocks by topology optimization. In *Proceedings of the 14th international conference on civil, structural and environmental engineering, Cagliari, Sardinia, Italy*.

CEN. (1993). *Thermal bridges in building construction − Heat flows and surface temperatures − Part 1−General calculation method*. Brussels, Belgium.

CEN. (2002). *EN 1745: 2002 eurocode masonry and masonry products − Methods for determining design thermal values*. Brussels, Belgium.

CEN. (2004). *EN 1998-1: Design of structures for earthquake resistance − Part 1: General rules, seismic actions and rules for buildings*. Brussels, Belgium.

CEN. (2005). *EN 1996-1-1: Eurocode 6 − Design masonry structures. Part 1-1: General rules for reinforced and unreinforced masonry structures*. Brussels, Belgium.

CSTB. (2008). *NF DTU 20.1-Travaux de bâtiment. Ouvrage en Maçonnerie de Petits Éléments − Parois et Murs*. CD Reef, Paris, France.

del Coz Díaz, J. J., Álvarez Rabanal, F. P., García Nieto, P. J., Domínguez Hernández, J., Rodríguez Soria, B., & María Pérez-Bella, J. (2013). Hygrothermal properties of lightweight concrete: experiments and numerical fitting study. *Construction and Building Materials, 40*, 543−555.

del Coz Díaz, J. J., García Nieto, P. J., Álvarez Rabanal, F. P., Alonso-Martínez, M., Domínguez Hernández, J., & María Pérez-Bella, J. (2014). The use of response surface methodology to improve the thermal transmittance of lightweight concrete hollow bricks by FEM. *Construction and Building Materials, 52*, 331−344.

del Coz Díaz, J. J., García Nieto, P. J., Álvarez Rabanal, F. P., & Domínguez Hernández, J. (2012). Non-linear thermal analysis of the efficiency of light concrete multi-holed bricks with large recesses by FEM. *Applied Mathematics and Computation, 218*(20), 10040−10048.

del Coz Díaz, J. J., García Nieto, P. J., Betegón Biempica, C., & Prendes Gero, M. B. (2007). Analysis and optimization of the heat-insulating light concrete hollow brick walls design by the finite element method. *Applied Thermal Engineering, 27*(8−9), 1445−1456.

del Coz Díaz, J. J., García Nieto, P. J., Díaz Pérez, L. M., & Riesgo Fernández, P. (2011). Nonlinear thermal analysis of multi-holed lightweight concrete blocks used in external and non-habitable floors by FEM. *International Journal of Heat and Mass Transfer, 54*(1−3), 533−548.

del Coz Díaz, J. J., García Nieto, P. J., Domínguez Hernández, J., & Álvarez Rabanal, F. P. (2010). A FEM comparative analysis of the thermal efficiency among floors made up of clay, concrete and lightweight concrete hollow blocks. *Applied Thermal Engineering, 30*(17-18), 2822−2826.

del Coz Díaz, J. J., García Nieto, P. J., Domínguez Hernández, J., & Suárez Sánchez, A. (2009). Thermal design optimization of lightweight concrete blocks for internal oneway spanning slabs floors by FEM. *Energy and Buildings, 41*(12), 1276−1287.

del Coz Díaz, J. J., García Nieto, P. J., Suárez Sierra, J. L., & Betegón Biempica, C. (2008). Nonlinear thermal optimization of external light concrete multi-holed brick walls by the finite element method. *International Journal of Heat and Mass Transfer, 51*(7−8), 1530−1541.

del Coz Díaz, J. J., García Nieto, P. J., Suárez Sierra, J. L., & Peñuelas Sánchez, I. (2008). Non-linear thermal optimization and design improvement of a new internal light concrete multi-holed brick walls by FEM. *Applied Thermal Engineering, 28*(8−9), 1090−1100.

European Parliament. (2011). Laying down harmonised conditions for the marketing of construction products and repealing. *Official Journal of the European Union.* Regulation (EU) no 305/2011 of 9 March, Council Directive 89/106/EEC. *88*(4), 5−43.

Evins, R. (2013). A review of computational optimization methods applied to sustainable building design. *Renewable and Sustainable Energy Reviews, 22*, 230−245.

Forth, J. P., Dao, D. V., Toropov, V. V., & Vu, H. M. (2010). Experimental and mathematical optimisation of a novel sustainable masonry unit. *Masonry International, 23*(3), 103−111.

Gosselin, L., Tye-Gingras, M., & Mathieu-Potvin, F. (2009). Review of utilization of genetic algorithms in heat transfer problems. *International Journal of Heat and Mass Transfer, 52*(9−10), 2169−2188.

Javidan, F., Safarnejad, M., & Shahbeyk, S. (2013). Shape optimization of hollow concrete blocks using the lattice discrete particle model. *Iranica Journal of Energy & Environment, 4*, 243−250.

Kreith, F., & Bohn, M. (2000). *Principles of Heat Transfer* (6th ed.). Thomson Learning.

Kreith, F., & Bohn, M. S. (2001). *Principles of heat transfer* (6th ed.). Pacific Grove, California: Brooks/Cole Publishers.

Pierzchlewicz, J. (1996). Modern concrete wall-units with improved thermal resistance for housing in hot climate. *Science and Technology, 1*, 69−80.

Portugal − Leis, Decretos, etc. (2006). *Regulamento das Características de Comportamento Térmico dos Edifícios*. Diário da República. Decreto-Lei no 80/2006 (in Portuguese).

Sousa, L. C., Castro, C. F., António, C. C., & Sousa, H. (2011). Topology optimisation of masonry units from the thermal point of view using a genetic algorithm. *Construction and Building Materials, 25*(5), 2254−2262.

Sousa, R., Guedes, J., & Sousa, H. (2013). Diagonal compressive strength of masonry samples−experimental and numerical approach. *Materials and Structures, 46*(5), 765−786.

Sousa, R., & Sousa, H. (2010). Experimental evaluation of some mechanical properties of large lightweight concrete and clay masonry and comparison with EC6 expressions. In *Proceedings of the 8th international masonry conference, Dresden, Germany*.

Sousa, R., & Sousa, H. (2011). Influence of head joints and unreinforced rendering on shear behaviour of lightweight concrete masonry. In *Proceedings of the 9th Australasian masonry conference, Queenstown, New Zealand*.

Sousa, R., & Sousa, H. (2012). Numerical simulations of masonry laboratory tests: a sensitivity analysis of the compressive behaviour. In *Proceedings of the 15th international brick and block masonry conference, Florianópolis, Brazil*.

Sousa, H., Sousa, L. C., Castro, C. F., António, C. C., & Sousa, R. (2011). A new lightweight concrete single leaf masonry wall system development approach. In *Proceedings of the 9th Australasian masonry conference, Queenstown, New Zealand*.

Sousa, L. C., Sousa, H., Castro, C. F., António, C. C., & Sousa, R. (2013). A new lightweight masonry block: thermal and mechanical performance. *Archives of Civil and Mechanical Engineering, 14*(1), 160−169.

Svoboda, Z., & Kubr, M. (2010). Numerical simulation of heat transfer through hollow bricks in the vertical direction. *Journal of Building Physics, 34*(4), 325−350.

Vu, H. M., Forth, J. P., Dao, D. V., & Toropov, V. V. (2013). The use of optimisation for enhancing the development of a novel sustainable masonry unit. *Applied Mathematical Modelling, 38*(3), 853−863.

The properties and durability of fly ash-based geopolymeric masonry bricks

12

M.M.A. Abdullah, W.M.W. Ibrahim, M.F.M. Tahir
Universiti Malaysia Perlis, Perlis, Malaysia

12.1 Introduction

Bricks are considered to be one of the oldest and the most environmentally friendly building materials. Bricks are usually used in the construction of buildings as walls, paving, and flooring. Bricks are made from a variety of materials like calcium silicate, and concrete and bricks made from clay are the most common. However, production of clay bricks requires high-temperature (900−1000 °C) kiln firing and also releases a substantial quantity of greenhouse gases (Ahmari & Zhang, 2012). Uses of fly ash in making bricks have many advantages over conventional clay bricks as they do not emit any pollutant or greenhouse gas during and after manufacturing, they require much less energy consumption, and their manufacture costs about 20% less than clay bricks (Kayali, 2005). Fly ash is a fine particulate material separated from the flue gas of coal-fired power stations that is rich in alumina and silica. As the production of fly ash rises continuously and creates serious environmental pollution problems, fly ash should be treated as a valuable resource or reused as raw material in new technology with good properties. Class F fly ash has been considered as pozzolanic materials or porcelain and can be activated by high alkaline solutions to act as a binder through chemical polymerization reactions (Swanepoel & Strydom, 2002). This reaction transforms aluminosilicate materials (fly ash) into aluminosilicate polymers known as geopolymers. Geopolymer is one of the new materials and has been investigated, studied, and utilized for some decades by several researchers throughout the world. Geopolymer was first used by Prof. Joseph Davidovits in St. Quentin, France in the 1970s (Davidovits, 1989). The main properties of geopolymers are high compressive strength, low shrinkage, acid resistance, fire resistance, and low thermal conductivity depending on the raw material used and processing conditions (Duxson et al., 2007). The geopolymer-based material involves a chemical reaction known as the geopolymerization process and yields polymeric Si−O−Al bonds. The geopolymerization process involves a substantially fast chemical reaction under alkaline solutions on silica-alumina materials that results in a three-dimensional polymeric chain and ring structure (Provis, Duxson, Van Deventer, & Lukey, 2005; Van Deventer, Provis, Duxson, & Lukey, 2007). This chapter presents a design and performance evaluation of fly ash-based geopolymeric masonry brick. It proposes new technology of masonry brick production in Malaysia

Eco-efficient Masonry Bricks and Blocks. http://dx.doi.org/10.1016/B978-1-78242-305-8.00012-7

and widens the possibilities to recycle waste (fly ash) to useful products, especially building materials that can contribute to environmental and economical benefits. The properties and durability of geopolymeric masonry brick were measured based on physico-mechanical properties present in the masonry brick, which are compressive strength, water absorption, and density.

12.2 Mix design parameters

12.2.1 Influence of fly-ash-to-sand ratio, by mass

The ratio of fly ash to sand, by mass, has been varied from 1:2 to 1:5. The compressive strength of fly ash-based geopolymeric masonry bricks was decreased as the ratio of fly ash to sand, by mass, increased. The fly ash-based geopolymeric masonry bricks were cured in the oven at 60 °C for 24 h. The compressive strengths and water absorption for the test masonry bricks were measured after aging for 7 days. The measured seventh-day compressive strengths of test bricks are shown in Figure 12.1, while the results for water absorbed by the bricks are given in Figure 12.2.

From the data obtained, the compressive strength of geopolymer bricks was decreased as the ratio of fly ash to sand, by mass increased. When the ratio of fly ash to sand increased, the mass of sand used also increased. Therefore, the geopolymeric masonry bricks became crumbly and caused the decrease in strength of geopolymeric masonry bricks. Thakur and Ghosh (2009) also found that further increases in sand content drastically reduced the compressive strength of fly ash-based geopolymer composites. As seen from Figure 12.1, the ratio 1:2 of fly ash to sand, by mass, produced the highest compressive strength, compared to others, which is 17 MPa. However, the 1:2 ratio does not have good structure and shape when removed from the mold due to the flaccid samples and poor workability. For this reason, a 1:3 ratio of fly ash to sand, by mass, was selected as the most suitable and basic mixture for further study of other parameters. This is because the 1:3 ratio by mass has obtained

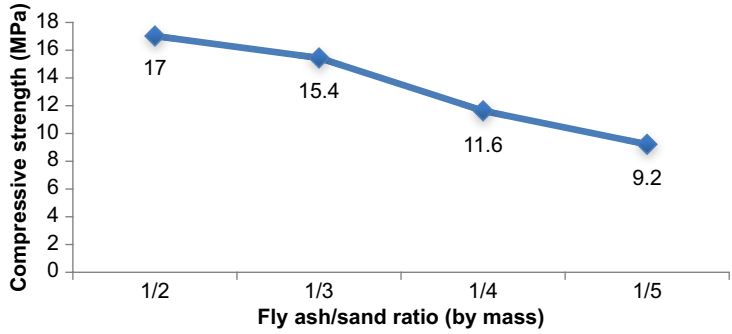

Figure 12.1 Compressive strength of different ratios, fly ash to sand.

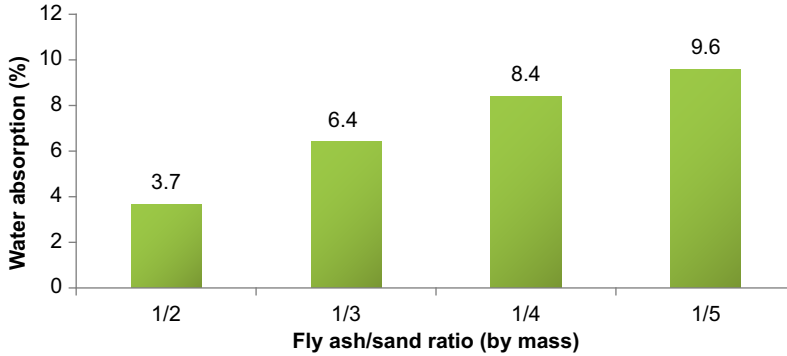

Figure 12.2 Water absorption of different ratios, fly ash to sand.

more satisfactory workability with good structure and shape. Furthermore, it shows the second highest strength after the 1:2 ratio, by mass, which is 15.4 MPa. The lowest strength of fly ash-based geopolymeric masonry bricks are 9.2 MPa, exhibited by geopolymeric masonry bricks with a 1:5 ratio of fly ash to sand, by mass.

Figure 12.2 represents the results of water absorption for geopolymer bricks with different ratios of fly ash to sand, by mass. From the data obtained, it shows that the water absorption increased as the ratio of fly ash to sand increased. The previous research also shows that the water absorption increased as the ratio of fly ash to sand increased. This might be due to the capillary effect on the geopolymeric masonry bricks which allowed the water to penetrate the geopolymer (Anas, 2011). A geopolymeric masonry brick with a 1:5 ratio of fly ash to sand, by mass, gives the highest percentage of water absorption compared to the others, which is 9.6%. The lowest water absorption was presented by a 1:2 ratio of fly ash to sand, by mass, which is 3.7%.

12.2.2 *Influence of curing time*

The results from the previous study on the influence of curing time onto the fly ash-based geopolymeric masonry bricks have demonstrated that the compressive strength increases with increase in curing time. However, it was found that seven days' water absorption decreased with increase in curing time from 1 h to 24 h. The compressive strength and water absorption of fly ash-based geopolymer bricks on the seventh day with different curing times is shown in Figures 12.3 and 12.4, respectively. The geopolymeric masonry bricks, cured at 60 °C for 24 h, produced the highest compressive strength (15.4 MPa) compared to others. On the contrary, the geopolymeric masonry bricks cured for 24 h reported lower water absorption (6.4%) as compared to the others. The lowest compressive strength (5.9 MPa) and highest water absorption percentage (10.3%) was shown by the geopolymeric masonry bricks cured for a period of 1 h at 60 °C. It was found that prolonging the curing time has enhanced the polymerization process resulting in higher compressive strength. Heat-curing time need not be more than 24 h in practical applications because the rate of increase in strength went up rapidly to 24 h of curing time; beyond 24 h, the gain in

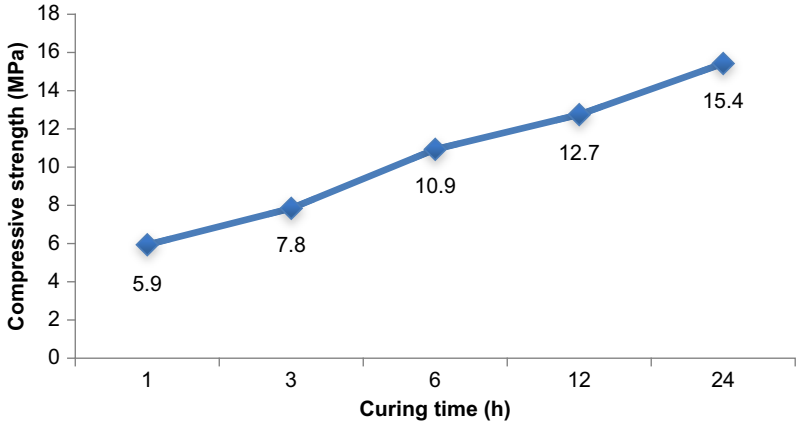

Figure 12.3 Compressive strength of different curing times.

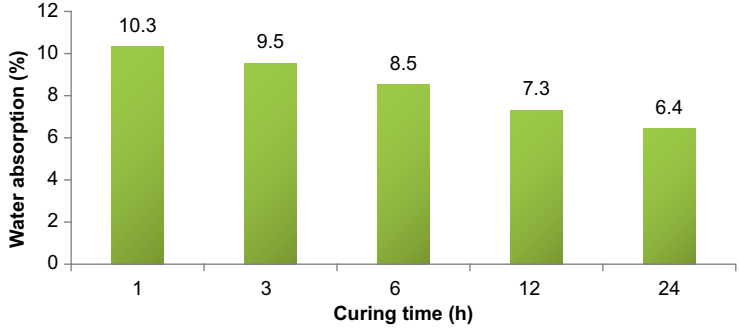

Figure 12.4 Water absorption of different curing time.

strength is only moderate (Rangan, Hardjito, Wallah, & Sumajouw, 2005). Figure 12.4 depicts that longer curing time provides the lowest water absorption of geopolymer bricks. The trend of these test results is similar to that observed by Omar, Mustafa Al Bakri, Kamarudin, & Khairul Nizar (2012) in their study on fly ash-based geopolymer materials. Bakharev (2005) also reported that the first 6 h of heat curing started to make significant changes in the geopolymeric materials, and the reactions that occurred did not stop after heat exposure but continued for further growth in strength.

12.2.3 *Influence of curing temperature*

For the geopolymeric masonry bricks, curing temperature plays an important role in strength development. A higher temperature of 40 to 95 °C is necessary for the formation of a sufficiently interconnected network of bonds within the geopolymer on the basis of fly ash (Skvara, Jilek, & Kopecky, 2005). Figures 12.5 and 12.6 show the effect of curing temperature on the compressive strength and water absorption of fly

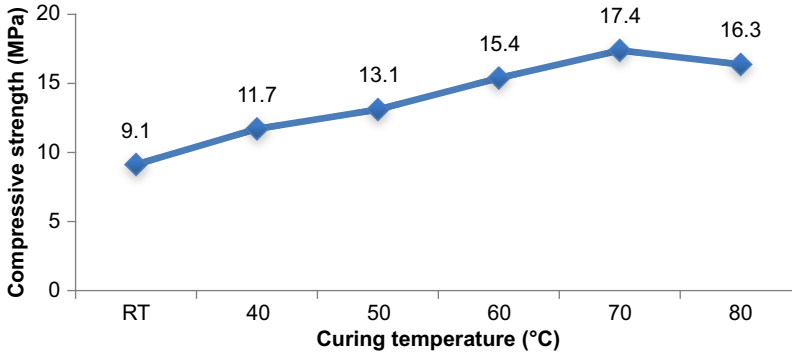

Figure 12.5 Compressive strength of different curing temperatures.

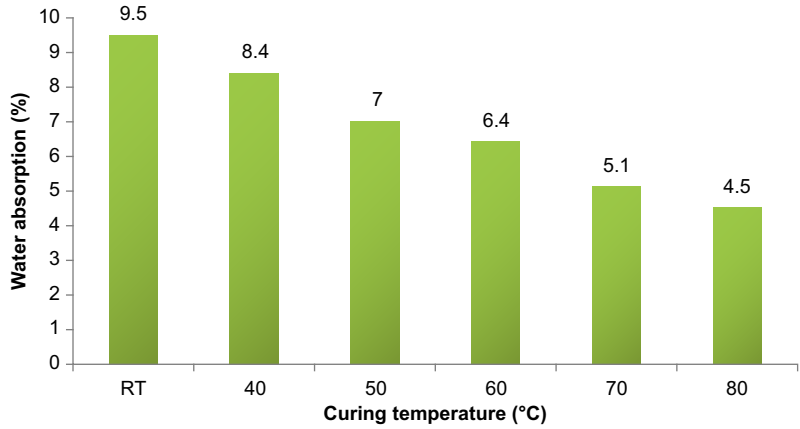

Figure 12.6 Water absorption of different curing temperatures.

ash-based geopolymer bricks, respectively. The geopolymer brick samples were tested at seven days of aging. Compressive strength results, shown in Figure 12.5, indicate that increasing the curing temperature from room temperature to 70 °C increases the compressive strength of the geopolymeric masonry bricks. Nevertheless, the compressive strength of geopolymeric masonry bricks slightly decreased from 18.9 to 17.4 MPa with an increase in the curing temperature from 70 to 80 °C. The results from this research agreed with that of other researchers who also studied the effect of curing temperature on the properties of fly ash-based geopolymeric materials (Fareed, Muhd Fadhil, Samuel, & Nasir, 2011; Hardjito, Wallah, Sumajouw, & Rangan, 2004; Mustafa Al Bakri et al., 2011; Swanepoel & Strydom, 2002). Therefore, it can be concluded that the rate of geopolymerization reaction depends on the heat treatment for the strength development of geopolymeric masonry bricks. An increase in the processing temperatures has a spectacular effect on the dissolution rate of the amorphous silica particles, thereby affecting the gel formation (Simonsen, Sonderby, & Sogaard,

2009). Mustafa Al Bakri et al. (2011) stated that curing at high temperature causes the loss of moisture in the geopolymer samples. The geopolymer reaction requires the presence of moisture for good strength development. Hence, most of the geopolymeric materials based on fly ash were cured at temperatures below 90 °C.

The results from Figure 12.6 show that increasing the curing temperature decreases the percentage of water absorbed by the geopolymer bricks. Water absorption tests were carried out according to ASTM C140. Curing at 80 °C has a lower percentage of water absorption (10.5%), while the highest percentage of water absorption is 13.5%, for samples cured at room temperature. Increased temperature has probably accelerated the geopolymerization reaction and, therefore, the amount of reaction products increased, because at higher temperatures, the geopolymerization degree is higher. This may be a result of the pore structure and size shifts toward smaller pores caused by the gradual filling of larger pores with reaction products as the geopolymerization proceeds (Rovnanik, 2010).

12.3 Mix details of fly ash-based geopolymeric masonry bricks

12.3.1 Mixture proportion

The mixture proportions of fly ash-based geopolymeric bricks were determined using the trial and error method and also based on the previous work done by several researchers (Abdullah et al., 2011; Mustafa Al Bakri et al., 2012) on our CEGeoGTech team on geopolymer pastes. The ratio of fly ash to sand was found by trial mixing and varied from 1:2 to 1:5 ratio, by mass. Then the ratio was fixed in a 1:3 ratio, by mass, for most of the mixtures based on their good workability and highest strength development with lower water absorption. The ratio of sodium silicate solution to sodium hydroxide solution was fixed at a 2.5 ratio, by mass, and the ratio of solid to liquid (fly ash to alkaline activator) was fixed at a 2.0 ratio, by mass, for all the mixtures based on studying done by Mustafa Al Bakri et al. (2012) which gives the highest compressive strength for geopolymer-based materials. Fly ash (class F ASTM) was used 100% in this study as cement replacement.

12.4 Mixing and curing processes

12.4.1 Mixing process

The materials (fly ash, sand, sodium hydroxide solution, and sodium silicate) were weighed according to the ratio given and prepared appropriately before mixing. The materials were put into the mixer following the sequence. The sequence is important as different materials have different properties. Fly ash and sand is mixed first for 5 min before the alkaline activator is added to the mixes. After the alkaline activator had been added, the mixture was mixed for 10 min or until all the mixture was

integrated. Then the mixes were weighed, approximately 2.5 kg for each sample of brick, then poured into the mold and compressed with the pressure of 10 MPa to get the compact sample bricks.

12.4.2 Curing process

In this research, curing time and curing temperature were set as the parameters for determination of the effect of curing condition of the properties of fly ash-based geopolymeric masonry bricks. The geopolymeric bricks were cured in the oven after removing the samples from the mold. Then, the bricks were taken out and air dried at room temperature until they were ready to be tested. For the determination of effect of different curing times and curing temperatures, the specimens were compressed and tested for water absorption at seven days. After finding the best time and temperature for the curing regime, the masonry bricks prepared for the next research had been left at room temperature after removing from the oven for 1, 3, 7, 28, and 60 days prior to being tested for mechanical performances.

12.5 Physical and mechanical properties

12.5.1 Compressive strength

From the structural point of view, the compressive strength of the unit is the controlling factor. Bricks of various strengths are available to suit the wide range of architectural and engineering requirements. The compressive strength values of the geopolymeric masonry bricks were tested at 1, 3, 7, 28, and 60 days of aging time. Five samples of bricks for each aging time have been tested to get the average data and comply with the ASTM C 67-11 standard. The compressive strength of geopolymer bricks was determined on their stretcher face only. The influences of geopolymer bricks' age to the compressive strength is shown in Figure 12.7. As seen in Figure 12.7, the compressive strength was increased as the age of geopolymer bricks increased up to 60 days. The least compressive strength is 9.4 MPa, and this satisfies the requirements of BS 6073 for compressive strength ($\geq$7 MPa). The highest strength of geopolymeric bricks was 20.3 MPa in the samples cured at 70 °C for 24 h after 60 days of aging. This indicated that the long curing period does affect compressive strength development of geopolymer bricks. It can be attributed to the continuous formation of aluminum silicate hydrate/calcium silicate hydrate gel. The minimum one-day strength attainable is sufficient for handling and transportation of geopolymer bricks and the minimum seven day's strength attained is sufficient for early masonry work (Manjunath, Radhakrishna, Giridhar, & Jadhav, 2011).

12.5.2 Water absorption

A good quality of bricks or blocks used in construction and building should absorb less water. The amount of water that a brick can absorb was measured by the water

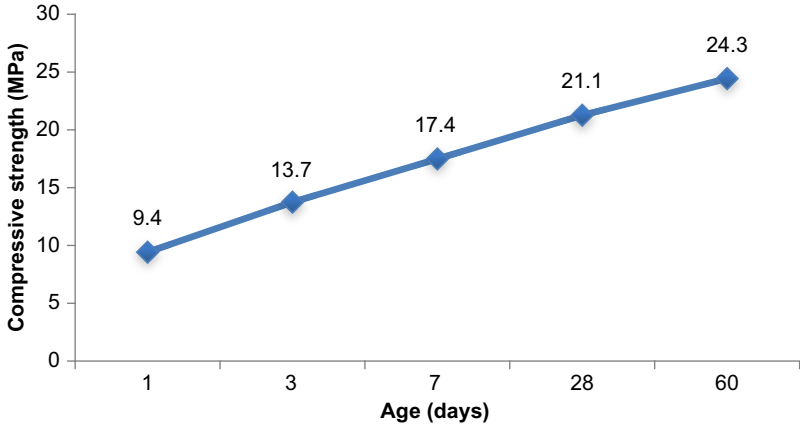

Figure 12.7 Compressive strength of different aging times.

absorption test. The water absorption of the 1, 3, 7, 28, and 60-day fly ash-based geopolymeric masonry bricks were tested. There were three samples of bricks for each proportion. The percentage of water absorbed by geopolymer bricks at different ages was summarized and is shown in Figure 12.8. From the data obtained, the water absorption of geopolymeric bricks could be decreased as the age of geopolymeric bricks increased. The water absorption of fly ash-based geopolymeric bricks ranged between 3.5 and 6.7%. The water absorption at 1 day (6.7%) of aging was higher, while the lowest percentage of water absorption was at 60 days (3.5%) of aging. This result obtained was due to the capillary effect on the pores of the masonry bricks; the pores will absorb water from mortar that lay on the bricks (Sukri, 2010). All of the test bricks/blocks met the standard specification for water absorption. It is believed that when the bricks have lower water absorption that this means the bricks are durable.

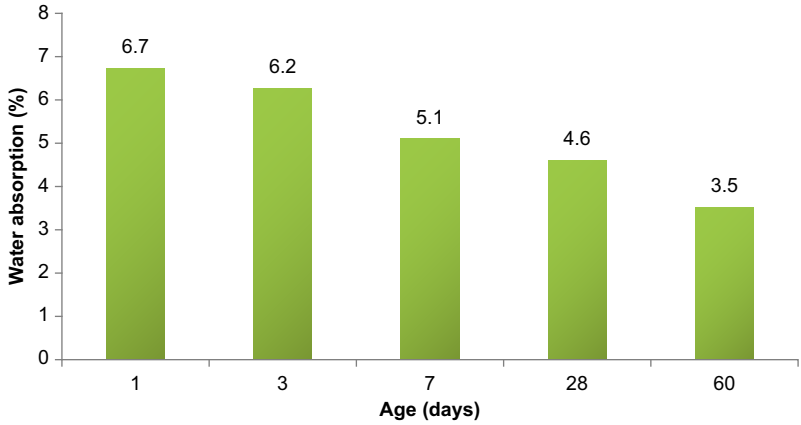

Figure 12.8 Water absorption of different aging times.

12.5.3 Density analysis

In general, the more dense a brick, the harder and stronger it is. The purpose of this test is generally to relate the density of the geopolymeric bricks with their strength performances. The density of the geopolymeric masonry bricks can be determined by dividing the weight of the bricks (kg) over the volume of unit brick (m^3). Three samples have been prepared for each age of the geopolymeric bricks prior to this research. Table 12.1 shows the density of fly ash-based geopolymer bricks at different ages. The density of fly ash-based geopolymer bricks ranged between 1800 kg/m^3 to 1950 kg/m^3. For the density test, the weight and volume of samples were taken at the average value. The geopolymeric bricks at 60 days of aging have the highest density; whereas, the geopolymeric bricks at 1 day of aging have the lowest density. An increase in the density from one day to 60 days of aging is caused by the complete reactions of geopolymerization that occurred in the geopolymer bricks. When the geopolymerization reaction has completed, the geopolymer structure becomes compact and denser; hence, it provides higher density. This result was associated with the compressive strength test results. As shown in Figure 12.9, the density and compressive strength of geopolymer

Table 12.1 Density of geopolymer bricks measured

Age (days)	Density (kg/m^3)
1	1813.5
3	1824.0
7	1828.2
28	1887.5
60	1915.4

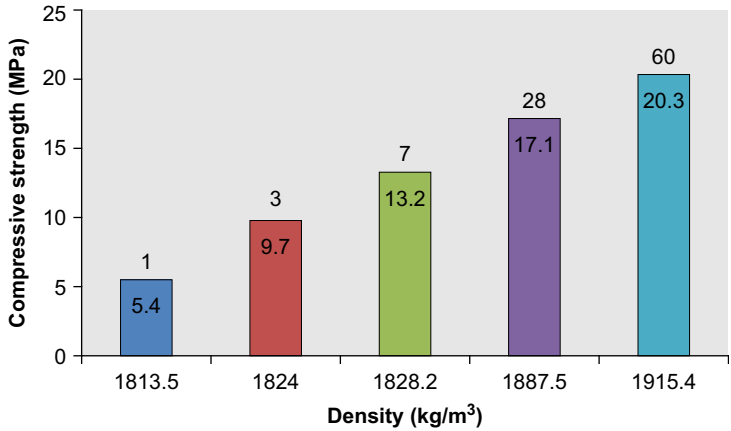

Figure 12.9 Relation of density and compressive strength of geopolymer bricks.

Table 12.2 Dimensions of bricks measured

Dimensions	Total measurement for 24 bricks (mm)	Mean measurement for individual brick (mm)
Length, *L*	5182	215.9
Width, *W*	2395	99.8
Height, *H*	1545	64.3

bricks are related to each other. The higher density of the bricks will provide the higher strength of bricks.

12.5.4 Dimensional tolerances

Measurement of the brick dimensions was done based on the procedures provided in BS 3921: 1985. Table 12.2 below shows the results obtained from the measurement of 24 bricks and individual measurements of bricks. The results obtained were compared with the work sizes stated in the BS 3921: 1985. The work sizes were as given in the BS for length, width, and height, i.e., 215, 102.5, and 65 mm, respectively. The mean measurement for individual length was 215.9 mm, exceeding the limit stated in BS 3921: 1985 by 0.9 mm. The individual measurement of width and height is still within the limits of BS 3921: 1985, which showed the value of 99.8 and 64.3 mm, respectively. Table 12.2 clearly demonstrates that the fly ash-based geopolymer bricks in this research had widths and heights marginally in agreement with the BS 3921: 1985 standards, but the lengths were oversized.

12.6 Microstructure properties

12.6.1 Scanning electron microscope analysis

Scanning electron microscopy (SEM) is a versatile and nondestructive technique that can be used to observe the morphology and to measure the particle size of raw materials of geopolymeric bricks. The SEM analysis of the microstructure of geopolymeric bricks was analyzed under 2000× magnification, while the original fly ash was analyzed under 5000× magnification. Figure 12.10 shows the micrograph of original fly ash before the activation takes place. The original fly ash consists of a series of spherical vitreous particles of different sizes, but with a regular smooth texture. These particles are usually hollow, and some spheres may contain other particles of a smaller size in their interiors.

Figure 12.11 shows the results of fly ash activation with alkaline solution at room temperature (a), at 70 °C (b), at 7 days of aging (c), and 60 days of aging (d), respectively. The number of unreacted fly ash particles decreases as the temperature and age of geopolymeric bricks increased. It was observed in Figure 12.11; that the unreacted

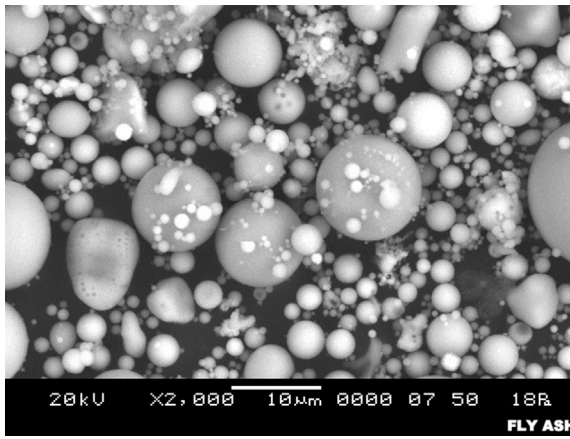

Figure 12.10 SEM micrograph of class F fly ash with amplified 5000× magnification.

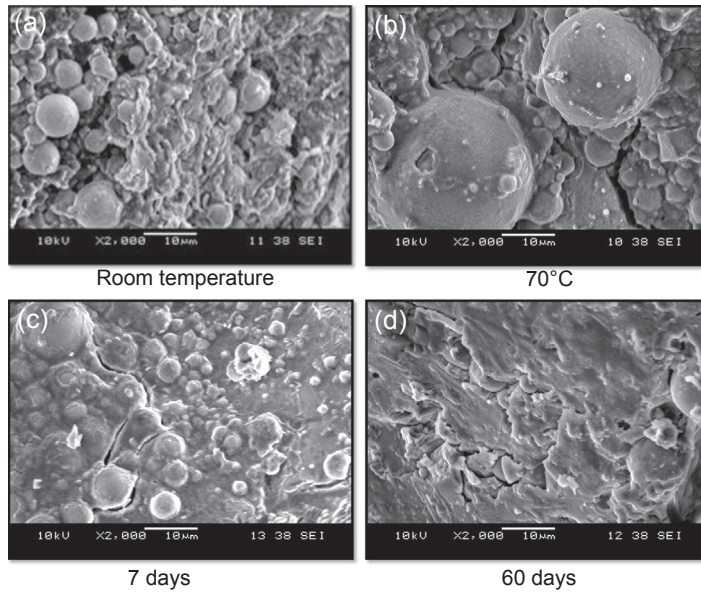

Figure 12.11 SEM micrograph of geopolymer bricks/blocks.

ash particles are embedded in the binder and display some dissolved particles of ash together with the gel formation. It is clear that there is an intimate bond between the aggregate and geopolymer binder. Measly formed micro-cracks were also found on the surface of the geopolymer brick structure. Curing at room temperature (a) presents a scarcely compact structure in which numerous unreacted spherical fly ash particles are clearly visible. On the other hand, when curing is carried out at 70 °C

for 24 h (b), unreacted spherical ash particles are embedded in the matrix and irregularly shaped micro cracks are clearly seen between the unreacted fly ash particles and the geopolymeric matrix.

In the micrograph, the presence of gel (sodium aluminosilicate hydrate) that forms the cementitious matrix could be observed alongside the spheres of unreacted ash particles (Criado, Fernandez-Jimenez, & Palomo, 2010). Hence, the geopolymerization without thermal activation could be regarded as a superficial reaction based on diffusion mechanisms rather than on a complete dissolution and subsequent formation of species (Izquierdo et al., 2009). The microstructure of geopolymer bricks at 60 days of aging (c) shows the disappearance of sphere-shaped fly ash particles and the microstructure of the geopolymeric brick/block became relatively compacted compared to the microstructure of geopolymer bricks at 7 days of aging (d). The compactness of geopolymer materials, improved by duration of activation, attributed to the formation of a greater amount of aluminosilicate gel (Kumar & Kumar, 2011).

12.6.2 X-ray diffraction analysis

Fly ash-based geopolymeric bricks prepared at different conditions were analyzed using X-ray diffraction analysis (XRD) mainly for the determination of active phases, structure, and crystallinity. Normally, the structure of geopolymeric compounds is either crystalline or noncrystalline (amorphous or glassy structure). The degree of disorder in a geopolymer can be determined by the way it diffracts X-rays to form a pattern (Davidovits, 2011). The diffractograms for all the geopolymer bricks studied at different conditions, as well as for the original fly ash, are represented in Figure 12.12. The main phases formed in the XRD pattern of the geopolymeric bricks are amorphous or noncrystalline content. In a noncrystalline state, diffraction of X-rays resulted in a broad, diffuse halo rather than sharp diffraction peaks. The broad peak of amorphous structure can be observed around 22° 2θ. From the results, it shows that the major mineral components of the original fly ash samples were mullite, quartz, and magnetite. The diffractogram for the original fly ash changed perceptibly when the ash was activated by alkaline solutions, which the halo attributed to the vitreous phase of the original ash slightly shifting from 25 to 40° 2θ values. This change indicates the formation of an alkaline aluminosilicate hydrate gel that has been identified as the primary reaction product and the characteristic diffraction patterns of geopolymeric (Criado et al., 2010). The XRD pattern obtained shows that there is a marked shift in the halo to the higher 2θ values with increasing curing temperature and age of geopolymer bricks. The halo exhibits at least two highest intensities with low angle composition at $2\theta = 20^\circ$ to $2\theta = 27^\circ$ compatible to three-dimensional networks and a high angle composition at $2\theta = 30^\circ$ to $2\theta = 39^\circ$ compatible to low molecular weight silicate (dimer, monomer) (Davidovits, 2011). The most intense halo peak was registered between $2\theta = 20^\circ$ and $2\theta = 30^\circ$ and was attributed to an amorphous silicate phase consisting of a SiO_4 tetrahedra sharing oxygen atoms (Dimas, Giannopoulou, & Panias, 2009).

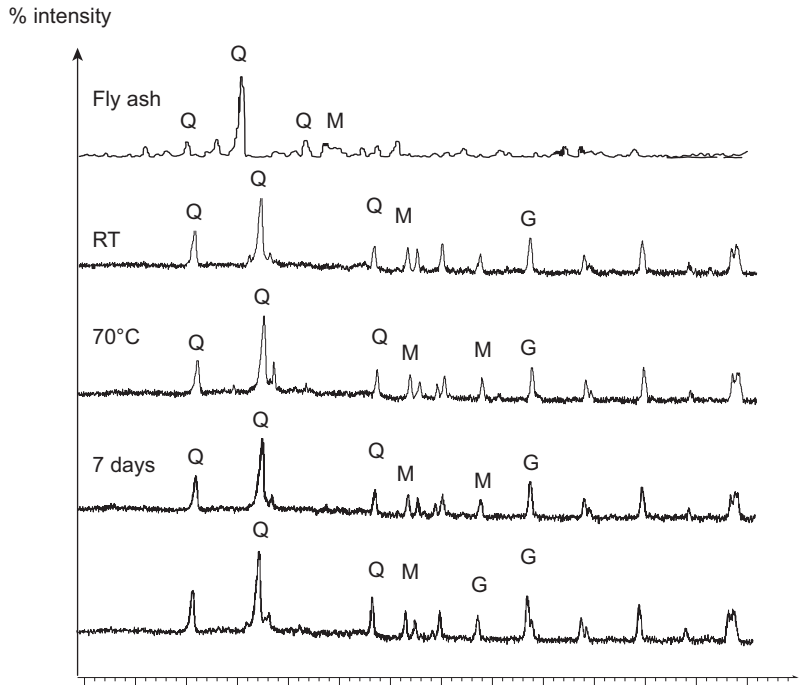

Figure 12.12 Diffractograms for geopolymer bricks/blocks and original fly ash. Q, Silicon Oxide (Quartz); M, Aluminium Silicate (Mullite); G, Magnetite.

12.7 Future research trends

Further investigations are needed in order to improve, to extend, and to explore the current work for development of fly ash-based geopolymeric masonry bricks, such as:

1. It is suggested to diversify the mix proportion by using other types of waste or by-product material for replacement of sand to observe the physical and strength changes.
2. Different class, batch, source, and properties of fly ashes should be considered as the fly ash is effective in enhancing the compressive strength and reducing the requirements of alkaline solution.
3. Various parameters can be investigated for producing fly ash-based geopolymeric masonry bricks/blocks to identify the workability of geopolymeric bricks and suitability of fly ash as a source material.
4. Detailed study of the properties of geopolymeric bricks, like drying shrinkage and also transverse strength, should be carried out so that the behavior of bricks is well understood.
5. Further study of the mechanical properties of fly ash-based geopolymeric masonry bricks such as flexural strength, thermal resistance, fire resistance, and efflorescence testing is needed.

References

Abdullah, M. M. A., Kamarudin, H., Mohammed, H., Khairul Nizar, I., Rafiza, A. R., & Zarina, Y. (2011). The relationships of NaOH molarity, Na_2SiO_3/NaOH ratio, fly ash/alkaline activator ratio, and curing temperature to the strength of fly ash-based geopolymer. *Advanced Materials Research, 328−330*, 1475−1482.

Ahmari, S., & Zhang, L. (2012). Production of eco-friendly bricks from copper mine tailings through geopolymerization. *Construction and Building Materials, 29*, 323−331.

Anas, M. A. L. (2011). *Engineering properties of geopolymer mortar bricks*. Malaysia: UniversitiTeknologi.

Bakharev, T. (2005). Geopolymeric materials prepared using class F fly ash and elevated temperature curing. *Cement and Concrete Research, 35*, 1224−1232.

Criado, M., Fernandez-Jimenez, A., & Palomo, A. (2010). Alkali activation of fly ash. Part III: effect of curing conditions on reaction and its graphical description. *Fuel, 89*, 3185−3192.

Davidovits, J. (1989). Geopolymers and geopolymeric materials. *Journal of Thermal Analysis, 35*, 429−441.

Davidovits, J. (2011). *Geopolymer chemistry and applications* (3rd ed.). Saint-Quentin: Institute Geopolymer.

Dimas, D., Giannopoulou, I., & Panias, D. (2009). Polymerization in sodium silicate solutions: a fundamental process in geopolymerization technology. *Journal of Material Science, 44*, 3719−3730.

Duxson, P., Fernandez-Jimenez, A., Provis, J. L., Lukey, G. C., Palomo, A., & Van Deventer, J. S. J. (2007a). Geopolymer technology: the current state of the art. *Journal of Material Science, 42*, 2917−2933.

Duxson, P., Provis, J. L., Lukey, G. C., & Van Deventer, J. S. J. (2007b). The role of inorganic polymer technology in the development of 'green concrete'. *Cement and Concrete Research, 37*, 1590−1597.

Fareed, A. M., Muhd Fadhil, N., Samuel, D., & Nasir, S. (2011). Effect of curing conditions on strength of fly ash-based self-compacting geopolymer concrete. *International Journal of Civil and Environmental Engineering, 3*(3), 183−186.

Hardjito, D., Wallah, S. E., Sumajouw, D. M. J., & Rangan, B. V. (2004). Factors influencing the compressive strength of fly ash-based geopolymer concrete. *Civil Engineering Dimension, 6*(2), 88−93.

Izquierdo, M., Querol, X., Davidovits, J., Antenucci, D., Nugteren, H., & Fernandez-Pereira, C. (2009). Coal fly ash-slag-based geopolymers: microstructure and metal leaching. *Journal of Hazardous Materials, 166*, 561−566.

Kayali, O. (2005). High performance bricks from fly ash. In: *Proceedings from: 2005 World of Coal Ash (WOCA) conference. Lexington, KY, USA*.

Kumar, S., & Kumar, R. (2011). Mechanical activatin of fly ash: effect on reaction, structure and properties of resulting geopolymer. *Ceramics International, 37*(2), 533−541.

Manjunath, G. S., Radhakrishna, Giridhar, C., & Jadhav, M. (2011). Compressive strength development in ambient cured geo-polymer mortar. *International Journal of Earth Sciences and Engineering, 4*(6), 830−834.

Mustafa Al Bakri, A. M., Kamarudin, H., Bnhussain, M., Khairul Nizar, I., Zarina, Y., & Rafiza, A. R. (2011). The effect of curing temperature on physical and chemical properties of geopolymers. *Physics Procedia, 22*, 286−291.

Mustafa Al Bakri, A. M., Kamarudin, H., Khairul Nizar, I., Bnhussain, M., Zarina, Y., & Rafiza, A. R. (2012). Correlation between Na_2SiO_3/NaOH ratio and fly ash/alkaline activator ratio to the strength of geopolymer. *Advanced Materials Research, 341−342*, 189−193.

Omar, A. A., Mustafa Al Bakri, A. M., Kamarudin, H., & Khairul Nizar, I. (2012). The influence of curing periods on the compressive strength of fly ash-based geopolymer at different aging times. *Advanced Materials Research, 479−481*, 512−516.

Provis, J. L., Duxson, P., Van Deventer, J. S. J., & Lukey, G. C. (2005). The role of mathematical modeling and gel chemistry in advancing geopolymer technology. *Chemical Engineering Research and Design, 83*, 853−860.

Rangan, B. V., Hardjito, D., Wallah, S. E., & Sumajouw, D. M. J. (2005). Geopolymer concrete: curing of fly ash-based geopolymer concrete. In J. Davidovits (Ed.), *Geopolymer chemistry and applications* (pp. 561−584). France: Institute Geopolymere.

Rovnanik, P. (2010). Effect of curing temperature on the development of hard structure of Metakaolin-based geopolymer. *Construction and Building Materials, 24*, 1176−1183.

Simonsen, M. E., Sonderby, C., & Sogaard, E. G. (2009). Synthesis and characterization of silicate polymers. *Journal of Sol-gel Science and Technology, 50*, 372−382.

Skvara, F., Jilek, T., & Kopecky, L. (2005). Geopolymer materials based on fly ash. *Ceramics-Silicaty, 49*(3), 195−204.

Sukri, D. (2010). *Investigation of compressive strength foam brickwall panel with different bonding by using stretcher and Flemish bond*. University Malaysia Pahang.

Swanepoel, J. C., & Strydom, C. A. (2002). Utilisation of fly ash in a geopolymeric material. *Applied Geochemistry, 17*, 1143−1148.

Thakur, R. N., & Ghosh, S. (2009). Effect of mix composition on compressive strength and microstructure of fly ash based geoolymer composites. *ARPN Journal of Engineering and Applied Sciences, 4*(4), 68−74.

Van Deventer, J. S. J., Provis, J. L., Duxson, P., & Lukey, G. C. (2007). Reaction mechanisms in the geopolymeric conversion of inorganic waste to useful products. *Journal of Hazardous Materials, 139*, 506−513.

The properties and durability of mine tailings-based geopolymeric masonry blocks

13

S. Ahmari[1], *L. Zhang*[2]
[1]Cornerstone Engineering Inc., Louisville, KY, USA; [2]University of Arizona, Tucson, AZ, USA

13.1 Introduction

Mine tailings (MT) are pulverized rock that remains after the valuable metal-bearing minerals have been extracted in physical separation processes. MT are generally uniform in character and size and usually consist of hard, angular particles with a high percentage of fines. The major constituents of MT are silica and alumina although in many cases they also contain traces of heavy metals. Disposal of MT causes major concerns in the mining industry. Although there are alternative ways such as underwater storage for disposal of MT, they are commonly disposed of in large tailings impoundments, which are costly and occupy large areas of land. Disposal of MT in impoundments may also cause environmental and safety problems, including contamination of surface water, groundwater and soils, and collapse of tailings dams. In addition, tailings are also susceptible to erosion and dust generation due to wind.

Researchers have been working on the recycling and utilization of MT to produce construction materials, which not only addresses the problems related to MT disposal but also reduces the demand for natural materials that would need quarrying. To use MT as construction material, they need to be stabilized, not only to improve their engineering properties but also to encapsulate and immobilize the potential contaminants. Research has been conducted on stabilization of MT using calcium-based products such as ordinary Portland cement (OPC) (Sultan, 1978, 1979). Stabilization of MT with other type of additives such as asphalt, fly ash, and cement kiln dust (CKD) has also been reported by researchers (Teredesai, 2005). The results show enhanced mechanical properties of MT after stabilization with the mentioned additives. However, the stabilization of MT based on reaction with calcium is associated with several disadvantages including low acid resistance, poor immobilization of contaminants, and high energy consumption and greenhouse gas emissions related to production of OPC. A sustainable way to recycle and reuse MT is based on the geopolymerization technology (Ahmari, Chen, & Zhang, 2012; Ahmari, Zhang, & Zhang, 2012; Ahmari & Zhang, 2012; Giannopoulou & Panias, 2006; He, Jie, Zhang, Yu, & Zhang, 2013; Pacheco-Torgal, Castro-Gomes, & Jalali, 2010; Pacheco-Torgal, Castro-Gomes, Jalali, 2008a; Southam et al., 2007). In this method, MT are mixed with an alkaline solution and cured at ambient or slightly elevated temperature depending on the MT chemical properties and the synthesis condition. Different applications of MT-based geopolymer

Eco-efficient Masonry Bricks and Blocks. http://dx.doi.org/10.1016/B978-1-78242-305-8.00013-9

have been suggested, including road base material, cover material for tailings dam, masonry blocks, and construction concrete. This chapter discusses MT-based geopolymer masonry blocks.

Masonry blocks are a widely used construction material. They are mainly used to construct walls and partitions; however, they can also be used as load bearing components. Production of traditional masonry blocks is energy intensive and consumes a significant amount of natural materials, mainly clay. Quarrying for natural materials adversely affects the natural landscape and can release high level of waste materials. In order to reduce the consumption of natural materials, much research has been done on the utilization of waste materials to replace natural materials in production of masonry blocks (Zhang, 2013). For example, Chen, Zhang, Chen, Zhao, & Bao (2011) mixed hematite MT with fly ash and clay to produce masonry blocks and concluded that up to 84% of clay can be replaced with MT. However, the production process required firing at 980−1030 °C and thus was very energy intensive. Other researchers also showed that clay can be partially or fully replaced with waste materials such as fly ash and mixture of MT and Portland cement to produce masonry blocks (Freidin, 2007; Liu et al., 2011; Morchhale, Ramakrishnan, & Dindorkar, 2006; Roy, Adhikari, & Gupta, 2007). Of all the different methods for utilizing waste materials to produce masonry blocks, geopolymerization is a promising one (Freidin, 2007; Zhang, 2013).

13.2 Mine tailings (MT)-based geopolymer

Geopolymer is a family of aluminosilicates synthesized by alkali activating Si- and Al-rich materials and polycondensing tetrahedral silica (SiO_4) and alumina (AlO_4). The molecular expression of geopolymer gel can be represented by the following formula:

$$M_n\left[-(SiO_2)_z-AlO_2^-\right]_n \tag{13.1}$$

where M is the cation (sodium or potassium), n the degree of polymerization, z the Si/Al molar ratio that is normally in the range of 1−15 and can be up to 300 (Davidovits, 1982, 1994). The geopolymerization process can be described as a series of reactions that interact with each other: (1) dissolution of amorphous aluminosilicate raw materials in an alkaline solution, (2) formation of Si and/or Si−Al oligomers in the aqueous phase, and (3) polycondensation of the oligomers to form a three-dimensional aluminosilicate framework. The alkaline solution has two functions. First, it breaks the silica and alumina bonds in the initial material and dissolves them. Second, the cation in the alkali solution acts as a charge balancing agent for aluminum in the geopolymer structure. In principle, a wide range of materials, both natural minerals and industrial by-products, provided that they contain sufficient amorphous silica and alumina, can be used to synthesize geopolymer. However, the phase composition of the initial material determines its reactivity and thus the degree of geopolymerization. It is known

that metakaolin is one of the most reactive materials for geopolymerization owing to its amorphous structure resulting from the high temperature it has experienced. MT are typically crystalline materials depending on their origin and the mineral operation they underwent in the past. They contain a substantial amount of silica as quartz. Quartz is one of the most stable materials and does not easily dissolve in alkaline solution. It makes MT less reactive in ambient temperature compared to other geopolymer source materials. Figure 13.1 shows the XRD pattern of a copper MT sample. It can be clearly seen that the major phase is crystalline, containing mainly quartz. The amorphous phase which emerges as a broad hump on the spectrum stretching from 18 to 34° is very minor. Therefore, MT without pretreatment can only be partially geopolymerized.

Another distinct characteristic of MT is their variability in terms of chemical composition, particularly the silica to alumina ratio (Si/Al), which is also an important factor that affects the geopolymerization process and the properties of the final geopolymer product. Table 13.1 summarizes the information on different types of MT used by researchers for geopolymer synthesis. High variations in the Si/Al ratio and its dependence on the source material can be clearly seen. In most of the reported cases, MT were cured at slightly elevated temperature, which is consistent with the above discussion about the low reactivity of MT. Room cured MT-based geopolymer products may be used as low specification construction materials such as the material for capping tailings dam (Van Jaarsveld, Lukey, van Deventer, & Graham, 2000). The reactivity of MT can be improved using different methods such as heating to high temperature and then rapid cooling to break down the crystalline structure. The crystalline nature of silica in MT can also be compensated by using sodium silicate solution as an activator to provide external soluble silica. In this case, the sodium silicate solution not only acts as the activating agent but also provides soluble silica monomers, which readily take part in the reaction.

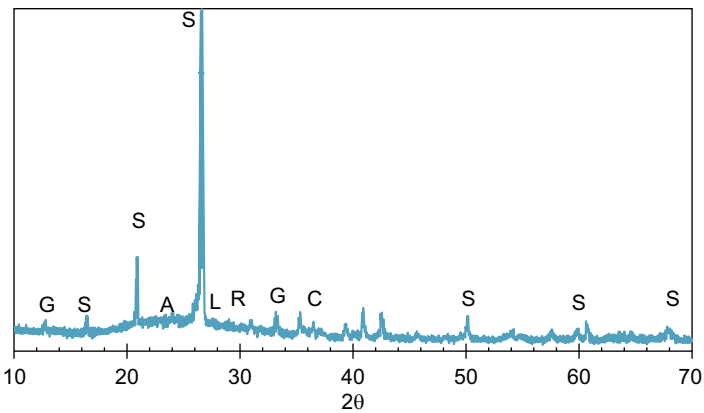

Figure 13.1 XRD pattern of MT (A: Anorthite, C: Cuprite, G: Gypsum, L: Labradorite, R: Calcium Carbonate, S: SiO_2).
Zhang et al. (2011).

Table 13.1 Summary of information on different types of MT used by different researchers for geopolymer synthesis

Source of MT	Initial Si/Al	Product application	Curing temperature (°C)	Improvement method	References
Copper mine	7.8	Undefined	60	Addition of fly ash	Zhang et al. (2011)
Copper mine	7.8	Masonry block	90	Elevated curing temperature/ precompression	Ahmari and Zhang (2012)
Tungsten mine	2.73	Undefined	Room	Dehydroxylation	Pacheco-Torgal et al. (2008a, 2010)
Copper and gold mine	2.69−14.4	Mining backfill	70	Addition of fly ash or slag	Southam et al. (2007)
Red mud	0.3	Building materials	60	Addition of ferronickel slag	Giannopoulou et al. (2009)
Gold mine	3.5−4.5	Capping of hypersaline MT	Room	Addition of fly ash	Van Jaarsveld et al. (2000)
Copper mine	6.7	Stabilization of tailings	60	Addition of fly ash	Giannopoulou and Panias (2006)

13.2.1 Dehydroxylation of MT

Dehydroxylation involves the heating process through which the hydroxyl group (OH) is released by forming a water molecule (Frost & Vassallo, 1996). The generally accepted mechanism of dehydroxylation of kaolinite is the interaction between two liberated hydroxyl as below:

$$\begin{aligned} &OH^- \leftrightarrow H^+ + O^{2-} \\ &H^+ + OH^- \leftrightarrow H_2O \end{aligned} \tag{13.2}$$

The process requires proton delocalization at specific hydroxyl sites. The consequence of the release of structural water through dehydroxylation is distortion and buckling of polymeric structure of aluminosilicates, resulting in disordered structure (Sperinck et al., 2011).

Pacheco-Torgal & Jalali (2010) studied dehydroxylation of tungsten mine waste with and without adding sodium carbonate. They heated the mine waste and cooled it down rapidly to assure that the crystalline structure is transformed to an amorphous one. The reason for the addition of sodium carbonate was to reach the criteria $Na_2O/SiO_2 > 0.2$ given by Davidovits (Davidovits, 1999). The study indicated that with no addition of sodium carbonate, dehydroxylation at 960 °C resulted in the highest compressive strength of the geopolymer product. The addition of sodium carbonate did not lead to an optimal temperature (dehydroxylation state) although the compressive strength of sodium carbonate-added specimens was higher.

The dehydroxylated tungsten MT-based geopolymer concrete exhibited good physical and mechanical properties (Pacheco-Torgal et al., 2008a). The water absorption by immersion (WAI) after 24 h immersion in water was on average below 3.4%. The capillarity water absorption coefficient (CWAC) was below 0.015 g/cm^2. Comparison between the CWAC of the geopolymer concrete and that of the aggregates indicated that the measured values (0.0007−0.005 g/cm^2) primarily represent the water absorption of the geopolymer paste. The measured static elastic modulus (29.7−34.9 GPa) showed dependence on the type and size of the aggregates used. The compressive strength after 50 days of curing was reported to increase to about 40 MPa for hardened geopolymer paste and more than 90 MPa for geopolymer concrete. This indicates the effectiveness of dehydroxylation for pretreatment of MT. However, since the main goal for using MT-based geopolymer is to develop sustainable materials and considering the energy intensiveness of the dehydroxylation process, commercialization of this process is still questionable.

13.2.2 Addition of other aluminosilicate source material

Production of hybrid MT-based geopolymer by adding other source material containing reactive aluminosilicates is another option to improve the properties of MT-based geopolymer products. Dissolution of alumina tends to be easier than silica as it takes less energy to dissolve it. The major problem with MT is the high stability of silica. Addition of a more reactive source material such as fly ash or slag will mainly help

provide an additional source of silica although it may be a source of alumina as well. Mixture of MT with fly ash or slag creates a new system with a different Si/Al ratio from the initial one. Therefore, it is important to proportion the mixture in a way to achieve the optimal Si/Al ratio. Addition of fly ash to MT helps produce a geopolymer with better properties not only due to the increased reactivity and adjustment of the Si/Al ratio, but also due to the filling effect of fly ash particles, which are much smaller than MT particles. Fly ash particles fill the voids between MT particles and form a denser microstructure, which eventually leads to higher compressive strength. Zhang, Ahmari, & Zhang (2011) showed the increase of compressive strength from approximately 3−20 MPa for copper MT-based geopolymer paste after curing at 60 °C for seven days due to the addition of fly ash. Their study indicated that the amount of added fly ash did not have an effect on the curing time required to reach the ultimate strength, and all specimens gained their ultimate strength within seven days. The addition of fly ash also led to an obvious change in the mode of failure and the ductility of the geopolymer paste specimens. It was shown that the pure MT-based geopolymer specimen failed with no distinct peak stress while the fly ash-added MT-based geopolymer specimen failed with a sharp peak and at larger strains.

Giannopoulou, Dimas, Maragkos, & Panias (2009) studied the production of geopolymer using a mixture of metakaolin and red mud. The mixture by weight comprised 15% metakaolin. In the optimum condition corresponding to 8 M NaOH concentration, the compressive strength up to about 20 MPa and the water absorption of 1.9% were obtained. It is noted that for any geopolymer system, there is an optimum NaOH concentration depending on the type of source materials.

13.2.3 Utilization of soluble silica in activation solution

Additional silica can also be provided by adding a soluble silica source such as sodium silicate to the activation solution. Mixed NaOH and sodium silicate solution is commonly used in the synthesis of geopolymers. This makes geopolymerization faster because the silica species are already available in the activation solution. Addition of sodium silicate up to a certain level results in higher strength, and beyond that, the strength declines. Ahmari et al. (2012a) found that for copper MT, the amount of sodium silicate corresponding to $SiO_2/Na_2O = 1.0-1.26$ is the optimum one and further addition of sodium silicate results in strength loss. This is possibly because too much sodium silicate hinders evaporation of water and formation of polymeric structure by preventing the contact between the solid material and the activation solution through precipitation of the Si−Al phase (Cheng & Chiu, 2003; Lee & Van Deventer, 2002). The study also indicated that despite the high initial Si/Al ratio, addition of sodium silicate still improved the mechanical properties of the geopolymer binder. The reason is because although the initial Si/Al ratio is high, only a small amount of silica is available for geopolymerization. The initial or nominal Si/Al accounts for both the crystalline and amorphous phases of silica, but the amorphous phase is the major part participating in geopolymerization. That is why addition of sodium aluminate to the NaOH solution did not result in improvement of strength.

13.2.4 Use of appropriate curing temperature

Curing temperature is a crucial factor in geopolymerization of MT due to its lower reactivity compared to other source materials. By increasing curing temperature, more energy is delivered to dissolve the silica and alumina species from the surface of MT particles. It is known that geopolymerization of an aluminosilicate-containing material leads to the highest strength at a certain temperature. This optimum temperature was found to be 90 °C for copper MT (Ahmari et al., 2012a). A summary of the optimum curing temperatures for different source materials and NaOH concentrations is shown in Table 13.2. The optimum curing temperature decreases when the source material is more reactive or the NaOH concentration is lower. The MT-based geopolymer binder reaches the highest strength at 75 °C for 5 or 10 M NaOH and 90 °C for 15 M NaOH, respectively. Ahmari et al. (2012a) conducted leaching tests on MT powder to better understand the relationship between dissolution of silica and alumina species and temperature (see Table 13.3). From 60 °C to 90 °C, there is a significant increase in dissolution of Si and Al. Elevated NaOH concentration has a similar effect on dissolution of Si and Al but the effect of temperature is prevalent. The increased dissolution of Si and Al explains why the compressive strength of MT-based geopolymer binder increased from about 3 to 20 MPa when the curing temperature was increased from 60 to 90 °C. The kinetics of dissolution of Si and Al also explains why sodium aluminate is an effective activator at 90 °C but not at 60 °C. The reason

Table 13.2 Optimum curing temperatures from different researchers for different source materials

Source material	Optimum curing temperature (°C)	NaOH concentration (M)	References
Natural zeolite	40	7	Villa, Pecina, Torres, and Gómez (2010)
Glass cullet	40	5−10	Cyr, Idir, and Poinot (2012)
Class C fly ash	60	8.1	Guo, Shi, and Dick (2010)
Class F fly ash	75	7.5	Van Deventer et al. (2006)
Class C fly ash	75	8.1	Guo et al. (2010)
Class F fly ash	80	7	Yunfen, Dongmin, Wenjuan, Hongbo, and Lin (2009)
Metakaolin	85	13.6	Yao, Zhang, Zhua, and Chen (2009)
MT	75	5 and 10	Ahmari et al. (2012a)
MT	90	15	Ahmari et al. (2012a)

Ahmari et al. (2012a).

Table 13.3 Leaching test results on Si and Al concentration of MT powder soaked in NaOH of different concentrations at two different temperatures

Temperature (°C)	60			90		
NaOH (M)	5	10	15	5	10	15
Si (ppm)	71	171	233	1846	3970	4570
Al (ppm)	28	76	121	299	319	550
Si/Al	2.44	2.16	1.85	5.93	11.9	7.98

is that the Si/Al ratio is very high at 90 °C and the addition of sodium aluminate helps decrease this ratio in the aqueous phase to be closer to the optimum one.

13.2.5 Addition of calcium

Other additives may also be used to enhance the mechanical properties of MT-based geopolymer. However, the improvement might not be necessarily due to the enhanced geopolymerization process. For example, calcium-containing material such as calcium hydroxide can be added to MT. Pacheco-Torgal, Castro-Gomes, & Jalali (2008b) studied the effect of added calcium hydroxide on geopolymerization of tungsten mine waste and noted that addition of more than 10% calcium hydroxide leads to strength decrease after 14 days. This is possibly due to the formation of CSH gel and the competition between geopolymer and CSH gel for silicates. Other possible reasons are the occurrence of shrinkage cracks at the interface of binder and aggregates and the formation of ettringate.

Ahmari and Zhang (2013b) also studied calcium added MT-based geopolymer. They added CKD to improve the durability of copper MT-based geopolymer bricks. The study indicated that the compressive strength and durability of the geopolymer binder improved significantly after the addition of CKD.

The effect of calcium on the geopolymerization process is still not completely known. Some researchers believe that calcium also takes place in geopolymerization and serves as a charge balancing agent. The other possible effect of calcium on geopolymerization is the increase of alkalinity of the activation solution and consequently the improvement of dissolution of silica and alumina species.

13.3 Synthesis and physical and mechanical properties of MT-based geopolymer masonry blocks

13.3.1 Synthesis of MT-based geopolymer masonry blocks

The conventional process (Figure 13.2(a)) for producing masonry blocks is energy intensive and consumes natural materials (mainly clay). The

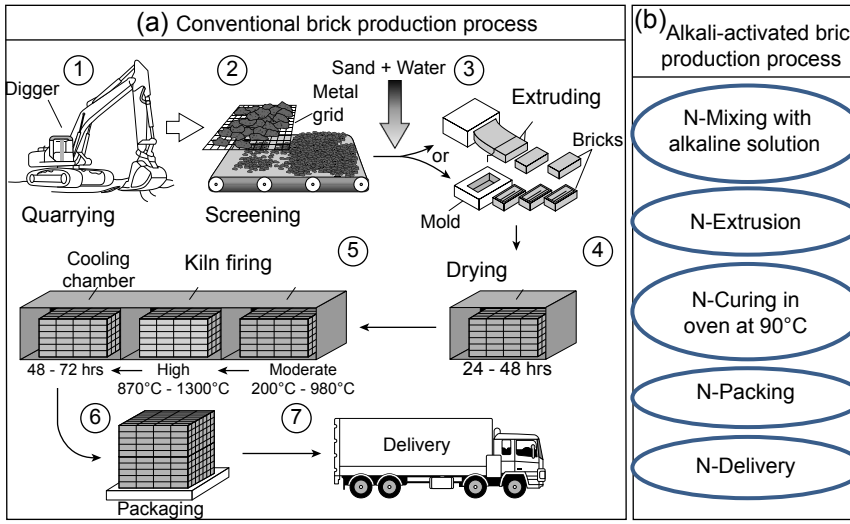

Figure 13.2 Schematic demonstration of production of masonry blocks: (a) using conventional method and (b) using geopolymerization method.

geopolymerization method for producing masonry blocks from MT (Figure 13.2(b)) includes fewer steps and consumes much less energy than the conventional method.

To produce MT-based geopolymer masonry blocks, first MT is mixed with an alkaline solution prepared in advance at a specified water to solid ratio. Ahmari and Zhang (2012) used only NaOH to prepare the activation solution. MT were used as received from the tailings dam except that the agglomerated particles were crushed by hand. The resulant mixture can vary from semidry to semipaste. Then the mixture is compressed with a forming machine to a certain pressure (usually no water should be squeezed out of the mold). After the forming pressure is released, there might be a slight rebound due to the elastic deformation; however, the major portion of the deformation is plastic and related to the elimination of air voids inside the mixture. The relative amount of elastic deformation decreases with a slower loading rate. The study by Ahmari & Zhang (2012) indicated that 10 min is an appropriate forming time. After the blocks are formed, they are placed in an oven for curing at a specified temperature. Ahmari & Zhang (2012) showed that for copper MT-based geopolymer masonry blocks using an NaOH activation solution, 90 °C is the optimum temperature. It is noted that the optimum curing temperature may change for different types of MT or different types of activation solutions. As discussed earlier, the optimum curing temperature decreases when the reactivity of the source material is higher. Figure 13.3 shows some of the MT-based geopolymer blocks produced in the laboratory following the above procedure. For commercial production, the cured blocks will then be packed and delivered.

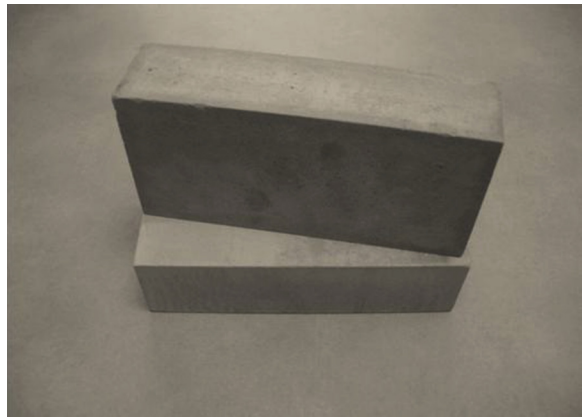

Figure 13.3 MT-based geopolymer blocks produced in laboratory.

13.3.2 Physical and mechanical properties of MT-based geopolymer masonry blocks

The physical and mechanical properties of MT-based geopolymer masonry blocks are affected by several factors. Due to the crystalline characteristics of MT, curing temperature has an especially important effect. Increasing curing temperature up to the optimum level results in dissolution of more amorphous silica and alumina species from the MT particles and thus higher compressive strength of the geopolymer product. However, further increase in curing temperature above the optimum level results in a decrease of the compressive strength. Too high a curing temperature results in not only rapid dissolution of silica and alumina but also accelerated polycondensation. Rapid polycondensation causes fast growth of geopolymer gel and inhibits further dissolution of silica and alumina species. Too high a curing temperature also causes fast dehydration of the blocks, especially when the blocks are uncovered, and leads to incomplete geopolymerization.

Initial water content and forming pressure are other important factors affecting the properties of MT-based geopolymer blocks. Sufficient water is required for dissolution of silica and alumina species and initiation of polycondensation of the dissolved species. The forming pressure needs to be selected based on the initial water content so that the mixture is compressed to the highest degree without squeezing out the activation solution during the forming process. This means for an initial water content, there is a corresponding optimum forming pressure. The study by Ahmari & Zhang (2012) indicated that the increase of initial water content from semidry to semipaste consistency results in higher compressive strength of the MT-based geopolymer blocks. This is because, first, as mentioned earlier, water serves as a medium for geopolymerization and lack of water results in incomplete geopolymerization. Second, higher initial water content means more NaOH at a constant NaOH concentration. NaOH has two important roles in geopolymerization: dissolution of Si and Al and charge balancing of alumina tetrahedral in geopolymer structure. Figure 13.4 shows the effect

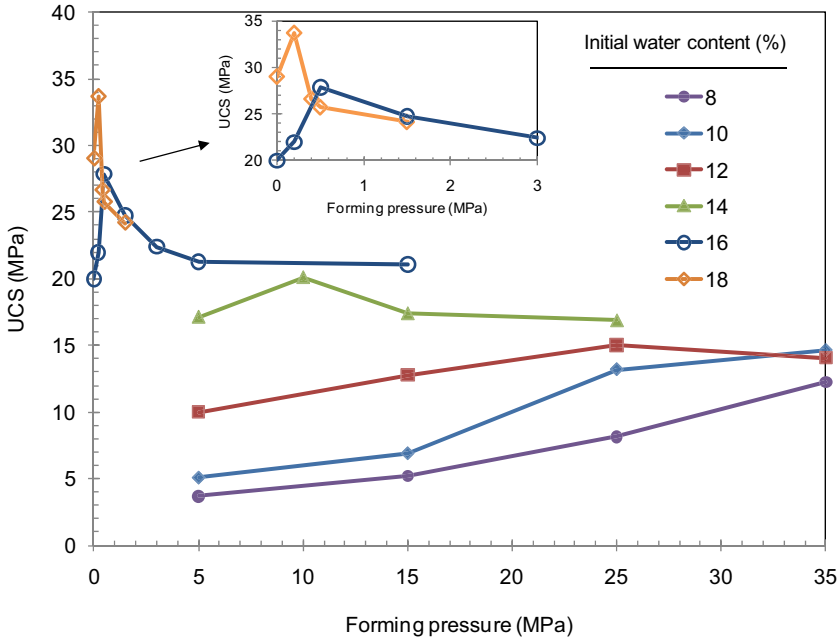

Figure 13.4 Unconfined compressive strength (UCS) versus forming pressure for MT-based geopolymer blocks prepared at different initial water contents and 15 M NaOH concentration and cured for seven days at 90 °C.
Ahmari & Zhang (2012).

of initial water content and forming pressure on the compressive strength of MT-based geopolymer blocks synthesized with 15 M NaOH solution and cured at 90 °C for seven days. It can be seen from the figure that there are two ways to increase the compressive strength of the blocks: using lower initial water content and higher forming pressures or using higher initial water content and lower forming pressures. Increasing the amount of NaOH solution is much more effective than increasing the forming pressure for improving the compressive strength of the MT-based geopolymer blocks. The NaOH solution affects the chemical reaction and thus the amount of generated geopolymer gels, but the forming pressure influences the physical structure by compacting the MT matrix. Figure 13.5 compares the micrographs of two blocks prepared respectively at 12% and 16% initial water contents and the corresponding 25 and 0.5 MPa forming pressures. The 16%/0.5 MPa block has a denser microstructure than the 12%/25 MPa one.

Table 13.4 shows the compressive strength, unit weight, water absorption, and abrasion index (resistance) of MT-based geopolymer blocks prepared with 16% initial water content and different forming pressures and cured at 90 °C for seven days. The compressive strength was measured using unconfined compression tests. The unit weight was measured by simply using the compressive strength samples. The water absorption was determined by soaking the blocks in water for a certain period of time and then measuring the weight increase of the blocks. And the abrasion index

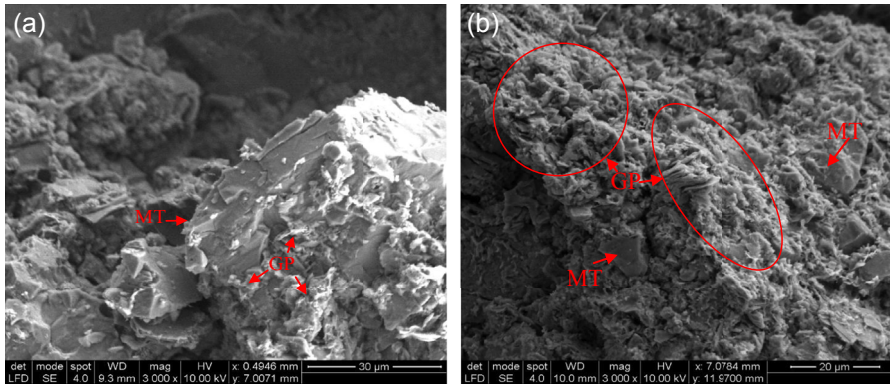

Figure 13.5 SEM micrographs at initial water content/forming pressure combinations of 12%/25 MPa (a) and 16%/0.5 MPa (b) for the specimens cured at 90 °C for seven days (GP: geopolymer, MT: mine tailings particle).
Ahmari & Zhang (2012).

Table 13.4 Physical and mechanical properties of MT-based geopolymer blocks prepared at 16% initial content and cured at 90 °C for seven days

Forming pressure (MPa)	UCS (MPa)/(psi)	Unit weight (kN/m^3)	24 h water absorption (%)	Abrasion index
0.5	28/4040	19.66	0.93	0.02
1.5	25/3591	19.70	2.18	0.06
3.0	22/3250	19.89	2.92	0.09
5.0	21/3086	19.93	3.45	0.11
15.0	21/3059	19.96	3.15	0.10

was determined from the unconfined compressive strength (UCS) and water absorption using the following expression:

$$\text{Abrasion Index} = \frac{100 \times \text{absorption}\ (\%)}{\text{UCS}\ (\text{psi})} \tag{13.3}$$

The American Society for Testing and Materials (ASTM) has different requirements for the different applications of bricks and blocks (see Table 13.5). The minimum required UCS varies between 4.8 MPa for load bearing wall tiles and 55.2 MPa for severe exposure (SX) grade pedestrian and light traffic paving bricks. The maximum water absorption varies between 8% for SX grade pedestrian and light traffic paving bricks to 25% for load bearing nonexposed wall tiles. The requirements

Table 13.5 ASTM specifications for different applications of bricks and blocks

Title of specification	ASTM designation	Type/grade	Minimum UCS (MPa)	Maximum water absorption (%)	Abrasion index	
Structural clay load bearing wall tile	C34-03	LBX	9.6	16	NA	
		LBX	4.8	16	NA	
		LB	6.8	25	NA	
		LB	4.8	25	NA	
Building brick	C62-10	SW	20.7	17	NA	
		MW	17.2	22	NA	
		NW	10.3	No limit	NA	
Solid masonry unit	C126-99	Vertical coring	20.7	NA	NA	
		Horizontal coring	13.8	NA	NA	
Facing brick	C216-07a	SW	20.7	17	NA	
		MW	17.2	22	NA	
Pedestrian and light traffic paving brick	C902-07	SX	55.2	8	Type I	0.11
		MX	20.7	14	Type II	0.25
		NX	20.7	No limit	Type III	0.50

Notes: LBX = load bearing exposed; LB = load bearing nonexposed; SW = severe weathering; MW = moderate weathering; NW = negligible weathering; SX = severe exposure; MX = moderate exposure; NX = negligible exposure; and Type I, II, and III = subjected to extensive, intermediate, and low abrasion, respectively.

for abrasion resistance only apply to pedestrian and light traffic paving bricks and the maximum abrasion index values are between 0.11 and 0.5. The MT-based geopolymer blocks prepared with 16% initial water content and different forming pressures and cured at 90 °C for seven days (see Table 13.4) meet all the ASTM requirements for different types of applications except for the SX grade pedestrian and light traffic paving bricks.

The mechanical properties of MT-based geopolymer blocks can be improved by adding other higher reactivity source materials. Figure 13.6 shows the UCS of MT-based geopolymer blocks containing different amounts of ground furnace slag (GFS). Addition of GFS results in a significant increase of UCS. The improving effect of GFS can be attributed to a number of factors such as the favorable physical and chemical properties and phase composition of the GFS. GFS is much more amorphous than MT due to the extremely high temperature and subsequent rapid cooling it has experienced. This contributes to easier dissolution of silica as a major component of GFS in alkaline solution. GFS may contain crystalline minerals of Si such as fayalite (Fe_2SiO_4), but the silica in fayalite is easier to liberate and dissolve in alkaline solution than that in quartz. Another advantage of adding GFS to MT is that GFS improves the workability of the mixture and thus less water is required for constant consistency. For example, at 10% water content, GFS-added MT shows the same consistency as the pure MT at 16% water content. Ahmari & Zhang (2013b) also investigated the improvement of properties of MT-based geopolymer blocks by adding CKD. CKD is a by-product of the Portland cement production process, which is collected from cement kiln exhaust gases. CKD mainly contains Ca and Si, which are beneficial for geopolymerization. The addition of CKD reduced the workability of the mixture mainly due to the fast dissolution of calcium and the very fine size of the CKD

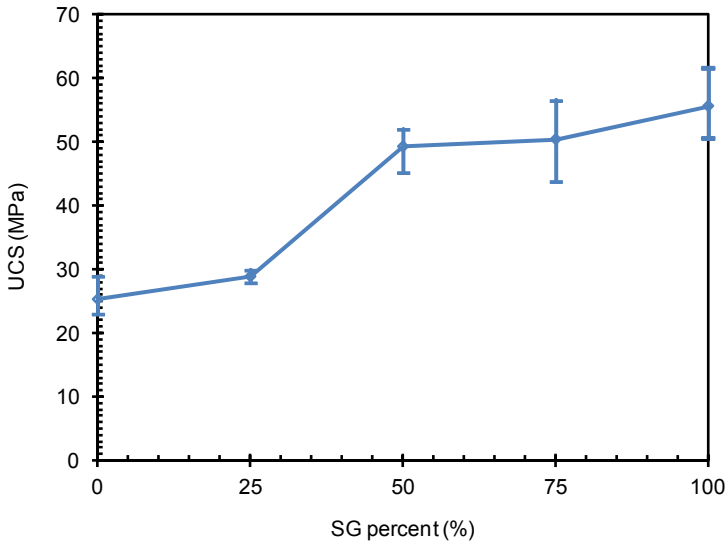

Figure 13.6 UCS versus slag content for geopolymer blocks prepared at 15 M NaOH and cured at 90 °C for seven days.

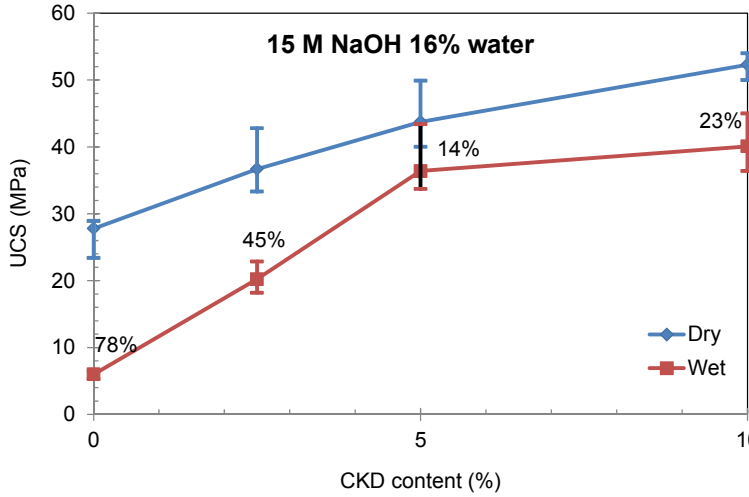

Figure 13.7 Dry and wet UCS (before and after immersion in water) versus CKD content for geopolymer block specimens prepared with 16% initial water content, 15 M NaOH, and cured at 90 °C for seven days. (The percentage numbers show the percentage loss of strength after immersion in water for seven days.)

particles. However, as discussed in the next section (see Figure 13.7), the addition of CKD significantly increased the strength of the MT-based geopolymer blocks.

13.4 Durability of MT-based geopolymer masonry blocks

The durability of geopolymer in an aggressive environment depends on a variety of factors such as the source material of geopolymer, the type of activator, and the type of aggressive ions. The more reactive source materials result in a higher degree of geopolymerization and denser microstructure and thus higher resistance to acid attack. Ahmari & Zhang (2013a) studied the durability of MT-based geopolymer blocks in water and nitric acid with a pH of respectively 7 and 4. They reported a significant strength loss after immersion for about four months. They accounted partial geopolymerization of the MT as one of the reasons for the strength loss. Similarly, Silva, Castro-Gomes, & Albuquerque (2010) reported significant strength loss of MT-based geopolymer used as artificial aggregates for wastewater treatment plant after immersion in water. The strength loss was attributed to the dissolution of unreacted NaOH particles that fill the voids, which leads to increase of porosity of the geopolymer matrix and migration of the aggressive solution into the micropores. Migration of reacted cations into the solution can also account for the strength loss. It is likely that the cations in the geopolymer structure are replaced with the cations in the solution if geopolymer binder is immersed in salt such as sodium sulfate (Bakharev, 2005). In this case, the cation exchange rate depends on the pore size. Bakharev (2005) showed that

the exchange rate is higher when potassium hydroxide (KOH) instead of NaOH is used as the activation solution, due to larger pore size. That is why larger cracks were observed in the specimens activated with KOH.

Pacheco-Torgal, Castro-Gomes, & Jalali (2010) studied the durability of tungsten MT-based geopolymer concrete with different types of aggregates including schist, limestone, and granite and immersed in 5% sulfuric, hydrochloric, and nitric acid solutions for 28 days. Overall, the geopolymer concrete blocks were more durable than the Portland cement concrete blocks. The calcium in Portland cement reacts to the acid anions and forms soluble salts, resulting in more porous matrix and further invasion of acid into the matrix. The geopolymer concrete specimens exhibited variable durability depending on the aggregate type and the acid type. All the geopolymer concrete specimens immersed in the hydrochloric acid solution exhibited low weight loss regardless of the aggregate type. The specimens made with schist aggregate exhibited good durability in most of the acids. The specimens made with limestone aggregates showed expansion and cracks in sulfuric acid. This was due to the reaction of sulfate in the solution with limestone and the formation of expanding minerals (Pacheco-Torgal et al., 2010). It needs to be noted that because it was calcined, the used tungsten MT was highly reactive. In addition, they added calcium hydroxide to improve the mechanical properties of the tungsten MT-based geopolymer concrete. This can be the reason why the tungsten MT-based geopolymer concrete exhibited better durability than the pure MT-based geopolymer blocks studied by Ahmari & Zhang (2013a) and Silva, Castro-Gomes, & Albuquerque (2010).

As discussed in Section 12.3, lower forming pressure associated with higher water content (which means more NaOH at the same NaOH concentration) results in stronger MT-based geopolymer blocks. The UCS of 16%/0.5 MPa blocks (prepared at 16% initial water content and 0.5 MPa forming pressure) was higher than that of 12%/25 MPa blocks. However, both types of blocks exhibited significant strength loss after immersion in water or nitric acid. Nevertheless, the durability of the 12%/25 MPa blocks was slightly better. This means the durability requirement favors the utilization of a higher forming pressure. The denser microstructure of the 16%/0.5 MPa blocks resulted due to the formation of larger amounts of geopolymer gels, but the dissolution finally resulted in a more porous microstructure. In contrast, the compact microstructure of the 12%/25 MPa specimens resulted due to the physical compaction of the MT and although smaller amounts of geopolymer gels were generated, a slightly more compact microstructure remained after immersion.

Ahmari & Zhang (2013b) added CKD to improve the durability of MT-based geopolymer blocks. Figure 13.7 shows the UCS of CKD-added MT-based geopolymer blocks prepared at 16% initial water content and formed at 0.5 MPa, before and after immersion in water, respectively. Addition of a small amount of CKD results in significant improvement of strength of the geopolymer blocks, due to several reasons. Dissolution of CKD in alkaline solution leads to release of a substantial amount of calcium cations, which further increases the alkalinity of the activation solution. As discussed earlier, higher alkalinity of the activation solution results in dissolution of larger amounts of silica and alumina from MT. Soluble calcium also leads to the formation of $Ca(OH)_2$, which eventually yields $CaCO_3$ due to a reaction to air. This acts like a

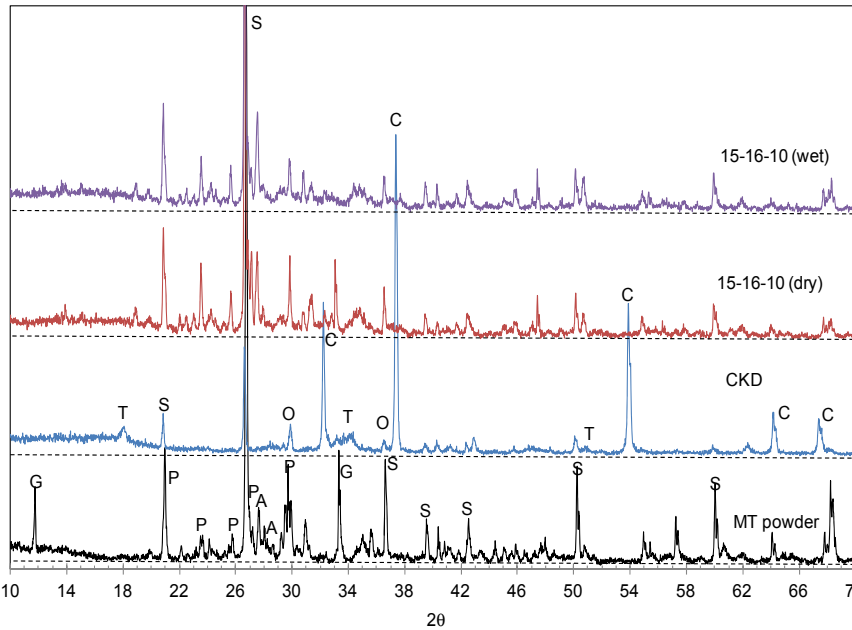

Figure 13.8 XRD patterns of MT and CKD powders and geopolymer blocks prepared at 15 M NaOH, 16% initial water content, 10% CKD, and cured at 90 °C for seven days and before and after immersion in water (A: albite, G: gypsum, P: sanidine, S: quartz, C: CaO, O: $CaCO_3$, S: SiO_2, T: $Ca(OH)_2$).

cementing agent and decreases the porosity of the geopolymer matrix. $CaCO_3$ has good stability in water and alkaline condition and thus further enhances the durability of the MT-based geopolymer blocks. Figure 13.8 shows the XRD spectra of MT and CKD and the 16%/0.5 MPa blocks before and after immersion in water. It can be seen that the calcium in CKD as CaO and $Ca(OH)_2$ disappears after geopolymerization, but the peak corresponding to $CaCO_3$ increases. CKD contains a substantial amount of silica, which after dissolution can take part in geopolymerization. These all indicate formation of a denser microstructure and consequently more durable geopolymer blocks. The released calcium can also serve as charge balancing agent for the geopolymer structure. One reason for the deterioration of geopolymer is cation exchange and release of alkali cations. Since calcium has a low tendency to cation exchange, the durability of the geopolymer blocks will increase.

13.5 Environmental performance of MT-based geopolymer masonry blocks

MT are susceptible to acid mine drainage, meaning that the sulfide minerals such as pyrite in MT oxidize and result in generation of sulfuric acid. The generated sulfuric acid lowers the environment pH and consequently results in release of heavy metals.

Therefore, it is important to ensure that MT-based geopolymer blocks are stable and will not release toxic substances such as heavy metals. The environmental safety of MT-based geopolymers has been studied by different researchers. Pacheco-Torgal et al. (2010) demonstrated that the concentration of released heavy metals from the tungsten MT-based geopolymer concrete is below the Portuguese standard limits for irrigation purposes but above those for potable water. There was a high concentration of Na in the leachate due to the dissolution of unreacted NaOH.

Giannopoulou & Panias (2006) performed leaching analysis on fly ash-added MT-based geopolymer and showed that the MT powder in acidic condition (1 M sulfuric acid) released a significant amount of Mn, Fe, Mg, Mn, K, Na, Ca, and Si. However, in a neutral condition Mg, Ca, Si, and Al exhibited the highest release rate. This is because of the dependence of solubility of heavy metals on pH. The concentration of released heavy metals from MT-based geopolymer was below the Greek standard thresholds and significantly lower than that from the MT powder.

Ahmari & Zhang (2013a) also evaluated the environmental performance of MT-based geopolymer blocks. They immersed the blocks in nitric acid (pH = 4) and water (pH = 7) for three months and monitored the concentration of different heavy metals in the liquid. The study showed that there was a significant amount of heavy metals released from the MT powder, especially at pH = 4. At neutral condition, Na, Mg, K, and Ca exhibited a high release rate while in acidic condition, besides them, Mn, Cu, and Zn also had a high concentration in the liquid. For geopolymer blocks, the concentration of all these released metals (except for Na, which was due to unreacted NaOH) dropped significantly. As and Mo exhibited higher concentrations in the case of geopolymer blocks due to their higher solubility in alkaline condition. Overall, for all geopolymer blocks, the leached heavy metals showed a concentration much lower than the USEPA standard limits.

From the discussion on durability and leaching analysis, it appears that higher forming pressures favor durability and immobilization efficiency although lower UCS is obtained. To avoid compromising strength with durability and immobilization efficiency, hybrid systems such as CKD or slag-added MT geopolymer blocks can be used.

13.6 Conclusions and future trends

MT are a potential source material for producing geopolymer masonry blocks despite their dominant crystalline phase. The low activity of MT can be addressed using different methods such as dehydroxylation, addition of other more reactive materials, utilization of soluble silica in the activation solution, optimization of the synthesis condition such as curing temperature, and addition of calcium. The research has indicated that the physical and mechanical properties of MT-based geopolymer blocks can meet the ASTM standard requirements for most applications of bricks. The research has also shown the durability and environmental safety of MT-based geopolymer blocks.

Since most of the research so far is in laboratory scale, further research in full-scale should be conducted in order to promote the production and utilization of MT-based geopolymer masonry blocks in practice. The full-scale study should investigate the

different practical aspects such as the commercial production method, the costs, and the long-term performance.

References

Ahmari, S., Chen, R., & Zhang, L. (2012b). Utilization of mine tailings as road base material. *GeoCongress, 2012*, 3654−3661.

Ahmari, S., & Zhang, L. (2012). Production of eco-friendly bricks from copper mine tailings through geopolymerization. *Construction and Building Materials, 29*, 323−331.

Ahmari, S., & Zhang, L. (2013a). Durability and leaching behavior of mine tailings-based geopolymer bricks. *Construction and Building Materials, 44*, 743−750.

Ahmari, S., & Zhang, L. (2013b). Utilization of cement kiln dust (CKD) to enhance mine tailings-based geopolymer bricks. *Construction and Building Materials, 40*, 1002−1011.

Ahmari, S., Zhang, L., & Zhang, J. (2012a). Effects of activator type/concentration and curing temperature on alkali-activated binder based on copper mine tailings. *Journal of Materials Science, 47*(16), 5933−5945.

Bakharev, T. (2005). Durability of geopolymer materials in sodium and magnesium sulfate solutions. *Cement and Concrete Research, 35*, 1233−1246.

Cheng, T. W., & Chiu, J. P. (2003). Fire resistant geopolymer produced by granulated blast furnace slag. *Journal of Mineral Engineering, 16*, 205−210.

Chen, Y., Zhang, Y., Chen, T., Zhao, Y., & Bao, S. (2011). Preparation of eco-friendly construction bricks from hematite tailings. *Journal of Construction and Building Materials, 25*, 2107−2111.

Cyr, M., Idir, R., & Poinot, T. (2012). Properties of inorganic polymer (geopolymer) mortars made of glass cullet. *Journal of Materials Science, 47*(6), 2782−2797.

Davidovits, J. (1982). Mineral polymers and methods of making them, US patent 4349386, 14.09.82.

Davidovits, J. (1994). Properties of geopolymer cements. In *First international conference on alkaline cements and concretes, Scientific Research Institute on Binders and Materials, Kiev State, Technical University, Kiev, Ukraine*.

Davidovits, J. (1999). Chemistry of geopolymeric systems, terminology. In *Proceedings of 99 geopolymer conference, The Geopolymer Institute, Saint Quentin, France* (pp. 9−40).

Freidin, C. (2007). Cementless pressed blocks from waste products of coal-firing power station. *Construction and Building Materials, 21*, 12−18.

Frost, R. L., & Vassallo, A. M. (1996). The dehydroxylation of the kaolinite clay minerals using infrared emission spectroscopy. *Clays and Clay Minerals, 44*(5), 635−651.

Giannopoulou, I. P., Dimas, D., Maragkos, I., & Panias, D. (2009). Utilization of metallurgical solid by-products for the development of inorganic polymeric construction materials. *Global NEST Journal, 11*(2), 127−136.

Giannopoulou, I. P., & Panias, D. (2006). Development of geopolymeric materials from industrial solid wastes. In *2nd international conference on advances in mineral resources management and environmental geotechnology, AMIREG 2006, Hania, Greece*.

Guo, X., Shi, H., & Dick, W. A. (2010). Compressive strength and microstructural characteristics of class C fly ash geopolymer. *Cement and Concrete Composites, 32*, 142−147.

He, J., Jie, Y., Zhang, J., Yu, Y., & Zhang, G. (2013). Synthesis and characterization of red mud and rice husk ash-based geopolymer composites. *Cement and Concrete Composites, 37*, 108−118.

Lee, W. K. W., & Van Deventer, J. S. J. (2002). The effects of inorganic salt contamination on the strength and durability of geopolymers. *Colloid Surface, 211*, 115−126.

Liu, Z., Chen, Q., Xie, X., Xue, G., Du, F., Ning, Q., et al. (2011). Utilization of the sludge derived from dyestuff-making wastewater coagulation for unfired bricks. *Construction and Building Materials, 25*(4), 1699−1706.

Morchhale, R. K., Ramakrishnan, N., & Dindorkar, N. (2006). Utilization of copper mine tailings in production of bricks. *Journal of Industrial Engineering Indian Civil Engineering Division, 87*, 13−16.

Pacheco-Torgal, F., Castro-Gomes, J., & Jalali, S. (2008a). Properties of tungsten mine waste geopolymeric binder. *Construction and Building Materials, 22*(6), 1201−1211.

Pacheco-Torgal, F., Castro-Gomes, J. P., & Jalali, S. (2008b). Investigations on mix design of tungsten mine waste geopolymeric binder. *Construction and Building Materials, 22*, 1939−1949.

Pacheco-Torgal, F., Castro-Gomes, J., & Jalali, S. (2010). Durability and environmental performance of alkali-activated tungsten mine waste mud mortars. *Journal of Materials in Civil Engineering, 22*, 897−904.

Pacheco-Torgal, F., & Jalali, S. (2010). Influence of sodium carbonate addition on the thermal reactivity of tungsten mine waste mud based binders. *Construction and Building Materials, 24*, 56−60.

Roy, S., Adhikari, G. R., & Gupta, R. N. (2007). Use of gold mill tailings in making bricks: a feasibility study. *Waste Management Research, 25*, 475−482.

Silva, I. C., Castro-Gomes, J., & Albuquerque, A. (2010). Evaluation of the stability of waste-based geopolymeric artificial aggregates for wastewater treatment processes under different curing conditions. *Advances in Science and Technology*, 86−91.

Southam, D. C., Brent, G. F., Felipe, F., Carr, C., Hart, R. D., & Wright, K. (2007). *Towards more sustainable mine fills — Replacement of ordinary Portland cement with geopolymer cements*. Australia: World Gold Conference.

Sperinck, S., Raiteri, P., Marks, N., & Wright, K. (2011). Dehydroxylation of kaolinite to metakaolin−a molecular dynamics study. *Journal of Materials Chemistry, 21*, 2118−2125.

Sultan, H. A. (1978). *Utilization of copper mill tailings for highway construction, Final tech. report*. Washington DC: National Science Foundation.

Sultan, H. A. (1979). Stabilized copper mill tailings for highway construction. *Transportation Research Record, 734*, 1−7.

Teredesai, R. V. (2005). *Stabilization of pile run chat for roadway base application* (MS thesis). University of Oklahoma.

Van Deventer, J. S. J., Lukey, G. C., & Xu, H. (2006). Effect of curing temperature and silicate concentration on fly-ash-based geopolymerization. *Industrial and Engineering Chemistry Research, 45*(10), 3559−3568.

Van Jaarsveld, J. G. S., Lukey, G. C., van Deventer, J. S. J., & Graham, A. (2000). The stabilisation of mine tailings by reactive geopolymerisation. In *MINPREX 2000, Melbourne, Australasian Institute of Mining and Metallurgy* (pp. 363−371).

Villa, C., Pecina, E. T., Torres, R., & Gómez, L. (2010). Geopolymer synthesis using alkaline activation of natural zeolite. *Construction and Building Materials, 24*, 2084−2090.

Yao, X., Zhang, Z., Zhua, H., & Chen, Y. (2009). Geopolymerization process of alkali−metakaolinite characterized by isothermal calorimetry. *Thermochimica Acta, 493*(1−2), 49−54.

Yunfen, H., Dongmin, W., Wenjuan, Z., Hongbo, L., & Lin, W. (2009). Effect of activator and curing mode on fly ash-based geopolymer. *Journal of Wuhan University of Technology−Material Science Edition, 24*(5), 711−715.

Zhang, L. (2013). Production of bricks from waste materials — a review. *Construction and Building Materials, 47*, 643−655.

Zhang, L., Ahmari, S., & Zhang, J. (2011). Synthesis and characterization of fly ash modified mine tailings-based geopolymers. *Construction and Building Materials, 25*(9), 3773−3781.

The properties and performance of red mud-based geopolymeric masonry blocks

14

S. Kumar
CSIR-National Metallurgical Laboratory, Jamshedpur, India

14.1 Introduction

Red mud is a by-product generated during the Bayer's process of alumina and aluminum production. The Bayer's process accounts for the majority of the world's production of alumina. In this process, the milled bauxite is digested in caustic soda, and then during the solid liquid separation stage the leach residue red mud is collected (Figure 14.1). Before it is sent for disposal, it is washed several times to recover the soda. Typically the red mud generation varies between 0.7 and 2 tons per tons of alumina produced (World Aluminum, 2013; Report on Bauxite Residue Management: Best Practice, 2013). According to Statistics, 2014, published by the International Aluminium Institute at http://www.world-aluminium.org (2014), the total alumina production in the year 2013 was 107,120,000 metric tonnes. So even with the very conservative estimate of 0.7 ton red mud/ton of alumina produced, the total red mud generation was 74,984,000 tonnes, which is an enormous quantity. The total inventory of red mud would be severalfold larger, as it is getting deposited from many

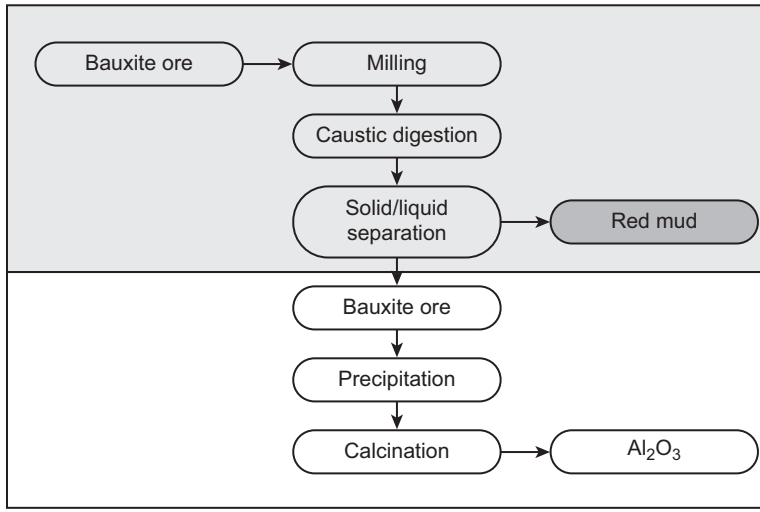

Figure 14.1 Bayer's process for alumina extraction showing point of generation of red mud.

Eco-efficient Masonry Bricks and Blocks. http://dx.doi.org/10.1016/B978-1-78242-305-8.00014-0

years with very low or no utilization. Red mud falls under the category of nonhazardous waste. However due to its enormous quantity, high alkalinity and very fine particle size, its safe disposal remains a challenging task.

The major constituent of red mud is oxides and hydroxides of Fe, Al and Si along with minor quantities of CaO and TiO_2, and it is alkaline in nature (Piga & Stoppa, 1993). As it contains a significant quantity of iron oxides, various efforts have been made to extract iron from red mud (Kumar, Kumar, Alex, & Bandopadhyay, 2006). Balomenos et al. (2011) developed a process of making pig iron by carbothermic reduction of red mud in an electric arc furnace. Research on use of red mud for product development is mainly directed towards brick making, either by sintering or by lime stabilization (Kawas, 2006; Yang & Xiao, 2008), glass ceramics (Marabini, Plescia, Maccari, Burragato, & Pelino, 1998; Yang, Zhang, Hou, He, & Xiao, 2008), cement (Senff, Hotza, & Labrincha, 2011; Tsakiridis, Agatzini-Leonardou, & Oustadakis, 2004; Xiaoming & Zhang, 2011) and glazes (Yalcin & Sevinc, 2000). In spite of extensive research conducted, most of the processes developed at lab scale remained confined to lab scale or pilot scale. This is mainly due to associated scientific problems such as presence of undesirable constituents, high pH and high conductivity; technical problems such as handling of very fine particle size; and other problems like commercial viability, health and safety.

One of the promising areas that has potential to use red mud is geopolymer technology. The term geopolymer is used for aluminosilicate polymers formed in alkaline environments (Davidovits, 1989). During the process of geopolymerization, aluminosilicates are dissolved into alkali solution to form free SiO_4 and AlO_4 tetrahedral units. Further, these SiO_4 and AlO_4 tetrahedrons are linked alternatively where charge-balancing cations are provided by alkali metal cations and yield polymeric precursors ($-SiO_4-AlO_4-$ or $-SiO_4-AlO_4-SiO_4-$ or $-SiO_4-AlO_4-SiO_4-SiO_4-$) by sharing all oxygen atoms between two tetrahedral units and forming monolithic geopolymer products (Davidovits, 1989; Xu & Van-Deventer, 2000). The recent focus in geopolymer research is use of industrial waste and by-products. Some of the most commonly used waste and by-products are fly ash and granulated blast furnace slag, which has shown excellent properties and performance in geopolymers (Kumar & Kumar, 2011; Kumar, Kumar, & Mehrotra, 2010). Some of the other wastes that are under experimental stage are steel slag, tailings and red mud. The use of red mud as one of the constituents for geopolymers is based on such facts as: (1) red mud contains Al_2O_3 and SiO_2, which is desirable to form the network structure of geopolymers; (2) the presence of caustic soda is sought after for the alkaline activation and also provides a washed surface of Al_2O_3 and SiO_2 for reaction; (3) part of the iron oxide and hydroxide may participate in geopolymerization by forming ferrosialate; and (4) geopolymer has emerged as an effective binder for stabilization of toxic materials, and thus apprehension of leaching of metals from red mud can be minimized.

Many researchers have studied the role of red mud in geopolymer systems. These studies can be broadly categorized into two: (1) studies based on red mud metakaolin mixtures; and (2) studies based on red mud fly ash mixtures. Scanty information is available on the use of only red mud for geopolymerization. This may be because only red mud does not give sufficient strength during early geopolymerization. This

observation was also supported by Cundi et al. (2005), who studied the geopolymerization of red mud and pressurized fluidized bed boiler ash (PFBC ash). They reported that red mud behaves as inactive filler, which can be solidified with the help of active PFBC ash. Use of red mud and metakaolin mixture was tried by many researchers (Dimas, Giannopoulou, & Panias, 2009; Hajjaji et al., 2013). They have obtained compressive strength in the range of 2−13 MPa with red mud addition up to 40%. Almost similar results were obtained with red mud and fly ash mixture (Zhang, He, & Gambrel, 2010), where with class C fly ash an unconfined compressive strength in the range of 7−13 MPa was reported.

14.2 Characterization of red mud

During the Bayer's process, bauxite is fine milled. As a consequence, the red mud generated has a very fine particle size distribution. The particle size analysis of red mud was carried out using a laser particle size analyzer (MASTERSIZER S, Malvern, UK). Figure 14.2 shows the particle size distribution of red mud received from ALCOA, Australia. The characteristic particle diameter X_{90}, X_{50} and X_{10} is 56.88, 1.57 and 0.37 μm. The pH of this red mud was 12.5 and specific gravity 2.88.

The chemical and mineralogical composition of red mud depends largely on the nature of bauxite ore and the extraction process. Thus there is wide variation in chemistry of red mud, as follows: Fe_2O_3 20−60 wt%, Al_2O_3 10−30 wt%, SiO_2 02−20 wt%, TiO_2 0−28 wt%, Na_2O 2−10 wt% and CaO 2−8 wt%. It also contains small quantities of minor elements such as V, Ga, Cr, P, Mn, Cu, Cd, Ni, Zn, Pb, Mg, Zr, Hf, Nb, U, Th, Y, K, Ba, Sr, and traces of rare earth elements (Kalkan, 2006; Singh, Upadhayay, & Prasad, 1996; Singh, Upadhayay, & Prasad, 1997; Tsakiridis et al., 2004).

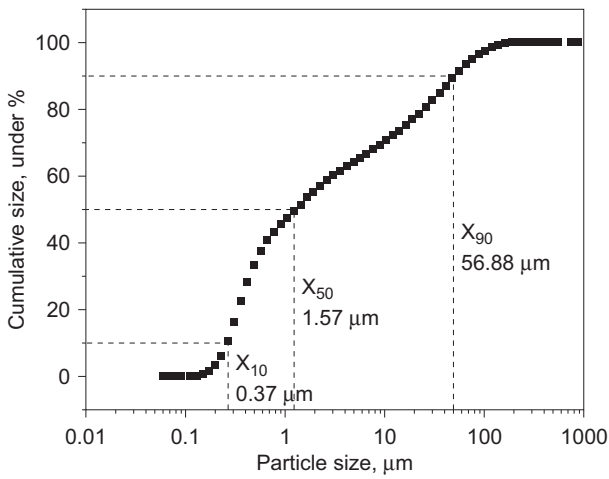

Figure 14.2 Particle size distribution of red mud. Characteristic particle diameters X_{10}, X_{50} and X_{90} are marked in the figure.

Table 14.1 Chemical analysis of two types of red mud

Component	NALCO red mud, wt%	ALCOA red mud, wt%
Fe_2O_3	49.91	31.50
Al_2O_3	15.16	15.20
SiO_2	9.20	29.2
CaO	2.8	04.50
TiO_2	3.82	–
Na_2O	3.98	3.1

Table 14.1 shows the chemical analysis of two red muds, NALCO red mud from India and ALCOA red mud from Australia, carried out using a combination of conventional method, atomic absorption spectroscopy and X-ray fluorescence. The NALCO red mud contains a higher amount of iron oxides, whereas the ALCOA red mud is rich in SiO_2. Chemistry-wise, silica-rich red mud seems more suitable for geopolymerization and the silica-to-alumina ratio is 2:1, which is the desirable range. Thus, for further studies ALCOA red mud was used.

Like its chemistry, red mud also shows variation in its mineralogical composition. XRD analysis of ALCOA red mud has been carried out using a SIEMENS X-ray diffractometer (Model D500), with Co$K\propto$ radiation and Fe-filter. A scanning speed of 1 °/min was used and the samples were scanned from 15 to 65 °C. Figure 14.3 shows the mineralogical composition of ALCOA red mud. The main mineralogical phases were identified as haematite (Fe_2O_3), Goethite (FeO(OH)) and quartz (SiO_2). In addition, peaks of cancrenite ($Na_6Ca_2Al_6Si_6O_{24}(CO_3)_2$) and sodalite ($Na_8(Al_6Si_6O_{24})Cl_2$) were found, mostly overlapping with each other. Some of the phases,

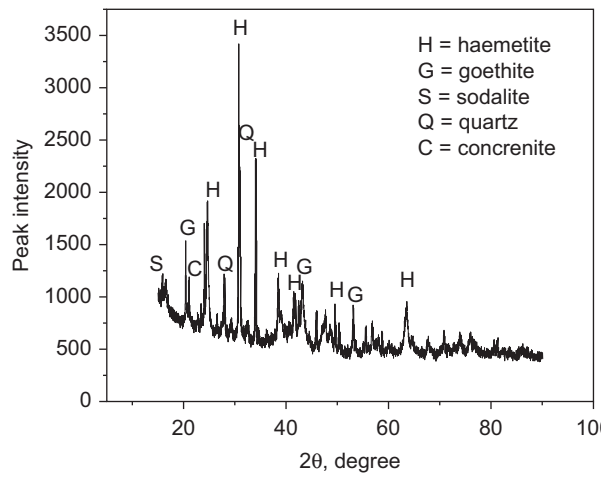

Figure 14.3 X-ray diffractrogram of red mud showing major mineralogical phases.

such as haematite and quartz, derived from parent bauxite, whereas some of the peaks, such as sodalite and cancrenite, were formed during the processing stage.

14.3 Suitability of red mud for geopolymeric masonry block

Earlier, red mud was not considered a suitable material for geopolymer due to its high Fe content. Little information was available on the role of iron oxides and hydroxides in geopolymer cements. Previously developed geopolymer composition contains very small amounts of iron oxides as it was believed that iron oxide reduces the compressive strength. However, some of the recent studies showed that Fe plays an important role in geopolymer structure. Davidovits, Davidovits, Davidovits, & Davidovits (2012) patented a new geopolymeric binder that has a molecular structure consisting of Fe atoms as tetrahedral Fe [IV] in structural position within the ferrosialate geopolymeric sequence [-Fe-O-Si-O-Al-O-]. The formation of ferrosialate forms the scientific basis of using red mud in geopolymer.

To understand whether only red mud can be used for geopolymerization, isothermal conduction calorimetry was used (TAM AIR, Thermometric AB, Jarafalla, Sweden) to measure the heat evolution during the reaction of red mud with 6 M NaOH solution ($d\propto/dt$). Figure 14.4 shows the calorimetric curve of red mud geopolymer obtained at 60 °C. The curve of fly ash has also been included in the same graph for comparison. It is interesting to note that the red mud has not shown any significant calorimetric peak even after 16 h of reaction, whereas the fly ash has shown a wide peak corresponding to geopolymerization. In order to further explore the reactivity of red mud, samples were prepared with 6 M NaOH solution and with Na_2SiO_3 solution. The samples with NaOH solution had not set even after 24 h, whereas the sample with Na_2SiO_3 had set, but no strength had developed in

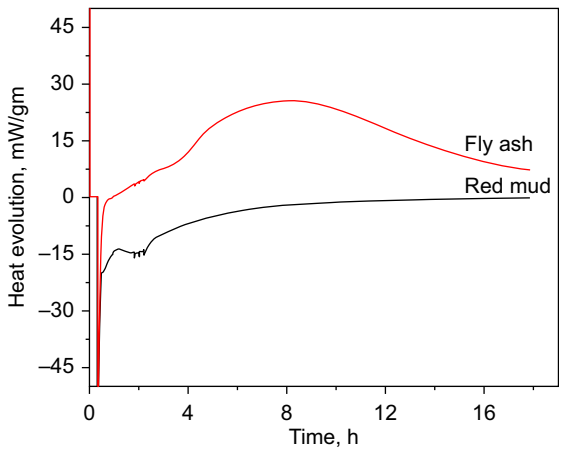

Figure 14.4 Isothermal conduction calorimetric curve of red mud and fly ash with 6 M NaOH solution at 60 °C.

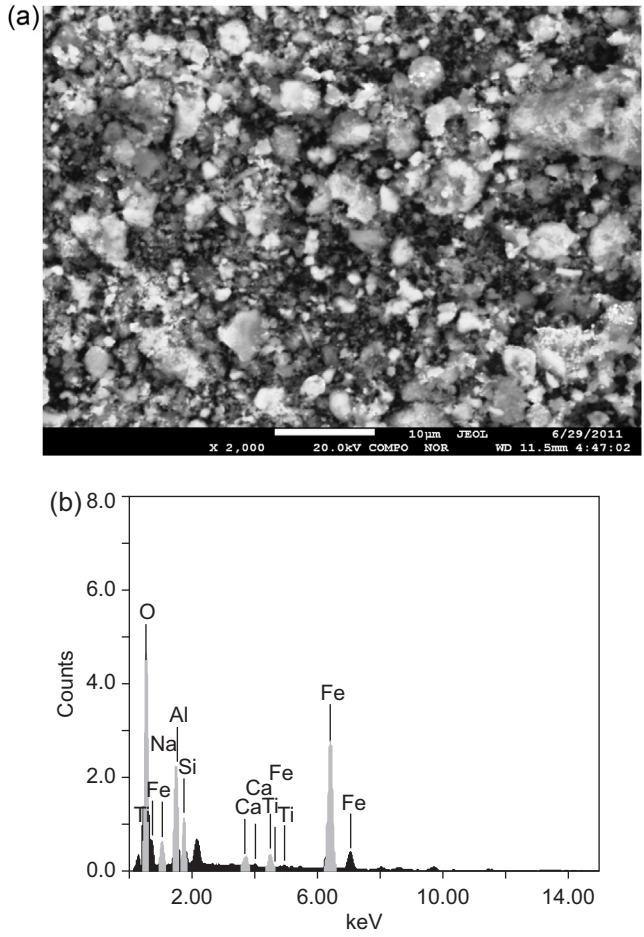

Figure 14.5 (a) SEM micrograph of red mud geopolymer with NaOH activator. (b) EDS analysis of red mud geopolymer showing the presence of elements.

3 days. Further, scanning electron microscopy−energy dispersive X-ray spectroscopy (SEM-EDS) analysis was carried out for the red mud geopolymer samples prepared with NaOH solution; the micrographs and EDS plot are given in Figure 14.5(a) and (b), respectively. No major gel-type morphology was detected. The microstructure contained many pores and most of the grains are showing a diffused boundary. The spherical grain belongs to the iron-rich phase haematite. Bulk EDS analysis (Figure 14.5(b)) shows that the main elements are Fe, Al, Si and Na, along with minor amounts of Ti and Ca. Based on calorimetric results, compressive strength observations and SEM-EDS analysis, the following possible reasons can be given for not using red mud alone for geopolymerization:

1. X-ray diffraction (XRD) results (Figure 14.3) indicated that SiO_2 was in the form of quartz, which has no solubility in alkaline solution.

2. Due to aqueous conditions in the red mud pond, the aluminosilicate fractions, which reacted under alkali conditions, formed a very dilute gel phase that was not giving any binding properties.
3. The amount of reactive SiO_2 and Al_2O_3 was not adequate to form the network structure that could hold the materials with relatively lower or no reactivity, such as Fe_2O_3 and TiO_2.
4. The diffused boundary of grains is possibly due to the presence of NaOH solution, which altered the surface by reacting with it, but the gel formation was not enough to hold the structure.

14.4 Synergy of red mud with other waste

As we have seen that only red mud has limited potential for geopolymerization, it is often used with a reactive material. The two most commonly used materials are metakaolin and fly ash. From the resource conservation and waste utilization point of view, fly ash is the most desirable material for blending. Further, many aluminum plants have captive coal-based power plants where fly ash is generated. This makes for a synergy of red mud and fly ash, as no or very low transportation of waste material is involved.

14.4.1 Isothermal conduction calorimetric studies

To understand the co-geopolymerization behavior of red mud and fly ash, isothermal conduction calorimetric studies have been carried out using different combinations. High-silica red mud from ALCOA, Australia and fly ash from Tata Power, India have been used in all subsequent studies. Two types of samples have been prepared: one with 20% red mud and 80% fly ash (FARM20) and the other with 40% red mud

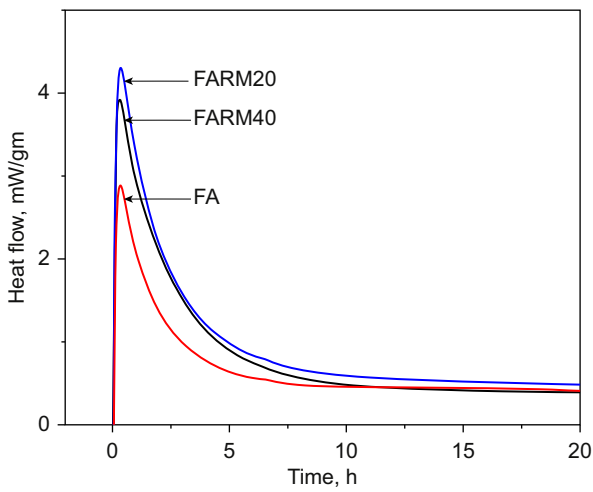

Figure 14.6 Isothermal conduction calorimetric curve of red mud-based geopolymer at ambient temperature (27 °C).

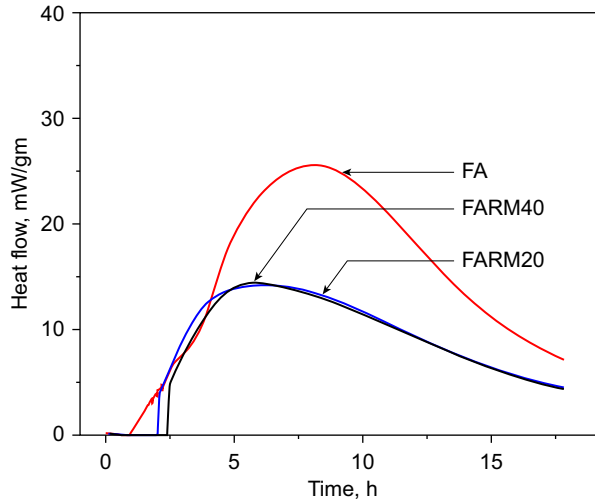

Figure 14.7 Isothermal conduction calorimetric curve of red mud-based geopolymer at elevated temperature (60 °C).

and 60% fly ash (FARM40). Only fly ash was used as reference. Figure 14.6 shows the heat evolution curve obtained by isothermal conduction calorimetry of the samples at 27 °C for 24 h. In all the samples, only one peak was observed. As there was no major peak shift or change in peak behavior, the reaction mechanism was believed to be broadly similar in all samples. The peak intensity of red mud-containing samples was more than the fly ash sample. Interestingly the intensity was more when 20% red mud was used and decreased slightly when 40% red mud was used. The change in peak intensity with addition of red mud can be attributed to change in dissolution

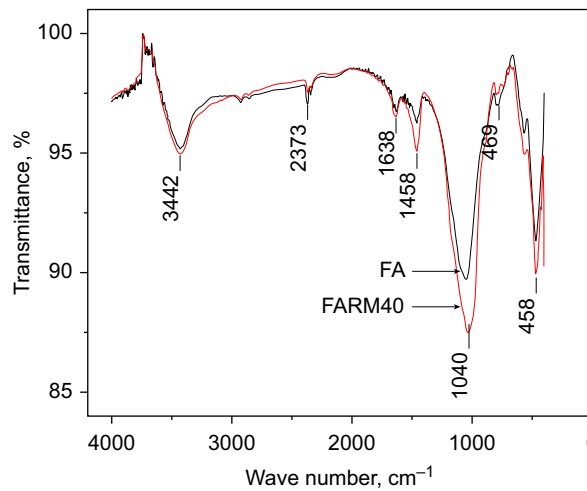

Figure 14.8 FTIR spectra of red mud-based geopolymer.

behavior due to addition of Al_2O_3, SiO_2 and CaO derived from red mud. However, the calorimetric peak obtained at 60 °C has shown a different trend (Figure 14.7). Samples with only fly ash have shown the higher peak intensity, whereas samples with red mud have shown lower peak intensity. This can be explained with the help of the SiO_2/Al_2O_3 ratio, which decreased from 2.14 in fly ash to 2.12 in FARM20 and 2.08 in FARM40. Furthermore, the loading of iron oxide also increased from 4.52 to 9.91 to 15.31 wt% in the same order. Based on the calorimetric peak at both the temperatures, it can be observed that red mud addition influenced the ambient temperature reactions such as dissolution and precipitation; however, at 60 °C red mud behaved as a less reactive constituent than fly ash.

14.4.2 Fourier transform infrared spectroscopy

Figure 14.8 shows the Fourier transform infrared spectroscopy (FTIR) spectra of FARM40 samples. The spectrum of the fly ash sample was taken as reference. The positions of the absorption bands were nearly similar in both cases, but relative intensity was greater in FARM40. The broad band at ∼3442/cm and a weak peak at ∼1638/cm is due to the stretching vibrations of O−H bonds and H−O−H bending vibrations of interlayer adsorbed H_2O molecules, respectively. The change in intensity of these peaks can be attributed to the presence of structural water in red mud (Armstrong & Dann, 2000; Gok, Omastova, & Proke, 2007). The band near 1638/cm can be ascribed to the water molecules occluded inside the aluminosilicate structure (Gok et al., 2007; Linares, Sanchez, Urbina de Navarro, Rodrıguez, & Goldwasser, 2005). The absorption bands at ∼1458/cm corresponding to stretching vibrations of C = O confirmed the presence of carbonate groups (Huang & Kerr, 1960; Yip, Lukey, Provis, & Van-Deventer, 2008). Characteristic bands corresponding to Si−O vibration were detected at ∼1040/cm (Farmer, 1974). Peaks at ∼569/cm and ∼458/cm were

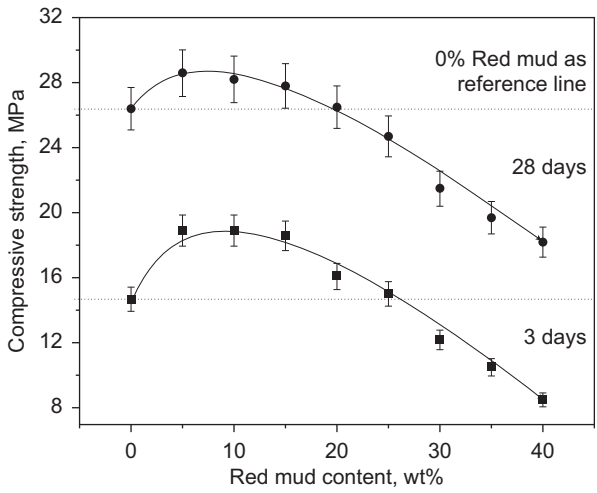

Figure 14.9 Variation in compressive strength of geopolymer with respect to red mud content.

due to bending vibration of Si−O−Al and stretching vibrations of Fe−O bonds, respectively (Farmer, 1974; Gadsden, 1975). Increased intensities of these peaks in FARM40 confirmed the enhanced dissolution of silicate minerals.

14.4.3 Mechanical properties

Figure 14.9 shows the variation in compressive strength with respect to red mud addition. The compressive strength of geopolymer containing 5%, 10%, 15%, 20%, 25%, 30%, 35% and 40% red mud has been tested after 3 and 28 days using an automatic compression testing machine (AIMIL, India). The fly ash sample has been used as reference. It is very interesting to note that the compressive strength increased when red mud in the range of 5−15% was added. Afterwards, it started decreasing. At up to 20% replacement of fly ash by red mud, the compressive strength was more than or equal to the fly ash-based geopolymer used as reference. This trend was similar in both 3 day and 28 day strength.

14.4.4 Microstructural characterization

As was discussed in our earlier studies, the microstructure consists of partially reacted cenosphere from fly ash, platy structure corresponding to N-A-S-H gel and microspheres of haematite (Kumar & Kumar, 2013). Elemental mapping of red mud-based geopolymer and red mud and fly ash mixture-based geopolymer treated at 60 °C has been carried out using a JEOL JXA-8230F electron probe microanalyzer (EPMA) at 15 KV, 50 nA. The elements that have been mapped are Fe, Al, Si, Ca, Na and Ti (Figure 14.10(a) and (b)). An average of 10 measurements was taken for each set of mapping. To understand the relation between various elements, the photographs were superimposed. In the case of red mud geopolymer it was observed that the majority of the elements are independent of each other, whereas in the case of red mud fly ash mixture-based geopolymer it was observed that Al, Si and Na are overlapping. This gives an indication that reaction has taken place and has resulted in formation of A-S-H gel ($A = Al_2O_3$, $S = SiO_2$, $H = H_2O$). This observation was supported by the EDS analysis of the gel. Some Fe was also observed overlapping with Al, Si and Na, which might be due to the formation of ferrosialate, where Fe substituted Al in the structure.

14.5 Production of masonry blocks

Based on the scientific understanding, masonry block has been produced at pilot scale using the FARM20 and FARM40 composition. The alkaline activator used was 6 M NaOH solution and Na_2SiO_3 in a 1:1 ratio. The rationale for using Na_2SiO_3 was to gain sufficient compressive strength during the green handling stage. Because during the drying, fine cracks were appearing due to the very fine particle size of red mud and fly ash, river sand was added as filler. The samples

were produced using the process flow diagram shown in Figure 14.11. The following procedure was used:

1. Red mud and fly ash were dry mixed in a planetary mixer for 3 min followed by mixing with alkali solution for another 3 min. After uniform mixing was achieved, river sand was added and mixed for another 2 min.

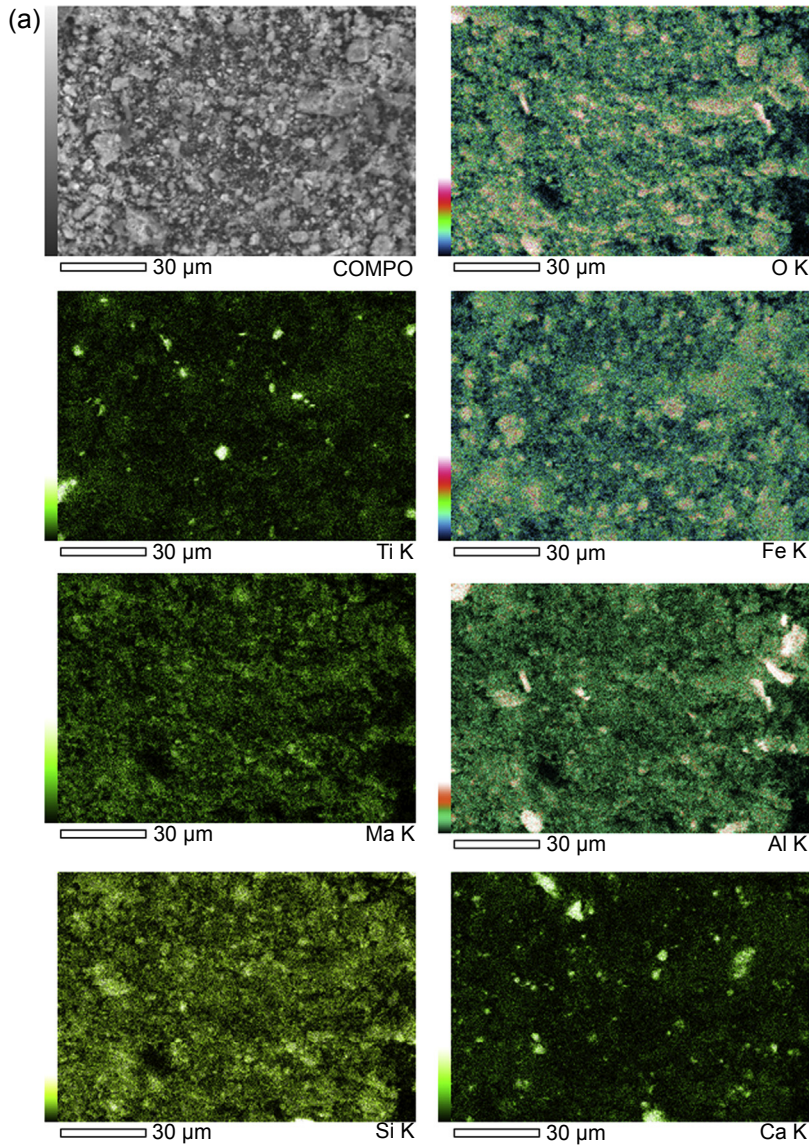

Figure 14.10 (a) Elemental mapping by EPMA of only red mud geopolymer. (b) Elemental mapping by EPMA of only FARM40 geopolymer.

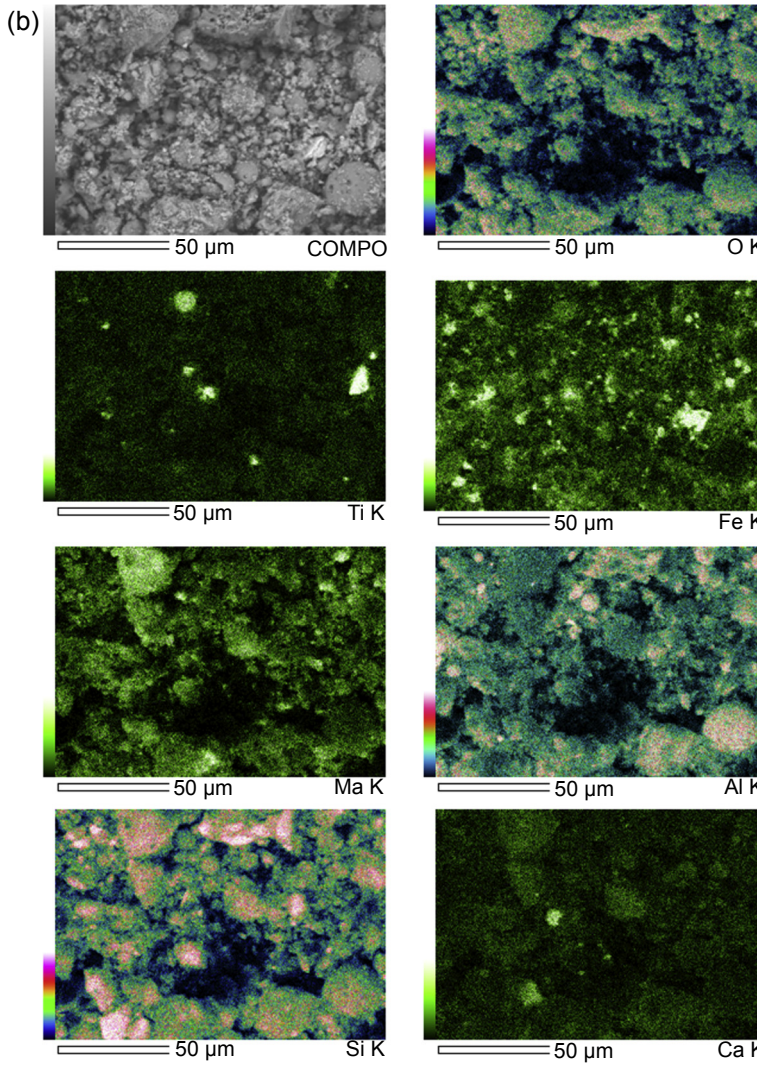

Figure 14.10 Continued.

2. The mixture was discharged onto a conveyer belt through a pneumatically operated discharge gate. Then it was transferred to a feeding hopper. From the hopper, it was fed to the mold, vibrated for 10 s and then hydraulically pressed using a 100 kg/cm^2 load. After compaction, the masonry blocks were discharged onto a pallet and then transferred to the curing chamber.
3. Curing was done at ambient temperature in closed conditions to retain the moisture. After curing, the samples were subjected to various tests.
4. The physical properties of the paving blocks were tested as per IS 15658 specifications; the results are summarized in Table 14.2.

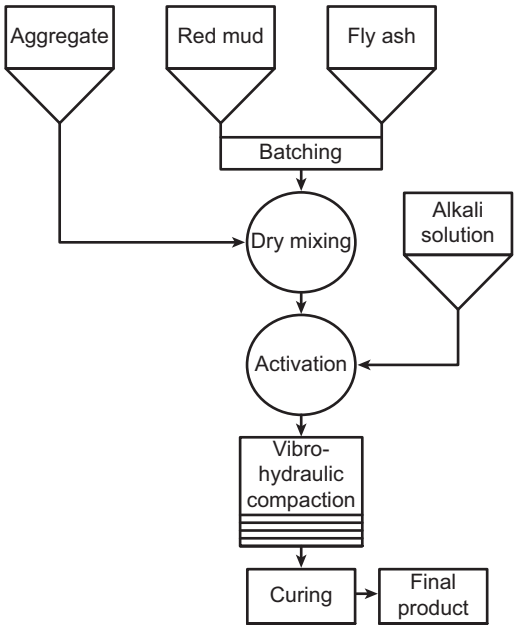

Figure 14.11 Process flow sheet adopted at pilot-scale production of masonry block.

Table 14.2 Properties of masonry block and its compliance with IS specification

Sl. No	Property	IS 15658: 2006 Specification	FARM20	FARM40
Obligatory requirements				
1	Visual inspection	95% free from visual defects	95% free from visual defects	95% free from visual defects
2	Size tolerance, mm (L + W)	±2	±1	±1
3	Water absorption, %	7	7	7
4	Compressive strength, N/mm^2	30	>30	>25
Optional requirements				
5	Tensile splitting strength, MPa	No spec	>2.1	>2.0
6	Flexural strength, MPa	3	>3.2	>2.8
7	Abrasion resistance, mm	2	0.78	1.22

From Table 14.2, it can be seen that the block prepared from FARM20 was equivalent to M30 grade concrete, whereas the one prepared from FARM40 was equivalent to M25 grade concrete. All other properties conformed to IS 15658 standard specification.

14.5.1 Durability behavior

Calcium-rich cements such as Portland cement and alkali-activated slag are generally prone to acid attack as the hydration products CSH and CH are quickly dissolved,

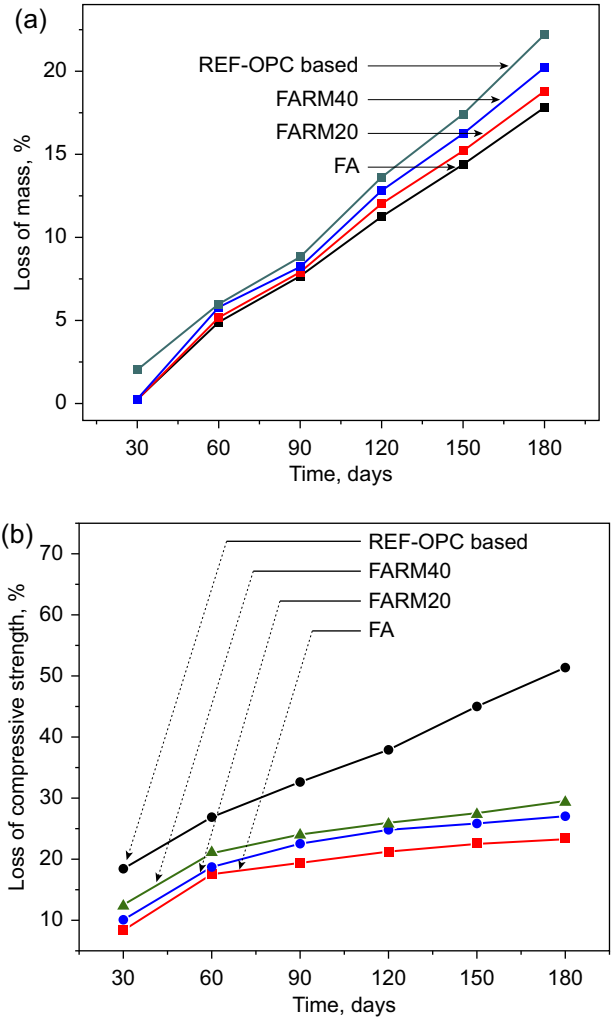

Figure 14.12 (a) Loss in mass of geopolymer samples with respect to time. (b) Loss in compressive strength of geopolymer samples with time.

Table 14.3 TCLP test results of masonry blocks

Elements	USEPA, ppm	FARM20, ppm	FARM40, ppm
Toxic metals			
Hg	5.0	Not found	Not found
Ag	5.0	Not found	Not found
Cd	1.0	0.030	0.055
Cr	5.0	Not found	Not found
Se	1.0	0.114	0.194
As	5.0	Not found	Not found
Ba	100.0	Not found	Not found
Pb	5.0	0.018	0.030
Nontoxic metals			
Al	No spec.	2.92	4.10
Fe	No spec.	6.44	10.68

leaving a skeleton of silica and gypsum, as per the following equation (Neville, 1995):

$$H_2SO_4 + Ca(OH)_2 \rightarrow CaSO_4 + 2H_2O \tag{5.1}$$

$$H_2SO_4 + C-S-H \rightarrow CaSO_4 + SiO_2 \tag{5.2}$$

Durability behavior of fly ash, FARM20 and FARM40 geopolymers was studied using test samples of size 75 mm diameter × 75 mm long. A Portland cement-based masonry block was also prepared to use as reference sample. The samples were exposed to 2% sulfuric acid solution for up to 180 days. The physical condition and change in mass were observed at periodic intervals while the loss in compressive strength was measured at monthly intervals. Figure 14.12(a) shows the loss in mass of geopolymer samples with respect to time. The mass loss in fly ash, FARM20 and FARM40 was comparable up to 30 days. After 30 days, a clear trend was observed between increase in mass loss and increase in red mud percentage. However, the mass loss was significantly lower than in the Portland cement-based reference material. A similar trend was observed in loss of compressive strength with time (Figure 14.12(b)). Fly ash samples showed minimum strength loss, followed by FARM20 and FARM40 samples. The improved durability of red mud geopolymer in comparison to Portland cement-based geopolymer can be ascribed to its aluminosilicate composition with low amount of CaO (<4%). The decrease in acid resistance with increase in red mud content can be explained by taking into consideration the behavior of iron oxide, which is more soluble in acidic regions (Wagh & Douse,

1991). However the strength and mass loss was not very high. Some of the Fe ions replaced the Al ions in the structure, and thus could not undergo dissolution even in the acidic environment.

14.5.2 Environment suitability

Although red mud does not fall under hazardous waste, it is always under the scanner for environment compatibility due to various hazards encountered in the recent past. Toxicity characteristic leaching procedure (TCLP) has been carried out as per USEPA 1311 process to evaluate the leachability behavior of red mud containing geopolymer and the results are given in Table 14.3. Results showed that leaching of toxic metals are either negligible or within permissible limit. In addition leaching of two major non-toxic elements Fe and Al has also been tested and found to be very low.

14.6 Summary and conclusions

Red mud fly ash mixture seems to be most suitable feedstock for geopolymer masonry blocks, as it not only results in good properties but also looks commercially attractive. In addition, both of these components are by-products, and in many cases fly ash is available from the captive power plant of alumina industry. It is interesting to note that red mud alone does not show good reactivity with alkali solutions and does not develop compressive strength, but it has shown good properties when used with fly ash. The reason for improvement in compressive strength in red mud geopolymer can be explained by the help of mineral phases present in both red mud and fly ash. From the red mud, the main reactive phases were alumina, sodium hydroxide, sodium aluminate and part of the iron hydroxide. From fly ash the reactive fractions of silica and alumina participated in the reaction. The main crystalline phases (haematite and calcite in red mud and quartz and mullite in fly ash) acted as filler material. The development in strength was influenced by both physical processes, such as particle shape, size and packing, and chemical process like gel formation, interfacial bonding between gel and filler, Si/Al ratio, Na/Si ratio and formation of ferrosialate. The pilot-scale production of red mud masonry block by geopolymerization depicts its potential for upscaling. Further, the durability and leachability studies let us know about its good long-term performance and environmental stability. The following conclusions can be drawn from the study:

1. Red mud has the potential to be used as one of the raw materials for geopolymer synthesis. The combination of red mud and fly ash gives properties that are suitable for masonry blocks.
2. Masonry blocks using 20–40% red mud have been developed that meet IS 15658 specifications. Blocks with 20% and 40% red mud have shown compressive strength equivalent to M35 and M25 grade concrete, respectively.
3. The masonry blocks meet USEPA 1311 specifications and are environmentally safe.
4. These blocks have potential for upscaling.

Acknowledgment

The authors are grateful to Dr S. Srikanth, Director, CSIR-National Metallurgical Laboratory, Jamshedpur, India for his kind permission to publish the paper. The red mud used in the study was received from ALCOA, Australia and NALCO, India and fly ash was received from Tata Power, India and is gratefully acknowledged.

References

Armstrong, J. A., & Dann, S. E. (2000). Investigation of zeolite scales formed in the Bayer process. *Microporous and Mesoporous Materials, 41*, 89−97.

Balomenos, E., Gianopoulou, I., Panias, D., Paspaliaris, I., Perry, K., & Boufounos, D. (2011). Efficient and complete exploitation of the bauxite residue (red mud) produced in the Bayer process. In *Proceedings of efficient and complete exploitation of the bauxite residue (EMC), Greece*.

Cundi, W., Hirano, Y., Terai, T., Vallepu, R., Mikuni, A., & Ikeda, K. (2005). Preparation of geopolymeric monoliths from red mud−PFBC ash fillers at ambient temperature. In J. Davidovits (Ed.), *Proceedings of 4th world congress on geopolymer. France* (pp. 85−87).

Davidovits, J. (1989). Geopolymers and geopolymeric materials. *Journal of Thermal Analysis and Calorimetry, 35*, 429−441.

Davidovits, J., Davidovits, M., Davidovits, F., & Davidovits, R. (2012). *Geopolymer cement of the calcium ferroaluminosilicate polymer type and production process*, Patent No. EP 2632870A0 published under World Intellectual Property Organization under number WO/2012/056125.

Dimas, D. D., Giannopoulou, I. P., & Panias, D. (2009). Utilization of alumina red mud for synthesis of inorganic polymeric materials. *Mineral Processing and Extractive Metallurgy Review, 30*, 211−239.

Farmer, V. C. (1974). *The infrared spectra of minerals*. London: Mineralogical Society.

Gadsden, J. A. (1975). *Infrared spectra of minerals and related inorganic compounds*. London: Butterworths.

Gok, A., Omastova, M., & Proke, J. (2007). Synthesis and characterization of red mud/polyaniline composites: electrical properties and thermal stability. *European Polymer Journal, 43*, 2471−2480.

Hajjaji, W., Andrejkovičova, S., Zanelli, C., Alshaaer, M., Dondi, M., Labrincha, J. A., et al. (2013). Composition and technological properties of geopolymers based on metakaolin and red mud. *Materials and Design, 52*, 648−654.

Statistics on the website of International Aluminium Institute (2014). http://www.world-aluminium.org.

Huang, C. K., & Kerr, P. F. (1960). Infrared study of the carbonate minerals. *American Mineralogist, 45*(2), 311−324.

Kalkan, E. (2006). Utilization of red mud as a stabilization material for the preparation of clay liners. *Engineering Geologist, 87*(3−4), 220−229.

Kawas, T. (2006). Use of boron waste as fluxing agent in the production of red mud bricks. *Building and Environment, 41*(12), 1779−1783.

Kumar, A., & Kumar, S. (2013). Development of paving blocks from synergistic use of red mud and fly ash using geopolymerization. *Construction and Building Materials, 38*, 865−871.

Kumar, S., & Kumar, R. (2011). Mechanical activation of fly ash: effect on reaction, structure and properties of resulting geopolymer. *Ceramics International, 37*, 533−541.

Kumar, S., Kumar, R., & Mehrotra, S. P. (2010). Influence of granulated blast furnace slag on the reaction, structure and properties of fly ash based geopolymer. *Journal of Material Science, 45*, 607−615.

Kumar, S., Kumar, R., Alex, T. C., & Bandopadhyay, A. (2006). Innovative methodologies for the utilisation of wastes from metallurgical and allied industries. *Resource Conservation Recycling, 48*, 301−314.

Linares, C. F., Sanchez, S., Urbina de Navarro, C., Rodrıguez, K., & Goldwasser, M. R. (2005). Study of cancrinite-type zeolites as possible antiacid agents. *Microporous and Mesoporous Materials, 77*, 215−221.

Marabini, A. M., Plescia, P., Maccari, D., Burragato, F., & Pelino, M. (1998). New materials from industrial and mining wastes: glass-ceramics and glass and rock-wool fibre. *International Journal of Mineral Processing, 53*, 121−134.

Neville, A. M. (1995). *Properties of concrete*. UK: Prentice Hall.

Piga, F. P., & Stoppa, L. (1993). Recovering metals from red mud generated during alumina production. *JOM, 45*(11), 55−59.

Senff, L., Hotza, D., & Labrincha, J. A. (2011). Effect of red mud addition on the rheological behaviour and on hardened state characteristics of cement mortars. *Construction and Building Materials, 25*(1), 163−167.

Singh, M., Upadhayay, S. N., & Prasad, P. M. (1996). Preparation of special cements from red mud. *Waste Management, 16*(8), 665−670.

Singh, M., Upadhayay, S. N., & Prasad, P. M. (1997). Preparation of iron rich cements using red mud. *Cement and Concrete Research, 27*, 1037−1046.

Tsakiridis, P. E., Agatzini-Leonardou, S., & Oustadakis, P. (2004). Red mud addition in the raw meal for the production of Portland cement clinker. *Journal of Hazardous Materials, 116*(1−2), 103−108.

Wagh, A. S., & Douse, V. E. (1991). Silicate bonded unsintered ceramics of Bayer process waste. *Journal of Materials Research, 6*, 1094−1102.

World Aluminium. (2013). *Report on bauxite residue management: Best practice by European aluminum association*.

Xiaoming, L., & Zhang, N. (2011). *Waste Management Research, 29*, 1053. http://dx.doi.org/10.1177/0734242X11407653.

Xu, H., & Van-Deventer, J. S. J. (2000). The geopolymerisation of aluminosilicate materials. *International Journal of Mineral Processing, 59*, 247−266.

Yalcin, N., & Sevinc, V. (2000). Utilization of bauxite waste in ceramic glazes. *Ceramics International, 26*, 485−493.

Yang, J., & Xiao, B. (2008). Development of unsintered construction materials from red mud wastes produced in the sintering alumina process. *Construction and Building Materials, 22*(12), 2299−2307.

Yang, J., Zhang, D., Hou, J., He, B., & Xiao, B. (2008). Preparation of glass ceramics from red mud in the aluminium industries. *Ceramic International, 34*(1), 125−129.

Yip, C. K., Lukey, G. C., Provis, J. L., & Van-Deventer, J. S. J. (2008). Carbonate mineral addition to metakaolin-based geopolymers. *Cement Concrete Composite, 30*(10), 979−985.

Zhang, G., He, J., & Gambrel, R. P. (2010). Synthesis, characterization, and mechanical properties of red mud based geopolymers. *Transportation Research Record: Journal of the Transportation Research Board, 2167*, 1−9.

Design and properties of fly ash, ground granulated blast furnace slag, silica fume and metakaolin geopolymeric based masonry blocks

15

Radhakrishna
R V College of Engineering, Bangalore, India

15.1 Introduction

Geopolymer is the name given to a wide range of alkali or silicate-activated aluminosilicate binders. Since the chemical reaction that takes place in this case is a polymerization process, Davidovits (1994, p. 9, 1999) coined the term 'geopolymer' to represent these binders. The dominant aluminosilicates are class F fly ash and ground granulated blast furnace slab (GGBS).

Provis (2014) reports that the chemistry of low calcium ("geopolymer") and high calcium (blast furnace slag-derived) alkali-activated material differ from each other. He also reports that the underlying mechanisms of degradation in such materials may not be always the same for alkali-activated binders as for Portland cement-based binders. According to Chao, Sun, & Longtu (2010), there are two main models of alkali-activated cements. They are activation of slag and metakaolin. In the first case of alkali activation of GGBS, the Si + Ca system dominates. In the second case of a geopolymer made with metakaolin and fly ash, Si + Al dominate. The main drawback in this case is a very high water requirement, which in turn causes difficulties related to drying shrinkage and cracking of the material.

Geopolymer composites have a very small greenhouse footprint when compared to traditional cement composites. The study by Shi & Fernandez-Jiménez (2006) concludes that alkali-activated cements are a better matrix for solidification/stabilization of hazardous and radioactive wastes than ordinary Portland cement. Geopolymer concrete possesses excellent similar strength and appearance similar to conventional concrete made from Portland cement (Hardjito, Wallah, Sumajouw, & Rangan, 2004). It is also well-known that geopolymers possess excellent mechanical properties, fire resistance and acid resistance (Davidovits & Davidovits, 1988; Palomo, Macias, Blanco, & Puertas, 1992).

The choice of the source materials for making geopolymers depends on availability, cost, type of application, etc. Studies by Zhao, Ni, Wang, and Liu (2007) have confirmed the formation of mainly ettringite and calcium silicate hydrate gel in the

Eco-efficient Masonry Bricks and Blocks. http://dx.doi.org/10.1016/B978-1-78242-305-8.00015-2

activation of GGBS and class F fly ash pastes. According to Astutiningsih & Liu (2005), the strength of alkali-activated slag decreases as the water content increases.

According to Montes, Islam, Shi, Kupwade-Patil, & Allouche (2013), the materials prepared by geopolymerization of fly ash and GGBS offer considerable resistance to freeze-thaw action, sulfate attack, sulfuric acid attack and nitric acid attack compared to Portland cement products. Sakkas, Nomikos, Sofianos, & Panias (2014) report that the sodium-based geopolymer from slag would be an appropriate material for passive fire protection systems. In the absence of long-term durability of geopolymers, comparable in scale and longevity to Portland cement, well-established testing methods and research are essential to validate the laboratory trials. Van Deventer, Provis, & Duxson (2012) are of the opinion that colloid and interface science, gel chemistry, phase formation, reaction kinetics, transport phenomena, communication, particle packing and rheology play a salient role in the development of geopolymer technology.

A report by Dahmen & Muñoz (2014) indicates that geopolymerization of abundant minerals such as aluminosilicates has the capacity to radically transform traditional cement-based masonry products on a global scale.

It is possible to tailor the geopolymer material to attain the required strength and durability to optimize the cost. Given the correct mix design and formulation development, geopolymeric materials derived from fly ash and GGBS can exhibit superior chemical and mechanical properties over those of OPC composites. But no literature is reported so far about the logical mix proportioning of the geopolymer mix except those of Rangan (2008a, 2008b). Trial mix is essential for exact proportions of the concrete mix. As geopolymers are highly complex and yet relatively poorly understood, there are clearly many areas in which further work is required (Duxson, Provis, Lukey, & Van deventer, 2007). There are attempts to develop phenomenological models to reproportion geopolymer mortar and concrete (Radhakrishna, Madhava, Manjunath, & Venugopal, 2013; Radhakrishna & Udayashankar, 2008; Radhakrishna, Udayashankar, & Renuka Devi, 2010). Such models were reported for fly ash, as well as lime-based masonry blocks (Radhakrishna & Niranjan, 2013).

The vast majority of research conducted in the field of geopolymers has to date focused on manipulation of engineering properties, short-term durability and waste immobilization efficacy. The objective of this chapter is therefore to remedy this situation by developing methods to reproportion the geopolymer mortar under the framework of scientific laws rather than simply by empirical mix formulation. The possibility of developing phenomenological models to take care of this situation merits examination. Methods of accounting different parameters involved in strength development of fly ash and GGBS-based thermal cured/ambient cured geopolymer masonry blocks is the major outcome of this chapter.

15.2 Characteristics of geopolymer mortar

To get the maximum dry density and optimum moisture content, Standard Proctor's compaction test was conducted on fresh geopolymer mortar. The fluid media to prepare the mortar was water and various alkaline solutions of different molarities for

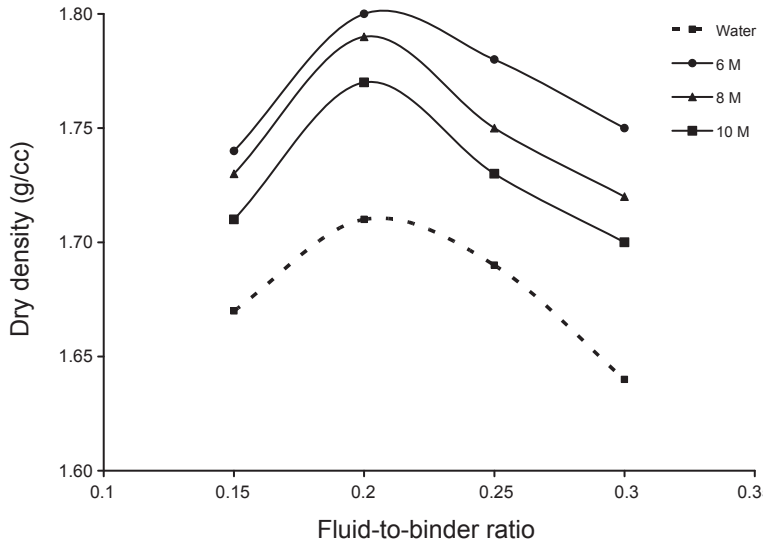

Figure 15.1 Variation of dry density of blocks with various molar solutions.

comparison. The variation of the dry density with fluid-to-binder (f/b) ratio is shown in Figure 15.1. As in any of the particulate material with the interaction of water, the dry density increases and then decreases. At f/b ratio of 0.2, the mix would attain maximum dry density for all the fluids. It can be seen that compaction characteristics would be marginally affected by the fluid medium.

The fresh geopolymer mortar sample having f/b ratio of less than 0.10 would be in a very dry powdery form. It would be very difficult to compress the material to get the block of required size and density. Even after casting with great difficulty, the samples would crack immediately after casting without any cohesiveness. In the range of 0.150−0.225 fluid-to-binder ratio the mixture was in the desired wet condition and interaction of the particles was homogeneous. At this range of f/b ratio, the mortar would be in a three-phase system with solids, liquid and air content. Casting of the geopolymer mortar specimens was possible at this range. However, compaction effort would be essential to cast the cylindrical specimens of mortar. Normally, in the range of 0.225−0.250 clusters would form in the mortar mix. At the f/b ratio of 0.250 and above, the mix attains full saturation resulting in a two-phase system with solids and liquid without any air content. It would not be possible to cast blocks in this system. However, the consistency of the mortar mainly depends on the combination of the materials along with the f/b ratio. A specially fabricated "static compaction device" was used to prepare cylindrical specimens to test in a laboratory.

15.3 Static compaction device

A static compaction device can be used to cast the compressed cylindrical blocks of geopolymer mortar at laboratory. This device can be fixed to a platform as shown in

Figure 15.2 Static compaction device.

Figure 15.2. The device essentially consists of a brass tubing of 38 mm internal diameter and 240 mm in length. Both the ends of the cylinder would be threaded to fit cylinder caps. These caps are machined to have suitable length of external bosses. Two piston rods of 25 mm diameter work from both ends in the bosses provided in the cylinder covers. The diameter of the piston rod governs the structural strength and the external bosses of the cylinder caps offer lateral rigidity to the piston rod. A number of threads per unit length of the piston rod control the sensitivity of the device. The position of the locknuts on the piston rods controls the final length of the sample to 76 mm. The piston head with a sliding fit in the cylinder is mounted on the ball bearing rigidly fixed to the piston rod. This prevents the rotational motion of the piston rod being transferred to the material. The compacted sample can be removed by using "sample extruder". This device provides an easy way of casting geopolymer mortar compressed blocks by manual operation.

A sample cylinder prepared using a static compaction device is shown in Figure 15.3. The ratio of height-to-diameter was maintained at 2. This type of cylindrical specimen was used for the laboratory study. However, the compressive strength was also correlated with the actual masonry block/brick used in practice.

15.4 Strength development with degree of saturation

The blocks with a constant density were cured at a temperature of 60 °C and above normally for 24 h (Radakrishna et al., 2013). The samples were left in open air after thermal curing. The variation of the unconfined compressive strength of the cylinders is shown in Figure 15.4 for three different ages. It can be noticed that the strength

Figure 15.3 Geopolymer mortar cylinders.

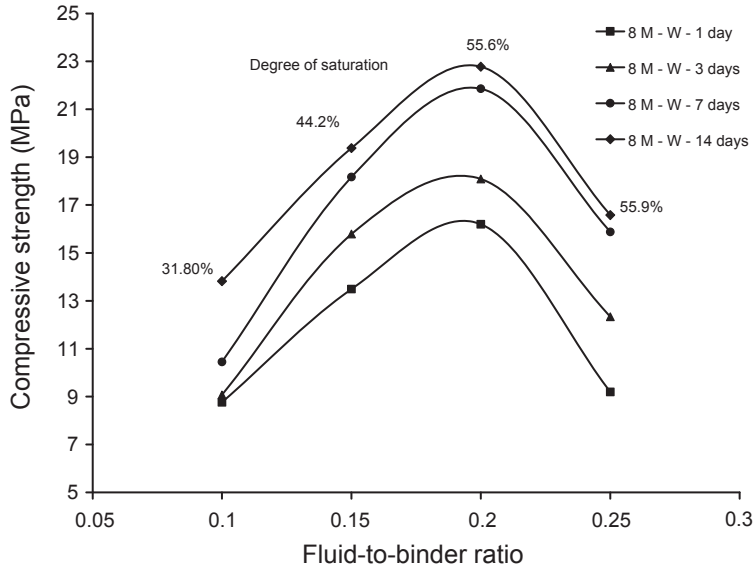

Figure 15.4 Compressive strength variation at constant density.

increases with f/b ratio and then decreases. This contradicts the trend of strength development according to Abrams' law (1918), p. 20.

In the case of cement mortar/concrete, strength decreases as the air content increases at saturated condition. In the case of partially saturated compressed mortar cylinders, the degrees of saturation at various dry density values were calculated and indicated in Figure 15.4. In the case of a partially saturated system, the material would be in a three-phase system – solids, liquid and air. Based on this system, to calculate the degree of saturation, the following basic relation of soil mechanics (Eqn (15.1)) was used.

$$\gamma = \left\{ \frac{\gamma_w G}{\left(1 + \frac{WG}{S_d}\right)} \right\} \tag{15.1}$$

where,

γ = Density in g/cc
γ_w = Density of water in g/cc
G = Specific gravity of the material used
W = Water content in percent
S_d = Degree of saturation in percent

From Eqn (15.1), it can observed that as the water content (W) increases, the degree of saturation (S_d) and air content in the mortar increases. For different f/b ratios, degree of saturation is shown in Figure 15.4. It can be seen that as the f/b increases the degree of saturation (air content) gradually increases. It can be seen that initially, as the f/b ratio increases from 0.10 to 0.20, strength increases (which is contrary to Abrams' Law). However from f/b ratio 0.20 to 0.25 (i.e. at more or less the same saturation level of 55.6% and 55.9%), the strength drops down as per Abrams' law. This suggests that when degree of saturation is maintained constant, the effects of f/b ratio get truly reflected in the strength development. Hence the study of strength development of compressed blocks at a constant degree of saturation can be made.

To maintain a constant degree of saturation (specified constant air content) in the compacted state, adjustment of dry density would be essential by varying water content using Eqn (15.1). If the water content (W) is known, the f/b ratio of the mortar can be calculated. This can be carried out by precalculations as is done in gravimetric and volumetric calculations in particulate material such as soils.

The proportioning of thermally cured and ambient cured geopolymer mortar is discussed in this chapter under two headings:

- Thermal cured geopolymer blocks
- Ambient cured geopolymer blocks

The masonry block used for the study is shown in Figure 15.5. The dimensions of the block are $200 \times 110 \times 60$ mm and cured either in an oven or in open air as indicated.

Figure 15.5 Masonry block used for the study.

15.5 Thermal cured geopolymer blocks

A typical series of geopolymer mortar blocks having constant binder-to-aggregate ratio and other parameters are shown in Table 15.1.

The various parameters considered for thermal cured compressed blocks include the following:

- Molarity of alkaline activator: 8, 10, 12, 14 M
- Age of the specimen: 1, 3 and 7 days
- Fine aggregate: Sand and quarry dust
- Curing conditions: in oven – wrapped and unwrapped

The compressive strength development in geopolymer mortar for various parameters is discussed in this section.

15.5.1 Strength variation at initial constant degree of saturation

From the laboratory trials, it can be observed that it is possible to cast the compressed blocks at the degree of saturation of 44% without any practical difficulties.

Table 15.1 Mix proportions of thermal cured geopolymer compressed blocks

Sl no	Series ID	Fine aggregate	Age (days)	Molarity	W/UW
1	10M-Sand-W-7 Days	Sand	7	10	W
2	10M-Sand-W-7 Days	Sand	7	10	W
3	10M-Sand-W-7 Days	Sand	7	10	W
4	10M-Sand-W-7 Days	Sand	7	10	W
5	12M-Sand-W-3 Days	Sand	3	12	W
6	12M-Sand-W-3 Days	Sand	3	12	W
7	12M-Sand-W-3 Days	Sand	3	12	W
8	12M-Sand-W-3 Days	Sand	3	12	W
9	14M-Sand-W-1 Day	Sand	1	14	W
10	14M-Sand-W-1 Day	Sand	1	14	W
11	14M-Sand-W-1 Day	Sand	1	14	W
12	14M-Sand-W-1 Day	Sand	1	14	W
13	14M-QD-W-7 Days	Quarry dust	7	14	W
14	14M-QD-W-7 Days	Quarry dust	7	14	W
15	14M-QD-W-7 Days	Quarry dust	7	14	W
16	14M-QD-W-7 Days	Quarry dust	7	14	W
17	14M-QD-UW-3 Days	Quarry dust	3	14	UW

M, molarity; QD, quarry dust; W, wrapped; UW, unwrapped.

This degree of saturation can be maintained constant for thermal cured blocks. In Figure 15.6 the strength variation is shown with f/b ratio at a constant degree of saturation of 44%. The molarities of the alkaline activator solutions were 6 and 8.

The strength development, particularly at a low f/b ratio, despite the degree of saturation being constant, did not reflect the strength levels as per Abrams' law. But distinctly, with an alkaline solution of molarity 10 the strength levels would be practically in tune with f/b ratios as shown in Figure 15.7. Owing to low molarity (concentration of alkaline salts) in a low f/b ratio (volume of fluid), the strength developed would be less. This is also another factor that influences strength development. With an increase in molarity, the concentration of alkaline salts would be adequate enough to push the strength levels to be in tune with Abrams' law as expected.

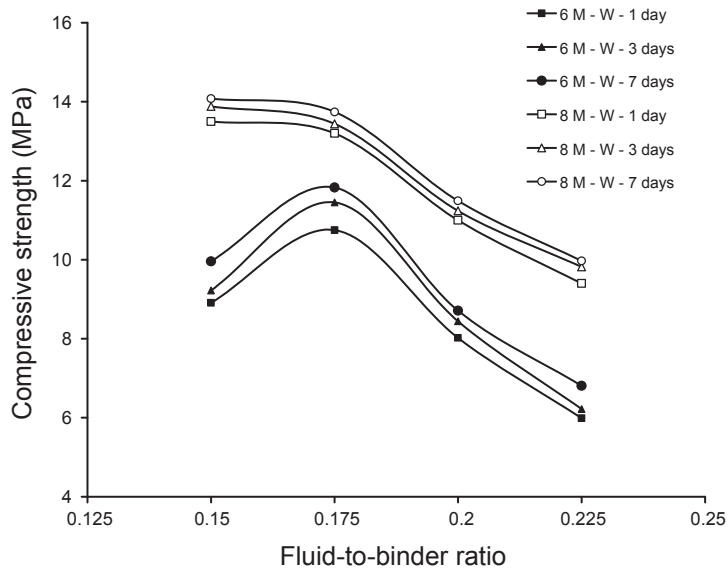

Figure 15.6 Compressive strength for the molarity of 6 and 8.

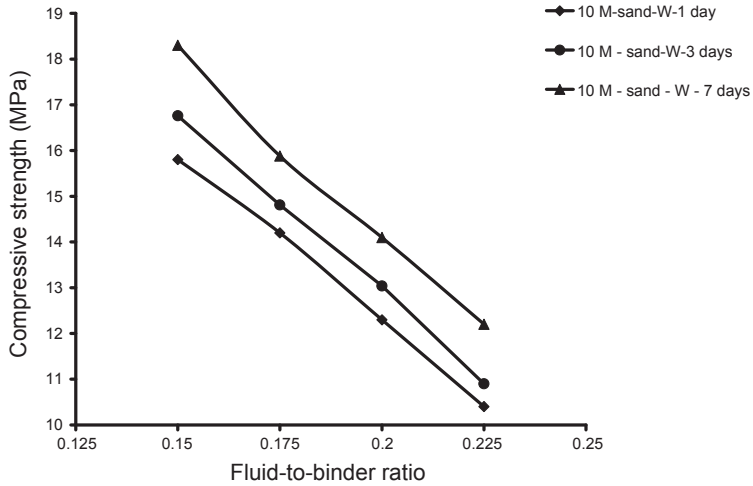

Figure 15.7 Compressive strength at a constant degree of saturation 44%.

Alkaline fluid of molarity of 10 and beyond with a constant degree of saturation could impart strength development in accordance with f/b ratios. Similar observations have been made by Chindaprasirt, Jaturapitakkul, Chalee, & Rattanasak (2009) for geopolymer concrete.

15.5.2 Effect of fine aggregate on strength

After identifying the role of degree of saturation, the influence of fine aggregate on strength development of fly ash-based geopolymer mortars merits examination. Apart from conventional fine aggregate (sand), the possibility of using other marginal aggregates need to be explored for sustainable development. The alternative fine aggregate quarry dust was also used. A typical variation of the compressive strength with f/b ratio is shown in Figure 15.8 for sand and quarry dust as fine aggregate for 14 M.

The strength development in the case of quarry dust as aggregate was marginally higher compared to natural river sand having the same fineness modulus. It can be noticed that the strength development with age would not be affected in any noticeable way with change of fine aggregate from sand to quarry dust. This is in order since both sand and quarry dust are noninteracting particulate materials with water. They are basically quartz with change in specific surface. Due to the fine size of particles in quarry dust, there would have been better particle packing in the mortar.

15.5.3 Strength development with/without loss of moisture

Fly ash-based geopolymer mortar blocks are normally cured in an oven at an elevated temperature. At a temperature of 60 °C, it can be realized that there would be a loss of moisture that would affect optimal strength development. The loss of moisture at low fluid content would be more crucial. This loss can be considerably prevented by wrapping them with aluminum foils. But from a practical viewpoint, this may not be desirable since the production of compressed blocks would be hampered. The purpose of this study was to assess the strength development in unwrapped and wrapped conditions. The compressed blocks were tightly wrapped in aluminum foil with the least air trapped in between them before keeping in the oven. The strength data of such samples after curing is shown in Figure 15.9.

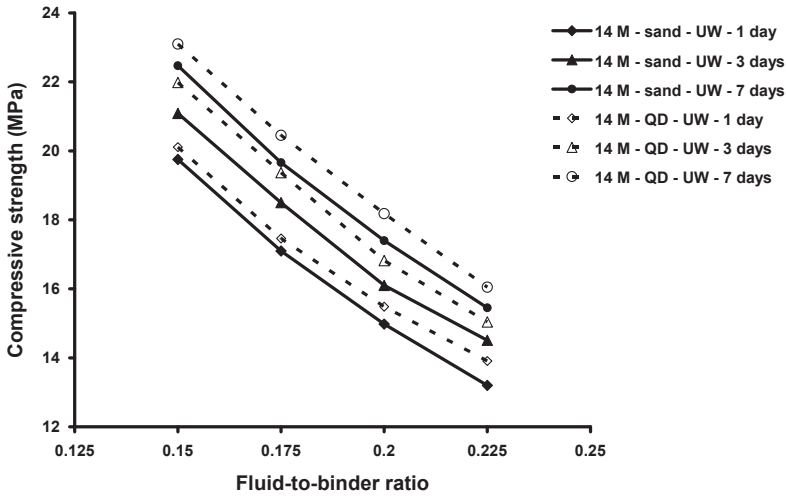

Figure 15.8 Variation of strength for sand and quarry dust as aggregate.

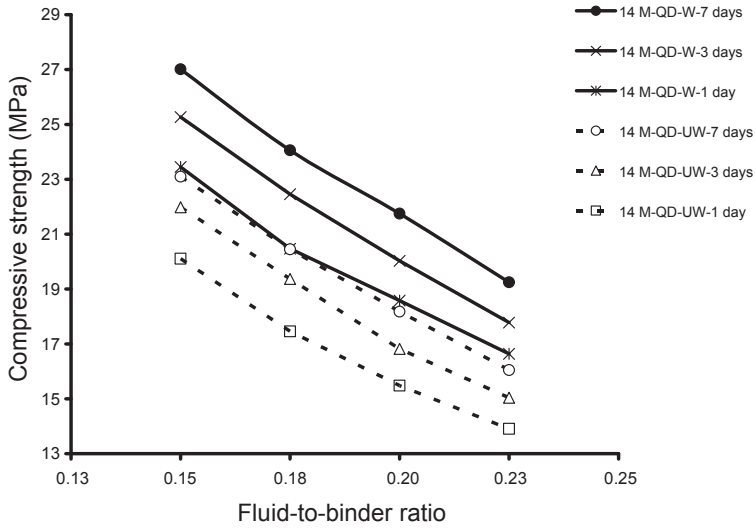

Figure 15.9 Effect of compressive strength for wrapping and unwrapping.

The comparison of data in Figure 15.9 indicates that owing to prevention of loss of moisture the strength developed would be higher. This increase can be seen at all ages to the extent of 20−25% and can be attributed to greater reaction of salts with fly ash to promote higher strength development.

The compressive strength with f/b ratio of all the series having a molarity of 10 and above is shown (all together) in Figure 15.10 at a constant degree of saturation of 44%. The compressive strength with binder-to-fluid (b/f) ratio is linear as shown all together in Figure 15.11.

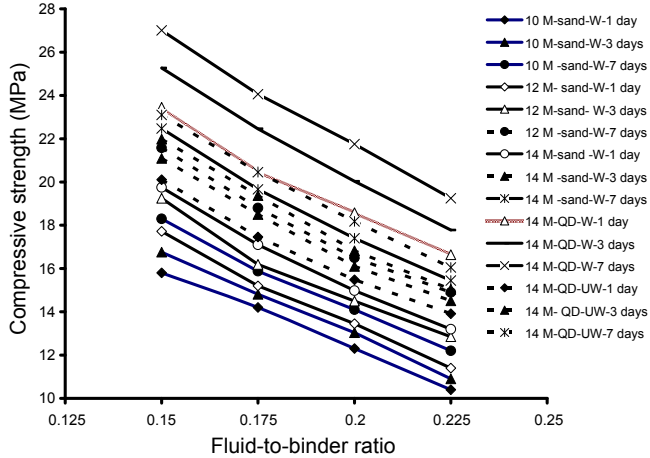

Figure 15.10 Strength variation with fluid-to-binder ratio.

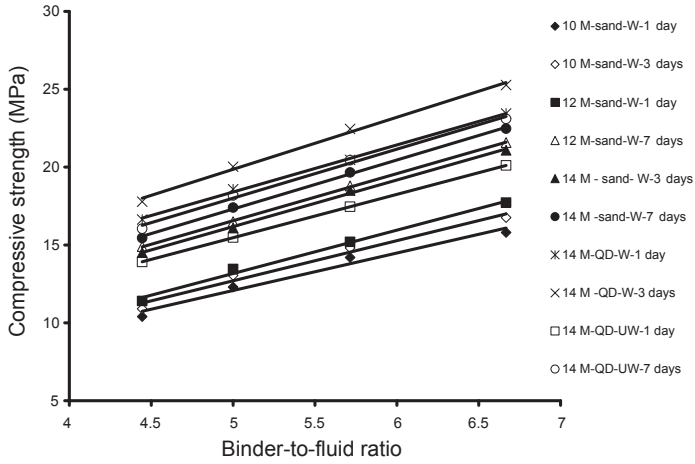

Figure 15.11 Strength development with binder-to-fluid ratio.

In summary, the analysis of all test results of thermal cured fly ash-based geopolymer mortar blocks shows that strength development would influence basically by f/b ratio. Unlike in a saturated (two-phase) system, degree of saturation was another variable parameter in compressed blocks, which has been maintained constant in all the series of experiments. The trend remains the same in all the cases. Similar trends can be seen in the case of cement compressed blocks as reported by Prasad, Narasimhulu, Nagaraj, Naidu, and Ifthakaruddin (2005).

15.5.4 Proportioning of geopolymers

Proportioning of geopolymer composites is scarcely reported in the open literature. The available literature focuses more on strength, durability and performance of geopolymer composites. Also, the research on partially saturated geopolymer mortar is rare. However, Radhakrishna et al. (2008) and Radhakrishna et al. (2010, 2013) have reported that heat-cured geopolymers can be reproportioned by generalized Abrams' (Abram, 1918, p. 20; Nagaraj & Banu, 1996, 1999) and Bolomey's laws (1927). As per the reported research, by using a single input parameter in the model, the b/f ratio for any other desired strength can be calculated using the phenomenological model.

15.5.5 Development of phenomenological model – thermal cured blocks

A rational, rapid and simple method to arrive at the combination of ingredients to realize a specific value of strength development at a required age is desirable. It is due to the following situations that may arise during handling of large volumes of waste materials.

1. The strength requirements and the age at which this is required vary depending upon end usage. As such, to arrive at the required f/b ratio, simple procedures are needed.
2. As the density, molarity of solution and curing conditions (thermal and ambient conditions) could vary, it is rather difficult to arrive at the required f/b ratio with minimum trials.
3. The batches of these materials may vary from time to time, which needs required control to recheck the mix proportions with minimum test data and computations.

In a wider context, if the method advanced has a rational basis it lends additional support and confidence to employ the same in practice.

In the case of OPC composites, water-to-cement ratio rules the strength development when other factors are kept constant (Nagaraj & Banu, 1996). In a similar manner, within the range of values of b/f ratio considered in this investigation inverse of f/b ratio of 0.2 (b/f ratio of 5.0) can be considered as a reference for normalization. This chosen value of b/f ratio of the compressed blocks is arbitrary. There is no other significance. The resulting functional relation by regression analysis is as shown in Eqn (15.2) and Figure 15.12 having R^2 value of 0.98. This is a phenomenological model for assessment of thermal cured geopolymer mortar blocks.

$$\left\{\frac{S}{S_{@b/f=5}}\right\} = 0.1833\left\{\frac{b}{f}\right\} + 0.0747 \tag{15.2}$$

where S is strength for which b/f ratio is to be calculated.

$S_{@b/f=5}$ is strength of mixture at f/b ratio of 0.2 (inverse = 5.0);
b/f is inverse of f/b ratio;
0.1833 and 0.0747 are constants.

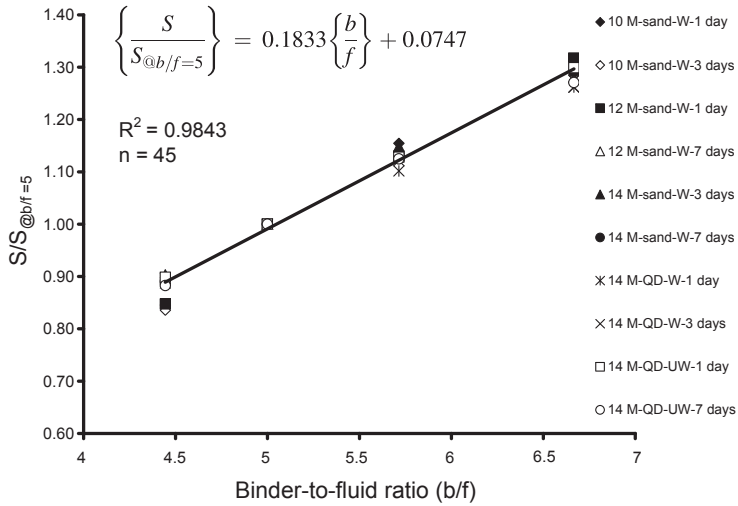

Figure 15.12 Graphical representation of the model (Eqn (15.2)).

15.5.6 Validation of the proposed model

To use this relation (Eqn (15.2)) for a given set of materials, the strength developed at a specified age for a b/f ratio of 5.0 needs to be determined. Using this as an input parameter in the equation, the b/f ratio for any other desired strength can be calculated using the phenomenological model. Using the calculated b/f ratio, all other ingredients in the mortar mix can be determined. Hence the mix proportions for the required strength can be arrived at.

To carry out this exercise, a series of experimental data with different conditions were considered. This was an independent set of data which is not a part of data analyzed in the formulation of the phenomenological model. Binder-to-fluid ratio (b/f) is an independent variable in each of the sets.

In the same range of b/f ratio, the strength developed in each set varies due to variation of other parameters. From each of these sets, the compressive strength at reference b/f ratio can be taken into consideration in the denominator of the left-hand side of phenomenological model (Eqn (15.2)). The strength developed at other f/b ratios can be calculated. The comparisons with experimental values are as shown in Table 15.2. There is very close match between the experimental and predicted values reinforcing the applicability of this model practically.

15.6 Ambient cured geopolymer blocks

It is a well-established fact that class F fly ash can be activated with thermal input with higher molarity of alkaline solution. However, it would not be an economical option to produce compressed blocks with fly ash alone as binder. In view of this, strength development of compressed blocks can be studied by the addition of GGBS and other binders.

The mix details are shown in Table 15.3. The blocks were cured in ambient conditions (around 24 °C) and prepared using different binders as indicated in the table.

In this section, strength development of geopolymer compressed blocks at ambient temperature is discussed considering various parameters. The parameters considered for the study are as follows:

- Age of the sample: 1, 3, 7, 14, 28, 56, 90, 120 and 180 days.
- Fly ash: FA1, FA2, FA3 and FA4.
- Alkaline activator: Sodium hydroxide and potassium hydroxide.
- Ratio of binder-to-aggregate: 1:1, 1:2 and 1:3.
- Degree of saturation: 40% and 60%.
- Molarity of alkaline solution: 8, 10, 12 and 14 M.
- Fine aggregate: Sand, quarry dust and pond ash.
- Temperature: 25, 30, 40, 50, 60, 70 and 80 °C.
- Binder: fly ash, GGBFS, silica fume and metakaolin.
- Sample size and shape: PB1, PB2, PB3, CB1, CB2 and CB3.

The effects of each of these parameters on the strength development are discussed below.

Table 15.2 A typical comparison of experimental and predicted compressive strengths

f/b ratio	b/f ratio	Series ID	ES (MPa)	PS (MPa)	ES/PS
0.150	6.67	10M-Sand-W-7 Days	18.3	18.29	1.00
0.175	5.71	10M-Sand-W-7 Days	15.88	15.81	1.00
0.200	5.00	10M-Sand-W-7 Days	14.1	14.1	1.00
0.225	4.44	10M-Sand-W-7 Days	12.2	12.52	0.97
0.15	6.67	12M-Sand-W-3 Days	19.25	18.8	1.02
0.175	5.71	12M-Sand-W-3 Days	16.19	16.25	1.00
0.200	5.00	12M-Sand-W-3 Days	14.5	14.5	1.00
0.225	4.44	12M-Sand-W-3 Days	12.85	12.88	1.00
0.150	6.67	14M-Sand-W-1 Day	19.75	19.43	1.02
0.175	5.71	14M-Sand-W-1 Day	17.1	16.79	1.02
0.200	5.00	14M-Sand-W-1 Day	14.98	14.98	1.00
0.225	4.44	14M-Sand-W-1 Day	13.2	13.3	0.99
0.150	6.67	14M-QD-W-7 Days	27.01	28.2	0.96
0.175	5.71	14M-QD-W-7 Days	24.06	24.38	0.99
0.200	5.00	14M-QD-W-7 Days	21.75	21.75	1.00
0.225	4.44	14M-QD-W-7 Days	19.25	19.32	1.00
0.150	6.67	14M-QD-UW-3 Days	21.98	21.82	1.01
0.175	5.71	14M-QD-UW-3 Days	19.37	18.86	1.03
0.200	5.00	14M-QD-UW-3 Days	16.82	16.82	1.00
0.225	4.44	14M-QD-UW-3 Days	15.04	14.95	1.01

ES, experimental strength; PS, predicted strength.

15.6.1 Strength development with age

The pattern of strength development of the geopolymer blocks with age for different f/b ratios is shown in Figure 15.13. The strength of compressed blocks increases with age and its development would rapidly increase during the early age compared to the later age. Ambient cured geopolymer blocks attain strength with age, owing to the continuous formation of CSH gel since GGBS was used as part of the binder. It is interesting to note that ambient cured blocks would develop strength of more than 1 MPa within 24 h. This strength would be sufficient to handle the blocks for the purpose of transportation. A minimum strength of 3 MPa can be achieved at the age of 7 days. This is again advantageous as the blocks can be used for masonry works early.

Table 15.3 Typical mix proportions of ambient cured geopolymer compressed blocks

Series ID	Binder-to-aggregate ratio	Fly ash type	Binder composition	Degree of saturation (%)	Alkaline activator with molarity	Curing temperature (°C)	Fine aggregate
ABS1	1:1	FA1	FA:GGBFS = 1:1	40	NaOH 14 M	Ambient	Sand
ABS2	1:2	FA1	FA:GGBFS = 1:1	40	NaOH 14 M	Ambient	Sand
ABS3	1:3	FA1	FA:GGBFS = 1:1	40	NaOH 14 M	Ambient	Sand
ABS4	1:2	FA1	FA:GGBFS = 1:1	40	NaOH 8 M	Ambient	Sand
ABS5	1:2	FA1	FA:GGBFS = 1:1	40	KOH, 8 M	Ambient	Sand
ABS6	1:2	FA1	FA:GGBFS = 1:1	40	NaOH 10 M	Ambient	Sand
ABS7	1:2	FA1	FA:GGBFS = 1:1	40	NaOH 12 M	Ambient	Sand
ABS8	1:2	FA4	FA:GGBFS = 1:1	40	NaOH 14 M	Ambient	Sand
ABS9	1:2	FA3	FA:GGBFS = 1:1	40	NaOH 14 M	Ambient	Sand
ABS10	1:2	FA2	FA:GGBFS = 1:1	40	NaOH 14 M	Ambient	Sand
ABS11	1:2	FA2	FA:GGBFS = 1:1	40	NaOH 14 M	Ambient	QD
ABS12	1:2	FA2	FA:GGBFS = 1:1	60	NaOH 14 M	Ambient	Sand
ABS13	1:2	–	GGBFS: MTK = 1:1	40	NaOH 14 M	Ambient	Sand
ABS14	1:2	–	GGBFS:SF = 1:1	40	NaOH 14 M	Ambient	Sand
ABS15	1:1	FA1	FA:GGBFS = 2:3	60	NaOH 12 M	Ambient	Sand
ABS16	1:2	FA1	FA:GBFS = 1:1	40	NaOH 14 M	30–80 °C	Sand
ABS17	1:2	FA1	FA:SF = 1:1	40	$Na(OH)_2$, 14 M	Ambient	Sand
ABS18 (size and shape)	1:2	FA1	FA:SF = 1:1	40	$Na(OH)_2$, 14 M	Ambient	Sand
ABS19	1:2	FA1	FA:GGBFS = 1:1	40	$Na(OH)_2$, 14 M	Ambient	Pond ash

QD, quarry dust; MTK, metakaolin; SF, silica fume.

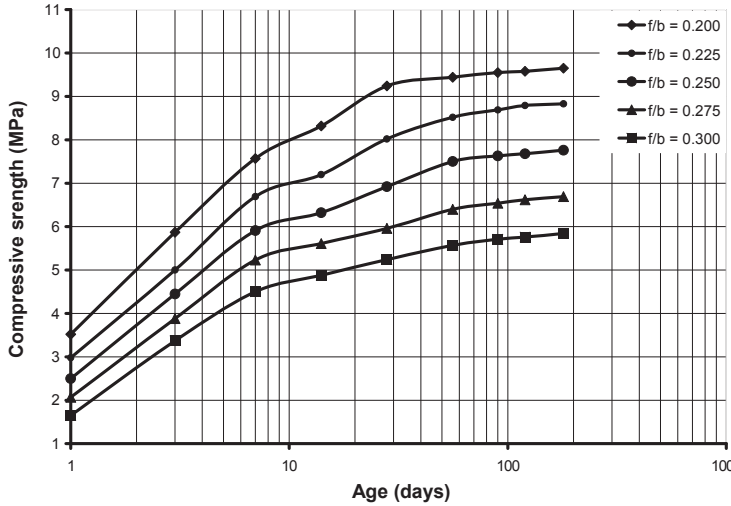

Figure 15.13 Strength development with age (Series ABS15).

15.6.2 Strength development with type of fly ash

Fly ash may vary in characteristics based on the source. It may become necessary to study strength development for various fly ash samples procured from different sources. This is required to assess a particular fly ash for use in making geopolymer compressed blocks. The strength development pattern of the blocks with different fly ash samples is shown in Figure 15.14.

The order of the fly ash samples with fineness is FA1, FA2, FA3 and FA4. The strength developed would be proportional to the fineness of the ash used. FA1 is finest among all the fly ash samples and FA4 is the coarsest. Fineness plays a significant role

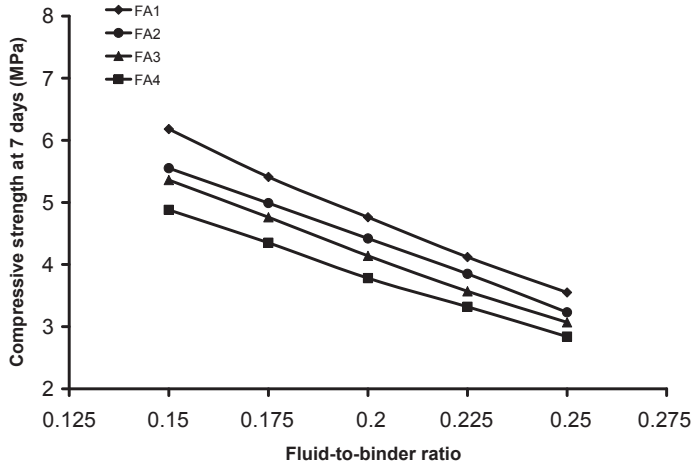

Figure 15.14 Strength development of blocks with different fly ashes.

in pozzolanic action in concrete incorporating fly ash. The same is true in the case of geopolymer blocks.

15.6.3 Strength with alkaline solution

Different alkaline solutions can be used to activate the binders in developing geopolymers. Among all the activators, sodium hydroxide and potassium hydroxide are the popular choice because of their easy availability. However, the latter is more expensive. The strength development for both the activators is shown in Figure 15.15.

The use of potassium hydroxide as an activator increases the strength of the compressed blocks compared to sodium hydroxide with the same molarity. Since potassium hydroxide is expensive, its use would not be economical, but economy can be compromised for strength.

15.6.4 Strength development with binder-to-aggregate ratio

The binder-to-aggregate ratio plays a role in the development of geopolymer compressed blocks. As in the case of OPC mortars, in geopolymers it is to be considered as a parameter to influence strength.

It can be noticed from Figure 15.16 that as the binder-to-aggregate ratio increases, strength also increases and vice versa. This parameter helps in economizing the product cost. At the lower f/b ratio of 0.15, the variation of strength with binder-to-aggregate ratio would be marginal.

15.6.5 Strength development with degree of saturation

Since dry mortar would be partially saturated material, the degree of saturation affects strength. It may not be possible to cast the mortar blocks for the degree of saturation

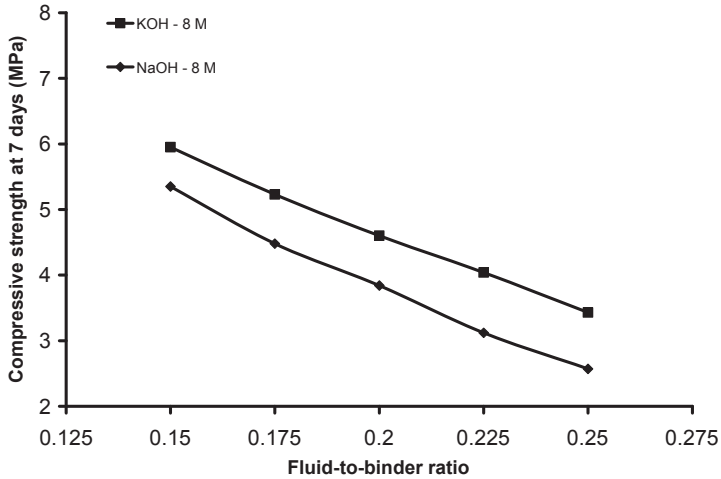

Figure 15.15 Strength development with different alkaline solutions.

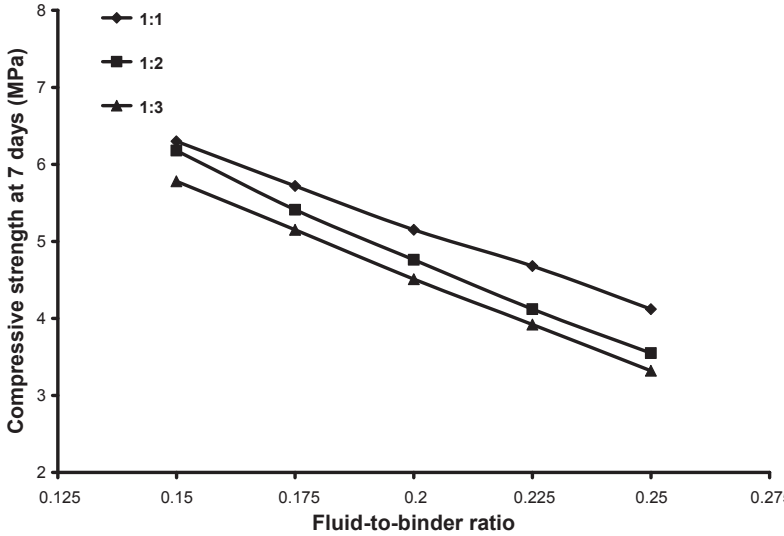

Figure 15.16 Strength development with binder-to-aggregate ratio.

below 40% and above 60% due to practical difficulties. The strength development of the compressed blocks with two degrees of saturations – 40% and 60% – is shown in Figure 15.17.

Degree of saturation (S_d) is the index of air content present in a three-phase material like geopolymer mortar. It is well-known that as the air content increases the strength decreases. This is true even in the case of geopolymer compressed blocks. The blocks with 40% degree of saturation would possess higher strength compared to the blocks

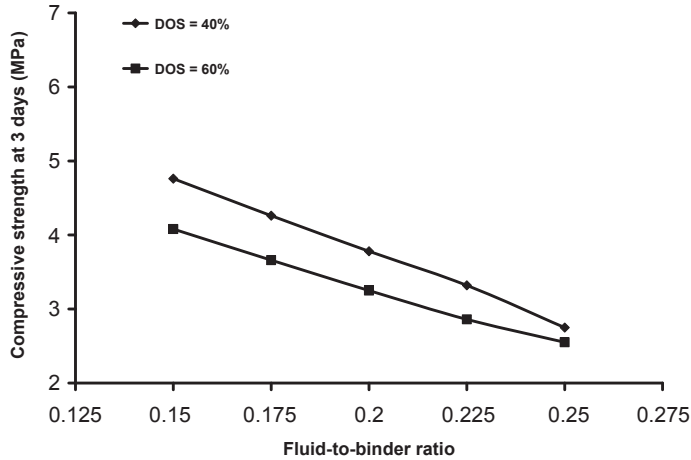

Figure 15.17 Variation of strength with the degree of saturation.

with a higher degree of saturation of 60%. It should be noted that as the degree of saturation increases, the mortar becomes too wet and cannot be used to cast blocks. On the other hand, if the degree of saturation is less, the effort required to cast the samples becomes too high. Hydraulic machines can be used to cast the samples at lower degree of saturation.

15.6.6 Strength development with molarity of alkaline solution

Molarity (M) of the alkaline solution represents the concentration of the salts in the solution. As molarity increases, the basic material required to prepare the solution increases. Molarity plays a major role in strength development.

Strength developed is always proportional to the molarity of the alkaline solution used. As the molarity of the solution increases, the formation of aluminosilicates and CSH gel increases (Figure 15.18). This results in higher strength. It is to be noted that at molarity less than 8, the strength developed would be much less and hence may not be considered for practical application. The solution of higher molarity of more than 14 cannot be prepared easily. As the molarity increases beyond 14, more salts would be deposited, and it becomes extremely difficult to maintain a homogeneous solution.

15.6.7 Strength development with fine aggregate

Natural river sand is turning scarce and hence should be preserved. Efforts are being made in the construction industry to use material alternate to sand. Hence, the alternatives such as quarry dust and pond ash as fine aggregate can be used.

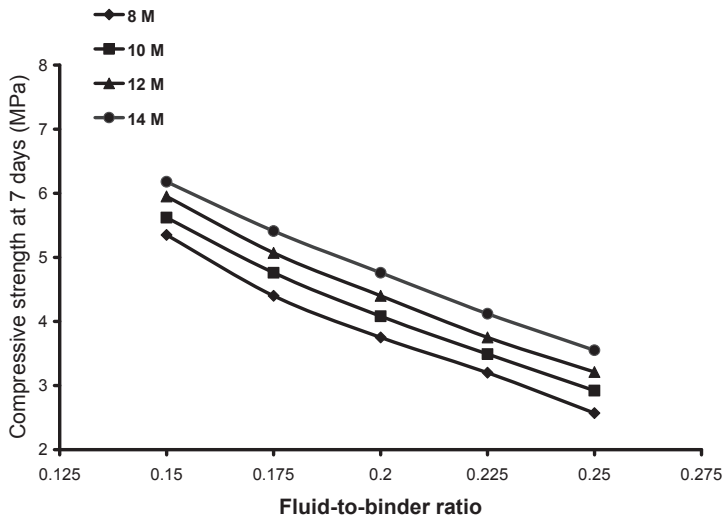

Figure 15.18 Variation of strength with molarity of alkaline solution.

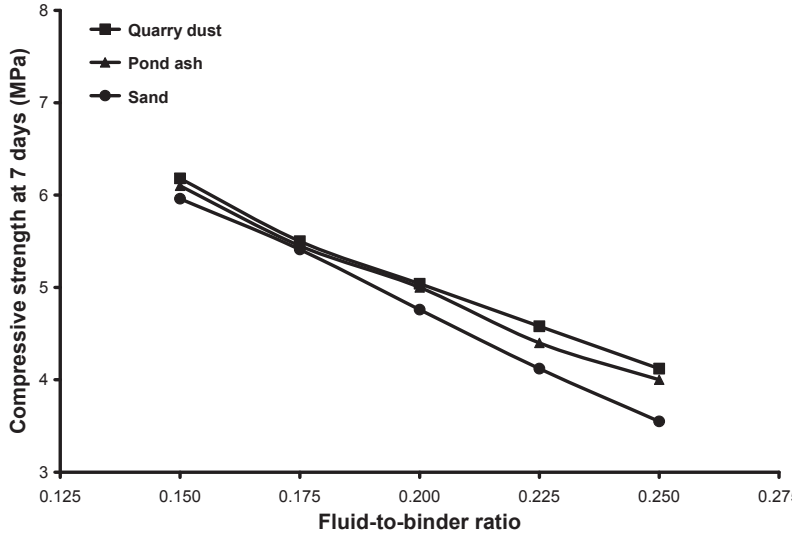

Figure 15.19 Variation of compressive strength with varied fine aggregates.

The use of quarry dust and pond ash with the same fineness moduli as fine aggregates strengthens the blocks marginally higher (Figure 15.19). This reinforces the possibility of using both pond ash and quarry dust in place of sand.

15.6.8 Strength development with binder

The properties of binders vary with the source. The strength development in the compressed blocks depends on the properties of the binder. Different binders can be used to prepare geopolymer composites apart from fly ash. The base materials used should be rich in alumina and silica. For this, a combination of three binders – GGBS, silica fume and metakaolin with/without fly ash – can be considered. The variation of strength with these binders is shown in Figure 15.20.

It is interesting to note that, with the use of silica fume as part of binder, strength development would be almost four times that of other combinations. At the age of 7 days and f/b ratio of 0.15, the strength would be more than 23 MPa. The reason for higher strength is due to the higher silica content and its higher surface area. If the strength requirement is more, silica fume can be recommended as binder in making the geopolymer compressed blocks. The finished block would be very light in color (creamy white) compared to other blocks. These blocks can be used for architectural purposes. But the cost of silica fume is to be considered before using it as binder in making the blocks. The strength developed with GGBS as binder would be marginally higher compared to metakaolin. It is advantageous to use GGBS in place of metakaolin, which is expensive.

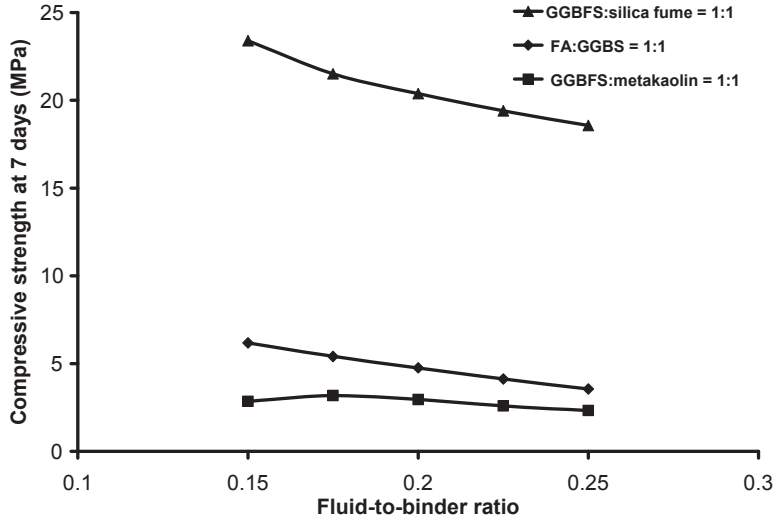

Figure 15.20 Strength development with different binders.

The compressive strength of ambient cured blocks in this study varies in the range 1−30 MPa for different parameters. This would cover a wide range of strength. Based on the end use, the raw materials and methods are to be selected to get the required strength. Blocks having any strength in this range can be prepared at ambient conditions without any special curing.

15.6.9 Development of phenomenological model − ambient cured blocks

It is interesting to note from the voluminous experimental data that at a constant degree of saturation, f/b ratio alone determines the strength development with all other parameters remaining unchanged. This was observed in thermal cured compressed blocks as discussed in the previous section. Keeping this in mind, another phenomenological model can be developed as that of thermal cured blocks.

When the compressive strength was generalized with reference to strength at b/f ratio of 5.0, the model Eqn (15.3) can be obtained.

$$\left\{\frac{S}{S_{@b/f=5}}\right\} = 0.2164\left\{\frac{b}{f}\right\} - 0.108 \tag{15.3}$$

The above model resembles Eqn (15.2) developed for thermal cured blocks in the previous section of this chapter with marginal variation in the constants. This strongly implies that the strength development in thermal cured and ambient cured blocks follows the same trend. This model is shown graphically in Figure 15.21 with R^2 value of 0.94. The data used to develop the model was not part of the data used for the

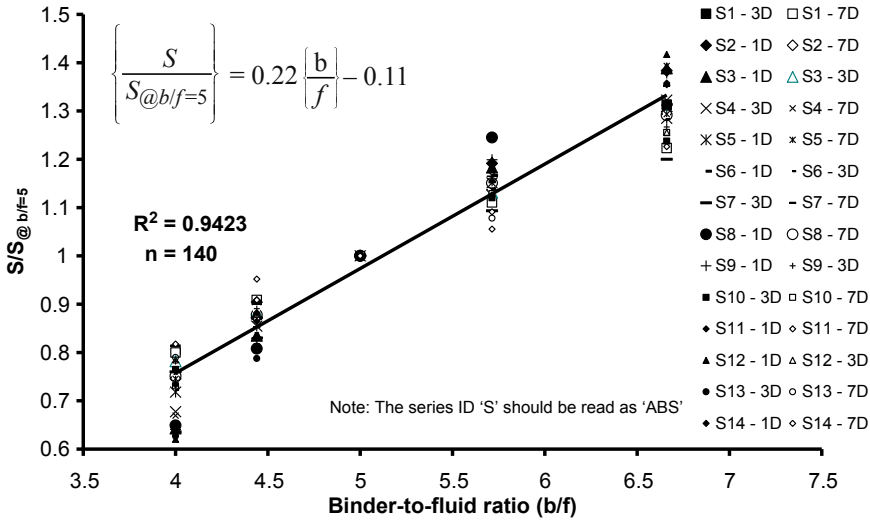

Figure 15.21 Graphical representation of the model (Eqn (15.3)).

prediction of the strength. The compressive strengths of thermal cured blocks can be predicted using Eqn (15.3) and of ambient cured blocks using Eqn (15.2) and vice versa with minimum error.

15.6.10 Validation of the model

To use the relation Eqn (15.3), for a given set of materials, the strength developed at a specified age for a b/f ratio of 5.0 (or f/b = 0.2) is to be determined experimentally. Using this as an input parameter in the equation, the b/f ratio of any other desired strength can be calculated using the phenomenological model.

A separate series of experimental data was generated to examine the predictions made using the phenomenological model. The strength developed at other f/b ratios is calculated and tabulated in Table 15.4 for comparison with experimental values. The correlation between experimental and predicted strength values is shown in Figure 15.22. There is a close match between the experimental and predicted values reinforcing the applicability of the phenomenological model. With more data being generated for a still wider range of b/f ratio the scope of this phenomenological model can further be enhanced.

15.6.11 Strength development with size and shape

The majority of the compressed blocks were either cylinders of 38 mm diameter and 76 mm height or the blocks of size 200 × 110 × 60 mm, which were prepared with manual compression. To correlate the compressive strength of these blocks, a series of blocks were prepared using a motorized hydraulic compressed machine. The shape

Table 15.4 Comparison of strength data using Eqn (15.3)

Series ID	Fluid-to-binder ratio	Binder-to-fluid ratio	Predicted value (MPa)	Experimental value (MPa)	Error (%)
ABS1 − 1D	0.15	6.66	4.43	4.26	−3.90
	0.175	5.714	3.75	3.78	0.88
	0.2	5	3.23	3.32	2.60
	0.225	4.44	2.83	2.75	−2.96
	0.25	4	2.52	2.5	−0.61
ABS2 − 3D	0.15	6.66	5.04	4.76	−5.87
	0.175	5.714	4.27	4.26	−0.14
	0.2	5	3.68	3.78	2.60
	0.225	4.44	3.22	3.32	2.90
	0.25	4	2.86	2.75	−4.14
ABS3 − 7D	0.15	6.66	6.01	5.78	−4.03
	0.175	5.714	5.09	5.15	1.17
	0.2	5	4.39	4.51	2.60
	0.225	4.44	3.85	3.92	1.88
	0.25	4	3.42	3.32	−2.91
ABS4 − 1D	0.15	6.66	2.68	2.92	8.23
	0.175	5.714	2.27	2.44	7.04
	0.2	5	1.96	2.01	2.60
	0.225	4.44	1.71	1.6	−7.14
	0.25	4	1.52	1.5	−1.52
ABS5 − 3D	0.15	6.66	5.39	5.2	−3.58
	0.175	5.714	4.56	4.62	1.32
	0.2	5	3.93	4.04	2.60
	0.225	4.44	3.45	3.49	1.28
	0.25	4	3.06	2.95	−3.75
ABS6 − 7D	0.15	6.66	5.44	5.62	3.21
	0.175	5.714	4.60	4.76	3.27
	0.2	5	3.97	4.08	2.60
	0.225	4.44	3.48	3.49	0.30
	0.25	4	3.09	2.92	−5.86

Table 15.4 Continued

Series ID	Fluid-to-binder ratio	Binder-to-fluid ratio	Predicted value (MPa)	Experimental value (MPa)	Error (%)
ABS7 − 1D	0.15	6.66	3.20	3.2	0.01
	0.175	5.714	2.71	2.79	2.92
	0.2	5	2.34	2.4	2.60
	0.225	4.44	2.05	2.02	−1.32
	0.25	4	1.82	1.8	−1.01
ABS8 − 3D	0.15	6.66	3.81	3.78	−0.87
	0.175	5.714	3.23	3.27	1.30
	0.2	5	2.79	2.86	2.60
	0.225	4.44	2.44	2.52	3.21
	0.25	4	2.17	2.15	−0.78
ABS9 − 7D	0.15	6.66	5.52	5.36	−2.98
	0.175	5.714	4.67	4.76	1.85
	0.2	5	4.03	4.14	2.60
	0.225	4.44	3.53	3.57	1.10
	0.25	4	3.14	3.07	−2.16
ABS10 − 1D	0.15	6.66	3.51	3.66	4.20
	0.175	5.714	2.97	3.12	4.87
	0.2	5	2.56	2.63	2.60
	0.225	4.44	2.24	2.24	−0.13
	0.25	4	1.99	1.87	−6.55
ABS11 − 3D	0.15	6.66	4.17	4.25	1.81
	0.175	5.714	3.53	3.74	5.56
	0.2	5	3.05	3.13	2.60
	0.225	4.44	2.67	2.82	5.34
	0.25	4	2.37	2.2	−7.79
ABS12 − 7D	0.15	6.66	4.57	4.24	−7.85
	0.175	5.714	3.87	3.82	−1.33
	0.2	5	3.34	3.43	2.60
	0.225	4.44	2.93	3.02	3.14
	0.25	4	2.60	2.7	3.76

Continued

Table 15.4 Continued

Series ID	Fluid-to-binder ratio	Binder-to-fluid ratio	Predicted value (MPa)	Experimental value (MPa)	Error (%)
ABS13 − 1D	0.15	6.66	1.69	1.77	4.34
	0.175	5.714	1.43	1.44	0.47
	0.2	5	1.24	1.27	2.60
	0.225	4.44	1.08	1.15	5.82
	0.25	4	0.96	1.01	4.74
ABS14 − 3D	0.15	6.66	20.97	20.22	−3.72
	0.175	5.714	17.75	17.25	−2.91
	0.2	5	15.32	15.73	2.60
	0.225	4.44	13.41	14.64	8.37
	0.25	4	11.92	12.5	4.66

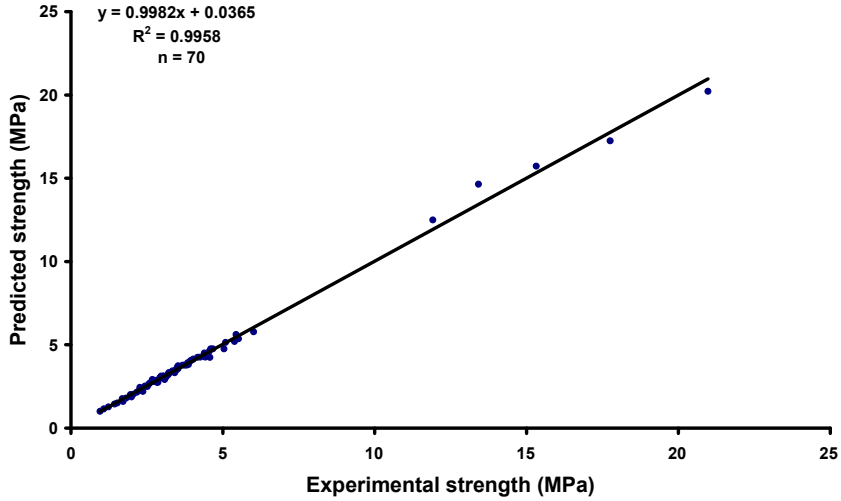

Figure 15.22 Experimental and predicted strength (Eqn (15.3)).

and size of the blocks selected were such that they could be directly used in the field once prepared. For speedier production and commercial usage, the blocks should be made using a motorized hydraulic compressed machine, which is currently in use to make cement blocks. Compressed blocks of PB1, PB2, PB3 and CB1 were made by employing the motorized hydraulic machine and of CB2 and CB3 with a manually

operated device. Size and shapes of the blocks are shown in Table 15.5 and Figure 15.23. The results of the compressive strength test of various blocks are shown in Figures 15.24 and 15.25. It can be seen from these figures that strength development is the same for different sizes and shapes of the blocks and pavers. There is no effect of scale and size of the blocks on the strength development. This encourages the use of these blocks as masonry blocks and pavers.

Table 15.5 Dimensions of the blocks

Sl no.	Block ID	Size (mm)
1	PB1	220 × 150 × 60 (outer to outer)
2	PB2	200 × 160 × 60 (outer to outer)
3	PB3	200 × 120 × 60 (outer to outer)
4	CB1	200 × 110 × 60
5	CB2	Cylinder, dia = 38, ht = 76
6	CB3	230 × 190 × 90

Paver Block 1 (PB1)

Paver Block 2 (PB2)

Paver Block 3 (PB3)

Compressed Block 1 (CB1)

Compressed Block 2 (CB2)

Compressed Block 3 (CB3)

Figure 15.23 Shapes of pavers and compressed blocks.

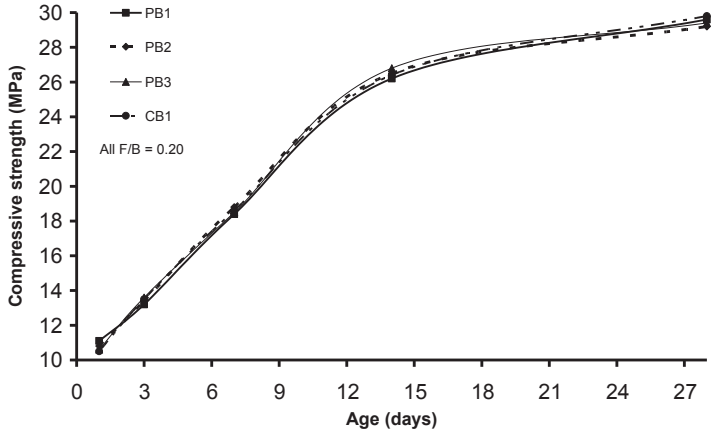

Figure 15.24 Compressive strength of paver and compressed blocks of various sizes and shapes.

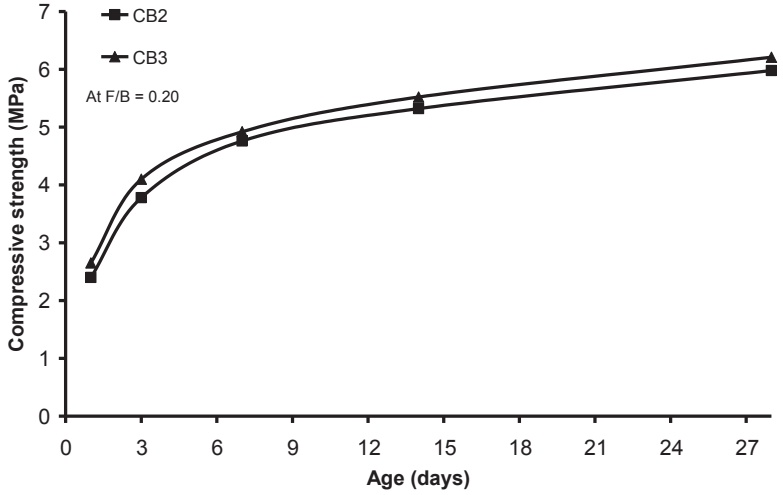

Figure 15.25 Compressive strength of compressed blocks of various sizes and shapes.

15.7 Conclusions and future trends

It was noted that, apart from f/b ratio, air content in compressed blocks (degree of saturation) also affects strength development with age. If the air content is maintained constant then the strength development is in accordance with Abrams' law for the specified range of f/b ratio. Silica fume can be used as one of the components of binder if the strength required is high and also in situations where architectural aesthetic appeal is called for. Phenomenological models can be developed to reproportion the materials for making geopolymer compressed masonry blocks. The phenomenological model developed can be used for a given set of materials and conditions. If there is any

change in the properties of materials or conditions, a fresh reference value of strength at f/b ratio of 0.2 ($S_{f/b} = 0.2$) shall be generated to make use of the model. A wide range of reference strength data would be useful to proportion the materials for the given strength at ambient conditions. The masonry blocks can be made using locally available materials, which are rich in silica and alumina.

Further research about geopolymer mortar masonry blocks is needed in order to clarify several aspects that current knowledge does not, such as the following:

1. The f/b ratio can be further decreased for better strength and use of appropriate plasticizers need to be invented to compensate the workability without compromising the economy.
2. Various combinations of locally available aluminosilicates as base materials need to be investigated.
3. The use of silica fume as a base material needs to be further investigated without compromising autogenous shrinkage, compressive strength, color and economy. The surface finish and color of the blocks may avoid plastering. The attractive light color of the blocks may influence the architects to use them as facade elements.
4. Long-term field studies need to be carried out to establish endurance of the blocks.
5. The commercialization of geopolymer masonry blocks may be possible only if the properties are comparatively better than the conventional masonry units available in the market without compromising the economy.

References

Abrams, D. (1918). *Design of concrete mixtures*. Bulletin No. 1. Chicago: Structural Materials Research Laboratory, Lewis Institute.

Astutiningsih, S., & Liu, Y. (2005). Geopolymerization of Australian slag with effective dissolution by the alkali, geopolymer. Green Chemistry and Sustainable Development Solutions. In *Proceedings of world congress geopolymer*. Peer-Reviewed by Geopolymer Institute Publication Policy.

Bolomey, J. (1927). Durecissenment des mortiers ets benton. *Technique Suisse Romande Nos,* Published by F. Rouge et Cie S.A, 1936 (in French)*, 16*(22), 24−2.4.1.

Chao, L., Sun, H., & Longtu, L. (2010). A review: the comparison between alkali-activated slag (Si + Ca) and metakaolin (Si + Al) cements. *Cement and Concrete Research, 40*, 1341−1349.

Chindaprasirt, P., Jaturapitakkul, C., Chalee, W., & Rattanasak, U. (2009). Comparative study on the characteristics of fly ash and bottom ash geopolymers. *Waste Management, 29*(2), 539−543.

Dahmen, J., & Muñoz, J. F. (June 2014). Earth masonry unit: sustainable CMU alternative. *International Journal of Geomate, 6*(2) (Sl. no. 12), 903−909.

Davidovits, J. (1994). *Properties of geopolymer cements*. Kiev Ukraine: Alkaline Cements and Concretes. Proceedings of first international Conference on Alkaline Cements and Concretes, Scientific Research institute on Binders and Materials, Ukraine, pp. 131−149.

Davidovits, J. (1999). Chemistry of geopolymeric systems, terminology. In *Geopolymer international conference, France*.

Davidovits, J., & Davidovits, M. (1988). Geopolymer room temperature ceramic matrix for composites. *Ceramic Engineering and Science Proceeding, 9*, 842−853.

Duxson, P., Provis, J. L., Lukey, G. C., & Van deventer, J. S. J. (2007). The role of inorganic polymer technology in the development of 'green concrete'. *Cement and Concrete Research, 37*, 1590−1597.

Hardjito, D., Wallah, S. E., Sumajouw, D. M. J., & Rangan, B. V. (2004). On the development of fly ash based geopolymer concrete. *ACI Material Journal, 101*, 467−472.

Montes, C., Islam, R., Shi, J., Kupwade-Patil, K., & Allouche, E. (2013). Towards a pre-cast geopolymer concrete pipe. In *Pipelines 2013* (pp. 534−542). http://dx.doi.org/10.1061/9780784413012.049.

Nagaraj, T. S., & Banu, Z. (1996). Generalization of Abrams' law. *Cement and Concrete Research, 26*(6), 933−942.

Nagaraj, T. S., & Banu, Z. (1999). Relative efficacies of the different concrete mix proportioning methods. *Journal of Structural Engineering, 26*(2), 107−111.

Palomo, A., Macias, A., Blanco, M. T., & Puertas, F. (1992). Physical, chemical and mechanical characterization of geopolymers. In *Proceedings of the 9th international congress on the chemistry of cement* (pp. 505−511).

Prasad, K. N., Narasimhulu, M. L., Nagaraj, T. S., Naidu, J. S., & Ifthakaruddin, S. (2005). Strength development in compressed cement blocks − analysis and assessment. *Indian Concrete Institute Journal, 79*(4), 49−54.

Provis, J. L. (2014). Geopolymers and other alkali activated materials: why, how, and what? *Materials and Structures, 47*, 11−25. http://dx.doi.org/10.1617/s11527-013-0211-5.

Radhakrishna, Venu Madhav, T., Manjunath, G. S., & Venugopal, K. (2013). Phenomenological model to re-proportion the ambient cured geopolymer compressed blocks. *International Journal of Concrete Structures and Materials, 7*(3), 193−202.

Radhakrishna, & Niranjan, P. S. (2013). Prediction of the compressive strength in Fal-G compressed blocks. *i-manager's Journal on Civil Engineering, 3*(1), 45−49.

Radhakrishna, Shashishankar, A., & Udayashankar, B. C. (2008). Analysis and assessment of strength development in class F fly ash based compressed geopolymer blocks. *Indian Concrete Journal, 82*(8), 31−37.

Radhakrishna, Shashishankar, A., Udayashankar, B. C., & Renuka Devi, M. V. (June 2010). Compressive strength assessment of geopolymer composites by a phenomenological model. *Journal of Reinforced Plastics and Composites, 4*(29), 840−852.

Rangan, B. V. (2008a). *Fly ash-based geopolymer concrete*. Research Report GC4 Engineering Faculty Curtin University of Technology Perth, Australia.

Rangan, B. V. (2008b). Mix design and production of fly ash based geopolymer concrete. *The Indian Concrete Journal, 82*(5), 7−15.

Sakkas, K., Nomikos, P., Sofianos, A., & Panias, D (February 26, 2014). Sodium-based fire resistant geopolymer for passive fire protection. Fire and Materials (Special issue), Available online doi:10.1002/fam.2244.

Shi, C., & Fernandez-Jiménez, A. (2006). Stabilization/solidification of hazardous and radioactive wastes with alkali-activated cements. *Journal of Hazardous Materials, B137*, 1656−1663.

Van Deventer, J. S. J., Provis, J. L., & Duxson, P. (2012). Technical and commercial progress in the adoption of geopolymer cement. *Minerals Engineering, 29*, 89−104.

Zhao, F.-Q., Ni, W., Wang, H.-J., & Liu, H.-J. (2007). Activated fly ash/slag blended cement. *Resources, Conservation and Recycling, 52*, 303−313.

The properties and durability of adobe earth-based masonry blocks

16

E. Quagliarini, M. D'Orazio, S. Lenci
Universitá Politecnica delle Marche, Ancona, Italy

16.1 Introduction

Earth is an economical, environmentally friendly and abundantly available building material and is probably one of the oldest building materials known. Nowadays, earth constructions are an area of growing interest, both for rescuing heritage and for a rediscovered eco-sustainability material. However, because earth constructions are a forgotten technique, a lack of skilled people at all levels in this area can be found, from designers to masons, as well as problems of how to carry out compatible conservation works on earthen heritage. This chapter tries to fill this gap for a peculiar earthen construction technique, namely adobe, in which raw earth is mixed and molded to form blocks to make a bearing wall. The following sections, after a brief historical digression, will deal with how manufacturing adobe earth-based masonry blocks, their typical dimensions, which soil is suitable and which stabilization materials are currently used for enhancing their properties. Then, the principal mechanical and hygro-thermal properties of adobe blocks, how to determine them and which parameters influence them will be provided, as well as methods of testing adobe blocks for durability and practical advice on how to maintaining or improving it will be supplied. Finally, environmental and economic benefits potentially associated with the use of adobe earth-based masonry blocks, including new ways to reuse bulk industrial waste as stabilizers, will be addressed.

16.2 Adobe technique and materials

Earth has been extensively used for the construction of walls and buildings for 1000 years around the world (some recorded cases of the use of earth blocks date back to Mesopotamia around 10,000 BC (Quagliarini, Lenci, & Iorio, 2010)), particularly in all hot-dry, subtropical and moderate climates and in those countries where there is not much vegetation, so there is a lack of wood (Ren & Kagi, 1995). Approximately 30% of the world's present population still lives in earthen structures (Cofirman, Agnew, Auiston, & Doehne, 1990). For many centuries, hand-molded unburnt earthen blocks (adobes) have been used for load-bearing masonry structures.

Eco-efficient Masonry Bricks and Blocks. http://dx.doi.org/10.1016/B978-1-78242-305-8.00016-4

In particular, adobe earth construction was prolific in the ancient world, and archaeologists discovered surviving examples in many different places. Earth block buildings were found in Turkistan (dating back to about 8000−6000 BC), in Assiria (from about 4000 BC) and monumental earth structures can be observed still today in upper Egypt (from about 3200 BC). The historical city of Shibam in the south of Yemen is completely built by adobe (about fifteenth century). For centuries, Indians in New Mexico built their houses by earth blocks. During the seventeenth and eighteenth centuries, this technique was commonly used in England and Scandinavia, and European immigrants brought it to the United States, where a large number of earth houses were built between the eighteenth and nineteenth centuries (Minke, 2000). These earthen ancient constructions are precious cultural heritages and their artistic value is immeasurable (Heathcote, 1995). Adobe in fact is a very simple earth building technique and maybe this is the reason why most ancient constructions were made of adobe. The word "adobe" seems to come from the Arab *attob*, which means sun-dried brick (Pacheco-Torgal & Jalali, 2012). The production of adobe blocks generally consists of manually filling a wooden mold (Figures 16.1−16.3), which is first wet with water and scattered inside with sand so as to reduce water absorption by wood and facilitate the removal of the earth block, with wet earth (this molding reduces the quantity of voids between grains and thus gives a form to the mixture thanks to cohesion) and allowing to dry in natural environmental conditions, under the sun or, preferably, the shade. Usually, adobe walls consist of rectangular blocks arranged next to one another and put with alternate joints. The adobe blocks are generally stacked nearly dry, with a thin layer of clay or mortar made by their same composition (Figure 16.4).

Although adobes are most used for lightly loaded single and two-storey residential buildings, adobes have also been used to build up to 10-storey high buildings

Figure 16.1 Typical wooden mold used to make an adobe block. The mold is first wet with water and scattered inside with sand so as to reduce water absorption by wood and facilitate the removal of the earth block.

Figure 16.2 The production of an adobe block. The wooden mold is manually filled with wet earth.

Figure 16.3 A typical prismatic adobe block.

(Houben & Guillaud, 1994). Nowadays, the material is mostly used for restoration purposes. In addition, adobe is currently introduced in contemporary sustainable architecture (Illampas, Ioannou, & Charmpis, 2014).

The soil used for making adobe generally refers to an *in situ* sandy loam subsoil. Topsoil is in fact unsuitable mainly due to the significant amount of organic matter present that biodegrades, absorbs water and is highly compressible. Recent studies (Kouakou & Morel, 2009) showed that the suitable soil should contain less than 20% clay minerals. In particular, (Quagliarini & Lenci, 2010) have underlined that a

Figure 16.4 An adobe wall under construction made by rectangular blocks arranged next to one another and put with alternate earth mortar joints.

preferable clay content into the bearing adobe block elements should be between 12% and 16% (by weight). Cohesion, indeed, is the most important property that earth should have to be used for construction purposes (Houben & Guillaud, 1994), so the presence of clay is essential because it acts as a natural binder.

Romans usually used *in situ* raw earth as a building material (Adam, 1984). Vitruvius himself (Barbaro, 1997), in fact, states that earth can be used as a building material if it is *cretosa*, that is guaranteed by a great presence of clay. Moreover, he suggested producing adobe blocks during spring or autumn because the sun is not so strong and thus there is not a rapid drying process that can produce cracks. Only if it is really necessary to produce them in summer or winter is it good to adopt some precautions: In the first case blocks have to be covered with wet straw to avoid excessive drying whereas in the second case they have to be covered with dry sand in order to allow good seasoning of earth blocks also in humid and cold weather. The standard dimensions of Roman adobe blocks as Vitruvius (Barbaro, 1997) states are 1 foot per 1.5 feet per one palm ($0.296 \times 0.444 \times 0.074\ m^3$), but different, even if similar, dimensions of the blocks can be found in some Roman archaeological sites (i.e. $0.31 \times 0.46 \times 0.13\ m^3$ (Quagliarini et al., 2010)). In general, their dimension is highly variable, ranging in length from 0.25 to 0.6 m (Houben & Guillaud, 1994). The method of production, in general nonindustrial, enables the manufacturer to vary block size and shape to suit requirements by using mold inserts (Figure 16.2).

Anyway, ancient masons well knew that it was hardly possible to use only earth to produce large adobe bearing blocks because of their excessive shrinkage and consequently cracking and because of the limited workability of the mixture. In this way, sand or coarse sand was added into the mixture (Quagliarini et al., 2010) to "degrease" clay and to allow making it into a mixture. Sand, in fact, reduces the clay fraction relative to other components and allows a lower shrinkage due to the smaller presence of

the component (clay) prone to this phenomenon. The components of adobe earth material, in fact, can be considered as analogous to those of concrete: The inert aggregate fraction is represented by granular soils (sand and gravel) and the binder fraction is represented by cohesive soils (silt and clay) (Hall & Djerbib, 2004).

Moreover, ancient masons often put vegetable fibers into the mixture such as straw or dry grass (Houben & Guillaud, 1994). This can reduce hygrometric shrinkage because of both their traction strength and above all their capability of releasing water slowly (Quagliarini & Lenci, 2010). However, this position is not unanimous because vegetable fibers could rot, leading to the appearance of fungi (Pacheco-Torgal & Jalali, 2012). However, fibers, when present, were added randomly but possibly in a homogeneous way to the wet soil and mixed until getting a complete homogeneous composite. It is known that, in practice, straw fiber addition is suggested to be about $5-10\ kg/m^3$; however, as clay content increases, this proportion can be increased, even if some authors recommend that the fiber content should be restricted about 0.5% by weight (Yetgin, Çavdar, & Çavdar, 2006).

As a matter of fact, ancient brick-makers have not had a chance to do scientific experimental investigation on the balance of ingredients and on the optimization of this production, and it is likely that no weight balance was present on-site many years ago; thus, the components were mixed using different volume quantities. In this way, different quantities in volume of sand (or coarse sand) and fibers (i.e. straw) were usually added to the *in situ* soil. Then a variable volume of water was added to reach a sufficient workability of the mixture: When the sand and fiber content was increased, water content also increased a little. It could be said that addition of sand generally improved workability whereas reducing the sand and vegetable fibers clay fraction became dominant in reducing workability.

Nowadays, a promising way to improve the characteristics of the soil so that the resulting adobe units can bear greater loading and perform better when exposed to weathering is stabilization. Soil stabilization means changing the soil characteristics in order to improve its mechanical or physical behavior. The stabilization processes aim at the reduction of the soil plasticity and improvement of its workability, its compressive strength and its resistance to erosion.

In general, there are three types of stabilization: The first is the mechanical stabilization, the second is the physical stabilization and the third is the chemical stabilization (Medjo Eko, Dieudonné Offa, Yatchoupou Ngatcha, & Seba Minsili, 2012). Mechanical stabilization relates to the densification of soil through compaction. Physical stabilization modifies the soil properties through processes such as soil texture improvement, firing, freezing or electro-osmosis. Chemical stabilization modifies soil properties through mixing with chemical additives such as cement or lime (i.e. combining with 4−10% cement stabilization significantly improves compressive strength and water resistance in comparison with traditional adobe blocks (Morel, Pkla, & Walker, 2007)). The most effective method to modify the adobe is its stabilization with additives. Molasses, bitumen, cow-dung and saw dust could be used as stabilizers (Pacheco-Torgal & Jalali, 2012). In addition, plasticizers used in the concrete industry could be used, such as lignins or naphthalene sulfonates, which are readily available and cheap. Resin or pozzolan can also be used. Natural fibers such as straw,

coconut and sisal can be used for additive. Artificial fibers can also be used in adobes, such as plastic or polystyrene fabrics. Bitumen emulsion can be used to prevent the water absorption of fibers (Yetgin et al., 2006).

It is important to underline that if we want to manufacture eco-efficient adobe blocks, the stabilization through, for example cement or lime, could be somewhat inadequate. In fact, this stabilization does not enable the recycling of the material, and this is not good from a sustainable development standpoint. Furthermore, the use of cement or lime (for example) could also meet an economic problem and the availability of these materials in the market in some countries and regions (Bui, Morel, Reddy, & Ghayad, 2009). Anyway, in some specific cases, it could be the only solution for some applications (i.e. low-cost buildings in India subject to the monsoon to avoid having to rebuild every year) (Morel, Aubert, Millogo, Hamard, & Fabbri, 2013).

16.3 Adobe blocks properties

This section provides the principal mechanical and hygro-thermal properties of adobe blocks, how to determine them and which parameters influence them.

16.3.1 Mechanical properties

The adobe does not reach mechanical strength as high as concrete or fired brick. However, some studies observed that the adobe is strong enough, ductile and resistant against earthquakes (Yetgin et al., 2006). In the literature, many studies elaborate on the mechanical properties of adobe bricks (see for example Binici, Aksogan, & Shah, 2005; Bouhicha, Aouissi, & Kenai, 2005; Clementi, Lenci, & Sadowski, 2008; Kumar, Walia, & Mohan, 2006; Lenci, Clementi, & Sadowski, 2011, 2012; Piattoni, Quagliarini, & Lenci, 2011; Quagliarini & Lenci, 2010; Quagliarini et al., 2010; Yetgin et al., 2006). As for stone or brick masonry, the capacity of adobe masonry in compression is strongly related to the compressive strength of its blocks as well as mortar strength, bonding pattern and many other factors. Thus, compressive strength has become a basic and universally accepted unit of measurement to specify the quality of masonry units. The relative ease of undertaking laboratory compressive strength testing has also contributed to its universality as an expression of material quality (Morel et al., 2007).

Considerable variations in the composition of the used soil make the measurement of compressive strength of adobe blocks an important quality control measure for manufacturers and builders. Even if standardized testing methods for evaluating the unconfined compressive strength of cohesive soils are present in literature, they examine earthen materials from the scope of geomechanics rather than in the context of common building applications (Illampas et al., 2014). Thus, quality control strength testing of adobe blocks has often followed procedures developed for fired clay and concrete block units (Morel et al., 2007). However, the suitability of these procedures has largely not been checked by scientific study. The compressive strength of adobe blocks can be many times lower than similar fired bricks. In addition, compressive strength is

improved by compaction effort (density) and cement content but reduced by increasing moisture content and clay content. National and international guideline documents have also been developed for earth block test procedures (14.7.4NMAC, 2009; New Zealand Standard 4298, 1998; NTE E0.80, 2000; Standards Australia Handbook 194, 2002). These documents include specific references to testing methodologies and prescribe permissible strength values. Nevertheless, there is little general consensus on test procedure, and some questions, such as how the dimensional effects (i.e. aspect ratio) and platen restraint have to be taken into account, still remain without a unique answer.

Considerable differences also occur in the treatment of samples prior to testing. Specimens may be stored under stable thermo-hygrometric conditions for a certain period of time, oven-dried at a certain temperature up to constant weight or placed outdoors under direct sunlight or in the shade so as to replicate traditional production methods (Illampas et al., 2014).

In general, geometrical effects on single adobe block compressive strength are treated in one of two ways. In many standard test procedures, platen restraint effects are usually neglected. Average or characteristic compressive strength is simply expressed following statistical manipulation of individual test results (Morel et al., 2007), in which these results are often obtained by dividing the net force by the area of the specimen (i.e. by considering the average or nominal stress) and by measuring the vertical displacements only at the center of the block. In this way, the possible nonparallelism between the two platens is missed, as well as the induced combined compressive and bending stresses.

In an alternative approach, used in both Australia (Middleton, 1992; Standards Australia Handbook 194, 2002) and New Zealand (New Zealand Standard 4298, 1998), platen restraint effects are catered for by factoring test values with an aspect correction factor. Correction factors used are typically the same as derived for fired clay units (Figures 16.5−16.6), although other work has suggested alternatives (Heathcote & Jankulovski, 1992). Hence, direct comparison of the test results obtained by different researchers is not always possible.

The methodology adopted in many national standards and codes of practice is similar to that used for fired clay and concrete blocks (Morel et al., 2007). Single units are capped and tested directly between platens. Block surfaces are usually sufficiently flat and parallel to achieve a uniform distribution of the compressive load, and capping with plywood, softwood, mortar, cardboard or a layer of sand (Illampas et al., 2014; Piattoni et al., 2011) can be applied on the specimens' surfaces. Alternatively, smoothening of irregularities by abrasion may be carried out (Illampas et al., 2014). Adobe samples obtained from existing walls, cut from full-size bricks or formed through mold casting have also been examined in the literature (Illampas et al., 2014).

The test units include full size bricks; prisms with length-to-width ratios from 2 to 0.5 and cubes with edges of 40, 50, 100 and 150 mm (Illampas et al., 2014; Piattoni et al., 2011; Quagliarini & Lenci, 2010). The use of cylinders with 1:1 and 2:1 aspect ratios and diameters ranging from 50 to 150 mm is also quite common (Illampas et al., 2014). A scheme is reported in Table 16.1.

Figure 16.5 A typical compressive test on an adobe block specimen.

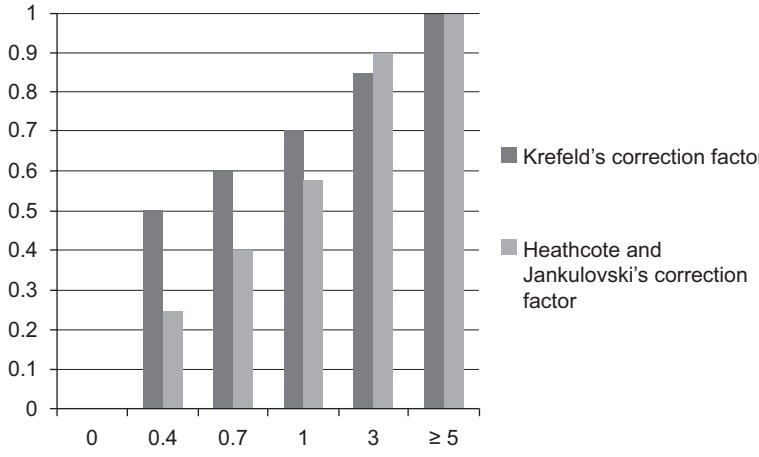

Figure 16.6 Correction factors for confined compressive strength. Data elaborated from Morel et al. (2007).

Table 16.1 Typical geometrical dimensions of specimens tested for determining the compressive strength of adobe blocks

Full size brick	As manufactured
Prisms (aspect ratio)	0.5−2
Cubes (mm)	40−150
Cylinders (aspect ratio)	1−2
Cylinders (diameter, mm)	50−150

Blocks are generally tested along the direction in which they have been pressed, which is also the direction in which they are generally laid. Test samples generally comprise between five and ten blocks. Compressive loading is imposed following either a load-controlled (Quagliarini & Lenci, 2010) or a displacement-controlled (Lenci, Piattoni, Clementi, & Sadowski, 2011) procedure. The aim of the latter is to provide information regarding the post-yield behavior of the material. In load-controlled tests, typical applied compression rates are set to between 0.03 and 0.1 MPa/s (Quagliarini & Lenci, 2010; Silveira, Varum, & Costa, 2013). In displacement-controlled tests, constant vertical displacement is imposed at a rate between 0.5 and 7 mm/min (Bouhicha et al., 2005; Ghavami, Filho, & Barbosa, 1999; Kouakou & Morel, 2009; Silveira et al., 2012, 2013; Villamizar, Spinosi Araque, Ríos Reyes, & Sandoval Silva, 2012).

The results of compression tests reported in the literature vary from 0.6 to 8.3 MPa, the most common values being between 0.8 and 3.5 MPa. The lowest strength limits set in national directive documents range from 1.2 to 2.1 MPa (Illampas et al., 2014). Hence, because a single- or a two-storey dwelling usually has a downward thrust from about 0.1 to 0.2 MPa, earthen adobe walls could generally withstand this with a reasonable safety factor.

Apart from the mere determination of the failure stress, constitutive models describing the compressive stress−strain response of adobes have also been developed (Silveira et al., 2013). Recent results have shown how the granular content controls the Young's modulus of the adobe blocks whereas natural fibers control the "plastic" behavior and influence the way they break (Quagliarini & Lenci, 2010).

In addition, stabilization created by stiffening the material will induce a commonly observed behavior in brittle materials as concrete or stone. In contrast, the unstabilized material is likely to be closer to the conventional behavior of soils. In this case, the soil behavior elasto-plastic models are a priori better suited to earthen materials (Morel et al., 2013).

16.3.2 Hygro-thermal properties

Adobe blocks made by unfired clay and straw in different percentages were commonly used in many regions of the world, not only for their mechanical properties, as shown

above, but also for the comfort level of buildings made with earth. Because of its high thermal capacity, earth could store heat absorbed during the day, keeping the interior of a dwelling constructed from earth relatively cool (Parra-Saldivar & Batty, 2006). When the outside temperature drops at night, the walls would emit the heat stored during the day inside of the building. The specific heat capacity of the adobe material is considered to be a key factor in its ability to moderate temperature peaks in buildings because adobe materials have relatively high thermal conductivities. In fact, Maniatidis & Walker, (2003) report conductivities of rammed earth of about 0.58 W/m K according to Delgado & Guerrero (2006) and other authors. Some values collected in literature (Acosta, Diaz, Zarazua, & Garcia, 2010) in comparison with other materials are reported in Table 16.2.

The little amount of straw added to the soil in order to reduce shrinkage of adobe blocks does not affect in a strong way the thermal conductivity. Figure 16.7 reports thermal conductivity of adobe block with different straw percentages.

Finally, the ability of adobe blocks to conduct heat also depends on the moisture content (Hall & Djerbib, 2004, 2006a,b) because of the strong relationship between water content and heat conduction (Rees, Zhou, & Thomas, 2001). In moderate and hot climates, the moisture content of adobe blocks could be an advantage because of the phase transition of the water. When the material starts to dry, water evaporates; therefore, heat loss in the form of latent heat occurs, which in turn causes the external surface temperature to decrease. Thus, considering the overall rate of heat transfer, the U-value for a 300 mm-thick earth wall can reach 1.9–2.0 W/m^2 K, even if Delgado & Guerrero (2006) report lower U-values (1.5 W/m^2 K).

With these data, it is clear that earth could not be considered a good insulation material, but even a poor insulating material can insulate effectively if it is large enough (Acosta et al., 2010) and if it can "absorb" heat (Di Perna, Stazi, Casalena, & D'Orazio, 2011). In fact, several studies show that an adobe house can maintain natural thermal comfort throughout the whole year (Eben Saleh, 1990). The adobe house buildings have a natural air conditioning effect because the temperature of rooms tends to be cool during daytime and warm during nighttime (Chel & Tiwari, 2009; Coffman, Duffin, & Knowles, 1980).

Table 16.2 Thermal conductivity of adobe block in comparison with other materials

Type of adobe	Thermal conductivity (W/m K)
Fired adobe	0.244
Concrete brick	0.6277
Adobe	0.24
Straw bales	0.05–0.08
Adobe with straw (5–10%)	0.180
Expanded polystyrene	0.036

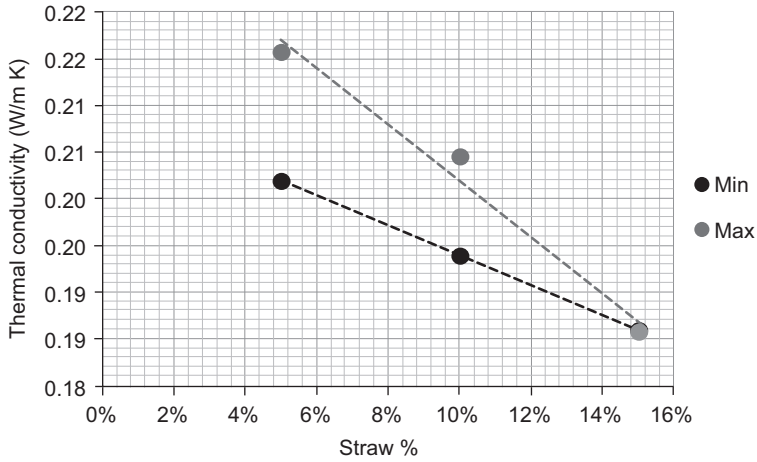

Figure 16.7 Relationship between straw content and thermal conductivity.

The comparison of the thermal behavior of an adobe house with a modern concrete house in Yemen showed the benefit of mud as construction material for energy saving in houses (Algifri, Bin Gadhi, & Nijaguna, 1992). Bahadori & Haghighat (1985) and Chel & Tiwari (2009) predicted the room air temperature and energy saving potential of adobe houses with a vault roof structure. Martín, Mazarrón, & Cañas, (2010) analyzed the comfort conditions inside earth buildings in Spain. Finally, Parra-Saldivar & Batty, (2006) analyzed the effects of window size, the position of and the presence or absence of internal walls and type of roof constructions on the thermal performance of adobe constructions. They show that the adobe walls grant decrements of the indoor temperature with respect to external temperature; however, the percentage decrement is strongly related to the window dimension.

The thermal performance of adobe blocks is measured in a number of different ways. Millogo, Morel, Aubert, & Ghavami (2014) report conductivity values of pressed adobe blocks measured in a transient state with a hot wire probe, which is also a heating resistor. Govaer (1987) uses a similar procedure with cylindrical specimens. However, more accurate measurement in a steady state can be realized with a hot-guarded plate apparatus (Gonçalves & Bergmann, 2007) according to ASTM C 177 or ASTM E1225-13. Another method is the calibrated hot box method according to ASTM C1363-11. This method provides laboratory measurement of heat transfer through a specimen under controlled air temperature, air velocity and radiation conditions established in a metering chamber on one side and in a climatic chamber on the other side.

Another advantage of adobe blocks is related to their ability in moderating changes of indoor relative humidity. An unfired clay block is, in fact, much superior to burnt brick as a humidity buffer, and its hygroscopic behaviour can be more effective in reducing the indoor air relative humidity than the use of ventilation (Padfield, 1998). Some investigations show that earth blocks can absorb 10 times more weight moisture than ceramic bricks and that an earth construction is capable of keeping

the relative humidity of indoor air between 40% and 60%, which is the optimum range for human health (Pacheco-Torgal & Jalali, 2012).

16.4 Durability of adobe blocks

This section outlines the present methods of testing adobe blocks for durability and suggests practical advice on how to maintain or improve it. The durability of adobe structures is testified by the fact that some of these buildings last for hundreds of years. It usually depends on appropriate maintenance and repairs that are compatible with the original construction. In general, adobe structures may be protected by correctly designing the roof or protecting them (i.e. by plaster). Anyway, water is the main potential drawback for adobe blocks.

Adobe walls can, in fact, erode under rain impact and can collapse when exposed to continuous rain for several hours. In addition, water absorption may cause the swelling of clay minerals whereas evaporation of water from the clay gives rise to shrinkage and cracking. Therefore, adobe walls that are not protected suffer greatly from durability problems due to water erosion, penetration and evaporation.

In order to improve the durability of exposed adobe blocks, cement has been used to stabilize them by mixing up to 15% cement with soil, and bitumen emulsion has also been used to stabilize earth blocks and to reduce the water absorption of them; up to 20% bitumen emulsion has been mixed with the soil (Ren & Kagi, 1995). However, the use of either cement or bitumen emulsion can be, in general, impractical because of the mixing problems and the cost of the large quantities of these materials needed to increase the durability of the adobe. Materials such as soluble silicate, ethyl silicate, silanes or siloxanes, isocyanates and various polymers have been also used as consolidation or waterproofing agents to treat the earth-block surface through impregnation. However, these treatments may be applied with caution, because of their costs, to the use of large quantities of undesirable organic solvents (an environmental problem) and to the often unsatisfactory waterproof results (Ren & Kagi, 1995).

Impregnating the adobe block with soluble sodium silicate followed by water-based organic silicone emulsion has been tested for its consolidating and waterproofing. The durability of the treated blocks was found to be significantly increased compared with that of the untreated ones; in addition, very low concentrations of both sodium silicate and silicone emulsion were used, and there were no organic solvents involved in the treatment. Therefore, the cost of the treatment was low and could be acceptable for increasing the durability of structures.

Several types of durability tests (Cid-Falceto, Mazarrón, & Cañas, 2012) are proposed for earthen materials, obtaining dispersed results because of the variability of their technical test specifications (Hall, 2007; Mbumbia, Mertens de Wilmars, & Tirlocq, 2000; Ogunye & Boussabaine, 2002; Ola & Mbata, 1990; Reddy & Jagadish, 1987).

However, recent studies have shown that these tests could be too severe and unrealistic because unstabilized earth blocks could often not pass these tests whereas

existing traditional unstabilized earth walls have undergone more than 100 years of weathering (Bui et al., 2009). That is why the development of new suitable durability tests accounting for, for example, the different climatic conditions is a main issue and further studies need to be carried out. This could be also important to decide when the stabilization is needed.

The most common durability tests currently used are the spray erosion test and the drip erosion test. These are mentioned for adobe blocks in several national standards (Cid-Falceto et al., 2012).

These tests have been also proposed in numerous documents and are usually considered empirical: The spray erosion test is usually referred to as a direct replica of the erosion originated by rain water, studying its application on real conditions, whereas the drip erosion test is a good, cheap test for testing blocks in areas of little rain (Cid-Falceto et al., 2012).

All of the tests are based on the same ground of subjecting a test tube to a pressure spray for a certain amount of time or until specimen is penetrated (spray erosion), or to a constant waterfall for a certain amount of time (drip erosion), in order to evaluate afterward the damage caused in both cases.

In the spray erosion test, parameters such as tested side, number of samples to be tested, exposed area, spray time, observations, application distance (nozzle-specimen) and pressure are defined. The height of the waterfall or the slope of the sample to be tested are instead provided for the drip erosion test.

16.5 Future trends for eco-efficient constructions

This section deals with the environmental and economic benefits potentially associated with the use of adobe earth-based masonry blocks, including new ways to reuse bulk industrial waste as stabilizers. Nowadays, the use of nonindustrial materials has been rediscovered because of environmental problems caused by the excessive use of the industrial materials. The concept of nonindustrial building materials means local materials manufactured using a simple, quick process with low embodied energy using raw materials from the site or nearby (Kouakou & Morel, 2009). The use of soil as a raw material can be considered a way to perform it. The soil should be taken from the construction site or nearby in order to limit transportation and must contain clay particles to reduce or avoid the use of industrial binders such as lime and cement (see previous sections). Thus, similar to dry stonemasonry, soil can represent one of the few construction materials that can be easily reused and does not generate waste (Kouakou & Morel, 2009). At the end of a building's life, an unstabilized adobe block can be easily reused by grinding or wetting, or it can be returned to the ground with no environmental hazard involved; in fact, it is able to be returned to its initial state (as a soil) by simply wetting.

Even when the soil is stabilized with cement or lime, it could potentially be reused for this type of construction (Pacheco-Torgal & Jalali, 2012), even if this is not a unanimous standpoint in the literature (Morel et al., 2013). By using adobe blocks, an economic impact may be also pursued: The slight cost of raw material, local skills and

employment can be developed because of their simple manufacturing, and auto-construction can be promoted.

Another advantage of using adobe blocks could be associated with no indoor air volatile organic compounds; thus, the dwellers should have better indoor air quality (Pacheco-Torgal & Jalali, 2012). Although data on waste-material-reinforced unfired blocks are still limited, new ways to reuse bulk industrial waste as stabilizers for adobe blocks can be followed too. Replacing natural soils, aggregates and typically employed stabilizers with industrial wastes is highly desirable so as to offer a substantial environmental contribution to society. In some cases, a by-product could be inferior to traditional earthen materials, but, because of its lower cost, this could be an attractive alternative if adequate performance can be obtained.

The worldwide development of the agroindustry annually produces large volumes of agricultural wastes, and their disposal causes major challenges and serious economic and environmental problems (Villamizar et al., 2012). During recent years, alternative uses of these wastes have been carried out to reduce their amount, and some first results have also been provided to develop their use in the manufacture of earth blocks with initial good results. In fact, several types of organic fibres can be produced from a relevant number of agroindustrial wastes. Thus, they could be included within a mixture so as to reinforce adobe blocks, although they do not provide adequate durability alone (Villamizar et al., 2012).

A huge quantity of straw is produced every summer, and farmers often burn this material, giving rise to ecological problems: instead of burning, this material could be used in adobe block production. However, locally available materials such as barley straw, bamboo, sisal, coconut and *Hibiscus cannabinus* fibers were also tested in earth construction (Bouhicha et al., 2005; Ghavami et al., 1999; Millogo et al. 2014). The rice hull ash was also studied as an earthen stabilizer, and the incorporation of craft paper fibers from discarded cement bags was studied for the production of earthen blocks (Lima, Varum, Sales, & Neto, 2012). In addition, other studies suggested that synthetic fibres recovered from various waste streams, such as plastic fibers and polystyrene fabric or salvaged steel fibers, rather than deteriorating the environment could be used for the reinforcement of earthen blocks (Medjo Eko et al., 2012).

16.6 Sources of further information and advice

Suggested general standards or handbooks on adobe block are the following:

- ASTM C177-13. Standard Test Method for Steady-State Heat Flux Measurements and Thermal Transmission Properties by Means of the Guarded-Hot-Plate Apparatus, ASTM International, West Conshohocken, PA, 2013.
- ASTM C1363-11. Standard Test Method for Thermal Performance of Building Materials and Envelope Assemblies by Means of a Hot Box Apparatus, ASTM International, West Conshohocken, PA, 2011.
- ASTM D2166-06. Standard Test Method for Unconfined Compressive Strength of Cohesive Soil. West Conshohocken, PA: ASTM International; 2006.

- ASTM E1225-13. Standard Test Method for Thermal Conductivity of Solids Using the Guarded-Comparative-Longitudinal Heat Flow Technique, ASTM International, West Conshohocken, PA, 2013.
- Earth Building Association of Australia (EBAA). Earth Building Book. Draft for Comment. Draft Code 05/01. Wangaratta, Australia: Earth Building Association of Australia, 2001.
- Houben, H., Guillaud, H. (1994) Earth construction. A comprehensive guide. CRATerre-EAG, London, ITDG publishing
- Middleton G.F., 1987 (revised by Schneider L.M.) Fourth Edition. Bulletin 5. Earth Wall Construction. North Ryde, Australia: CSIRO Division of Building, Construction and Engineering, 1992.
- Minke G. (2000) Earth construction handbook, WIT press, Southampton, Boston.
- MOPT. Bases Para el Diseno y Construccion con Tapial. Madrid, Spain: Centro de Publicaciones, Secretaría General Tecnica, Ministerio de Obras Publicas y Transportes, 1992.
- NMAC New Mexico Administrative Code 14.7.4. 2009 New Mexico Earthen Building Materials Code. Santa Fé, NM: Construction Industries Division (CID) of the Regulation and Licensing Department, 2009.
- SAZ. Standards Association Zimbabwe Standard (SAZS) 724:2001: Standard Code of Practice for Rammed Earth Structures. Harare: Standards Association of Zimbabwe, 2001.
- SENCICO. Norma Técnica Edificación NTE E 0.80 Adobe. Reglamento Nacional de Construcciones. Lima: SENCICO, 2000.
- SNZ. New Zealand Standard 4297:1998. Engineering design of earth buildings. Wellington: Standards New Zealand, 1998.
- SNZ. New Zealand Standard 4298:1998. Materials and workmanship for earth buildings. Wellington: Standards New Zealand, 1998.
- SNZ. New Zealand Standard 4299:1998. Earth buildings not requiring specific design. Wellington: Standards New Zealand, 1999.
- Standards Australia Handbook 194. The Australian earth building handbook. Standards Australia, Sydney, Australia; 2002.
- Standards Australia and Walker P. HB 195: The Australian earth building handbook. Sydney (Australia): Standards Australia, 2002.

References

Acosta, J. D. R., Diaz, A. G., Zarazua, G. M. S., & Garcia, E. R. (2010). Adobe as a sustainable material: a thermal performance. *Journal of Applied Science, 10*, 2211−2216.

Adam, J. P. (1984). *L'arte di costruire presso i romani*. Milano (in Italian): Longanesi.

Algifri, A. H., Bin Gadhi, S. M., & Nijaguna, B. T. (1992). Thermal behaviour of adobe and concrete houses in Yemen. *Renewable Energy, 2*, 597−602.

Bahadori, M. N., & Haghighat, F. (1985). Weekly storage of coolness in heavy brick and adobe walls. *Energy and Buildings, 8*, 259−270.

Barbaro, D. (1997). *Lucio Vitruvio Pollione. I dieci libri dell'architettura (rist. anast. 1567)*. Il Polifilo (in Italian).

Binici, H., Aksogan, O., & Shah, T. (2005). Investigation of fibre reinforced mud brick as a building material. *Construction and Building Materials, 19*(4), 313−318.

Bouhicha, M., Aouissi, F., & Kenai, S. (2005). Performance of composite soil reinforced with barley straw. *Cement and Concrete Composites, 27*(5), 617−621.

Bui, Q. B., Morel, J. C., Reddy, B. V. V., & Ghayad, W. (2009). Durability of rammed earth walls exposed for 20 years to natural weathering. *Building and Environment, 44*, 912−919.

Chel, A., & Tiwari, G. N. (2009). Performance evaluation and life cycle cost analysis of earth to air heat exchanger integrated with adobe building for New Delhi composite climate. *Energy and Buildings, 41*, 56−66.

Cid-Falceto, J., Mazarrón, F. R., & Cañas, I. (2012). Assessment of compressed earth blocks made in Spain: International durability tests. *Construction and Building Materials, 37*, 738−745.

Clementi, F., Lenci, S., & Sadowski, T. (2008). Fracture characteristics of unfired earth. *International Journal of Fracture, 149*, 193−198.

Coffman, C. V., Duffin, R. J., & Knowles, G. P. (1980). Are adobe walls optimal phase-shift filters? *Advances in Applied Mathematics, 1*, 50−66.

Cofirman, R., Agnew, N., Auiston, G., & Doehne, E. (October 1990). Adobe mineralogy: characterisation of adobes from around the world. In *Proceedings of the 6th International Conference on the Conservation of Earthen Architecture* (pp. 14−19). Las Cruces, NM.

Delgado, M. C. J., & Guerrero, I. C. (2006). Earth building in Spain. *Construction and Building Materials, 20*, 679−690.

Di Perna, C., Stazi, F., Casalena, A. U., & D'Orazio, M. (2011). Influence of the internal inertia of the building envelope on summertime comfort in buildings with high internal heat loads. *Energy and Buildings, 43*, 200−206.

Eben Saleh, M. A. E. (1990). Adobe as a thermal regulating material. *Solar and Wind Technology, 7*, 407−416.

Ghavami, K., Filho, R. D. T., & Barbosa, N. P. (1999). Behaviour of composite soil reinforced with natural fibres. *Cement and Concrete Composites, 21*, 39−48.

Gonçalves, M. R. F., & Bergmann, C. P. (2007). Thermal insulators made with rice husk ashes: production and correlation between properties and microstructure. *Construction and Building Materials, 21*, 2059−2065.

Govaer, D. (1987). Apparent thermal conductivity of a local adobe building material. *Solar Energy, 38*, 165−168.

Hall, M. R. (2007). Assessing the environmental performance of stabilised rammed earth walls using a climatic simulation chamber. *Building and Environment, 42*, 139−145.

Hall, M., & Djerbib, Y. (2004). Moisture ingress in rammed earth: Part 1—the effect of soil particle-size distribution on the rate of capillary suction. *Construction and Building Materials, 18*, 269−280.

Hall, M., & Djerbib, Y. (2006a). Moisture ingress in rammed earth: Part 2 − the effect of soil particle-size distribution on the absorption of static pressure-driven water. *Construction and Building Materials, 20*, 374−383.

Hall, M., & Djerbib, Y. (2006b). Moisture ingress in rammed earth: Part 3 − sorptivity, surface receptiveness and surface inflow velocity. *Construction and Building Materials, 20*, 384−395.

Heathcote, K. A. (1995). Durability of earthwall buildings. *Construction and Building Materials, 9*, 185−189.

Heathcote, K., & Jankulovski, E. (1992). Aspect ratio correction factors for soilcrete blocks. In *Australian civil engineering transactions* (vol. CE34, pp. 309−312). Australia: Institution of Engineers, 4.

Houben, H., & Guillaud, H. (1994). *Earth construction. A comprehensive guide*. CRATerre-EAG. London: ITDG publishing.

Illampas, R., Ioannou, I., & Charmpis, D. C. (2014). Adobe bricks under compression: experimental investigation and derivation of stress−strain equation. *Construction and Building Materials, 53*, 83−90.

Kouakou, C. H., & Morel, J. C. (2009). Strength and elasto-plastic properties of non-industrial building materials manufactured with clay as a natural binder. *Applied Clay Science, 44*, 27−34.

Kumar, A., Walia, B. S., & Mohan, J. (2006). Compressive strength of fiber reinforced highly compressible clay. *Construction and Building Materials, 20*(10), 1063−1068.

Lenci, S., Clementi, F., & Sadowski, T. (2012). Experimental determination of the fracture properties of unfired dry earth. *Engineering Fracture Mechanics, 87*, 62−72.

Lenci, S., Piattoni, Q., Clementi, F., & Sadowski, T. (2011). An experimental study on damage evolution of unfired dry earth under compression. *International Journal of Fracture, 172*, 193−200.

Lima, S. A., Varum, H., Sales, A., & Neto, V. F. (2012). Analysis of the mechanical properties of compressed earth block masonry using the sugarcane bagasse ash. *Construction and Building Materials, 35*, 829−837.

Maniatidis, V., & Walker, P. (2003). *A review of rammed earth construction*. Univ. Bath.

Martín, S., Mazarrón, F. R., & Cañas, I. (2010). Study of thermal environment inside rural houses of Navapalos (Spain): the advantages of reuse buildings of high thermal inertia. *Construction and Building Materials, 24*, 666−676.

Mbumbia, L., Mertens de Wilmars, A., & Tirlocq, J. (2000). Performance characteristics of lateritic soil bricks fired at low temperatures: a case study of Cameroon. *Construction and Building Materials, 14*, 121−131.

Medjo Eko, R., Dieudonné Offa, E., Yatchoupou Ngatcha, T., & Seba Minsili, L. (2012). Potential of salvaged steel fibers for reinforcement of unfired earth blocks. *Construction and Building Materials, 35*, 340−346.

Middleton, G. F. (1992). *Earth-wall construction, Bulletin 5, CSIRO Division of building, construction and engineering* (4th ed.) (Sydney [revised by Schneider, L.M.]).

Millogo, Y., Morel, J.-C., Aubert, J.-E., & Ghavami, K. (2014). Experimental analysis of pressed adobe blocks reinforced with *Hibiscus cannabinus* fibers. *Construction and Building Materials, 52*, 71−78.

Minke, G. (2000). *Earth construction handbook*. Southampton, Boston: WIT press.

Morel, J. C., Aubert, J. E., Millogo, Y., Hamard, E., & Fabbri, A. (2013). Some observations about the paper "Earth construction: Lessons from the past for future eco-efficient construction" by F. Pacheco-Torgal and S. Jalali. *Construction and Building Materials, 44*, 419−421.

Morel, J. C., Pkla, A., & Walker, P. (2007). Compressive strength testing of compressed earth blocks. *Construction and Building Materials, 21*, 303−309.

14.7.4NMAC. (2006). New Mexico earthen building materials code. *New Mexico State Construction Industries Division Regul Licensing Department*.

New Zealand Standard 4298. (1998). *Materials and workmanship for earth buildings*. Wellington: Standards New Zealand.

NTE E0.80. (2000). *Adobe: Norma Técnica de Edificación. Lima*. Ministerio de Transportes, Comunicaciones, Vivienda y Construcción.

Ogunye, F. O., & Boussabaine, H. (2002). Development of a rainfall test rig as an aid in soil block weathering assessment. *Construction and Building Materials, 16*, 173−180.

Ola, S. A., & Mbata, A. (1990). Durability of soil-cement for building purposes − rain erosion resistance test. *Construction and Building Materials, 4*, 182−187.

Pacheco-Torgal, F., & Jalali, S. (2012). Earth construction: Lessons from the past for future eco-efficient construction. *Construction and Building Materials, 29*, 512−519.

Padfield, T. (1998). *The role of absorbent building materials in moderating changes of relative humidity* (Ph.D. thesis). Department of Structural Engineering and Materials, The Technical University of Denmark, http://www.natmus.dk/cons/tp/phd/phd-indx.htm.

Parra-Saldivar, M. L., & Batty, W. (2006). Thermal behaviour of adobe constructions. *Building and Environment, 41*, 1892−1904.

Piattoni, Q., Quagliarini, E., & Lenci, S. (2011). Experimental analysis and modelling of the mechanical behaviour of earthen bricks. *Construction and Building Materials, 25*(4), 2067−7.

Quagliarini, E., & Lenci, S. (2010). The influence of natural stabilizers and natural fibres on the mechanical properties of ancient Roman adobe bricks. *Journal of Cultural Heritage, 11*, 309−314.

Quagliarini, E., Lenci, S., & Iorio, M. (2010). Mechanical properties of adobe walls in a Roman Republican domus at Suasa. *Journal of Cultural Heritage, 11*, 130−137.

Reddy, B. V. V., & Jagadish, K. S. (1987). Spray erosion studies on pressed soil blocks. *Building and Environment, 22*, 135−140.

Rees, S. W., Zhou, Z., & Thomas, H. R. (2001). The influence of soil moisture content variations on heat losses from earth-contact structures: an initial assessment. *Building and Environment, 36*, 157−165.

Ren, K. B., & Kagi, D. A. (1995). Upgrading the durability of mud bricks by impregnation. *Building and Environment, 30*(3), 433−440.

Silveira, D., Varum, H., Costa, A., Martins, T., Pereira, H., & Almeida, J. (2012). Mechanical properties of adobe bricks in ancient constructions. *Construction and Building Materials, 28*, 36−44.

Silveira, D., Varum, H., & Costa, A. (2013). Influence of the testing procedures in the mechanical characterization of adobe bricks. *Construction and Building Materials, 40*, 719−728 (Special Section on Recycling Wastes for Use as Construction Materials).

Standards Australia Handbook 194. (2002). *The Australian earth building handbook*. Sydney, Australia: Standards Australia.

Villamizar, M. C. N., Spinosi Araque, V., Ríos Reyes, C. A., & Sandoval Silva, R. (2012). Effect of the addition of coal-ash and cassava peels on the engineering properties of compressed earth blocks. *Construction and Building Materials, 36*, 276−286.

Yetgin, Ş., Çavdar, Ö., & Çavdar, A. (2006). The effects of the fiber contents on the mechanic properties of the adobe. *Construction and Building Materials, 22*, 222−227.

The properties of compressed earth-based (CEB) masonry blocks

17

F.V. Riza, I.A. Rahman
Universiti Tun Hussein Onn Malaysia, Jalan, Malaysia

17.1 Introduction

Generally, compressed earth-based masonry blocks will give an illustration of the block that is made up of earth-based materials and produced by a masonry method that has been going through a compression process. The definition of compressed earth-based masonry blocks may vary from one country to another, especially with the word 'blocks'. In masonry, the words "block" and "brick" are not strictly categorized, as can be seen from the description from the standards or from expert definitions.

In British Standard BS 3921: 1985, *Clay brick* is defined as "a masonry unit not exceeding 337.5 mm in length, 225 mm in thickness (referred to as width in one of the standards) or 112.5 mm in height". As for block, BS 6073: Part 1: 1981 specification for precast concrete masonry unit states, when used in its normal aspect, it exceeds the length or width or height specified for brick (Thomas, 1996). CDI (1998) defined compressed earth block as "masonry elements principally made of raw earth, which are small in size and which have regular dynamic compression of earth in a humid state followed by immediate demoulding." Morton (2008) even gave a lighter definition for brick and block as a small masonry unit, liftable with one hand, and a large masonry unit liftable with two hands for the latter. Hence, for the rest of this chapter, the use of the word "block" can be interchangeable with "brick" in definition; for that reason CEB can stand for compressed earth block or compressed earth brick.

The main focus of this chapter is the properties of CEB, and as a complement, the properties of CEB made out of agro-waste material, such as rice husk ash (RHA), palm oil fuel ash (POFA) and cassava peels, will be elaborated on briefly.

17.2 Properties of compressed earth-based masonry blocks

This chapter will discuss properties of CEB including its mechanical, physical and thermal properties on a single CEB or prism.

17.2.1 Compressive strength

Apparently, of the physical properties of CEB, compressive strength is the most universally accepted value for determining the quality of bricks. Nevertheless, it is

Eco-efficient Masonry Bricks and Blocks. http://dx.doi.org/10.1016/B978-1-78242-305-8.00017-6

intensely related to the soil types and stabilizer content. Typically, determination of compressive strength in wet conditions will give the weakest strength value. Reduction in compressive strength under saturation conditions can be attributed to the development of pore water pressures and the liquefaction of unstabilized clay minerals in the brick matrix. Factors affecting the CEB brick strength are cement content, types of soil (plasticity index), compaction pressure and types of compaction.

Optimum cement content for the stabilization is in the range of 5 to 10%, where addition above 10% will affect the strength of the bricks in a negative way. Plasticity index of the clay soil is usually in the range of 15 to 25%. The best earth soils for stabilization are those with low plasticity index. But for plasticity index >20, it is not suitable with manual compaction (Walker, 1995). Anifowose (2000) found that the presence of iron in the soil is responsible for low compressive strength in the soil stabilization process. The strength of the CSEB can be increased by adding natural fibers where they can improve the ductility of tension. The improvement is by retarding the tensile crack propagation after initial formation and also the shrinkage cracking (Mesbah, Morel, Walker, & Ghavami, 2004).

Since there is no standard testing for CEB, most researchers determined the compressive strength using the testing method used for fired-clay brick and concrete masonry block such as ASTM 1984, BS 6073-1:1981, BSI 1985, BS EN 772 1998, BS 1924-2:1990, Standard Australia 1997 and Australian Standard 2733 (Oti et al., 2009a, 2009b; Walker, 1995, 2004).

The direct testing and alternative RILEM test usually measures the compressive strength of the CEB. Figure 17.1 shows the effect of CEB height to its compressive strength, indicating that CEBs with greater height tend to have higher compressive strength (Morel, Pkla, & Walker, 2005). Compressive strength of CEB prism with a RILEM test and a direct test is shown in Figure 17.2.

The unconfined compressive test needs expensive equipment and must be carried out in the laboratory. Hence, some researchers suggest using an indirect compressive test (i.e. flexural test/modulus of rupture/three-point bending test). These indirect tests provide simple, inexpensive and fast assessments of *in situ* bending strength of the brick (Morel & Pkla, 2002; Morel et al., 2005). Walker (1995, 2004) suggested using factors where the modulus of rupture is equivalent to one-sixth of its compressive strength, and in his latest experiment suggested that unconfined compressive strength is about five times the bending strength.

Compacting procedure also considerably affects the compressive strength of the CEB brick. Guettala, Houari, Mezghiche, & Chebili (2002) concluded that by increasing the compacting stress from 5 to 20 MPa, it will improve the compressive strength up to 70%. His conclusion was strengthened by Bahar, Benazzoug, & Kenai (2004), who observed that by using dynamic compaction energy, dry compressive strength increases by more than 50%, but for vibro-static, compaction increases slightly by about 5%.

Brick strength and brick characteristic flexural bond strength are factors that limit the bond strength between bricks and mortar in wall panels made from CEB (Walker, 1999). Hence, types of bricks such as solid, interlocking or hollow and types of bonds like English, Flemmish or Rat trap bond also play an important role in the flexural strength of the panels (Jayasinghe & Mallawaarachchi, 2009).

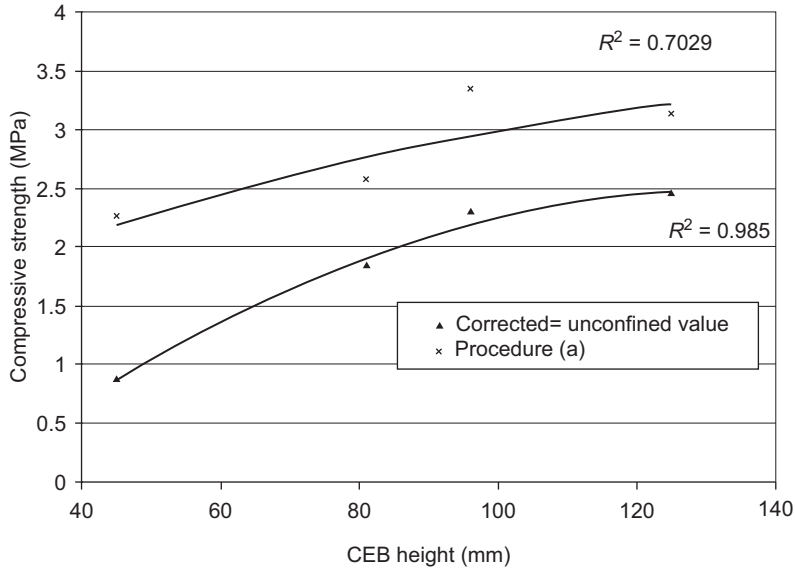

Figure 17.1 Effect of block height on RILEM test compressive strength (Morel et al., 2005).

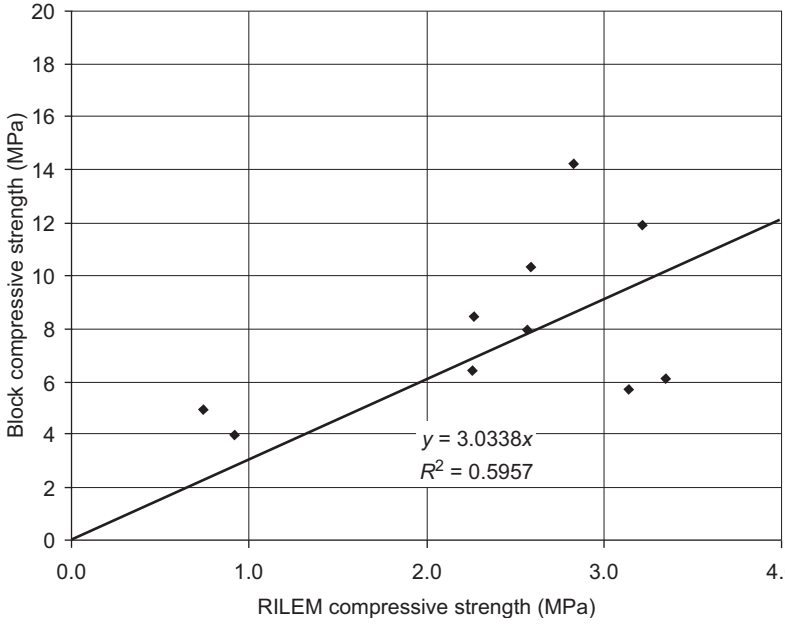

Figure 17.2 Comparison between RILEM prism strength and direct block strength (Morel et al., 2005).

Additional of natural fiber content such as palm date fibers will decrease the tensile strength with the increase of fiber content, but only causes a slight reduction in compressive strength (Taallah, Guettala, Guettala, & Kriker, 2014). However, the addition of natural fiber has unfavorable results on wet compressive strength of the CEB.

17.2.2 Density

Commonly, most researchers found that the density of compressed stabilized earth bricks is within the range of 1500−2000 kg/m^3. Density of the compressed earth brick is consistently related to its compressive strength and compactive force applied during production. The dry density is largely a function of the constituent material's characteristics, moisture content during pressing and the degree of compactive load applied and even in India compressive strength is controlled by density. Types of compaction applied such as dynamic, static and vibro will also affect the density. The density of brick can be determined through standard procedure such as ASTM C 140 and BS 1924-2 (1990) and others (Bahar et al., 2004; Morel et al., 2005; Oti et al., 2009b, 2009c; Walker, 1999).

17.2.3 Water absorption and moisture content

Masonry construction will take on water, with or without coating. Although the mortar and grout in the gutter considerably affect the water resistance of masonry construction, in this section, however, we will only discuss single CEB water absorption and moisture content. As earth masonry, CEBs will absorb more moisture compared with other building materials as shown in Figure 17.3. The results showed that CEB can absorb 10 times more air moisture than fired bricks (Morton, 2008).

Water absorption is a function of clay and cement content and usually related with the strength and durability of earth bricks, and therefore, it is important to determine the rate of water absorption of earth bricks. Oti et al. (2009c) stated that water absorption rate decreases with increasing age of earth bricks. High rate of water absorption of a specimen may cause swelling of stabilized clay fraction and result in losing strength with time. As observed by Walker (Walker & Stace, 1996), water absorption, as well as porosity, increases with clay content and decreasing cement content.

Between cement, lime, cement-lime and cement-resin, a combination of cement and resin stabilization shows the lowest water absorption both in capillary absorption and total absorption (Guettala, Abibsi, & Houari, 2006). Freidin & Erell (1995) tried to reduce the water uptake by adding a hydrophobic material; in this case, siloxane-polymethylhydrohen-siloxane was combined with slag + fly ash, which is highly absorbent, and the result showed that the water uptake with the addition of 0.5% siloxane was less than a quarter of the water uptake of fly ash−slag without additive.

Sand content in the mixes apparently can reduce water absorption and weight loss even though it does not affect the compressive strength significantly (Guettala et al., 2002). The standards used to determine water absorption are ASTM C 140 (total water

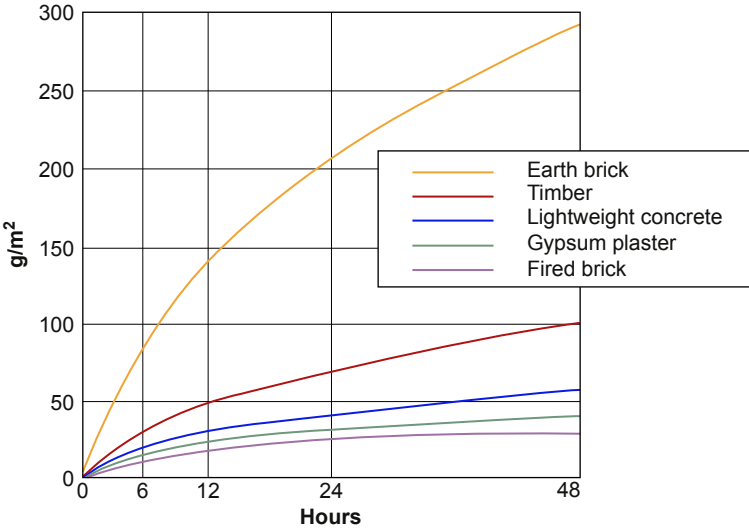

Figure 17.3 The weight of moisture absorbed by different materials after an increase in relative humidity from 50% to 80% RH (Morton, 2008).

absorption), BS EN 771-2 and Australian Standards 2733 (initial rate of absorption) (Oti et al., 2009b; Walker, 1999; Walker & Stace, 1996).

Moisture content affects strength development and durability of the material and has a significant influence on the long-term performance of stabilized soil material, especially on bonding with mortars at the time of construction. When the brick is dry, water is rapidly sucked out of the mortar, thereby preventing good adhesion and proper hydration of the cement, and when the brick is very wet, the mortars tend to float on the surface without gaining proper adhesion (Oti et al., 2009c; Walker, 1999).

Types of compaction affect the optimum water content in the stabilized mixes. Dynamic compaction can reduce the optimum water content from 12% to 10% with the compressive strength increased for about 50%. Bahar et al. (2004) stated the optimum water content ranges between 10% and 13% for static compaction, whereas vibro-static compaction slightly increases compressive strength with the same water content for low compressive load. According to Osula (1996) soil-lime mixes required higher optimum moisture content than soil-cement mixes. Standards conform to determine water content such as ASTM D 558, Australian Standards 1289, BS 1924-2 (1990) and BS EN 1745 (Oti et al., 2009b, 2009c; Walker, 1999; Walker & Stace, 1996).

The addition of natural fiber such as date palm fibers will increase the total water absorption of CEB (Taallah et al., 2014). Figure 17.4 indicates that longer immersion times will cause higher total absorption. Absorption is the process in which a fluid is dissolved by a liquid or a solid (absorbent), while adsorption is the process in which atoms, ions or molecules from a substance (it could be gas, liquid or dissolved solid) adhere to a surface of the adsorbent.

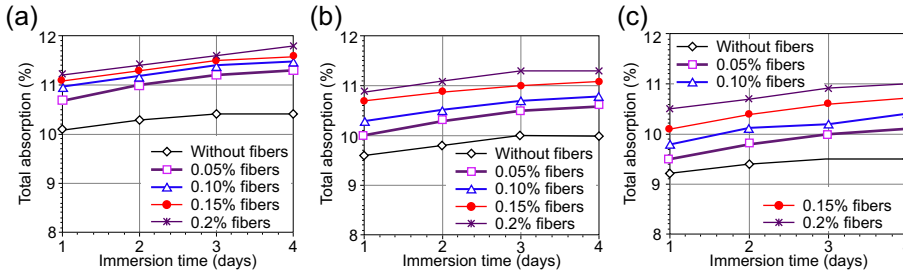

Figure 17.4 Effect of fiber content on the total absorption in time of CEB (with 10 MPa compaction pressure): (a) 5% cement; (b) 6.5% cement; (c) 8% cement (Taallah et al., 2014).

Moisture absorption or desorption properties of CEB can be used as a way to improve indoor air quality and save energy, also known as moisture buffering (Rode & Grau, 2008). Things that affect the practical moisture buffering value (MBV) are open surface and relative humidity, as stated in the report by Rode et al. (2005). Among the conditions that influenced the moisture buffering measurement of CEB is the addition of stabilizers (Figure 17.5).

17.2.4 Shrinkage

Drying shrinkage of the bricks was primarily governed by the plasticity index and cement content. Water loss also contributes to the shrink of the clay fraction. For low clay mineral content (index plasticity below 20%), drying shrinkage showed a steady increase with the increase of clay content, but for a plasticity index beyond 25−30%, drying shrinkage increased rapidly as the clay content also increased. Soil with a plasticity index <20% is good for cement stabilization with cement content 10%. And, the commonly used drying shrinkage limit is from 0.008% to 0.10% (Walker, 1995, 1999; Walker & Stace, 1996).

Sand as part of the mix seems to have significant influence in shrinkage, although sand content does not significantly affect the compressive strength as stated by Guettala (Guettala et al., 2002). However, Rahman (1987) found out it can decrease plasticity, linear shrinkage and warping.

Bahar et al. (2004) reported that shrinkage increases rapidly during the first four days for cement-stabilized earth bricks, and the addition of sand reduces the shrinkage as sand particles oppose the shrinkage movement. He also observed that the addition of cement content can reduce the shrinkage up to 44% for 10% cement content added. BSI 6073 and Australian Standards 2733 can be used to measure the drying shrinkage (Walker, 1995; Walker & Stace, 1996). The addition of natural fiber content can increase the swelling of CEB (Taallah et al., 2014).

17.2.5 Thermal conductivity

In the growing concern of energy consciousness and ecological awareness, thermal comfort in building materials is an important aspect that attracts great attention

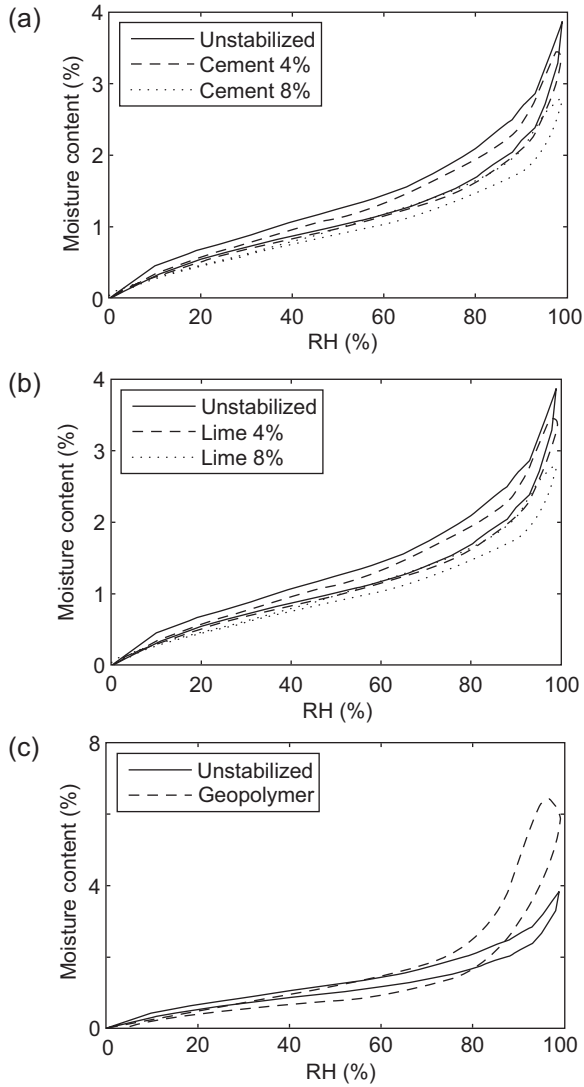

Figure 17.5 DVS water vapor sorption isotherms for different stabilizers: (a) cement, (b) lime, (c) geopolymer (McGregor, Heath, Fodde, & Shea, 2014).

nowadays since building regulations are now stressing more of the thermal performance of the buildings compared to the past. As a building material, brick has quite excellent thermal conductivity. Oti (Oti et al., 2009b) observed that thermal conductivity is a function of the material density and moisture content. Thus, the design value for thermal conductivity can be determined through experimental and theoretical methods. CEB showed better thermal conductivity values compare to the fired-clay bricks.

- Lime-GGBS-based: 0.2545 ± 0.0350 W/m K
- Cement-GGBS-based: 0.2612 ± 0.0350 W/m K
- Fired clay bricks: 0.4007 ± 0.0350 W/m K

Bahar et al. (2004) noted that the addition of cement and sand content can slightly decrease the conductivity of the brick. The advantage of having low thermal conductivity can result in energy efficiency, cost reduction of heating in winter and air conditioning in summer, and the environmental friendliness of a building. Fired-clay bricks have higher conductivity values because the firing process of clay bricks makes the clay partially combine to form a glassy product, so as to give the product the strength and durability. It is also a result from the breakdown of the original clay mineral and the formation of new crystalline material and glass phases.

To determine the thermal value of CEB, one can utilize the following standards: BS EN 1745 (thermal conductivity and thermal resistance), ASTM C 518-91 and ASTM C 1132-89 (thermal value) (Oti et al., 2009b).

17.3 Integration of agricultural waste materials

The depleting resources and escalating price of building materials have evoked the creative side of human nature. With the abundant agricultural waste, especially in developing countries, some experiments to produce CEB have been made by using RHA and POFA. The use of agricultural waste not only helps people to obtain cheaper sustainable building materials, at the same time, it has also solved the environmental problems caused by its disposal.

17.3.1 Rice husk ash

Rice husk ash (RHA) is an abundantly available and renewable agriculture by-product from rice milling in the rice-producing countries. It has the highest proportion of silica content among all plant residues (Siddique, 2008; Xu, Lo, & Memon, 2012; Yalçin & Sevinç, 2001). A rice mill turns the paddy plant into 78% rice, 20% rice husk and 2% is lost in the process (Ash, 2010). The rice husk contains about 50% cellulose, 25−30% lignin and 15−20% silica (Ismail & Waliuddin, 1996). Hence, after the combustion, one-fifth to one-quarter of the rice husk will change into ash.

Rice husk is difficult to ignite and does not burn easily with an open flame, unless air is blown through the husk. Also, it has a high average calorific value of 3410 kcal/kg. Therefore, it is a good, renewable energy source. Rice husk can be used as an alternative energy source, i.e. as the fuel in the boiler of a rice-milling kiln to generate electricity where the heating value of the husk ranges from 12.6 MJ/kg (Xu et al., 2012) to 13.34−16.20 MJ/kg (Mansaray & Ghaly, 1997) to 15.7 MJ/kg, of which 18.8% is carbon, 62.8% is volatile materials, and 9.3% is moisture content (Ekasilp, Soponronnarit, & Therdyothin, 1995; Thorburn, 1982), and even up to 17 MJ/kg (Ferraro, Nanni, Vempati, & Matta, 2010).

The end product of RH in the boiler is RHA, which for the most part will end up as waste since it has little or no commercial value. Its disposal also evokes environmental problems because RHA does not biodegrade easily (Beagle, 1978) and it generates pollution, which has caused health problems to the inhabitants. In Uruguay, RHA was thrown into the river and brought about great contamination and ecological concern (Sensale, 2006).

CEB made of clay, calcium hydroxide ($Ca(OH)_2$) and fine-grind uncontrolled burnt RHA can reach a maximum dry compression strength up to 20.7 MPa, with the best proportion of lime and RHA 1: (Muntohar, 2011). In another experiment (Riza, 2011), the best result in compressive strength was attained by a sample with a ratio of RHA and lime equal to 0.25:0.75 in the fourteenth day, with 3.62 MPa, and its twenty-eighth-day strength was 3.48 MPa. Overall trends indicate that increasing RHA proportion in a mix ratio will consequently reduce the strength.

17.3.2 Palm oil fuel ash

Palm Oil Fuel Ash (POFA) is a by-product of palm oil processing. It is considered to be a waste and is abundantly available in Indonesia and Malaysia. For every 100 tons of fresh fruit bunches supplied to the mill, 20% of it is nut shells and 7% is fibers that have no further use. It was found out that the nut shells and their fibers can be utilized as a fuel in the boiler at 800−1000 °C to produce steam for generating electricity in order to extract palm oil (Chindaprasirt, Rukzon, & Sirivivatnanon, 2008). From this incineration process in the steam boiler, 5% POFA was produced from the total solid waste used (Sata, Jaturapitakkul, & Kiattikomol, 2004). By using POFA, it is part of the green activity that turns the waste into a useful product.

Some researchers (Illston & DOmone; Ismail, Ismail, Lau, Muhammad, & Majid, 2010; Jaturapitakkul, Kiattikomol, Tangchirapart, & Saeting, 2006; Tangchirapat, Tangpakasit, Waew-kum, & Jaturapitakkul, 2003; Tay & Show, 2003) have confirmed the presence of pozzolanic properties in POFA, which indicates silica content that has the ability to create cementitious material in the presence of moisture and chemically reacts with calcium hydroxide (Massaza, 2002). Nevertheless, most of the researchers worked on the utilization of POFA as a supplementary cementing material in concrete production, and apparently, they always focused on the ground form because finer particle size will have higher pozzolanic reactivity, which in turn will make the production cost higher. Moreover, the application of POFA in the compressed earth bricks (CEB) is not attractive enough for most researchers.

Addition of unground POFA apparently showed an increase in the compressive strength of the control sample at 28 days, but there was no visible trace of strength gained for early age strength development at seven days. On the contrary, for seven days strength development, addition of POFA apparently will reduce the brick strength (Riza, Rahman, & Zaidi, 2013).

Maximum strength was achieved by 40% addition of POFA for 28 days at 13.89 MPa where the control sample strength was 12.93 MPa. In fact, the CEB compressive strength for all additional proportions of POFA at 28 days was still higher than compressive strength of the control sample. It reached 13.44, 13.12 and

13.07 MPa for 20%, 60% and 80% POFA addition, respectively (although, the trend is decreasing for further POFA addition beyond 40%).

This finding corroborated the work of Abdullah, Hussin, Zakaria, Muhammad, and Hamid (2006) which proved that replacement of POFA until 40% displayed significant increase in concrete strength from 7 to 28 days, even though they worked on POFA as a cement replacement for aerated concrete. Further addition of POFA seemingly has no contribution to the strength gain; instead, the strength reduced gradually, but still the total strengths were higher than the control mix.

According to Ahmad, Omar, Malek, Noor, & Thiruselvam (2008), strength gained can be originated from the silica oxide content in POFA, which reacts with calcium hydroxide [$Ca(OH)_2$] from OPC in the hydration process and resulted in a gel compound of C-S-H (Calcium Silicate Hydrate) whereas at the same time reducing the amount of calcium hydroxide. This is certified by Zhang, Lastra, & Malhotra (1996) investigation which stated that pozzolanic reaction in the OPC will create lower calcium hydroxide, therefore, affected the amount of it in the interfacial transition zone which in turns the existing interfacial transition zone will undergo densification resulting in increasing strength.

Addition of POFA was proven to decrease water absorption of compressed bricks for all stages of strength development (7 and 28 days), as shown in Figure 8. For control specimens, water absorption for 7 days is 17.5% and is 16.4% for 28 days. From the compressive strength test, it was determined that the best additional proportion of POFA is 40%, and its water absorption rate is 15.9% and 15.3% for 7 and 28 days testing, respectively. For bricks with 80% POFA addition, water absorption showed a significant decrease to 14.3% and 13% for 7 and 28 days, respectively.

Compared with the water absorption of paper sludge−POFA brick, which reached 39.6%, Ismail et al. (2010) found that the water absorption of the bricks with the addition of POFA is far lower for every additional composition of POFA. These findings are consistent with the results of Tangchirapat, Jaturapitakkul, & Chindaprasit (2009), which also showed the reduction of water permeability for high-strength concrete, and this could be attributed to the pozzolanic reaction and filler effect of POFA that filled voids. Decreases in water absorption can result in improving brick durability. This confirms the findings of Raimondo, Dondi, Gardini, Guarini, & Mazzanti (2009) that stated that the ability of brick to absorb water is dependent on its microstructural characteristics, especially amount, size and shape of pores. According to Lewis, Sear, Wainwright, & Ryle (2003), fineness of particles affects the water required for concrete workability. This can be implemented to the bricks with the finer particles; it will reduce water necessity in the mix.

17.3.3 Cassava peels

Cassava has been a staple food in some developing countries for centuries, and its processing contributes to environmental pollution. As a waste, cassava peels are available in abundant quantities in those countries. Waste materials from cassava processing are divided into four categories: peels, fibers, starch and waste water (Ubalua, 2007). Cassava is different from RHA and POFA, where their ash was used as a binder

together with lime. Cassava peels are used for their organic fiber within the mixture to reinforce CEB, although the fiber does not provide adequate durability (Chen, 2009).

CEB experiments in Colombia (Villamizar, Araque, Reyes, & Silva, 2012) utilizing clay-rich soil, coal ash and cassava peels produced a compressive strength of CEB with composition 90:7.5:2.5 ranging between 2.43 and 2.6 MPa, lower than that of CEB from RHA and POFA. The water absorption of cassava CEB reached 27.77%, which showed low-resistance contact with water. Hence, it has unsatisfactory durability properties.

17.4 Future trends

Nowadays, the use of CEB is still very uncommon despite its huge advantages, especially from the environmental and sustainability points of view. In the future, where the cost-effective, long-term energy conservation and ease of use material are the objectives, CEB is the perfect choice for energy efficiency and durability.

Innovation in CEB, with its interlocking shapes, can add versatility and help to reduce the skill level needed for homeowners to build their own homes utilizing locally available soils (Nelson, 2010). And the development of a CEB machine from manual, mechanical to motor-driven presses could hopefully motivate people to "do it yourself" with their own houses. Furthermore, the materials of CEB could vary in line with the effort to use greener and more environmental friendly substances.

References

Abdullah, K., Hussin, M. W., Zakaria, F., Muhammad, R., & Hamid, Z. A. (2006). *POFA: A potential partial replacement material in aerated concrete*. Paper presented at the Asia-Pacific Structural Engineering and Construction Conference (APSEC), Kuala Lumpur, Malaysia.

Ahmad, M. H., Omar, R. C., Malek, M. A., Noor, N. M., & Thiruselvam, S. (2008). *Compressive strength of palm oil fuel ash concrete*. Paper presented at the International Conference on Construction and Building Technology, Kuala Lumpur, Malaysia.

Anifowose, A. Y. B. (2000). Stabilisation of lateritic soils as a raw material for building blocks. *Bulletin of Engineering Geology and the Environment, 58*, 151−157.

Ash, R. H. (2010). *Rice husk ash*. from http://www.ricehuskash.com/.

Bahar, R., Benazzoug, M., & Kenai, S. (2004). Performance of compacted cement-stabilised soil. *Cement and Concrete Composites, 26*(7), 811−820.

CDI. (1998). *Compressed earth blocks: Standards (N. C, Trans.)*. Brussels, Belgium: CDI and CRATerre-EAG Publication.

Chen, G. Y. Y. (2009). *Analysis of stabilized adobe in rural East Africa*. San Luis Obispo: Master of Science, California Polytechnic State University.

Chindaprasirt, P., Rukzon, S., & Sirivivatnanon, V. (2008). Resistance to chloride penetration of blended Portland cement mortar containing palm oil fuel ash, rice husk ash and fly ash. *Construction and Building Materials, 22*(5), 932−938.

Ekasilp, W., Soponronnarit, S., & Therdyothin, A. (1995). Energy analysis in white rice and par-boiled mills for cogeneration in Thailand. *RERIC International Energy Journal, 17*(2), 83−92.

Ferraro, R. M., Nanni, A., Vempati, R. K., & Matta, F. (2010). Carbon neutral off-white rice husk ash as a partial white cement replacement. *Journal of Materials in Civil Engineering (ASCE), 22*(10), 1078−1083. http://dx.doi.org/10.1061/(ASCE)MT.1943-5533.0000112.

Freidin, K., & Erell, E. (1995). Bricks made of coal fly-ash and slag, cured in the open air. *Cement and Concrete Composites, 17*(4), 289−300.

Guettala, A., Abibsi, A., & Houari, H. (2006). Durability study of stabilized earth concrete under both laboratory and climatic conditions exposure. *Construction and Building Materials, 20*(3), 119−127.

Guettala, A., Houari, H., Mezghiche, B., & Chebili, R. (2002). Durability of lime stabilized earth blocks. *Courrier du Savoir, 02*, 61−66.

Heath, A., Lawrence, M., Walker, P., & Fouride, C. (2009). *The compressive strength of modern earth masonry*. Paper presented at the International Conference on Non-conventional Materials and Technologies (NOCMAT 2009), Bath, UK.

Illston, J. M., & DOmone, P. L. J. *Construction material: Their nature and behaviour* (3rd ed.). Taylor and Francis Group.

Ismail, M., Ismail, M. A., Lau, S. K., Muhammad, B., & Majid, Z. (2010). Fabrication of brick from paper sludge and palm oil fuel ash. *Concrete Research Letters, 1*(2), 60−66.

Ismail, M. S., & Waliuddin, A. M. (1996). Effect of rice husk ash on high strength concrete. *Construction and Building Materials, 10*(7), 521−526.

Jaturapitakkul, C., Kiattikomol, K., Tangchirapart, W., & Saeting, T. (2006). Evaluation of the sulfate resistance of concrete containing palm oil fuel ash. *Construction and Building Material, 21*, 1399−1405.

Jayasinghe, C., & Mallawaarachchi, R. S. (2009). Flexural strength of compressed stabilized earth masonry materials. *Materials & Design, 30*(9), 3859−3868.

Lewis, R., Sear, L., Wainwright, P., & Ryle, R. (2003). Cementitious additions. In J. Newman, & B. S. Choo (Eds.), *Advanced concrete technology: Constituent materials*. Oxford: Elsevier.

Mansaray, K. G., & Ghaly, A. E. (1997). Physical and thermochemical of rice husk. *Energy Sources, 19*(9), 989−1004.

Massaza, F. (2002). Properties and application of natural pozzolanas. In J. Bensted, & P. Barnes (Eds.), *Structure and performance of cements*. New York: Spon Press − Taylor & Francis Group.

McGregor, F., Heath, A., Fodde, E., & Shea, A. (2014). Conditions affecting the moisture buffering measurement performed on compressed earth blocks. *Building and Environment, 75*, 11−18.

Mesbah, A., Morel, J. C., Walker, P., & Ghavami, K. (2004). Development of a direct tensile test for compacted earth blocks reinforced with natural fibers. *Journal of Materials in Civil Engineering, 16*(1), 95−98.

Morel, J. C., & Pkla, A. (2002). A model to measure compressive strength of compressed earth blocks with the '3 points bending test'. *Construction and Building Materials, 16*(5), 303−310.

Morel, J.-C., Pkla, A., & Walker, P. (2005). Compressive strength testing of compressed earth blocks. *Construction and Building Materials, 21*(2), 303−309.

Morton, T. (2008). *Earth masonry design and construction guidelines*. Berkshire: Construction Research Communications Limited.

Muntohar, A. S. (2011). Engineering characteristics of the compressed-stabilized earth brick. *Construction and Building Materials, 25*(11), 4215−4220. http://dx.doi.org/10.1016/j.conbuildmat.2011.04.061.

Nelson, W. (2010). *Compressed earth blocks*. Retrieved 19.02.10, from Natural Building Colloquium http://www.networkearth.org/naturalbuilding/ceb.html.

Osula, D. O. A. (1996). A comparative evaluation of cement and lime modification of laterite. *Engineering Geology, 42*(1), 71−81.

Oti, J. E., Kinuthia, J. M., & Bai, J. (2009a). Compressive strength and microstructural analysis of unfired clay masonry bricks. *Engineering Geology, 109*(3−4), 230−240.

Oti, J. E., Kinuthia, J. M., & Bai, J. (2009b). Design thermal values for unfired clay bricks. *Materials & Design, 31*(1), 104−112.

Oti, J. E., Kinuthia, J. M., & Bai, J. (2009c). Engineering properties of unfired clay masonry bricks. *Engineering Geology, 107*(3−4), 130−139.

Rahman, M. A. (1987). Properties of clay-sand-rice husk ash mixed bricks. *International Journal of Cement Composites and Lightweight Concrete, 9*(2), 105−108.

Raimondo, M., Dondi, M., Gardini, D., Guarini, G., & Mazzanti, F. (2009). Predicting the initial water absorption in clay bricks. *Construction and Building Material, 23*, 2623−2630.

Riza, F. V. (2011). Application of RHA pozzolanic properties in CEB production. *International Journal of Sustainable Construction Engineering and Technology (IJSCET), 2*(2).

Riza, F. V., Rahman, I. A., & Zaidi, A. M. A. (2013). Influence of unground palm oil fuel ash (UPOFA) in compressed earth brick (CEB) properties. *Advanced Materials Research Journal, 488*, 188−193.

Rode, C., & Grau, K. (2008). Moisture buffering and its consequence in whole building hygrothermal modeling. *Journal of Building Physics, 31*(4), 333−360.

Rode, C., Peuhkuri, R., Mortensen, L. H., Hansen, K. K., Time, B., Gustavsen, A., et al. (2005). *Moisture buffering of building materials:* Department of Civil Engineering, Technical University of Denmark.

Sata, V., Jaturapitakkul, C., & Kiattikomol, K. (2004). Utilization of palm oil fuel ash in high strength Concrete. *Journals of Materials in Civil Engineering, ASCE, 16*, 623−628.

Sensale, G. R. (2006). Strength development of concrete with rice-husk ash. *Cement and Concrete Composites, 28*(2), 158−160.

Siddique, R. (2008). *Waste materials and by-products in concrete*. Berlin: Springer-Verlag Berlin Heidelberg.

Taallah, B., Guettala, A., Guettala, S., & Kriker, A. (2014). Mechanical properties and hygroscopicity behaviour of compressed earth block filled by date palm fibers. *Construction and Building Material, 59*, 161−168.

Tangchirapat, W., Jaturapitakkul, C., & Chindaprasit, P. (2009). Use of palm oil fuel ash as a supplementary cementitious material for producing high strength concrete. *Construction and Building Material, 23*, 2641−2646.

Tangchirapat, W., Tangpakasit, J., Waew-kum, S., & Jaturapitakkul, C. (2003). A new pozzolanic material from palm oil fuel ash. *KMUTT Research and Development Journal, 26*(4), 459−473.

Tay, J.-H., & Show, K.-Y. (2003). Use of ash derived from oil-palm waste incineration as a cement replacement material. *Resources, Conservation and Recycling, 13*(1), 27−36.

Thomas, K. (1996). *Masonry wall: Specification and design* (1st ed.). London: Butterworth-Heinemann.

Thorburn, C. (1982). *Rice husk as a fuel*. Indonesia: Tekton Books.

Ubalua, A. O. (2007). Cassava wastes: treatment options and value addition alternatives. *African Journal of Biotechnology, 6*(18), 2065−2073.

Villamizar, M. C. N., Araque, V. S., Reyes, C. A. R., & Silva, R. S. (2012). Effect of the addition of coal-ash and cassava peels on the engineering properties of compressed earth blocks. *Construction and Building Materials, 36*(0), 276−286. http://dx.doi.org/10.1016/j.conbuildmat.2012.04.056.

Walker, P. J. (1995). Strength, durability and shrinkage characteristics of cement stabilised soil blocks. *Cement and Concrete Composites, 17*(4), 301−310.

Walker, P. J. (1999). Bond characteristic of earth block masonry. *Journal of Materials in Civil Engineering, 11*(3), 249−256.

Walker, P. J. (2004). Strength and erosion characteristics of earth blocks and earth block masonry. *Journal of Materials in Civil Engineering, 16*(5), 497−506.

Walker, P. J., & Stace, T. (1996). Properties of some cement stabilised compressed earth blocks and mortars. *Materials and Structures/Mat4riaux et Constructions, 30*(November 1997), 545−551.

Xu, W., Lo, T. Y., & Memon, S. A. (2012). Microstructure and reactivity of rich husk ash. *Construction and Building Materials, 29*(0), 541−547.

Yalçin, N., & Sevinç, V. (2001). Studies on silica obtained from rice husk. *Ceramics International, 27*(2), 219−224.

Zhang, M. H., Lastra, R., & Malhotra, V. M. (1996). Rice-husk ash paste and concrete: some aspects of hydration and the microstructure of the interfacial zone between the aggregate and paste. *Cement and Concrete Research, 26*(6), 963−977.

The durability of compressed earth-based masonry blocks

18

J.M. Kinuthia
University of South Wales, Pontypridd, UK

18.1 Introduction

Building bricks and blocks are common wall material options for housing, although there may be other applications in general construction, such a paving, drains and canal lining, among other uses. The history of bricks is long, and brick technologies also have a long history, including the sustainable use of unfired bricks as well as composite material usage – by, for example, incorporating straw to provide extra strength (particularly flexural strength) and to minimize cracking and disintegration during service (Aubert & Gasc-Barbier, 2012; Böke & Akkut, 2003; Cid-Falceto, Mazarron, & Cañas, 2012; Guinea, Hussein, Elices, & Planas, 2000; Heathcote, 1995; Moropoulou, Bakolas, & Anagnostopulou, 2005; Walker, 2004). The selection of materials used for brick making has tended to depend on both location and environment. Most communities have successfully managed to utilize clays of varying plasticities to provide the basic cementation capability. Egyptians and Romans managed to develop lime-based cementitious systems at an early stage, thus obviating the over-reliance on clay plasticity to provide basic cementation (Aubert & Gasc-Barbier, 2012; Moropoulou et al., 2005). The Egyptians, for example, had dual systems, utilizing straw brick construction, and later developed lime-based technologies by calcining gypsum as the basic raw material for sourcing quicklime. The quicklime would then be used in various ways, the most notable being as binder in clay–lime pozzolanic cementitious systems. The Romans used an alternative approach for sourcing quicklime, by calcining limestone. They then developed further technology by using accelerated pozzolanicity provided by volcanic ash rather than relying on the much slower cementation process using raw clay soil. Volcanic activity inputs energy into rock and earth materials, disordering the microstructure to provide a material structure that is readily broken chemically, resulting in higher reactivity. Other innovations, such as appropriate use of varied material densities to produce durable and complex structural forms, further refined and enhanced the sustainability of the Roman infrastructure. The structures made using these technologies and innovations are still evidenced today by the robust durability and complexity demonstrated by the survival to date of the Coliseum and Pantheon, among other Roman structures and ruins (Aubert & Gasc-Barbier, 2012; Moropoulou et al., 2005).

This chapter focuses on the durability of earth bricks and blocks. It endeavors to provide a detailed analysis of the factors at play in the determination of durability of

Eco-efficient Masonry Bricks and Blocks. http://dx.doi.org/10.1016/B978-1-78242-305-8.00018-8

earth bricks and blocks. It also aims at raising awareness of the durability tests for compressed earth units that are more commonly encountered at present. In addition, is postulates the likely future scenario in terms of materials research and development (R & D) on compressed earth masonry, and the complex interplay of this R & D with a wide range of the most key stakeholders, from government, materials researchers and users to those involved in the entire housing and construction sectors.

Because the durability aspects of masonry and of concrete are broadly similar, and because there is by far a larger body of research work in concrete, this chapter borrows heavily, but carefully, from the factors relevant to the durability of concrete. The durability of a brick or brick system will most probably depend on a wide range of factors, including the brick materials used, the adopted brick technology, the prevailing environment, appropriateness of use, and care during service, among other possible factors. The detailed analysis of these factors, together with a view of future trends, is the main aim of this chapter.

18.2 Factors influencing durability of earth-based masonry

The durability of a brick or brick system will most probably depend on a holistic interplay of many factors (Lanas & Alvarez, 2003). These factors are likely to fall under one or more of the following categories:

1. Materials used
2. Technology and resultant material engineering properties
3. Prevailing environment
4. Appropriateness and care.

18.2.1 Materials used

Materials used and technologies adopted with these materials are perhaps the two most important factors that will determine durability during service. It is well known that cement-based bricks are typically more durable than clay bricks, especially if the latter are made in unfired processes. However, in both fired and unfired brick categories, the material ingredients are critical to durability of the bricks formulated from them. Both fired and unfired technologies for soil-based bricks are common, and both processes require some degree of plasticity, especially for non-cement-based soil bricks. This leaves out some categories of soils, such as low-plasticity silty and sandy soils, which mainly require cement for the provision of cementation.

Soil is virtually inexhaustible as a raw material. The cost and environmental benefits of its utilization in construction far outweigh those of stone or concrete. Unfortunately, in their natural state, soils generally have relatively low load-bearing capacities and often require stabilization. The strengthening can take the form of physical−mechanical approaches such as use of aggregates and/or other granular particulate material (including waste, such as aggregates sourced from waste tires among other industrial wastes) to

provide particle−particle resistance, and/or use of natural or synthetic fibers, and/or use of chemical approaches. Traditionally, chemical stabilization and strengthening has been by far one of the most common approaches to strengthening compacted earth, and has been achieved using expensive and environmentally undesirable materials (mainly lime and/or Portland cement (PC)), whose manufacture deplete energy resources and exacerbate pollution.

The effects of the nature of materials used in the formulation of the earth bricks and blocks on durability are very similar to those encountered in ordinary concrete, where cement/binder, aggregates and water are the key ingredients and hence the key determinants of durability. Thus, in compressed earth, the type of soil, the binder used (cement, lime, etc.) and the water used are the key material-related aspects that need detailed consideration.

Soil aggregates: "Soil" commonly refers to any loose material at the earth's crust, regardless of particle-size distribution, composition, or organic content. Soil has also been defined as "natural aggregate of mineral grains that can be separated by such gentle means as agitation in water" (Grim, 1968). The term "aggregate" is not commonly used with reference to soil − although, strictly speaking, soil particles are indeed aggregates, albeit weak ones. In concrete, the use of aggregates has the dual purpose of providing bulk volume as well as physical−mechanical strength, rather than cementitious (chemical) activity. In soil-based materials, the soil "aggregates" are expected to play the same role as normal aggregates in concrete: bulk volume and particle−particle interaction leading to strength. Therefore, irrespective of whether bricks or blocks are soil- or cement-based, weak aggregates are more likely to fail to provide high strength and hence are not able to impart durability under high stresses. Especially for concrete, reactive aggregates are undesirable, because any reactivity is likely to be gradual and slow, slowly and gradually affecting the robustness of any matrix form that may have already developed strength initially (Debieb, Courard, Kenai, & Degeimbre, 2010). The internal stresses due to these late reactions (for example, alkali−silica reactions) may weaken the compacted material.

Surface texture of aggregates affects both water absorption and adhesion to binder material, while excessive particle size would result in higher binder content requirements. The use of low amounts of binder is therefore very critical in cases of extreme excesses in either fine or oversize aggregates. For this reason, the achievement of a well-graded aggregate matrix is a common objective for optimal performance in cement-based bricks. Flaky and elongated aggregate particles are also susceptible to breakage upon stress and thus impact adversely on durability. From the foregoing, it is clear that for durability in aggregate-containing bricks and blocks, all the aggregate properties mentioned here need a very careful assessment before use. Other aggregate-related factors that may be of concern as far as durability is concerned include excessive water absorption and particle shape. Water absorption in aggregates is usually dependent on the aggregate surface texture. Wet aggregates are known to have lower crushing values, thus decreasing strength. On the other hand, elongated and/or flaky aggregates fracture easily, leading to reduced durability (Oti, Kinuthia, Snelson, & Bai, 2010f; Oti, Kinuthia, & Bai, 2010e). The use of sand in brick making should be seen in the same light as in the use of aggregates as discussed above. To most

practitioners, designers and standards, sand refers to the aggregate fraction where the particle size falls between 2 and 5 mm.

Cement/binder: Because cement is ordinarily made under very standard and controlled processes and conditions, it is normal and logical to anticipate durability when the right amounts of cement are used. However, because cement is the most expensive material ingredient in bricks and blocks, it is perhaps the most sensitive ingredient to any abuse. However, in most cases it is usually the amount, rather than the quality, of the cement that is more likely to affect durability. The standards have progressively changed from stipulating restrictive properties on building materials, and the emphasis is slowly shifting towards the need for product manufacturers to state the possible uses, appropriate or ideal situation of applicability, and the consequences of nonadherence, during service, to conditions of use recommended by the manufacturer. This shift has eased pressure that has traditionally been caused by a blanket expectation of product performance. It has also encouraged the uptake of a wider range of innovative materials and products with a wider range of performance characteristics. Thus, as long as the manufacturer has provided insight into the use of the final product, cement bricks and blocks with low cement content can now be used under limited conditions and applications as intended by the manufacturer. The challenge on the user is now to ensure that the material or product is applied as recommended, in order to expect or anticipate the appropriate durability, commensurate with the cement quantity used.

Water: Of the ingredients in bricks and concrete, water is perhaps the most readily available for many regions, in the quantity and quality necessary to ensure acceptable durability. Unless marine water is used, the quality of most other water sources is usually adequate for most cementitious applications, obviating costly water purification processes before use. It is the quantity of water used that is more likely to cause concern. There is a conflict between the amount of water needed for complete or optimal hydraulicity and that needed for material workability. The former requires far less water and thus, for profitability, the manufacturer has to try vibro-compaction or other techniques, depending on plant available, so as to result in a workable material that is as near as possible to the water level needed for optimal hydraulic potential. Excessive water absorption results in excess water in the cementitious system, and it is well known that strength in cementitious systems has an inverse relationship with the water content (or water/cement (or water/binder) ratio).

Other material factors: Most of the material effects observed in concrete can also be traced directly or indirectly in compressed/stabilized soil systems. The effects of excess lime in the jointing mortar or in the stabilization process are the same as excess lime produced during cement hydration (Dow & Glasser, 2003; Miqueleiz et al., 2012). The excess lime, as indeed any excessive salts in the material used, may cause discoloration of the brick or blocks, causing unsightly structures, as shown in Figure 18.1. Repeated wetting and evaporation exacerbates the process, explaining why it is possible to witness more efflorescence on the masonry in certain elevations and not in others. Care or caution must therefore be taken in the use of emergent newly researched materials, as in the attempts to utilize industrial and agricultural wastes. Such attempts must be accompanied by a thorough analysis of ingredients that may

Figure 18.1 Discoloration (efflorescence) of a masonry wall caused by excessive lime or other salts in the materials used.

cause discoloration or material disintegration. Work by Miquieleiz et al. (2012) has shown that excessive efflorescence can cause material disintegration. However, in most mild cases of efflorescence the damage is limited to the unsightly structure. The use of industrial and agricultural wastes in cement-bound bricks and blocks is dealt with in a dedicated section on sustainability later in this chapter.

18.2.2 Technology and resultant material engineering properties

Fired bricks: Fired bricks form a significant proportion of soil-based construction materials, providing the bulk of the engineering bricks used in wall materials. These bricks are stronger and more durable than their unfired counterparts, such as either stabilized or simply compressed earth (Oti, Kinuthia, & Bai, 2010a,b,c,d). However, blanket application of fired bricks for all situations has attracted criticism. With pressure mounting from the pursuance of sustainability, the cost of fuel for firing bricks has become unbearably critical. Thus, designers and practitioners have steered away from using fired bricks for all cases, preferring to use them only when strength and durability demands warrant their use, and opting for the unfired bricks and/or other cheaper alternatives where environmental and application requirements can allow.

The genesis of the desirable durability aspects of fired bricks is the sintering calcination process, resulting in robustness by way of high compressive strength and low water absorption as a result of low wetting tendency and low capillary suction. The calcination breaks down a clay soil in various stages:

- *100–250°C*: Removal of loosely held water (adsorbed or evaporable water).
- *300–400°C:* Beginning of the removal of the more strongly held water (combined or nonevaporable water) from the clay. This process is commonly referred to as the dehydroxylation of the clay (loss of −OH group [hydroxyl (OH^-) ions] in the clay).

- *500−600°C*: Rapid removal of combined water from the clay. This is the proper dehydroxylation temperature of the clay.
- *600−900°C:* Removal of carbon dioxide from the carbonates (if present). This process is commonly referred to as the decarboxylation of the clay (loss of carbon dioxide (CO_2) from the breakdown of any limestone (such as calcite) present).
- *Above 900°C:* New high-temperature phases begin to form, and although these are not desirable as pozzolanic materials for stabilization with for example lime (they are not easily dissolved, even at high pH), the phases are the genesis of the high fused strength that results in durability of fired bricks.

The losses of free and chemically bound water reduce the swelling potential associated with clay soils. Considering that some soils can exhibit very excessive swelling potential as high as 2000%, as can be seen in the section on unfired bricks, the calcination process is therefore beneficial in imparting volume stability on a target soil material. The strong bonding reduces the effects of porosity and imparts chemical resistance (Benavidez et al., 200; Molina et al., 2011).

Unfired bricks: When soils are used in an unstabilized form, serious volume instability may be encountered through excessive swelling. This is because hydrated cations (such as Li, Na, K and Ca) can usually find their way into the clay inter-layer spaces by various mechanisms (adsorption, diffusion, osmosis, etc.) (Kinuthia & Wild, 2001; Kinuthia, Wild, & Jones, 1999), as schematically illustrated in Figure 18.2. This is the origin of the inherent differences in the swelling potential of different clay soils further demonstrated in Figure 18.3.

Traditionally the high volume changes have been mitigated by enhancing flexural strength by incorporating fibrous constituents (Moropoulou et al., 2005; Khedari, Watsanasathaporn, & Hirunlabh, 2005). This is an old technology, and unfired bricks

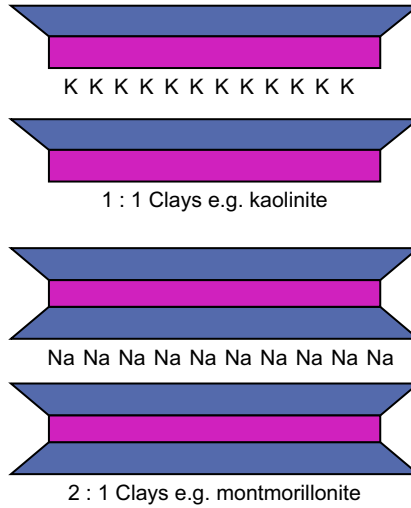

Figure 18.2 Clay structure, showing inter-layer cations that contribute to the swelling potential. K: potassium cations (K^+); Na: sodium cations (Na^+).

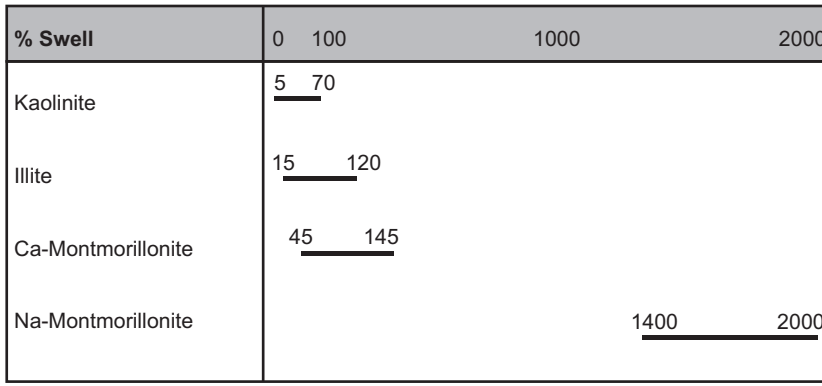

Figure 18.3 Common clay soil types and different typical free swell values.

have been strengthened with straw in practices that are centuries old. Soils can be strengthened by other unfired processes, such as soil stabilization techniques. When soils are stabilized with lime and/or Portland cement, a colloidal product predominantly composed of a calcium silicate hydrate (C-S-H) gel is formed, although aluminum phases may also be present. The complex gel gradually changes with time by partially crystallizing, resulting in strength gain in a mechanism very similar to that in Portland cement hydration. The composition of this colloidal product is dependent on material ingredients used: the compounds of calcium, silicon and aluminum coming from the lime or Portland cement used as stabilizer; aluminum and silicon from the soil; and finally the water added for the stabilization process. This colloidal $CaO\text{-}Al_2O_3\text{-}SiO_2\text{-}H_2O$ system is beneficial for strength development, although it is prone to ingress of water and other elements. The quantity and long-term development of this colloidal product influences the total porosity and affects strength and volume stability. The blocking of pores is obviously beneficial to strength in construction materials (Benavente, García, Fort, & Ordoñez, 2004; Molina et al., 2011). When well protected, all goes well, and hence we have roads, foundations, brick walls and other products of unfired soil stabilization. Depending on prevailing environment, things could go wrong, as both the residual unbound ingredients and the hydration products (from lime and Portland cement) and the complex C-A-S-H gel are prone to attack in aggressive solutions (Beaudoin, Catinaud, & Marchand, 2001; O'Farrell, Wild, & Sabir, 1999; O'Farrell, Wild, & Sabir, 2000; Snelson & Kinuthia, 2010; McCarthy, Csetenyi, Sachdeva, & Dhir, 2014; Wild, Kinuthia, Robinson, & Humphries, 1996; Wild, Kinuthia, Jones, & Higgins, 1998; Wild, Kinuthia, Jones, & Higgins, 1999).

As will be observed in section 17.4 on durability, some engineering material properties (such as strength, density and porosity, for example) are commonly used as indicators of durability. Water absorption affects all these parameters; hence water ingress will feature prominently in this section. Guetalla et al. (2006) has observed that smooth faces on which water will have less action enhance water resistance. However, in general, any aspect of the masonry that affects water intake – particle size, surface

finish, total porosity and void size distribution (affects capillary suction) − plays an important role in determining durability.

18.2.3 Prevailing environment

The prevailing environment is very critical to the durability of masonry. For this reason, regular inspection of masonry cannot be overemphasized. Problems should be pinpointed long before they become severe. Early micro-cracking that may go unchecked could lead to very expensive remedial measures if left unattended.

Damage due to water ingress is perhaps the most common in masonry, as materials in general lose strength upon wetting (Adedeji, 2002; Baojian, Chisun, & Caijun, 2013; Forth, Brooks, & Tapsir, 2000; Kelman & Spence, 2004; Walker, 2004; Obuzor, Kinuthia, & Robinson, 2011a,b; Obuzor, Kinuthia, & Robinson, 2012). Water ingress can be due to flooding or underground water flows or by way of capillary rise. Capillary rise is much dependent on pore structure of the masonry. Kelman & Spence (2004) have reported that capillary effects occur in pores between about 0.1 and 100 μm diameter. Not only does the water weaken the compressed/stabilized material, but any freezing and thawing of the water tests any masonry to the limit. A thorough inspection after every freeze−thaw cycle or season is recommended, and this should be accompanied by a detailed description of any cracking or spalling and any other observations. Whenever possible, photographic evidence or record of the condition of the masonry should be maintained. The inspection should not merely consider the brick or block system, but should be comprehensive, assessing covings, damp proof courses, pointing mortar, adjacent ground slopes, and differential damage due to orientation and wall heights, among other relevant details (Jansen et al., 2012). It is anticipated that masonry zones near the ground are more likely to be more moisture prone and hence more at risk of freeze−thaw and other moisture-related damage.

There are other mechanisms by which water can reduce the durability of otherwise robust brick and compressed earth masonry. The $CaO\text{-}Al_2O_3\text{-}SiO_2\text{-}H_2O$ colloidal product mentioned earlier can be very water absorbent under certain environments. In sulfate environments, for example, the "good" strength-enhancing colloidal material can absorb sulfate ions if these gain access to the masonry or any stabilized material, gradually replacing the silica in the "good" system. This is when compounds of calcium (from lime or Portland cement), aluminum and silicon from the soil (or Portland cement), and sulfate (if in excess in the Portland cement or from any other sources, such as ground water, gritting salts, industrial effluents, etc.) all come together in the presence of excess water. Eventually, within this colloidal product, a compound with little or no silica in it, commonly known as ettringite, is precipitated. Ettringite may be represented either in the structural chemistry notation as $Ca_6[Al(OH)_6]_2(SO_4)_3 26H_2O$, or in the cement chemistry notation as $C_3A3C\underline{S}H_{32}$ or $C_6AS_3H_{32}$ (i.e. $3CaO.Al_2O_3.3CaSO_4.32H_2O$) [where C = CaO; A = Al_2O_3; S = SiO_2; $\underline{S}$ = SO_3; H = H_2O].

This ettringite compound stands out for its variable behavior, ranging from desirable strength-enhancing aspects to what may be associated with the genesis of adverse loss in material strength and volume stability. If formed during the early

malleable stages of stabilization, such as soon after compression, ettringite may be beneficial to strength development as long as its formation is readily stopped by lack of feedstock. If, however, excess water absorption continues, or the reaction starts in some shape or form after the material has already set or gained strength, the now 'delayed' ettringite formation and subsequent excessive water absorption can be very disruptive. This can occur especially when the prerequisite reactive raw material ingredients necessary for ettringite formation are introduced late, when the cementitious material has already hardened. Common sources of this late ingress include flooding, underground water flows, unforeseen industrial effluents, or any other late introduction of sulfate-bearing contaminants (Kelman & Spence, 2004; Wild et al., 1998, 1999). Under flooding conditions, salt water, sewage, and industrial chemicals, among other deleterious contaminants, are a significant risk to masonry. Any bricks made from soil stabilization and in these environmental conditions are susceptible to reduced durability. This has been visually demonstrated in Figure 18.4, which shows linear expansion that takes place when a non-sulfate-bearing kaolin clay soil of high purity was artificially dosed with sulfate (gypsum). Figure 18.5 graphically confirms this expansion potential, demonstrated using lime stabilization of a natural sulfate-bearing clay soil (Kimmeridge clay from Oxfordshire in the United Kingdom) (Higgins, Kinuthia, & Wild, 1998; Higgins, Thomas, Kinuthia, 2002; Kinuthia, Nidzam, Wild, & Robinson, 2003; Wild et al., 1998, 1999).

In the advent of usage of various industrial and agricultural waste and by-product materials in brick manufacture in the pursuance of sustainability, it is easily feasible to recreate the situations narrated here, leading to strong unfired brick systems, but that are susceptible, in the special environmental circumstances already mentioned, to sulfate attack depending on material ingredients and service conditions. Only with a thorough understanding of the brick material constituents, chemical compositions and the chemistry involved is one able to design mitigating steps to enhance the

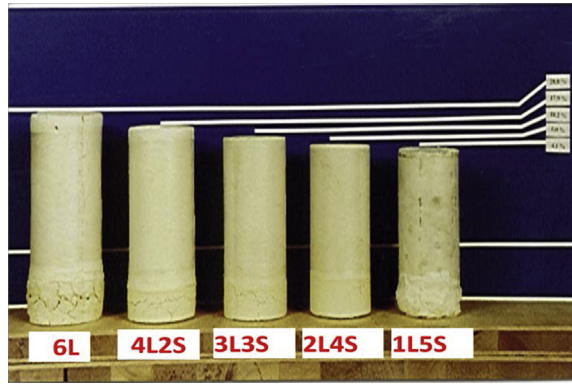

Figure 18.4 Physical demonstration of linear expansion of lime-stabilized non-sulfate-bearing clay soil (kaolin clay) when sulfate (in the form of 8% gypsum) was artificially introduced. There was gradual reduction in expansion as the lime was gradually replaced with an industrial by-product material (GGBS).

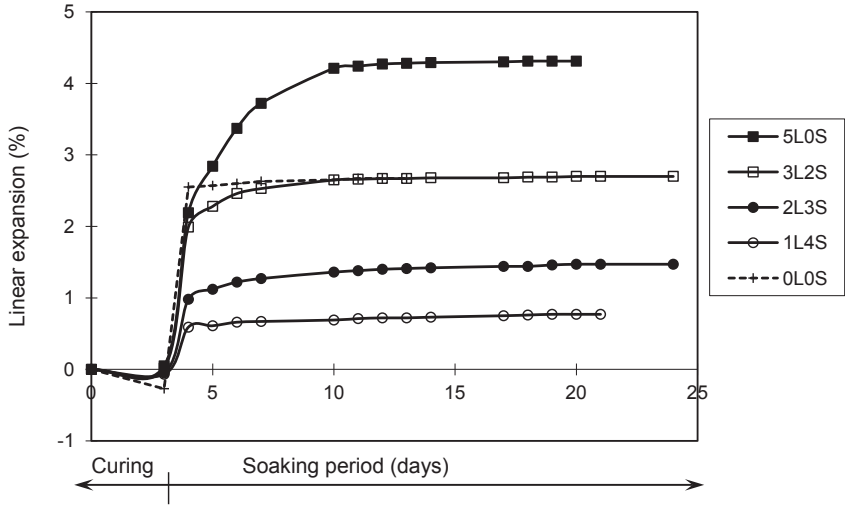

Figure 18.5 Graphical demonstration of linear expansion of lime-stabilized of a natural sulfate-bearing clay soil (Kimmeridge clay) (5L0S) and the gradually reduced expansion as the lime was gradually replaced with an industrial by-product material (GGBS).

durability of bricks incorporating industrial waste and by-products. For this reason, this chapter includes a section dedicated to the use of waste and by-products in brick manufacture, to showcase only a few experiences.

18.2.4 Appropriateness and care

The analysis of the influence of the material ingredients that constitute masonry systems, together with the prevailing environmental conditions, on the durability of masonry has suggested that the limits of applicability and care during service are very critical considerations. Masonry systems exposed to the elements have far higher expectations in terms of robustness compared to those used for internal walls or other protected environments (Dias et al., 2013). On the other hand, the level of care during service is also critical. Careful maintenance regimes are recommended for any masonry. Biological actions including microorganisms and plant growth thrive in damp conditions, particularly molds and fungi. Other effects such as torn or inelastic sealants, cracked pointing mortar, blocked weep holes, standing water, missing damp-proofing, and worn coatings, among other critical issues, are key factors, and mitigating or remedial steps should be taken as early as possible, together with a strict adherence to manufacturer recommendations (Kelman & Spence, 2004). Any reported cases of flooding of masonry should be carefully analyzed to characterize the flood's depth, salinity, contaminants and duration, among other factors. To prevent the biological actions mentioned, thorough disinfecting of flooded buildings is necessary to prevent mold growth. In case of problems, a thorough problem analysis is necessary before any remedial action. Covering problems (for example, cracks, loose material

and effloresced salts) with render or paint only helps to delay and exacerbate the problem, leading to more expensive remedial measures later. In addition, expert help may sometimes be found necessary, as inappropriate remedy or workmanship can appear an attractive repair and maintenance option but may have consequences at a later date, including serious ones such as loss of life.

18.3 Use of industrial and agricultural wastes and by-products

Due to various forces such as pursuance of environmental care, low cost, technological advances and/or other drivers, there are no longer what may be considered conventional or classical materials for masonry. Changes have been encountered either in the materials used or in the nonclassical applications. For this reason, marginal natural materials that have hitherto not been considered in building and construction, such as expansive clays and weathered, flaky and/or elongated aggregates, as well as contaminated soils, have been considered in ambitious research programmes for potential sources of materials for masonry. In addition, industrial or agricultural waste and by-product materials have also found their way into masonry.

Marginal natural materials can have applications in masonry. The use of nonindustrial harvesting of stone, coral limestone, chalk and gravels has been attempted for sourcing materials for masonry. Use of marginal naturally occurring materials does not, however, attract much attention compared with the use of industrial and agricultural waste streams, primarily because of the negative environmental impact of these waste and by-product materials.

Ground granulated blast-furnace slag (GGBS): This is an industrial by-product material that results from the manufacture of steel from iron ore in a blast furnace. The material has successfully been applied in the concrete industry, where it results in reduced use of Portland cement, an energy-intensive material with a significant negative environmental impact. Use of GGBS also results in improved durability in concrete. The material has had very little impact in masonry until recent times. The reduction in swelling potential in lime-stabilized clay soils by gradually replacing the lime used in the stabilization process with GGBS was demonstrated earlier in Figures 18.4 and 18.5. Figure 18.6 further shows that higher compressive strength values were obtained using a combination of 3% lime and 5% slag (GGBS), i.e. combination 3(5), as opposed to using the traditional lime on its own (combination 8[0]). Considering that slag is a by-product material that is in most cases less expensive compared to lime or Portland cement, there are benefits in using a blended binder that results in the use of reduced amounts of traditional binders in masonry.

In an attempt to exploit the strength enhancement and volume stability imparted by the incorporation of GGBS in stabilized soils, a large research team (comprising Kinuthia et al., 1999; Wild et al., 1996, 1998, 1999; Kinuthia & Oti, 2012; Oti & Kinuthia, 2012; Oti, Kinuthia, & Bai, 2008a,b; Oti et al., 2010a,b,c,d) has comprehensively researched the use of lime−GGBS blended binders, including in the

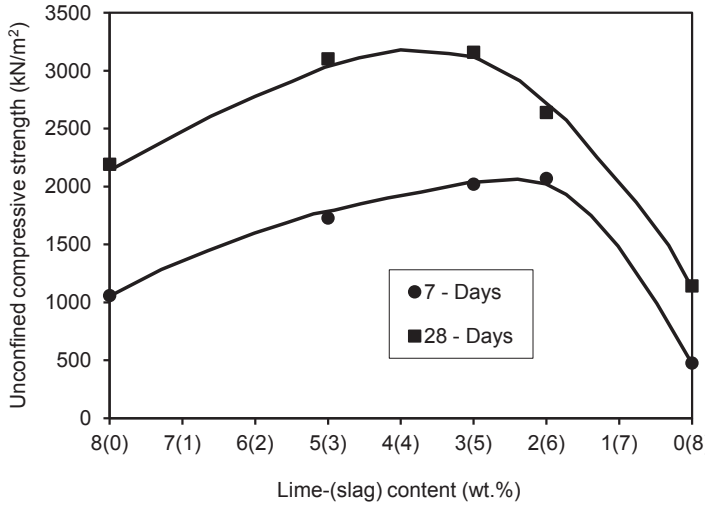

Figure 18.6 Evidence of superior performance in terms of compressive strength of compressed Kimmeridge clay soil, a troublesome sulphate-bearing clay soil, stabilized using sustainable blended binders containing GGBS (slag), relative to use of the traditional lime stabilizer on its own.

development of a robust masonry system. Figure 18.7 shows unfired building bricks made with a sulfate-bearing clay soil (Lower Oxford Clay from Oxfordshire in the United Kingdom), stabilized using combined lime and GGBS, obviating the brick firing process and also reducing the use of traditional binders of lime or PC. The bricks were made in a trial at Hanson Brick Company Ltd at their fired clay brick plant at Stewartby, in Bedfordshire. Hanson Brick Company Ltd is one of the largest manufacturers of the well-known "London" (fired) clay brick in the UK, whose mold was used in the trials for the bricks shown in Figure 18.7. The bricks have shown resistance to repeated freezing and thawing, which is one of the harshest tests for robustness of construction materials (Oti et al., 2010c).

Pulverized fuel ash (PFA): For many years, coal has been a dominant source of energy in America, Europe, Asia, Australia and parts of Africa. The waste from this big industry ranges from the unusable mining debris (collectively referred to in various terms, such as simply coal mining waste, colliery spoil, colliery waste, coal mine tailings, and possibly other terms) to the waste resulting from the burning of coal as a fuel. The burnt waste is predominantly the fine particulate material collected from the flue gases, mainly by electrostatic precipitation. It is commonly referred to as fly ash (FA) in America and other places, or as pulverized fuel ash (PFA), as in the United Kingdom and some other places in Europe and beyond. There is also the relatively coarser waste referred to as bottom ash, which, as the name suggests, is collected at the bottom of the coal-burning boilers. Although PFA's classical application is in concrete – where the benefits include enhanced workability, reduction in the amount of Portland cement used, improved later strength, and enhanced durability such as increased resistance to sulfate and chloride forms of attack – its use in masonry is not very widespread.

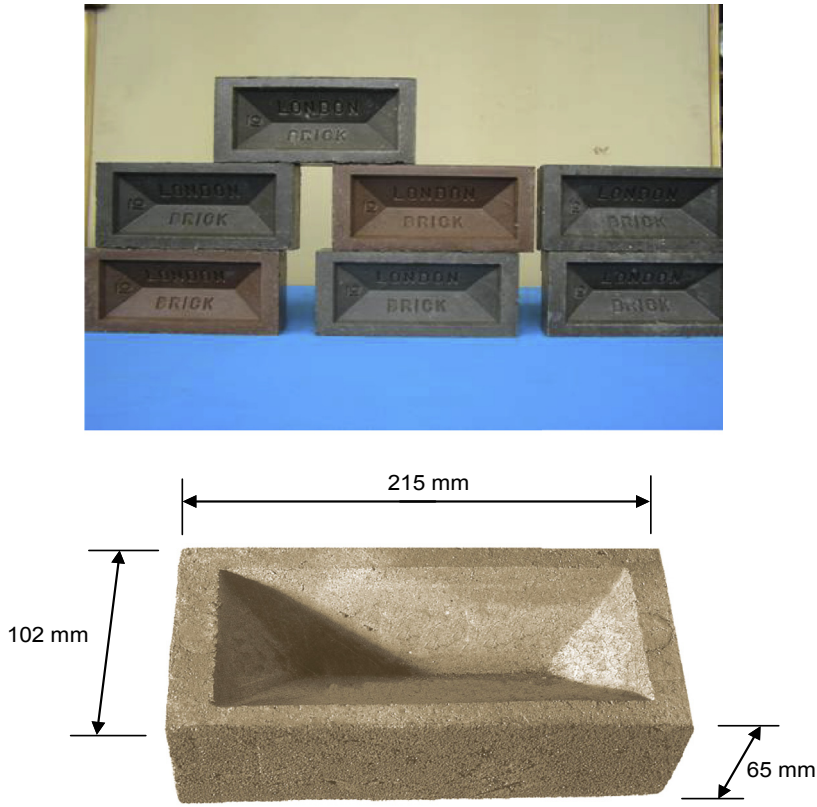

Figure 18.7 Unfired building bricks made with combined lime and GGBS (industrial pilot-scale trials carried out at Hanson Brick Company, using their "London" brick mold). Oti, Kinuthia, and Bai (2010a,b,c,d).

As with GGBS, it has been demonstrated that PFA can also be used in the manufacture of durable masonry (McCarthy et al., 2014; Rahmat, Ismail, & Kinuthia, 2011). The compressed clay−PFA blocks shown in Figure 18.8 have not been commercially tested, but work (Rahmat et al., 2011) has suggested that durable compressed masonry

Figure 18.8 Clay−PFA "Eco-brick" made sustainable by using the already proven sustainable lime−GGBS blended binder.

block can be made using this industrial waste or by-product material that is readily available worldwide.

Wastepaper sludge ash (WSA): Most paper is normally coated with clay and limestone to create the smooth surfaces that we are all familiar with. When paper is recycled, the clay and the limestone remain in the sludge from which the recyclable cellulose fibrous material is removed during recycling of paper. When this sludge is combusted to reduce volume of landfilled waste, the clay and limestone are heated in the process. Combusting wastepaper sludge inadvertently produces a waste material that has undergone more or less a similar heat process as Portland cement, albeit at lower temperatures. For many years, this wastepaper sludge ash material has ended up in landfill, without the knowledge that this is weak cement. Successful development of novel cement utilizing wastepaper ash and blast-furnace slag has been reported by Nidzam & Kinuthia (2010, 2011a,b). The cement was developed by combining an industrial waste (WSA) with a by-product material (GGBS) for replacement of Portland cement. This has enabled the development of "green" cement for masonry. The "green" cement has performed very well in terms of strength and durability, and sometimes better in terms of appearance compared with the traditional Portland cement. The demonstration of success has been carried out using concrete block making, as shown in Figure 18.9. However, as has been demonstrated using GGBS and PFA, it is also possible to utilize WSA, and indeed any other waste that has shown success in concrete trials, in compressed earth masonry (Kinuthia et al., 2003; Nidzam & Kinuthia, 2011b). Figure 18.10 shows successful suppression of swelling potential using WSA−GGBS blended binder on the same expansive Lower Oxford clay used in demonstration projects earlier.

In the examples shown here, utilization of a waste in combination with a by-product material has resulted in superior performance relative to the use of a classical or traditional building material. Because such hybrid binders do not usually have excess

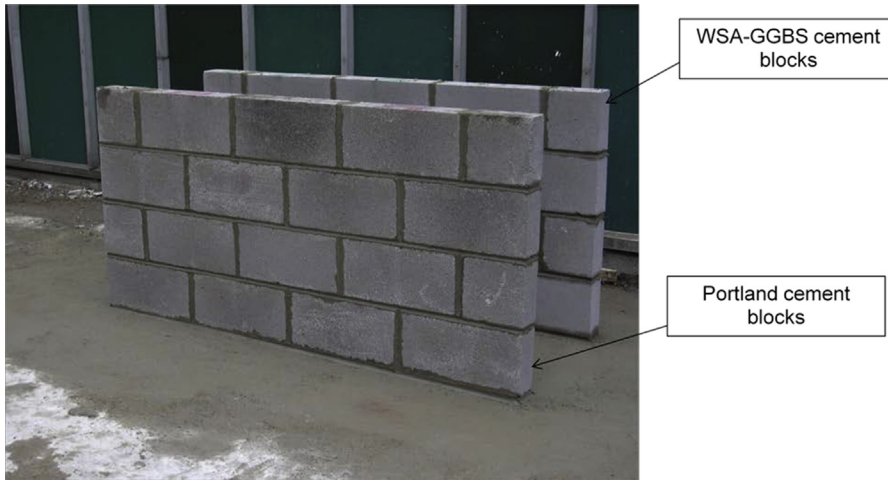

Figure 18.9 Demonstration of two concrete block walls showcasing the utilization of WSA in the development of "green" cement for the manufacture of building blocks.

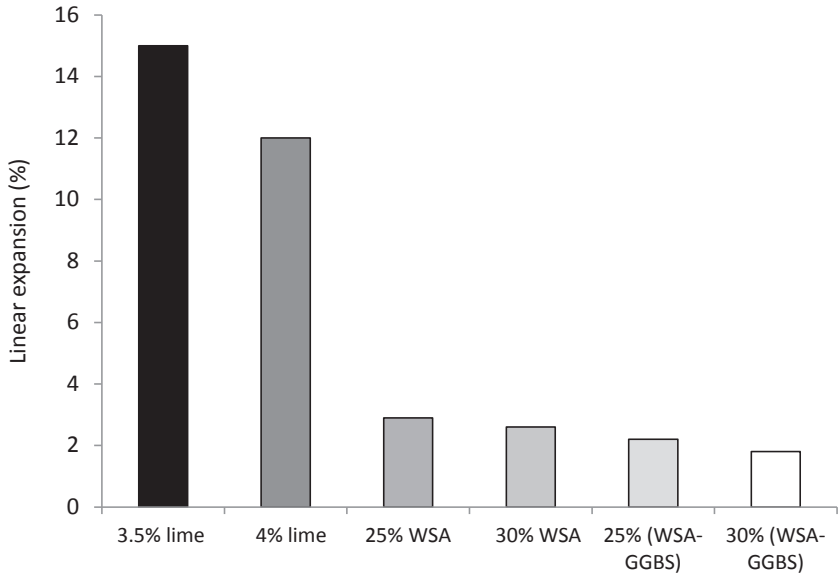

Figure 18.10 Significant reduction in linear expansion by the combined use of WSA and GGBS in the stabilization of an expansive sulfate-bearing clay soil.

lime, the common discoloration in the typical use of lime and/or Portland cement (efflorescence) (seen earlier in Figure 18.1) was not observed in the lime−GGBS, lime−PFA, or WSA−GGBS clay systems. Indeed, GGBS, PFA and WSA all thrive by utilizing any excess lime for their activation to form additional cementitious products. Similar approaches are possible elsewhere, using waste and/or by-product materials that are available in significant quantities, including agricultural waste. Other examples of commonly encountered industrial waste and by-product materials that have applicability in both soil- and cement-based building and construction materials and components include waste glass (Chidiac & Mihaljevic, 2011); waste tires (Snelson, Kinuthia, Davies, & Chang, 2009); shale, slate, colliery waste and other forms of recycled aggregates (Baojin et al., 2013; Bryson, Gutierrez, & Hopkins, 2012; Corinaldesi, 2009; Debieb et al., 2010; Kinuthia, Snelson, & Gailius, 2009; Oti et al., 2010f,e); brick dust (Kinuthia & Nidzam, 2011; O'Farrell, Wild, & Sabir, 2000, 1999).

Agricultural waste: For many countries, the major industrial activities are directly or indirectly related with agriculture. For these countries, any major breakthrough in the development of sustainable infrastructure cannot afford to ignore waste from the agricultural sector. Initial focus has been in activities that produce large agricultural waste streams, including the growing of palm oil and sugarcane (Mofor, Kinuthia, Melo, & Djialli, 2009), rice (Billong, Melo, Kamseu, Kinuthia, & Njopwouo, 2011), and fibrous materials for fiber-based soil−cement blocks − e.g. bagasse, straw, kenaf, bamboo, jute, coir, durian (Khedari, Watsanasathaporn, & Hirunlabh, 2005). The research and commercial application of masonry products made by incorporating agricultural materials and agricultural waste and by-product materials is in its

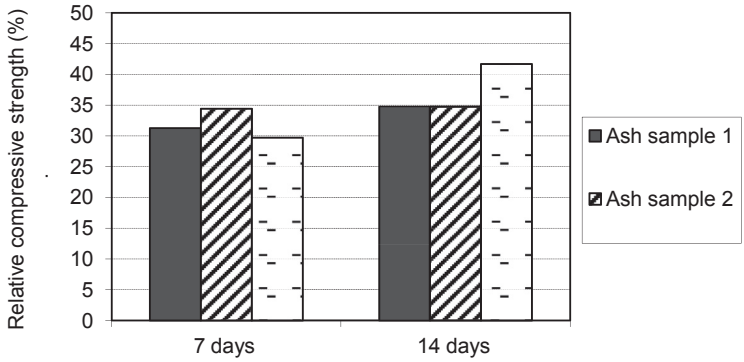

Figure 18.11 Relative compressive strength (%) of concrete cubes where 50% of the Portland cement was partially replaced with sugarcane waste ash.
Mofor et al. (2009).

formative years. Most research groups have only managed to demonstrate potential. Preliminary work by Mofor et al. (2009) on bagasse ash from the growing of sugarcane has demonstrated possible potential savings in Portland cement of about 50%, as demonstrated in Figure 18.11. However, the durability of masonry made using both fibrous and nonfibrous agricultural waste is ongoing, particularly on waste ash resulting from the burning of waste from the growing and processing of cereals, such as rice husks and bagasse from sugarcane (Khedari et al., 2005).

18.4 Tests and indicators of durability

For a long time, compressive strength has been employed by many users as an indicator of durability. While to some degree this does reflect possible outcome during service life, it has also been established in both soil- and cement-based materials that strength alone is only one of the many factors determining durability. In concrete, for example, tests involving ingress of water and chemicals, especially for applications of concrete in either marine or buried environments, are among the severe test environments under which durability of concrete may be assessed. Unless there are freezing conditions anticipated during service life, pure water often does not pose any significant danger to well-designed concrete. For compressed earth, however, even without the presence of any chemicals, soaking in water has a significant influence on the durability of the masonry. For this reason, applications of buried compressed earth masonry are rare and are strongly discouraged. Indeed, there are practically few or no examples of applications of compressed earth in wet buried conditions. The water absorption capacity tests are therefore very strong indicators of durability. Indeed, all the common tests for durability of compressed earth units are water-based or water-related. Broadly, these tests fall under four overlapping categories, viz:

1. *Category 1* – Laboratory-based tests for durability indicators such as compressive strength and water absorption, usually with attempts to simulate certain rain characteristics,

2. *Category 2* − Laboratory-based tests with little or no regard for particular rain characteristics,
3. *Category 3* − Laboratory-based tests commonly of a very high degree of severity, usually attempting to adopt tests more suited for other materials (e.g. rocks, concrete) or components, and
4. *Category 4* − Both laboratory and, more commonly, nonlaboratory tests attempting to simulate prevailing environmental conditions (holistic variations in weather: sunlight, rain, wind, temperature, flooding etc.).

Category 1: It is common to first test for the durability indicators of compressive strength and water absorption. For this reason, these tests are more or less routine tests for compressed earth masonry. Compressive strength tests are in this regard commonly carried out in the basic mode without test specimen confinement and without mortar capping, although the use of soft leveling materials such as cardboard is sometimes common. For water absorption, water uptake by capillary suction and/or by fully soaking test specimens in water is common. Due to the large variations in soils and additives used in compressed earth masonry, together with an equally large variation in the methods of manufacture, it is neither possible nor helpful to attempt to quote en masse test results for water absorption and for compressive strength in this chapter. For compressed earth blocks, these values vary greatly, and the situation is in many cases exacerbated by lack of standards for these materials, for either their manufacture or the testing procedures. This situation is perhaps due to the already mentioned variability in soil types and additives to compressed earth units. Notwithstanding, Guetalla et al. (2006) report a recommended maximum value for water absorption of 15%, while that for capillary suction is 2.5%. This value is not far from the recommended value of less than 14% by Heathcote (1995) for stabilized well-graded sandy soils. The work reported by Guetalla et al. (2006) shows total water absorption values for stabilized earth masonry within the range of 5.3−9.9%, which was 2.5−4 times the corresponding values for water absorption by capillary action. In contrast, work by Oti et al. (2009) reported on very robust bricks of compressed earth stabilized using a blended lime−GGBS binder, despite observing water absorption values within the range of 16−22%, outside the recommended value of 15% as reported by Guetalla et al. (2006). It is precisely for this reason that this chapter has deliberately opted for generic coverage, preferring generic factors and trends, as opposed to over-reliance on specifically quoted values on durability in the literature.

In terms of damage caused by absorbed water, compressive strength test results in the soaked condition have been used, relative to unsoaked strength values, as indicative pointers to durability. The water spray method (see typical set-up in Figure 18.12) is also fairly common for assessing water damage and durability (Guetalla et al., 2006; Obonyo, Exelbirt, & Baskaran, 2010; Cid-Falceto et al., 2012, among others). Typical erosion rates for various masonry materials upon water spraying of unfired masonry are provided in Table 18.1, after the research work by Obonyo et al., 2010), while Table 18.2 shows typical strength reduction values for compressed earth stabilized using a blended binder consisting of lime and GGBS, from work by Obuzor, Kinuthia, & Robinson (2012). It is reiterated that these typical values by Obonyo et al. (2010) or by Obuzor et al. (2012) can change significantly upon changes in material composition and small

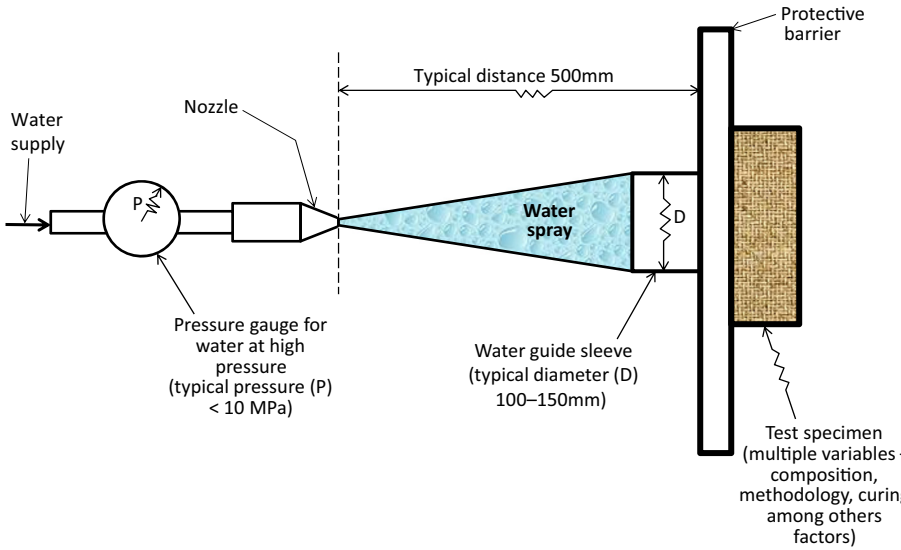

Figure 18.12 Schematic drawing of the water spray test for the durability of compressed earth masonry.

changes in test conditions, among other factors, and should be interpreted, used or extrapolated with great caution and care, as the following analysis will demonstrate. The work by Guettala et al. (2006) used a target material with the following soil characteristics: 64% sand, 18% silt, and 18% clay, with a chemical composition analysis showing 5.81% sulfate as SO_3. Using these values alone, an experienced researcher in this field may be able to approximately establish that this material is best suited for cement stabilization, with possible good results being also expected from an alternative blended binder comprising cement and lime. The cement would target the 64% sand, while the lime would target the 18% clay content present. The results in Table 18.3 (after Guettala et al., 2006) confirm this argument. Guettala et al. (2006) ranked the holistic performance on durability of the material as (1) cement, (2) cement + lime, and (3) lime, a further confirmation of prediction. A similar order of performance was observed by Oti et al. (2009) with a completely different composition, using a fine-grained clay soil with no sand at all (Lower Oxford clay). This shows that different compressed earth materials can show identical behavior, and thus extrapolation of results in the literature without due care or consideration of the fine details of the circumstances of the data capture may be risky.

Some users are prepared to use unconfined compressive strength and/or water absorption by either capillary or soaking as indicators of durability. However, with some modifications, durability tests have been formulated to advance these indicators to full-fledged durability tests. As argued earlier, it is rare to find durability tests that are based on ingress of chemicals such as chlorides or sulfates for compressed earth masonry. This is due in part to the care taken in the selection of situations for applications of compressed earth units. A significant section of this chapter has been devoted

Table 18.1 Brick erosion test results at a spray pressure of 4.13 MPa

Type of brick	Time (minutes)	Depth of erosion	Rate of erosion (mm/minute)
Soil-cement-lime-fluid	15 30 45 60	17.5 20 25 30	0.50
Interlocking bricks	15 30 45 60	0.1 0.2 0.2 0.2	0.003
Soil-cement	15 30 45 60	0.5 0.6 0.7 0.8	0.013
Soil-cement-lime	15 30 45 60	17.5 18.5 19.5 20	0.333
Soil-cement-fiber	15 30 45 60	25 35 45 55	0.917

Source: Obonyo et al. (2010).

Table 18.2 Loss of strength upon soaking a sulfate-bearing clay soil (Lower Oxford clay) stabilized with lime−GGBS blended binder (4 lime−12 GGBS)

Curing time (days)	Original (unsoaked) samples		Partially soaked samples		Completely soaked samples	
	16L (Control)	4L-12G	16L (Control)	4L-12G	16L (Control)	4L-12G
7	1.30	2.00	0.20	2.30	0.15	1.80
14	1.400	2.50	0.25	2.40	0.08	2.00
28	1.75	2.60	0.50	2.70	0.50	2.30
56	1.80	4.05	0.60	2.80	0.50	2.50
91	1.60	4.70	F0.75	4.40	0.50	2.90

Source: Obuzor et al. (2012).

Table 18.3 Loss of strength upon soaking a sulfate-bearing silty-clayey sand stabilized with various binders

Bricks characteristics	Different wall treatments					
	Cement (%)		Lime (%)		Cement + lime (%)	
	5	8	8	12	5 + 3	8 + 4
Compressive strength in dry state (MPa)	15.4	18.4	15.9	17.8	17.5	21.5
Compressive strength in dry state (MPa)	9	12.7	10.1	11.7	12.3	15.6
Water strength coefficient	0.58	0.69	0.64	0.66	0.63	0.7
Capillary absorption (%)	2.35	2.2	3.7	2.9	2.3	2
Total absorption (%)	8.27	7.35	9.8	9.02	8.1	7.9
Weight loss (wet−dry) (%)	1.4	1.25	2.3	2.1	1.2	1.0
Weight loss (freeze−thaw) (%)	2.35	2.23	3.7	2.9	2.3	2.0

Source: Guettala et al. (2006).

to the causes of volume changes that can occur when sulfates are present in the masonry material ingredients. This attention is primarily because the masonry need not be in a buried situation for sulfates to affect the masonry. Normal water ingress is capable of kick-starting sulfate-induced expansion when all the other prerequisite ingredients are present, either during service or during manufacture. As was demonstrated by Figure 18.4, sulfate-induced water absorption and expansion can be so severe in terms of magnitude and disruptive capacity, compared to normal water-induced expansion, that significant expansion and disintegration is bound to be picked up during the ordinary analysis for water absorption by capillary or by full soaking. There is perhaps no need, therefore, for further testing of compressed earth masonry using ingress of chemicals.

Category 1 tests also assess the depth of erosion, material loss and/or disintegration or closely similar assessments. Some approaches attempt to simulate wind-driven rain in a water spray and/or water drip erosion methodology. They aim to focus on what may be considered to be the relevant or appropriate rain characteristics, such as

intensity/speed, angle of approach or impact or raindrop size, among other rain characteristics (Ogunye & Boussabaine, 2002a,b; Obonyo et al., 2010; Aubert & Gasc-Barbier, 2012; Erkal et al., 2012). Obonyo et al. (2010) assessed the rate of erosion of compressed earth units upon varied pressure of water spray. Two spray pressure levels were adopted, at 2.07 and 4.13 MPa. Table 18.1 shows the reproduction of the test results obtained at the higher spray pressure of 4.13 MPa. The table also gives an indication of the variability of material ingredients for compressed masonry units, suggesting, as argued earlier, the complexity in any over-reliance on typical strength or durability values in a generic publication such as this chapter without due attention to the relevant test conditions used in each case. For unstabilized soil blocks, some researchers have shown preference to total material loss rather than depth or erosion. Cid-Falceto et al. (2012) observed that the maximum erosion produced on unstabilized compressed earth blocks in a water drip test was not due to the direct fall of the drop of water, but rather to the run-off that takes place. They recommended weight losses within the range of 5−10% as the limiting performance criteria for unstabilized compressed earth blocks. In comparison, observation by Oti et al. (2009) on the weight losses for lime−GGBS stabilized earth blocks using the much more severe freeze−thaw tests were within 1.5−2%, demonstrating the wide durability range that is likely to be encountered in practice when dealing with both stabilized and unstabilized compressed earth units.

Another test approach within this category focuses on strength loss either upon varying compaction moisture content or upon water absorption by water spraying, capillary action and/or full immersion in water. Varying compaction moisture content may be considered as a mix design issue and not necessarily an indicator for durability. Such variations in moisture content have been exercised by many researchers during materials design (Rahmat et al., 2011; Obuzor et al., 2011a,b, 2012, among others). In the assessment of strength loss upon water absorption of cured test specimens as a durability test, Obuzor et al. (2012) established significant strength loss of lime-stabilized sulfate-bearing clay soils. In a rare occurrence, the researchers also observed strength increase upon soaking compressed earth units, when the lime binding material was partially replaced with a lime−slag blended binder. Sample results have been reproduced in Table 18.2 and also in Figure 18.13. This work clearly shows that water need not always be a bad thing in some well-researched formulations. Similar observations are reported by Guetalla et al. (2006) for work carried out using earth masonry with microsilica (silica fume) addition. The beneficial cementitious qualities of GGBS have been discussed in slightly more detail in Section 18.3. It is hypothesized that both GGBS and microsilica thrive in a water-cured environment, producing more C-S-H gel such that the high water-cured strength results enable significant water resistance and hence better durability. In another research work by Taallah, Guettala, Guettala, & Kriker (2014) on the mechanical properties and hygroscopicity behavior of compressed earth blocks incorporating date palm fibers, a series of cement-stabilized compressed earth blocks were fabricated at various compacting stresses. The addition of fibers was observed to have an adverse effect on the properties of some of the blocks. The fibers were observed to be of low tensile strength and very high water absorption. The use of fibers in this case would not be conducive for durability.

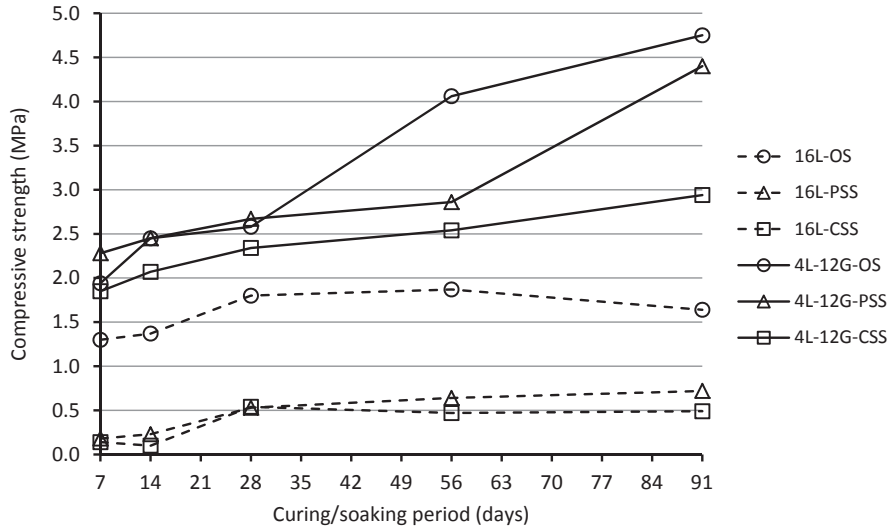

Figure 18.13 Loss of strength upon soaking a sulfate-bearing clay soil (Lower Oxford clay) stabilized with lime−GGBS blended binder (4 lime−12 GGBS).
Obuzor et al. (2012)

Category 2: This category of durability tests has little or no regard for rain characteristics, focusing rather on the amount of water absorbed, materials loss and/or disintegration (see Figure 18.14, after Oti et al., 2010c) and/or visual block integrity, and possibly other related or relevant observations (edge wear, cracking, efflorescence, etc.), relative to the variations in environmental situations and conditions simulated in the test. The test recognizes that it is not easy to design reproducible environmental situations and conditions, and it is also not easy to overcome the hardships in the attempt to model rain and/or in the adaptation of tests meant for rocks or concrete.

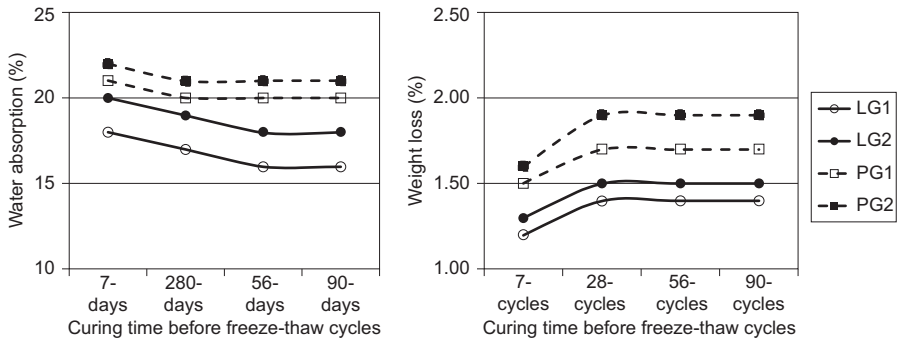

Figure 18.14 Water absorption and subsequent weight loss during freeze−thaw tests of masonry units stabilized with lime−GGBS blended binder.
Oti et al. (2010c).

Whenever possible or available, test facilities with carefully controllable environments (temperature, humidity etc. against time, among other relevant factors) are preferable and commonly adopted. Some freeze−thaw tests offer such conditions, using computer-controlled chambers (Oti et al., 2010c; Pan, Li, & Liao, 2014).

Freeze−thaw tests come in many guises, with all manner of variations in test specimen preparation, curing regimes before testing, water or moisture introduction methodologies and cyclic freeze−thaw cycles. It is therefore not appropriate to discriminate and cite here any particular regime or its test results. For this reason, only the nature of factors leading to the attraction to, and common features of freeze−thaw cycles need be analyzed.

Freeze−thaw tests have been adopted either for zones subject to freezing and thawing conditions in nature or as standalone tests for soaked material fatigue or robustness, irrespective of whether the region in mind is prone to freezing conditions. The freeze−thaw effects have been shown to be very severe tests for any construction material or component (Oti et al., 2010c, 2009; Pan et al., 2014). For relatively weak materials such as compressed earth, the freeze−thaw tests are perhaps among the severest tests for mechanical stresses and response to water ingress. This observation notwithstanding, not all freeze−thaw test conditions have proved to be very severe or disruptive. Research work by Aubert & Gasc-Barbier (2012) on freeze−thaw effects on compressed earth masonry sprayed with water resulted in hardening of the clayey soil blocks during freezing and thawing cycles. The decision to spray the test specimens rather than to immerse them in water was based on the weak nature of the test specimens. The specimens were not rehumidified after the initial spray, and this led to their desiccation and hardening. It is arguable that under such circumstances, unless a one-off water spray in a freeze−thaw test is seen as the best simulation of the likely prevalent environmental conditions, such a "soft" approach may be considered risky, due to the possibility of misleading apparent durability. Aubert & Gasc-Barbier (2012) have noted this risk in their research, by stating that freeze−thaw cycles on clayey soil blocks will need to be representative of the real risks encountered by these blocks during their service life, and setting up such tests still requires thought and discussion among experts on the topic.

Category 3: This category of durability tests attempts to adopt tests that are more suited to other materials, particularly and mainly tests for rocks and concrete. The previous section highlighted the hardships encountered in the attempts to model real-life environmental situations and conditions. However, with caveats and care in results interpretation and extrapolation, it is possible to have meaningful test regimes for durability of compressed masonry units. It is arguable that water absorption tests, compressive strength tests on noncylindrical test specimens, and most freeze−thaw cycles adopted by many researchers are adaptations of tests for concrete, carefully varied to suit conditions for tests on earth-based materials.

Other innovative adaptations are also common under this test category. Aubert & Gasc-Barbier (2012) and Aldaood, Bouasker, & Al-Mukhtar (2014), for example, both used wave velocity for the assessment of durability of masonry units upon freeze−thaw and wetting and drying cycles, respectively. The wave technologies were adopted from approaches commonly used in tests on rocks and concrete, for

the assessment of the effects of water ingress. It is generally observed that the higher the degree of saturation, the more significant is the increase in wave velocity. Aubert & Gasc-Barbier (2012) and Aldaood et al. (2014) used this observation to monitor the degree of water absorption in compressed earth blocks, noting that any cracking due to freezing and thawing or wetting and drying cycles is bound to lead to more water absorption, and hence to changes in wave velocity.

Category 4: These are both laboratory and, more commonly, nonlaboratory tests, attempting to simulate the naturally and actually prevailing environmental conditions to which the compressed earth masonry under test is likely to be subjected. The tests usually aim for the actual holistic variations in weather, leaving nothing behind and looking, for example, to take into account exposure conditions of prevailing sunlight, various rain characteristics (duration, drop size, intensity, etc.), wind, temperature, and flooding, among other details. This category of tests has been found appropriate by some researchers (Guettala et al., 2006, among others) who have either facilities for out-of-laboratory capacity for construction of full or sample masonry units for exposure, or a strong belief or view that immersion of masonry blocks under simulated laboratory conditions is very severe and perhaps unrealistic. They argue that soaking tests sometimes do not adequately reflect the equivalent of the actual environmental conditions of the regions where the masonry units are to be applied. Some water spray or wet and drying methodologies may equally be very violent, with tests involving freezing and thawing being the most severe (Guettala et al., 2006).

Most other accelerated laboratory tests are seen as too severe and hard to validate to natural aging processes. Guettala et al. (2006) are of the view that such tests often cause controversy as one cannot simulate in the laboratory the complex succession of the multiple climatic phenomena. Due to the flexibility of the water spray method, and the fact that it is widely seen as realistic in nature, some researchers have come to the conclusion that among the accelerated tests for the durability of compressed masonry, this is the method that stands the best chance of a close simulation of natural aging.

18.5 Future trends

There is an observable increase in the researched use of compressed earth masonry units. These units are increasingly being seen as industrialized materials, and are no longer considered as only appropriate or applicable to traditional approaches for self-construction of infrastructure in the built environment (Cid-Falceto et al., 2012). Many examples exist of the increasing use of industrial and agricultural waste and by-product materials in compressed earth masonry, and it is not possible to cover or quote all of them here. However, a brief survey of the materials, techniques and applications of today's masonry suggests a thriving ongoing research and innovation-led development of compressed earth masonry technology. There is also a gradual shift from the traditional fired clay masonry categories to unfired categories. While the fired categories adopted a blanket approach of firing clay irrespective of clay composition, there is a far wider variety in material selection and technology adopted for the

unfired masonry category. This is because the durability imparted by the firing process is harder to mimic or achieve in unfired systems, resulting in the pursuance of alternative approaches to materials usage to include industrial and agricultural waste and by-product materials. There is also increasing use of synthetic (industrial) and natural fibers for reinforcement, chemical cementation, attention to particle matrix configurations and variable and careful selection of applicability scenarios. Fortunately, as mentioned earlier, there is also a gradual shift in emphasis away from a blanket stipulation of standard properties and material expectations, relying rather on recommendations by the manufacturer for the appropriate usage, and also for the possible consequences of lack of adherence by the end user to these recommendations. The future will therefore most likely witness enhanced end-user sensitivity to global changes in materials technology and materials failure mechanisms, and better or closer liaison with material manufacturers, coupled with a keen(er) awareness of relevant government policies, guidance and legislation. This development or trend is likely to enhance reliability of compressed earth masonry than witnessed in the past, and it is hoped that the mortgage lenders and insurance industries will be quick to respond to the fast-changing landscape, resulting in an ever-increasing adaptation of compressed earth masonry in future social and commercial housing. These scenarios suggest an urgent need for a near-universal harmonization, consensus building and characterization and/or classification of compressed earth-based building and construction materials, taking into account the wide range of materials likely to be encountered and variable manufacturing methodologies. In terms of the further research work needed, tests on durability need to be clearly and well delineated, with those for fired systems adopting considerations that suit fired systems and separate from those best suited for the unfired systems. Those for the unfired systems need, in turn, to differentiate between stabilized and nonstabilized compressed earth systems. Both test categories should embrace and embed the indicative tests of compressive strength and water absorption. The more severe cyclic freeze−thaw and wet−dry tests should be more in reference to stabilized systems, with the water and spray and drip test methodologies being in specific reference to unstabilized systems. This task is beyond the remit intended for this chapter, but the chapter has managed to cite most of the factors that determine the durability of compressed earth units and a few of the tests that are commonly encountered at present.

References

Adedeji, A. A. (2002). Estimation of service life of coated brickwork mortar joint. *Cement and Concrete Research, 32*, 199−203.

Aldaood, A., Bouasker, M., & Al-Mukhtar, M. (2014). Impact of wetting−drying cycles on the microstructure and mechanical properties of lime-stabilized gypseous soils. *Engineering Geology, 174*, 11−21.

Aubert, J. E., & Gasc-Barbier, M. (2012). Hardening of clayey soil blocks during freezing and thawing cycles. *Applied Clay Science, 65−66*, 1−5.

Baojian, Z., Chisun, O., & Caijun, S. (2013). CO_2 curing for improving the properties of concrete blocks containing recycled aggregates. *Cement and Concrete Composites, 42*, 1−8.

Beaudoin, J. J., Catinaud, S., & Marchand, J. (2001). Volume stability of calcium hydroxide in aggressive solutions. *Cement and Concrete Research, 31*, 149−151.

Benavente, D., García, M. A., Fort, R., & Ordoñez, S. (2004). Durability estimation of porous building stones from pore structure and strength. *Engineering Geology, 74*, 113−127.

Billong, N. A. B., Melo, U. C., Kamseu, A. B. E., Kinuthia, J. M., & Njopwouo, B. (2011). Improving hydraulic properties of lime−rice husk ash (RHA) binders with metakaolin (MK). *Construction and Building Materials, 25*, 2157−2161.

Böke, H., & Akkut, S. (2003). Ettringite formation in historic bath brick-lime plasters. *Cement and Concrete Research, 33*, 1457−1464.

Bryson, L. S., Gutierrez, I. C. G., & Hopkins, T. C. (2012). Development of a new durability index for compacted shale. *Engineering Geology, 139−140*, 66−75.

Cid-Falceto, J. C., Mazarron, F. R., & Cañas, I. (2012). Assessment of compressed earth blocks made in Spain: International durability tests. *Construction and Building Materials, 37*, 738−745.

Chidiac, S. E., & Mihaljevic, S. N. (2011). Performance of dry cast blocks containing waste glass powder or polyethylene aggregates. *Cement and Concrete Composites, 33*, 855−863.

Corinaldesi, V. (2009). Mechanical behavior of masonry assemblages manufactured with recycled-aggregate mortars. *Cement and Concrete Composites, 31*, 505−510.

Debieb, F., Courard, L., Kenai, S., & Degeimbre, R. (2010). Mechanical and durability properties of concrete using contaminated aggregates. *Cement and Concrete Research, 32*, 421−426.

Dias, J. L., Silva, A., Chai, C., Gaspar, P. L., & de Brito, J. (2013). Neural networks applied to service life prediction of exterior painted surfaces. *Building Research & Information, 42*(3), 371−380.

Dow, C., & Glasser, F. P. (2003). Calcium carbonate efflorescence on Portland cement and building materials. *Cement and Concrete Research, 33*, 147−154.

Erkal, A., D'Ayala, D., & Sequeira, L. (2012). Assessment of wind-driven rain impact, related surface erosion and surface strength reduction of historic materials. *Building and Environment, 57*, 336−348.

Forth, J. P., Brooks, J. J., & Tapsir, S. H. (2000). The effect of unit water absorption on long-term movements of masonry. *Cement and Concrete Composites, 22*, 273−280.

Grim, R. E. (1968). *Clay Mineralogy* (2nd· ed.). McGraw Hill Book Company.

Guetatala, A., Abibsi, A., & Houari, H. (2006). Durability study of stabilized earth concrete under both laboratory and climatic conditions exposure. *Construction and Building Materials, 20*, 119−127.

Guinea, G. V., Hussein, G., Elices, M., & Planas, J. (2000). Micromechanical modeling of brick-masonry fracture. *Cement and Concrete Research, 30*, 731−737.

Heathcote, K. A. (1995). Durability of earthwall buildings. *Construction and Building Materials, 9*, 185−189.

Higgins, D. D., Kinuthia, J. M., & Wild, S. (1998). Soil stabilisation using lime-activated ground granulated blastfurnace slag (GGBS). In V. M. Malhotra (Ed.), *Proceedings of the 6th CANMET/ACI Int. Conf. On fly ash, silica fume, slag and natural Pozzolans in Concrete, 1998, 2, SP, 178−55* pp. 1057−1074. Bangkok, Thailand, May 31st-June 5th, 1998, Libr. Of Congr. Catal. Card No. 98-85145. pp. 1057−1074.

Higgins, D. D., Thomas, B., & Kinuthia, J. (2002). Pyrite oxidation, expansion of stabilised clay and the effect of ggbs. In S. E. Zoorob, A. C. Collop, & S. F. Brown (Eds.), *Proceedings of the 4th European Symposium, Bitmat4, on performance of bituminous and hydraulic materials in pavements* (pp. 161−168), ISBN 90 5809 375 1. Published by Nottingham University, UK, 11−12 April 2002.

Janssen, H., Derluyn, H., & Carmeliet, J. (2012). Moisture transfer through mortar joints: a sharp-front analysis. *Cement and Concrete Research, 42*, 1105−1112.

Kelman, I., & Spence, R. (2004). An overview of flood actions on buildings. *Engineering Geology, 73*, 297−309.

Khedari, J., Watsanasathaporn, P., & Hirunlabh, J. (2005). Development of fiber-based soil-cement block with low thermal conductivity. *Cement and Concrete Composites, 27*, 111−116.

Kinuthia, J. M., & Nidzam, R. M. (2011). Towards zero industrial waste: utilization of brick dust waste in sustainable construction. *Waste Management, 31*, 1867−1878.

Kinuthia, J. M., Nidzam, R. M., Wild, S., & Robinson, R. B. (2003). Strength and swelling properties of sulphate-bearing soil stabilised utilising wastepaper sludge ash (WSA). In Andrew R. Dawson (Ed.), *Proceedings of UNBAR 6−6th International Symposium on Pavements unbound! Nottingham, England, 6th−8th July 2004*. Balkema Publishers, ISBN 90 5809 699 8.

Kinuthia, J. M., & Oti, J. E. (2012). Designed non-fired clay mixes for sustainable and low carbon use. *Applied Clay Science, 59/60*, 131−139.

Kinuthia, J. M., Snelson, D. G., & Gailius, A. (2009). Sustainable medium-strength concrete (CS-Concrete) from colliery spoil in South Wales UK. *Civil Engineering and Management, 15*, 149−157.

Kinuthia, J. M., & Wild, S. (2001). Effects of some metal sulfates on the strength and swelling properties of lime-stabilised kaolinite. *International Journal of Pavement Engineering (IJPE), 2*, 103−120.

Kinuthia, J. M., Wild, S., & Jones, G. I. (1999). Effects of monovalent and divalent metal sulphates on consistency and compaction of lime-stabilised kaolinite. *Applied Clay Science, 14*, 27−45.

Lanas, J., & Alvarez, J. I. (2003). Masonry repair lime-based mortars: factors affecting the mechanical behavior. *Cement and Concrete Research, 33*, 1867−1876.

McCarthy, M. J., Csetenyi, L. J., Sachdeva, A., & Dhir, R. K. (2014). Engineering and durability properties of fly ash treated lime-stabilized sulfate-bearing soils. *Engineering Geology, 174*, 139−148.

Miqueleiz, L., Ramirez, F., Oti, J. E., Seco, A., Kinuthia, J. M., Oreja, I., et al. (2013). Alumina filler waste as clay replacement material for unfired brick production. *Engineering Geology, 163*, 68−74.

Miqueleiz, L., Ramirez, F., Seco, A., Nidzam, R. M., Kinuthia, J. M., Abu Tair, A., et al. (2012). The use of stabilised Spanish clay soil for sustainable construction material. *Engineering Geology, 133−134*, 9−15.

Mofor, L., Kinuthia, J. M., Melo, U. C., & Djialli, D. (2009). Energy in Cameroon: the potential for transporting waste to riches. *Materials Solutions, 1*, 18−21.

Molina, E., Cultrone, G., Sebastián, E., Alonso, F. J., Carrizo, L., Gisbert, J., et al. (2011). The pore system of sedimentary rocks as a key factor in the durability of building materials. *Engineering Geology, 118*, 110−121.

Moropoulou, A., Bakolas, S., & Anagnostopulou, S. (2005). Composite materials in ancient structures. *Cement and Concrete Composites, 27*, 295−300.

Nidzam, R. M., & Kinuthia, J. M. (2010). Sustainable soil stabilisation with blastfurnace slag (GGBS) − a review. *Construction Materials, 163*, 157−165.

Nidzam, R. M., & Kinuthia, J. M. (2011a). Compaction of fills involving stabilisation of expansive soils. *Geotechnical Engineering, 164*, 113−126.

Nidzam, R. M., & Kinuthia, J. M. (2011b). Effects of mellowing sulfate-bearing clay soil stabilized with wastepaper sludge ash for road construction. *Engineering Geology, 117*, 170−179.

Obonyo, E., Exelbirt, J., & Baskaran, M. (2010). Durability of compressed earth bricks: assessing erosion resistance using the modified spray testing. *Sustainability, 2*, 3639−3649.

Obuzor, G. N., Kinuthia, J. M., & Robinson, R. B. (2011a). Enhancing the durability of flooded low-capacity soils by utilizing lime-activated ground granulated blastfurnace slag (GGBS). *Engineering Geology, 123*, 179−186.

Obuzor, G. N., Kinuthia, J. M., & Robinson, R. B. (2011b). Utilisation of lime activated GGBS to reduce the deleterious effect of flooding on stabilised road structural materials: a laboratory simulation. *Engineering Geology, 122*, 334−338.

Obuzor, G. N., Kinuthia, J. M., & Robinson, R. B. (2012). Soil stabilisation with lime-activated-GGBS—A mitigation to flooding effects on road structural layers/embankments constructed on floodplains. *Engineering Geology, 151*, 112−119.

Ogunye, F. O., & Boussabaine, H. (2002a). Development of a rainfall test rig as an aid in soil block weathering assessment. *Construction and Building Materials, 16*, 173−180.

Ogunye, F. O., & Boussabaine, H. (2002b). Diagnosis of assessment methods for weatherability of stabilized compressed soil blocks. *Construction and Building Materials, 16*, 163−172.

Oti, J. E., & Kinuthia, J. M. (2012). Stabilised unfired clay bricks for environmental and sustainable use. *Applied Clay Science, 58*, 52−59.

Oti, J. E., Kinuthia, J. M., & Bai, J. (2008a). Developing unfired stabilized building materials in the UK. *Engineering Sustainability, 161*, 211−218.

Oti, J. E., Kinuthia, J. M., & Bai, J. (2008b). Using slag for unfired-clay masonry-bricks. *Construction Materials, 161*, 147−155.

Oti, J. E., Kinuthia, J. M., & Bai, J. (2009a). Compressive strength and Microstructural analysis of unfired clay masonry bricks. *Engineering Geology, 109*, 230−240.

Oti, J. E., Kinuthia, J. M., & Bai, J. (2009b). Design Thermal values for unfired clay bricks. *Materials Design, 31*, 104−112.

Oti, J. E., Kinuthia, J. M., & Bai, J. (2009c). Engineering properties of unfired clay masonry. *Engineering* Geology*, 107*, 130−139.

Oti, J. E., Kinuthia, J. M., & Bai, J. (2009d). Unfired clay bricks: from laboratory to industrial production. *Proceedings of the Institution of Civil Engineers (ICE), Engineering Sustainability, 162*, 229−237.

Oti, J. E., Kinuthia, J. M., & Bai, J. (2010a). Design Thermal values for unfired clay bricks. *Materials and Design, 31*, 104−112.

Oti, J. E., Kinuthia, J. M., & Bai, J. (2010b). Engineering properties of concrete made with slate. *Proceedings of the Institution of Civil Engineers (ICE), Construction Materials, 163*, 131−142.

Oti, J. E., Kinuthia, J. M., & Bai, J. (2010c). Freeze-thaw of stabilised clay brick. *Proceedings of the Institution of Civil Engineers (ICE), Waste and Resource Management, 163*, 129−135.

Oti, J. E., Kinuthia, J. M., & Bai, J. (2010d). Sustainable masonry mortar for brick joint and plaster in the UK. *Proceedings of the Institution of Civil Engineers (ICE), Construction Materials, 163*, 87−96.

Oti, J. E., Kinuthia, J. M., & Bai, J. (2010e). Unfired clay masonry incorporating slate waste. *Proceedings of the Institution of Civil Engineers (ICE), Waste and Resource Management, 163*, 17−27.

Oti, J. E., Kinuthia, J. M., Snelson, D. G., & Bai, J. (2010f). Applications of slate waste material in the UK. *Proceedings of the Institution of Civil Engineers (ICE), Waste and Resource Management, 163*, 9−15.

O'Farrell, M., Wild, S., & Sabir, B. B. (1999). Resistance to chemical attack of ground brick-PC mortar, Part I. Sodium sulphate solution. *Cement and Concrete Research, 29*, 1781−1790.

O'Farrell, M., Wild, S., & Sabir, B. B. (2000). Resistance to chemical attack of ground brick-PC mortar, Part II. Synthetic seawater. *Cement and Concrete Research, 30*, 757−765.

Pan, Y. W., Li, K. W., & Liao, J. J. (2014). Mechanics and response of a surface rock block subjected to pressure fluctuations: a plucking model and its application. *Engineering Geology, 171*, 1−10.

Rahmat, M. N., Ismail, N., & Kinuthia, J. M. (2011). The potential of utilising industrial waste as lightweight building components − a preliminary investigation. *Modern Applied Science, 4*, 35−46.

Snelson, D. G., & Kinuthia, J. M. (2010). Resistance of mortar containing unprocessed pulverised fuel ash (PFA) to sulphate attack. *Cement and Concrete Composites, 32*, 523−531.

Snelson, D. G., Kinuthia, J. M., Davies, P. A., & Chang, S. (2009). Sustainable construction: composite use of tyres and ash in concrete. *Waste Management, 29*, 360−367.

Taallah, B., Guettala, A., Guettala, S., & Kriker, A. (2014). Mechanical properties and hygroscopicity behavior of compressed earth block filled by date palm fibers. *Construction and Building Materials, 59*, 161−168.

Walker, P. J. (2004). Strength and erosion characteristics of earth blocks and earth block masonry. *Journal of Materials in Civil Engineering, 16*, 497−506.

Wild, S., Kinuthia, J. M., Jones, G. I., & Higgins, D. D. (1998). Effects of partial substitution of lime with ground granulated blastfurnace slag (ggbs) on the strength properties of lime-stabilised sulphate bearing clay soils. *Engineering Geology, 51*, 37−53.

Wild, S., Kinuthia, J. M., Jones, G. I., & Higgins, D. D. (1999). Suppression of swelling associated with ettringite formation in lime-stabilised sulphate-bearing clay soils by partial substitution of lime with ground granulated blastfurnace slag (GGBS). *Engineering Geology, 51*, 257−277.

Wild, S., Kinuthia, J. M., Robinson, R. B., & Humphries, I. (1996). Effects of ground granulated blastfurnace slag (ggbs) on the strength and swelling properties of lime-stabilised kaolinite in the presence of sulphates. *Clay Minerals, 31*, 423−433.

Topology optimization for the development of eco-efficient masonry units

19

M. Bruggi, A. Taliercio
Politecnico di Milano, Milan, Italy

19.1 Introduction

With the progressive decrease in available energy sources and the need for reducing energy consumption, one of the primary objectives in the design of new buildings is to increase their thermal insulation. Different strategies can be adopted to achieve this goal, including passive heating, proper building exposure, ground source heat pumps, and use of innovative mixes to produce building blocks with enhanced insulating properties. The latter possibility has received much attention in the last decade: in particular, the use of wastes of different types, e.g., PET bottles or rubber tires (Yesilata, Isiker, & Turgut, 2009), fabrics (Briga-Sá et al., 2013), corn cobs (Pinto et al., 2012), and industrial wastes of various nature (Huang, Ranade, Zhang, Ni, & Li, 2013) has been shown to be an effective and eco-friendly means to obtain high-performance insulation materials, mainly concrete. These wastes can be added to the concrete mix in the form of shreds or used to fill air boxes in multileaf walls. Also, adding cork to mortar mixes (Brás, Leal, & Faria, 2013) can reduce thermal bridges.

In the case of masonry walls made up of concrete or clay blocks, thermal efficiency can be quantified through the so-called "thermal transmittance" (usually denoted by U), that is, the heat flow per square meter divided by the difference in temperature between the faces of the wall; accordingly, U is expressed in W/m^2K. U can be decreased by including in the mix design materials with insulating properties, such as expanded clay (Bastos, Sousa, & Melo, 2005), perlite (Topçu & Isikdağ, 2007), or diatomite (Ünal, Uygunoğlu, & Yildiz, 2007). Air cells in concrete units and mortar joints are also found to decrease the thermal conductivity of a wall, as experimentally shown by Abdou & Murali (1994).

Another possibility is designing masonry (or concrete) units of innovative shape, in order to decrease their thermal transmittance (that is, to increase their thermal resistance) compared to standard hollow blocks. Several authors have addressed the problem of finding the geometry of a masonry block that allows the thermal insulation of any building to be maximized. Pierzchlewicz (1996), for instance, analyzed the thermal and strength properties of 13 kinds of hollow blocks with aligned or staggered holes. A similar investigation was later carried out by Al-Jabri, Hago, Al-Nuaimi, & Al-Saidy (2005) on lightweight concrete hollow blocks. Recently, Sousa, Sousa,

Eco-efficient Masonry Bricks and Blocks. http://dx.doi.org/10.1016/B978-1-78242-305-8.00019-X

Castro, Antònio, & Sousa (2011), Sousa, Castro, Antònio, & Sousa, (2011) used a genetic algorithm to define the geometry of lightweight hollow concrete blocks that minimizes their transmittance by varying a finite number of parameters that define the position, size, and spacing of rectangular, evenly spaced holes within the block. The holes can be either aligned or staggered.

In this chapter, a problem similar to that studied by Sousa, Sousa, et al. (2011), Sousa, Castro, et al. (2011) is dealt with using a more general approach. Topology optimization (see, for example, Bendsøe & Sigmund, 2003) is employed to determine the distribution of a prescribed amount of material over a given design domain, which minimizes the thermal transmittance of a masonry wall. As the heat flux is supposed to be uniform along the wall height, a 2D optimization problem has to be solved, and the design domain represents the cross-section of any masonry block. No a priori assumption is made about the geometry of the holes in the block so as to fully exploit the potentials of topology optimization. Indeed, topology optimization differs from shape optimization, as the final topology of the design domain generally differs from that at the beginning of the optimization process. Unlike shape optimization, topology optimization allows material layouts characterized by voids and multiplies connected regions to be obtained, even if the original design domain is simply connected.

A broad and updated survey of the established numerical methods developed in structural topology optimization can be found in Rozvany (2009) or Sigmund & Maute (2013). Topology optimization has been widely used by many authors: in most applications, the material distribution that maximizes the stiffness or strength properties of bi- and three-dimensional bodies is sought. Only recently, a few authors have applied topology optimization to thermal problems. Li, Steven, Querin, & Xie (1999), Li, Steven, Xie, & Querin (2004) applied evolutionary structural optimization (ESO) to get the topology that maximizes heat transfer for a prescribed material volume under steady-state assumption, or to minimize the temperature at a given location in heat-conducting fields.

In the field of building technology, topology optimization can help in designing buildings with reduced energy consumption. To this end, the results obtained by Munoz, Allaire, & Bendsøe (2007) can be exploited. The authors aim at finding the optimal distribution of a fixed amount of insulating material around a conductive domain heated by an internal source, which basically amounts to defining the optimal layout of an insulator around an indoor environment with prescribed radiators. More recently, Bruggi & Cinquini (2011) developed an algorithm to minimize the transmittance of walls, floors, and ceilings, and to reduce the effects of undesirable thermal bridges. The procedure is based on the steady-state heat equation, with boundary conditions of convective type.

Extending the proposal by Bruggi & Cinquini (2011), in this chapter an approach is followed which also takes into account mechanical constraints. The thermal transmittance of any masonry block is minimized, assuming the in-plane and the out-of-plane stiffness of the block is higher than a given minimum value. These mechanical constraints indirectly allow for the requirements prescribed by the current standards on the percentage of holes in structural blocks. Also, controlling the in-plane stiffness of the wall is an expedient way to increase the resistance to in-plane shear

actions, as required by recent regulations for the use of masonry blocks in areas prone to earthquakes.

The outline of the chapter is as follows. In Section 19.2 the equations governing two-dimensional heat conduction problems under steady-state conditions are recalled. In Section 19.3.1 the fundamentals of topology optimization are briefly reviewed, and the optimization problem to be dealt with is described in detail. To avoid convergence problems related to the abrupt transition of any element from full to empty (or vice versa) during the iterative optimization scheme, the classical so-called RAMP method is employed, according to which the thermomechanical properties of the material are related to the design variable (i.e., the material density) through continuous functions (Section 19.3.2). The governing equations are reformulated in a weak (Section 19.3.3) and discrete (Section 19.3.4) form, in view of their implementation in a finite element code. In Section 19.4 the optimal material distributions obtained for blocks of square or rectangular section, with flat (Section 19.4.1) or indented (Section 19.4.2) sides, are presented and critically discussed. The proposed technique is shown to spontaneously lead to layouts characterized by the presence of holes of general shape, which may serve as a basis for the practical realization of blocks with nontraditional geometries. The gain in terms of thermal efficiency compared to existing blocks is also shown (Section 19.4.3). Finally, in Section 19.5, the main results of the work are summarized, and possible future developments are outlined.

From here onward, vectors and tensors will be denoted by italic boldface symbols; arrays and matrices by single and double underline, respectively.

19.2 The steady-state heat conduction problem

The fundamentals of the heat conduction problem in steady-state conditions over any plane domain are briefly recalled, in view of the formulation of the topology optimization problem for thermal insulation in Section 19.3. The formulation is limited to the 2D case, according to the simplifying assumptions made in Section 19.1.

19.2.1 Governing equations

Let $\Omega \in R^2$ denote the design domain, $\partial\Omega$ its regular boundary, and $\boldsymbol{k}$ the second-order thermal conductivity tensor of the material at any point in Ω. Under steady-state conditions, the unknown temperature field T over Ω is governed by the well-known heat conduction equation:

$$\operatorname{div}(\boldsymbol{k}\nabla T) + b = 0 \tag{19.1}$$

where b is the heat energy generated per unit volume. In particular, for isotropic materials $\boldsymbol{k} = k\boldsymbol{I}$, where k is the thermal conductivity and $\boldsymbol{I}$ is the identity tensor. For homogeneous isotropic domains, Eqn (19.1) reduces to $k\Delta T + b = 0$, with Δ being the Laplace operator.

The boundary of Ω usually consists of a part Γ_T where a temperature distribution T_0 is prescribed, and another part Γ_f over which a heat flux q is prescribed. Thus, the boundary conditions for Eqn (19.1) read:

$$T = T_0 \text{ over } \Gamma_T, \quad -(\boldsymbol{k}\nabla T)\cdot\boldsymbol{n} = q \text{ over } \Gamma_f, \tag{19.2}$$

with $\boldsymbol{n}$ being the unit outward normal vector to Γ_f. The case where a convective heat transfer is prescribed through a part Γ_c of $\partial\Omega$ is included in the latter condition. In this case, the heat flux per unit area q_c is proportional to the difference between the temperature of the body surface and the ambient temperature T_a, i.e.,

$$q_c = h_c(T - T_a), \tag{19.3}$$

with h_c being the so-called convective heat transfer coefficient. This coefficient takes globally into account the heat fluxes affecting the body surfaces under laminar flow conditions. See, for example, the ISO standards 6946:2007 (2007).

The problem defined by Eqns (19.1)–(19.3) can be stated in weak formulation as (Gosz, 2006): find T such that $T_{|\Gamma_T} = T_0$ and

$$\int_\Omega \nabla w\cdot(\boldsymbol{k}\nabla T)\mathrm{d}V = \int_{\Gamma_T} wq_{\text{react}}(T_0)\mathrm{d}S - \int_{\Gamma_f} wq\mathrm{d}S - \int_{\Gamma_c} wh_c(T - T_0)\mathrm{d}S + \int_\Omega wb\mathrm{d}V, \ \forall w, \tag{19.4}$$

where w can be interpreted as a "virtual" temperature field, and $q_{\text{react}}(T_0)$ stands for the "reactive" heat flux acting on T_0. Eqn (19.4) can be rewritten in compact form as

$$a(w, T) + < w, h_cT>_{\Gamma_c} = < w, q_{\text{react}}(T_0)>_{\Gamma_T} - < w, q>_{\Gamma_f} + < w, h_cT_a>_{\Gamma_c} + < w, b >, \tag{19.5}$$

where $a(w, T)$ is the left-hand side of Eqn (19.4). The definition of the bilinear forms $<*>$ in Eqn (19.5) is straightforward.

19.2.2 Transmittance and thermal compliance

In linear elasticity, the structural compliance C^S of any body Ω is defined as

$$C^S(\boldsymbol{u}) = \int_\Omega C_{ijhk}\varepsilon_{ij}(\boldsymbol{u})\varepsilon_{hk}(\boldsymbol{u})\mathrm{d}V, \tag{19.6}$$

where C_{ijhk} are the components of the fourth-order elasticity tensor, ε_{ij} are infinitesimal strains, and $\boldsymbol{u}$ is the small displacement vector. At the equilibrium, assuming the body

to be subjected only to prescribed tractions $\boldsymbol{t}_0$ over the portion Γ_T of its boundary, $C^S(\boldsymbol{u}) = \int_{\Gamma_T} t_0 \cdot \boldsymbol{u}\, \mathrm{d}\Gamma$.

In analogy to the structural compliance C^S, it is expedient to define a "thermal compliance" C^T as (see Gao, Zhang, Zhu, Xu, & Bassir, 2008; Iga, Nishiwaki, Izui, & Yoshimura, 2009)

$$\begin{aligned} C^T(T) &= < T,\, q_{\text{react}}(T_0) > \Gamma_T - < T,\, q > \Gamma_f + < T,\, h_c T_a > \Gamma_c + < T,\, b > \\ &\equiv a(T,\, T) + < T,\, h_c T > \Gamma_c. \end{aligned} \tag{19.7}$$

Let any building envelope be modeled as a conduction-dominated solid domain that exchanges heat fluxes with fluid regions across its surfaces. No heat source b, heat flux q, or temperature T are supposed to be prescribed within the domain or over its boundary. Assume that only a convective heat flux takes place across the external surfaces of the building, conforming with Eqn (19.3). The indoor and outdoor ambient temperatures, denoted by T_{ai} and T_{ao}, respectively, are given over the corresponding parts of $\Gamma_c = \Gamma_{ci} \cup \Gamma_{co}$. The heat flux might also be prescribed to vanish across a certain part Γ_f of $\partial\Omega$, e.g., due to symmetry conditions. According to the above assumption, assuming $T_{ai} > 0$ and assuming the outdoor ambient temperature T_{ao} to vanish, for the sake of simplicity, Eqn (19.7) can be rewritten as

$$C^T(T) = < T,\, h_c T_{ai} > \Gamma_{ci} \big(= a(T,\, T) + < T,\, h_c T > \Gamma_c \big). \tag{19.8}$$

As the heat diffusion depends on the magnitude of the convective flux across Γ_{ci}, i.e., $h_c(T_{ai} - T)$, the thermal compliance $C^T(T)$ given by Eqn (19.8) can be spontaneously adopted as an objective function to minimize or maximize the heat transfer through Ω. Indeed, minimizing C^T, the optimal thermal conductor is found; conversely, maximizing C^T, the optimal thermal insulator is obtained.

Under the above assumptions, the thermal transmittance of any wall of the building separating the inner environment from the outer environment can be defined as

$$U = \frac{1}{|\Gamma_{ci}|} \int_{\Gamma_{ci}} h_c(T_{ai} - T)\mathrm{d}\Gamma. \tag{19.9}$$

Maximizing C^T amounts at minimizing U.

It is worth noting that, according to existing engineering codes, h_c takes different values at the surfaces in contact with the inner and the outer environment, denoted by h_{ci} and h_{co}, respectively. The values suggested by the ISO standards, for instance, are $h_{ci} = 7.7$ W/(m^{2}K) and $h_{co} = 25$ W/(m^{2}K). Only the value of h_{ci} is of interest for the numerical applications shown in Section 19.4, according to the definition of U, Eqn (19.9).

19.3 Optimal design for thermal insulation: problem formulation

In Section 19.2 the fundamentals of the heat conduction problem considered herein have been shown, and a suitable objective function for the optimal design of thermal conductors/insulators has been defined. In this section, the proposed optimization procedure is outlined, and details on the numerical procedure implemented are given.

19.3.1 Introductory remarks on topology optimization

Topology optimization is a design tool that allows a prescribed amount of material to be distributed over a given design domain to minimize a scalar objective function for a fixed set of constraints. In the original formulation by Bendsøe & Kikuchi (1988), the distribution of isotropic material that maximizes the structural stiffness (i.e., that minimizes the structural compliance) for an available amount of material is sought. The elastic properties of the material are assumed to depend point-wise on a continuous density function, which plays the role of design variable and takes values in [0,1]. Suitable interpolation laws are conceived to penalize the material stiffness at intermediate densities with the aim of achieving a design characterized only by "voids" and "solid regions."

In discrete form, the topology optimization problem can be straightforwardly solved through minimizers based on mathematical programming, coupled with finite element techniques to enforce the elastic equilibrium equation in terms of displacements. The formulation for minimum structural compliance can be extended to cope with another classical problem of optimal design, i.e., the optimization for minimum thermal compliance (Cherkaev, 2000). The former involves a vector (displacement) field; whereas, the latter is written in terms of the scalar temperature field. In the thermal case, conductivity is assumed to depend on density through a suitable interpolation function, with the aim of achieving optimal material layouts.

Both problems will be dealt with in detail in the next section, and the key elements of the proposed theoretical framework for the optimal thermomechanical design of masonry blocks will be illustrated.

19.3.2 Interpolation model for the thermal and mechanical properties of the material

Topology optimization by distribution of isotropic material is based on the adoption of a suitable interpolation scheme (Bendsøe & Sigmund, 2003; Rozvany, 2009) to approximate the mechanical and physical properties of the material, herein, the thermal conductivity k and the Young's modulus E, depending on the design variable ρ. Design variable ρ can be interpreted as a nondimensional material density that ranges between 1 (full material) and 0 (void). Intermediate values of ρ correspond to a sort of porous material.

The procedure proposed hereafter implements the so-called RAMP (rational approximation of material properties) model (Stolpe & Svanberg, 2001). For thermal conductivity, the proposed interpolation reads:

$$k(\rho) = k_0 + \frac{\rho}{1 + p(1-\rho)}(k_1 - k_0). \tag{19.10}$$

A similar interpolation law will be also used for the material elastic modulus. k ranges between two extreme values, $k_0 = k(\rho = 0)$ and $k_1 = k(\rho = 1)$, with $k_1 > k_0$. According to the EN 1745 standards (EN 1745:2012.(2010)), k_0 can be interpreted as the equivalent thermal conductivity of the voids (see also Sousa, Castro, Antònio, et al., 2011). For $p = 0$, the RAMP model provides a linear interpolation. As p increases, the interpolation law strongly penalizes the intermediate material densities and spontaneously leads to pure 0-1 designs. In the numerical applications presented in Section 19.4, $p = 3$ is assumed: this choice allows black-and-white layouts to be obtained without any appearance of gray areas.

Other interpolation schemes could be used instead of Eqn (19.10): the SIMP model (Bendsøe, 1989) is probably the most frequently used, but is not suitable to interpolate material variables if the extreme values are both nonvanishing.

19.3.3 Continuous formulation

The problem of finding the optimal material distribution over a design domain Ω which minimizes the heat diffusivity through Ω (or maximizes the heat conduction, i.e., C^T—see Eqn (19.8)) with prescribed convective boundary conditions (see Eqn (19.4) and constraints on the elastic stiffness) can be stated as follows:

$$\begin{aligned}
&\text{Find} \quad \max_{\rho \in R_0^+} C^T = a(T,\, T) + <T,\, h_c T>_{\Gamma_c} \quad \text{such that} \\
&\int_\Omega \nabla w \cdot (\boldsymbol{k}(\rho)\nabla T)\mathrm{d}V = \int_{\Gamma_c} w h_c (T - T_a)\mathrm{d}S \\
&C_h^S(\boldsymbol{u}) / C_{0h}^S \le \alpha_h, \quad h = 1 \ldots n \\
&\int_\Omega \boldsymbol{\varepsilon}(\boldsymbol{u}) :\, \boldsymbol{C}(\rho) :\, \boldsymbol{\varepsilon}(\boldsymbol{u})\mathrm{d}V = \int_{\Gamma_t} \boldsymbol{t}_{oh} \cdot \boldsymbol{u}\mathrm{d}S \\
&0 \le \rho \le 1.
\end{aligned} \tag{19.11}$$

In Eqn (19.11) the dependence of the thermal conductivity tensor $\boldsymbol{k}$ on the unknown design variable ρ, according to Eqn (19.10), has been pointed out. The coefficients h_c are referred to a fixed boundary Γ_c and are assumed to be independent of ρ.

The third row in Eqn (19.11) represents a set of constraints on the overall stiffness, prescribing the structural compliance C_h^S, computed for any load case h, be greater than a minimum value $\alpha_h C_{0h}^S$, with C_{0h}^S being the compliance evaluated for a homogeneous solid block, and α_h (≥ 1, $h = 1 \ldots n$) a value selected to match any desired structural

performance. In the applications shown in Section 19.4, these constraints will be specialized to loads acting perpendicular to the wall ($h = 1$) and loads acting parallel to the wall mid-plane ($h = 2$). These constraints can be replaced, or complemented, by other technological constraints.

Finally, the fourth row in Eqn (19.11) represents the elastic equilibrium conditions in weak form for the body, under prescribed boundary tractions $\boldsymbol{t}_{0h}$ corresponding to the h-th load case. On the left-hand side all the coefficients of the elasticity tensor $\boldsymbol{C}$ can be expressed as a function of the design variable ρ according to a RAMP-like law similar to Eqn (19.10).

19.3.4 Discrete formulation

The numerical solution of Eqn (19.11) resorts to the finite element discretization of the density field, and to the approximation of the state equations for the thermal and the elastic problem. A mesh consisting of quadrilateral finite elements with bilinear shape functions is used to discretize both the temperature and the displacement fields, considering only one density unknown for each element (see, for example, Bendsøe & Sigmund, 2003; Sigmund, 2001). Mathematical programming is used to cope with the minimization problem. In discrete form, the thermal compliance C^T in the first row of Eqn (19.11) can be expressed as:

$$C^T = \underline{\theta}^T \left(\underline{\underline{K}}_t(\underline{x}) + \underline{\underline{H}}_t \right) \underline{\theta}, \tag{19.12}$$

where $\underline{x} = \{x_1, x_2, \ldots, x_N\}^T$ is an array gathering the unknown densities of the N elements, $\underline{\theta}$ is the array of the nodal temperatures, $\underline{\underline{K}}_t$ is the matrix of the elemental conductivities, and $\underline{\underline{H}}_t$ is the heat transfer matrix. From an operational point of view, the objective function is computed as the sum of N quadratic forms depending on the sub-array $\underline{\theta}_i$ of the elemental nodal temperatures, the elemental conductivity matrix $\underline{\underline{K}}_{ti}$, and the elemental heat transfer matrix $\underline{\underline{H}}_{ti}$:

$$C^T = \sum_{i=1}^{N} \underline{\theta}_i^T \left(k(x_i) \underline{\underline{K}}_{t0,i} + \underline{\underline{H}}_{ti} \right) \underline{\theta}_i. \tag{19.13}$$

To explicit the dependence on the density, the conductivity matrix of the i-th element was expressed as $k(x_i)\underline{\underline{K}}_{t0,i}$, where $\underline{\underline{K}}_{t0,i}$ refers to a unit thermal coefficient. The convective matrix $\underline{\underline{H}}_{ti}$ is independent of x_i, as discussed in Section 19.3.3.

Similarly, in discrete form, the structural compliance C^S in Eqns (19.6) and (19.11) can be rewritten as

$$C^S = \underline{U}^T \underline{\underline{K}}_s \underline{U} = \sum_{i=1}^{N} \underline{U}_i^T E(x_i) \underline{\underline{K}}_{s0,i} \underline{U}_i, \tag{19.14}$$

where $\underline{U}$ is the array of the nodal displacements, $\underline{U}_i$ is the sub-array of the nodal displacements of the i-th element, and $\underline{\underline{K}}_s$ is the stiffness matrix of the entire body.

Assuming the material to be isotropic, and adopting a RAMP-like interpolation for the elastic modulus E, the stiffness matrix of any element can be expressed as $E(x_i)\underline{\underline{K}}_{s0,i}$, where $\underline{\underline{K}}_{s0,i}$ refers to a unitary elastic modulus. E ranges between $E_0 = E(\rho = 0)$ and $E_1 = E(\rho = 1)$.

The ensuing discrete formulation reads:

$$\begin{aligned}
&\text{Find} \quad \max_{\underline{x}} C^T = \sum_{i=1}^{N} \underline{\theta}_i^T \left(k(x_i)\underline{\underline{K}}_{t0,i} + \underline{\underline{H}}_{ti} \right) \underline{\theta}_i \quad \text{such that} \\
&\left(\underline{\underline{K}}_t(\underline{x}) + \underline{\underline{H}}_t \right) \underline{\theta} = \underline{F}_t \\
&C_h^S(\underline{u}) \Big/ C_{0h}^S \leq \alpha_h, \quad h = 1 \ldots n \\
&\underline{\underline{K}}_s(\underline{x})\underline{U} = \underline{F}_s \\
&0 \leq x_i \leq 1, \quad i = 1 \ldots N,
\end{aligned} \tag{19.15}$$

where the arrays $\underline{F}_t$ and $\underline{F}_s$ can be straightforwardly derived from Eqn (19.11).

If a gradient-based algorithm is used to solve problem Eqn (19.15), the sensitivities of the discrete thermal compliance, Eqn (19.13), and the discrete structural compliance, Eqn (19.14), must be evaluated. The derivative of C^T with respect to the j-th design variable x_j can be directly computed as

$$\frac{\partial C^T}{\partial x_{ji}} = -\underline{\theta}_j^T \frac{\partial k(x_j)}{\partial x_{ji}} \underline{\underline{K}}_{t0,j} \underline{\theta}_j. \tag{19.16}$$

Similarly, the derivative of C^S with respect to the j-th design variable is given by

$$\frac{\partial C^S}{\partial x_{ji}} = -\underline{U}_j^T \frac{\partial E(x_j)}{\partial x_{ji}} \underline{\underline{K}}_{s0,j} \underline{U}_j \tag{19.17}$$

The sensitivities of the constraints in Eqn (19.11) can be easily computed using Eqn (19.17).

Note that numerical instabilities may arise in the optimization procedure if low-order finite elements are adopted in the discretization, along with an element-wise constant density approximation (see, among the others, Bruggi, 2008; Sigmund & Petersson, 1998). Undesired "checkerboard" patterns and mesh dependence may also arise in the case of thermal insulation problems, as outlined by Munoz et al. (2007). A classical remedy consists in the adoption of filtering schemes, which also allow for a heuristic control of the minimum thickness of the members arising in the optimal design. Instead of the conventional filters on the sensitivities of the objective function employed in Bruggi & Cinquini (2011), in this work an approach based on the density filter is implemented, as proposed by Bourdin (2001) or Bruns &

Tortorelli (2001). The original design variables x_i are transformed into a new set of unknowns $\tilde{x}_i$ defined by

$$\tilde{x}_i = \frac{\sum_N H_{ij} x_j}{\sum_N H_{ij}}, H_{ij} = \sum_N \max\left(0, r_{\min} - \mathrm{dist}(i,j)\right), \tag{19.18}$$

where dist(i,j) is the distance between the centroids of the i-th and the j-th elements, and $r_{\min}$ is the filtering radius.

19.4 Numerical investigations

To illustrate the capabilities of the algorithm described in Section 19.3, the optimal material distribution that minimizes the heat conduction of masonry blocks will be now sought. Heat is supposed to flow across the wall only horizontally, so that the problem can be effectively analyzed as two-dimensional. The effect of the prescribed structural compliance on the optimal layout are discussed for blocks of square or rectangular cross-section with flat sides (Section 19.4.1). The changes in the optimal material layout due to the presence of indentations along the boundary of the design domain existing in most real blocks are also investigated (Section 19.4.2). Finally, the increase in thermal efficiency of the optimized blocks compared to commercially available blocks is discussed in Section 19.4.3.

The material properties employed in the applications are listed in Table 19.1: refer to Section 19.3 for the meaning of the symbols. The Poisson's ratio ν of the material is supposed to be unaffected by the material density. The value of the equivalent thermal conductivity of the voids, k_0, was taken from the EN 1745 standards (2010). The "void" regions were given a negligible elasticity modulus E_0.

Two self-equilibrated load cases are considered in the analyses: a uniform out-of-plane compression $t_{01} = 1$ N/m, acting on the opposite sides of the block belonging to the surfaces of the wall, and a uniform in-plane compression $t_{02} = 1$ N/m, acting on the other two faces of the block along the wall thickness. The compliance of the solid design domain in the two load cases will be denoted by C_{01}^S and C_{02}^S, respectively.

Table 19.1 Thermomechanical properties of the materials employed in the numerical applications

	k_0 [W/m/K]	k_1 [W/m/K]	E_0 [N/mm^2]	E_1 [N/mm^2]	ν
Clay	0.050	0.7	0.01	10,000	0.25
Lightweight concrete	0.050	0.8	0.015	15,000	0.20

In all the applications, the thickness of the finite elements discretizing the design domain Ω is arbitrarily taken equal to 1. The elements along $\partial\Omega$, forming a strip 10 mm thick, are given a fixed density $\rho = 1$. The filtering radius $r_{\min}$ is taken equal to 2.5 mm. Filtering also allows for a heuristic control of the minimum thickness of the "webs" that characterize the optimal design, which will not be thinner than 4 mm, accordingly (Bendsøe & Sigmund, 2003).

In all the figures shown hereafter, the vertical sides of the design domain correspond to the surfaces crossed by the heat flux; the horizontal sides of the design domain are parallel to the wall thickness.

19.4.1 Influence of the block shape: square versus rectangular clay blocks

Consider a clay block of square cross-section, with side length 0.30 m, and a clay block of rectangular cross-section, 0.30 × 0.50 m. Only half the block is discretized in the latter case. The design domain is subdivided into approximately 65,000 elements. First, the effect of the prescribed minimum value of the out-of-plane structural compliance of the wall (C_1^S) on the optimal material layout that maximizes the thermal compliance is studied. The normalized in-plane structural compliance, $\alpha_2 = C_2^S/C_{02}^S$, is taken equal to 2.5.

Figure 19.1 shows the optimal material distribution obtained for increasing values of α_1, that is, for decreasing values of the out-of-plane stiffness. For both types of block, as the required out-of-plane stiffness decreases, the thermal transmittance U decreases, and the percentage of voids V_f increases. The values of U and V_f computed for the

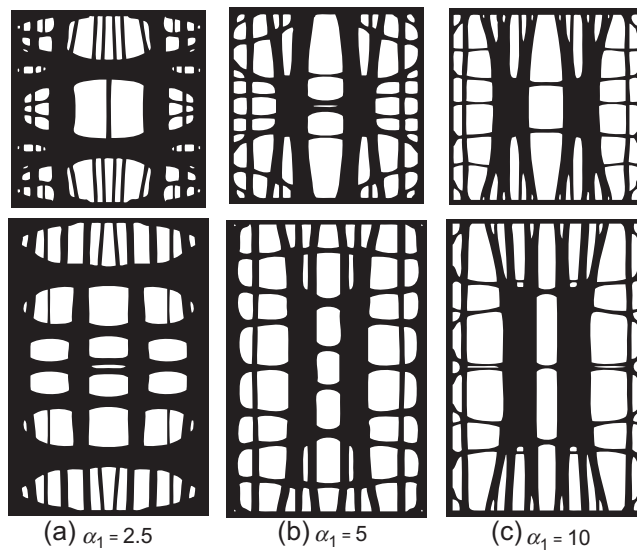

Figure 19.1 (a–c) Square versus rectangular clay blocks: optimal design for a fixed normalized in-plane compliance $\alpha_2 = 2.5$ and different values of the normalized out-of-plane compliance α_1.

Table 19.2 Thermal transmittance (U) and percentage of voids (V_f) for the optimized clay blocks with square and rectangular sections shown in Figure 19.1 ($\alpha_2 = 2.5$)

		Square block		Rectangular block	
Figure 19.4	α_1	U [W/m^2/K]	V_f [%]	U [W/m^2/K]	V_f [%]
(a)	2.5	0.919	35	0.898	38
(b)	5	0.678	48	0.657	48
(c)	10	0.543	53	0.526	52

material layouts shown in Figure 19.1 are reported in Table 19.2. Note that the decrease in U is matched by staggered material layouts, which lengthen the path that the heat flux must follow. For the smallest value of α_1, several thermal bridges arise (see Figure 19.1(a)). As α_1 increases (see Figure 19.1(b) and (c)), material localizes at the center of the block; the number of connections of the inner core with the vertical surfaces of the wall decreases, which contributes to further reduce the block transmittance. Also note that, for a given out-of-plane stiffness, the rectangular block has a lower transmittance than the square block, although the percentage of voids is similar.

When load bearing masonry is employed in seismic areas, blocks with suitable mechanical and geometrical characteristics must be employed. The Italian Standards NTC 2008 (2008) currently in force, for instance, prescribe conditions on the maximum admissible percentage of voids (45% in the zones of higher seismicity) and on the minimum strength properties of the blocks, both vertically ($f_{bk} = 5$ N/mm^2) and out-of-plane ($f'_{bk} = 1.5$ N/mm^2). The prescription regarding the out-of-plane performances of the blocks are strictly connected with limitations on the out-of-plane compliance, i.e., α_1. Accordingly, assuming the normalized out-of-plane compliance α_1 to take a prescribed value (5, in the numerical applications), a parametric study was carried out to investigate the effect of a change in the normalized in-plane compliance, α_2, on the layout of the block that minimizes its thermal transmittance. The analysis was limited to square blocks. The results obtained are shown in Figure 19.2; the relevant values of the transmittance and the percentage of voids are reported in Table 19.3. As α_2 increases, the percentage of voids increases, and the thermal transmittance decreases, as a consequence of the reduction of the number of webs connecting the two sides of the wall.

19.4.2 *Influence of the side geometry: clay blocks with flat or indented sides*

It was already pointed out that the sides of most real masonry blocks have grooves to improve interlocking and facilitate laying. Shear keys are also required in seismic regions to resist out-of-plane forces between adjacent blocks. An additional set of simulations is performed to assess the influence of indentations along two of the block

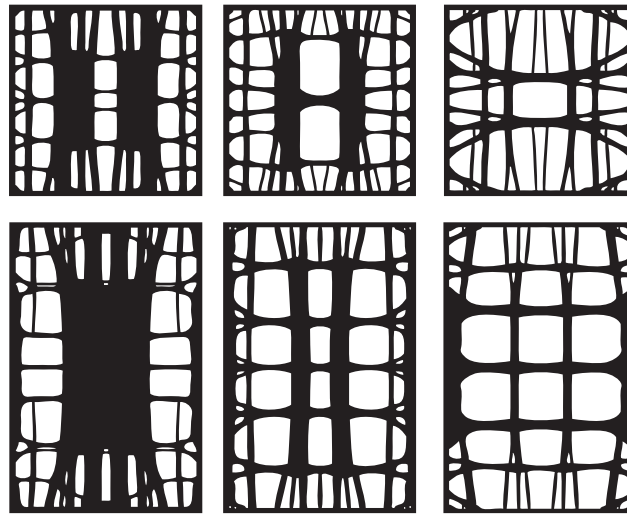

Figure 19.2 (a–c) Square versus rectangular clay blocks: optimal design for a fixed normalized out-of-plane compliance $\alpha_1 = 5$ and different values of the normalized in-plane compliance α_2.

Table 19.3 Thermal transmittance (U) and percentage of voids (V_f) for the optimized clay blocks with square section shown in Figure 19.2 ($\alpha_1 = 5$)

		Square block		Rectangular block	
Figure 19.2	α_2	U [W/m^2/K]	V_f [%]	U [W/m^2/K]	V_f [%]
(a)	2	0.707	40	0.718	38
(b)	3	0.659	53	0.636	53
(c)	5	0.619	62	0.603	63

sides on the thermal performances of square clay blocks. The optimal geometry and thermal transmittance are compared with those obtained in Section 19.4.1 for blocks with flat sides with the same mechanical performances. Figure 19.3 shows the geometry of the design domain with shear keys; again, the region along the boundary 10 mm thick has a fixed density $\rho = 1$.

Figure 19.4 shows the optimal material distribution in blocks with square section and indented sides, for increasing values of the normalized out-of-plane compliance of the wall, α_1, and for a given normalized in-plane structural compliance ($\alpha_2 = 2.5$). Comparing Figure 19.4 with the first row of Figure 19.1, one can see that the indentations in the boundary of the design domain deeply affect the optimal material distribution for given mechanical performances.

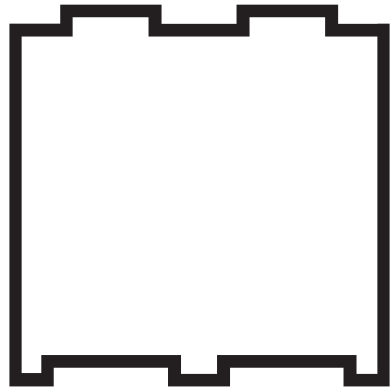

Figure 19.3 Square blocks with indented sides: geometry of the design domain.

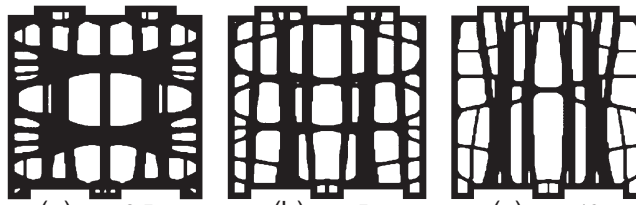

Figure 19.4 (a–c) Square blocks with indented sides. Optimal design for a fixed normalized in-plane compliance $\alpha_2 = 2.5$ and different values of the normalized out-of-plane compliance α_1.

The presence of shear keys also affects the thermal transmittance for prescribed mechanical performances, as shown in Table 19.4. The indented blocks have poorer thermal performances: for $\alpha_1 = 10$, for instance, the thermal transmittance increases from 0.543 W/m^2/K for blocks with flat sides to 0.6 W/m^2/K for blocks with shear keys, although the two blocks have nearly the same percentage of voids. Similarly to blocks with flat sides, as the required out-of-plane stiffness decreases, the thermal transmittance U decreases and the percentage of voids V_f increases. Again, the decrease in U is matched by staggered void regions (see Figure 19.4(c)).

Table 19.4 Thermal transmittance (U) and percentage of voids (V_f) for the optimized clay blocks with flat and indented sides shown in Figure 19.4 ($\alpha_2 = 2.5$)

		Flat sides		Indented sides	
Figure 19.4	α_1	U [W/m^2/K]	V_f [%]	U [W/m^2/K]	V_f [%]
(a)	2.5	0.911	36	0.944	40
(b)	5	0.678	48	0.717	50
(c)	10	0.543	53	0.600	54

19.4.3 Enhancement of the thermal efficiency of commercially available blocks

It is worthwhile to compare the thermal performances obtained with the proposed optimization procedure with those of commercially available blocks. Two lightweight concrete blocks are considered, labeled Block 1 and Block 2 hereafter: their cross-sections are shown in Figure 19.5. Block 1 is 298 mm wide and 263 mm thick. Block 2 is 245 mm wide and 269 mm thick.

The structural compliances of the blocks under loads acting along the two directions, C_1^S and C_2^S, and their thermal transmittance U are first evaluated: their values are reported in the first row of Table 19.5, along with the percentage of voids of the blocks. The topology optimization procedure is then applied to identify the optimal material layouts for blocks with the same structural compliance and the same boundary geometry. The design domain was divided into approximately 20,000 finite elements in the case of Block 1 and into approximately 17,000 elements in the case of Block 2. The vertical grooves and the horizontal slot at the center of Block 1 (Figure 19.5(a)) are supposed to be part of the design domain. The geometry of the optimized blocks is shown in Figure 19.6, and the corresponding values of U, together with the percentage of voids, are reported in the last row of Table 19.5.

Optimizing Block 1, a decrease in transmittance of about 4% in respect to the commercial block is obtained. This is basically due to the higher percentage of voids of the optimized block. The thermal performances of the two blocks, however, are not

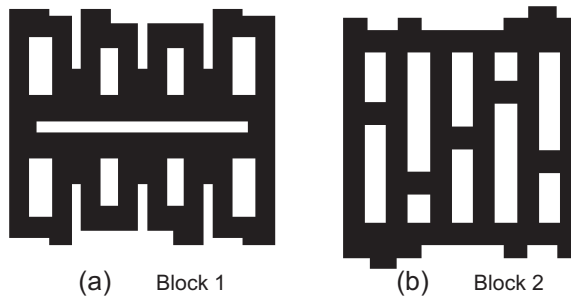

Figure 19.5 (a,b) Cross-sections of two commercially available lightweight concrete blocks.

Table 19.5 Comparison between the thermal performances of the commercial blocks and the companion optimized blocks

	Block 1				Block 2			
Figures	α_1	α_2	V_f [%]	U [W/(m^{2}K)]	α_1	α_2	V_f [%]	U [W/(m^{2}K)]
19.5	2.160	5.379	25	1.094	7.187	2.085	48	0.940
19.6			44	1.050			58	0.860

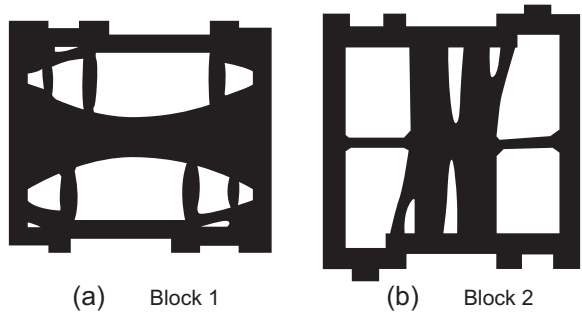

Figure 19.6 (a,b) Optimized material distribution for the blocks shown in Figure 19.5.

significantly different: indeed, the requirement of a high out-of-plane stiffness limits the amount of voids that can be placed across the wall thickness, which would resist the heat flux. The optimization procedure definitely decreases the amount of material with respect to the commercial solution. Optimizing Block 2, a decrease in transmittance of about 9% is obtained compared to the commercial block (see the last column of Table 19.5). The higher thermal efficiency of the optimized block is due, on the one hand, to the increased percentage of voids, and on the other hand, to the limited presence of thermal bridges across the wall thickness as a consequence of the reduced out-of-plane stiffness.

Finally, the influence of the prescribed mechanical stiffness on the optimal shape of the two blocks is investigated. First, the out-of-plane compliance (i.e., α_1) is varied, keeping the normalized in-plane compliance α_2 equal to 2.5. The optimal layouts are shown in Figure 19.7 for increasing values of α_1 (i.e., decreasing out-of-plane stiffness). Once again, the percentage of voids increases with α_1, the thermal transmittance

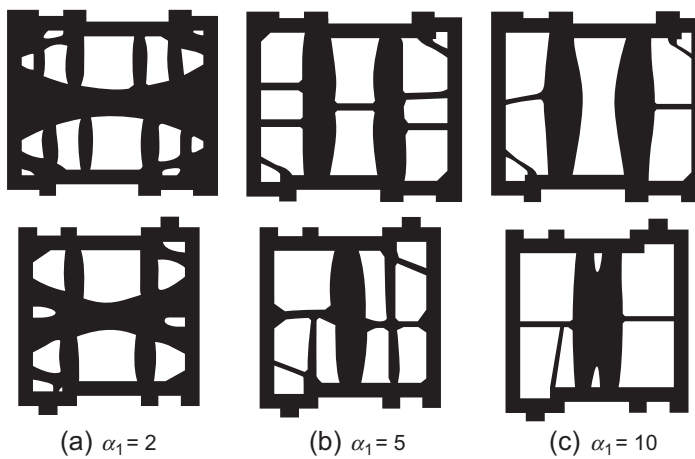

Figure 19.7 (a–c) Optimized material distribution for the blocks shown in Figure 19.5, for increasing values of the out-of-plane stiffness ($\alpha_2 = 2.5$). First row = Block 1; second row = Block 2.

Table 19.6 Comparison between the thermal performances of blocks 1 and 2 for different prescribed values of the out-of-plane stiffness α_1 ($\alpha_2 = 2.5$)

		Block 1		Block 2	
α_1	Figure 19.7	V_f [%]	U [W/(m^{2}K)]	V_f [%]	U [W/(m^{2}K)]
2.0	(a)	39	1.069	45	1.201
5.0	(b)	58	0.760	61	0.896
10.0	(c)	61	0.663	66	0.809

decreases, and the number of thermal bridges along the direction of the heat flux decreases as well. The values of U and V_f corresponding to the different layouts are reported in Table 19.6. Then, the out-of-plane compliance is kept constant ($\alpha_1 = 5$), and the normalized in-plane compliance is increased from 2 to 5. The optimal layouts obtained are shown in Figure 19.8, and the corresponding values of U and V_f are summarized in Table 19.7. As the in-plane compliance increases, the percentage of voids increases and the thermal transmittance decreases, as a consequence of the decrease in size of the webs connecting the two sides of the wall. Note that, for the lowest prescribed in-plane stiffness ($\alpha_2 = 5$, Table 19.7), the decrease in thermal transmittance compared to the commercially available solutions exceeds 30% in the case of Block 1.

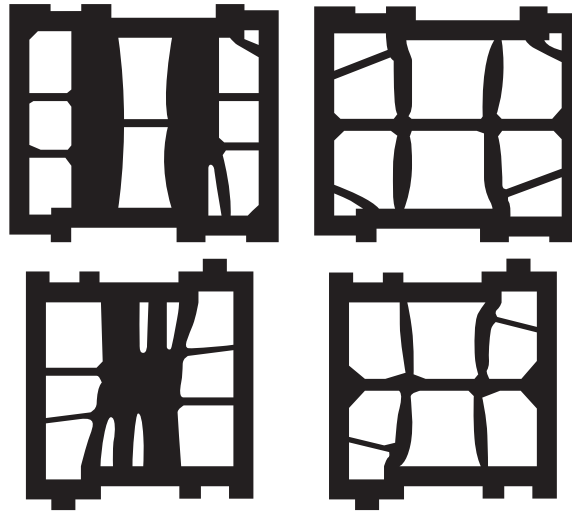

Figure 19.8 (a,b) Optimized material distribution for the blocks shown in Figure 19.5, for increasing values of the in-plane stiffness ($\alpha_1 = 5$). First row = Block 1; second row = Block 2.

Table 19.7 Comparison between the thermal performances of blocks 1 and 2 for different prescribed values of the in-of-plane stiffness α_2 ($\alpha_1 = 5$)

		Block 1		Block 2	
α_2	Figure 19.8	V_f [%]	U [W/(m^{2}K)]	V_f [%]	U [W/(m^{2}K)]
2.0	(a)	50	0.785	54	0.930
5.0	(b)	74	0.735	76	0.865

19.5 Conclusion and future trends

A topology optimization procedure has been illustrated to achieve the layout of hollow masonry blocks that minimizes their thermal transmittance for given mechanical performances (Section 19.3). The potentials of the procedure have been illustrated through numerical applications (Section 19.4). The optimal material distributions obtained can be exploited to achieve the predesign of new and nonstandard types of blocks.

The optimal block topology is found to be deeply affected by the mechanical prescriptions. Referring to the attempt of enhancing the thermal performances of two commercially available blocks (Section 19.4.3), for instance, it was shown that in the case of Block 1, the effectiveness of topology optimization was limited by the need of placing an appropriate amount of conductive material along the direction of the heat flux, to provide the block with sufficient out-of-plane stiffness (Figure 19.6(a)). Conversely, as Block 2 has reduced out-of-plane stiffness, the connections between the sides of the wall could be reduced by the optimization procedure (Figure 19.6(b)), and a significant decrease in transmittance could be obtained.

It is worth emphasizing that the optimization procedure allows technological constraints to be taken into account, directly or indirectly. This was done in Section 19.4.2, where blocks endowed with shear keys were analyzed. Holes of given shape and position can also be easily taken into account in the optimization procedure to provide handgrips and facilitate lifting and gripping (Bruggi & Taliercio, 2013). The presence of holes in the optimized layout of the blocks, however, is a typical outcome of topology optimization. Also, the minimum thickness of the webs can be controlled by properly selecting the value of the filtering radius in Eqn (19.18) to avoid, for instance, buckling phenomena of the vertically compressed webs. By varying the filtering radius, the density of the optimal layout can be tuned, and smaller or larger holes can be obtained. Note, however, that increasing $r_{\min}$ increases the thermal transmittance, and the attempt to optimize the thermal performances of the block can be nullified.

So far, the heat flux was assumed to be uniform across the height of the wall, and a two-dimensional problem could be dealt with. Indeed, the presence of concrete layers at the top of the blocks or strip bed joints requires the problem to be modeled as 3D, as pointed out by Sousa, Castro, Antònio, et al. (2011). This will be done in the continuation of the research, at the cost of a significant increase in the computational burden.

References

Abdou, O. A., & Murali, K. S. (1994). The effect of air cells and mortar joints on the thermal resistance of concrete masonry walls. *Energy and Buildings, 21*(2), 111−119. http://dx.doi.org/10.1016/0378-7788(94)90004-3.

Al-Jabri, K. S., Hago, A. W., Al-Nuaimi, A. S., & Al-Saidy, A. H. (2005). Concrete blocks for thermal insulation in hot climate. *Cement and Concrete Research, 35*(8), 1472−1479. http://dx.doi.org/10.1016/j.cemconres.2004.08.018.

Bastos, A. M., Sousa, H., & Melo, A. F. (2005). Methodology for the design of lightweight concrete with expanded clay aggregates. *Masonry Society Journal, 23*(1), 73−84.

Bendsøe, M. P. (1989). Optimal shape design as a material distribution problem. *Structural Optimization, 1*, 193−202. http://dx.doi.org/10.1007/BF01650949.

Bendsøe, M. P., & Kikuchi, N. (1988). Generating optimal topologies in structural design using a homogenization method. *Computer Methods in Applied Mechanics and Engineering, 71*(2), 197−224. http://dx.doi.org/10.1016/0045-7825(88)90086-2.

Bendsøe, M. P., & Sigmund, O. (2003). *Topology optimization − Theory, methods and applications*. Berlin, Heidelberg, New York: Springer-Verlag.

Bourdin, B. (2001). Filters in topology optimization. *International Journal for Numerical Methods in Engineering, 50*, 2143−2158. http://dx.doi.org/10.1002/nme.116.

Briga-Sá, A., Nascimento, D., Teixeira, N., Pinto, J., Caldeira, F., Varum, H., et al. (2013). Textile waste as an alternative thermal insulation building material solution. *Construction and Building Materials, 38*, 155−160. http://dx.doi.org/10.1016/j.conbuildmat.2012.08.037.

Brás, A., Leal, M., & Faria, P. (2013). Cement-cork mortars for thermal bridges correction. Comparison with cement-EPS mortars performance. *Construction and Building Materials, 49*, 315−327. http://dx.doi.org/10.1016/j.conbuildmat.2013.08.006.

Bruggi, M. (2008). On the solution of the checkerboard problem in mixed-FEM topology optimization. *Composite Structures, 86*(19−20), 1819−1829. http://dx.doi.org/10.1016/j.compstruc.2008.04.008.

Bruggi, M., & Cinquini, C. (2011). Topology optimization for thermal insulation: an application to building engineering. *Engineering Optimization, 43*(11), 1223−1242. http://dx.doi.org/10.1080/0305215X.2010.550284.

Bruggi, M., & Taliercio, A. (2013). Design of masonry blocks with enhanced thermomechanical performances by topology optimization. *Construction Building Materials, 48*, 424−433. http://dx.doi.org/10.1016/j.conbuildmat.2013.07.023.

Bruns, T. E., & Tortorelli, D. A. (2001). Topology optimization of non-linear elastic structures and compliant mechanisms. *Computer Methods in Applied Mechanics and Engineering, 190*, 3443−3459. http://dx.doi.org/10.1016/S0045-7825(00)00278-4.

Cherkaev, A. (2000). *Variational methods for structural optimization*. Berlin, Heidelberg, New York: Springer-Verlag.

EN 1745:2012. (2010). *Masonry and masonry products − Methods for determining thermal properties*.

Gao, T., Zhang, W. H., Zhu, J. H., Xu, Y. J., & Bassir, D. H. (2008). Topology optimization of heat conduction problem involving design-dependent heat load effect. *Finite Elements in Analysis and Design, 44*, 805−813. http://dx.doi.org/10.1016/j.finel.2008.06.001.

Gosz, M. R. (2006). *Finite element method: Applications in solids, structures, and heat transfer*. Boca Raton (FL), USA: CRC Press, Taylor & Francis.

Huang, X., Ranade, R., Zhang, Q., Ni, W., & Li, V. C. (2013). Mechanical and thermal properties of green lightweight engineered cementitious composites. *Construction Building Materials, 48*, 954−960. http://dx.doi.org/10.1016/j.conbuildmat.2013.07.104.

Iga, A., Nishiwaki, S., Izui, K., & Yoshimura, M. (2009). Topology optimization for thermal conductors considering design-dependent effects, including heat conduction and convection. *International Journal of Heat and Mass Transfer, 52*, 2721−2732. http://dx.doi.org/10.1016/j.ijheatmasstransfer.2008.12.013.

ISO 6946:2007. (2007). *Building components and building elements − Thermal resistance and thermal transmittance − Calculation method*.

Li, Q., Steven, G. P., Querin, O. M., & Xie, Y. M. (1999). Shape and topology design for heat conduction by evolutionary structural optimization. *International Journal of Heat and Mass Transfer, 42*, 3361−3371. http://dx.doi.org/10.1016/S0017-9310(99)00008-3.

Li, Q., Steven, G. P., Xie, Y. M., & Querin, O. M. (2004). Evolutionary topology optimization for temperature reduction of heat conducting fields. *International Journal of Heat and Mass Transfer, 47*(23), 5071−5083. http://dx.doi.org/10.1016/j.ijheatmasstransfer.2004.06.010.

Munoz, E., Allaire, G., & Bendsøe, M. P. (2007). On two formulations of an optimal insulation problem. *Structural and Multidisciplinary Optimization, 33*(4−5), 363−373. http://dx.doi.org/10.1007/s00158-006-0085-z.

NTC 2008. (2008). *Italian technical standards for constructions*.

Pierzchlewicz, J. (1996). Modern concrete wall-units with improved thermal resistance for housing in hot climate. *Science and Technology, 1*, 69−80.

Pinto, J., Vieira, B., Pereira, H., Jacinto, C., Vilela, P., Paiva, A., et al. (2012). Corn cob lightweight concrete for non-structural applications. *Construction Building Materials, 34*, 346−351. http://dx.doi.org/10.1016/j.conbuildmat.2012.02.043.

Rozvany, G. I. N. (2009). A critical review of established methods of structural topology optimization. *Structural and Multidisciplinary Optimization, 37*(3), 217−237. http://dx.doi.org/10.1007/s00158-007-0217-0.

Sigmund, O. (2001). A 99 line topology optimization code written in Matlab. *Structural and Multidisciplinary Optimization, 21*, 120−127. http://dx.doi.org/10.1007/s001580050176.

Sigmund, O., & Maute, K. (2013). Topology optimization approaches. *Structural and Multidisciplinary Optimization, 48*(6), 1031−1055. http://dx.doi.org/10.1007/s00158-013-0978-6.

Sigmund, O., & Petersson, J. (1998). Numerical instabilities in topology optimization: a survey on procedures dealing with checkerboards, mesh-dependencies and local minima. *Structural and Multidisciplinary Optimization, 16*(1), 68−75. http://dx.doi.org/10.1007/BF01214002.

Sousa, H., Sousa, L. C., Castro, C. F., Antònio, C. C., & Sousa, R. (2011). A new lightweight concrete single leaf masonry wall system development approach. In *Proceedings of 9th Australasian Masonry Conference, Queenstown (NZ)*, 10 pp. (CD Rom).

Sousa, L. C., Castro, C. F., Antònio, C. C., & Sousa, H. (2011). Topology optimisation of masonry units from the thermal point of view using a genetic algorithm. *Construction Building Materials, 25*, 2254−2262. http://dx.doi.org/10.1016/j.conbuildmat.2010.11.010.

Stolpe, M., & Svanberg, K. (2001). An alternative interpolation scheme for minimum compliance optimization. *Structural and Multidisciplinary Optimization, 22*, 116−124. http://dx.doi.org/10.1007/s001580100129.

Topçu, B., & Isikdağ, I. B. (2007). Manufacture of high heat conductivity resistant clay bricks containing perlite. *Building and Environment, 42*(10), 3540−3546. http://dx.doi.org/10.1016/j.buildenv.2006.10.016.

Ünal, O., Uygunoğlu, T., & Yildiz, A. (2007). Investigation of properties of low-strength lightweight concrete for thermal insulation. *Building and Environment, 42*, 584−590. http://dx.doi.org/10.1016/j.buildenv.2005.09.024.

Yesilata, B., Isiker, Y., & Turgut, P. (2009). Thermal insulation enhancement in concretes by adding waste PET and rubber pieces. *Construction Building Materials, 23*(5), 1878−1882. http://dx.doi.org/10.1016/j.conbuildmat.2008.09.014.

Environmental performance and energy assessment of fired-clay brick masonry

20

D. Hotza, B.G.O. Maia
Federal University of Santa Catarina, Florianópolis, Brazil

20.1 Introduction

The concept of sustainability in construction and building has evolved in recent years. Emphasis has been placed on how to deal with limited resources, both raw materials and energy, and on how to reduce negative impacts on the natural environment (UNEP, 2001). Issues related to building materials and components, as well as construction technologies and design, have been extensively investigated (Pacheco-Torgal, Cabeza, Labrincha, & Magalhães, 2013). Assessing the energy and environmental impact is of critical importance toward designing and developing eco-efficient building processes and materials, particularly in masonry constructions.

Masonry refers to the technique of building up structures out of individual units laid in and bound together by mortar. The most common masonry units are ceramic bricks and concrete blocks. Other important products applied are natural stones (marble, granite, limestone, among many others), glass (in windows, doors, and/or ceilings) and wall, floor, and roof tiles. Mortar itself might be considered a masonry unit since it becomes hard when it sets, resulting in a rigid material. Although polymers (e.g., polyvinyl chloride (PVC) tubes) or metals (e.g., steel reinforcements in concrete) may be present as accessories in a typical masonry construction, the major materials employed worldwide are either clay-based or cement-based ceramic materials (Hendry, Sinha, & Davies, 2004).

Ceramic products are manufactured from natural raw materials. Most commonly, bricks are made of clay, quartz, and feldspar, which might be present in a mixture as single or several raw materials. Concrete, on the other hand, is a composite comprised of coarse, granular aggregates or fillers (mainly sand or gravel) embedded in a hard matrix of cement. By its turn, Portland cement, which is by far the most common type of cement in use, is manufactured basically from limestone and clay (or marl) with lower amounts of gypsum. This basic standardized composition is referred to as "ordinary Portland cement," although many other specifications of cement might be produced from blends of Portland cement and common particulate wastes, such as fly ash or blast furnace slag (Neville & Brooks, 2008).

Fabricating ceramic products includes mechanical and thermal processes, which induce physical and/or chemical transformations from raw materials to final products. Mechanical processes are normally related to comminution (milling, crushing),

Eco-efficient Masonry Bricks and Blocks. http://dx.doi.org/10.1016/B978-1-78242-305-8.00020-6

mixing, and separation (screening, filtering) steps. Thermally driven processes are basically drying for elimination of water from raw or intermediate materials, and firing or sintering for densification of powders at high temperatures (Reed, 1995). The latter process is the most energy-consuming step corresponding to the clinker production in cement fabrication and to the firing of ceramic bricks.

Life cycle assessment (LCA) is an important tool to evaluate the environmental impact of processes and products. LCA has been widely applied to many construction and building materials, considering extraction, manufacturing, use, and post-use steps (Ortiz, Castells, & Sonnemann, 2009). Particularly in this reference book, the environmental impact assessment of cement and concrete-based products is extensively reviewed. Thus, the scope of this work will be restricted to clay-based materials, particularly those used for fabrication of bricks in the construction industry.

When LCA is carried out on manufacturing and use of ceramic masonry units, usually the highest impact associated from both the environmental and energy perspective is the firing step. This process requires a high amount of heat that is generally gained from the combustion of fossil and biomass fuels. The focus of this work is to analyze the use of conventional and alternative fuels to produce ceramic bricks, considering the manufacturing plant as a system boundary. Process efficiency and environmental impacts are assessed and compared.

20.2 Life cycle assessments of ceramic masonry units

Soares & Pereira (2004) presented inventory data related to the consumption of raw materials and energy, and the generation of residues, associated with the manufacture of 1 m^2 of floor tiles and ceramic bricks in Santa Catarina, Brazil. In the case of bricks, they compared two factories, both using sawdust as fuel for firing in a bottle and tunnel kiln, respectively. The obtained data can be used as environmental indicators for comparisons to other materials that perform the same function, or as a spatial and temporal reference for the products and processes described.

Koroneos & Dompros (2007) analyzed the different stages of brick production in Greece, including materials and energy balances, raw material acquisition, industrial production, packaging, and transportation. The main energy inputs to the production system are electricity, diesel, and solid fuel. The environmental burdens that arise from the operation of a brick industry are mainly due to air emissions derived from fossil fuel utilization.

Bribián, Capilla, & Usón (2011) performed an LCA study comparing the most commonly used building materials with some eco-materials. They showed that the impact of construction products can be significantly reduced by promoting the use of the best techniques available in production plants, substituting the use of finite natural resources for waste generated in other production processes, preferably available locally. Selected results for ceramic masonry units are presented in Table 20.1.

Comparing both ceramic products, roof tiles are those that have the highest primary energy demand, mainly due to the high consumption of water in their manufacture

Table 20.1 LCA results for ceramic bricks and roof tiles

Building product	Density (kg/m^3)	Thermal conductivity (W/mK)	Primary energy demand (MJ/kg)	Global warming potential ($kgCO_2/kg$)	Water demand (l/kg)
Ordinary brick	1800	0.95	3.562	0.271	1.890
Roof tile	2000	1	4.590	0.406	2.456

Adapted from Bribián et al. (2011).

stage. On the other hand, the firing stage can account for more than 80% of the total consumption in the production plant (Bribián et al., 2011).

It is important to note the potential for reducing existing impacts in ceramic products associated with technological improvements, particularly in the manufacture of bricks. For example, the replacement of intermittent kilns by tunnel kilns would generate increased energy efficiency (Elmi, 1993). The use of high-speed burners and the recovery of the heat from the exhaust gases to preheat/dry the product to be fired can lead to a reduction in the consumption of the kiln (Bovea et al., 2010). Finally, the implementation of fast firing schedules in continuous kilns (García, Klein, & Hotza, 2012), may lead to a further reduction in the energy consumption. In this case, "fast" refers to firing cycles in roller kilns in less than 6 h (cold-to-cold) and, e.g., a hold time of 30 min at the peak temperature (1080 °C), in comparison to "slow" firing in tunnel kilns, e.g., carried for 24 h (cold-to-cold) at maximum temperatures of 990 ± 10 °C (Dondi, Marsigli, & Venturi, 1999).

Quinteiro et al. (2012) quantified the carbon footprint and the greenhouse gas emissions during the life cycle of an earthenware ceramic piece in Portugal from the extraction of raw materials, through the production, use, and recycling, to the disposal of the used product. The manufacture represents almost 90% of the carbon footprint of the piece. A complementary investigation from the same authors (Quinteiro et al., 2012) showed that the energy consumption and costs and the emissions of the studied ceramics are strongly dependent on their mass and volume. These results suggested some improvement measures to reduce the consumption of electricity and natural gas in firing cycles.

Gomes, Salgado, & Hotza (2012) performed a comparative LCA study between two ceramic brick production units in Brazil. Key impact categories, including fossil fuel use, global warming, ozone depletion, ecotoxicity, and human toxicity were assessed. The critical point has been found in the fuel used in the furnace for firing the bricks that is responsible, during the firing process, for the relevant CO_2 emissions and for the highest energy consumption.

Haddad et al. (2013) summarized different LCA studies that addressed the life cycle of ceramic bricks in Brazil and compared them to studies in Greece and Germany. The review included inventories of production phase, identifying differences in modeling

processes, and in inputs and outputs. The results pointed out to homogeneity in process description and to a lack of correspondence of inputs and outputs with functional units adopted.

20.3 Environmental and energy assessments in ceramic manufacturing plants

From the LCA studies performed on ceramic bricks, three relevant outcomes can be summarized:

- Among the life cycle steps analyzed (raw materials, manufacture, use, and disposal) the fabrication process causes the major energy and environmental impacts.
- Within the manufacturing process itself, the firing step is responsible for the highest energy consumption and for the highest level of gaseous emissions that are environmentally harmful.
- Since firing relies on the combustion of fossil fuels, the main energetic and environmental impacts of the manufacturing process are directly related to fossil fuels.

This kind of relation was already highlighted by Rydh & Sun (2005), who performed a cradle-to-gate life cycle inventory with different parameters for more than 200 materials. The study showed a high correlation ($R^2 = 0.93$) between primary energy use and CO_2 emissions. Primary energy was calculated from the lower heating value of the energy carriers, embodied in natural resources (e.g., coal, oil, and natural gas), used along the manufacturing chain of those materials. The relationships stem from energy generation that is mainly based on combustion of carbon-containing fuels. The amounts of emission depend on the energy conversion efficiency and carbon content of different fuels. The average carbon intensity for energy use was 52 g CO_2/MJ considering all materials classes, with the values for ceramics being the highest (71 g CO_2/MJ) among them all (Rydh & Sun, 2005).

In this regard, this section will focus on a brief review of comparative studies of energy consumption and gaseous emissions in the ceramic industry. Moreover, traditional and alternative fuels will be considered in relation to their energetic potential and environmental aspects during firing of bricks.

20.3.1 Mass and energy flows in ceramic plants

The ceramic processing may be divided into three main steps: powder processing, shaping, and firing (Ring, 1996). A typical brick manufacturing process, Figure 20.1, starts with the raw materials being shipped from different locations to the manufacturing plant, where they are stocked for later use. Brick manufacturers generally are located near the clay deposits to reduce raw material shipping cost. For a brick formulation, one or more clays are needed. The raw materials are ground and/or mixed in pug or roll mills. Bricks are then shaped by extrusion from pastes, whereas for roof tile forming, uniaxial pressing is applied to a plastic body using different die designs for several shapes and sizes. After shaping, excess moisture is evaporated by natural or

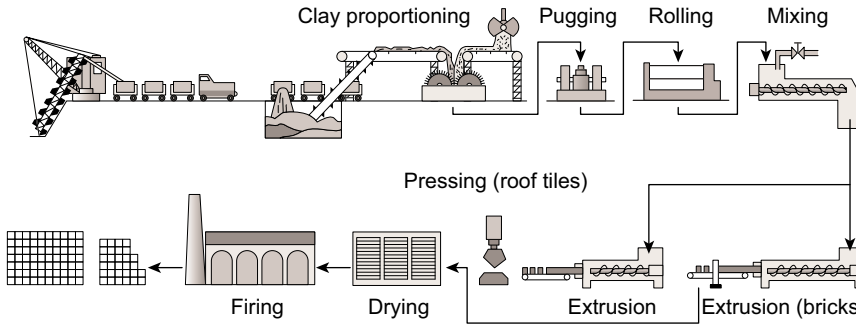

Figure 20.1 Flowchart of a modern brick and roof tile manufacturing plant. Adapted from Bender, Hadley, Hellerstein, & Hohman (2011).

forced drying. In the case of some roof tiles, a glazing step follows. Finally, firing is performed in intermittent kilns (mostly) or tunnel kilns (in modern brick plants). After firing, the products are inspected, packed, and stored for later shipping.

Along the ceramic manufacturing process, the main mass inputs are in the powder processing step where the solid raw materials are homogenized, eventually with the addition of recycled raw materials. After shaping, excess water is removed by drying, which is accomplished in dryers or, in some cases, in an ambient room. Finally, gases originating from raw material decomposition or burning out of organic matter and additives are released during the firing schedule before the bodies are densified by sintering. Table 20.2 summarizes the main inflows and outflows occurring along a typical manufacturing process of ceramic bricks.

The energy consumption is also considered in Table 20.2. In the case of mechanically driven equipment, such as mills, presses, extruders, and glazing machines, electric energy must be supplied. On the other hand, dryers and kilns need electric power—for controlling measures and mechanical actions—and thermal energy—required by the mass transfer and diffusion phenomena occurring in the ceramic pieces being heated. Particularly in firing processes, heat is usually generated from combustion of fossil fuels, which may be solid (such as coal or biomass), liquid (such as liquefied petroleum gas (LPG)), or gaseous (such as natural gas (NG)). Excess heat is also released with hot gas emissions, which may be eventually partially recovered for drying or preheating purposes (Mallol & Moreno, 2001).

20.3.2 Solid wastes, liquid effluents, and gaseous emissions

From the point of view of outputs, a typical ceramic process may produce solid wastes (powder after milling, broken green parts after shaping, or discharged sintered pieces after inspection), liquid effluents (in the wet milling of glaze raw materials and during glazing), and also gaseous emissions during thermal treatments (drying and firing). In the latter case, the gases are originated both from volatilized species from the ceramic body and from combustion products from the fuel, including particulate matter (fly ash). When solid fuels are used, such as coal or firewood, a solid waste (bottom ash) is also generated (Blasco, 1992).

Table 20.2 Mass and energy inputs and outputs for manufacturing ceramic bricks and roof tiles

Mass input	Energy input	Process step	Mass output	Energy output
Raw materials, water, additives, recycled materials	Electric	Milling/mixing	Liquid/solid wastes[a]	
	Electric	Extrusion[b]	Solid wastes[a]	
	Electric	Pressing[c]	Solid wastes[a]	
Fuel[c]	Electric and/or thermal	Drying	Water vapor	Heat (hot gases)
	Electric	Glaze milling/mixing[a,c]	Liquid effluents[a]	
	Electric	Glazing[a,c]	Liquid effluents[a]	
Fuel	Electric and/or thermal	Firing	Water vapor, gases, particulates	Heat (hot gases)
	Electric	Inspection	Selected/discharged pieces	

[a]Eventually.
[b]Typically for bricks.
[c]Typically for roof tiles.

Table 20.3 summarizes the inventory data collected by Soares & Pereira (2004) related to the generation of residues in the fabrication of ceramic tiles and bricks in Santa Catarina, Brazil. Two brick factories using sawdust as fuel for firing in a bottle and tunnel kiln, respectively, were studied. In all cases, 1 m^2 of produced bricks was chosen as a functional unit, for the sake of comparison of the processes.

The water vapor generation in both plants is similar. On a weight basis, the water evaporated in plants A and B is around 50% of the produced tiles or bricks. However, plant A employs more water than plant B, and the output of vapor is proportional to that number. Sawdust is used as fuel for firing bricks in factories A and B: 31.11 and 26.23 kg/m^2 product, respectively (Soares & Pereira, 2004). Nevertheless, the fuel consumption in plant A is 25% higher than in plant B (0.33 and 0.27 kg/kg product, respectively). Additionally, the CO_2 emissions are also much higher in plant A (0.45 kg/kg product) than in plant B (0.22 kg/kg product). Moreover, the amount of CO produced in process A is more than 10 times higher than in process B, meaning that the combustion was not well conducted in the first case. The reason of this discrepancy lies on the type of kilns used: plant A employs an intermittent bottle kiln, whereas

Table 20.3 Typical outputs (amounts expressed in kg) of ceramic brick plants

Process step	Output	Plant A[a]	Plant B[b]
Drying and firing	Water vapor	53.580	50.110
Firing	Ash	0.370	0.250
	CO	0.560	0.051
	CO_2	41.880	21.410
	NO_x	0.022	0.011
	Bricks	93.690	97.670
	Broken bricks	1.190	1.940

[a]Based on 1 m^2 or 35.76 bricks (6-hole, 19.5 × 17.0 × 12.0 cm^3).
[b]Based on 1 m^2 or 32.18 bricks (6-hole, 23.0 × 17.0 × 11.8 cm^3).
Adapted from Soares & Pereira (2004).

plant B has a continuous tunnel kiln, which is more energy efficient. To compensate, the electric energy consumption in plant B (3.7 kW) is 12 times higher than in plant A (0.3 kW), considering the production of 1 m^2 of bricks (Soares & Pereira, 2004). In this case, the more advanced technology employed in plant B demands more electric energy.

20.3.3 Energy consumption and fuels for firing ceramics

The energy consumption, particularly thermal energy produced from combustion of fossil fuels and used for the firing step, has been extensively addressed for brick fabrication processes. Nevertheless, only a few studies presented an international perspective, comparing manufacturing techniques and/or specific producing countries and regions.

In the case of ceramic brick manufacturing, an energy assessment is not straightforward. First, the technological variants are countless, so are the shapes and dimensions of final products. Bricks are fabricated literally all over the world, and available raw materials, labor expertise, and technological background are locally defined. Brick manufacturing tends to involve local suppliers and local markets due to the cost of shipping of the finished product.

Depending on the type of clay, which is the main constituent of bricks, firing is carried out at temperatures between 900 and 1200 °C in a multitude of types of kilns (Remmey, 1994). Kilns for firing bricks are being developed and used for centuries with very different levels of technology and, thus, of energy efficiency and quality of products. Fundamentally, continuous kilns are more efficient than batch kilns. Continuous kilns typically use hot gases to preheat unfired bricks. Moreover, the structure of the kiln does not need to be heated up for each batch of bricks. Finally, fast

firing schedules might be implemented in continuous kilns, making it possible to obtain products with equal or even better properties than those achieved with traditional firing cycles (Dondi et al., 1999). However, the high costs of equipment and service associated with continuous processing limits its use for large production plants. A detailed description of kiln design and operation is out of the scope of this review though.

Much of the energy consumed in the world comes from nonrenewable resources, such as coal, oil, and natural gas. However, in a carbon constraint economy, which is limited by dwindling fossil fuel reserves and climate change, renewable energy is becoming increasingly important in highly developed countries and/or in those with abundant natural resources (Pottmaier et al., 2013).

For the sake of comparison, Table 20.4 presents default gas emission factors for various types of fuel used for generating heat in ceramic plants worldwide, as proposed by the US Environmental Protection Agency (EPA, 2009), as well as their default heating values, according to the U.S. Department of Energy (DOE, 2011).

Natural gas (NG) is the fossil fuel with the lowest CO_2 emission factor (IPCC, 2006). Compared to coal or coke, it does not contain sulfur or give off soot and other particulate matter, and emissions of CH_4 and NO_x are equally low. In a ceramic plant, NG can be used not only in dryers and kilns, but also for power cogeneration and mechanical operation of machinery. It has a homogenous composition, high combustion yield, and lower demand for combustion air, which reduces waste heat in the firing process. Additionally, NG does not need to be stored at the factory and dispenses preheating or heat pumping for transfer, avoiding equipment maintenance and consumption of electricity. Moreover, it extends the useful life of equipment in relation to solid fuels. It also ensures higher quality (better uniformity, color, and finishing), increasing the value added of the final product. The productivity is increased, and the automation of the process is enabled. All these advantages contribute to a positive balance of impacts when conducting an LCA of ceramics produced with NG as a fuel since all stages of the production chain are covered (Schwob, Henriques, & Szklo, 2009). Nevertheless, the capital investment associated with the firing kiln and accessories and the fuel costs are high when compared to the technologies based on solid fuels.

Despite the nature of hydrocarbon fossil fuels, such as oil and coal, and their potential for pollution, they play an important role in the energy matrix of several ceramic-producing regions, such as in Europe (European Commission, 1998). Fuel oil and LPG present high heating values and are, thus, efficient fuels. On the other hand, coal and coke have the highest greenhouse gas emissions among common fossil fuels (IPCC, 2006). Particularly in the case of coal, studies to enhance efficiency in gasification as well as carbon capture and sequestration have significantly advanced (Hester & Harrison, 2009), but to effectively mitigate the negative impacts of the use of fossil fuels, further developments are needed (Abbasi & Abbasi, 2011). Moreover, when using coal as fuel in ceramic plants, associated issues related to emission of highly abrasive particulate matter, sulfur, and acids—such as degradation of bearings, lubrication systems, and refractory bricks in kilns, must also be addressed. However, due to favorable costs and local availability, coal continues to be an adequate fuel in many circumstances.

Table 20.4 Default high heating values and gas emission factors for various types of fuel

Fuel	Heating value		Emission factor		
	Lower[a] (MJ/kg)	Higher[b] (MJ/kg)	CO_2 (kg/GJ)	CH_4 (kg/GJ)	N_2O (kg/GJ)
Gaseous					
Natural gas	47.14	52.22	50.26	8.53×10^{-4}	9.48×10^{-5}
Biogas[c]	n/a	n/a	49.36	n/a	n/a
Liquid					
Fuel oil	39.47	42.21	74.64	2.84×10^{-3}	5.69×10^{-4}
LPG	46.61	50.15	59.70	9.48×10^{-4}	9.48×10^{-5}
Solid					
Coal[d]	22.73	23.97	89.01	9.48×10^{-3}	1.42×10^{-3}
Coke[d]	28.61	29.86	96.72	2.84×10^{-3}	5.69×10^{-4}
Wood[e]	19.55	20.59	88.91	2.84×10^{-2}	3.79×10^{-3}
Biomass[e]	17.21	18.12	88.91	2.84×10^{-2}	3.79×10^{-3}

[a]The lower heating value (LHV, also known as net calorific value) of a fuel is defined as the amount of heat released by combusting a specified quantity (at 25 °C) and returning the temperature of the combustion products to 150 °C, which assumes the latent heat of vaporization of water in the reaction products is *not* recovered. The LHV is frequently used in Europe.
[b]The higher heating value (HHV, also known as gross calorific value) of a fuel is defined as the amount of heat released by a specified quantity (at 25 °C) once it is combusted and the products have returned to a temperature of 25 °C, which takes into account the latent heat of vaporization of water in the combustion products. The HHV is frequently used in the United States for solid fuels.
[c]Data for biogas were eventually not available since its composition varies to a large extent.
[d]Wet basis.
[e]Dry basis.
Adapted from DOE (2011) and EPA (2009), respectively.

In many countries in Latin America, Africa, and Asia (Schilderman, 2007), ceramic bricks and tiles are fired using native wood as fuel. Residues from the wood processing industry, such as sawdust and chips, are also widely employed as fuel. The unrestrained consumption of fuel wood may cause deforestation and soil erosion problems. Moreover, firewood does not allow achieving good energy performance in industrial ceramic kilns, due to relatively low heating values when compared to fossil fuels. This may lead to high losses of energy, low productivity, and low-quality products (Schwob et al., 2009). Additionally, emissions of greenhouse gases from burned wood are in the same order of magnitude as those of coal. Nevertheless, wood is a renewable source and, provided that there is a commitment to a suitable forest management, the advantages in terms of sustainability must be considered.

The use of sawdust and wood chips has technical advantages over natural wood and even planted forest wood because of the lower demand for combustion air, allowing more efficient burning. However, the burning of sawdust gives off unhealthful smoke

and raises machinery maintenance costs due to accelerated corrosion and wear. Moreover, the use of firewood and their residues as fuels have further drawbacks in ceramic plants due to variations of moisture, lower heating value, and particle size, which lead to variable quality of the final products (Schwob et al., 2009).

The biomass obtained from agricultural, domestic, and industrial wastes is one of the sources for energy with the highest growth potential in the coming years. Biomass is considered one of the main alternatives for diversification of energy sources and the consequent reduction of the dependence on fossil fuels, as well as for reducing deforestation to obtain firewood. Additionally, in rural areas biomass is often the only accessible and affordable source of energy.

The use of biomass fuels provides substantial benefits as far as the environment is concerned. Biomass absorbs carbon dioxide during growth and emits it during combustion, offering the advantage of a renewable and CO_2-neutral fuel. Although the compositions of biomass differ considerably, some properties of the biomass samples such as the hydrogen content, the sulfur content, and the ignition temperatures changed in a narrow interval as can be observed in Table 20.5 (Demirbas, 2004).

To increase process efficiency and reduce environmental impacts, more efficient conversion technologies have been developed (Basu, 2010). Biomass can be transformed into liquid, solid, and gaseous fuels with the help of some physical, chemical, and biological conversion processes, such as gasification and pyrolysis.

Although biomass contains much less carbon and more oxygen and has a lower heating value in comparison with solid fossil fuels, the burning velocity of pulverized biomass fuels is considerably higher than that of coals (Demirbas, 2004). The

Table 20.5 Ultimate analyses of typical fuel samples

Fuel sample	Composition (wt%)[a]				
	C	H	N	S	O
Alfalfa stalk	45.4	5.8	2.1	0.09	36.5
Corn stover	42.5	5.0	0.8	0.2	42.6
Cotton gin	42.8	5.4	1.4	0.5	35.0
Hazelnut shell	52.8	5.6	1.4	0.04	42.6
Peach pit	53.0	5.9	0.3	0.05	39.1
Poplar	48.4	5.9	0.4	0.01	39.6
Rice husk	47.8	5.1	0.1	–	38.9
Sawdust	46.9	5.2	0.1	0.04	37.8
Sugarcane bagasse	44.8	5.4	0.4	0.01	39.6
Switchgrass	46.7	5.9	0.8	0.19	37.4

[a]Dry basis, including ash.
Adapted from Dermirbas (2004).

pulverized biomass fuels can be burned in a flame in the same way as oil or gas fuels and at the same high-power output. However, the use of biomass as fuel could present some drawbacks. First, by the combustion of biomass, noncombustible by-products and harmful substances are produced, such as ashes. In many cases, though, provided that there is careful selection of the biomass that is burned, ashes can be incorporated in the cement products (Zhang & Malhotra, 1996) or used as ceramic raw materials (Della, Kuhn, & Hotza, 2002).

Another issue associated with the use of biomass as fuel is the eventual need of some type of preparation of the raw material such as milling, drying, and/or pressing (in the case of briquettes and pellets). All those steps involve energy costs and waste generation, which must be taken into account in an LCA study. In addition, although agricultural and industrial wastes present lower prices than natural wood, delivering them to the destination may still involve considerable freight costs due to the distance between supplier and consumer.

Finally, according to Williams, Jones, Ma, & Pourkashanian (2012), biomass feedstock expansion can have adverse impacts on the environment. For instance, in regions where there has been a major change of land-use, such as deforestation, there can be little or no savings in greenhouse gas emissions. In this respect, economic and life cycle analyses are helpful. Those studies can eventually identify the benefit of specific strategies of processing biomass into an environmental friendly and affordable fuel alternative.

20.4 Conclusions

The case studies discussed in this review indicate that the fabrication is indeed the most impacting step of the life cycle of ceramic tiles and bricks. During manufacturing, the highest energy consumption takes place due to the high temperatures needed for firing ceramics. The combustion of fuels in firing kilns accounts for the generation of high levels of greenhouse gases, among other harmful emissions.

Notably, fossil fuels such as natural gas, fuel oil, or coal are used in technologically developed countries. Nevertheless, the carbon footstep is not favorable in those cases. Renewable fuels offer the advantage of sustainable development, provided that the biomass sources are properly managed.

Environmental and energy assessment tools, such as LCA, can assist the process of making decisions regarding the economical choices and technical changes to be made in the ceramic manufacturing industry so that sustainable products are produced.

References

Abbasi, T., & Abbasi, S. (2011). Decarbonization of fossil fuels as a strategy to control global warming. *Renewable and Sustainable Energy Reviews, 15*(4), 1828−1834.

Basu, P. (2010). *Biomass gasification and pyrolysis: practical design and theory*. Burlington, MA: Academic Press.

Bender, J., Hadley, J., Hellerstein, J., & Hohman, C. (2011). Glass, ceramics and related materials. In J. Stellman (Ed.), *Encyclopedia of occupational health and safety* (pp. 1−35). Geneva: International Labor Organization.

Blasco, A. (1992). *Tratamiento de emisiones gaseosas, efluentes líquidos y residuos sólidos de la industria cerámica*. Castellón: ITC/UJI.

Bovea, M. D., Díaz-Albo, E., Gallardo, A., Colomer, F. J., & Serrano, J. (2010). Environmental performance of ceramic tiles: improvement proposals. *Materials & Design, 31*(1), 35−41.

Bribián, I., Capilla, A., & Usón, A. (2011). Life cycle assessment of building materials: comparative analysis of energy and environmental impacts and evaluation of the eco-efficiency improvement potential. *Building and Environment, 46*(5), 1133−1140.

Della, V., Kuhn, I., & Hotza, D. (2002). Rice husk ash as an alternate source for active silica production. *Materials Letters, 57*(4), 818−821.

Demirbas, A. (2004). Combustion characteristics of different biomass fuels. *Progress in Energy and Combustion Science, 30*, 219−230.

DOE. (2011). *Lower and higher heating values of gas, liquid and solid fuels. U.S. Department of Energy*. [Online] Available at http://cta.ornl.gov/bedb/appendix_a.shtml. Accessed March 2014.

Dondi, M., Marsigli, M., & Venturi, I. (1999). Microstructure and mechanical properties of clay bricks: comparison between fast firing and traditional firing. *British Ceramic Transactions, 98*(1), 2−18.

Elmi, G. (1993). Fast firing technology in the brick and tile industry — a technical evaluation. *Brick and Tile Industry International, 46*(3), 168−170.

EPA. (2009). *Mandatory reporting of greenhous. U.S. Government Printing Office*. [Online] Available at http://www.gpo.gov/fdsys/pkg/FR-2009-04-10/pdf/E9-5711.pdf. Accessed March 2014.

European Commission. (1998). *Energy saving in the brick and tile industry*. Luxembourg: European Communities.

García, D., Klein, A., & Hotza, D. (2012). Advanced ceramics with dense and fine-grained microstructures through fast firing. *Reviews on Advanced Materials Science, 30*(3), 273−281.

Gomes, J., Salgado, A., & Hotza, D. (2012). Life cycle assessment of ceramic bricks. *Materials Science Forum, 727−728*, 815−820.

Haddad, A. N., de Moraes Sedrez, M., de Macedo Pires Condeixa, K., Evangelista, A. C. J., & Boer, D. T. (2013). Life cycle assessment: a comparison of ceramic brick inventories to subsidize the development of databases in Brazil. *Applied Mechanics and Materials, 431*, 370−377.

Hendry, A., Sinha, B., & Davies, S. (2004). *Design of masonry structures* (3rd. ed.). London: Chapman & Hall.

Hester, R., & Harrison, R. (2009). *Carbon capture*. London: Royal Society of Chemistry.

IPCC. (2006). *Guidelines for national greenhouse gas inventories. United Nations Intergovernmental Panel on Climate Change*. [Online] Available at http://www.ipcc-nggip.iges.or.jp/public/2006gl/vol1.html Accessed March 2014.

Koroneos, C., & Dompros, A. (2007). Environmental assessment of brick production in Greece. *Building and Environment, 42*(5), 2114−2123.

Mallol, G., & Moreno, A. (2001). *Depuración de los gases de combustión en la industria cerámica*. Castellón: ITC.

Neville, A., & Brooks, J. (2008). *Concrete technology*. Essex: Pearson.

Ortiz, O., Castells, F., & Sonnemann, G. (2009). Sustainability in the construction industry: a review of recent developments based on LCA. *Construction and Building Materials, 23*(1), 28−39.

Pacheco-Torgal, F., Cabeza, L., Labrincha, J., & Magalhães, A. (Eds.). (2013). *Eco-efficient construction and building materials: Life cycle assessment (LCA), eco-labelling and case studies*. London: Woodhead.

Pottmaier, D., Melo, C. R., Sartor, M. N., Kuester, S., Amadio, T. M., Fernandes, C. A. H., et al. (2013). The Brazilian energy matrix: from a materials science and engineering perspective. *Renewable and Sustainable Energy Reviews, 19*, 678−691.

Quinteiro, P., Araújo, A., Dias, A. C., Oliveira, B., & Arroja, L. (2012a). Allocation of energy consumption and greenhouse gas emissions in the production of earthenware ceramic pieces. *Journal of Cleaner Production, 31*, 14−21.

Quinteiro, P., Araújo, A., Oliveira, B., Dias, A. C., & Arroja, L. (2012b). The carbon footprint and energy consumption of a commercially produced earthenware ceramic piece. *Journal of the European Ceramic Society, 32*(10), 2087−2094.

Reed, J. (1995). *Principles of ceramics processing* (2nd. ed.). New York: Wiley.

Remmey, G., Jr. (1994). *Firing ceramics*. London: World Scientific.

Ring, T. (1996). *Fundamentals of powder processing and synthesis*. New York: Academic Press.

Rydh, C., & Sun, M. (2005). Life cycle inventory data for materials grouped according to environmental and material properties. *Journal of Cleaner Production, 13*, 1258−1268.

Schilderman, T. (2007). *Ten rules for energy-efficient, cost-effective brick firing. Practical Action*. [Online] Available at http://practicalaction.org/ten-rules-for-energy-efficient-cost-effective-brick-firing. Accessed March 2014.

Schwob, M., Henriques, M., Jr., & Szklo, A. (2009). Technical potential for developing natural gas use in the Brazilian red ceramic industry. *Applied Energy, 86*, 1524−1531.

Soares, S., & Pereira, S. (2004). Inventário da produção de pisos e tijolos cerâmicos no contexto da análise do ciclo de vida. *Ambiente Construído, 4*(2), 83−94.

United Nations Environmental Programme. (2001). *Energy and cities: sustainable building and construction.* [Online] Available at: http://www.unep.or.jp/ietc/focus/EnergyCities1.asp Accessed March 2014.

Williams, A., Jones, J., Ma, L., & Pourkashanian, M. (2012). Pollutants from the combustion of solid biomass fuels. *Progress in Energy and Combustion Science, 38*, 113−137.

Zhang, M., & Malhotra, V. (1996). High-performance concrete incorporating rice husk ash as a supplementary cementing material. *Materials Journal, 93*(6), 629−636.

Assessment of the energy and carbon embodied in straw and clay masonry blocks

21

A.D. González
CONICET and Universidad Nacional del Comahue, Bariloche, Argentina

21.1 Introduction

Far from industrial centers, buildings in cities located in rural or touristic areas carry the burden of long distance transport of construction supplies. As we will see in the case studied here, the transportation on difficult roads and the lack of proper logistics increase costs and reduce the options for materials. For instance, in Patagonia, the cost to transport lightweight but voluminous expanded polystyrene makes this insulation material less affordable, more so for housing in areas in which efficiency would greatly reduce the demand for energy resources. In the case of heavy loads like fired clay bricks and cement, consumption of fuel in transport on small roads might also increase fuel consumption between 20% and 30% (González, 2014).

In addition, regions supplied with construction materials from long-distance locations may suffer social disadvantages for not participating in the manufacturing process, which requires labor, machinery, techniques, and concentration of business in value-added activities that process primary resources. On the other hand, the benefits of constructions with renewable and local resources include social benefits from local labor and businesses; lower impacts and recycling at construction and demolition; autonomy that increases resilience to future fossil fuel scarcity; adaptation of materials and techniques to local requirements; and mitigation of environmental impacts as energy and carbon footprints. Even though techniques and characteristics of materials and skills in this area would not apply in a standard way in the majority of cases, the niche experience and lessons can bring up good practices in mainstream constructions, and therefore, energy policies promoting local manufacturing of building elements should be considered (Seyfang, 2010).

For these and other reasons that will be explained below, using local primary materials to manufacture construction elements might introduce a variety of benefits, both ecological as well as social. Adobe is a known example of a technique that has traditionally solved housing demands worldwide, though it is best suited to areas with temperate climate and no seismic activity. The choice for a technique that takes advantage of local resources depends not only on the availability of basic materials and skilled labor, but also on weather and geological conditions affecting comfort demands and durability. A particular technique may be convenient in one region

Eco-efficient Masonry Bricks and Blocks. http://dx.doi.org/10.1016/B978-1-78242-305-8.00021-8

but not elsewhere. For instance, adobe without the addition of thermal insulation, as mostly used, is not an efficient choice for a cold region such as Patagonia (González, 2009).

Thus, the high relevance of the operational phase in buildings, both in energy consumed and maintenance, should be considered when local renewable materials are chosen. Whether operational energy and carbon emissions were high, lower embodied burdens could be compensated in short periods of time. Besides thermal efficiency, durability is a key factor as well, because embodied burdens would become larger if the construction's lifespan is shortened.

Cereal straw has traditionally been used as a base material to make building envelopes. Unlike grass cuttings, straw contains a large percentage of carbon in a cellulose-bind structure and a small amount of nitrogen, which reduces the degradation rate and gives chemical stability. Straw-bale constructions have been extensively studied, and the benefits documented (Ashour, Georg, & Wu, 2011). When combining good thermal properties and large wall thicknesses, straw-bale constructions offer very high thermal efficiency. However, the use of straw bales as wall elements requires a large cultivation area per m^2 of wall, and therefore, sustainability concerns arise when a large number of constructions based on this technique are considered. Depending on weather requirements, certain locations may not need as high a thermal efficiency and allow a compromise between embodied and operational resources used.

The construction system investigated in the present chapter attempts to keep the benefits of using cereal straw but increase the wall surface covered per hectare of cultivation. Straw is a lightweight and voluminous material that requires large truck capacity for long-distance hauling. Thus, local production is relevant if embodied burdens are to be low.

The results show that energy use and greenhouse gas (GHG) emissions per wall surface unit of all straw options are significantly lower compared to fired clay bricks or to concrete blocks. Furthermore, the current building envelopes used in the region of the study (fired clay bricks or concrete blocks) have significantly worse thermal performance than all straw options.

21.2 Current materials and building efficiency in the region

The construction techniques introduced here were developed near the city of El Bolsón, in the northern Andean Patagonian region (González, 2014). This region is characterized by very cold climate, with an annual average temperature ranging from 7 to 9 °C, and heating degree days (HDD) ranging from 3000 to 4500, while cooling degree days are negligible (IRAM, 1996). Climate requirements are similar to those found in the north of Europe and parts of Scandinavia. In spite of this, at present, 97% of buildings lack the basic thermal insulation which would reduce energy consumption for heating (González, Carlsson-Kanyama, Crivelli, & Gortari, 2007). For instance, the majority of houses are built of fired clay bricks and/or concrete

blocks, to which plaster of sand and cement is applied for finishing in both interior and exterior, with no thermal insulation added neither from the outside nor the inside.

Reinforced concrete framing is most commonly preferred, which is built on-site after the fired clay brick walls are set, partially using the brick wall as framing. Thus, the fired clay bricks and concrete envelope actually exposes large areas with thermal bridges not covered by insulation materials. At present, a minor percentage of houses in the Argentinean Patagonia are made of wood. In these cases, the preferred framing is wood and the envelope might be either particle boards or metal sheets, with minimal insulation in cavities. The most chosen standard roofing includes particle board, wood framing and metal sheet on top, and in the best cases, filled with 2−5 cm of glass wool. Building bases and ground floors are very seldom thermally insulated. Building codes in Argentina classify envelopes by establishing four levels of thermal insulation depending on climate requirements. Nevertheless, the efficiency classification in the codes is given as a reference, but it is not mandatory to actually choose improved efficiency, not even in very cold climates as found in the Andean region of Patagonia.

21.2.1 Energy use in buildings with fired clay bricks and concrete walls

It is interesting to note that building techniques in Argentina do not change with climate requirements. In spite of the early studies and publications by architects from Universidad de Buenos Aires (De Schiller & Evans, 1990), at present, building techniques still do not show sensitivity to regional climate requirements. In a previous work, the same thermal behavior for houses in Patagonia and in temperate Buenos Aires was demonstrated, and the contrast to higher efficiency buildings in northern Europe shown (González, 2009).

In the region of interest for this chapter, households with provision of natural gas in the city of Bariloche have been surveyed, showing an average consumption of approximately 5000 m^3/year. The contribution of space heating was found to be 85%, followed by 10% in sanitary water and 5% in cooking. Electricity consumption in Bariloche was less than 5% of total residential energy (González et al., 2007). The use of heating energy was also found to be very high in the temperate city of La Plata, near Buenos Aires, where investigations from Universidad Nacional de La Plata show electricity consumption to be less than 10% of total residential energy (Rosenfeld et al., 2003). Again, the use of gas in heating was the main contribution. In the Patagonian city of Río Grande, high consumption in heating was even found during the summer months (Díaz & Czajkowski, 2006). The observation suggests that dwellings with no thermal insulation lose heat fast and may fall below comfort standards during cold summer nights.

Low efficiency in Argentinean buildings is also due to furnace preferences. In previous works, we have investigated in detail the most common gas furnace in use in Argentina. This is a metal device with direct entrance and outlet chimneys, and has been shown to have a thermal efficiency between 45% and 63%, depending on the chimney's design (Juanicó & González, 2008a). Furthermore, commercial heaters could be greatly improved by simple modifications and low-cost additions, which

would not add more than 10% to the sale value but give as much as 50% more thermal efficiency (Juanicó & González, 2008b). Although these research findings were widely communicated to authorities and industries, so far, the improvements suggested have not been implemented.

A useful parameter to assess envelope efficiency is the actual energy use in heating divided by HDD, which accounts for climate requirements. This parameter is around 40 MJ/HDD per year for houses in both very cold and in temperate regions of Argentina, and around 13 MJ/HDD per year for houses in Stockholm, Sweden (Schueftan & González, 2013). Note that this parameter represents actual consumption, and thus, it is relevant to know how such a high amount of energy is obtained and afforded.

21.2.2 How can households afford very high energy consumption?

Energy prices for households and businesses have been regulated since 2003 in Argentina. A distinctive feature of the regulation is the state subsidy applied to natural gas, bottled gas and electricity; however, the largest subsidy is given to natural gas for households. At present, for instance, 1 m^3 of natural gas in the region of study has a final price for households 30 times lower than the average paid in European countries (a detailed comparison was published in González, 2009). Compared to neighboring countries, like Chile for example, with a minimum salary, a household in Argentina buys four times more electricity and 10 times more bottled gas than those in Chile. Natural gas is not common in all regions of Chile, but compared to firewood, a minimum salary buys 12 times more energy from natural gas in Argentina than energy from firewood in southern Chile (Schueftan & González, 2013). These comparisons are independent of currency differences because they are based on the minimum salary for each country.

Large subsidies in Argentina have led builders to save by cutting down on insulation materials, and hence, to produce low-efficiency constructions. Users, households, as well as businesses, do not notice the thermal failures of their properties because energy bills are easy to pay. For instance, in 2013, the average one-family house in Bariloche paid the equivalent of one large pizza per month of high winter gas consumption. Whether excess heat or cold affect indoor comfort due to lack of proper thermal design, it is simply solved by energy use in air conditioning (electricity) or heating (gas). The matter has serious consequences in an array of problems, among others: drainage of foreign currency to compensate for energy imported at international price and sold for less than a tenth of its value in the local market, paid for with local currency; sustain a building stock of very low efficiency that would require enormous investments to future energy reduction needs; delay and lose educational and technical opportunities to enhance design and building capacity to improve the use of resources, and social unrest in case subsidies can no longer be paid. An attempt to raise prices in 2009 caused such social pressure that tariffs had to be returned to their original low levels, but state subsidies on limited resources cannot be maintained endlessly. The assessment of risks related to heavy subsidies to fuel consumption in Argentina has been reported in detail elsewhere (González, 2013).

Recall that Argentina was a natural gas exporter until 2004, but gas production has declined steadily in the last decade. In 2008, the imports of liquefied natural gas (LNG) by vessels from Trinidad Tobago, Qatar and Russia have started. To this purpose, two major gasification ports have been set in the Province of Buenos Aires. Investments in prospection and production were not incentivized by low prices paid for gas produced within the country. On the contrary, these low prices were part of the regulation of the activity, decreasing the amount of subsidies to national producers. However, for imported resources, international prices had to be paid for both LNG shipments and gas provision by pipelines from Bolivia. In 2012, around 65 shipments of LNG by tankers arrived at the two ports, and in 2013 nearly 85 shipments were needed. Together with imports by pipelines from Bolivia, the total imported gas accounts for 20% of consumption. Households in the region covered by the present research pay an end-user price of around $0.70 per MBTU, while gas from Bolivia costs around $10 per MBTU at pipeline, and LNG by tankers costs around $17 per MBTU at port of entry. Nationally produced natural gas costs less than $4 per MBTU at the well head, but since 2012 arrangements were made to raise this price to $7.50 per MBTU for certain new wells. This comparison helps to assess the magnitude of the pressure exerted on construction materials and designs not to have incentives for technological updating. In addition, the delivery of gas to the building sector (residential, public and commercial), has priority when supplies are short in certain periods of winter time. At these periods, industry is forced to either slow down production or to stop it completely until climate permits. These enforcements and loss of productivity would not be needed if buildings had a fair thermal efficiency.

21.2.3 Natural gas is a key energy resource for constructions

Construction-related industries in Argentina are highly dependent on natural gas; therefore, the current fragile energy status causes concerns that these industrial activities might be affected. The total energy production in the country, mainly fossil fuels, reached a maximum in 1999 and has levelled off since. Whether in the construction stage or in the building operation phase, fossil fuels are key energy resources for sustainability analysis for the building sector in Argentina.

Regular construction materials like fired clay bricks, cement and iron, are manufactured using natural gas, which is also the main fuel for generating electricity (51% in 2009), and furthermore contributes 52% to the total primary energy supply of the country (IEA, 2014). Thus, fossil fuels, but particularly natural gas, are at present a key component in the energy supply in Argentina.

Manufacturing of fired clay bricks, cement and metals relies heavily on the use of natural gas, and thus production facilities concentrate along pipelines located mainly in the provinces of Mendoza, Neuquén, Chubut and Buenos Aires. Therefore, to deliver construction materials to the Andean Patagonia requires long-distance transportation between 700 and 2000 km. To the area of study, transportation takes place by truck along narrow highways comprising nearly 400 km across mountain roads. No railways are used for this transport in Patagonia. Cement is transported between 700 and 1000 km, steel between 1500 and 1800 km, and fired clay bricks between 700 and 1000 km, depending on the

city in question. Wood is mostly local and the availability regular, whether from plantations or native varieties. Insulation materials are also delivered from long distances: expanded polystyrene from 700 km and glass wool from 2000 km. Particle boards are mostly imported from Brazil, delivered by truck at least 3000 km, and from Chile, transported around 500 km to the area of interest here.

From the aforementioned, it is clear that both manufacturing and delivering material to construction sites in the Andean Patagonia are energy and carbon intense activities, which need a large and diverse supply of fossil fuels. Even though we focus here on a specific region, it is believed that a similar situation may be found in other regions or countries worldwide. However, the particular energy status of Argentina raises more concerns on future sustainability, and it is one of the major incentives to investigate local low-energy production of construction materials, which should provide, simultaneously, buildings with higher efficiencies than present ones.

21.3 Farming walls

Building with straw bales is a technique that has traditionally been used worldwide. Protected from excess moisture, straw is a durable material, and there are century-old constructions in regular use (Goodhew, Griffiths, & Wooley, 2004). Cereal straw is the preferred based material, having advantages over grass cuttings in durability and thermal properties. The particular cellulose structure, including chemical factors as crystallinity and lignifications, makes it difficult for bacteria to degrade straw, to the extent that straw does not constitute a suitable feed component without further treatment even for ruminants (Sun Rang-Can, 2010).

As soon as machinery was available, bales were traditionally used due to the simplicity of shaping them into blocks that are easy to bind and make building envelopes. However, the direct use of straw in quincha-type walls is practiced where baling is not possible. In quincha with straw, a wooden frame serves as the main structure and a large number of smaller size beams or canes are fastened to the main structure. Straw and clay is then positioned between the smaller beams forming a cavity wall with fair thermal resistance.

Cereals are the major food group consumed worldwide, and straw is regularly a by-product. In general, for each ton of grain, an additional ton of straw is obtained; however, as we will discuss below, soil sustainability requires that not all residues should be extracted. Straw from all cereals is suitable as construction material, and the convenience of a certain variety is determined by climate and cultivation potential. For instance, rye gives good yields in colder climates, while in temperate climates, wheat and barley may be convenient. Modern high-yield wheat varieties have short stems and produce less straw, though more grain. Thus, the variety of straw or cereal depends on a diversity of local conditions and the purpose of the cultivation. Where there is a market for straw, the farmer can choose a variety that yields fair grain but also large amount of straw. Actually, in areas with high demands for straw, its value can be as high as that of grain. While if grain is the only product sought, straw would become just a residue of lower value. In any case, it is relevant to note that straw is a light

voluminous material, and long-distance transportation may add significant costs and environmental impacts. Therefore, the advantages of using straw as building material are enhanced with local production.

In the Andean Patagonia, different techniques use cereal straw as a key component in buildings: (1) quincha-type walls filled with mixed straw, clay and soil; (2) on-site framing straw and clay into a wall shape; (3) direct use of straw bales for walls, whether in whole or in halves; and (4) building with blocks manufactured locally with straw and clay. The present chapter will focus on the last two techniques.

21.3.1 Straw-bale options

The performance of straw bales in housing has been demonstrated by several researchers, and recently, a house built in the south of Germany proved again to have very good thermal response of straw bale walls to cold conditions (Ashour et al., 2011). Measurements of moisture content also showed safe levels for straw durability. Nevertheless, this old but unusual type of construction faces a number of barriers in order to be massively implemented. These barriers are not necessarily technically related but rather originated in market preferences and regulations. Usually builders stay attached to known techniques and materials, even unsustainable ones. On the other hand, rigid codes and strict regulations, together with the lack of information, make it difficult to get alternative projects approved (Deverell, Goodhew, Griffiths, & de Wilde, 2009). In the cases presented here, a key factor that led the initiative to gain support for several projects was not the existence of special regulations, but rather the lack of rigid codes that allowed small enterprises and private organizations to adapt building techniques to local requirements. Besides, in a large area of the Andean Patagonia, no codes are enforced at all, leading to an unusual number of constructions with local materials that have been built and used for decades. Therefore, the particular experience is unique and valuable in order to study further improvements and possibilities for sustainable construction techniques.

Whole straw bales usually measure around $1 \times 0.5 \times 0.4$ m and lead to finished wall thickness of 0.45 to 0.55 m. Thermal conductivity of straw is around 0.07/0.09 W/°C m, which is fair compared to expanded polystyrene (0.04 W/°C m). Due to the large thickness, thermal resistance (i.e. thickness divided by conductivity) of straw-bale envelopes suits even the strictest building codes (Goodhew & Griffiths, 2005). However, the use of whole straw bales involves large wall thicknesses that are not always possible or desired in the design. Experimental constructions with half straw bales were also found to be convenient (González, 2014, Figures 5 and 6). In this case, a finished wall of around 25 cm has similar thermal resistance as 10 cm of expanded polystyrene, results far more efficient than current conventional solutions using fired clay bricks.

On the other hand, the use of whole straw bales requires large amounts of resources, needing areas of cultivation or, if not available, transported from elsewhere. Therefore, even though straw bales are a proven solution for efficient, sustainable constructions, the search for improving resource utilization has led to the manufacturing of blocks with cereal straw and earth bindings (see Figure 21.1).

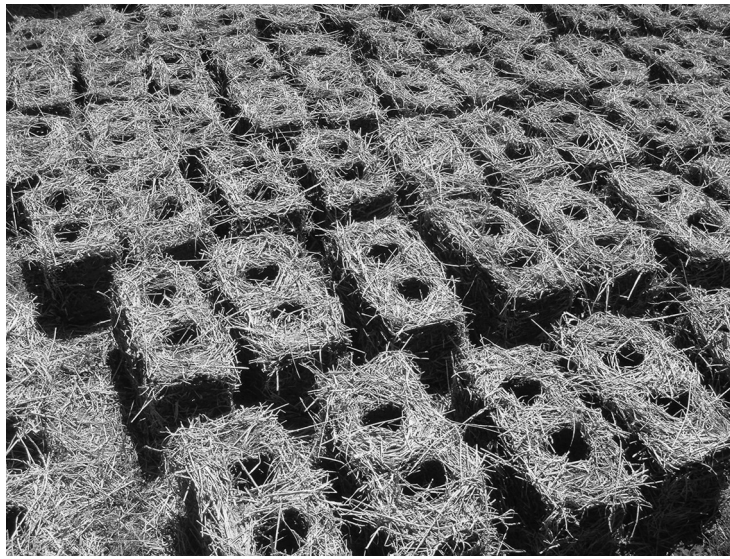

Figure 21.1 Straw-clay blocks air drying for further use.

21.3.2 Sustainability issues limit straw availability

As mentioned, the extraction of straw from the cultivation field cannot be 100% if soil quality is to be preserved. Soil degradation by decreasing soil organic carbon can be avoided by leaving crop residue on the field. A minimum of around 50−70% of straw should be left on the ground to maintain the amount of organic carbon stable in agricultural soils under no tillage practices (Lal, 2011).

However, this percentage varies depending on soil structure and climate. In addition, leaving the root of crops also incorporates a significant amount of organic matter in soils, as shown by researchers in Sweden for a climate condition similar to the area of study (Kätterer, Bolinder, Andrén, Kirchmann, & Menichetti, 2011). The farm that was surveyed to assess the life cycle inventory of wheat production followed both good practices, leaving roots and part of the straw. By empirically determining the level of residues needed to maintain soil quality, the farmer reported that 50% of residues left on the field were enough for the region. In the past, pressure from various ongoing constructions and the high price of straw bales made farmers harvest all straw from wheat and rye fields, but soil degradation was soon detected. Other locations and climates might permit different levels of residue removals. In the area of study, in addition to climate and soil conditions, the choice for low input agriculture and no tillage also contributes to the percentage of straw that can be removed.

21.3.3 Energy and carbon embodied in wheat straw

Here we will discuss the case of straw production in the Golondrinas Valley (42°04S latitude, 71°30W longitude), located in the northern part of the Chubut Province, in

Argentina. However, the same procedure can be followed for every other location given that farm inputs and cultivation practices are detailed. Energy and carbon per kg of straw needs to be obtained to assess afterwards embodied impacts of bales and/or straw and clay blocks. For every kg of grain cultivated approximately another kg of straw is produced. As explained above, assuming 50% extraction from the field a total of 0.50 kg of straw per kg of grain can be used in construction.

Life cycle inventories of wheat and other cereal grains have been obtained for different countries and conditions of cultivation. European production of oats, rye, barley and wheat lead to a similar energy and carbon footprint at farm gate, around 2 MJ/kg grain and 0.40 kg CO_2eq/kg grain (see González et al., 2011 and references therein). These productions are characterized by high yields made possible by high input of fertilizers. In general, fertilizers are the main burden in conventional farming, and diesel for machinery is the main burden in organic farming. Assuming high-yield intensive farming, both methods are substantially different in practice, but result in similar energy and carbon impacts per kilogram of grain. The major producer of cereal grain and straw in the Golondrinas valley considered here uses a mixed method, no tillage, low inputs of fertilizers, and obtains lower yields than found in European productions.

In spite of adverse climate conditions, cereal production in the Andean Patagonia was a major activity until the 1950s. Winter cultivation is the preferred method as timing for moisture, temperature and drought makes it profitable. Average annual temperatures between 8 and 10 °C are found in the region, favoring wheat, rye, barley, and oat cultivation. All these cereals provide straw suitable for construction. Demand of straw is so high that farmers in the area are booked a year in advance for straw required by customers for construction. The price of straw is thus similar to that of grain, but is convenient compared to long-distance transport if straw would be bought elsewhere. Therefore, since straw is as much appreciated as grain, and even the commercial value is similar, allocation of embodied energy and carbon to grain and straw is done on an equal basis. This assumption may not be valid for other locations.

No-tillage cultivation reduces soil degradation and energy use in machinery. Previous to the cultivation cycle, herbicide is applied for weed control. Seed is self-provided, saved from previous harvests. Sowing is done in autumn, harvest in summer, and no irrigation is applied to the fields surveyed. Climate conditions do not permit a second cultivation within the same season. The harvest is done with a combine, which separates grain and cuts straw to a chosen height. Bailing is done afterwards using another machine. On average, 150 straw bales of 10 kg each are obtained per ha (González, 2014). Embodied energy and carbon dioxide for this case results in 1.2 MJ/kg grain and 0.11 kg CO_2eq/kg grain if only grain is harvested, and 0.92 MJ/kg and 0.085 kg CO_2eq/kg if grain and straw are harvested, respectively. Local yield is 3000 kg/ha for grain, plus 1500 kg/ha for straw. A bale weighs 10 kg on average and has the dimensions $0.90 \times 0.45 \times 0.35$ m.

It is interesting to compare these results to any of the average European productions. For instance, for the United Kingdom, Williams, Audsley, & Sandars (2010) reported more than double the yield of grain/ha (7700 kg/ha) achieved with an energy

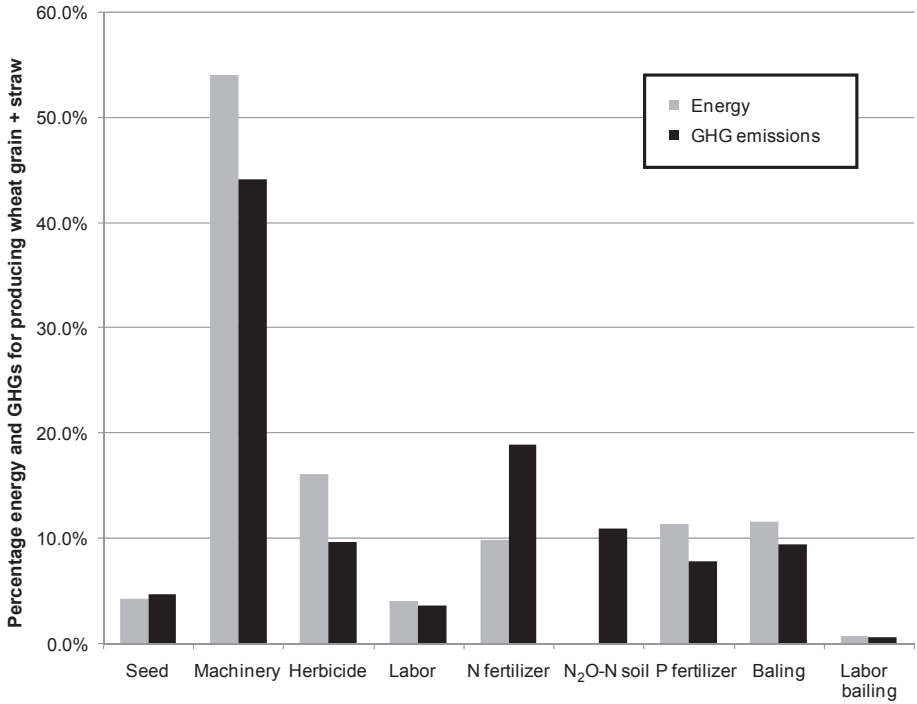

Figure 21.2 Partial contribution of energy and greenhouse gases (GHGs) for each stage/activity in the production of grain and straw.

footprint of 2.4 MJ/kg for only grain and GHG emissions of 0.70 kgCO_2eq/kg grain. Assuming similar conditions for straw extraction, the combined grain + straw would result in 1.6 MJ/kg and 0.46 kg CO_2eq/kg. These footprints are larger than those for the low-yield, low-input cultivation in Andean Patagonia, though, it is important to stress the advantage that higher yields reduce cultivation area needed to satisfy the requirements for both food and construction materials.

In Figure 21.2, the contribution to energy and carbon embodied in each step in the cultivation process is depicted. The main energy embodied to obtain straw corresponds to diesel combustion on machinery, followed by the manufacturing of agrochemicals. Due to emissions of N_2O from agricultural soils under fertilization (occurring with synthetic fertilizer and manures, Carlsson-Kanyama & González, 2007), embodied carbon is as significant for fertilizers as for diesel in machinery. Nevertheless, the carbon footprint of all agrochemicals added results are higher than for fuels.

The impact of the seed required is minor, given that it is produced and saved by the same farmer. Labor will be discussed with more detail below; however, for grain and straw production its impact is small compared to fuels and agrochemicals. It is relevant to note which steps contribute the larger percentages, because the observation provides experience to evaluate life cycle inventories in simple forms, that otherwise could be very complex. For instance, in most grain production studies on life cycle assessment

labor is not taken into account, and, as we have seen, this is correct due to the low influence of the contribution. We will see below that in the labor-intensive activity of manufacturing blocks, labor must be considered in embodied burdens.

21.4 Straw and clay blocks

Concrete blocks are manufactured in the region using cement delivered from 700 km away. Sand and gravel are mixed locally with cement and made into blocks. The result is a 13.5 kg block with two large holes that allow air convection and overall low thermal resistance. To improve insulation properties, Mansour, Srebric, & Burley (2007) experimented with a mixture of rice straw, cement and the addition of salts for adhesion, obtaining good results. The scheme, sand-cement or straw-cement mixture is similar to the straw and clay masonry blocks, which are at present extensively used in the region of study.

Straw is mixed with clay which has been soaked in water. The mix is then set in casts of rectangular shape with dimensions $0.50 \times 0.25 \times 0.21$ m with two holes of 10 cm diameter vertically oriented (see Figure 21.1). At the instance of setting the blocks to make the wall, the holes are filled with loose straw, improving thermal insulation by avoiding air convection. Once in the cast, the mix of straw and clay is pressed and unmolded, to be thereafter placed in the open air for drying. A number of small, local enterprises specialize in the manufacturing and further building with these blocks. When set to make walls, they are bound with a mix of straw, clay and sand, which is also covered with rough plasters of 1.5 to 2 cm. To finish the surface and control moisture, a finer plaster that includes flax oil and pigments is applied. Examples of houses built using the technique can be seen in González (2014).

Embodied energy and carbon estimated here are based on input data provided by one of the local enterprises, which, by 2013, had built 10 one-family houses with living areas ranging from 65 to 170 m^2 in suburban and rural areas and a large public building of 600 m^2 dedicated to a private clinic. This large building is located in downtown El Bolsón, and it is the largest constructed with renewable and recycling materials and the first to pass inspections and code requirements by municipality regulations. The codes define the region as seismically sensitive and enforce structures to be adequate. The structure of the 600 m^2 building was made of steel tubing recycled from the oil industry. The tubing is originally used in setting oil and gas wells and afterwards discarded. As such, it can be bought at a convenient price and transported between 500 and 600 km to the construction site. This material will not be included in the analysis below given that it is explained here solely to illustrate construction trends that are new in the region. After the structure was secured and inspected, the envelope of straw and clay blocks was set. Around 6000 blocks were used, which were manufactured elsewhere and transported 15 km to the construction site.

The houses and the large business building mentioned comply with all modern standards for comfort and safety. However, systematic investigations on durability have not yet been done, mainly due to the short time elapsed since being finished. Nevertheless, so far it is noted that the large percentage of local labor and businesses that were

involved in the projects and the significant amount of human labor involved. The enterprise surveyed is organized as a labor cooperative, and earnings were higher than average for construction in the region. According to the entrepreneurs, the cost to build with straw-clay blocks is in the end similar to that with fired clay bricks; however, the distribution of economical resources among stakeholders is different. It is interesting to know that, at present, the general construction activity is depressed in the region; however, building, whether with straw bales or blocks, has not seen a decrease in demand. There can be observed a slow, but steady increase of preference of house owners to buy local materials and services. As Seyfang (2010) pointed out, the experience of community-led initiatives for sustainable development like the one described here have the potential to create green niches that might influence the transformation of mainstream society.

The technique is also suitable for thermal refurbishment of existing houses. In González (2014, Figure 4), an example of retrofitting a wooden cabin was depicted. The improved house was originally built with a wooden envelope and no thermal insulation. Straw-clay blocks were set on the outside covering the original wooden wall. The technique is convenient not only to improve thermal resistance but also to control air infiltration, as clay in the mortar and plasters clogs any possible infiltration existing in the original wooden envelope.

21.4.1 Input data from small enterprises

Like the farming activities discussed above, the life cycle inventory for straw and clay blocks requires input data for the analysis. Bales are transported to the construction site to minimize work and volume in transport, and the blocks are preferably manufactured on site. Clay is mined nearby and transported by a 10-ton truck for a distance on average of 20 km. A gasoline-powered drum mixer is used to mix straw and clay, and then the material is set on a large 300 μm-thick plastic for further checking of the appropriate level of humidity, and finally distributed using wheel barrels to the points where casting is done. A wooden cast is used to shape blocks into $0.25 \times 0.21 \times 0.50\ m^3$, and then they are air dried outdoors. An average density of $280\ kg/m^3$ is obtained, but large variations are expected in the mostly handmade manufacturing process. Dry straw-clay blocks weigh between 5.5 and 7 kg (note that even smaller size concrete blocks weigh 13.5 kg). As mentioned, the mix used for binding masonry blocks and for rough plasters also includes sand, and the plaster density is estimated at $400\ kg/m^3$.

The enterprise surveyed dedicated groups of three to four people to manufacture blocks. In 240 h of labor, around 1000 blocks are usually made and set to dry. This number of blocks is enough to fill the envelope of a $120\ m^2$ one-family house (on average $1\ m^2$ of wall requires seven blocks). The specialized worker can produce between 35 and 40 straw-clay blocks per day. These data, along with the standard use of gasoline in the mixer and bulk transportation of straw and clay, will be needed to assess energy and carbon embodied. As it is clear, in this activity, human labor is significant and must be considered, for which an estimation of energy and carbon footprint of human labor is in order.

21.4.2 Assessing embodied human labor

Energy and GHG assessment of human labour are needed in cases where large parts of the life cycle is based on labor. This was noted early by Giampietro & Pimentel (1990) who, based on the concept of power, give a detailed account on the difference between machine labor and human or animal labor. Besides, Pimentel (2009) showed with examples the differences in cereal production in the United States and in African countries where animal and human force replace machinery.

On the other hand, note that in some studies on natural buildings, human labor is not included. For instance, adobe usually requires a significant amount of working force, which is commonly excluded from the economical and environmental analysis. For the case discussed here, the entrepreneur estimates that the cost of building with straw-clay blocks results about the same as when using fired clay bricks and cement (Tognetti, 2013). In the former, labor is the major cost, while in the latter buying ready-to-use materials from long distances accounts for the item with higher cost.

Even so, we will see below that for straw solutions the environmental burden is much smaller than for fired clay bricks or concrete blocks, even accounting for the energy and carbon embodied in human labor.

Footprints for human labor are difficult to assess accurately. In a previous work, we discussed two different approaches: (1) based on country energy and carbon data, and (2) based on local consumption of food, housing and energy. For the region considered, the two approaches gave similar results, and the values of 10.6 MJ/h for energy embodied and 0.88 kg CO_2/h for carbon were considered for an hour of human labor in the Andean Patagonia, respectively (González, 2014).

In any case, there are not only large differences among countries (as shown by Pimentel, 2009), but even within the country there may be large differences in energy and technology availability, food habits, means of transport, and lifestyles with regional variability. For instance, the northeast of Argentina has warm subtropical weather, no provision of cheap natural gas and fewer subsidies for electricity. Therefore, in the northeast, household energy can be 20 times lower than the average for the Andean Patagonia, and this fact would lower embodied energy for human labor to nearly 3 MJ/h and GHGs to 0.3 kg CO_2eq/h when the estimation is based on consumption. This estimate is far below the one obtained with country-based data, which results in 9.5 MJ/h and 0.74 kg CO_2eq/h. Although in the case study presented here, the two approaches, country-based and consumption-based, give similar results. We wanted to show the general difficulties to assess the environmental burden of human labor; however, the large incidence in some activities certainly requires including it.

21.4.3 Energy and carbon embodied in straw and clay blocks

The construction system with straw-clay blocks was described in previous sections. To manufacture the blocks, gasoline for drum mixers, diesel for transport, straw and clay, water, and human labor are required, meaning that energy and carbon footprint should be assessed for each input. As explained in González (2014), to manufacture 1000 straw-clay blocks of $0.21 \times 0.25 \times 0.50$ m^3 requires the use of 180 straw bales

(1800 kg of wheat straw); 4 m^3 of dry clay; 12 L of gasoline; 240 h of human labor; 2 m^3 of water (which includes the cleaning of the equipment); and the transportation of straw and clay. Straw bales are transported 20 km from the farm to the construction site on a 10-ton truck that loads 105 bales. Bales are low density and imply large volumes to transport, and so two truckloads are required from the farm to the construction site. Clay is mined from a location 40 km away, depending on the construction site, and it is also transported by a 10-ton truck. With these data and with the embodied energy and carbon for each specific item (see Table 1 in González, 2014), the result for straw-clay blocks is 5.7 MJ/block and 0.47 kg CO_2eq/block for energy and CO_2, respectively. In the next section, these values will be compared to fired clay bricks, concrete blocks, particle boards and insulation materials.

Figure 21.3 shows the percentage of energy and carbon in each step for the manufacturing of blocks. Human labor is the major impact, followed by the production of straw, which was described in detail in Section 21.3.3. Transports of clay and straw add slightly higher embodied burdens than the gasoline used in the drum mixer. The use of 2 m^3 of water for manufacturing 1000 blocks implies an energy and carbon embodied of 11 MJ and 1 kg CO_2eq, respectively, which are negligible compared to the other items (see Table 3 in González, 2014).

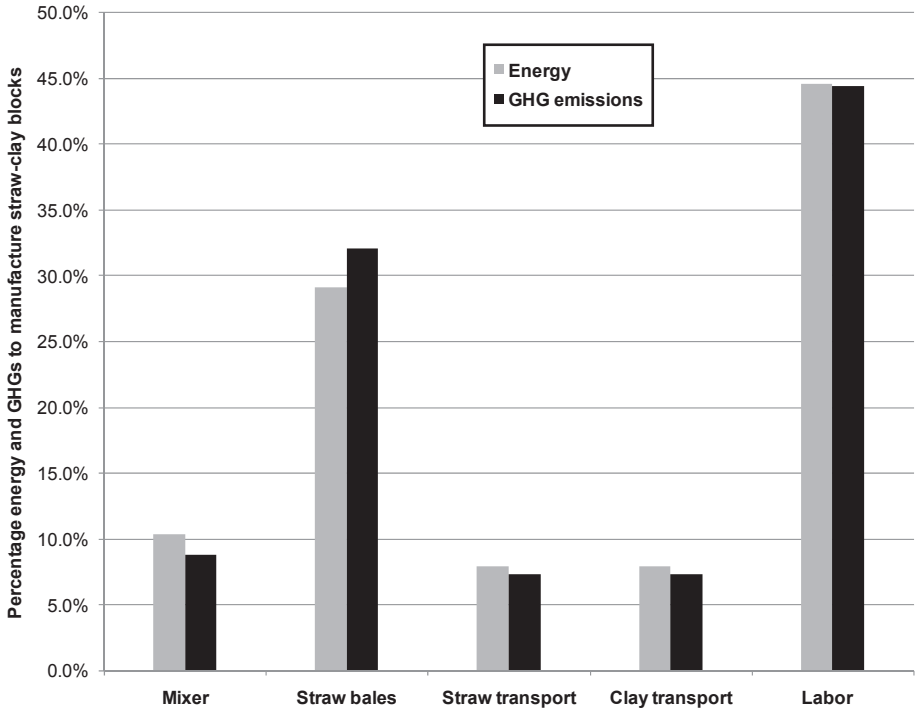

Figure 21.3 Relative importance of different steps in energy and carbon dioxide embodied in the life cycle for manufacturing straw and clay blocks. GHG, greenhouse gas.

As mentioned, input data for resources and labor were obtained from professional work in a small-size local enterprise. Nevertheless, it is common practice in community-based natural building to organize working groups with some professionals and some voluntaries. If this would be the case, energy and carbon embodied would be somewhat higher, as nonprofessionals would cause the same impacts per hour of labour but would produce fewer blocks. This matter is stressed here to distinguish that although voluntaries may not count (or partially count) on economical costs, they would add embodied burdens to materials as well as professionals.

21.4.4 Thermal efficiency of wall elements compared

So far, the thermal conductivity for the present straw-blocks was not measured and will be estimated here based on similar materials reported by other authors. Goodhew & Griffiths (2005) investigated different combinations of straw and clay, and reported a thermal conductivity of 0.18 W/m K for straw and clay mix with a density of 440 kg/m^3. The blocks studied here have a lower density (around 300 kg/m^3) and when forming walls, the large holes are filled with loose straw, which improves thermal resistance. Thus, we will consider the value 0.18 W/m K as an upper limit for the conductivity of straw and clay blocks in order to compare to other options. Thermal conductivity of straw bales is between 0.07 and 0.09 W/m K for a density range of 60 kg/m^3 to 90 kg/m^3. The bales described in Section 21.3.3 have a density c. 70 kg/m^3, and a conductivity of 0.08 W/m K is assumed here.

In Table 21.1, a comparison of different solutions to fill an envelope wall is depicted. Data for embodied energy and carbon for fired clay bricks, cement, and transport were reported in a previous work (González, 2014, Tables 1 and 4). Here we will make a comparison based on equal thermal resistance for straw-clay blocks and conventional fired clay brick/block elements and the option of drywall. Therefore, a layer of 3.5 cm EPS insulation is added to fired clay bricks and concrete blocks, respectively, and in the option of a cavity wall with two OSB boards, EPS fills a 4 cm gap. These particular EPS insulation thicknesses are solely chosen to equal the thermal resistance of 1.16 m^{2}K/W, which corresponds to straw-clay blocks. Hence, the embodied values in the comparison are for solutions leading to similar operational energy and carbon emissions. Whole straw bales of 0.45 m thickness have higher thermal resistance. In González (2014), an option of half bales was shown and analysed. For the comparison in Table 21.1, we have included an option of straw packed with a thickness that equals the thermal resistance of straw-clay blocks. This solution can be realized in practice by the technique of framed straw already reported (González, 2014). Not having local data on embodied energy and carbon for EPS and OSB boards, data from Bribián, Usón, & Scarpellini (2009) were used. For fired clay bricks and concrete blocks, data are obtained as explained in González (2014).

Following the initial discussion on the influence of operational and embodied energy, Table 21.1 helps to illustrate that, for equal thermal resistance, straw-clay blocks result in far smaller embodied energy and carbon than conventional solutions. The option with straw framed on wood has lower embodied values, but it cannot be considered yet since it has not been systematically implemented, and only pilot

Table 21.1 Energy and carbon embodied in different materials to cover 1 m^2 of wall

Elements required to cover 1 m^2 of wall envelope	Thermal conductivity (W/m K)	Thermal resistance m^2 K/W)	Energy per m^2 wall (MJ/m^2)	GHG emissions per m^2 wall (kg CO_2/m^2)
85 fired bricks + 1 m^2 EPS 3.5 cm thickness	0.90[a] 0.04	1.14	535[b]	37
11 concrete blocks + 1 m^2 EPS 3.5 cm thickness	0.64[a] 0.04	1.18	218[c]	16
2 m^2 1.1 cm OSB board + 1 m^2 EPS 4.0 cm thickness	0.13 0.04	1.16	256[d]	27
7 straw-clay blocks	0.18[e]	1.16	40	3.4
3 parts of straw bale, framed 9.5 cm thickness	0.08[e]	1.16	6.2[f]	0.6[f]
3 straw bales	0.08[e]	5.6	28	2.5

GHG, greenhouse gas.
[a]Lahv (2014).
[b]Includes 700 km transport for bricks and EPS.
[c]Includes 700 km transport for EPS and 10% of weight due to cement.
[d]OSB transported 600 km from Chile, embodied data from Bribián et al. (2009).
[e]Goodhew and Griffiths (2005).
[f]Only the straw, and not the frame, is accounted for.

experiences have been performed. Whole straw bales have the best operational performance and the lowest embodied burdens, at least on energy and carbon emissions. However, building with straw bales requires more land for cultivation. For instance, in the conditions of the region studied, a typical one-family house of 120 m^2 living area demands the use of 420 bales and 2.8 ha of cultivation; while covering the same envelope with straw-clay blocks would demand 980 blocks and 1.2 ha. Although building with straw bales results in better thermal conductivity, straw-clay walls have three to four times better thermal insulation than major conventional solutions used currently in the region. It can be clearly seen in Table 21.1 that common fired clay bricks and concrete blocks need the addition of EPS to achieve the same thermal performance of straw-clay blocks.

A word on durability is in order. All constructions based on straw should be well protected from moisture. The possible damage to straw and clay blocks may vary

significantly with weather conditions. The area of study here has a cold, humid climate in at least 8 months per year, and so it would provide a good indication of durability for straw and clay masonries. The majority of constructions made so far with the technique are less than five years old, and the general opinion of users does not give indications of degradation problems so far; although, a systematic study on the durability has not yet been done. Several strategies are currently applied to protect straw-clay masonries: large roof overhangs; appropriate interior and exterior plasters; waterproof wall bases to avoid moisture reaching upwards, among others (González, 2014). In addition, the fair thermal properties of straw reduce the probability of condensation. Other authors have reported on successful moisture management in straw-based constructions also placed in cold, humid environments and summarized moisture management along with techniques for monitoring (Ashour et al., 2011; Goodhew et al., 2004). To my knowledge, there have not been reports on degradation of straw by termites, while this is not common in the region. Since straw must be protected with plasters, these act as termite and as fire protection as well. The technique using a steel structure encased with straw and clay masonry seems to be appropriate for termite and fire hazards, though moisture should be carefully checked.

21.5 Conclusions and future trends

At present, most construction materials require large amounts of energy resources and are in general produced far away from the building's location. This results in high emissions of GHGs, which are to be mitigated if climate is to be checked within safe limits. Therefore, there are increasingly more drivers promoting sustainable constructions, i.e. the ones using fewer resources, emitting fewer gases, and disposing of as little as possible of nondegradable items. Sustainable constructions must also be efficient because the operational phase of buildings may result in larger impacts than the embodied burdens.

On the other hand, the sustainability of constructions should not only consider the environmental consequences, but also the social issues involved. For instance, while most materials are mass produced in large-scale operations, an increasing number of regions worldwide suffer unemployment, in particular with higher rates within the younger population. The case studied here depicted a variety of stakeholders in a local community that found their hard work creative and highly motivating, and through the construction method we see an experience of a local community developing its own way of using local resources for building and employing.

Due to the use of fossil fuels in agriculture and transport and the use of mined clay, straw-clay blocks should not be considered sustainable. Even the straw, in appearance renewable, needs nonrenewable inputs to be produced. However, relative to the options of long-distance delivered fired clay bricks and cement, the initiative can be considered a positive step towards sustainability, both environmentally and socially. Hybrid approaches that combine alternative low-impact materials with technological advances can also improve sustainability. For instance, modern insulation and structural materials combined with straw, corns cobs, hemp, and clay, among others, can

lower embodied as well as operational burdens. Nevertheless, moisture penetration, plaster stability and durability studies should be performed in future works to assess these relevant aspects of sustainability.

Energy and carbon embodied in wall elements based on wheat straw were investigated for local conditions in the Andean Patagonia. Wheat is cultivated by local farmers in low-input agriculture that harvest a maximum of 50% straw to let the rest and the roots degrade in soils. For the area, it is found that no-tillage practice and returning straw and roots guarantee soil organic carbon content and fertility. The straw is baled and sold for construction applications, which have been high in demand for the last decade, to the extent that straw and grain are sold at similar prices. Other sources of straw would be at least 700 km away, and transportation of this lightweight bulky material would add unaffordable cost and environmental burdens. The straw has been used in straw-bale housing, and lately, a systematic manufacturing of blocks with straw and clay was developed and used in envelopes for houses and large public buildings. Considering the actual harvest yield, the straw-clay option allows the coverage of 120 m^2 of wall per ha of cultivation, in contrast to straw bale constructions that cover 50 m^2 of wall per ha. Local manufacturing of straw-clay blocks and the building activity associated became a relevant business with a diversity of benefits for the local community. The activity, as it is currently managed, demands a substantial part of human labor, which is mainly done by young people. Although this is still a niche successful experience, it can be concluded that the activity has the potential to greatly benefit a net of stakeholders, from farmers to building owners as well. On the other hand, straw-clay blocks have significantly better thermal performance than fired clay bricks or concrete blocks, which are at present the most common wall envelopes in the region of study. In addition, embodied energy and carbon dioxide in the local straw solutions were found far smaller than fired clay bricks, concrete blocks and insulated cavity walls. At present, thermal insulation in buildings is rarely applied in the region interested in this work, causing consumption of natural gas and firewood per m^2 to be between four and five times larger than for similar climates in Europe. Thus, either straw bales or straw-clay blocks would improve operative energy use in buildings in the very cold region of Andean Patagonia, as well as significantly lower energy and carbon embodied in walls.

Acknowledgments

I am indebted to Simón Van den Heede, farmer, and to Conrado Tognetti, builder's entrepreneur, for the valuable information that made this research possible. Partial supports by project CONICET-PIP 00107 and by Universidad Austral de Chile during the author's sabbatical in 2013 are also acknowledged.

References

Ashour, T., Georg, H., & Wu, W. (2011). Performance of straw bale wall: A case of study. *Energy and Buildings, 43*, 1960−1967.

Bribián, I. Z., Usón, A. A., & Scarpellini, S. (2009). Life cycle assessment in buildings: state-of-the-art and simplified LCA methodology as a complement for building certification. *Building and Environment, 44*, 2510−2520.

Carlsson-Kanyama, A., & González, A. D. (2007). *Non-CO_2 greenhouse gas emissions associated with food production: Methane (CH_4) and nitrous oxide (N_2O)*. KTH Report http://www.ima.kth.se/eng/respublic/emissions_report_17_set_ACK.pdf.

De Schiller, S., & Evans, J. M. (1990). Bridging the gap between climate and design at the urban and building scale: research and application. *Energy and Buildings, 15/16*, 51−55.

Deverell, R., Goodhew, S., Griffiths, R., & de Wilde, P. (2009). The noise insulation properties of non-food-crop walling for schools and colleges: a case study. *Journal of Building Appraisal, 5*, 29−40.

Díaz, C., & Czajkowski, J. (2006). Auditorías energéticas en viviendas de interés social en Río Grande, Tierra del fuego. *Avances Energía Renovable Medio Ambiente, 10*, 07.33−07.38.

Giampietro, M., & Pimentel, D. (1990). Assessment of the energetics of human labour. *Agriculture Ecosytems and Environment, 32*, 257−272.

González, A. D. (2009). Energy subsidies in Argentina lead to inequalities and low thermal efficiency. *Energies, 2*, 769−788.

González, A. D. (2013). Management of disaster risks derived from very large fuel subsidies of natural gas in Argentina. In W. Leal (Ed.), *Climate change management* (pp. 463−473). Berlin: Springer-Verlag. Part 3. http://link.springer.com/chapter/10.1007%2F978-3-642-31110-9_30

González, A. D. (2014). Energy and carbon embodied in straw and clay wall blocks produced locally in the Andean Patagonia. *Energy and Buidlings, 70*, 15−22.

González, A. D., Carlsson-Kanyama, A., Crivelli, C., & Gortari, S. (2007). Residential energy use in one-family households with natural gas provision in a city of the Patagonian Andean region. *Energy Policy, 35*, 2141−2150.

González, A. D., Frostell, B., & Carlsson-Kanyama, A. (2011). Protein efficiency per unit energy and per unit greenhouse gas emissions: Potential contribution of diet choices to climate change mitigation. *Food Policy, 36*, 562−570.

Goodhew, S., & Griffiths, R. (2005). Sustainable earth walls to meet the building regulation. *Energy and Buildings, 37*, 451−459.

Goodhew, S., Griffiths, R., & Wooley, T. (2004). An investigation of the moisture content in the walls of a straw-bale building. *Building and Environment, 39*, 1443−1451.

IEA. (2014). *Argentina: Statistics*. International Energy Agency. http://www.iea.org/stats/countryresults.asp?COUNTRY_CODE=AR&Submit=Submit.

IRAM. (1996). Acondicionamiento térmico de edificios: clasificación bioambiental de la República Argentina. *Norma IRAM, 11603*. Instituto Argentino de Normalización de Materiales.

Juanicó, L., & González, A. D. (2008a). Thermal efficiency of natural gas balanced-flue space heaters: Measurements for commercial devices. *Energy and Buildings, 40*, 1067−1073.

Juanicó, L., & González, A. D. (2008b). Savings on natural gas consumption by doubling thermal efficiencies of balanced-flue space heaters. *Energy and Buildings, 40*, 1479−1486.

Kätterer, T., Bolinder, M. A., Andrén, O., Kirchmann, H., & Menichetti, L. (2011). Roots contribute more to refractory soil organic matter than above-ground crop residues, as revealed by a long-term field experiment. *Agriculture Ecosystems & Environment, 141*, 184−192.

Lahv. (2014). *Cálculo de transmitancia térmica de sistemas constructivos* (online tool). Laboratorio de Ambiente Humano y Vivienda. http://www.cricyt.edu.ar/lahv/pruebas/conductancia/principal.htm.

Lal, R. (2011). Sequestering carbon in soils of agro-ecosystems. *Food Policy, 36*, S33−S39.

Mansour, A., Srebric, J., & Burley, B. J. (2007). Development of straw-cement composite sustainable building material for low-cost housing in Egypt. *Journal of Applied Sciences Research, 3*, 1571−1580.

Pimentel, D. (2009). Energy inputs in crop production. *Energies, 2*, 1−24.

Rosenfeld, E., Díscol, C., Martini, I., Czajkowski, J., San Juan, G., Barbero, D., et al. (2003). El uso de la energía en el sector residencial del Gran La Plata. Discriminación de consumos, cambios tecnológicos y opinión de los usuarios en las décadas del '80 y '90. *Avances Energía Renovable Medio Ambiente, 7*, 07.25−07.30.

Schueftan, A., & González, A. D. (2013). Reduction of firewood consumption by households in south-central Chile associated with energy efficiency programs. *Energy Policy, 63*, 823−832.

Seyfang, G. (2010). Community action for sustainable housing: building a low-carbon future. *Energy Policy, 38*, 7624−7633.

Sun Rang-Can. (2010). *Cereal straw as a resource for sustainable biomaterials and biofuels chemistry, extractives, lignins, hemicelluloses and cellulose*. Amsterdam, NL: Elsevier.

Tognetti, C. (2013). Builder entrepreneur, Personal communication.

Williams, A. G., Audsley, E., & Sandars, D. L. (2010). Environmental burdens of producing bread wheat, oilseed rape, and potatoes in England and Wales using simulation and system modelling. *International Journal of Life Cycle Assessment, 15*, 855−868.

Earth-block versus sandcrete-block houses: embodied energy and CO_2 assessment

22

H. Abanda[1], *J.H.M. Tah*[1], *G. Elambo Nkeng*[2]
[1]Oxford Brookes University, Oxford, UK; [2]Ecole Nationale Supérieure des Travaux Publics, Cameroun, Africa

22.1 Background

According to the recent Fifth Assessment Report of the Intergovernmental Panel on Climate Change (IPCC), in 2010, the building sector accounted for approximately 32% of global final energy consumption and of energy-related CO_2 emissions. Also, the built environment consumes more natural resources than necessary and therefore generates a large amount of waste (Osmani, 2011). The high energy consumption, high CO_2 emissions, and wasteful resources all have huge negative impacts on the environment. Although the greatest share of emissions has so far been from developed countries, the greatest burden of the impacts is on developing countries. Thus, there is an urgent need for concerted efforts from the developed and developing countries to minimize or eliminate activities that negatively alter climate systems. The increasing concern from developing countries has steadily been reflected in their participation in some high-profile international conferences such as Conference of the Parties (COP) 15-Copenhagen; COP17-Durban; COP 18-Doha and lastly COP 19-Warsaw in 2009, 2011, 2012 and 2013 respectively.

Therefore, the built environment is a major sector to consider in designing strategies for combating the impacts of climate change. Some examples of strategies include the improvement of construction and energy efficiency processes/techniques/technologies, adoption of passive design, use of renewable energy and the appropriate selection of building materials. The focus of this chapter will be on building materials used for housing construction because the share of materials often used in construction is huge and most other factors depend on them. Also, building materials constitute a significant share of house construction cost. Adedeji (2010) noted that about 60% of the total house construction cost goes toward the purchase of construction materials. Embodied energy and CO_2 are currently two main parameters commonly used in assessing the importance of building materials (Hammond & Jones, 2008). The European Union (EU) Construction Products Directive has recommended embodied energy as a key factor in the selection of building materials or construction products (Edwards, 2010). Although CO_2 is the least potent of all of the Kyoto greenhouse gases, it is by far the most plentiful and largest contributing compound to the greenhouse effect (Ürge-Vorsatz & Novikova, 2008). Hence, in this

Eco-efficient Masonry Bricks and Blocks. http://dx.doi.org/10.1016/B978-1-78242-305-8.00022-X

chapter, the shares of embodied energy from the two most common house types in Cameroon will be investigated. The findings from this paper are important to Cameroon given that housing in that country has recently become too expensive for local residents, especially in urban areas where the cost of imported building materials is reported to be too exorbitant and less environmentally friendly than the locally available building materials (Meukam, Jannot, Noumowe, & Kofane, 2004). Cerutti et al. (2010) argued in Robiglio et al. (2010) that most of Cameroon's market for domestic timber, for example, has been on the rise. Thus, it is imperative to use parameters (e.g. embodied energy and CO_2) to guide the selection of environmentally benign materials from a list of options for alternative uses in buildings. On the basis of the review of the literature, there is a lack of quantitative studies in Cameroon regarding embodied energy and CO_2 of buildings (see Section 22.2). To facilitate understanding, embodied energy and CO_2 concepts have been examined in the ensuing section.

22.2 Embodied energy and CO_2: an overview

Although embodied energy has recently gained ground, the concept has been around for at least three decades, perhaps used for different purposes. Input-output techniques developed by Leontief (1966) for analyzing the industrial interdependencies in a national or regional economic system today constitute solid theoretical underpinnings for embodied energy assessment (e.g. Treloar, 1997; Treloar, Gupta, Love, & Nguyen, 2003). Since then, it has been common to also find embodied energy concepts being used in industrial and chemical processes. Van Gool (1980) evaluated the product ("process" plus "embodied") energy required of chemical process equipment, often termed "unit operations". A typical trade-off between process and embodied energy (Hammond, 2007), in which a minimum total energy requirement can be observed that is somewhat greater than the thermodynamic minimum (based on the so-called Gibbs free energy; Van Gool, 1980), is presented in Figure 22.1.

Before the recent applications of input–output technique (e.g. Treloar, 1997; Treloar et al., 2003) in embodied energy analysis, the technique had already been featured in environmental applications (Leontief, 1970) in the 1970s. Specifically, Hannon (1973) adopted the input–output technique (Leontief, 1966) in embodied energy analysis to describe ecosystem energy flows. Similar to Leontief input–output theory, energy inputs to a system are aggregated from all subsidiary pathways to yield the total embodied energy or gross energy requirement (Cabeza et al., 2013).

There are two forms of embodied energy in buildings (Harries, 2007; Shrivastava & Chini, 2012): the initial embodied energy, which consists of the nonrenewable energy required to extract and process its raw materials (indirect energy) and the energy used to transport the finished product to the job site and install it (direct energy) (Harries, 2007; Shrivastava & Chini, 2012). The recurring embodied energy of a building component can be defined as the nonrenewable energy consumed to

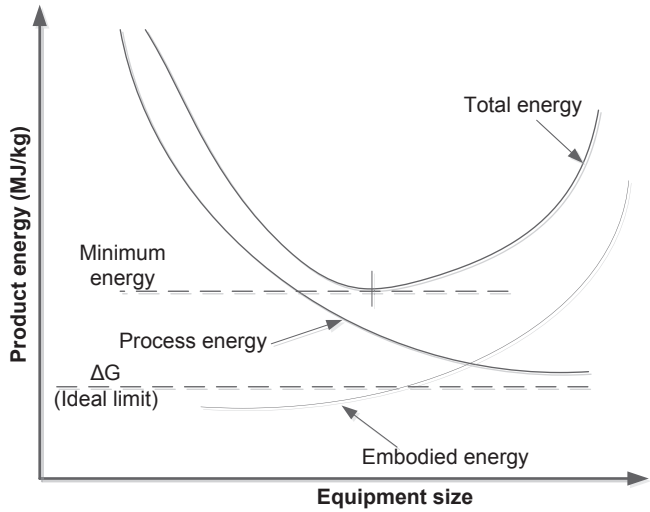

Figure 22.1 Product (process + embodied) energy requirements associated with process equipment.
Source: Adopted from Cabeza et al. (2013).

maintain and replace it as well as recycle it or dispose of it at the end of its useful life (Harries, 2007; Shrivastava & Chini, 2012). The operational energy of buildings is the energy required for maintaining comfort conditions and day-to-day maintenance of the buildings by operating processes such as heating and cooling, lighting and appliances and air conditioning (Ramesh, Prakash, & Shukla, 2010). For many years, the embodied energy content of a building was assumed to be small compared with the operational energy (Cabeza, Rincón, Vilariño, Pérez, & Castell, 2014; Dixit, Fernandez-Solis, Lavy, & Culp, 2012; Pacheco-Torgal, Faria, & Jalali, 2013). Pacheco-Torgal et al. (2013) reported that embodied energy represents between 10% and 15% of the operational energy. Cabeza et al. (2014) reported that embodied energy constituted 10−20% of the life cycle energy of a building. Some studies have reported even very low figures, as low as 2%; for example, Sartori and Hestnes (2007) reported that embodied energy could account for 2−38% of the total life cycle energy of a conventional building and 9−46% for a low-energy building. Consequently, most energy-related research efforts have been directed toward reducing the operational energy largely by improving the energy efficiency of the building envelope.

In addition to embodied energy, the production of building materials (e.g. extraction, transportation and manufacturing processes) releases CO_2 mainly because of the use of fuel or electricity. This is often called "embodied CO_2". Thormark (2006) reported that the embodied energy in traditional buildings can be reduced by approximately 10−15% through proper selection of building materials with low environmental impacts. González & Navarro (2006) estimated that

the selection of building materials with low impacts can reduce CO_2 emissions by up to 30%. In the United Kingdom, Sturgis & Roberts (2010) predict the proportion of embodied carbon to increase from 30% to 95% whereas operational will reduce to 5% from 70% for a domestic dwelling over the coming 7−10 years with improved legislation. The effective implementation of policies such as the Energy Performance Building Directive could see a significant reduction in operational energy whereas embodied energy could increase to almost 400% of the operational energy in the near future (Cabeza et al., 2013). Thus, embodied energy and CO_2 are quite important in environmental building assessment. Cabeza et al. (2014) provide an extensive review of studies about the selection of environmentally preferred materials for buildings. Before embarking on their assessment methodology, it is important to gain insights into the content of peer-reviewed literature about embodied energy and CO_2 in Africa in general and Cameroon in particular.

22.3 Embodied energy and CO_2-related studies

To gain insights into how similar studies on embodied energy and CO_2 might have been conducted in the African continent and Cameroon in particular, a literature review was conducted. A systematic search of key peer-reviewed papers from renowned databases including ScienceDirect (http://www.sciencedirect.com/), EI Compendex (http://www.ei.org/) and EBSCO (http://www.ebsco.com/index.asp) about embodied energy and CO_2 analysis was conducted. These searches yielded few results with little relevance. The first overarching outcome was the general agreement among peer-reviewed literature about the importance of embodied energy and CO_2 in the assessment of building impacts on the environment (Adedeji & Fa, 2012; Bashir, Iro, & Babanyara, 2013; Bruelisauer, 2007; Mohammed & Mu'azu, 2011; Mpakati-Gama, Wamuziri, & Sloan, 2011; Nwokoro & Onukwube, 2011). The second outcome was that, despite acknowledgment of the need to consider embodied energy and CO_2 in building impact analysis, very few quantitative studies have been conducted in this respect. Hugo, Stoffberg, & Barker (2012) computed the embodied energy and CO_2 of construction materials of three South African Bus Rapid Transit stations. Irurah & Holm (1999) demonstrated discrepancy and conflicts of data of basic embodied energy intensities of building construction materials between building systems and building types. An extensive study of the embodied energy of various wall, floor, and roofing systems in India has been reported in Reddy (2009). The discrepancies of embodied energy values can also be noted for some selected countries presented in Table 22.1.

What emerges from these findings is that studies on building embodied energy and CO_2 assessment with regards to Africa in general and Cameroon in particular are scarce. This outcome underpins the motivation for this study. The assessment methodologies based on life cycle analysis of the embodied energy and CO_2 are examined in the ensuing section.

Table 22.1 Some embodied energy values for selected African countries and India

Hydraform brick hydraulically compressed soil-cement mixture, used in domestic dwelling	0.635 MJ/kg	Hydraform brickhouse in Lynedoch Ecovillage, Stellenbosch, South Africa	Roux and Alexander in The Sustainability Institute (2009)
Fly ash brick cement-based brick used for construction of toilets	0.632 MJ/kg	South Africa	Roux and Alexander in The Sustainability Institute (2009)
Fired clay bricks	4.25 MJ/brick	Uganda	Esteban and Aimee (2012)
Compressed earth masonry unit produced using manual press	≈0	Uganda	Esteban and Aimee (2012)
Dimensional, rough-sawn, timber	1.5 MJ/timber	Kimomba, Uganda	Esteban and Aimee (2012)
Timber with steel connections	1.5 MJ/kg, 35 MJ/kg	Gita, Uganda	Esteban and Aimee (2012)
Site felled timber	≈0	Lutisi, Uganda	Esteban and Aimee (2012)
G + 1 reinforced concrete[a] structure (R.C.C.) structure	3702.344 MJ/m^2	India	Gumaste (2006)
G + 2 R.C.C. structure[b]	2911.233 MJ/m^2	India	Gumaste (2006)
G + 7 R.C.C. structure[b]	3611.977 MJ/m^2	India	Gumaste (2006)

[a]Construction materials are cement, sand, aggregate, bricks, glass, tiles, timber, steel and paint.
[b]Construction materials are cement, sand, aggregate, bricks, glass, aluminum, tiles, timber, steel and paint.
Source: Authors' collection.

22.4 Assessment methodology

The dissipation of embodied energy and the emission of CO_2 are directly associated with each phase of a building's life cycle and vary by building types (Verbeeck & Hens, 2010). Although there is a lack of consensus as to the different types of phases

in a building life cycle, the product phase (raw materials supply, transport and manufacturing), construction phase (transport and construction-installation on-site processes), use phase (maintenance, repair and replacement, refurbishment, operational energy use; heating, cooling, ventilation, hot water and lighting and operational water use) and end-of-life phase (deconstruction, transport, recycling/re-use and disposal) (Blengini & Carlo, 2010) are generally quite common and encompass most other life cycle classifications. The increased awareness of the importance of environmental protection and the possible impacts associated with construction processes have increased interest in the development of methods to better understand and address these impacts. The most widely used technique is the life cycle assessment (LCA), which considers the building's life cycle (Blengini & Carlo, 2010; Cabeza et al., 2014). LCA is the most comprehensive tool in the assessment of environmental impacts and has been adopted for use in many types of products and processes by reputable institutions such as the International Standard Organisation (i.e. ISO 14,040 environmental management standards), the U.S. Environmental Protection Agency, the European Union (i.e. European Standard) and the United Kingdom (i.e. British Standard).

In this study, the assessment methodology adopted follows the European Standard, which has been adopted as part of the British Standard for evaluating environmental impacts of building projects (BS EN, 2011). The standard provides the calculation method, based on the LCA, to assess and evaluate the environmental performance; thus, it provides design options and specifications for new and existing buildings. The main guidelines of the standard stipulated in European and British standards (BS EN, 2011) are the description of the object of the assessment, the system boundary that applies at the building level, the procedure to be used for inventory analysis and the requirements for the data necessary for the calculation. The applications of these guidelines and their rationale will be examined in the ensuing sections.

22.5 The description of the object of the assessment and system boundary

The object refers to what is being developed or is in the process of being developed and the process of development and/or its existence after development has impacts on the environment. In this study, two residential buildings are the objects of assessments. The two buildings represent typical houses common in Cameroon. One is predominantly made up of what is generally referred to as imported materials (i.e. sandcrete-block house); the other is constructed predominantly out of local building materials (i.e. earth-block house). Here, a block is considered to mean an object that cannot be held or carried with one hand as compared with a brick that can completely be held with a single adult's palm. The drawings depicting the dimensions of the two types of blocks are presented in Figures 22.2 and 22.3, respectively.

According to ISO 14040, the system boundary is a set of criteria specifying which unit processes are part of a product system. It also describes the limits of what is

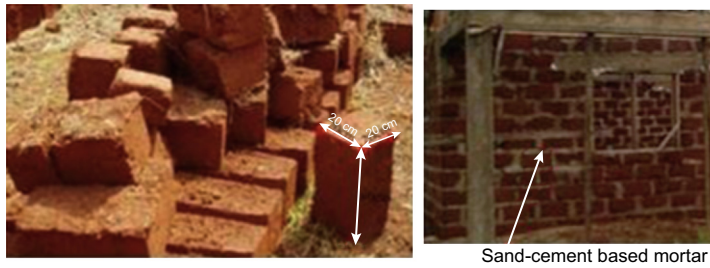

Figure 22.2 Earth-block.
Source: Adapted from http://www.villageaid.org/index.php?id=411.

Figure 22.3 Sandcrete block.
Source: Adapted from http://www.trophees-solidaires.fr/projets/yega.

included or not included in the assessment of the whole life cycle for a new building or any remaining cycle stages for the existing building. Figure 22.4 is used to clarify the boundaries considered in this study.

The first boundary to be defined is around the product phase. On the basis of Figure 22.4, this boundary includes the extraction of material from its original sources and the transportation to the production unit where manufacturing into different products is undertaken. The manufactured components are then transported to the construction site where the construction phase begins. Thus, the physical boundary considered is from cradle to gate. This choice has a major advantage in that it provides the possibility to directly use the inventory of carbon and energy for construction materials developed by Bath University in the United Kingdom (Hammond & Jones, 2008). With respect to the boundary on processes or activities, the material extraction, material transportation, material transformation and transportation of components from gate to construction site have been considered.

The second is about the construction phase. In practice, two major categories of activities that have impacts on the environment occur. The categories consist of erecting a new or renovating (upgrade/maintenance) an existing building. The main activities in each of these tasks are site installation, the transportation of plants/equipment, plant/equipment use, the use of temporary materials and the construction of a site office. Also, there are induced activities that occur during

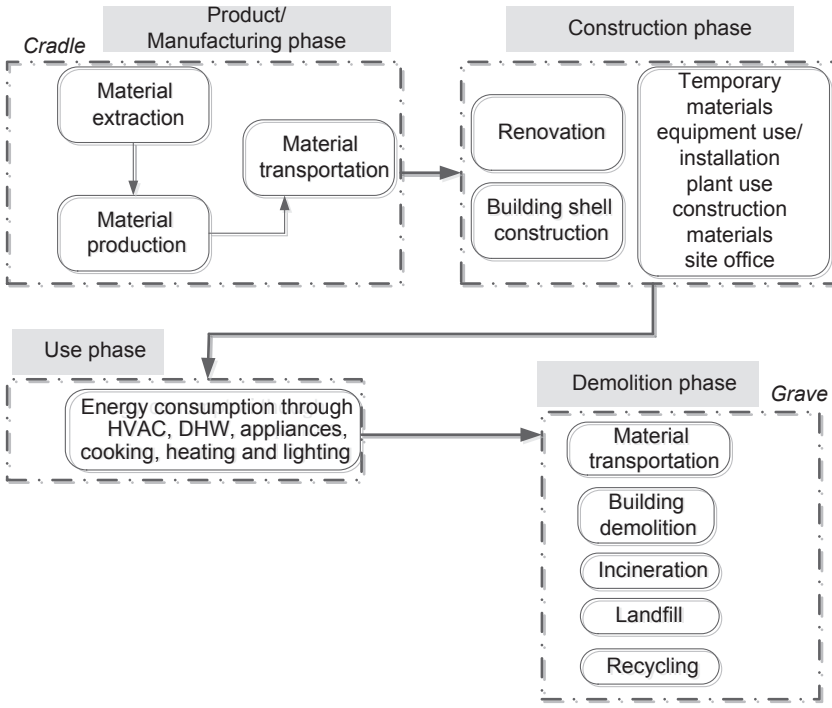

Figure 22.4 Life cycle phases of a typical house building project.

the erection of the building. This includes on-site construction waste and the transportation of waste from packaging. These activities are out of the scope of this chapter. In particular, on the basis of the limited information about site installation, only the embodied energy and CO_2 of building materials used in erecting the houses will be considered whereas the transportation of plants/equipment is also out of scope. It is important to note that the impacts from erecting a new building or renovating an existing house can be determined using the same methods. If the renovation work entails repairs or replacement of materials originally installed, then the frequency of repairs will be required. However, because of limited data and information about the replacement of building components in Cameroon, only on-site construction, specifically the erection of a new building in the construction phase, will be considered.

The use phase of a building consists of the operational energy use for heating, ventilation and air conditioning; domestic hot water; appliances; cooking; heating and lighting. The impacts from building use are determined from appliances' characteristics in the building and thus constitute operation energy or operation CO_2. Any building has a life cycle that begins with extraction of building materials and ends with demolition of the building when it becomes obsolete. When a building becomes obsolete, it is demolished or deconstructed and the materials are recycled for use, dumped in a landfill, taken to the incinerator or a combination

of the three. Similar to the construction phase, the impacts from the demolition phase can be determined. However, data and information about building demolition waste in Cameroon are not available, hence, they will not be considered in this study. After the establishment of the physical and process boundaries, the assessment methods considered in this study will be examined in the ensuing section.

22.6 The methods of assessment

In this section, the different embodied energy and embodied CO_2 assessment methods are examined. The aim is to establish which method(s) to use. In the literature, three methods of assessment are quite common: input-output analysis, process analysis and hybrid analysis.

Input-output LCA is a top-down method for analyzing the environmental interventions of a product using a combination of national sector-by-sector economic interdependent data that quantify the dependencies between sectors with sector-level environmental effects and resource use data (Seo & Hwang, 2001; Treloar et al., 2003). Using matrix operations, a change in economic demand from a sector can be quantified in environmental effects or resource use. For example, the purchase of a construction crane would directly impact steel, aluminum and plastic. Other examples are the indirect impacts from the production of steel as well as the entire supply chain of the plant through the economy.

In process LCA, known environmental inputs and outputs are systematically modeled through the utilization of a process flow diagram. The process LCA is often called a 'bottom-up approach'. This is because the subjects of analysis in process LCA are individual processing units and the flow rate and composition of streams entering and exiting such units. For example, a steel mill requires iron ore, coal and electricity and this will often be considered in process LCA. However, indirect supplies such as office equipment, food and vehicles are generally excluded to keep the analysis simple and manageable.

The above two life cycle methods of assessment have advantages and disadvantages that have been extensively discussed in Treloar et al. (2003), Goggins, Keane, & Kelly (2010), Crawford & Treloar (2003) and Dixit, Fernandez-Solis, Lavy, & Culp (2010). To justify the choice of the methods used in this project, a summary of the advantages and disadvantages of the preferred choice is examined.

Input-output analysis suffers from a lack of representativeness being used because of over-aggregation of data. Also, national sector-by-sector economic interdependent data or a sectoral matrix are often too old and out of date in developed countries and worse in developing countries. Process-based LCA allows for a detailed analysis of a specific process at a point in time and space. Nonetheless, it is often criticized for its subjectivity in the definition of the processes that should be considered and the data sources to be used. Also, process LCA can be complex if the building has so many different types of building materials. Furthermore, the emerging building information modeling (BIM) can be used to model a building that can systematically simplify the

complexity of building materials and hence facilitate the task of embodied energy and CO_2 assessment. In this study, BIM was employed to simplify and validate results obtained from manual implementation of the process-based method.

22.7 Data collection methods

The British Standard and PAS-2050 recommend that the data sources and key assumptions are to be explicitly stated to facilitate the verification of the environmental emissions quantified at the end of the assessment. To measure embodied energy and CO_2, building processes need to be identified first. Then, the activities involved and materials used in the processes are determined. Advanced draughting and modeling software applicable to the design of buildings (e.g. Revit) allow users to generate building quantities automatically from the three-dimensional models. The generated quantities represented by the physical dimensions need to be converted to masses using relevant densities and then multiplied by suitable CO_2 emission factors from embodied energy and CO_2 inventories. Although embodied energy and CO_2 inventories for developing countries are lacking, they are quite common in the developed countries and are often used in environmental impact assessment studies. These inventories developed in developed countries are now also being used in developing countries (Hugo et al., 2012).

22.8 Inventory sources

The computation of environmental emissions depends largely on the accuracy, relevance and completeness of inventory data. However, in most cases complete data are often impossible to obtain and the computation of emissions is often found on the "best evidence" as a compromise. Because individual data inventories do not contain all of the emission factors for the estimation of embodied CO_2 for all building processes, a combination of various inventories are often used to carry out the estimation. The common embodied energy and CO_2 emission inventories used include the following:

- The Bath Inventory of Carbon and Energy (ICE), which contains emission factors for construction materials. This is the most popular and most widely used emission factors dataset developed by the Sustainable Energy Research Team at the University of Bath (Hammond & Jones, 2008). The current version, ICE V2.0, was developed in 2011.
- Eco-inventory database developed by the Swiss Centre for Life Cycle Inventories.
- Bilan carbon six developed by the French Environment and Energy Management Agency.
- Emission factors for road vehicles by the UK Department of Transport (Boulter, Barlow, & McCrae, 2009).
- Emission factors for off-road equipment by the Department of Environment, Food and Rural Affairs (McGinlay, 2004).
- IPCC Emission Factor Database: This is a web-based tool developed by IPCC that contains greenhouse emission factors for use by the community.

On investigating the different impact factors' inventories aforementioned, the Bath ICE is more specific to buildings than all of the others. Furthermore, it is widely used in Europe and already being used in other countries other than the usual Anglo-American and European countries (e.g. in South Africa; Hugo et al., 2012). Consequently, Bath ICE will be used in this study. To maintain the applied objectivity of this study, the embodied energy and CO_2 results obtained from using the Bath ICE should be used in a comparative sense. To facilitate understanding of computation variables, mathematical models relating the different impact factors to the building material quantities will be examined in Section 22.9.

22.9 Mathematical models underpinning the process analysis approach

The main reason for using emission or impact factors is to facilitate computation of emissions. By using emission factors, tedious tasks that would have involved chemical equations are avoided. This is because emission factors are expressed as a quantity of embodied energy or CO_2 per functional unit. For example, according to Bath ICE, the emission factor of virgin aluminum is 11.46 $kgCO_2/kg$. The functional unit is the kilogram in the denominator because it denotes quantity of virgin aluminum in 1 kg. Therefore, to compute the emission from a given quantity of virgin aluminum, a simple multiplication of the total quantity and the emission factor is conducted. If there are several construction materials considered, then the products of the emission from different materials are added. This is modeled mathematically as in Eqns (22.1) and (22.2).

$$\mathrm{EE}_k = \sum_{k=1}^{n} (1 + \xi_k) \cdot Q_k \cdot I_k \tag{22.1}$$

$$\mathrm{EC}_k = \sum_{k=1}^{n} (1 + \xi_k) \cdot Q_k \cdot I_k \tag{22.2}$$

where:

- EE_k and EC_k are the embodied energy and embodied CO_2 of material type k with units MJ and $kgCO_2$, respectively;
- ξ_k is the waste factor (dimensionless) of material type k and
- Q_k is the total functional quantity of material;
- I_k is the embodied energy factor or embodied CO_2 factor with units of MJ/functional unit and $kgCO_2$/functional unit of material, respectively.

Because of lack of information about waste data in Cameroon, the waste factor was considered to be zero.

22.10 Calculations and the use of tools

There are available calculation tools in the market for the computation of emissions. For example, the Greenhouse Gas Protocol Initiative toolset based on an Excel spreadsheet can be used to calculate the various greenhouse gases of different products. There are also emerging BIM authoring tools that can be used to automate the computational process of embodied energy and CO_2. Some of these tools (e.g. Revit, Bentley Systems and Tekla) have been reviewed in Kurul, Abanda, Tah, & Cheung (2013), hence, their work will not be duplicated here. Given that some of these tools are not affordable, especially from developing countries' perspectives, a manual computation process was adopted (see Section 22.12.4) and then Revit, a BIM tool, was used to validate the manual computational results.

22.11 Data aggregation

Aggregation is a straightforward task. First, the emissions from a category are added independently. In other words, emissions from all of the different construction materials, equipment/plants and personnel transport types used are independently computed. Then, the emissions from the three different categories are summed up to obtain a total. Sections 22.1–22.11 have all been about embodied energy and CO_2

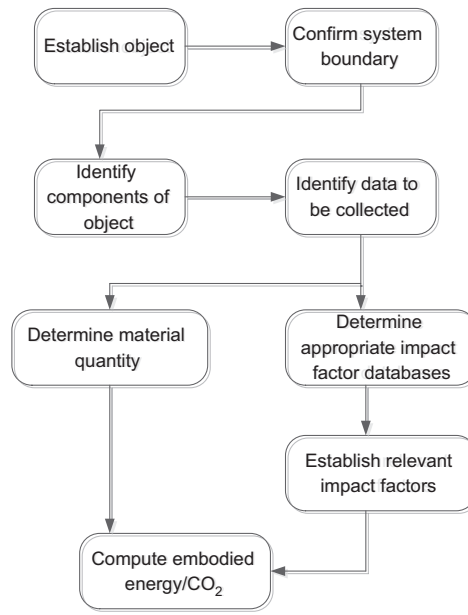

Figure 22.5 Steps for the computation of embodied energy and CO_2 of building materials.

assessment. These steps have been summarized in Figure 22.5 and will now be implemented in assessing the embodied energy and CO_2 of the two case studies considered.

22.12 Assessments of embodied energy and CO_2: case studies' applications

22.12.1 Description of case studies

Because of the complexity and variety of housing types in the construction sector, the Ministry of Housing and Urban Development (MINHUD) of Cameroon has categorized houses according to sizes and content. MINHUD categorizes domestic dwellings according to the following minimum requirements: (1) gross floor area (GFA), usually denoted (T1: GFA $\geq 20\,m^2$, T2: GFA $\geq 32\,m^2$, T3: GFA $\geq 62\,m^2$, T4: GFA $\geq 89\,m^2$, T5: GFA $\geq 106\,m^2$, T6: GFA $\geq 130\,m^2$); (2) all of the dwellings except T1 must contain a kitchen, corridors, lounge and dining room; (3) T1 and T2 should contain one bedroom each whereas T3, T4, T5 and T6 should contain two, three, four and five bedrooms, respectively and (4) T1, T2 and T3 should contain 1 toilet each and T4 and T5 should contain two toilets whereas T6 should contain three toilets. For purposes of this study T3 and T4 were employed as case studies for earth-

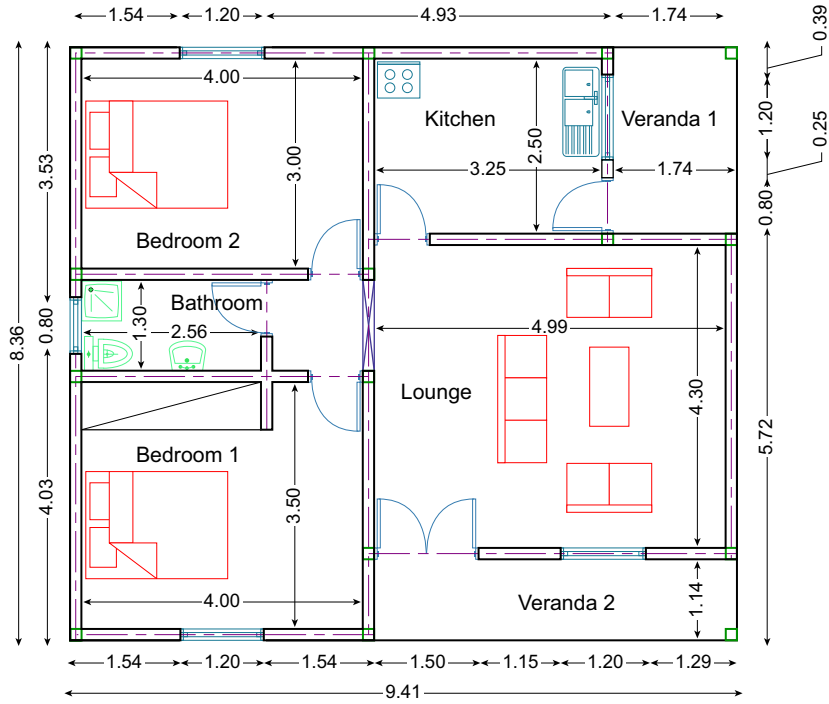

Figure 22.6 T3 earth-block house.

block and sandcrete-block houses, respectively. Their choice is based on their popularity of use in Cameroon. The two-dimensional drawings of T3 and T4 are presented in Figures 22.6 and 22.7.

22.12.2 Sample computation of a component

In this section, only the foundation components of the buildings have been chosen to illustrate the computation process of embodied energy and CO_2. The foundations of both T3 and T4 are geometrically the same in form except differences in dimensions. Consequently, for illustrative purposes, detailed steps in the computation of embodied energy and CO_2 performed on T3 will be presented. The results for the computation of the complete houses will be presented in summarized tabular forms.

The emission intensities used in the computation of the emissions consider the product phase excluding the manufacturing of components in the fabrication shop. Although construction waste has recently been noted to be significant in Cameroon (Cout & Trois, 2010; Fombe & Ntani, 2012), no studies have actually determined the share or fraction of construction waste in relation to the various construction materials used. Consequently, in this study, the value for the construction waste factor is assumed to be zero. The quantity of the various parts of the foundation were measured and multiplied by the density of the respective materials to deduce their weight for the calculation of the emissions.

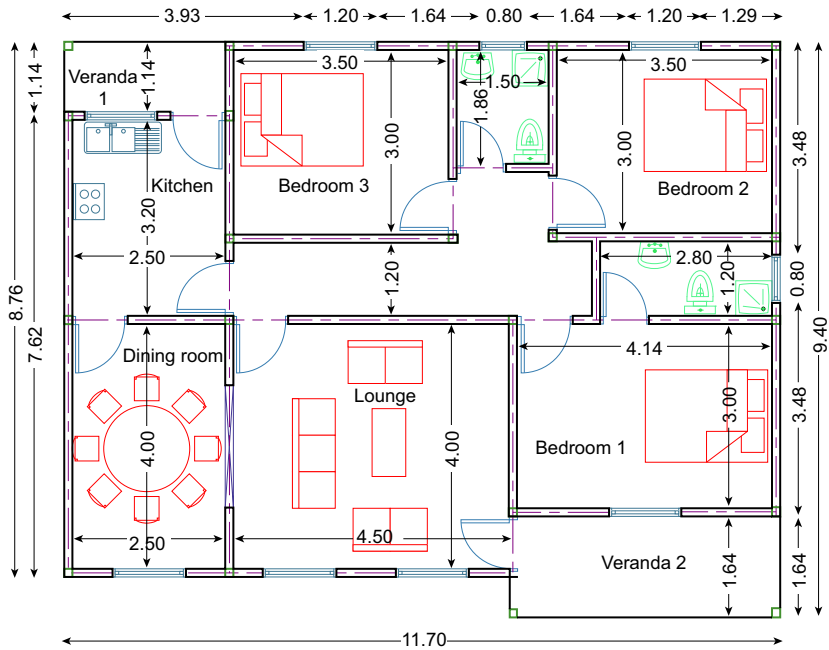

Figure 22.7 T4 sandcrete-block house.

22.12.3 Specimen calculation of foundation

According to the architect's specifications, the foundations have been used in bearing the concrete slab floor. The foundation dimensions are shown in Figure 22.8. The different foundation material components are as follows:

- Lean concrete: Its role is to provide the uniform surface to the foundation concrete and to prevent the direct contact of foundation concrete with the soil. Its thickness is 5 cm. It is mixed at 150 kg/m^3.
- Concrete for ground beam, column footings: This is mixed at 350 kg/m^3.
- Ground floor slab: This is concrete with a cement finish. The concrete is mixed at 300 kg/m^3.
- Foundation wall: This wall is made up of sandcrete blocks of dimension 20 × 20 × 40 cm completely filled with concrete.
- Damp-proof course of thickness 0.05 cm.
- Substrate of gravel.
- Sand.

22.12.4 Calculation of the mass of the different materials in the foundation

In general, the mass, Q, of any substance is related to the volume (V), through the formula $Q = \rho V$, where ρ is the material density.

$$\text{Volume } (V) = \text{Length} \times \text{Width} \times \text{Thickness}$$

22.12.4.1 Lean concrete

Volume of lean concrete.

$$V_1 = 3\ \text{m}^3$$

Therefore, the total mass of lean concrete (Q_l) is given by

$$Q_1 = \left(22\text{kN}/\text{m}^3\right) \times 3\ \text{m}^3$$

$$Q_l = 6600\ \text{kg}$$

The embodied energy is defined by $EE_{tp} = Q_{tp} \times I_{p(ee)}$, where $I_{p(ee)}$ is the embodied energy factor for concrete. In Bath ICE, the embodied energy and CO_2 intensities of concrete dosed at 150 kg/m^3 have not been provided. However, values for concrete dosed at 120 and 200 kg/m^3 have been provided. From Bath ICE, the embodied energy intensities for concrete dosed at 120 and at 200 kg/m^3 are 0.49 and 0.67 MJ whereas embodied carbon intensities are 0.06 and 0.091 kgCO_2, respectively. Although using the lower or upper values would be an underestimation or overestimation, an average of both values is most probable, especially because these intensities are increasing functions.

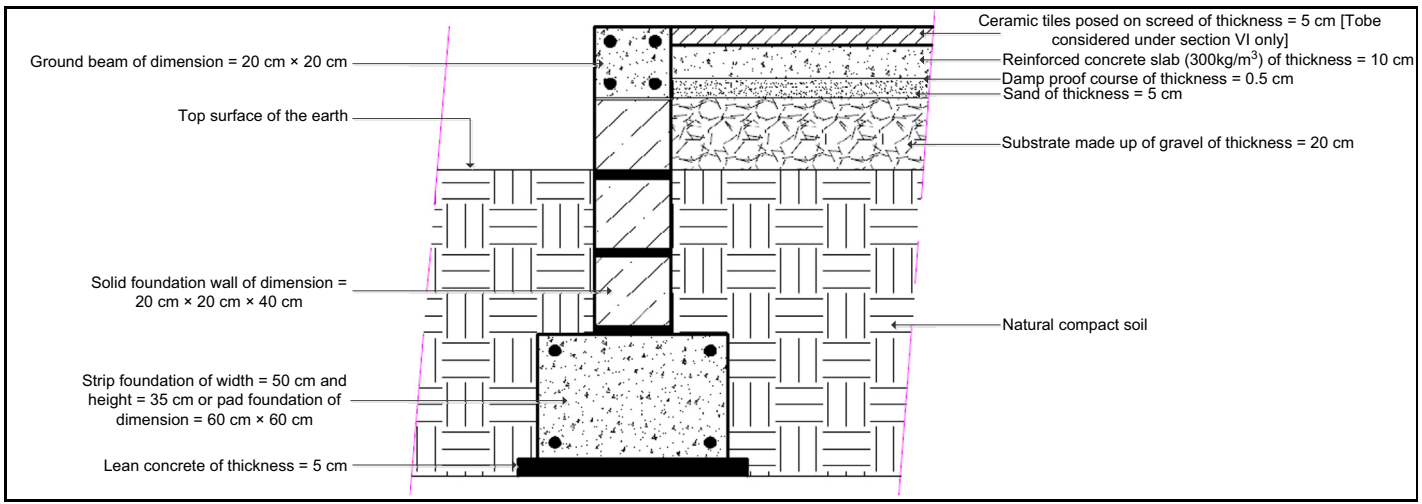

Figure 22.8 Cross-section of foundation.

On the basis of this assumption, the computed embodied energy and CO_2 intensities for lean concrete dosed at 150 kg/m^3 are 0.58 MJ {=(0.58 + 0.67)/2} and 0.0755 kgCO_2 {=(0.06 + 0.091)/2}.

$$EE_l = 6600\ \text{kg} \times (0.58\ \text{MJ/kg})$$

$$EE_l = 3828\ \text{MJ}$$

The embodied CO_2 $EC_l = Q_l \times I_{l(CO_2)}$, where $I_{l(CO_2)}$ is the embodied CO_2 factor for concrete:

$$EC_l = 6600\ \text{kg} \times (0.0755\ \text{kg}CO_2/\text{kg})$$

$$EC_l = 498.3\ \text{kg}CO_2$$

22.12.4.2 Damp-proof course

The plastic used for damp proof is a general type and has a thickness of 5×10^{-4} m. The floor covered by the plastic is slightly higher than the gross internal floor area. The value is 100 m^2. Therefore, the volume is 100 m^2 × 5×10^{-4} m = 0.05 m^3. The density of general plastic is 960 kg/m^3.

Therefore, mass $Q_{dp} = 0.05\ \text{m}^3 \times 960\ \text{kg/m}^3 = 48\ \text{kg}$.

From the Bath ICE, the embodied energy and CO_2 intensities for general plastic are 80.5 MJ/kg and 2.73 kgCO_2/kg, respectively. Therefore, the embodied energy and CO_2 are

$$EE_{dp} = 48\ \text{kg} \times 80.5\ \text{MJ/kg} = 3864\ \text{MJ}$$

$$EC_{dp} = 48\ \text{kg} \times 2.73\ \text{kg}CO_2/\text{kg} = 131.04\ \text{kg}CO_2$$

22.12.4.3 Solid foundation wall

The solid foundation wall is made up of sandcrete blocks of dimensions 20 × 20 × 40 cm. It is arrayed in two columns along the perimeter of the T3 floor plan as indicated in Figure 22.6. The total volume is 11.65 m^3. From the Bath ICE, its density, embodied energy and CO_2 are 1900 kg/m^3, 1.33 MJ/kg and 0.208 kgCO_2/kg, respectively. Therefore, the embodied energy and CO_2 emissions are

$$EE_{sw} = 11.65\ \text{m}^3 \times 1900\ \text{kg/m}^3 \times 1.33\ \text{MJ/kg} = 29439.6\ \text{MJ}$$

$$EC_{sw} = 11.65\ \text{m}^3 \times 1900\ \text{kg/m}^3 \times 0.208\ \text{kg}CO_2/\text{kg} = 4604.1\ \text{kg}CO_2$$

22.12.4.4 Mortar for foundation wall joints

The volume of the mortar for the foundation wall is estimated at 1.93 m^3. On the basis of the Bath ICE, the density, embodied energy and CO_2 intensities are

1650 kg/m^3, 1.11 MJ/kg and 0.171 kgCO_2/kg. Therefore, the embodied energy and CO_2 emissions are

$$EE_{mf} = 1.93\ m^3 \times 1650\ kg/m^3 \times 1.11\ MJ/kg = 3535\ MJ$$

$$EC_{mf} = 1.93\ m^3 \times 1650\ kg/m^3 \times 0.171\ kgCO_2/kg = 544.55\ kgCO_2$$

22.12.4.5 Concrete for ground beam, column footings

The total mass of concrete (Q_g) is given by

$$Q_g = \left(24\ kN/m^3\right) \times 4\ m^3$$

$$Q_g = 9600\ kg$$

On the basis of this assumption, the computed embodied energy and CO_2 intensities for concrete dosed at 350 kg/m^3 are 1.025 MJ {=(0.91 + 1.14)/2} and 0.1505 kgCO_2 {=(0.06 + 0.091)/2}.

$$EE_g = 9600\ kg \times \left(1.025\ MJ/kg\right)$$

$$EE_g = 9840\ MJ$$

The embodied CO_2 $EC_g = Q_g \times I_{g(CO_2)}$, where $I_{g(CO_2)}$ is the embodied CO_2 factor for concrete:

$$EC_g = 9600\ kg \times 0.1505\ kgCO_2/kg$$

$$EC_g = 1445\ kgCO_2$$

22.12.4.6 Timber for formwork

The volume of the timber for the foundation wall formwork is estimated at 0.7 m^3. On the basis of the Bath ICE, the density, embodied energy and CO_2 intensities are 90 kg/m^3, 10 MJ/kg and 0.71 kgCO_2/kg. Therefore, the embodied energy and CO_2 emissions are

$$EE_{mf} = 0.7\ m^3 \times 90\ kg/m^3 \times 10\ MJ/kg = 630\ MJ$$

$$EC_{mf} = 0.7\ m^3 \times 90\ kg/m^3 \times 0.71\ kgCO_2/kg = 45\ kgCO_2$$

22.12.4.7 Ground floor slab

The total mass of concrete (Q_s) is given by

$$Q_s = \left(24\ kN/m^3\right) \times 8.69\ m^3$$

$$Q_s = 20{,}860\ kg$$

On the basis of the Bath ICE, the embodied energy and CO_2 intensities for concrete dosed at 300 kg/m^3 were available and directly used. The values are 0.91 MJ and 0.131 kgCO_2, respectively.

$$EE_s = 20{,}860\ \text{kg} \times 0.91\ \text{MJ/kg}$$

$$EE_s = 18{,}979\ \text{MJ}$$

Total embodied CO_2 $EC_s = Q_s \times I_{s(CO_2)}$, where $I_{s(CO_2)}$ is the embodied CO_2 factor for concrete:

$$EC_s = 20{,}860\ \text{kg} \times 0.131\ \text{kg}CO_2\text{/kg}$$

$$EC_s = 2733\ \text{kg}CO_2$$

22.12.4.8 Substrate of gravel

The substrate used is made up of crushed rocks of an average thickness of 2 cm. The volume of substrate is estimated at 0.17 m^3. On the basis of the Bath ICE, the density, embodied energy and CO_2 intensities are 2240 kg/m^3, 0.083 MJ/kg and 0.0048 kgCO_2/kg. Therefore, the embodied energy and CO_2 emissions are

$$EE_{sg} = 0.17\ \text{m}^3 \times 2240\ \text{kg/m}^3 \times 0.083\ \text{MJ/kg} = 32\ \text{MJ}$$

$$EC_{sg} = 0.17\ \text{m}^3 \times 2240\ \text{kg/m}^3 \times 0.0048\ \text{kg}CO_2\text{/kg} = 1.83\ \text{kg}CO_2$$

22.12.4.9 Sand

The volume of sand is estimated at 0.04 m^3. On the basis of the Bath ICE, the density, embodied energy and CO_2 intensities are 0.2240 kg/m^3, 0.081 MJ/kg and 0.0048 kgCO_2/kg. Therefore, the embodied energy and CO_2 emissions are

$$EE_{sa} = 0.04\ \text{m}^3 \times 2240\ \text{kg/m}^3 \times 0.081\ \text{MJ/kg} = 7.30\ \text{MJ}$$

$$EC_{sa} = 0.04\ \text{m}^3 \times 2240\ \text{kg/m}^3 \times 0.0048\ \text{kg}CO_2\text{/kg} = 0.43\ \text{kg}CO_2$$

Thus, the total embodied energy and CO_2 values for the foundation are 70,154.9 MJ and 10,003.25 kgCO_2, respectively. Similarly, the embodied energy and CO_2 for the other components are computed and the summation taken to obtain the embodied energy and CO_2 for the whole T3 house as 137,934.91 MJ and 15,665.56 kgCO_2, respectively. Similarly, the embodied energy and CO_2 for the whole T4 house are 292,326.81 MJ and 378,290.19 kgCO_2, respectively.

22.13 Validation of results using building information modeling (BIM) software

On the basis of the computation of embodied energy and CO_2 of the foundation, the challenges encountered in doing the same for the whole building cannot be

underestimated. This is a key weakness of manual computation, in which mundane computational tasks are repeated for each identified building material. Furthermore, the manual process is very susceptible to errors, and the chances of identifying the errors are slim. As discussed earlier in Section 22.6, emerging BIM can be used to enhance the accuracy of process-based methods in the computation of embodied energy and CO_2. BIM also serves as an alternative to validate the computational results manually obtained. On the basis of literature review (e.g. Kurul et al., 2013), there are many BIM software products that have emerged and are currently being applied to model buildings. Revit is quite popular in the BIM software market. A major advantage of Revit is that its building models can readily be converted into interoperable or communicable formats that can be processed by other software (Abanda, Zhou, Tah, & Cheung, 2013). Comma-separated values (CSV) is a common, relatively simple file format that is easily supported by Revit and Microsoft Excel. Data stored in CSV format can be read by Excel. Outputting or representing building model information in CSV can be read by Revit or Microsoft Excel. The computational power of Microsoft Excel makes it a great choice in modeling Eqns (22.1) and (22.2), which are subsequently used in computing embodied energy and CO_2. Also, Microsoft Excel can easily be used to present computational results according to standard formats such as new rules of measurements in the United Kingdom and the Cahier des Prescriptions Techniques in France. These are rules of construction quantity measurements and output presentation. The latter was adopted for this study because it is more commonly used in Francophone countries, including Cameroon. On the basis of the two-dimensional drawings and architects' specification, T3 and T4 were modelled in Revit. The three-dimensional equivalents are presented in Figures 22.9 and 22.10.

Schedules and quantities are then generated from these models using the "Modify Schedules/Quantities" function under the "View" tab in Revit 2014. The output is converted to CSV format using the "Export" function in Revit 2014. The CSV format is stored in any preferred location on the computer and read with Microsoft Excel. Equations (22.1) and (22.2) are modelled in Excel and computations are easily conducted in this environment. The initial results obtained differ slightly from those obtained through manual computations in Section 22.12.4. The manual process is rechecked

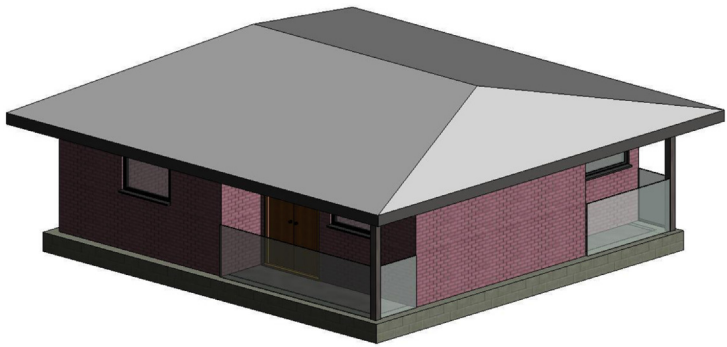

Figure 22.9 Three-dimensional T3 earth-block house Revit model.

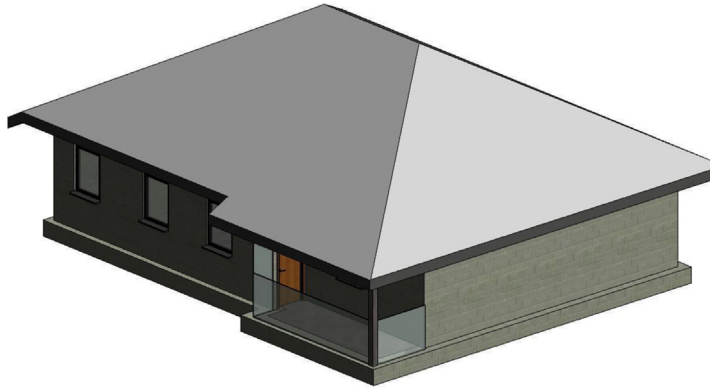

Figure 22.10 Three-dimensional T4 sandcrete-block house Revit model.

to identify and correct errors. Also, the BIM model is rechecked to identify missing components. These activities were conducted several times until common results were obtained. The results are presented in Tables 22.2 and 22.3.

22.14 Discussion and analysis

From the spreadsheet, the total embodied energy and total embodied CO_2 for the construction materials of the sandcrete-block house used in the sub-structure, superstructure, floor and wall finishes are 292,326.81 MJ and 37,829.19 $kgCO_2$ respectively. When converted to energy and carbon footprint (using gross internal area = 95.36 m^2), the values are 3065.51 MJ/m^2 and 396.7 $kgCO_2/m^2$, respectively. Other elements such as ceiling finishes, fittings and building services are not included in the result because of the lack of design specification data. Also, the embodied energy and CO_2 for the earth-block house are 137,934.91 MJ and 15,665.56 $kgCO_2$, respectively. By dividing by the GFA (68.7 m^2), the following values are obtained: 2007.8 MJ/m^2 and 228.03 $kgCO_2/m^2$, respectively.

Current available data or computation results about embodied energy and CO_2 for houses are scarce, and when they exist, they are very diverse and lack consistency. Hence, it is often too difficult to compare results from different research and draw generalizations. These disparities in results are often caused by differences in computational methods, boundary systems, construction materials, technologies and techniques used as well as discrepancies in the various database inventories used. However, to appreciate the findings of this study, results from other studies will be discussed. Pullen (2000) has reported an embodied energy value of 3.6 GJ/m^2 for a residential building. Hammond & Jones (2008) reported a mean of 5.3 GJ/m^2 and 403 $kgCO_2/m^2$ embodied energy and CO_2, respectively, for 14 residential case studies. Twelve of the 14 case studies are in the United Kingdom whereas the other 2 are in the United States. Dixit et al. (2010) also reported a mean of 5.506 GJ/m^2 of embodied energy for residential buildings. In India, Reddy & Jagadish (2003) reported embodied

Table 22.2 Embodied energy and CO_2 assessment of T3 earth-block house

No.	Description	Volume (m^3)	Density (kg/m^3)	Quantity (kg)	Embodied energy (EE) intensity (MJ/kg)	Embodied carbon (EC) intensity $kgCO_2/kg$	EE emissions (MJ)	EC emissions ($kgCO_2$)
0	**Site installation**	No data						
		Sub-total						
1	**Foundation**							
1.1	Lean concrete mix at 150 kg/m^3 of thickness = 5 cm	3.000	2200	6600	0.58	0.0755	3828	498.3
1.2	Damp-proof course/ membrane of thickness = 0.05 cm (plastic-general)	0.050	960	48	80.5000	2.7300	3864	131.04
1.3	Solid foundation wall of dimension 20 × 20 × 40 cm	11.650	1900	22,135	1.3300	0.2080	29,439.55	4604.08
1.4	Mortar for wall joints	1.930	1650	3184.5	1.1100	0.1710	3534.795	544.5495
1.5	Concrete mix at 350 kg/m^3 for footing, ground beam, sub-structure column	4.000	2400	9600	1.0250	0.1505	9840	1444.8
1.6	Timber for formwork (hardwood unspecified)	0.700	90	63	10.0000	0.7100	630	44.73

1.7	Concrete slab mix at 300 kg/m^3 of thickness = 10 cm	8.690	2400	20,856	0.91	0.131	18,978.96	2732.136
1.8	Substrate made of gravel and crushed rocks of thickness = 20 cm	0.170	2240	380.8	0.0830	0.0048	31.6064	1.82784
1.9	Sand of thickness 5 cm	0.040	2240	89.6	0.0810	0.0048	7.2576	0.43008
		Sub-total					**70,154.17**	**10,001.89**
2	**Elevations**							
2.1	Brick walls (mud)	29.400	1730	50,862	0.0000	0.0000	0	0
2.2	Mortar for wall joints	5.250	1650	8662.5	1.1100	0.1710	9615.375	1481.2875
2.3	Concrete mix at 350 kg/m^3 for super-structural beams and columns	3.000	2400	7200	1.0250	0.1505	7380	1083.6
2.4	Timber for formwork (hardwood unspecified)	1.400	90	126	10.0000	0.7100	1260	89.46
		Sub-total					**18,255.38**	**2654.35**
3	**Carpentry and roofwork**							
3.1	Timber joist of dimension 3 × 15 cm (sawn hardwood)	0.850	90	76.5	10.4000	0.8900	795.6	68.085
3.2	Roof battens of dimension 8 × 8 cm (sawn hardwood)	0.250	90	22.5	10.4000	0.8900	234	20.025

Continued

Table 22.2 Continued

No.	Description	Volume (m^3)	Density (kg/m^3)	Quantity (kg)	Embodied energy (EE) intensity (MJ/kg)	Embodied carbon (EC) intensity $kgCO_2/kg$	EE emissions (MJ)	EC emissions ($kgCO_2$)
3.3	Aluminum roof covering	0.060	2700	162.00	155.0000	8.2400	25,110	1334.88
3.4	Ceiling plywood	0.320	540	172.8	15.0000	1.0700	2592	184.896
3.5	Aluminum ridge board	0.002	2700	5.4	155.0000	8.2400	837	44.496
3.6	Wooden fascia (sawn hardwood)	0.030	700	21	10.4	0.89	218.4	18.69
3.7	Aluminum on fascia	0.006	2700	16.2	155.0000	8.2400	2511	133.488
		Sub-total					**32,298.00**	**1804.56**
4	**Electricity**	No data						
5	**Plumbing**	No data						
6	**Tiles and paintings**							
6.1	Bathroom wall ceramic tiles of dimension 30 × 30 cm	0.040	2000	80	10.0000	0.66	800	52.8
6.2	Bathroom tiles 15 × 15 cm	0.008	1700	13.6	29.0000	1.5100	394.4	20.536
6.3	Mortar for posing of tiles	0.009	1900	17.1	1.3300	0.2080	22.743	3.5568
		Sub-total					**1217.14**	**76.89**

7	**Wood and steel works**							
7.1	Wooden door panel of thickness 4 cm including frames	0.220	700	154	10.4	0.89	1601.6	137.06
7.2	Aluminum locks			3	155.0000	8.2400	465	24.72
7.3	Timber window including frames	0.200	700	140	10.4	0.89	1456	124.6
7.4	Glass louvres	0.090	25	2.25	15.0000	0.86	33.75	1.935
7.5	Aluminum glass louvres' holders			4	155.0000	8.24	620	32.96
7.6	Steel window protectors	0.075	7850	588.75	20.1	1.37	11,833.875	806.5875
		Sub-total					**16,010.23**	**1127.86**
	Grand total						**137,934.91**	**15,665.56**

Table 22.3 **Embodied energy and CO_2 assessment of T4 sandcrete-block house**

No.	Description	Volume (m^3)	Density (kg/m^3)	Quantity (kg)	Embodied energy (EE) intensity (MJ/kg)	Embodied carbon (EC) intensity $kgCO_2/kg$	EE emissions (MJ)	EC emissions ($kgCO_2$)
0	**Site installation**	No data						
1	**Foundation**							
1.1	Lean concrete mix at 150 kg/m^3 of thickness = 5 cm	3.850	2200	8470	0.58	0.0755	4912.60	639.49
1.2	Damp-proof course/ membrane of thickness = 0.05 cm (plastic-general)	0.070	960	67.20	80.5000	2.7300	5409.60	183.46
1.3	Solid foundation wall of dimension 20 × 20 × 40 cm	16.640	1900	31,616	1.3300	0.2080	42,049.28	6576.13
1.4	Mortar for wall joints	2.400	1650	3960	1.1100	0.1710	4395.60	677.16
1.5	Concrete mix at 350 kg/m^3 for footing, ground beam, sub-structure column	5.840	2400	14,016	1.0250	0.1505	14,366.40	2109.41
1.6	Timber for formwork (hardwood unspecified)	0.900	90	81.00	10.0000	0.7100	810.00	57.51

1.7	Concrete slab mix at 300 kg/m^3 of thickness = 10 cm	11.500	2400	27,600	0.91	0.1310	25,116.00	3615.60
1.8	Substrate made of gravel and crushed rocks of thickness = 20 cm	0.240	2240	537.60	0.0830	0.0048	44.62	2.58
1.9	Sand of thickness 5 cm	0.060	2240	134.40	0.0810	0.0048	10.89	0.65
		Sub-total					**97,114.99**	**13,861.97**
2	**Elevations**							
2.1	Sandcrete blocks for walls (cement-sand mix ratio 1:3)	38.000	1900	72,200	1.3300	0.2080	96,026.00	15,017.60
2.2	Wall joint mortar (cement-sand ratio 1:4)	6.100	1650	10,065	1.1100	0.1710	11,172.15	1721.12
2.3	Concrete mix at 350 kg/m^3 for superstructural beams and columns	4.000	2400	9600	1.0250	0.1505	9840.00	1444.80
2.4	Timber for formwork (hardwood unspecified)	1.700	90	153	10.0000	0.7100	1530.00	108.63
2.5	Mortar for wall plastering	4.300	1900	8170	1.3300	0.2080	10,866.10	1699.36
		Sub-total					**129,434.25**	**19,991.51**

Continued

Table 22.3 Continued

No.	Description	Volume (m^3)	Density (kg/m^3)	Quantity (kg)	Embodied energy (EE) intensity (MJ/kg)	Embodied carbon (EC) intensity $kgCO_2/kg$	EE emissions (MJ)	EC emissions ($kgCO_2$)
3	**Carpentry and roofwork**							
3.1	Timber joist of dimension 3 × 15 cm (sawn hardwood)	1.050	90	94.50	10.4000	0.8900	982.80	84.11
3.2	Roof battens of dimension 8 × 8 cm (sawn hardwood)	0.350	90	31.50	10.4000	0.8900	327.60	28.04
3.3	Aluminum roof covering	0.080	2700	216	155.0000	8.2400	33,480.00	1779.84
3.4	Ceiling plywood	0.480	540	259.20	15.0000	1.0700	3888.00	277.34
3.5	Aluminum ridge board	0.003	2700	8.10	155.0000	8.2400	1255.50	66.74
3.6	Wooden fascia (sawn hardwood)	0.026	700	18.20	10.4	0.89	189.28	16.20
3.7	Aluminum on fascia	0.007	2700	18.90	155.0000	8.2400	2929.50	155.74
		Sub-total					**43,052.68**	**2408.00**
4	**Electricity**	No data						
5	**Plumbing**	No data						

6	**Tiles and paintings**							
6.1	Bathroom wall ceramic tiles of dimension 30 × 30 cm	0.075	2000	150.00	10.0000	0.66	1500.00	99.00
6.2	Bathroom tiles 15 × 15 cm	0.015	1700	25.50	29.0000	1.5100	739.50	38.51
6.3	Mortar for posing of tiles	0.020	1900	38.00	1.3300	0.2080	50.54	7.90
		Sub-total					**2290.04**	**145.41**
7	**Wood and steel works**							
7.1	Wooden door panels of thickness 4 cm including frames	0.220	700	154.00	10.4	0.89	1601.60	137.06
7.2	Aluminum locks			4.00	155.0000	8.2400	620.00	32.96
7.3	Timber window including frames	0.200	700	140	10.4	0.89	1456.00	124.60
7.4	Glass louvres	0.130	25	3.25	15.0000	0.8600	48.75	2.80
7.5	Aluminum glass louvers' holders			6.00	155.0000	8.24	930.00	49.44
7.6	Steel window protectors	0.100	7850	785	20.1	1.37	15,778.50	1075.45
		Sub-total					**20,434.85**	**1422.31**
	Grand total						**292,326.81**	**37,829.19**

energy values of 4.21, 2.92 and 1.61 GJ/m^2 for clay brick masonry walls building with reinforced concrete structure, load-bearing brickwork and soil-cement block house, respectively. Also, another study in India revealed that the embodied energy for reinforced cement concrete and mud houses are 3702.3 and 2298.8 MJ/m^2, respectively (Chel & Tiwari, 2009). In the most recent, IPCC fifth assessment report, wood-based wall systems entail 10−20% less embodied energy than traditional concrete systems (Sathre & Gustavsson, 2009; Upton, Miner, Spinney, & Heath, 2008) and concrete-framed buildings entail less embodied energy than steel-framed buildings (Xing, Xu, & Jun, 2008).

What emerges from these studies is the fact that the values obtained for embodied energy and CO_2 for two typical houses in Cameroon are in the same range as those from other countries, especially India. The results reveal that a sandcrete-block house (T4) expends at least 1.5 times more embodied energy than an earth or earth-block house (T3). Furthermore, a sandcrete-block house emits at least 1.7 times more embodied CO_2 than an earth-block house.

Although embodied energy and CO_2 are important factors, it is also important to consider the effects of material choice on the energy requirements for cooling and heating over the lifetime of the building (Böjesson & Gustavsson, 2000; Lenzen & Treloar, 2002). Some studies have revealed embodied energy to be equivalent to a few years of operating energy (Levine et al., 2007), although cases in which embodied energy can be much higher have also been reported (Lippke, Wilson, Perez-Garcia, Bowyer, & Meil, 2004). In particular, in most developing countries, the embodied energy of most traditional buildings can be large compared with operating energy (Levine et al., 2007). This is mostly because most of the traditional buildings do not contain energy-intensive or energy-consuming appliances. What these discrepancies suggest is that a holistic approach should be undertaken when embodied energy and operational energy should be considered in assessing the energy use and environmental impacts of a building.

22.15 Conclusions

In this study, the process-based approach supported by some mathematical models was used to compute embodied energy and CO_2 for two typical houses in Cameroon. The process-based approach was manual, and because of the susceptibility of such an approach to errors, BIM software was used to validate the computational results. Because of the lack of data, embodied energy and CO_2 for site installation, electricity and plumbing were not computed. Also because of data scarcity, emissions from the transport of construction materials and personnel, on-site equipment such as concrete mixers and vibrators were not assessed. It is important to note that this is an emerging field, and knowledge in this field is gradually being explored. Hence, only emissions from construction materials were assessed. The results obtained were converted to per unit square meters to facilitate comparison. Furthermore, when compared with other studies, the computational results were in the same range, although they were significantly lower than values obtained in

the developed countries (e.g. United Kingdom). The comparison revealed that sandcrete-block houses consumed more embodied energy and CO_2 than earth-block houses.

References

Abanda, F. H., Zhou, W., Tah, J. H. M., & Cheung, F. (2013). Exploring the relationships between linked open data and building information modelling (BIM). In: *Proceedings of the sustainable building and construction (SB 13) conference; 2013 July 3−5*. UK: Coventry University.

Adedeji, Y. M. D. (2010). Technology and standardised composite cement fibres for housing in Nigeria. *Nigerian Institute of Architects Journal, 1*, 19−24.

Adedeji, Y. M. D., & Fa, G. (2012). Sustainable housing provision: preference for the use of interlocking masonry in housing delivery in Nigeria. *Environmental Research and Management, 3*(1), 009−016.

Bashir, U. M., Iro, A. I., & Babanyara, Y. Y. (2013). Inherent energy in demolition: re-use or recycle? (a case study of roads construction led demolition in Gombe Metropolis). *The International Journal of Engineering and Science, 2*(7), 19−24.

Blengini, G. A., & Carlo, T. D. (2010). The changing role of life cycle phases, subsystems and materials in the LCA of low energy buildings. *Energy and Buildings, 42*, 869−880.

Böjesson, P., & Gustavsson, L. (2000). Greenhouse gas balances in building construction: wood versus concrete from life-cycle and forest land-use perspectives. *Energy Policy, 28*(9), 575−588.

Boulter, P. G., Barlow, T. J., & McCrae, I. S. (2009). *Emission factors 2009: Report 3−exhaust emission factors for road vehicles in the United Kingdom*. UK: Department for Transport.

Bruelisauer. M. (2007). *Sustainable construction in South Africa−Theoretical and practical analysis of sustainable infrastructures in the case study of the Hawequas Straw Bale Accommodation* (Diploma thesis in Civil Engineering). Zurich: Institute for Transport Planning and Systems and Swiss Federal Institute of Technology.

BS EN. (2011). *BS EN 15978 sustainability of construction works assessment of environmental performance of buildings calculation method*. UK: BSI Group Headquarters.

Cabeza, L. F., Barreneche, C., Miró, L., Morera, J. M., Bartolí, E., & Fernández, A. I. (2013). Low carbon and low embodied energy materials in buildings: a review. *Renewable and Sustainable Energy Reviews, 23*, 536−542.

Cabeza, L. F., Rincón, L., Vilariño, V., Pérez, G., & Castell, A. (2014). Life cycle assessment (LCA) and life cycle energy analysis (LCEA) of buildings and the building sector: a review. *Renewable and Sustainable Energy Reviews, 29*, 394−416.

Chel, A., & Tiwari, G. N. (2009). Thermal performance and embodied energy analysis of a passive house-case study of vault roof mud-house in India. *Applied Energy, 86*(10), 1956−1969.

Cout, R., & Trois, C. (2010). Waste management activities and carbon emissions in Africa. *Waste Management, 31*(1), 131−137.

Crawford, R. H., & Treloar, G. J. (2003). Validation of the use of Australian input-output data for building embodied energy simulation. In: *Proceedings of the 8th international IBPSA conference, 2003 August 11−14, Eindhoven, The Netherlands*.

Dixit, M. K., Fernandez-Solis, J. L., Lavy, S., & Culp, C. H. (2010). Identification of parameters for embodied energy measurement: a literature review. *Energy and Buildings, 42*, 1238−1247.

Dixit, M. K., Fernandez-Solis, J. L., Lavy, S., & Culp, C. H. (2012). Need for an embodied energy measurement protocol for buildings: a review paper. *Renewable and Sustainable Energy Reviews, 16*, 3730−3743.

Edwards, B. (2010). *Rough guide to sustainability: A design primer*. UK: RIBA Publishing.

Esteban, W., & Aimee, P. C. B. (2012). Building tomorrow: a sustainable future starts in the classroom. In: *Proceedings of sustainable futures conference: Architecture and urbanism in the global south: Kampala, Uganda − June 25−30, 2012*.

Fombe, L. F., & Ntani, M. D. (2012). Building and endangering urban landscapes: the case of construction wastes in Bamenda, Cameroon. *Sustainable Development, 5*(10), 60−67.

Goggins, J., Keane, T., & Kelly, A. (2010). The assessment of embodied energy in typical reinforced concrete building structures in Ireland. *Energy and Buildings, 42*, 735−744.

González, M. J., & Navarro, J. G. (2006). Assessment of the decrease of CO_2 emissions in the construction field through the selection of materials: practical case study of three houses of low environmental impact. *Building and Environment, 41*(7), 902−909.

Gumaste, K. S. (2006). Embodied energy computations in buildings. In *National conference on advances in energy research (AER-2006) at IIT Bombay, Mumbai, 4th−5th December; 2006* (pp. 404−409).

Hammond, G. P. (2007). Industrial energy analysis, thermodynamics and sustainability. *Applied Energy, 84*, 675−700.

Hammond, G. P., & Jones, C. I. (2008). Embodied energy and carbon in construction materials. *Energy, 161*(EN2), 87−98.

Hannon, B. (1973). The structure of ecosystems. *Journal of Theoretical Biology, 41*(3), 535−546.

Harries, H. (2007). *Embodied energy: Masonry walling in South Africa*. Technical Note #7. [Online] http://www.claybrick.org/content/07-embodied-energy-masonry-walling-south-africa Accessed 10.05.10.

Hugo, J., Stoffberg, H., & Barker, A. (2012). Mitigating climate change by minimising carbon footprint and embodied energy of construction materials: a comparative analysis of three South African bus rapid transit (BRT) stations. *Acta Structilia, 19*(2), 21−45.

Irurah, D. K., & Holm, D. (1999). Energy impact analysis of building construction as applied to South Africa. *Construction Management and Economics, 17*, 363−374.

Kurul, E., Abanda, F. H., Tah, J. H. M., & Cheung, F. (2013). Rethinking the build process for BIM adoption. In: *Proceedings of the CIB world building congress construction and society; 2013 May 5−9, Australia*.

Lenzen, M., & Treloar, G. (2002). Embodied energy in buildings: wood versus concrete − reply to Börjesson and Gustavsson. *Energy Policy, 30*(3), 249−255.

Leontief, W. (1966). *Input-output economics*. New York, NY, USA: Oxford University Press.

Leontief, W. (1970). Environmental repercussions and the economic structure: an input-output approach. *Review of Economics and Statistics, 52*(3), 262−271.

Levine, M., Ürge-Vorsatz, D., Blok, K., Geng, L., Harvey, D., Lang, S., et al. (2007). Residential and commercial buildings. In: *Climate change 2007: Mitigation. Contribution of working group III to the fourth assessment report of the intergovernmental panel on climate change*. Cambridge, United Kingdom and New York, NY, USA: Cambridge University Press.

Lippke, B., Wilson, J., Perez-Garcia, J., Bowyer, J., & Meil, J. (2004). CORRIM: life-cycle environmental performance of renewable building materials. *Forest Products, 54*(6), 8−19.

McGinlay, J. (2004). *Non-road mobile machinery usage, life and correction factors*. Report to the Department for Transport. UK: Department for Transport.

Meukam, P., Jannot, Y., Noumowe, A., & Kofane, T. C. (2004). Thermo physical characteristics of economical building materials. *Construction and Building Materials, 18*(6), 437−443.

Mohammed, A., & Mu'azu, A. M. N. (2011). Energy efficient buildings as a tool for ensuring sustainability in the building industry. In: *Proceedings of the 2011 international conference on multimedia technology (ICMT), 26–28 July 2011, Hangzhou, China*.

Mpakati-Gama, E. C., Wamuziri, S., & Sloan, B. (2011). Applicability of inventory methods for embodied energy assessment of buildings in sub-Sahara Africa. *The Built & Human Environment Review, 4*(Special Issue 2).

Nwokoro, I., & Onukwube, H. (2011). Sustainable or green construction in Lagos, Nigeria: principles, attributes and framework. *Journal of Sustainable Development, 4*(4), 166–174.

Osmani, M. (2011). Construction waste. In T. M. Letcher, & D. A. Vallero (Eds.), *Waste: A handbook for management* (pp. 207–218). Burlington, MA: Academic Press.

Pacheco-Torgal, F., Faria, J., & Jalali, S. (2013). Embodied energy versus operational energy. Showing the shortcomings of the energy performance building directive (EPBD). *Materials Science Forum, 730–732*, 587–591.

Pullen, S. (2000). Estimating the embodied energy of timber building products. *Institute of Wood Science, 15*(3), 147–151.

Ramesh, T., Prakash, R., & Shukla, K. K. (2010). Life cycle energy analysis of buildings: an overview. *Energy and Buildings, 42*(10), 1592–1600.

Reddy, B. V. V. (2009). Sustainable materials for low carbon buildings. *International Journal Low-carbon Technologies, 4*, 175–181.

Reddy, B. V. V., & Jagadish, K. S. (2003). Embodied energy of common and alternative building materials and technologies. *Energy and Buildings, 35*, 129–137.

Robiglio, V., Ngendakumana, S., Yemefack, M., Tchienkoua, M., Gockowski, J., Tchawa, P., et al. (2010). *Reducing emissions from all land uses*. Report for REALU Project-Cameroon. ICRAF Working Paper no. XX. Nairobi: World Agroforestry Centre.

Sartori, I., & Hestnes, A. G. (2007). Energy use in the life cycle of conventional and low-energy buildings: a review article. *Energy and Buildings, 39*(3), 249–257.

Sathre, R., & Gustavsson, L. (2009). Using wood products to mitigate climate change: external costs and structural change. *Applied Energy, 86*, 251–257.

Seo, S., & Hwang, Y. (2001). Estimation of CO_2 emissions in life cycle of residential buildings. *Construction Engineering and Management, 127*(5), 414–418.

Shrivastava, S., & Chini, A. (2012). Using building information modeling to assess the initial embodied energy of a building. *The International Journal of Construction Management, 12*(1), 51–63.

Sturgis, S., & Roberts, G. (2010). *Redefining zero: Carbon profiling as a solution to whole life carbon emission measurement*. London: The Royal Institution of Chartered Surveyors.

The Sustainability Institute. (2009). *Sustainable neighbourhood design manual: A non-technical guide. Final draft for comment* [Online] http://www.sustainabledevelopmentnetwork.com/manual1/INTEGRATED%20SUSTAINABLE%20SETTLEMENTS.pdf Accessed 30.05.14.

Thormark, C. (2006). The effect of material choice on the total energy need and recycling potential of a building. *Building and Environment, 41*(8), 1019–1026.

Treloar, G. J. (1997). Extracting embodied energy paths from input-output tables: towards an input-output based hybrid energy analysis method. *Economic Systems Research, 9*(4), 375–391.

Treloar, G. J., Gupta, H., Love, P. E. D., & Nguyen, B. (2003). An analysis of factors influencing waste minimisation and use of recycled materials for construction of residential buildings. *Management of Environmental Quality: An International Journal, 14*(1), 134–145.

Upton, B., Miner, R., Spinney, M., & Heath, L. S. (2008). The greenhouse gas and energy impacts of using wood instead of alternatives in residential construction in the United States. *Biomass and Bioenergy, 32*, 1−10.

Ürge-Vorsatz, D., & Novikova, A. (2008). Potentials and costs of carbon dioxide mitigation in the world's buildings. *Energy Policy, 36*, 642−661.

Van Gool, W. (1980). Thermodynamic aspects of energy conservation. *Energy, 5*, 783−792.

Verbeeck, G., & Hens, H. (2010). Life cycle inventory of building: a calculation method. *Building and Environment, 45*, 1037−1041.

Xing, S., Xu, Z., & Jun, G. (2008). Inventory analysis of LCA on steel and concrete construction office buildings. *Energy and Buildings, 40*, 1188−1193.

Index

Note: Page numbers followed by f and t indicate figures and tables respectively.